Faculté des Sciences Appliquées
Département d'Architecture, Géologie, Environnement et Constructions
Secteur Ingénierie Structurale

Seismically retrofitting reinforced concrete moment resisting frames by using expanded metal panels

Thèse présentée par

PHUNG NGOC DUNG

en vue de l'obtention du grade de
Docteur en Sciences de l'Ingénieur

2011

Acknowledgments

I would like to express my deepest appreciation to my advisor Professor André Plumier for his guidance throughout my thesis, his kindness and encouragement and also many thanks to his nice family.

I am very grateful to Doctor Hervé Degée for helping me understand many fundamental things in dynamics of structures and direct displacement based design.

I would like to thank the Vietnamese Government and the French Community of Belgium for funding for the research.

I would like to thank all people in Structural Engineering Sector of ArGenCo department at the University of Liège.

I would like to thank my wife Minh Hien, my daughters Minh Thu and Minh Hoa, who are always by my side during my time at University of Liège.

ABSTRACT OF THE DISSERTATION

Reinforced concrete moment resisting frames (RC-MRFs) have been widely used as the main structural resisting systems for over 30 years based on their capacity in resisting both gravity loads and lateral forces like winds or earthquakes and on low cost of construction. However, there have been still many existing RC-MRFs not designed according to any modern seismic code. This may lead to some undesired failures under a rather low intensity earthquake. There are several existing retrofitting systems available for seismically retrofitting RC-MRFs, such as steel braces, steel plate or RC shear walls, base isolators…In those, some are able to increase the stiffness, strength, deformation and energy absorbing capacity of the structures and some are able to reduce the influence of the seismic actions on the structure. Despite having advantage in increasing the stiffness and strength for the buildings, the use of bulky systems like RC shear walls to retrofit buildings under seismic actions becomes more limited due to its complication in erection and high costs for foundation. The use of lighter retrofitting systems such as steel braces or shear walls made from steel or aluminium… has been becoming more favourable.

Made from sheet steel or various alloys by cutting and simultaneous stretching cold, expanded metal is considered as a macro-foam material. An expanded metal panel (EMP) with rectangular dimensions of 1.25m x 2.5m having many rhomb shape stitches with different geometrical sizes is the popular product. Currently it is employed primarily in the areas of protection (fencing, gates) and architecture. The final goal of this study is to consider a new application different in the field of civil engineering and more specifically that of the earthquake resistance of buildings. The work plan includes two main parts. This first part will set the EMP over existing techniques and see if its use is justified in the context of earthquake resistance. In addition, a more detailed description of the EMP is considered. In this way, the different data required for modelling the new resistance system are known and analyzes, tests and comparisons can be made in order to validate the use of EMP in the context of earthquake resistance. A complete study on pure shear behaviour of EMP under monotonic and quasi-static cyclic loading has been developed including experimental, theoretical and numerical investigations.

To apply EMP in seismically retrofitting RC-MRFs, thirty two RC-MRFs have been designed according to two codes EC2 and EC8. The seismic performance of the studied frames has been evaluated using Pushover and NLTH analyses. For the frames designed according to EC2 or EC8 with low ductility, some prominent deficiencies are found, such as incomplete load path or the soft-story failure. Based on the knowledge of deficiencies of the existing frames, many attempts to exploit EMP to seismically retrofit the existing frames have been made. All frames designed according to EC2 and EC8 with Low Ductility Class need to retrofit because they cannot reach the target displacements due to premature failure of beam-column joints. To seismically retrofit them by using EMP, a design procedure based on Direct Displacement Based Design (DDBD) has been proposed. The design is an iterative procedure, starting with the selection of the target displacements at the top based on the results from Pushover analysis. They are usually less than the limit displacements at which RC frames collapse due to crushing of the concrete at beam-column joints. These displacements are also the target ones for the retrofitted frames. The results from design procedure proposed are significantly affected by some typical factors such as selected target displacements and capacity of the existing frames contributing to overall resistance of the retrofitted frames, equivalent viscous damping of the EMP and MRFs as well as geometrical dimensions of the existing frames. The retrofitted design results, assessed by Pushover and NLTH analyses, have indicated that DDDB is a useful tool to design EMP to seismically retrofit the existing frames. With EMP, all retrofitted frames can reach target displacements under design earthquakes without any brittle failure, not like the original frames. However, EMP cannot improve the behaviour of the beam-column joints. Under the earthquakes greater than design ones, failure of the nodes is still observed in all retrofitted frames. The comparison of the seismic performance of the frames before and after being retrofitted has shown that EMP is able to reduce the influence of the earthquake on the original frames by increasing their strength and stiffness and by absorbing the seismic energy. Proposed design procedure of connection between EMP and the frame elements is applicable. This was verified in the experiments when connecting EMP with the steel testing frames. The design approach for the connection is based on Capacity Design, all starting with the maximum resistance of the bars in a rhomb-shape stitch of the EMP and the tension field action developed in the EMP during shear loading. However, it is necessary to perform tests on the connections between EMP and the RC beams and columns. Also, improved practical details can be developed.

LIST OF CONTENTS

LIST OF CONTENTS **7**

LIST OF TABLES **15**

LIST OF FIGURES **19**

LIST OF SYMBOLS AND ABBREVIATIONS **29**

1. INTRODUCTON **41**

1.1. Problem description and motivation 41

1.2. Objectives and Scope of the research 42

1.3. Organisation of the thesis 42

2. OVERVIEW OF SEISMIC EVALUATION AND RETROFIT OF REINFORCED CONCRETE MOMENT RESISTING FRAMES (RC-MRFS) **43**

2.1. Introduction 43

2.2. Determination of performance levels, seismic hazards, performance objectives, and deficiencies of the existing RC-MRFs 44

2.2.1. Performance levels 44

2.2.2. Seismic hazards 46

2.2.3. Performance objectives 47

2.2.4. Determination of deficiencies of an existing RC-MRFs 47

2.3. Analysis methods to evaluate the seismic performance and deficiencies of RC-MRFs 48

2.3.1. Capacity 49

2.3.2. Demand (displacement) 49

2.3.3. Performance 51

2.4. Retrofit strategies 51

2.4.1. Technical strategies 52

2.4.1.1. System completion 53

2.4.1.2. System strengthening and stiffening 53

2.4.1.3. Enhancing deformation capacity 54

2.4.1.4. Reducing earthquake demands 55

2.4.2. Management strategies 55

2.5. Recent Seismic Retrofitting systems for RC-MRFs 55

2.5.1. Retrofitting System using Conventional Steel Concentric Braces (CBFs) 55

2.5.1.1. Introduction 55

2.5.1.2. Configuration of CBFs 55

2.5.1.3. Experimental studies on CBF 56

2.5.1.4. Analytical studies and hysteretic behaviour of CBF 58

2.5.1.5. Design concepts of retrofit of RC-MRFs using CBF 59

2.5.2. Retrofitting system using Steel Buckling Restrained Braces (BRBs) 60

2.5.2.1. Introduction 60

2.5.2.2. Configuration of BRBs 60

2.5.2.3. Development and studies of BRBs 61
2.5.2.4. BRB hysteretic behaviour 63
2.5.2.5. BRB design concept 63
2.5.3. Retrofitting system using Steel Eccentric Braces (EBFs) 64
2.5.3.1. Introduction 64
2.5.3.2. Configuration of EBF 64
2.5.3.3. The hysteretic behaviour of the link 65
2.5.3.4. EBF design concept 65
2.5.4. Retrofitting system using Steel Plate Shear Walls (SPSWs) 66
2.5.4.1. Introduction 66
2.5.4.2. Analytical studies of shear walls under shear loading 67
2.5.4.3. Experimental and numerical studies 71
2.5.4.4. Contribution of the external frame to the overall resistance of SPSWs 76
2.5.4.5. Hysteretic behaviour of SPSW 78
2.5.4.6. Seismic Design of SPSWs 79
2.5.4.7. Behaviour or Response Modification factors of SPSWs 81
2.5.4.8. Connections between SPSW and the boundary frames 81
2.5.5. Retrofitting system using Low Yield Steel Shear Walls (LYSWs) 82
2.5.5.1. Introduction 82
2.5.5.2. Mechanical characteristics of the LYS 83
2.5.5.3. Experimental and numerical studies of LYSWs 84
2.5.6. Retrofitting system using Aluminium Shear Walls (ASWs) 85
2.5.6.1. Introduction 85
2.5.6.2. Mechanical properties of Aluminium 85
2.5.6.3. Experimental and numerical studies of ASWs 86
2.5.7. Retrofitting system using Perforated Shear Walls (PSWs) 88
2.5.8. Retrofitting system using Reinforced Concrete Shear Walls (RCSWs) 90
2.5.8.1. Introduction 90
2.5.8.2. Capacity design of the walls 91
2.5.8.3. Ductile walls 91
2.5.8.4. Large lightly reinforced walls 93
2.5.8.5. Prefabricated walls 94
2.5.9. Retrofitting system using Composite Shear Walls (CSWs) 94
2.6. Conclusions 98
3. INTRODUCTION ABOUT EXPANDED METAL PANELS (EMP) AND PREVIOUS STUDY ON EMP 101
3.1. Introduction about EMP 101
3.1.1. Introduction 101

3.1.2. Types of EMP and current applications 102
3.1.3. Mechanical properties of EMP 103
3.1.4. Conclusions 103
3.2. Previous studies on EMP 103
3.2.1. Pure plane shear behaviour 103
3.2.2. Complete 3D analytical model of EMP under shear loading 104
3.2.3. Ultimate behaviour of square EMP loaded in shear: 105
3.2.4. Some concluding remarks of the study by Pecquet (Pecquet, 2005) 106
4. EXPERIMENTAL STUDY ON EXPANDED METAL PANELS (EMP) 107
4.1. Introduction 107
4.2. Design Considerations and Objectives of Experiments 108
4.3. Specimens 109
4.3.1. Specimens for tensile tests 111
4.3.2. Specimens for shear tests in small scale 111
4.3.3. Specimens for shear tests in large scale 114
4.3.4. Test frame 116
4.3.4.1. Test frame in small scale tests 116
4.3.4.2. Test frame in large scale tests 119
4.4. Test procedures 120
4.4.1. Tensile tests 120
4.4.2. Monotonic test phase 121
4.4.3. Quasi-static cyclic test phase 121
4.5. Test observations 122
4.5.1. Tensile tests 122
4.5.2. Small scale tests 122
4.5.2.1. Monotonic loading test phase 122
4.5.2.2. Cyclic test phase 125
4.5.3. Tests in large scale 131
4.5.3.1. Monotonic loading phase 131
4.5.3.2. Cyclic loading phase 134
4.6. Summary of observations 137
5. SIMULATIONS OF THE TESTS AND PARAMETRIC STUDY OF EMP SUBJECTED TO SHEAR LOADING BY NUMERICAL APPROACH 139
5.1. Introduction 139
5.2. Numerical simulations of the tests 139
5.2.1. Description of the model 139
5.2.1.1. Modelling of the components of the test 139
5.2.1.2. Material properties 141

5.2.1.3. Initial conditions 142
5.2.1.4. Solution strategies 143
5.2.2. Comparison of numerical analysis and experimental studies of EMP under monotonic shear loading 144
5.2.3. Comparison of numerical analysis and experimental studies of EMP under cyclic shear loading 147
5.2.4. Summary and conclusions 149
5.3. Parametric study on EMP loaded in shear 149
5.3.1. Introduction 149
5.3.2. Description of the typical test model in the parametric study 150
5.3.2.1. Components of the model 150
5.3.2.2. Finite elements 150
5.3.2.3. Material characteristics of bars 151
5.3.2.4. Characteristics of the boundary frames 152
5.3.2.5. Initial conditions 152
5.3.2.6. Residual stress 152
5.3.2.7. Steps of analyses and solution strategy 152
5.3.3. Behaviour of the EMP under monotonic shear loading 153
5.3.3.1. Prior-to-buckling shear resistance of EMP 153
5.3.3.2. Effects of initial deformations or imperfections on ultimate resistance of the EMP 156
5.3.3.3. Maximum or post-buckling shear resistance of the single EMP and equivalent models 157
5.3.3.4. Shear resistance of a combined EMP 162
5.3.3.5. Drifts and Ductility of the EMP 164
5.3.4. Simplified behaviour of the EMP under cyclic shear loading 165
5.3.4.1. Cyclic shear loading behaviour of common structural systems 165
5.3.4.2. Comparison of the hysteresis behaviours 167
5.3.4.3. General steps to analyse EMP under quasi-static cyclic shear loading 167
5.3.4.4. Description of hysteretic behaviour of EMP loaded in shear by numerical simulations 168
5.3.4.5. Simplified analytical model for hysteretic behaviour of EMP loaded in shear 171
5.4. Conclusions 172
6. DESIGN OF REINFORCED CONCRETE MOMENT RESISTING FRAMES (RC-MRFS) 175
6.1. Introduction 175
6.2. General criteria and design steps pf RC-MRFs according to EC2 175
6.2.1. Preliminary design 175
6.2.2. Limit states 176
6.2.3. Material properties 176

6.2.3.1. Concrete 176
6.2.3.2. Steel 177
6.2.4. Design situations 178
6.2.5. Partial factors of safety 178
6.2.5.1. Partial factors of materials (γ_m) 178
6.2.5.2. Partial factors of actions (γ_f) 178
6.2.6. Actions 179
6.2.6.1. Characteristic values of actions 179
6.2.6.2. Load combinations at ultimate limit states: 180
6.2.6.3. Load combinations at serviceability limit states 180
6.2.7. Analysis of internal forces of RC-MRFs 180
6.2.7.1. Modelling and idealisation of the frames 180
6.2.7.2. Structural Analysis 181
6.2.7.3. Second order effects 181
6.2.8. Analysis of the sections at ultimate limit states 182
6.2.9. Check for serviceability limit states 183
6.3. Design of RC-MRFs according to EC2 and EC8 183
6.3.1. General introduction about seismic design 183
6.3.2. Design concepts, limitations of the studied RC-frames in accordance with EC8 184
6.3.3. General criteria of the design process 185
6.3.3.1. Design situations 185
6.3.3.2. Materials 186
6.3.3.3. Partial factors of safety 186
6.3.3.3.1. Partial factors of materials (γ_m) 186
6.3.3.3.2. Partial factors of actions (γ_f) 186
6.3.4. Actions 186
6.3.4.1. Actions in cases of persistent design situations 186
6.3.4.2. Actions in cases of seismic design situations 187
6.3.4.2.1. Ultimate limit states and no-collapse requirements (NCR) 187
6.3.4.2.1.1. Design peak ground acceleration (PGA) 187
6.3.4.2.1.2. Elastic spectra of the horizontal components in EC8 187
6.3.4.2.1.3. Design spectrum for elastic analysis 188
6.3.5. Ground types 189
6.3.6. Methods of analysis 189
6.3.7. Simplified modelling of the frames for linear analysis 190
6.3.8. Combinations of actions 192
6.3.8.1. Serviceability limit states – damage limitation state 192

6.3.9. Capacity design for longitudinal reinforcements of columns and transverse reinforcements of beams and columns 193
6.3.10. Detailing requirements 195
6.4. Case study structures 200
6.4.1. Description of case study RC-MRFs 200
6.4.2. RC-MRFs designed according to both EC2 and EC8 206
6.4.2.1. Global design results 208
6.4.2.2. Longitudinal reinforcement configurations of the RC-MRFs studied 211
6.4.2.3. Capacity design for transversal reinforcements of beams and columns 216
6.4.3. Some concluding remarks on the reinforcement configurations between DCL and DCM design of RC-MRFs in EC8-group 217
6.4.4. RC-MRFs designed according to EC2 217
6.4.4.1. Frame analysis 217
6.4.4.2. Longitudinal reinforcement configurations of the beams and columns of studied frames 219
6.4.4.3. Transversal reinforcement Configuration and Limitations of the studied RC-MRFs 221
6.5. Summary 222
7. SEISMIC EVALUATION OF EXISTING RC-MRFS 225
7.1. Introduction 225
7.2. Steps for seismic evaluation of the existing RC-MRFs 225
7.3. General models of RC-MRFs for seismic evaluation 226
7.3.1. Introduction 226
7.3.2. Modelling of beams and columns 226
7.3.2.1. Linear elastic beam element 227
7.3.2.2. Inelastic beam element 228
7.3.3. Damping 234
7.4. Seismic actions 235
7.5. Nonlinear methods of seismic evaluation of RC-MRF 236
7.5.1. Nonlinear static ('Pushover') analysis 236
7.5.2. Nonlinear dynamic (time-history) analysis (NLTH) 241
7.6. Seismic performance of the case study RC-MRFs 241
7.6.1. Introduction 241
7.6.2. Basic Assumptions and methodology for nonlinear analyses 241
7.6.2.1. Methodology 241
7.6.2.2. Detail modelling assumption and input data 242
7.6.2.3. Responses controlled the seismic performance of the studied RC-MRFs 248
7.6.2.4. Definition of ductility and ultimate response for the RC-MRFs 249
7.6.3. Evaluation of response of the RC-MRFs studied 250

7.6.3.1. Brief re-description of the existing RC-MRFs 250
7.6.3.2. Linear and nonlinear periods of the studied RC-MRFs 251
7.6.3.3. Nonlinear response of the studied RC-MRFs 253
7.7. Concluding remarks 268
8. ON THE USE OF EMP TO SEISMICALLY RETROFIT OR UPGRADE RC-MRFS .. 269
8.1. Introduction 269
8.2. Summary of geometrical characteristics and seismic behaviour of EMP under shear 269
8.2.1. Summary of typically geometrical configurations of EMP 269
8.2.2. Summary of seismic behaviour of EMP under shear 270
8.3. Background of Direct Displacement-Based Design (DDBD) 272
8.3.1. The need of Direct Displacement-Based Seismic Design approach for retrofitting RC-MRFs by using EMP 272
8.3.2. Background of Direct Displacement-Based Design (DDBD) for RC-MRFs 272
8.3.2.1. General background of DDBD 273
8.3.2.2. The main governing steps of DDBD for designing or retrofitting a frame structure 273
8.4. Application of DDBD for seismically retrofitting RC-MRFs by using EMP 276
8.4.1. General introduction 276
8.4.2. Target displacements or target drifts for the retrofitted RC-MRFs and maximum shear resistance of the RC-MRFs 276
8.4.3. Target displacement profiles for the retrofitted RC-MRFs 277
8.4.4. Equivalent Viscous Damping of RC-MRF with EMP 278
8.4.4.1. EVD of the reinforced concrete frames 279
8.4.4.2. EVD of the EMP 280
8.4.4.3. EVD of the retrofitted RC-MRFs with EMP 282
8.4.5. Design, selection and distribution of EMP for the RC-MRFs 282
8.4.6. Chart for design of EMP to seismically retrofit the frames 284
8.5. Design of EMP retrofitting in case study RC-MRFs using DDBD method 286
8.5.1. Case study example 1 286
8.5.2. Case study example 2 291
8.5.3. Verification of the proposed method and seismic evaluation of the case study RC-MRFs retrofitted by EMP using Pushover and NLTH analyses 296
8.5.3.1. Modelling of RC-MRFs and seismic input for nonlinear analyses 296
8.5.3.2. Modelling of EMP for nonlinear analyses 296
8.5.3.3. Seismic response of the retrofitted frames in comparison with the ones before retrofitting of the two examples by Pushover and NLTH analyses 297
8.5.4. General results of retrofitting design of the existing frames based on DDBD 300
8.5.4.1. RC-MRFs in EC2 group 300
8.5.4.2. RC-MRFs in EC8 group 302

8.6. Nonlinear response of the retrofitted structures in comparison with the structures before retrofitting 304
8.6.1. Periods 304
8.6.2. Comparison of nonlinear response of the studied RC-MRFs before and after retrofitted .. 305
8.7. Some existing practical solutions to retrofit beam-column nodes or to increase shear resistance of RC beams and columns 330
8.8. Design of connections of EMP with boundary elements of the frames 331
8.8.1. Description of the connection between EMP and the frame elements 332
8.8.2. Design of the connections between EMP and the frame's elements 332
8.8.2.1. Design of the connection between EM sheets to obtain a complete EMP 332
8.8.2.2. Design of the connection between EMP and the boundary frame elements 333
8.8.3. An example of designing the connections between EMP and the frame's elements 333
8.8.3.1. Connection between EM sheets to obtain a complete EMP 333
8.8.3.2. Connection between EMP and the boundary frame elements 334
8.9. Concluding remarks 338
9. CONCLUSIONS AND RECOMMENDATIONS 341
9.1. Conclusions 341
9.2. Recommendations 344
REFERENCES 345

LIST OF TABLES

Table 2-1 – Building performance levels in FEMA 356 (2000) 45
Table 2-2 – Structural performance levels and damage – Vertical Elements in FEMA 356 (2000) 45
Table 2-3 – Structural performance levels and damage – Horizontal Elements in FEMA 356 (2000) 46
Table 2-4 – Deficiencies in RC-MRFs (ATC 40, 1997) 48
Table 2-5 – R values for SPSW proposed by Astanaeh-Asl 81
Table 2-6 – Chemical composition of LYS (Nippon Steel Corp. standard) (Yamaguchi et al., 1998) 83
Table 2-7 – Mechanical properties of LYS (Nippon Steel Corp. standard) (Yamaguchi et al., 1998) 83
Table 2-8 – Chemical composition and mechanical properties of EN-AW 1050A (De Matteis et al., 2005) 86
Table 2-9 – Properties of the test specimens (Astaneh, 2000) 96
Table 2-10 – A comparison of R and q factors in US and Europe 98
Table 3-1 – Distinction between the name of normal and flattened types of EMP 102
Table 4-1 – Test specimens in small scale tests 113
Table 4-2 – Summary of all specimens in large scale tests 116
Table 4-3 – Exploiting the data from monotonic tests 121
Table 4-4 – Cyclic test procedures 121
Table 4-5 – Typical mechanical properties of an EM bar 122
Table 4-6 – Monotonic test results in small scale – weld specimens 125
Table 4-7 – First four cycle results of specimens with welded connections 127
Table 4-8 – Cyclic test results at displacements corresponding to maximum resistance in monotonic tests – welded specimens 127
Table 4-9 – Maximum shear resistance in cyclic tests and corresponding displacements – welded specimens 128
Table 4-10 – First four cycle results of specimens with epoxy-glued connections 128
Table 4-11 – Cyclic testing results at displacements corresponding to maximum resistance in monotonic tests – epoxy-glued specimens 129
Table 4-12 – Monotonic test results in large scale 131
Table 4-13 – First four cycle results of specimens with welded connections 135
Table 4-14 – Cyclic results at displacements corresponding to ultimate forces in monotonic tests (*Corres. – Corresponding) 136
Table 4-15 – Maximum shear forces in cyclic tests and corresponding displacements 136
Table 5-1 – Monotonic test results in small scale 145
Table 5-2 - Monotonic results of numerical simulations in small scale 145
Table 5-3 – Monotonic test results in large scale 145
Table 5-4 – Numerical results of monotonic loading in large scale 145
Table 5-5 – First four cycle results of the tests – small scale specimens 148
Table 5-6 – First four cycle results of the numerical simulations – small scale specimens 148
Table 5-7 – Maximum shear forces in cyclic tests and corresponding displacements – small scale specimens 149

Table 5-8 – Maximum shear forces in cyclic numerical simulations and corresponding displacements – small scale specimens 149
Table 5-9 – Material properties of EM bars 151
Table 5-10 – Summary of yield and ultimate values of loads and displacements of different square EMP made with A51-27-35-30 168
Table 5-11 – Some controlling parameters for cyclic analyses of different square EMP A51-27-35-30 169
Table 6-1 – Material properties of the concrete C25/30 176
Table 6-2 – Properties of reinforcement 177
Table 6-3 – Partial factors of safety applied to the material (γ_m) 178
Table 6-4 – Partial safety factors of the actions at the ultimate limit state (non seismic situations) 179
Table 6-5 – Partial safety factors of the actions at the serviceability limit state (non seismic situations) 179
Table 6-6 Classification of actions 179
Table 6-7 – Imposed loads on the studied buildings 180
Table 6-8 – Simplification of analysis of structures (Table 4.1 – EC8) 185
Table 6-9 – Partial factors of safety applied to the material (γ_m) 186
Table 6-10 – Partial safety factors of the actions at the ultimate limit state 186
Table 6-11 – Partial safety factors of the actions at the serviceability limit state 186
Table 6-12 – EC8 values of parameters S, T_B, T_C and T_D defining the elastic response spectrum Type 1 188
Table 6-13 – EC8 rules for detailing and dimensioning of primary beams (secondary beams: as in DCL) (Fardis, 2009) 195
Table 6-14 – EC8 rules for detailing and dimensioning of primary beams (secondary beams: as in DCL) (Fardis, 2009) (continue) 196
Table 6-15 – EC8 rules for detailing and dimensioning of primary columns (secondary columns: as in DCL) (Fardis, 2009) 197
Table 6-16 – EC8 rules for detailing and dimensioning of primary columns (secondary columns: as in DCL) (Fardis, 2009) (continued) 198
Table 6-17 – Hypothesis and motivation for defining different design in each Configuration 202
Table 6-18 – Hypothesis and motivation for defining different design in each Configuration (continued) 203
Table 6-19 – List of case study RC-MRFs 203
Table 6-20 – Geometrical dimensions of the components of frames studied (in meters) 204
Table 6-21 – Cross-sectional dimensions of the components of frames studied (in meters) 204
Table 6-22 – Cross-sectional dimensions of the components of frames studied (in meters) (continued) 205
Table 6-23 – Total seismic masses of buildings and studied frames 205
Table 6-24 – Total seismic masses of buildings and studied frames (in ton) (continued) 206
Table 6-25 – Design parameters of the frames in EC8-groups 206
Table 6-26 – Partial factors of main combinations of loads according to EC8 and EN1990 at the ultimate limit state of seismic situations 207
Table 6-27 – Partial factors of main combinations of loads according to EC8 and EN1990 at the serviceability limit state of seismic situations 208

Table 6-28 – Partial factors of loads for calculating effective seismic mass participating into the vibration modes of the frames according to EC8 208
Table 6-29 – Global results of the EC8 group 208
Table 6-30 – The values of design base shear and local ductility required 209
Table 6-31 – Maximum design and resisting moments of beams and columns (kNm) 211
Table 6-32 – Maximum design and resisting moments of beams and columns (kNm) (continued) 212
Table 6-33 – Reinforcement in all studied frames 212
Table 6-34 – Reinforcement in all studied frames 213
Table 6-35 – Reinforcement in all studied frames (continued) 214
Table 6-36 – Reinforcement contents (ρ, %) in comparison with criteria from EC8 214
Table 6-37 – Reinforcement contents (ρ, %) in comparison with criteria from EC8 215
Table 6-38 – Reinforcement contents (ρ, %) in comparison with criteria from EC8 216
Table 6-39 – Maximum design and resisting shears of beams and columns (kN) 216
Table 6-40 – Maximum design and resisting shears of beams and columns (kN) (continued) 217
Table 6-41 – Partial factors of some main combinations of loads according to EC2 and EN1990 at the ultimate limit state 218
Table 6-42 – Maximum design and resisting moments of beams and columns (unit: kNm) 219
Table 6-43 – Reinforcement Area from the analyses and chosen steel configurations of the frames in the EC2-group 220
Table 6-44 – Reinforcement Area from the analyses and chosen steel configurations of the frames in the EC2-group (continued) 221
Table 6-45 – Maximum shear forces generated during earthquake and shear resistance of beams and columns (kN) 222
Table 7-1 – Ductility parameters a, b, c for beams according to FEMA 356 247
Table 7-2 – Ductility parameters a, b, c for columns according to FEMA 326 (2000) 247
Table 7-3 – Fundamental periods of the RC-MRFs studied from linear and nonlinear dynamic analyses 252
Table 7-4 – Response of the frames by pushover analysis 267
Table 8-1 – Typical available EMP profiles 269
Table 8-2 – Typical available EMP profiles (continued) 270
Table 8-3 – Calculation of design properties of 6-story frame based on DDBD (Config. 1/Case EC2-0.3g) 287
Table 8-4 – Distributing the total base shear to the RC frame and to the EMP system and calculation of the shear story on the RC frame and on the EMP (Config. 1/Case EC2-0.3g) 287
Table 8-5 – EMP design ductility demand calculation summary (Config. 1/Case EC2-0.3g) 288
Table 8-6 – Overturning moment calculation from equivalent force profiles (Config. 1/Case EC2-0.3g) 288
Table 8-7 – Selection of EMP through out the frame (Config. 1/Case EC2-0.3g) 290
Table 8-8 – Stiffness of EMP through out the retrofitted frame (Config. 1/Case EC2-0.3g) 290
Table 8-9 – Profiles, shear resistance and secant stiffness of selected EMP through out the retrofitted frame (Config. 2/Case EC2-0.05g) 290
Table 8-10 – Design properties of 6-story frame based on DDBD (Config. 2/Case EC2-0.05g) 292

Table 8-11 – Distributing the total base shear to the RC frame and to the EMP system and calculation of the shear story on the RC frame and on the EMP (Config. 2/Case EC2-0.05g) 292

Table 8-12 – EMP design ductility demand calculation summary (Config. 2/Case EC2-0.05g) 293

Table 8-13 – Overturning moment calculation from equivalent force profiles (Config. 2/Case EC2-0.05g) 293

Table 8-14 – Selection of EMP through out the frame (Config. 2/Case EC2-0.05g) 295

Table 8-15 – Stiffness of EMP through out the retrofitted frame (Config. 2/Case EC2-0.05g) 295

Table 8-16 – Profiles, shear resistance and secant stiffness of selected EMP through out the retrofitted frame (Config. 2/Case EC2-0.05g) 296

Table 8-17 – Check of the necessity of upgrading the existing frames in EC2-group 301

Table 8-18 – Properties of the "substitute SDOF" structures 301

Table 8-19 – Properties of the "substitute SDOF" structures (continued) 302

Table 8-20 – Properties of the "substitute SDOF" structures 302

Table 8-21 – Check of the necessity of upgrading the existing frames in EC8-group 303

Table 8-22 – Properties of the "substitute SDOF" structures 304

Table 8-23 – Properties of the "substitute SDOF" structures 304

Table 8-24 – Fundamental periods of the RC-MRFs retrofitted in by linear and nonlinear time history analyses 305

Table 8-25 – Response of the frames by pushover analysis at the ultimate limit state 308

Table 8-26 – Response of the frames by pushover analysis at the ultimate limit state (continued) 309

LIST OF FIGURES

Figure 2-1 – Soft-story mechanism failure (Bendimerad, 2003) 43
Figure 2-2 – Direct and indirect ground effects caused by earthquakes (EN1998-1 (2004)) 46
Figure 2-3 – A typical capacity curve 49
Figure 2-4 – Response Spectra in Traditional and ADRS Formats 50
Figure 2-5 – Bilinear Representation of Capacity Spectrum for Capacity Spectrum Method 50
Figure 2-6 – Definition of the performance point 51
Figure 2-7 – Definitions in Capacity Curve 52
Figure 2-8 – Determination of Performance Point 52
Figure 2-9 – Effect of System Strengthening on Performance (ATC 40, 1997) 53
Figure 2-10 – Effect of System stiffening on Performance (ATC 40, 1997) 54
Figure 2-11 – Effect of Deformation Enhancement on Structural Performance (ATC 40, 1997) 54
Figure 2-12 – CBF systems to retrofit or upgrade structures 56
Figure 2-13 – Original brace models 59
Figure 2-14 – Idealised hysteretic behaviour of intermediate braces (Nakashima and Wakabayashi, 1992) 59
Figure 2-15 - Typical types of BRB (Tsai et al., 2004) 60
Figure 2-16 – Configuration of a BRB 61
Figure 2-17 – Buckling restrained braces sandwiched between precast concrete panels 61
Figure 2-18 – Sub-assemblage test of buckling-restrained braces sandwiched between precast concrete panels (a) Test setup; (b) hysteresis behaviour (Wakabayashi et al., 1973) 61
Figure 2-19 – Concept of sleeve column (Srihara, B.N., 1990) 62
Figure 2-20 – A typical hysteretic behaviour of the BRB 63
Figure 2-21 – Examples of frames with eccentric bracing (Plumier, 2008) 64
Figure 2-22 – Hysteretic behaviour of the EBF 65
Figure 2-23 – Design action in link for an inverted-Y-braced EBF configuration (Mazzolani et al., 2006) 65
Figure 2-24 – Plastic mechanisms of several EB configurations (Mazzolani et al. 2006) 66
Figure 2-25 – Configuration of steel plate shear walls (Mazzolani, 2006) 66
Figure 2-26 – Possibilities of the openings in SPSW and bracing systems (Astaneh-Asl, 2001) 67
Figure 2-27 – Stress state on the web of a stiffened beam subjected to shear (a) and corresponding principal stresses (b)(c) (Mazzolani et al., 2006) 67
Figure 2-28 – The development of the tensile stresses (Wagner theory) 69
Figure 2-29 – Model of Basler (1960) 69
Figure 2-30 – Equivalent diagonal method 70
Figure 2-31 – Strip model by Thorburn et al. (1983) 70
Figure 2-32 – A typical test specimen and typical hysteresis loops for 1mm plate (Sugii and Yamada, 1996) 72
Figure 2-33 – Specimens tested in UK and the effect of perforation on strength and stiffness of steel plate panels (Roberts, 1992) 72
Figure 2-34 – The model tested by Caccese, Elgaaly and Chen-1993 73

Figure 2-35 – The models tested by Timber and Kulak (1983) and by Tromposch and Kulak (1987) 74
Figure 2-36 – University of Alberta test setup and a sample of hysteresis behaviour 75
Figure 2-37 – One of the two University of British Columbia specimens with its hysteresis loops 75
Figure 2-38 – The specimen tested at the Uni. British Columbia and its response 76
Figure 2-39 – A typical test specimen and typical hysteresis loops for 1mm plate 76
Figure 2-40 – Strip model of single story wall and single story collapse mechanism 77
Figure 2-41 – Soft-story and uniform yielding mechanisms of multi-story SPSW 77
Figure 2-42 – Hysteretic behaviour of a stiffened shear wall 78
Figure 2-43 – Typically hysteretic behaviour of a slender shear wall 78
Figure 2-44 – Pinching effect on hysteretic behaviour of SPSW 79
Figure 2-45 – Hysteretic behaviour of the slender SPSWs (Tromposch and G. L. Kulak, 1987) 79
Figure 2-46 – Three regions of behaviour of SPSW 80
Figure 2-47 – Two possibilities to connect SPSW to the frame: bolted and welded 81
Figure 2-48 – Details of welded connections 82
Figure 2-49 – Details of bolted connections 82
Figure 2-50 – Comparison of the buckling loads of the plates made of common steel or LYS 83
Figure 2-51 – Comparison of stress – strain relationship between LYS and conventional steel 84
Figure 2-52 – The hysteretic behaviour of LYS panels (left) with horizontal and vertical stiffeners and (right) with vertical horizontal only 85
Figure 2-53 – Typical specimen dimensions (Vian and Bruneau, 2004) 85
Figure 2-54 – Hysteresis behaviour of the test specimens (Vian and Bruneau, 2004) 85
Figure 2-55 – Stress-strain relationships of different alloys 86
Figure 2-56 – Results of numerical studies of De Matteis et al. (2005) on shear walls made of aluminium 87
Figure 2-57 - Curve load/displacement of aluminium panels (SW1: 300x300 mm; SW2: 300x450 mm) (Roberts et al., 1992) 87
Figure 2-58 – The tested frame and aluminium panels (Mazzolani et al., 2006) 88
Figure 2-59 – Pushover curve of the studied frame with and without panels (Mazzolani et al., 2006) 88
Figure 2-60 – Non perforated panel curve/ Perforated panel curve with a circular hole d = 60 mm/ Perforated panel curve with a circular hole d = 150 mm (Roberts and Sabour-Ghomi, 1995) ... 89
Figure 2-61 – Experiments by Vian and Bruneau (2004) 89
Figure 2-62 – Hysteretic behaviour of the panels by Vian and Bruneau (2004) 90
Figure 2-63 – An example of configurations of RC wall systems 91
Figure 2-64 - Load displacement diagram of the wall before attaining large plastic deformations 93
Figure 2-65 - Load displacement diagram of the wall after attaining large plastic deformations 93
Figure 2-66 – Main components of the typical CSWs (Astaneh, 2002) 95
Figure 2-67 – View of traditional and "Innovative" CSWs (Astaneh, 2002) 96
Figure 2-68 – Test specimens of Zhao and Astaneh (1998-2000) 96
Figure 2-69 – Shear force drift behaviour of Specimens (Astaneh-Asl, 2002) 97
Figure 2-70 – Comparison of Damage to Concrete Wall in Innovative and Traditional 97

Figure 3-1 – Producing process of EMP 101
Figure 3-2 –Geometry of a rhomb shaped stitch 101
Figure 3-3 – Normal type of EMP 102
Figure 3-4 – Flattened type of EMP 102
Figure 3-5 – EMP used as front protector 102
Figure 3-6 – EMP as a fence 102
Figure 3-7 – Bar studied in pure plane shear behaviour 103
Figure 3-8 – Three components contributed to the resistance of the beam web 105
Figure 4-1 – Overview of all components of tests in small scale 109
Figure 4-2 – Geometry of a rhomb shaped stitch 109
Figure 4-3 – Overview of all components of tests in large scale 110
Figure 4-4 - Specimen for tensile tests 111
Figure 4-5 – Notions of sheet directions 112
Figure 4-6 – Overview of specimen A86-46-43-30 dir 1 – welded connections before testing 112
Figure 4-7 – Small EMP specimens – with welded connections 114
Figure 4-8 – Small EMP specimens – with glued connections 114
Figure 4-9 – EMP specimen in large scale tests 115
Figure 4-10 - Global view of the test frame for shear tests 117
Figure 4-11 – Section of the test frame and joint between two sides of the frame 117
Figure 4-12 – Additional fork for applying force 118
Figure 4-13 – Notions of shear loads acting on the frame 118
Figure 4-14 – Displacements measurements on an expanded metal sheer test 118
Figure 4-15 – Global view of tests in large scale 119
Figure 4-16 – Detail of connection between test frame and test EMP 120
Figure 4-17 – Test frame in large scale tests 120
Figure 4-18 – Tensile tests and proposed stress-strain curves for EM products 122
Figure 4-19 – Two possibilities of placing the EMP into the test frame: Direction 1 – Left; Direction 2 – Right 123
Figure 4-20 – Buckling shapes after testing of specimens 124
Figure 4-21 – Force–drift curve in monotonic tests of flattened types and analytical model by Pecquet (2005) 124
Figure 4-22 – Force–drift curves in monotonic tests of normal types and analytical model 124
Figure 4-23 – Global view of the specimen A86-46-43-30 dir2 before testing 125
Figure 4-24 – Broken bars appeared in the monotonic test of specimen A51-27-35-30 – direction 2 125
Figure 4-25 – Crack line and broken bars 128
Figure 4-26 – Hysteretic behaviour of flattened type specimens 129
Figure 4-27 – Hysteretic behaviour of normal type specimens – weld connection 130
Figure 4-28 – Hysteretic behaviour of flattened type specimens – glue connections 130
Figure 4-29 – Hysteretic behaviour of normal type specimens – glued connections 130

Figure 4-30 – Global buckling shapes of two sheets of the EMP panel 132
Figure 4-31 – Broken bars in monotonic large scale tests 132
Figure 4-32 – Broken bars of EMP at failures of the large scale tests 133
Figure 4-33 – Monotonic behaviour of specimen 1 – A51-27-35-30 133
Figure 4-34 – Global instability of the specimen in large scale tests 134
Figure 4-35 – Monotonic behaviour in large scale tests 134
Figure 4-36 – Broken bars of the sheets in large scale EMP specimen 135
Figure 4-37 – Hysteretic behaviour of the specimen A51-27-35-30 136
Figure 4-38 – Hysteretic behaviour of the specimen A86-46-43-30 137
Figure 5-1 – Bars of normal types of EM bars 140
Figure 5-2 – Bars of flattened types of EM bars 140
Figure 5-3 – Model of tests in large scale used in FINELG 141
Figure 5-4 – Model of tests in small scale used in FINELG (left: in the test; right: numerical simulation) 141
Figure 5-5 – View on a line of bars after failure 142
Figure 5-6 – Iterative procedures available in FINELG 143
Figure 5-7 – Load vs. deflection curves of the monotonic tests and the numerical simulations of A51-27-35-30 dir1 and A51-27-35-30 dir2- small scale tests 146
Figure 5-8 – Load vs. deflection curves of the tests and the models of A86-46-43-30 in large scale tests 146
Figure 5-9 – Out-of-plane deformations in the tests and in the numerical simulation during loading of A51-27-35-30 in large scale tests 146
Figure 5-10 – Deformations of the EMP at the test of A86-46-43-30 dir2 in small scale 147
Figure 5-11 – Fully yield bars (very large deformations – considered as failure) at the failure of the EMP A86-46-43-30 dir2 in small scale by the numerical simulation. 147
Figure 5-12 – Hysteretic curves of the cyclic tests and numerical simulations of the A51-27-35-30 dir1 - small scale tests 148
Figure 5-13 – Overview of typical finite element model for the parametric study 150
Figure 5-14 – Finite elements used in numerical simulations 150
Figure 5-15 – Material law for bars of EMP: (1) for determining the ultimate resistance; (2) for determining the ductility 151
Figure 5-16 – Plate model for a beam web 153
Figure 5-17 – Two directions of EMP loaded in shear [R3.3] 154
Figure 5-18 – Critical loads of different square EMP with different profiles subjected to shear. 155
Figure 5-19 – Critical loads of rectangular EMP with ratio 1x2 direction 1 subjected to shear 155
Figure 5-20 – Critical loads of rectangular EMP with ratio 1x2 direction 2 subjected to shear 156
Figure 5-21 – Shear behaviour of square EMP B=500mm MD51-27-35-30 with different imperfections 156
Figure 5-22 – Shear behaviour of three square EMP: type of A51-27-35-30 157
Figure 5-23 – Behaviour of rectangular EMP with ratio 1:2 and direction 1 subjected to shear 158
Figure 5-24 – Plastic resistance in function of the dimensions of square EMP subjected to shear 158

Figure 5-25 – Plastic resistance in function of the dimensions of rectangular EMP ratio 1:2 and direction 1 subjected to shear 159

Figure 5-26 – Plastic resistance in function of the dimensions of rectangular EMP ratio 1:2 and direction 2 subjected to shear 159

Figure 5-27 – Plastic resistance characterised by a single linear relation for all the commercial profiles .. 160

Figure 5-28 – Relationship between dimensions of ratio of square EMP and their plastic resistance divided by the product of diagonal length (l_{dia}), thickness (B), ultimate stress (f_u)and ratio of width to length of bars (A/l_{bar}) 160

Figure 5-29 – Relationship between dimensions of ratio of rectangular EMP ratio 2:1 direction 1 and their ultimate resistance divided by the product of diagonal length (l_{dia}), thickness (B), ultimate stress (f_u) and ratio of width to length of bars (A/l_{bar}) 161

Figure 5-30 – The equivalent band of the EMP 162

Figure 5-31 – Combination of two EMP A51-27-35-30 162

Figure 5-32 – The simplified model of a combined EMP with stiff intermediate gusset 163

Figure 5-33 – Influence of gusset plate on the shear behaviour of a combined EMP 163

Figure 5-34 – The simplified model of a combined EMP with non-stiff intermediate gusset 163

Figure 5-35 – Monotonic behaviour and displacement ductility of square EMP of A86-46-43-30 165

Figure 5-36 – Hysteresis behaviour of a Moment Resisting Frame (Popov E.P, 1980) 165

Figure 5-37 – Hysteresis behaviour of a Diagonally Braced Frame (Popov E.P, 1980) 165

Figure 5-38 – Hysteresis behaviour of a Reinforced Concrete Shear Wall (Oesterle, R.G, 1978) 166

Figure 5-39 – Hysteresis behaviour of an un-stiffened steel plate shear wall (Takahashi Y., Takeda, 1973) 166

Figure 5-40 – Hysteresis behaviour of a heavily stiffened steel plate shear wall panel (Takahashi Y., Takeda, 1973) 166

Figure 5-41 – Cyclic loading on EMP in numerical simulations 168

Figure 5-42 – First four cycle behaviour of 750mm square EMP with the profile of A51-27-35-30 direction 1 under shear loading 169

Figure 5-43 – First four cycle behaviour of 1000mm square EMP with the profile of A51-27-35-30 under shear loading 170

Figure 5-44 – Elastic buckling of the EMP 170

Figure 5-45 – Hysteretic behaviour of 500mm square EMP with the profile of A51-27-35-30 subjected to shear loading 170

Figure 5-46 – Hysteretic behaviour of 750mm square EMP with the profile of A51-27-35-30 subjected to shear loading 171

Figure 5-47 – The simplified hysteretic behaviour of EMP 172

Figure 5-48 – Comparison of hysteretic behaviour of analytical model and numerical model for a square EMP A51-27-35-30 with the dimension of 500mm 172

Figure 6-1 – Bilinear stress-strain relation of concrete for the design of cross-sections – EC2 177

Figure 6-2 – Idealised and design stress-strain diagrams for reinforcing steel (for tension and compression) 177

Figure 6-3 – Beam section with the strain diagram and the stress block 182

Figure 6-4 – Bending plus axial load with varying position of neutral axis in a column 182

Figure 6-5 – Recommended elastic response spectra for type 1 (left) and type 2 (right) 188
Figure 6-6 – Capacity design for the shear force in primary beams 194
Figure 6-7 – Case study structures: Configurations 1, 2, 3, 4 (dimensions in meters) 200
Figure 6-8 – Reinforcement configurations of the slab 202
Figure 6-9 – Cases of gravity loads and seismic forces on the studied frames for all limit states 207
Figure 6-10 – Design base shear coefficient (V_b/W) 209
Figure 6-11 – Maximum sensitivity coefficient in all stories (Max $\theta = N.\delta/V.h$) 209
Figure 6-12 – Top and maximum inter-story drift ratio (δ/h) for the four studied configurations 210
Figure 6-13 – Ratio of maximum inter-story drift to top drift for the studied frames 211
Figure 6-14 – Gravity, wind and snow load cases on the studied frames for all limit states 218
Figure 7-1 – Steps for seismic evaluation of the existing RC-MRFs 225
Figure 7-2 – Possibilities of decomposition of the beam to sub-elements 227
Figure 7-3 – Concentrated plasticity beam sub-elements 228
Figure 7-4 – Bilinear hysteresis model 229
Figure 7-5 – Clough's degrading stiffness model 229
Figure 7-6 – Takeda's degrading stiffness models 230
Figure 7-7 – Takeda-Takayanagi models (Takayanagi and Schnobrich, 1976): 230
Figure 7-8 – Degrading tri-linear model 231
Figure 7-9 – Pivot hysteresis loops (Dowell et al, 1998) 232
Figure 7-10 – Distributed inelasticity 233
Figure 7-11 – Section Modelling with Fibres 233
Figure 7-12 – Accelerograms for Nonlinear Dynamic Analyses 235
Figure 7-13 – Comparison of elastic response spectra from three accelerograms and EC8 of PGA of 0.15g soil C type 1 Earthquake 236
Figure 7-14 – Definition of factor α_u and α_1 on the basis of base shear versus top displacement diagram from pushover analysis 236
Figure 7-15 – Elastic and inelastic demand spectra versus capacity diagram (Faijar, 2000) 240
Figure 7-16 – Calculation of resistance of a beam in studied frames 243
Figure 7-17 – Calculation of resistance of a beam in studied frames 244
Figure 7-18 – Pivot hysteresis model for RC elements (Dowell et al., 1998) 245
Figure 7-19 – Generalized load deformation behaviour in a plastic hinge according to FEMA 356 246
Figure 7-20 – Rigid-plastic beam-column element in SAP 2000 in relevance with FEMA 356 246
Figure 7-21 – Determination of the resistance of compression strut at joint 249
Figure 7-22 – Definition of ductility capacity and ultimate response of the RC-MRFs 250
Figure 7-23 – Pushover curves and target drifts at design PGA established by Pushover analysis of RC-MRFs of Configuration 1 257
Figure 7-24 – Pushover curves and target drifts at design PGA established by Pushover analysis of RC-MRFs of Configuration 2 258

Figure 7-25 – Pushover curves and target drifts at design PGA established by Pushover analysis of RC-MRFs of Configuration 3 259

Figure 7-26 – Pushover curves and target drifts at design PGA established by Pushover analysis of RC-MRFs of Configuration 4 260

Figure 7-27 – Typical failure mechanisms of the studied frames in EC2 group (if node retrofitted) 261

Figure 7-28 – Typical failure mechanisms of the EC8-DCM frames and EC8-DCL if node retrofitted.. 261

Figure 7-29 – Top target displacements established by Pushover and maximum top displacements established by NLTH of studied RC-MRFs under design PGA (* - frames with node retrofitted) 262

Figure 7-30 – Design base shears, base shears corresponding to target displacements established by Pushover and maximum base shears established by NLTH of studied RC-MRF under design PGA (* - frames with node retrofitted) 263

Figure 7-31 – Maximum inter-story drifts at target displacements established by Pushover and maximum inter-story drifts established by NLTH of studied RC-MRFs under design (* - frames with node retrofitted) 264

Figure 7-32 – Ratios between maximum inter-story drifts and top drifts at target displacements of studied RC-MRFs under design PGA established by Pushover and NLTH analyses (* - frames with node retrofitted) 265

Figure 7-33 – Design and maximum resistible PGA of studied RC-MRFs established by Pushover analysis (* - the frames need node retrofitted) 266

Figure 8-1 – The equivalent band of the EMP 270

Figure 8-2 – The simplified hysteretic behaviour of EMP 271

Figure 8-3 – Key steps of DDBD for MDOF system (Maley, 2010) 273

Figure 8-4 – Simplified model of a multi-storey building 274

Figure 8-5 – Design displacement spectra 276

Figure 8-6 – Description of the selected displacement of the existing frames 277

Figure 8-7 – Definition of ductility capacity and ultimate response of the RC-MRFs 279

Figure 8-8 – A typical hysteretic behaviour of a square EMP A51-27-35-30 with the dimension of 500mm 280

Figure 8-9 – Takeda Thin hysteresis rule (Priestley, 2007) 280

Figure 8-10 – Strength assignment to determine the shear story and ductility of the EMP system 281

Figure 8-11 – Principle of designing EMP 283

Figure 8-12 – Design procedures of EMP 285

Figure 8-13 – Pushover curve of the existing frame and selected target drift (Case study EC2-0.05g) 286

Figure 8-14 – Obtaining effective period, T_{eff}, from design displacement, Δ_d, and reduced displacement design spectrum 289

Figure 8-15 – Obtaining effective period, T_{eff}, from design displacement, Δ_d, and reduced displacement design spectrum 289

Figure 8-16 – Pushover curve of the existing frame and selected target drift (Case study EC2-0.05g) 291

Figure 8-17 – Obtaining effective period, T_{eff}, from design displacement, Δ_d, and reduced displacement design spectrum 294

Figure 8-18 – Obtaining effective period, T_{eff}, from design displacement, Δ_d, and reduced displacement design spectrum 294

Figure 8-19 – Pivot hysteresis model in SAP 2000 for EMP (Dowell et al., 1998) 297

Figure 8-20 – Interstory drift and shear forces in retrofitted frame of the example Case 1/EC2-0.3g under earthquake at design PGA=a_{gR}=0.3g established by Pushover and NLTH analyses (left: the interstory drifts; right: displacement profiles) 298

Figure 8-21 – Interstory drift and shear forces in retrofitted frame of the example Case 2/EC2-0.05g under earthquake at design PGA=a_{gR}=0.15g established by Pushover and NLTH analyses (left: the interstory drifts; right: displacement profiles) 299

Figure 8-22 – Story shears of the examples under design PGA established by Pushover analysis (left: Case 1/EC2-0.3g; right: Case 2/EC2-0.05g) 299

Figure 8-23 – Seismic performance of the frame Case 1/EC2-0.3g before and after being retrofitted by Pushover analysis 300

Figure 8-24 – Seismic performance of the frame Case 2/EC2-0.05g before and after being retrofitted by Pushover analysis 300

Figure 8-25 – Pushover curves and target drifts by Pushover analysis of RC-MRFs of Configuration 1 . 309

Figure 8-26 – Pushover curves and target drifts by Pushover analysis of RC-MRFs of Configuration 1 (continued) 310

Figure 8-27 – Pushover curves and target drifts by Pushover analysis of RC-MRFs of Configuration 2 . 311

Figure 8-28 – Pushover curves and target drifts by Pushover analysis of RC-MRFs of Configuration 2 (continued) 312

Figure 8-29 – Pushover curves and target drifts by Pushover analysis of RC-MRFs of Configuration 3 . 313

Figure 8-30 – Pushover curves and target drifts by Pushover analysis of RC-MRFs of Configuration 3 (continued) 314

Figure 8-31 – Pushover curves and target drifts by Pushover analysis of RC-MRFs of Configuration 4 . 314

Figure 8-32 – Pushover curves and target drifts by Pushover analysis of RC-MRFs of Configuration 4 (continued) 315

Figure 8-33 – Typical failure mechanisms if all beam-column joints are well retrofitted 316

Figure 8-34 – Maximum values of top displacements of all RC-MRF studied under designed PGA by Pushover and NLTH analyses – Configurations 1 316

Figure 8-35 – Maximum values of top displacements of all RC-MRF studied under designed PGA by Pushover and NLTH analyses – Configuration 2 317

Figure 8-36 – Maximum values of top displacements of all RC-MRF studied under designed PGA by Pushover and NLTH analyses – Configurations 3 317

Figure 8-37 – Maximum values of top displacements of all RC-MRF studied under designed PGA by Pushover and NLTH analyses – Configurations 3 (continued) 318

Figure 8-38 – Maximum values of top displacements of all RC-MRF studied under designed PGA by Pushover and NLTH analyses – Configurations 4 318

Figure 8-39 – Design base shears and base shears generated in studied RC-MRFs at target displacements under design earthquakes established by Pushover, NLTH analyses – Configurations 1 319

Figure 8-40 – Design base shears and base shears generated in studied RC-MRFs at target displacements under design earthquakes established by Pushover, NLTH analyses – Configurations 2 319

Figure 8-41 – Design base shears and base shears generated in studied RC-MRFs at target displacements under design earthquakes established by Pushover, NLTH analyses – Configurations 2 (continued) 320

Figure 8-42 – Design base shears and base shears generated in studied RC-MRFs at target displacements under design earthquakes established by Pushover, NLTH analyses – Configurations 3 320

Figure 8-43 – Design base shears and base shears generated in studied RC-MRFs at target displacements under design earthquakes established by Pushover, NLTH analyses – Configurations 4 321

Figure 8-44 – Maximum interstory drift ratios at target displacements of studied RC-MRFs under design PGA established by Pushover and NLTH analyses – Configurations 1 321

Figure 8-45 – Maximum interstory drift ratios at target displacements of studied RC-MRFs under design PGA established by Pushover and NLTH analyses – Configurations 1 (continued) 322

Figure 8-46 – Maximum interstory drift ratios at target displacements of studied RC-MRFs under design PGA established by Pushover and NLTH analyses – Configurations 2 322

Figure 8-47 – Maximum interstory drift ratios at target displacements of studied RC-MRFs under design PGA established by Pushover and NLTH analyses – Configurations 3 323

Figure 8-48 – Maximum interstory drift ratios at target displacements of studied RC-MRFs under design PGA established by Pushover and NLTH analyses – Configurations 4 323

Figure 8-49 – Maximum interstory drift ratios at target displacements of studied RC-MRFs under design PGA established by Pushover and NLTH analyses – Configurations 4 (continued) 324

Figure 8-50 – Ratios between maximum interstory drifts and top drifts at target displacements of studied RC-MRFs under design PGA established by Pushover and NLTH analyses – Configurations 1 324

Figure 8-51 – Ratios between maximum interstory drifts and top drifts at target displacements of studied RC-MRFs under design PGA established by Pushover and NLTH analyses – Configurations 2 325

Figure 8-52 – Ratios between maximum interstory drifts and top drifts at target displacements of studied RC-MRFs under design PGA established by Pushover and NLTH analyses – Configurations 3 325

Figure 8-53 – Ratios between maximum interstory drifts and top drifts at target displacements of studied RC-MRFs under design PGA established by Pushover and NLTH analyses – Configurations 3 (continued) 326

Figure 8-54 – Ratios between maximum interstory drifts and top drifts at target displacements of studied RC-MRFs under design PGA established by Pushover and NLTH analyses – Configurations 4 326

Figure 8-55 – Design and maximum resistible PGA of retrofitted RC-MRFs by Pushover analysis – Configurations 1 327

Figure 8-56 – Design and maximum resistible PGA of retrofitted RC-MRFs by Pushover analysis – Configurations 2 327

Figure 8-57 – Design and maximum resistible PGA of retrofitted RC-MRFs by Pushover analysis – Configurations 2 (continued) 328

Figure 8-58 – Design and maximum resistible PGA of retrofitted RC-MRFs by Pushover analysis – Configurations 3 328

Figure 8-59 – Design and maximum resistible PGA of retrofitted RC-MRFs by Pushover analysis – Configurations 4 329

Figure 8-60 – Ratios of maximum resistible PGAs of RC-MRFs retrofitted using only EMP by Pushover analysis 329

Figure 8-61 – Ratios of maximum resistible PGAs of RC-MRFs retrofitted by EMP and node retrofitted established by Pushover analysis 330

Figure 8-62 – Retrofit of beam-column joints by using external prestressed bars with Dywidag type 331

Figure 8-63 – Retrofit of beams at critical regions with brittle failure due to shears by using external bolts or bar with epoxy injection to the cracks of concrete 331

Figure 8-64 – Description of the connection between EMP and the frame's elements..... 336
Figure 8-65 – Description of the connection between EMP and the frame's elements..... 337
Figure 8-66 – Steps to design connection between EM sheets 337
Figure 8-67 – Steps to design connection between EMP and the frame's elements..... 338
Figure 8-68 – Steps to design connection between EMP and the frame's elements..... 338
Figure 8-69 – Determination of bearing resistance per bolt 338

LIST OF SYMBOLS AND ABBREVIATIONS

A	= Width of the bars of the rhomb-shape stitch of EMP
A	= Accidental action
A	= Cross sectional area
A_c	= Cross sectional area of concrete
A_{Ed}	= Design value of seismic action ($\gamma_I.A_{Ek}$)
A_{Ek}	= Characteristic value of the seismic action for the reference return period
A_s	= Cross sectional area of reinforcement
A_{sh}	= Total area of horizontal hoops in a beam-column joint
A_{st}	= Area of one leg of transverse reinforcement
A_{sv}	= Total area of vertical reinforcement in the web of the wall
$A_{s,min}$	= Minimum cross sectional area of reinforcement
A_{sw}	= Cross sectional area of shear reinforcement
ASW	= Aluminium Shear Wall
B	= Thickness of the bars of the rhomb-shape stitch of EMP
BRB	= Buckling Restrained Brace
C	= Damping Matrix of MDOF structure
CSW	= Composite Shear Wall
CBF	= Concentric Braced Frame
CD	= Width of the rhomb-shaped stitch of EMP
DOF	= Degree Of Freedom
D_{pl}	= Flexural stiffness of a solid plate (under shear loading)
E	= Young's Modulus of the material
E	= Effect of action
E_c	= Tangent modulus of elasticity of normal weight concrete at a stress of $\sigma_c = 0$ and at 28 days
E_d	= Design value of action effects

E_{cd} = Design value of modulus of elasticity of concrete

E_s = Design value of modulus of elasticity of steel

E_{EM} = Elastic modulus of an Expanded Metal bar

$E_{str\text{-}EM}$ = Strain-hardening modulus of an Expanded Metal bar

EI = Bending Stiffness

EBF = Eccentric Braced Frame

EVD = Equivalent Viscous Damping

EMP = Expanded Metal Panel

F = Action

F_d = Design value of an action

F_k = Characteristic value of an action

G_k = Characteristic permanent action

H_e = Effective height of an equivalent SDOF system

H_i = Height of story i from the ground

H_n = Height of roof story from the ground

I = Second moment of area of concrete section

K = Stiffness

K = Stiffness matrix of a MDOF system

L = Length, Span

LD = Length of the rhomb-shaped stitch of EMP

$LYSW$ = Low Yield Steel Shear Wall

M = Bending moment

M = Mass matrix of a MDOF system

M_{Ed} = Design value of the applied internal bending moment

$M_{i,d}$ = End moment of a beam or column for the calculation of its capacity design shear

$M_{Rb,i}$ = Design value of beam moment of resistance of end i

$M_{Rc,i}$	= Design value of column moment of resistance of end i
$M_{OTM,MRF}$	= Overturning moment of the RC-MRF under lateral seismic forces
$M_{OTM,EMP}$	= Overturning moment of the EMP system in the retrofitted frames under lateral seismic forces
MDOF	= Multiple Degree Of Freedom
MRF	= Moment Resisting Frame
MRFs	= Moment Resisting Frames
N	= Axial force
N_{Ed}	= Design value of the applied internal axial force
R	= Response Modification Factor
R	= Resistance
RCSW	= Reinforce Concrete Shear Wall
PGA	= Peak Ground Acceleration
P_{NCR}	= Reference probability of exceedance in 50 years of the reference seismic action for the no-collapse requirement
P_{tot}	= Total gravity load at and above the story considered in the seismic design situation
Q	= Variable action
S	= First moment of area
S	= Soil Factor
$S_e(T)$	= Elastic horizontal ground acceleration response spectrum also called "elastic response spectrum". At T=0, the spectral acceleration given by this spectrum equals the design ground acceleration on type A ground multiplied by the soil factor S
$S_{de}(T)$	= Elastic displacement response spectrum
$S_d(T)$	= Design spectrum (for elastic analysis). At T=0, the spectral acceleration given by this spectrum equals the design ground acceleration on type A ground multiplied by the soil factor S
SDOF	= Single Degree Of Freedom
SPSW	= Steel Plate Shear Wall
SDM	= Spectral Difference Method

$SRSS$	= Square Root of the Sum of the Squares
ULS	= Ultimate limit state
T	= Period of vibration of a linear single degree of freedom system
T_e; T_{eff}	= Effective period of the SDOF system
T_1	= Fundamental period of the building in the horizontal direction of interest
T_C	= Corner period of at the upper limit of the constant acceleration region of the elastic spectrum
T_s	= Duration of the stationary part of the seismic action
T_{NCR}	= Reference return period of the reference seismic action for the no-collapse requirement
V	= Shear force
V_{base}	= Base shear of an equivalent SDOF system
V_{base}	= Total base shear of a MDOF system
V_{Rd}	= Design value of shear resistance
$V_{Rd,c}$	= Design value of shear resistance for members without shear reinforcement in accordance with EC2
V_{Ed}	= Design value of the applied shear force
V_{total}	= Total seismic shear at the considered level
V_{1y}; $V_{1,y}$	= Base shear corresponding to the first yield displacement
V_u	= Base shear corresponding to the ultimate displacement
$V_{EMP,i}$	= Shear at story i
$V_{b,EMP}$	= Shear strength of EMP system in DDBD
$V_{b,1Y,MRF}$	= Shear strength of MRF system in DDBD corresponding to first yield in MRF
$V_{b,Rd,MRF}$	= Shear Resistance of MRF system in DDBD
$V_{b,Rdmax,MRF}$	= Maximum shear Resistance of MRF system in DDBD
$V_{b,1Y,MRF+EMP}$	= Shear strength of MRF+EMP system in DDBD corresponding to first yield in MRF+EMP
$V_{b,Rd,MRF+EMP}$	= Shear Resistance of MRF+EMP system in DDBD

$V_{b,Rdmax,MRF+EMP}$ = Maximum shear Resistance of MRF+EMP system in DDBD

W = Effective width of EMP under shear

Ws = Wall system

a = Distance

a_{gR} = Reference peak ground acceleration on type A ground

a_g = Design ground acceleration on type A ground

b = Overall width of a cross-section, or actual flange width in a T or L beam

b_c = Cross-sectional dimension of column

b_{eff} = Effective length width of beam in tension at the face of a supporting column

b_w = Width of the web on T or I or L beams

b_0 = Width of the confined core of a column

d = Diameter; Depth

d = Effective depth of a cross section

d_e = Displacement induced by the design seismic action (EC8)

d_g = Design ground displacement

d_d = Displacement induced by a linear analysis based on the design response spectrum (EC8)

d_{bL} = Longitudinal bar diameter

d_{bW} = Diameter of hoop

d_r = Design story drift

d_{si} = Design lateral displacement at story i due to seismic action

d_{yEMP} = Yield lateral displacement of the EMP

d_{uEMP} = Ultimate lateral displacement of the EMP

e = Eccentricity

f = stress generated in equivalent band of EMP

f_c = Compressive strength of concrete

f_{cd} = Design value of concrete compressive strength

f_{ck} = Characteristic compressive cylinder strength of concrete at 28 days

f_{cm} = Mean value of concrete cylinder compressive strength

f_{ctk} = Characteristic axial tensile strength of concrete

f_{ctm} = Mean value of axial tensile strength of concrete

f_t = Tensile strength of reinforcement

f_{tk} = Characteristic tensile strength of reinforcement

f_y = Yield strength of reinforcement

f_{yd} = Design yield strength of reinforcement

$f_{yd,h}$ = Design value of yield strength of the horizontal web reinforcement

$f_{yd,v}$ = Design value of yield strength of the vertical web reinforcement

f_{yld} = Design value of yield strength of the longitudinal reinforcement

f_{ywd} = Design value of yield strength of the transverse reinforcement

f_{yk} = Characteristic yield strength of reinforcement

f_{ywd} = Design yield of shear reinforcement

f_{yEM} = Yield stress of the Expanded Metal material bar

f_{uEM} = Ultimate stress of the Expanded Metal material bar

f_{rEM} = Assumed remaining stress of the Expanded Metal material bar

g = Acceleration due to gravity

h = Height

h = Overall depth of a cross-section

h_c = Cross-sectional depth of column in the direction of interest

h_f = Flange depth

h_{jc} = Distance between extreme layers of column reinforcement in a beam-column joint

h_{jw} = Distance between beam top and bottom reinforcement

h_0 = Depth of confined core in a column (to centre line of hoops)

h_S = Clear story height

h_w = Cross-sectional depth of a beam

i = Radius of gyration

k_{bs} = Stiffness of building evaluated by a concentrated force

k_c = Spring constant of the connector modelling

k_e; k_{eff} = Effective stiffness of a SDOF system

$k_{e,EMP}$ = Elastic stiffness of the EMP system

$k_{s,EMP}$ = Secant stiffness of the EMP system

k_f = Final stiffness

k_w = Factor reflecting the prevailing failure mode in structural systems

k_p = Spring constant of the pounding modelling

k_{cpl} = generalised parameter of a solid plate

$k_{e,EMP}$ = elastic stiffness of EMP

$k_{s,EMP}$ = secant stiffness of EMP

l = Length, span

l_{cl} = Clear length of a beam or a column

l_{cr} = Length of critical region

l_{bar} = Length of the bars of the rhomb-shaped stitch of EMP

m = Mass

m_i = Mass of the floor i of the frame

m_e; m_{eff} = Effective mass of the equivalent SDOF system

n = Total number of longitudinal bars laterally engaged by hoops or cross ties on perimeter of column section

q = Behaviour factor

q_0 = Basic value of the behaviour factor

r = Radius

$1/r\ (=\varphi)$ = Curvature at a particular section

s = Spacing of transverse reinforcement

t = Thickness

x_u = Neutral axis depth

z = Internal lever arm

x, y, z = Coordinates

r_1 = The pseudo energy radii of structures 1

u_1 = Displacement of the first building

u_2 = Displacement of the second building

$\ddot{x}_g$ = Ground acceleration

$\ddot{x}_g$ = Ground acceleration

α = Angle between horizontal axis and diagonal of a story in multi-story frames

α = Ratio between the width and length of a bar in a rhomb-shaped stitch of EMP (A/l_{bar})

α = Confinement effectiveness factor

α_{cc} = Coefficient taking into account the long term effects on the compressive strength

α_0 = Prevailing aspect ratio of the structural system

α_1 = Multiplier of horizontal design seismic action at formation of first plastic hinge in the system

α_u = Multiplier of horizontal design seismic action at formation of global plastic mechanism

γ = Partial factor

γ = Factor used to determine equivalent band width of the EMP under shear

γ_A = Partial factor for accidental action A

γ_C = Partial factor for concrete

γ_G = Partial factor for permanent actions G

γ_f = Partial factor of actions

γ_m = Partial factor of materials

γ_I = Importance factor

γ_Q = Partial factor for variable actions Q

γ_{Rd} = Model uncertainty factor on design value of resistances in the estimation of capacity design action effects, accounting for various sources of overstrength

γ_S = Partial factor for reinforcement

γ_0, γ_1 = The proportionality factors for the calculation of damping

ε_c = Compressive strain in the concrete

ε_{c1} = Compressive strain in the concrete at peak stress f_c

ε_{cu} = Ultimate compressive strain in the concrete

ε_{cu2}, ε_{cu3} = Ultimate compressive strain in the unconfined concrete

$\varepsilon_{cu2,c}$; $\varepsilon_{cu3,c}$ = Ultimate compressive strain in the confined concrete

ε_u = Strain of the reinforcement at maximum load

ε_{uk} = Characteristic strain of the reinforcement at maximum load

ε_{suk} = Characteristic value of ultimate elongation of reinforcing steel

$\varepsilon_{sy,d}$ = Design value of steel strain at yield

ε_{yEM} = Yield strain of an expanded metal bar

ε_{u1EM} = Ultimate strain of an expanded metal bar

ε_{u2EM} = Assumed strain of an expanded metal bar corresponding to the f_{rEM}

θ = Interstory drift sensitivity coefficient

θ = Angle

$\theta_{EMP,i}$ = Drift of the EMP at story i

θ_{yEMP} = Yield drift of the EMP

θ_{uEMP} = Ultimate drift of the EMP

ξ, ξ_i = The viscous damping ratio (in percent)

ξ_0 = The critical damping ratio (in percent)

ξ_{hyst} = The hysteretic damping ratio (in percent)

ξ_{EVD} = The Equivalent Viscous Damping ratio (in percent)

ξ_{MRF} = The Equivalent Viscous Damping ratio (in percent) of RC-MRF

ξ = Normalised neutral axis depth

λ = Slenderness ratio

μ = Ductility demand

μ_d = Displacement Ductility

μ_ϕ = Curvature ductility factor

μ_δ = Displacement ductility factor

$\mu_{\varepsilon EM}$ = Strain ductility of an expanded metal bar

μ_{dEMP} = Displacement ductility of an expanded metal panel

$\mu_{dEMP,i}$ = Displacement ductility of EMP at story i

μ_{MRF} = Displacement ductility of a moment resisting frame

ν = Poisson's Ratio

ν = Strength reduction factor for concrete cracked in shear

ν, ν_d = Axial force in the seismic design situation, normalised to $A_c f_{cd}$

ρ = Oven-dry density of concrete in kg/m^3.

ρ_l = Total longitudinal reinforcement ratio

ρ = Tension reinforcement ratio for longitudinal reinforcement in beams

ρ' = Compression reinforcement ratio for longitudinal reinforcement in beams

ρ_{max} = Maximum allowed tension reinforcement ratio in critical regions of primary seismic beams

ρ_w = Reinforcement ratio for shear reinforcement

σ_c = Compressive stress in the concrete

σ_{cu} = Compressive stress in the concrete at ultimate compressive strain ε_{cu}

σ_{cr} = Critical stress in a solid plate

σ_1, σ_2 = Principal stress in a solid plate under shear loading

σ_t = Tensile stress in tension field action of a solid plate under shear loading

τ_{cr} = Shear critical stress in a solid plate under shear loading

ϕ = Diameter of reinforcement

Δ = Delta

Δ_c = Design displacement at critical story

Δ_d = Design displacement

Δ_i = Design displacement at story i

Δ_{limit} = Limit displacement for the existing frames

Δ_y = Yield displacement

Δ_{1y}; $\Delta_{1,y}$ = First yield displacement

$\Delta_{1Y,EMP}$ = First yield displacement of the EMP system

$\Delta_{1Y,MRF}$ = First yield displacement of the RC-MRF

$\Delta_{1Y,EMP+MRF}$ = First yield displacement of the retrofitted frames with EMP

Δ_{target} = Target displacement of the retrofitted frame

Δ_u = Ultimate displacement

δ_i = Design displacement at story i

δ_c = Design displacement at critical story

π = Pi

$\rho_{12}(\rho)$ = Correlation coefficient

τ = Time lag of the input ground motion

ω = The frequency of the ground motion

ω_n, ω_m = The two specified frequencies for the calculation of damping

ω_v = Mechanical ratio of vertical web reinforcement

ω_{wd} = Mechanical volumetric ratio of confinement reinforcement

ψ = Factors defining representative values of variable actions

ψ_0 for combination values

ψ_1 for frequent values

ψ_2 for quasi-permanent values

η = Damping correction factor

η = Reduction factor on concrete compressive strength due to tensile strains in transverse direction

$\sum M_{Rb}$	= sum of the design values of moments of resistance of the beams framing into a joint in the direction of interest
$\sum M_{Rc}$	= sum of the design values of moments of resistance of the columns framing into a joint in the direction of interest
ζ	= Ratio, $V_{Ed,min}/V_{Ed,max}$, between the minimum and maximum acting shear forces at the end section of a beam
$\boldsymbol{\Phi}$	Modal shape vector of a MODF system obtained by modal analysis

1. INTRODUCTON

1.1. Problem description and motivation

Reinforced concrete moment resisting frames (RC-MRFs) have been used as the main structural resisting systems for over 30 years in many countries all over the World. Thanks to rather high capacity in strength, stiffness and low cost of construction, this structural system is capable of resisting both gravity loads and lateral forces like winds or earthquakes. Many buildings using RC-MRFs as the main resistance component still have been building expansively. However, there have been still many existing RC-MRFs or even new ones, which have not been designed based on the modern seismic codes. This may lead to some undesired failures under a rather low intensity earthquake. This has been experienced in Turkey, Africa and Asia... In addition, in many regions like Turkey, Italia or Taiwan…, which are high seismic activity with frequently earthquake having probability of occurrence with large magnitude and intensity, this may leads to the increase of seismic hazards of those zones.

The main purpose of seismically retrofitting and/or upgrading a structure is to make it possible to succeed the intended seismic performance under a design earthquake. The retrofit has been required since the structure has not been designed according to a modern seismic code such as EC8. On the other hand, the upgrading becomes necessary if the recent seismic activities have lead to the modification of the seismic hazards. However, the retrofitting or upgrading of the existing buildings is a difficult task for engineers because of technical reasons and retrofitting costs. There are several existing retrofitting systems available for seismically retrofitting or upgrading RC-MRFs, such as conventional braces, eccentric braces, steel plate or reinforced concrete shear walls, base isolators or damper systems…In these systems, some are able to increase the stiffness, strength, deformation and energy absorbing capacity of the structures and some are able to reduce the influence of the seismic actions on the structure. The application in reality of these retrofitting systems is dependent on their effectiveness on the structures in both aspects: technique and construction costs.

In spite of having much advantage in increasing the stiffness and strength for the buildings, the use of bulky systems such as reinforced concrete shear walls to retrofit buildings under seismic actions becomes more and more limited due to its complication in erection and very high costs for foundation system because of high seismic forces acting on the walls. Therefore, the use of lighter retrofitting systems such as concentric braces, shear walls made from steel, low yield stress steel or aluminium… have been becoming more favourable. These retrofitting systems are able to increase the strength and stiffness of the structures. Also, they can provide an effective passive means to absorb the seismic energy during the earthquakes.

Made from sheet steel, aluminium or various alloys (copper, nickel, titanium) by cutting and simultaneous stretching cold (without loss of material), expanded metal is considered as a macro-foam material. A rectangular sheet with dimensions of 1250mm x 2500 mm having many rhomb shape stitches with different geometrical sizes is the popular product. The relatively low cost of expanded metal is a distinct advantage regardless of its use. Currently it is employed primarily in the areas of protection (fencing, gates) and architecture.

The aim is to consider a new application radically different in the field of civil engineering and more specifically that of the earthquake resistance of buildings. It is actually very common to apply the concept of shear walls. These are usually regarded as two main materials: concrete and steel. Despite acting as walls taking on the shear forces, walls of steel and concrete do not behave the same way. However, during an earthquake, these walls are able to withstand the horizontal forces that affect the structure in which they are used. The work here is to determine if the expanded metal can also take these horizontal forces and define the conditions under which this new system can be effectively considered. The work plan includes two main parts. In addition, since it is using expanded metal as a wall shear, a detailed study of these walls is performed in order to understand how they work, to highlight the advantages of such a system and new developments planned to improve them. This first part will set the expanded metal over existing techniques and see if its use is justified in the context of earthquake resistance. On the other hand, a more detailed description of the expanded metal is considered. In this way, the different data required for

modelling the new resistance system are known and analyzes, tests and comparisons can be made in order to validate the use of expanded metal in the context of earthquake resistance.

1.2. Objectives and Scope of the research

The first objective of the thesis is to investigate the behaviour of Expanded Metal Panels (EMP) under monotonic and quasi-static cyclic shear loading by experimental and numerical approaches. Analytical models which can be used to simplify the shear behaviour of EMP are the goal of this trend.

The second objective is to develop a complete procedure that can be used to design and select EMP in order to retrofit the existing reinforced concrete moment resisting frames under seismic actions. This will be fulfilled by numerical approach. Connections between EMP and the frames' elements are also under study.

1.3. Organisation of the thesis

The current thesis aims to develop a complete application of using expanded metal panels to retrofit RC-MRFs under seismic actions. This dissertation is organised into nine chapters with the following contents.

Chapter 1 is the introduction of the thesis.

Chapter 2 will focus on the overview of how to seismically retrofit or upgrade an existing RC-MRF. The common procedures of how to assess the seismic performance and detect the deficiencies of the existing RC frames will be introduced. Methods of retrofitting those frames will be presented as well. Different types of retrofitting systems will also be summarised and discussed.

In Chapter 3, general introduction about expanded metal panels (EMPs) is the main subject of discussion. Geometrical configuration, fabrication process, types and kinds of EMPs will be introduced. Current application of EMPs is also presented. Previous studies on EMPs under shear loading are summarised in detail.

A complete experimental study on EMPs loaded in shear will be described in Chapter 4. The tests on EMPs will be introduced from small scale tests to large scale ones under both monotonic and quasi-static cyclic shear loading.

Numerical simulations of the tests will be presented in Chapter 5. Based on numerical approach, parametric study to address shear behaviour of EMPs under monotonic and cyclic loading will be developed. A comparison of hysteretic behaviour of EMPs and other structural systems is also given. Analytical models that simplify the behaviour of the EMPs under shear loading are introduced as well.

A summary of designing RC-MRFs in accordance with EC2 and EC8 will be first summarised in Chapter 6. Designation of twenty planar RC frames is then presented. All parameters concerning the design processes are also given. Limitations of the studied frames will be discussed in this chapter.

Chapter 7 will first introduce the general methods and possibilities to evaluate the seismic performance of the existing RC-MRFs. Assessments of twenty frames designed in Chapter 6 are next presented in detail. Seismic performance and shortcomings or deficiencies of the existing RC-MRFs will be the results of the evaluation process.

Chapter 8 will develop a design process based on Direct Displacement-Based Design approach in order to use EMP to seismically retrofit the existing RC-MRFs which have been assessed in the Chapter 7. A comparison of seismic performance of the frames before and after being retrofitted will also be introduced. Advantages and disadvantages of using EMP will be discussed in detail. Furthermore, design of the connections between frames' elements and EMP will be presented as well.

To conclude, Chapter 9 shows a summary and a conclusion of this study and also gives some perspectives for future developments.

2. OVERVIEW OF SEISMIC EVALUATION AND RETROFIT OF REINFORCED CONCRETE MOMENT RESISTING FRAMES (RC-MRFS)

2.1. Introduction

In order to well behave under an earthquake, a building should possess adequate strength, redundancy and ductility. The response of a RC-MRFs building subjected to severe seismic forces depends primarily on those properties of its members and on detailing of its individual component and of connections between the components. Many RC-MRFs constructed and designed not according to seismic modern design code such as EC8 or before the development of rigorous seismic design codes and of detailing provisions may not have enough conditions for resisting the seismic actions. It has been clearly observed that many non-ductile RC-MRFs structures are severely damaged or collapsed during small earthquakes with undesirable failure modes such as soft-story mechanisms as shown in Figure 2-1.

Figure 2-1 – Soft-story mechanism failure (Bendimerad, 2003)

Generally, seismic upgrade and retrofit of such buildings to meet requirements of modern codes always pose a rather great effort to structural engineers. To help the owners clearly understand all retrofitting processes, it is very important for the engineers to know what are the seismic capacity and deficiencies of the existing RC-MRFs. In order to evaluate their capacity and the deficiencies, it is necessary to assess their seismic performances. The criteria, usually used to represent the overall seismic performances of a building or building's components, have been defined in some codes or reference documents (i.e. EC8-3, FEMA 356 (2000)…), depending on many aspects as seismic zones, types of the structures, seismic performances of the individual members, methods to evaluate, etc… In addition, many other tasks are needed to be done such as collecting the data on site, testing the material properties, determining the strategies and retrofit processes for the structures…In those, selecting the retrofitting system might be the biggest concern for engineers due to its important effects on the success of the project. The retrofitting system means the direct intervention techniques on the structure. It may cause significant changes of the behaviour of structures in stiffness, strength, ductility or foundation system.

Aiming at giving general points of how to seismically retrofit RC-MRFs, this chapter first presents the main steps of retrofitting or upgrading the RC-MRFs, including criteria of seismic performances, seismic characteristics and analytical tools to assess the existing buildings. Retrofit strategies are then introduced with the main focuses on the technical solutions. Most of recent advanced retrofitting systems are then introduced to generalize the existing methods to retrofit and/or upgrade the RC-MRFs. Finally, some assessments which compare the advantage and disadvantage of these systems are summarised in the concluding section.

2.2. Determination of performance levels, seismic hazards, performance objectives, and deficiencies of the existing RC-MRFs

2.2.1. Performance levels

Many methods for seismic design or retrofit of a building have been introduced to date. One of them, based on its seismic performance, is known as performance-based design. According to such approach, the overall behaviour of the building is dependent on the behaviour of its all parts. A building is constituted by structural and non-structural components therefore its seismic performance is a combination from the performance of these components.

In most of modern seismic codes and rehabilitation documents such as EC8 part 1 and 3, ATC 40 (1997), FEMA 356 (2000) or NEHRP (1997), depending on the consequences of an earthquake and/or on the damage states of the components and buildings, the building's seismic performance is divided into several performance levels.

EC8-3 defines three Limit States (LS) or building's performance levels, namely Near Collapse (NC), Significant Damage (SD), and Damage Limitation (DL), characterised as follows:

- LS of Near Collapse (NC): the structure is heavily damaged, with low residual lateral strength and stiffness, although vertical elements are still capable of sustaining vertical loads. Most non-structural components have collapsed. Large permanent drifts are present. The structure is near collapse and would probably not survive another earthquake, even of moderate intensity.
- LS of Significant Damage (SD): the structure is significantly damaged, with some residual lateral strength and stiffness, and vertical elements are capable of sustaining vertical loads. Non-structural components are damaged, although partitions and infill have not failed out-of-plane. Moderate permanent drifts are present. The structure can sustain after-shocks of moderate intensity. The structure is likely to be uneconomic to repair.
- LS of Damage Limitation (DL): the structure is only lightly damaged, with structural elements prevented from significant yielding and retaining their strength and stiffness properties. Non-structural components, such as partitions and infill, may show distributed cracking, but the damage could be economically repaired. Permanent drifts are negligible. The structure does not need any repair measures.

Also based on the performance and damage of the structures and their structural and non-structural components after an earthquake, ATC-40 (1997) defines 4 building performance levels as described hereafter:

- Operational: this performance level is related to functionality of the buildings. Damage to the building's structures is limited so that continued safe occupancy is not in question. Any required repair is minor and it is easy to carry out without big disturbances to occupants. All services inside and outside are usable.
- Immediate Occupancy: this level corresponds to the most widely used criteria for essential activities. The building's systems are expected to be reasonably usable but continuity of all services is not necessarily provided.
- Life Safety: at this level of building performance, the damage state presents an extremely low probability of threats to life safety
- Structural Stability: this damage state addresses only the main building frame and requires only stability under vertical loads. The performances of non structural elements are unreliable.

More detailed than EC8 part 3 and ATC-40 (1997), FEMA 356 (2000) not only defines the overall performance levels of buildings, as shown in Table 2-1, but also gives particular performance levels for different components of different structural types of buildings.

Particularly for RC-MRFs, FEMA 356 (2000) has introduced structural performance levels and damage of vertical elements (columns) and horizontal ones (beams) based on their seismic performance, as shown Table 2-2 and Table 2-3.

Table 2-1 – Building performance levels in FEMA 356 (2000)

	Building performance levels			
	Collapse Prevention Level	Life Safety Level	Immediate Occupancy Level	Operational Level
Overall Damage	Severe	Moderate	Light	Very Light
General	Little residual stiffness and strength, but load bearing columns and walls function. Large permanent drifts. Some exits blocked. Infills and un-braced parapets failed or at incipient failure. Building is near collapse.	Some residual strength and stiffness left in all stories. Gravity-load bearing elements function. No out-of plane failure of walls or tipping of parapets. Some permanent drift. Damage to partitions. Building may be beyond economical repair.	No permanent drift. Structure substantially retains original strength and stiffness. Minor cracking of facades, partitions, and ceilings as well as structural elements. Elevators can be restarted. Fire protection operable.	No permanent drift. Structure substantially retains original strength and stiffness. Minor cracking of facades, partitions, and ceilings as well as structural elements. All systems important to normal operation are functional.
Non structural components	Extensive damage.	Falling hazards mitigated but many architectural, mechanical, and electrical systems are damaged.	Equipment and contents are generally secure, but may not operate due to mechanical failure or lack of utilities.	Negligible damage occurs. Power and other utilities are available, possibly from standby sources.

Table 2-2 – Structural performance levels and damage – Vertical Elements in FEMA 356 (2000)

Elements	Type	Structural performance levels		
		Collapse Prevention Level	Life Safety Level	Immediate Occupancy Level
Reinforced Concrete Moment Resisting Frames	Primary	Extensive cracking and hinge formation in ductile elements. Limited cracking and/or splice failure in some non-ductile columns. Severe damage in short columns.	Extensive damage to beams. Spall of cover and shear cracking (<3.2 mm width) for ductile columns. Minor spall in non-ductile columns. Joint cracks <3.2 mm wide.	Minor hairline cracking. Limited yielding possible at a few locations. No crushing (strains below 0.003).
	Secondary	Extensive spall in columns (limited shortening) and beams. Severe joint damage. Some reinforcing buckled.	Extensive cracking and hinge formation in ductile elements. Limited cracking and/or splice failure in some non-ductile columns. Severe damage in short columns.	Minor spall in a few places in ductile columns and beams. Flexural cracking in beams and columns. Shear cracking in joints <1.6 mm width.
	Drift	4% transient or permanent	2% transient; 1% permanent	1% transient; negligible permanent

Table 2-3 – Structural performance levels and damage – Horizontal Elements in FEMA 356 (2000)

Elements	Structural performance levels		
	Collapse Prevention Level	Life Safety Level	Immediate Occupancy Level
Concrete Diaphragms	Extensive crushing and observable offset across many cracks.	Extensive cracking (<6.4 mm width). Local crushing and spall.	Distributed hairline cracking. Some minor cracks of larger size (<3.2 mm width).

2.2.2. Seismic hazards

Physically, an earthquake is a result of a sudden move between main tectonic plates, covering the surface of the globe. A seismic action, caused by an earthquake and applied to a structure, is a ground movement with horizontal and vertical components (Plumier, 2008). In general cases, the vertical component is about a half or even less of the horizontal component (Fardis, 2009). Because of less effect than horizontal component, the vertical component is usually neglected when designing a structure subjected to an earthquake; therefore from now on the horizontal component is likely assumed to be the uniquely specific feature in the present study. There are several procedures to represent the seismic actions such as map-based and site-specific procedures (Fardis et al., 2005).

Map-based procedures use maps of PGA to define seismic input at different hazard levels and under different site conditions (M.Fardis et al., 2005). With the aid of maps of PGA, the earthquake ground motion at a given site is usually characterized by the response spectrum or accelerograms (artificial or recorded accelerograms). The simplest way to apply the earthquake loads on the structures by using response spectrum is that seismic actions will be replaced by equivalent lateral forces or shear forces. Equivalent shear forces are dependent on the structure's properties (stiffness, mass, periods…) and on spectral acceleration ordinates that correspond to both PGA at a given site in and the structures' periods.

The seismic response of structures is significantly influenced by the soil conditions. Earthquakes may cause several types of ground effects including direct and indirect effects as defined in Figure 2-2 (EC8)

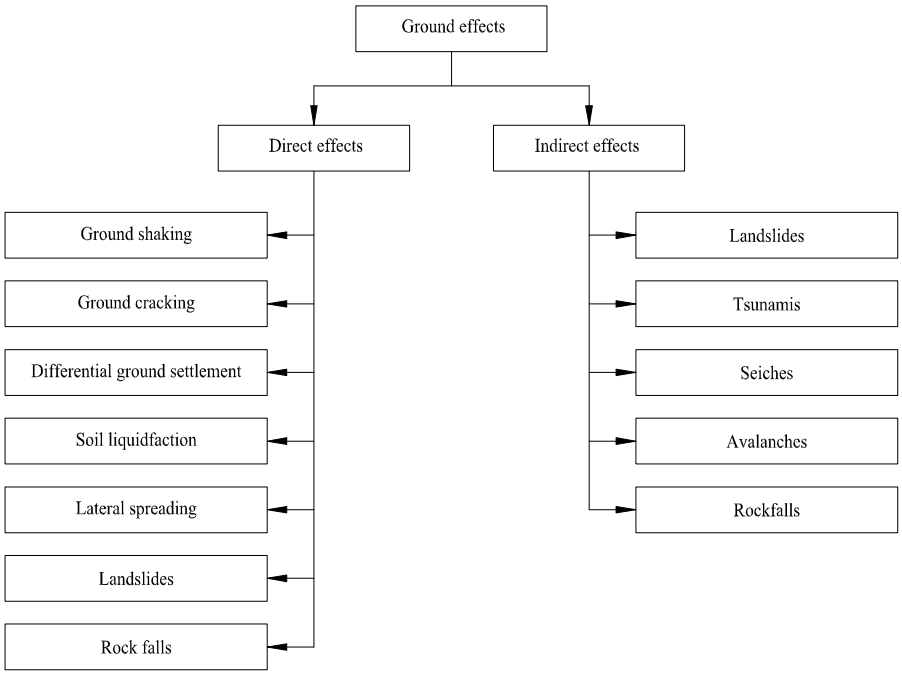

Figure 2-2 – Direct and indirect ground effects caused by earthquakes (EN1998-1 (2004))

To obtain the objectives of a seismic design or a seismic retrofit of the existing buildings, earthquake ground motions representing seismic hazards have to be defined. There are a number of ways in which

the seismic hazards can be expressed, depending on the approaches (such as deterministic or probabilistic ones). However, regardless of the approaches, the final aim is to present seismic engineering characteristics of the shaking at the site for a given earthquake.

According to EC8, the seismic hazard at a site can be expressed by a regional map or a hazard curve showing the probabilities of exceedance related to different levels of a given seismology parameter such as peak ground acceleration (PGA), velocity (PGV), displacement (PGD) and duration, for a given period of exposure. PGAs are widely used to represent hazard curves.

According to ATC-40, the seismic hazard can be defined either by specifying a level of shaking associated with a given probability of occurrence or a maximum level of shaking by a single event. The following three levels of earthquake ground motion are defined.

- The Serviceability Earthquake (SE): Ground motion with a 50 percent chance of being exceeded in a 50-year period.
- The Design Earthquake (DE): Ground motion with a 10 percent chance of being exceeded in a 50-year period.
- The Maximum Earthquake (ME): Maximum level of ground motion expected within the known geologic framework due to a specified single event or the ground motion of a 5 percent chance of being exceeded in a 50-year period.

2.2.3. Performance objectives

A seismic performance objective is defined by choosing a desired building performance level under a given earthquake ground motion. If the structures are chosen to satisfy two or more different desired performance levels, each for a different level of ground motion, a dual- or multiple-level performance objective will be created.

2.2.4. Determination of deficiencies of an existing RC-MRFs

If a structure is well seismically retrofitted or well seismically designed, it should meet its performance objectives when earthquakes occur. This means that during an earthquake horizontal and vertical resisting systems of the structures must be stable or comprise a complete seismic load path and the seismic forces are transferred from horizontal elements to vertical elements and then to the foundation systems without collapse. In all frame buildings, seismic inertial forces, originated in the components of the structures, will be transferred through the connections to horizontal diaphragm systems. These systems will distribute the inertial forces to vertical lateral force resisting components which in turn transfer these seismic forces to the foundations.

Deficiencies exist if seismic forces produce unacceptable limit states in components or connections of the structures or when vertical resisting systems are not capable of maintaining their capacity. These deficiencies can be due to a discontinuous load path, local failures, lack of redundancy in the vertical shear resisting systems, irregularities in plan or in vertical (abrupt changes in stiffness, strength or mass) or pounding. The seismic deficiencies of structural components could be ductile or brittle. Brittle mechanism, expressed by a rapid drop in stiffness and strength of the components, is an undesired failure mode. This causes abrupt rupture and subsequent rapid deterioration or disintegration of the material. On the contrary, the behaviour of a ductile member is characterised by essentially elastic performance until its critical force is attained beyond which deformation continues with little or no increase or decrease in capacity. At this stage, there are no abrupt changes in stiffness and strength and the component can continue to deform until material strain limits are exceeded. In that case, a sudden loss of stiffness and/or strength may occur.

It can be observed from past-earthquakes that there are several potential failure modes of RC-MRFs, including brittle column failure mode caused by shear failure or compression crushing of the concrete (due to combined axial, flexural and P-Δ effects) or lack of redundancy in the structures or weak story configurations leading to localized concentrations of drift, that directly affect the structure's capacity to

sustain vertical loads and maintain stable lateral behaviour. These failure modes are the result of deficiencies in the structures as summarised in Table 2-4.

Table 2-4 – Deficiencies in RC-MRFs (ATC 40, 1997)

Incomplete load path	Vertical Irregularities	Horizontal Irregularities	Week Column/Strong Beam
A complete load path of a structures assures that seismic forces will be completely transferred from all components in the structures to vertical resisting systems and then to the foundation.	Due to significant changes in building configuration such as setbacks, discontinuous vertical elements, vertical irregularities occur.	These deficiencies often cause significant differences between centers of mass and rigidity, resulting in the torsion response of the building.	Hinges at columns can lead to a soft story mechanism, creating large P-Δ effects and inelastic rotations at columns. Column hinging is undesirable since this may lead to loss of the column's gravity load carrying ability.

2.3. Analysis methods to evaluate the seismic performance and deficiencies of RC-MRFs

This section aims to briefly introduce all possible methods which can be used to evaluate seismic performance of RC-MRFs. There are a number of analysis procedures that compare measures of seismic capacity and demand to evaluate existing structures. These methods are useful to investigate deficiencies of the existing structures or verify the effectiveness of retrofit strategies mentioned in the next sections. The methods, which are chosen for the analyses and design of the frames throughout the thesis, will be re-presented in more detail in Chapter 6, Chapter 7 and 8.

EC8 proposes several methods to analyse the response of a structure subjected to an earthquake. The choice of method depends on the structure and on the objectives of the analysis.

- The standard method used in design is the modal response using a design spectrum. This is a linear method in which the inelastic behaviour is considered in the definition of the design spectrum, through the use of a behaviour factor q, accounting for the ductility and overstrength of the structure. This method is applicable to all types of buildings.
- The 'lateral force' method is a simplified version of the modal response method and is a static analysis which can only be employed for regular structures which respond essentially in one single mode of vibration. Similarly to the 'equivalent' force, F, applied to the mass m of the simple cantilever, it is possible to define in multi-storey buildings a set of 'storey' forces F_i, which are applied at each storey level and which induce the same deformed shape as the earthquake.
- The 'Pushover' analysis is a nonlinear static analysis carried out under constant gravity loads and monotonically increasing horizontal loads. It is applied essentially:
  - to verify or revise the overstrength ratio values α_u/α_1
  - to estimate the expected plastic mechanisms and the distribution of damage
  - to assess the structural performance of existing or retrofitted buildings
- Non-linear time-history analysis is a dynamic analysis obtained through direct numerical integration of the differential equations of motion. The earthquake action is represented by accelerograms (minimum 3). This type of analysis is often used for research and code background studies.

In countries which do not use Eurocodes, various analysis methods, both elastic (linear) and inelastic (nonlinear), can be used for the analysis of the existing RC-MFRs. The two elastic methods, namely equivalent lateral force and modal response spectrum analysis, are nearly similar to that of EC8-3. There are some differences such as behaviour factor q in EC8 being replaced by response modification factor R. The most basic inelastic analysis method, which is the completely nonlinear time history or nonlinear dynamic analysis, is the same as in EC8. Available simplified nonlinear analysis methods, referred to nonlinear static procedures, use the intersection of the capacity or pushover curve and a reduced response spectrum with damping taken into account to estimate the performance point; the displacement coefficient method (ATC 33) that transforms nonlinear pushover curve of a MDOF system into a bilinear

capacity curve of an equivalent SDOF system based on equal energy dissipation in two systems and determines maximum displacement of the real system; and the secant method (Priestley, 2007) that uses a substitute structure having secant stiffness. For the use of explaining technical strategies in the next sections, main steps of pushover analysis are briefly presented hereunder.

2.3.1. Capacity

Seismic resisting capacity of an existing structure depends on the strength and deformation capacities of its individual members. In order to determine the ultimate capacity of the structure, pushover analysis can be used. In pushover analysis, gravity loads are kept constant while lateral forces, vertically distributed to the structure and representing seismic actions, are gradually increased until the structure becomes unstable or predetermined limit is reached. In pushover procedure, lateral loads are first increased until first plastic hinge occurs anywhere in the structure. Then, the lateral load pattern can be adjusted to correlate with the deformation mode of the structure. Next, some more yields occur when the lateral loads are higher, leading to the reduction of overall stiffness and changes of dynamic deformation modes. The lateral load pattern can be readjusted again and then increased until the structure reach limits. Pushover analysis gives a capacity curve, which indicates how a structure behaves after exceeding its elastic limit; they are usually a plot of the force-displacement curve between the base shear and the roof displacement. The lateral load patterns are dependent on the mass of each story, first mode of vibration of the structure and on the change of structural properties after yielding. It is easy to obtain this curve if a completely nonlinear programme, such as FINELG or SEISMOSTRUCT or DRAIN-2DX..., is used. Four general steps to obtain capacity curve are summarised as follows:

- Step 1: Create a computer model of the structure. In order to obtain the more realistic seismic behaviour of the structure, all their components should be modelled based on their real behaviour. Nonlinearities in material and in geometry should be taken into account.
- Step 2: Apply lateral story shear force patterns to the structure. The gravity load should be imposed as well.
- Step 3: Create the analysis with the maximum desired top displacement.
- Step 4: Carry out the analysis until the desired top displacement is reached or the structure is unstable. The relationship between base shear and top displacement is recorded after each step of increasing displacement.

A typical capacity curve is depicted in Figure 2-3.

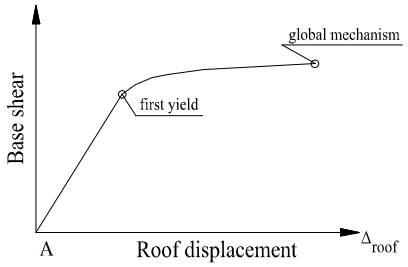

Figure 2-3 – A typical capacity curve

2.3.2. Demand (displacement)

During an earthquake, the ground will be moved and causes the movement of the structure. The displacements of the structure under a given ground motion are a function of time. Tracking these displacements at every time-step, with the aid of nonlinear time history analysis, consumes much time and is not an easy task. There are more simple methods to determine the demand due to seismic hazard by using pushover analysis. There are several types of Pushover analysis with different names: N2 method proposed in EC8 (developed by Faijar, 1997), the coefficient method (FEMA 356, 2000), or Capacity Spectrum Method (ATC 40, 1997) under a given ground motion, the displacement demand of the structure is an estimate of the maximum expected response of the building called target displacement. The basic meaning is nearly the same for all these methods, finding a point on the capacity spectrum,

which is a convert from capacity curve in Acceleration Displacement Response Spectrum (ADRS) format (S_a versus S_d). This point also lies on the appropriate demand response spectrum, reduced for nonlinear effects, and is called the performance point. This performance point represents the condition for which the seismic capacity of the structure is equal to the seismic demand imposed on the structure by the given ground motion. The procedures to determine performance point are presented herein:

- Step 1: Conversion from the Capacity Curve of a multi degree of freedom (MDOF) structure to the Capacity Spectrum of an equivalent single degree of freedom (SDOF) structure and from elastic response spectrum to ADRS format

The capacity curve of a MDOF structure, which is in terms of base shear and roof displacement, is transformed into what is called a capacity spectrum of an equivalent SDOF based on the first vibration mode, a representation of the capacity curve in ADRS format (S_a versus S_d). Base shear of the structure, calculated the product of the effective mass and the modal acceleration in the first mode vibration, will be converted to accelerations corresponding to each value of roof displacements. Displacements of the roof will be converted to modal displacements in the first mode vibration of the structure. Figure 2-4 presents response spectra in traditional S_a and T and in ADRS (S_a and S_d) formats.

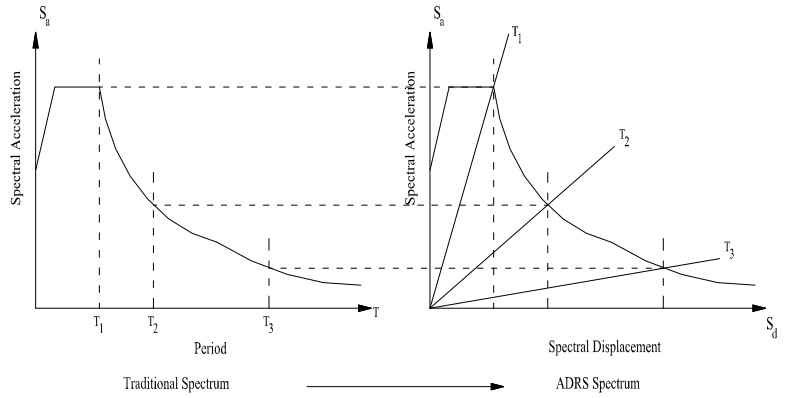

Figure 2-4 – Response Spectra in Traditional and ADRS Formats

- Step 2: Construction of bilinear representation of Capacity Spectrum

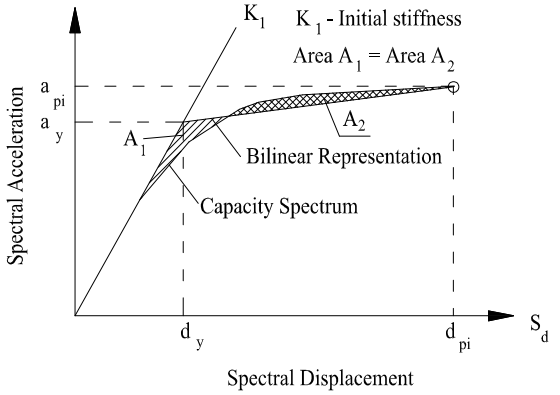

Figure 2-5 – Bilinear Representation of Capacity Spectrum for Capacity Spectrum Method

The elastic response spectrum of an earthquake, corresponding to a given ground motion, type of the soil..., is formed based on the response of a single degree of freedom (SDOF) structure under that motion, while capacity spectrum represents the seismic behaviour of a multi degree of freedom (MDOF) structure. To determine the performance point and/or dynamic responses corresponding to the response spectrum such as effective damping and appropriate reduction of spectral demand, capacity spectrum of the MDOF structure has to be transformed into an equivalent capacity spectrum of an equivalent SDOF structure. Generally, a bilinear spectrum is chosen to replace for the capacity spectrum. Construction of the bilinear representation is based on equating the displacement or dissipated energy of two systems. It

requires definition of the point a_{pi} and d_{pi}. This point is the trial performance point which is used to develop a reduced demand response spectrum. If the reduced response spectrum is found to intersect the capacity spectrum at the estimated a_{pi}, dpi point, then that point is the performance point. Figure 2-5 shows an example of determining a bilinear representation of capacity spectrum.

- Step 3: Estimation of damping and Reduction of 5 percent Damped Response Spectrum

Under a given ground motion, seismic hazard is represented by an elastic response spectrum. This spectrum corresponds to an elastic structure with the damping of 5%. However, the damping of a real structure when it is driven into the inelastic range by the earthquake consists of viscous damping that is inherent in the structure and hysteretic damping. The viscous damping is usually assumed to be constant and equal to 5%. Hysteretic damping is related to the energy that is dissipated by inelastic deformation. This energy is the area inside the loops that are formed when the earthquake force (base shear) is plotted against the structural displacement. In a SDOF system, hysteretic damping can usually be represented as equivalent viscous damping ATC 40 (1997).

- Step 4: Development of the Demand Spectrum

The 5% elastic response spectrum can be easily obtained from characteristics of the ground motion and of the soil. The demand spectrum of a given ground motion is determined by the product of 5 percent elastic response spectrum and the reduction spectral factor which represents the increase of damping in the structure due to hysteretic behaviour. These spectra are shown in Figure 2-6.

- Step 5: Intersection of Capacity Spectrum and Demand Spectrum

To obtain the performance point, it is necessary to perform a trial and error process. The performance point represents the maximum structural displacement expected for the demand earthquake ground motion. If the displacement of the trial point (a_{pi}, d_{pi}) is within 5 percent of the displacement at the intersection of demand and capacity spectra ($0.95d_{pi} \leq d_i \leq 1.05d_{pi}$), this point becomes the performance point. If the intersection is not within the acceptable tolerance, then a new trial point is selected and the process is repeated. This concept is illustrated in Figure 2-6.

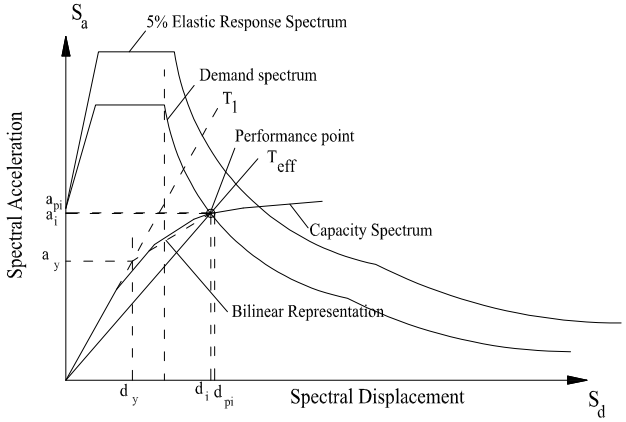

Figure 2-6 – Definition of the performance point

2.3.3. Performance

When a capacity curve and the demand displacement are defined, a performance check can be carried out. This verifies that structural and non-structural components are not damaged. With the demand displacement their behaviour is beyond acceptable limits of the performance objective.

2.4. Retrofit strategies

This section presents an overview of the process used to develop a retrofit strategy once deficiencies of the existing buildings have been detected and performance objectives have been apparently determined. A retrofit strategy comprises technical and management strategies. They are employed to obtain seismic risk reduction for the buildings.

2.4.1. Technical strategies

When a structure is subjected to earthquakes, lateral displacements and deformations of its members are generated. There will be no damage in the structure if its element deformations are in elastic range. At higher levels of response, element deformations will exceed their linear capacities and the structure will experience damage. In order to obtain good seismic performance, a structure must have a stable lateral force resisting system, which is capable of limiting lateral displacements and the damage so that their element deformations will be within acceptable levels for the intended performance objectives. The fundamental factors, referring to the capacity of the structure and demand parameters of the seismic hazard and affecting the lateral force resisting system, are mass, stiffness, strength, damping and configuration of the building; the deformation capacity of its elements; and the character of the ground motion. Technical strategies are approaches to modify these basic factors for Design Earthquake. These strategies include system completion, system strengthening, system stiffening, enhancing deformation capacity, increasing energy dissipation capacity and reducing seismic demand to the building. In order to explain for the physical and mechanical meaning of technical strategies, a capacity curve is used. There are some more definitions in the capacity curve in Figure 2-7.

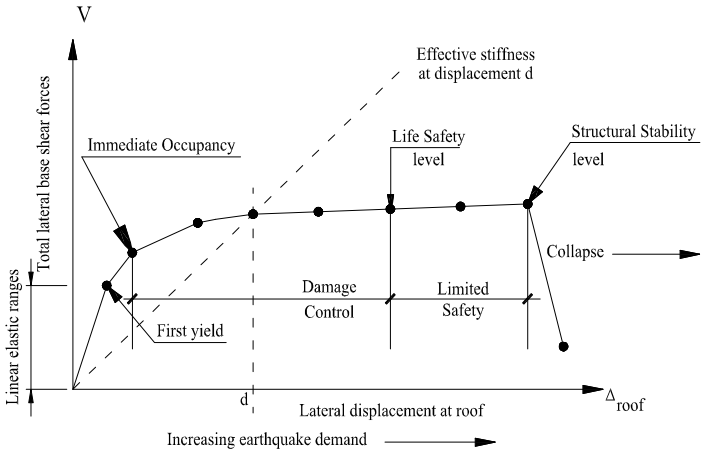

Figure 2-7 – Definitions in Capacity Curve

Capacity curve is a plot of base shears versus top displacements. Generally, if a building had infinite linear elastic capacity, this capacity curve would be a straight line with a slope equal to the global stiffness of the structure. However, since real buildings do not have infinite stiffness, the pushover curve typically includes a series of straight-line segments with decreasing slope, representing the gradual degradation of the structure's stiffness. This degradation is the result of yielding in some components of the structure. The slope of a straight line, drawn from the origin to a point on the curve at any displacement d, represents the secant or 'effective' stiffness of that structure. Based on the performance criteria, related to the displacements of the top, performance levels of the structure are also presented in Figure 2-7.

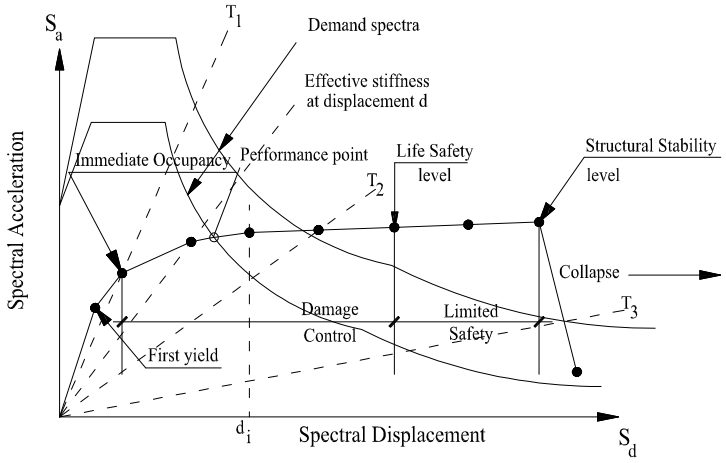

Figure 2-8 – Determination of Performance Point

In order to determine seismic performance of the structure under a given ground motion represented by a performance point, its capacity and seismic demand will be plotted in the same format and coordinates. In Pushover approach, ADRS format is used to visualise the seismic performance of the structure. As explained in the previous section, the capacity curve and reduced demand response spectrum will be converted to spectral acceleration S_a and spectral displacement S_d thanks to modal contributors such as the modal participation factor, the effective mass factor... The intersection of capacity and demand spectra is the performance point. Once performance point has been determined, the seismic performance of the structure can be judged in the comparison with the decided performance objectives. An example of determining the performance point is shown in Figure 2-8.

2.4.1.1. System completion

This strategy is usually used for the structures that have basic components of an adequate lateral force resisting system, but that lack some details which ensure that the system behaves as intended. The capacity spectrum of such a structure would intersect the demand spectra at an acceptable performance point. However, prior to reaching that point, some local failures would occur. These failures are caused by a lack of adequate chord, inadequate bearing length at precast element supports and inadequate anchorage or bracing of structural or non-structural elements. This strategy is often implemented together with other strategies to gain the desired seismic performance capacities of the structures.

2.4.1.2. System strengthening and stiffening

For structures that have inadequate lateral force resisting systems, system strengthening and stiffening are the most suitable strategies. They are closely related but differently. Strengthening makes the structures able to increase the capacities of carrying lateral forces. This means that the fundamental periods of the structures do not change after being retrofitted by strengthening. The effect of the strengthening is to permit the structures to obtain larger displacements without damage.

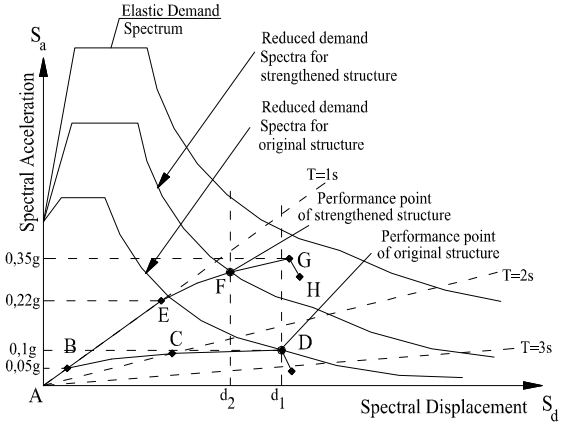

Figure 2-9 – Effect of System Strengthening on Performance (ATC 40, 1997)

The effect of system strengthening on seismic performance is clearly illustrated in Figure 2-9. The capacity spectrum represents seismic performance of an un-strengthened structure and is defined by the curve A-B-C-D. This structure has a fundamental period of 1s, a spectral acceleration capacity at first yield of 0.05g, an ultimate spectral acceleration capacity of 0.1g and the ultimate spectral deformation capacity of d_1. The performance point of this un-strengthened structure occurs at point 'D', at where the structure just reaches Structural Stability performance level. After being strengthened, the capacity spectrum of the new structure is represented by the curve A-B-E-F-G-H. It is worth noting that the fundamental period of the strengthened structure remains at 1s as the previous ones. This means that the structure has not been stiffened. In addition to that, the ultimate spectral deformation capacity still remains at approximately d_1. This indicates that there is no additional deformation capacity added to the strengthened structure. The advantages from this strengthening process is that there is an increase in its spectral acceleration capacity at first yield of 0.22g and an ultimate spectral acceleration capacity of 0.35g which are much higher than the un-strengthened structure. The new performance point for the strengthened structure under the same

earthquake is at F, corresponding to the spectral deformation capacity of d_2 which is much less than d_1 and well within the required performance.

Another very efficient strategy to increase the lateral force resisting systems of the structures is to make them stiffer. This strategy is quite different from strengthening system. The effect of stiffening a structure is explained in Figure 2-10. In the figure, capacity spectrum of an un-stiffened structure is represented by the curve A-B-C-D-E. This structure has an initial elastic period of approximately 1.5s, a spectral acceleration capacity at first yield of 0.22g and an ultimate spectral acceleration of 0.35g. After it has been stiffened, capacity spectrum is defined by the curve A-F-G-H-I. Since the stiffness of the structure has been increase, the initial elastic period of the stiffened structure is decreased and is 1s, while the spectral acceleration capacity at first yield and ultimate remain unchanged. The result of this stiffening process is to shift the performance point from a deflection of d_2 to a deflection d_3 which is less than d_2.

Strengthening and stiffening systems are usually used as concurrent strategies because most systems that strengthen a structure will also stiffen it and similarly, increasing the stiffness of the structure will also result in its strength increase.

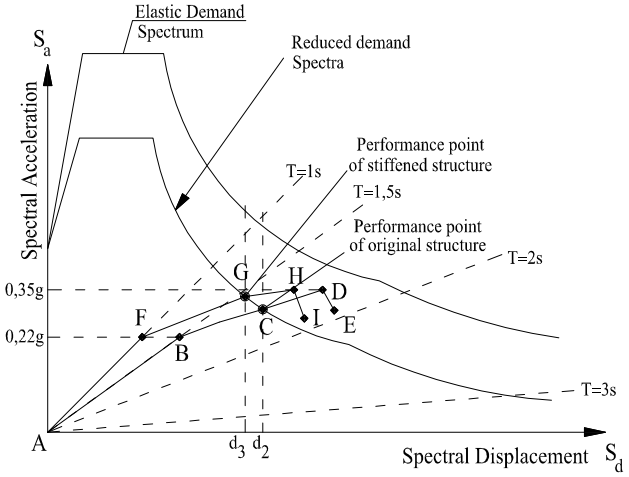

Figure 2-10 – Effect of System stiffening on Performance (ATC 40, 1997)

2.4.1.3. Enhancing deformation capacity

This technical strategy requires the improvement in the building seismic performance thanks to the enhancement of the capacity of individual elements. The effect of enhancing deformation capacity on building performance is illustrated in Figure 2-11.

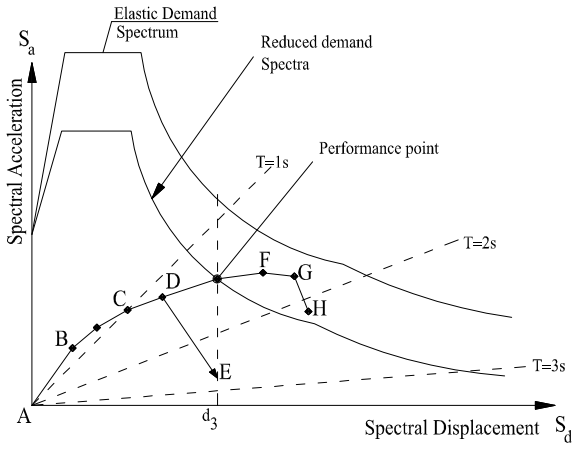

Figure 2-11 – Effect of Deformation Enhancement on Structural Performance (ATC 40, 1997)

The capacity spectrum of the original structure is represented by the curve A-B-C-D-E. This curve is unable to intersect the demand spectrum at a performance point because there are some critical failures of

an element occurring prior to this intersection. If this element is modified to obtain larger deformation capacity, the capacity spectrum of such a structure will be lengthen to larger spectral deformation capacity, as the curve A-B-C-D-F-G-H in Figure 2-11. This helps the structure to reach the target displacement or performance point at an acceptable structural performance level. This strategy can be obtained by adding some confinement to existing elements, making local reduction in stiffness to get larger deformation, modifying columns to alter their plastic mechanisms...

2.4.1.4. Reducing earthquake demands

Not modifying the capacity of seismic performance of the existing structures, this strategy proposes the solution to modify the response of the structures such that the demand forces and deformations are reduced. To obtain that, demand spectrum of seismic hazard will be modified rather than the capacity spectrum. Methods to obtain this strategy include reducing the building's mass and the installation of some systems such as base isolators, tuned mass dampers or viscous dampers to dissipate seismic energy.

2.4.2. Management strategies

Management strategies are typically more controlled by the owners than by the design teams. Therefore they are not of interest in the current study.

2.5. Recent Seismic Retrofitting systems for RC-MRFs

In the last few decades, many retrofit systems such as steel braces, steel plate shear walls, aluminium shear walls and reinforced concrete shear walls have been extensively studied and used to seismically retrofit and upgrade RC-MRFs. All these retrofitting systems modify capacity spectra of the existing RC-MRFs and provide more additional lateral stiffness and strength to the structures or change the demand spectra of the seismic hazard. Among those systems, steel braces (eccentric or concentric ones) and shear walls made from metal gain more advantages than reinforced concrete shear walls due to their efficiency in constructing on the site and in reducing costs of the foundations. Steel bracing systems can be applied externally even with few intervention on building occupants. Other approaches are to modify the response of the structures under given seismic ground shakings. These include adding base isolators, tuned mass dampers, or friction viscous dampers to the structures or reducing the buildings' mass with the aims to lengthen the structures' periods or to absorb seismic energy... This section briefly introduces these recent advanced retrofitting systems to date with the emphasis on their technical strategies, design concepts and hysteretic behaviour.

2.5.1. Retrofitting System using Conventional Steel Concentric Braces (CBFs)

2.5.1.1. Introduction

Prior to the 1994 Northridge earthquake, concentrically braced frames (CBFs) were mainly constructed in Japan. Then, they have been widely used as main lateral force resisting systems in US, Mexico... However, extensive damage has been clearly observed in CBFs following many recent earthquakes, including the 1985 Mexico (Osteraas, 1989), 1994 Northridge (Tremblay, 1995)… events. Due to these observations, US building codes stipulate low values for the response modification factor (R) used in design to account for the inherent ductility of a system. Furthermore, because many additional restrictions and complex and stringent guidelines for the design and construction of Steel MRFs with concentric braces located in regions of high seismic risk are required, a rapid increase in the use of CBFs has been recognised, especially for low- and mid-rise construction. Steel concentric braces can be divided into two groups: Conventional Concentric Braces and Restrained Buckling Braces. The latter has been developed more recently.

2.5.1.2. Configuration of CBFs

CBF systems applied for retrofitting reinforced concrete or steel structures contribute to lateral-load resistance, stiffness and to energy dissipation through the axial forces in their inclined braces. All possible

configurations of CBFs to date are illustrated in Figure 2-12. Tension braces are regarded as the dissipative elements. Most of appropriate concentric bracing systems are those with:

- X-diagonal ("cross-diagonal") bracings, along both diagonals of the braced bays (Figure 2-12, top-left). This is overall the preferable arrangement.
- Diagonal bracings, with a single diagonal per braced bay (Figure 2-12, top-right). The arrangement of bracings in different bays is able to give similar lateral resistance and stiffness for the X-diagonal ones in the plane of bracing.
- V-bracings or inverted-V ones (Figure 2-12 (bottom-left and right)), where a pair of inclined braces is connected to a single point close or at mid-span of a beam. Their advantages comprise the reduced un-braced length of the braces and the earlier flexibility of their strength and dissipation capacity. Chevron bracings in particular are most convenient for openings and passage through the braced bay. The horizontal member, to which the two braces connect, have to resist a transverse force equal to the difference in the vertical force components of the tension and compression braces. For this purpose, the post-buckling force of the compression brace is normally conservatively taken as 30% of the yield force or one-third of the buckling load (Fardis, 2009). If V-bracings are reversed in adjacent stories (with an inverted-V in one storey and a V-bracing in the storey above), the braces in consecutive stories are almost continuous and therefore there is no unbalanced transverse force on the beam (except the top beams).

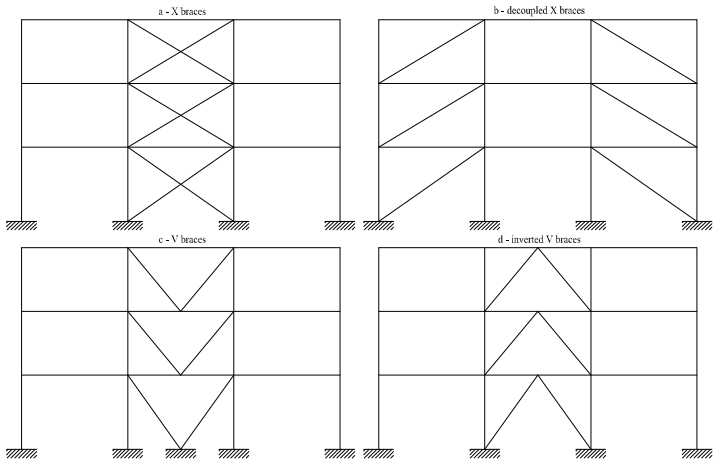

Figure 2-12 – CBF systems to retrofit or upgrade structures

- K-bracings, where the two inclined braces are connected to columns at about their mid-height, should be avoided, because the unbalanced force after buckling of the compression brace for V-bracings is applied to the columns and may lead to the failure of columns.

2.5.1.3. Experimental studies on CBF

Up to date, there have been a few studies on the behaviour of the CBF on RC-MRFs. There are several documents that have suggested for the use of the CBF to retrofit RC structures (FEMA356 (2000), Fardis (2009), Mazzolani (2006)). The analytical models of the CBF in such documents under monotonic and cyclic loading are based on many studies of the CBF on steel structures. Some selected studies are introduced herein, based on summaries of experimental results performed on CBF which have been prepared recently by Tremblay (2002) and Lee and Bruneau (2005).

Kahn and Hanson (1976) tested 16 small hot-rolled steel bars with a rectangular cross section of 25.4x12.7 mm. These bars were welded to steel plates at their ends and based on k.l/r ratios ranging from 85 to 210 with different lengths and end connections. Loads on bars were applied cyclically at both dynamic and quasi-static rates. The main goal of these experiments was to determine the effect of dynamic loading on the axial-force and axial-deformation relationship. It was found that the dynamic and static loading cases produce nearly identical hysteretic relationships.

One of the earliest shaking table experiments on CBF was conducted at the University of California by Ghanaat (1980). The three-story, 3/5-scale moment-frame specimen was designed for wind loading. It provided a test-bed structure to analyze the behaviour of different bracing systems: rod X-braces (kl/r=370 - slenderness), ¾-in (1.905 cm) diameter pipe X-braces (k.l/r = 125), and double-angle X-braces (k.l/r = 86). As a comparison, the moment frame without braces was also tested. The report from these tests concluded that the addition of braces designed primarily for wind can be effective in resisting intermediate-intensity earthquake induced shaking. However, the observed drifts were quite large with substantial damage to bracing elements. It was noted that the pinched hysteretic behaviour of all of the braces tested were undesirable for larger-magnitude earthquake loading. Finally, it was predicted that taller structures, where large P-Δ effects may be encountered, might be prone to collapse.

Tests representative of 1/6-scale tubular steel braces from a Southern California offshore platform (Zayas et al., 1980b) were carried out in support of subsequent cyclic inelastic tests on two complete 1/6-scale structures (Zayas et al., 1980a). The structures consisted of two full height X-brace stacked panels, with a final half-height panel with an inverted chevron-braced configuration. These cyclic tests were followed by a shake table test (Ghanaat and Clough, 1982) and pseudo-dynamic tests (Shing and Mahin, 1984) on the same structure. The brace component tests contained both fixed-ended and pin-ended configurations to bound actual boundary conditions expected in offshore platform construction. Comparisons of D/t (Diameters/thickness) ratios of 33 and 48 were made. In both D/t cases, after local buckling began, there was a rapid deterioration in the hysteretic behaviour and loss of strength. Another important observation that was similar to observations from past earthquakes is that the damage is concentrated in one half of a brace along the full diagonal. This led to further concentration of damage in the portion of the brace that buckled during subsequent cycles.

Experimental studies at the University of Michigan (El-Tayem and Goel, 1985) examined the effect of single-story X-bracing for use in seismic applications. A comparison of single-angle braces and double-angle braces was also performed. In all of the tests, only one half of the total brace buckled in compression. This study also reported that the effect of single-angle or double-angle shape did not greatly affect the hysteresis loops. However, local buckling led to rapid degradation of the moment capacity of the connection and, subsequently, the lateral strength of the entire sub-assemblage. The gusset plate details used were adapted from previous studies (Astaneh-Asl et al., 1985), and these connections behaved as expected. In general, failure mechanisms occurred typically at locations of local buckling or plastic hinging in the brace, and on a few occasions, they were due to fatigue failure of gusset plates or fracture of the welds connecting the brace to the gusset plate.

One-half-scale tests were conducted as prototype specimens for future full-scale tests on a chevron-configured frame (Fukuta et al. 1989). Six concentrically braced specimens were tested to observe the effect of in-plane versus out-of-plane buckling, beam versus column mode of failure for collapse, and the effect of the slenderness ratio (l/r = 70-120). Static cyclic loads were applied such that the relationship between the column axial force and the lateral shear force were maintained constant. These studies demonstrated that the compact braces [(D-2t)/t=6] (D- diameter and t – thickness of the braces) provided an excellent means of dissipating energy, and that the global hysteresis loops were similar to those of the moment frames. The members with slender sections [(D-2t)/t>20] experienced severe local buckling. The experimental assemblies had difficulty in reaching the tensile capacity of the brace due to large mid-span beam deflections.

Canadian researchers at the Ecole Polytechnique, Montreal, have more recently performed a large series of tests on concentrically braced steel frames using modern construction details similar to those found in the United States (Tremblay et al., 2002 …). In these tests, a series of 14 single diagonal and 10 single-story X-configurations were tested in a single-story single-bay testing rig. The rectangular hollow section braces tested in this configuration had relatively low width-to thickness ratios (8.9–13.8), where the width to thickness ratios is calculated by using the equation: (D-3t)/t. The slenderness of the braces, computed from gusset plate plastic hinge to gusset plate plastic hinge, were in the range of 100–160, and 60–110 for the single-diagonal and single-story X-braced configuration, respectively. As evidenced in previously described tests, the single-story X-configuration concentrates buckling and related damage in only one half of the compression brace. Thus, the plastic rotation demands in the plastic hinges are increased, leading to earlier initiation of fracture. Total normalized hysteretic energy dissipated by the single-diagonal configurations was greater than those of the single-story X-bracing configurations. These results again

highlight the strong correlation between fatigue life and the effective slenderness ratio of a brace. A maximum target displacement of 5 times the tension yield displacement was intended for each of the braces. As the geometry shown in the reports it results in a peak displacement drift of about 1.9%. The experiments were continued until each of the braces ruptured. It is important to note that few specimens reached drifts larger than 1.5% prior to fracture.

Tremblay (2002) examined the effect of the slenderness ratio, the section shape, the loading history, and other properties on the initial buckling capacity of the brace; the compression strength remaining when various amounts of normalized axial shortening were imposed; the amount of lateral displacement as a function of axial shortening; the amplitude of cyclic deformation when rupture occurred; and so on. Tremblay notes that braces are often stronger than predicted using code equations, and that this difference should be accounted for in analytical studies of performance. Similarly, the larger normalized displacements reached in compression for relatively slender braces prior to rupture suggested that more stringent width-to-thickness criteria would be appropriate for stocky braces.

Lee and Bruneau (2005) used virtually the same database, but focused on the deterioration of buckling load and energy dissipation in each cycle, from cycle to cycle, as a function of the slenderness ratio, the imposed deformation history, and the section shape. They concluded that tubular braces deteriorate slower than do non-tubular sections, especially in comparison with W-sections with slenderness ratios greater than 80. Interestingly, their results suggested that while more slender braces might be able to undergo larger inelastic displacements, the strength and energy-dissipation capacities deteriorated substantially during these excursions.

2.5.1.4. Analytical studies and hysteretic behaviour of CBF

Up to date, very few analytical studies have been carried out to examine the effectiveness and behaviour of CBF to retrofit the existing RC-MRFs. Since CBF have been mostly used for steel structures (in US, Japan), their behaviour in cooperation with steel structures have been experimentally and analytically studied. For retrofitting or upgrading RC-MRFs, design of CBF has been still based on their response in steel structures.

The behaviour of the RC-MRFs with the use of steel conventional concentric braces is a combination of two components: the behaviour of RC-MRFs without CBF and the individual behaviour of CBF. It has been modelled in several ways, resulted from experiments on individual steel braces or on the steel concentrically braced frames. Some previous simple models are illustrated in Figure 2-13, including (a) elastic behaviour, (b) tension-yield and compression-buckling and (c) tension-yield and compression-yield. The first model represents hysteretic behaviour for steel braces that work elastically and there is no yielding in either tension or compression. The second is appropriate for slender braces having very high slenderness causing the buckling in compression and the last ones is suitable for stocky braces that do not buckle in compression.

Apparently, there has been no model for the braces having intermediate lengths which either under-estimate or over-estimate the energy dissipated in the compression region of the hysteretic loop. For that reasons, some analytical studies have been focused on analytical modelling of intermediate length braces (Nakashima and Wakabayashi, 1992). Idealised hysteresis loop of a pin-ended brace obtained from those studies is illustrated in Figure 2-14. This loop is composed of some characteristic parts. From O to A, the brace works elastically up to its critical buckling load at A. Part A-B represents a constant axial load caused the buckling of the brace and accompanied by brace shortening due to lateral displacement, Δ. The second-order effect results in an increase of moment and a plastic hinge at mid-span of the brace. An instant mechanism is formed when this plastic hinge appears. Zone B-C describes the compression process with induced plastic rotation in this plastic mechanism. Parts from C to D and D to E represent the elastic unloading and tension reloading of the brace, respectively. Because of the residual curvature of the brace, the stiffness in these zones is significantly less than that in the stage O-A. Part EF describes an increase in axial load, resulting in an elongation and gradually straightening of the brace. This is accompanied by an increase in stiffness. The plastic hinge to rotate in the opposite sense is now formed due to P-Δ moment until all plastic rotation is recovered. The brace is straight at point F. Zone FG represents uniaxial yielding of the member. There may some increases in stiffness of the brace due to strain-hardening.

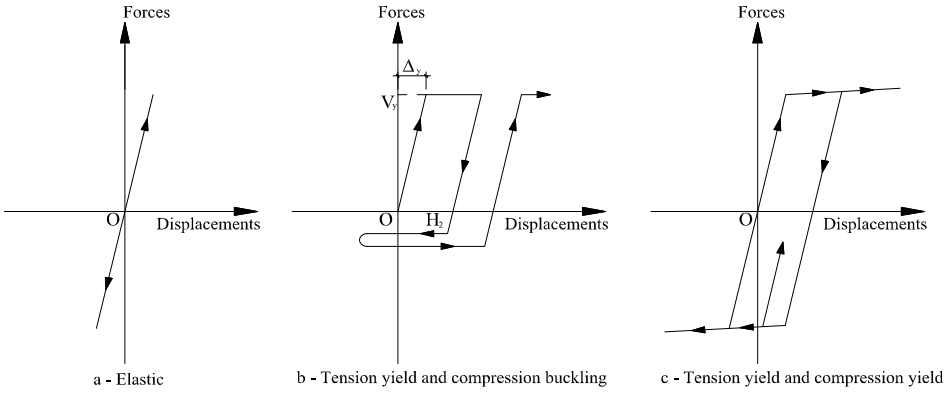

Figure 2-13 – Original brace models

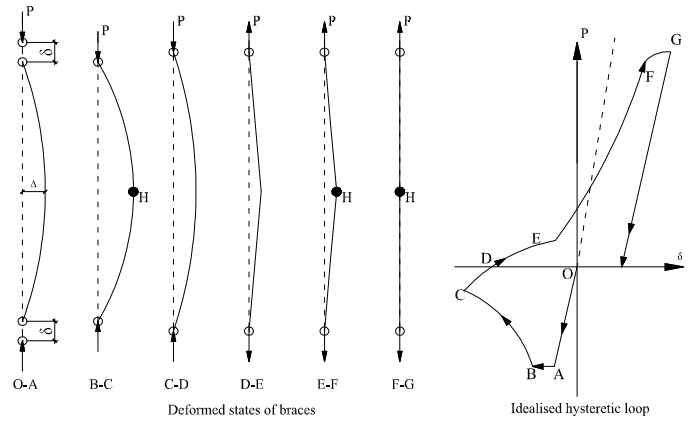

Figure 2-14 – Idealised hysteretic behaviour of intermediate braces (Nakashima and Wakabayashi, 1992)

2.5.1.5. Design concepts of retrofit of RC-MRFs using CBF

Performances of steel frames with CBFs from past earthquakes showed that they could fail mainly by failure of the braces and their connections after buckling. To enhance the behaviour of CBF, it is necessary to make them well able to withstand large post-buckling cyclic deformations. This can be done by preventing them from the adverse effects, like distortion and local buckling, early failure of welds, etc... Such phenomena may risk the full tensile capacity of a brace, after it is straightened back during the next half-cycle of the response. The post-buckling response of braces can be improved by welding closely spaced batten plates. Local buckling in compression bracings may cause fracture, owing to concentrations of strains or strain accumulation with cycling. To avoid this local buckling, "compact" sections should be used, with low width-to-thickness ratios. Due to that, for braces used in seismic design or retrofitting, the upper limit to this ratio should be considerably lower than for monotonic loads (e.g. by 50%, EC8-1). For new steel buildings, Part 1 of EC8 requires using:

– "class" 1 steel sections, if the q-factor 4 or more

– "class" 1 or 2 sections, for q between 2 and 4

– "class" 3 sections, with q between 1.5 and 2

These "classes" are defined in EN-Eurocode 3, Part 1, depending on the shape of the section and its width-to-thickness ratio. For bracings in seismic retrofitting it is strongly recommended avoiding "class" 3 sections. If possible, "class" 1 should be used. No matter whether compression braces are taken into account in the analysis for the retrofit design (as in V-bracings), or neglected (as may be the case in diagonal or X-braced systems), their slenderness should be limited. A sensible upper limit is the value of 2.0 imposed by EC8 to the non-dimensional slenderness $\bar{\lambda}$ (defined as the square root of the ratio of the member's yield force, f_{yA}, to its critical buckling load, N_{cr}) in new steel structures. EC8 provides a lower

limit of 1.3 on $\bar{\lambda}$ for compression braces, neglected in a linear analysis for the seismic action. This is to reduce the axial force that will inevitably develop in the (neglected) compression braces during the pre-buckling stage and prevent columns and beams from being overloaded with seismic action effects (much) higher than given by the linear analysis and damaged before the tension diagonals yield. If compression braces are included in a nonlinear analysis, there is little sense in observing a lower limit on $\bar{\lambda}$. Realistic end restraint assumptions should be made for the effective un-braced length of braces (Fardis, 2009).

2.5.2. Retrofitting system using Steel Buckling Restrained Braces (BRBs)

2.5.2.1. Introduction

To exploit ultimate capacity of the braces in both tension and compression under seismic excitations, steel conventionally concentric braces are improved by preventing them from buckling in compression. The retrofitting systems using these types of braces are called steel BRB systems. In fact, as it has been known that conventional braced frames have exhibited certain unfavourable modes of behaviour in past earthquakes: connection fracture, degradation of stiffness and strength under cyclic loading, and excessive flexure of beams in chevron-braced frames..., the concept of eliminating the compression buckling failure mode in intermediate and slender compression elements to avoid degradation of stiffness of the steel braces has long been a subject of discussion. For that reason, considerable research in recent years has focused on developing bracing elements with more favourable behaviour. BRBs achieve stable, balanced hysteretic behaviour by accommodating ductile compression yielding before the onset of buckling. Structural systems designed with these braces can achieve performance superior to that of CBFs at many aspects such as a comparable cost and capacity of energy dissipation. BRB frames are regarded as being capable of providing similar, or perhaps even better, performance than eccentrically-braced frames (EBFs), and with the added benefit of removing ductility and energy dissipation demands from the primary gravity load-supporting frame of the structure and confining it to structural elements by the BRBs. Similarly to EBFs, BRB systems are not only the affective solution for steel structures but also the excellent option for protecting reinforced concrete structures from severe earthquake damage (Mazolani, D'Aniello et al., 2006).

2.5.2.2. Configuration of BRBs

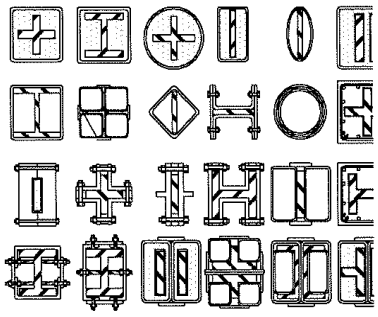

Figure 2-15 - Typical types of BRB (Tsai et al., 2004)

Generally, the theoretical solution for eliminating the buckling failure mode is very simple: laterally brace a compression element so that the compression element's un-braced length effectively approaches zero, as shown in Figure 2-16. Figure 2-15 illustrates different types of BRBs summarized by Tsai et al. (2004). BRBs have been studied based on the basic concept to use tubes for restraining lateral deformations while permitting axial deformations of the core. Usually, the restraining tube is filled with concrete and an un-bonding layer is placed at the contact surface between the concrete and core plates. This type of the BRB is called 'un-bonded braces'. Without friction at contact surface, the brace can freely slide inside the tube and transverse expansion of the brace can develop when the brace yields in compression. There is another type of the BRB known as 'only steel' brace, which includes two or more steel tubes contacting directly with the yielding plates. These restraining tubes can be connected by bolts which allow an easy inspection

and maintenance during the life-time or after a damaging earthquake (Tsai et al., 2004). A typical view of a BRB is shown in Figure 2-16.

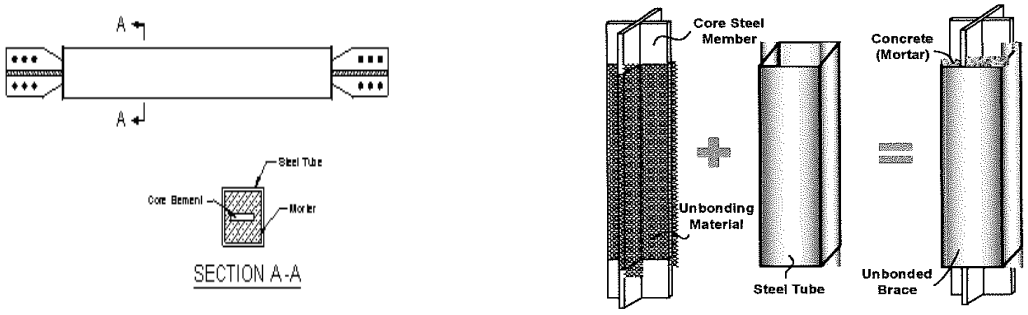

Figure 2-16 – Configuration of a BRB

2.5.2.3. Development and studies of BRBs

Up to present, this type of structure has been studied and developed expansively, mostly in Japan, US, Mexico. There are numerous tests and numerical studies performed with various types of the BRB. This section will briefly present some selected studies on the BRBs.

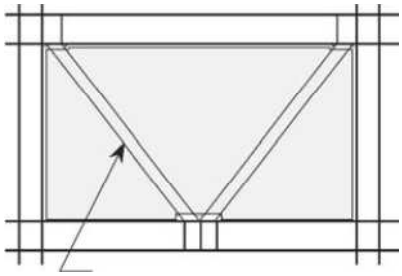

Figure 2-17 – Buckling restrained braces sandwiched between precast concrete panels

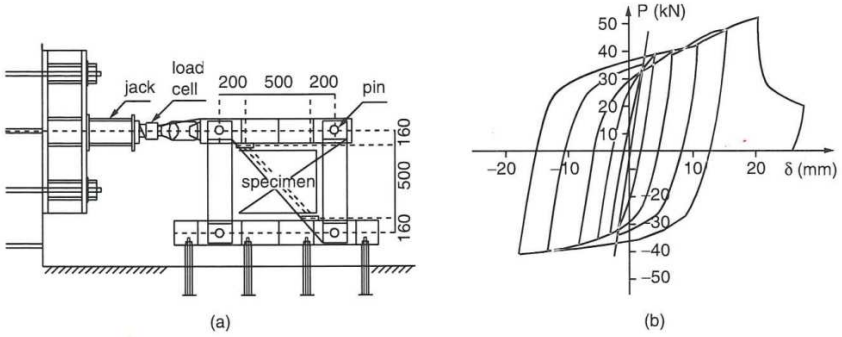

Figure 2-18 – Sub-assemblage test of buckling-restrained braces sandwiched between precast concrete panels (a) Test setup; (b) hysteresis behaviour (Wakabayashi et al., 1973)

The first work on BRBs was conducted by Wakabayashi et al. (1973), who developed a system in which braces made of steel flat plates were sandwiched between a pair of precast reinforced concrete panels (Figure 2-17). This research was performed in four stages: (1) pull-out tests to examine the methods of un-bonded, (2) compression tests of plates sandwiched between precast panels to examine the required stiffness and strength for the panels, (3) sub-assemblage tests to see the effectiveness of end connection details and (4) two-story frame tests for system verification. In the pull-out tests, epoxy resin, silicon resin, vinyl tapes, etc. were experimented as the un-bonded material. A total of 11 specimens were tested and it was concluded that a layer of epoxy resin covered by silicon resin was the most effective un-bonded material. In the compression tests, in which 21 specimens were tested, various reinforcing details were adopted for the precast concrete panels, and a special emphasis was placed on the reinforcement along the edges of the panels. Inadequate reinforcement at these locations was found to cause damage earlier in the

loading cycles because of the transverse forces that were produced by the out-of-plane deflection of the braces. In the sub-assemblage test, a pair of flat plates, arranged in either a diagonal or chevron pattern, was connected to a pin-connected steel frame and encased by precast concrete panels; the specimens were about 1/5 in scale (Figure 2-18a). An example of hysteresis behaviour is shown in Figure 2-18b.

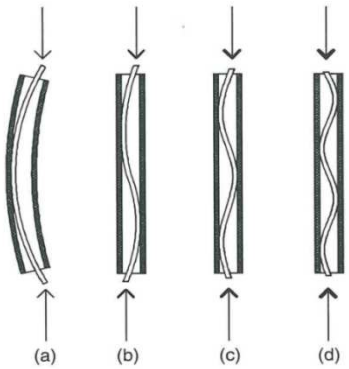

Figure 2-19 – Concept of sleeve column (Srihara, B.N., 1990)

Siridhara (1990) introduced sleeved column as a BRB. The idea was to decouple the compression load resistance of the core from the flexural buckling resistance of the sleeve. The behaviour of the steel core in a sleeve depends on the relative stiffness of the core and the sleeve. In a sleeve column, the core is loosely placed inside a sleeve and the load is applied only to the core. The core, under the action of the applied load, bends and presses against the inside surface of the sleeve, thus causing primarily bending stress in the sleeve. If the maximum bending stress in the sleeve is kept within the yield strength of the sleeve material, it is possible to stress the core to very high stress levels, much beyond the yield strength of the core material. Figure 2-19 shows the concept of the sleeved column. As the applied load is increased, the core will bear against the sleeve and buckle into higher modes.

A new study on BRBs to retrofit RC-MRFs under seismic actions was carried out by Bordea (2010). In this study, two experimental programs were performed. The first one was to address the behaviour of BRBs under monotonic and cyclic loading and the second was about the test of a one-story RC-MRF combined with BRBs. Numerical simulations with Pushover and Incremental dynamic analyses were used to evaluate the seismic performance of RC-MRFs. FEMA 356 was adopted as the criteria to clarify seismic behaviour of the system. From tests on BRBs, it was concluded that BRBs showed good performance and large deformation capacity. In addition, the values of the deformation capacity under monotonic tests showed similar results in both tension and compression; cyclic tests showed very stable and repeatable behaviour. Besides, the unbonding material may have an important influence on the deformation capacity of the BRBs. Numerical analysis on the RC-MRFs from this study showed that the initial structure MRF have limited ductility and did not attain the displacement demands for LS and CP levels. When the global retrofitting is accomplished MRF+BRB, the behavior is much improved. The stiffness and the strength were increased and the structure could attain the LS performance. The contribution of the local retrofitting is again very limited. Therefore, it is necessary to strengthen the columns and not only to confine them in order to fulfill the requirements for the three performance levels. Concerning about the behavior factor q, the mean value of q factor was larger than the initial value considered in the analysis. The retrofitting of existing RC frames with buckling restrained steel braces can be based of q factors amounting from 3 to 3.5. If higher q factors are used, the strengthening of the concrete elements is necessary. Two types of RC-MRFs with and without BRBs were tested monotonically and cyclically. Tests showed very good behavior of the retrofitted structure. The ductility of the structure was very much improved and the failure was caused by the failure of the steel brace in tension. The connections between BRB and RC elements performed very well. The workability of the system with pre-stressed ties was also tested. The connection devices used for installing BRB's within the frame took benefit from the friction resistant forces induced by the ties pretension and showed a very good behavior. In fact, reduced slips were observed, with very small influence on the hysteretic loops of the BRB system. Results recommend the application of this connecting system for such interventions. Moreover, in the case of multi-storey frames, such connecting systems also provide a beneficial confining effect at the frame joints, enhancing both strength and ductility of the MRF+BRB system. The q factor values for frames were evaluated and then compared to the theoretical values. There is a good agreement between the values used in design and

the values based on test. The difference between the q factor values corresponding to the positive and negative branches of envelope curves can be explained by the fact that the negative direction corresponds to the reversal cycle, after the damages have already occurred in the positive cycle. Values of the q factor between 3 and 4 were suggested for such types of retrofitted structures. Compared with initial RC frames, the values of the q factor are higher by approximately 50% for retrofitted frames.

2.5.2.4. BRB hysteretic behaviour

Many numerical studies have been performed to characterise the hysteretic behaviour of BRB (Clark et al., 1999; Menegato-Pinto; Mc Kenna, 1997…). All the studies were based on the approaches the same as used in characterizing the behaviour of CBF under cyclic loading, as mentioned in the previous sections. The results from these studies have shown that the hysteretic behaviour of BRB is stable, ductile in both tension and compression phases of loads. The typical hysteretic curve of the BRB is shown in Figure 2-20.

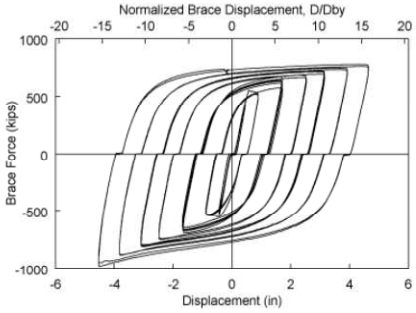

Figure 2-20 – A typical hysteretic behaviour of the BRB

2.5.2.5. BRB design concept

The design of BRB frames has not yet governed by any building code. Recommended provisions for the design of BRB frames are available, however, mostly in US and Japan. A set of Recommended Provisions for Buckling Restrained Braced Frames (Recommended Provisions) was developed by a joint AISC/SEAOC task group with the intention of including the provisions in the 2005 edition of the Seismic Provisions. The Recommended Provisions have been reviewed and have been included in Chapter 8 of FEMA 450. The design example found in section 3 of the Steel TIPS (Sabelli et al., 2004) report is based on the Recommended Provisions published in FEMA 450. Chapter 4 of FEMA 450 includes BRB system factors R, C_d, C_t (C_r), Ω_0... The Steel TIPS recommended taking the force reduction factor for BRB frame system R of 8.

In order to design the structure using the BRBs, the lateral equivalent force method is usually used. Two types of brace tests are required by FEMA 450. The first is a uniaxial test that requires the BRB specimen to be of a similar size to those used in the actual building project. In this test a BRB specimen is loaded axially and cycled through the prescribed displacements until it has dissipated a minimum amount of energy. This test is intended to verify the adequacy of the BRB design using representative proportions. The second type of brace test is called a sub-assemblage test. In this test, the BRB specimen is loaded axially while the end connections are rotated to simulate the conditions to be expected when the BRB is employed in a frame. This test is intended to verify that the brace-end rotational demands imposed by the frame action will not compromise the performance of the BRB. This test is not intended to test the performance of a frame. BRB frames can have braces in any one of a number of configurations. Because there is no strength or stiffness degradation in the braces, and because the tension and compression strengths are almost equal, the single diagonal configuration is permitted without any penalty. The single-diagonal configuration is an effective way to take advantage of the high strengths possible for BRB. The V and inverted-V configurations are also popular for BRB frames, as they allow some openness in the frame. Because of the balance between brace tension and compression strength, the beam is required to resist modest loads in comparison to CBF frames; a deflection limit is also imposed to prevent excessive vertical beam displacement. Other BRB frame configurations are also possible.

2.5.3. Retrofitting system using Steel Eccentric Braces (EBFs)

2.5.3.1. Introduction

EBF is one of recent advanced retrofitting techniques to improve the seismic performance of the existing RC-MRFs in last few decades. EBFs have more advantages than the CBFs thanks to less complicated connection details which reduce fabrication costs and may also simplify the erection of the structure and taking over some portions of gravity loads, providing an increase of overall stiffness of the structure (Plumier, 2008).

EBFs can be a laterally stiff framing system with significant energy dissipation capacity to accommodate large seismic forces (Popov, Charles Roeder, 1978). The main difference between the geometry of EBFs and that of CBFs is that there are some intentional eccentricities e in the layout of the elements in EBFs (see Figure 2-21), which generate bending moments and shears. The seismic forces, generated in the structures, are essentially resisted by axial loads in EBFs. However they are designed to yield first in shear or bending in what are called ductile steel links or the 'seismic links' while preventing buckling of the brace members. These links are created by positioning the ends of the braces away from the 'usual' intersection points with other elements (Plumier, 2008).

Many experimental and numerical studies on the behaviour of EBFs have been carrying out since mid-1970s (Roeder & Popov (1977), Roeder & Popov (1978) ...). Most of them were conducted mostly at the University of California. These studies focused both on behaviour and modelling of shear links or seismic links as components and systems. After that, relatively little was published related to EBFs design and behaviour until the design of shear links for the tower of the San Francisco-Oakland Bay Bridge East Bay self-anchored suspension span (McDaniel et al., 2003). This idea of shear links as a general ductile element that can be replaced after damage, has developed further in recent work by Dusicka et al. (2009).

Up to date, there are few researches on EBF to retrofit RC-MRFs. Brecchia et al. (2006) did the experimental and numerical studies on seismic links to retrofit RC-MRFs. The full scale tests performed on an existing RC structure equipped with eccentric braces were carried out. It is also found that EBF systems may be a viable solution for seismic retrofitting of RC structures.

2.5.3.2. Configuration of EBF

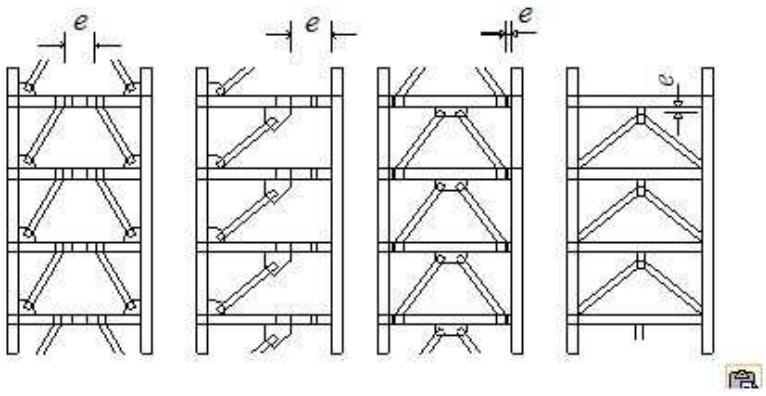

Figure 2-21 – Examples of frames with eccentric bracing (Plumier, 2008)

The most important part of an EBF is that at least one end of each brace is connected so as to isolate a segment of beam called 'seismic links'. In RC-MRFs, the concrete beams are incapable to perform as a ductile link like the steel beams for the EBF that is inserted in the frame bays. Therefore, it is necessary to adopt other solutions such as Y-inverted bracing configuration with a vertical steel link (Figure 2-21d). In addition, in order to be easily replaced, the connections in this configuration should be considered in the design and the bolted connection is a good choice. Since the diagonals are designed not to buckle under seismic actions, it is not necessary to perform the approximations made for frames like concentric bracing. These diagonals are non dissipative zones that are 'capacity designed' relative to the strength of the seismic links, in order to ensure they remain elastic and do not buckle. The inelastic behaviour of a link is

significantly influenced by its length. The four EBF are usually named as split-K-braced frame, D-braced frame, V-braced and Y or inverted-Y braced frames as shown in Figure 2-21.

2.5.3.3. The hysteretic behaviour of the link

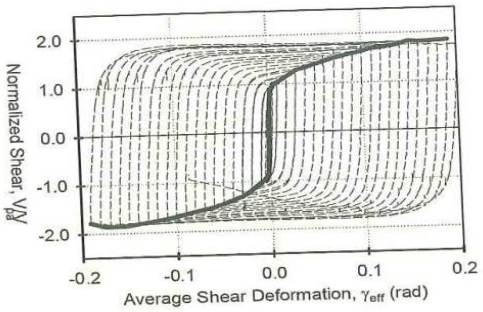

Figure 2-22 – Hysteretic behaviour of the EBF

The seismic response and the ultimate failure modes of long and short links are quite different. In short links, their hysteretic behaviour is controlled by shear while in long links it is controlled by flexure and for intermediate links the behaviour of the links is dependent on both shear and moments. However, regardless of the lengths of the links, if the web is not well stiffened, local failures may control the response of the links. According to the studies of Kasai & Popov (1986), the link mechanical behaviour is characterized by three stages: elastic, pre-buckling inelastic and post-buckling. These three stages correspond to three limit states of the link: yielding, buckling and failure. The link works elastically until reaching the yielding stress of the web. The web is now in pre-buckling inelastic range. This behaviour is characterized by a stable cyclic loop leading to a large amount of energy dissipated in this stage. When the web is buckled the behaviour of the link is changed. Due to buckling the stiffness and strength of the link reduce. However the link is still able to carry the forces and dissipate seismic energy through the so called tension field of the web. If the web is well braced to resist buckling, shear stresses will be uniformly distributed along the seismic link length and hysteretic behaviour of such links is stable. This post-buckling energy dissipation mechanism is less efficient than the pre-buckling one. When the link is not able to sustain loads and forces, the failure occurs. Figure 2-22 shows the hysteretic behaviour of a shear seismic link.

2.5.3.4. EBF design concept

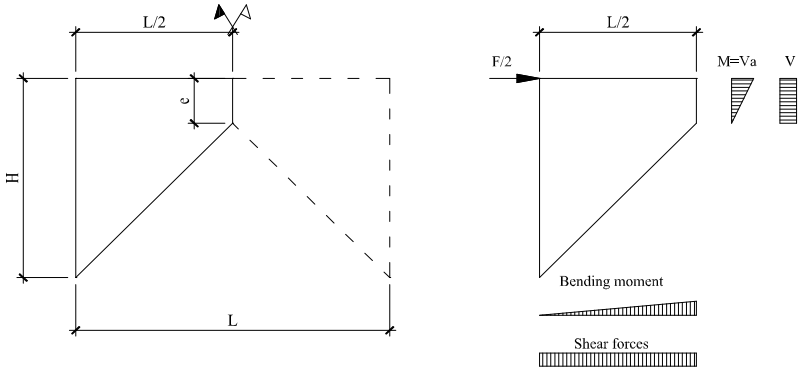

Figure 2-23 – Design action in link for an inverted-Y-braced EBF configuration (Mazzolani et al., 2006)

There are three main parameters which have to be determined in design of an EBF: the bracing configuration, the length and properties of the link and anticipated plastic mechanisms of the frame. During extreme seismic loading it is expected that most energy will be significantly dissipated through inelastic deformations of the link, while the other parts of the frame still remain elastic. Therefore, the main objective in the design of EBF is to choose the properties of seismic links so that they will perform appropriate inelastic deformations under shear or bending and to keep all frame components around the links in the elastic range by making them able to carry the maximum forces (full yielding and strain

hardening) that the link can developed. To do this it is necessary to explicate the distribution of internal actions in the EBF system and find a relationship between frame shear force and link shear force. Depending on the configuration of EBF in the frame, this relationship can be determined based on the equilibrium between earthquake base shear forces and response generated in seismic links. For example in an inverted-Y braced EBF (Figure 2-23), with the assumption that the moment at brace connection is equal to zero (pinned braces), the link shear force can be expressed as: V=F; where F is the lateral shear force.

A very important aspect in the design of EBF is the desired plastic mechanism. It is known that energy dissipated in the frames is based on the plastic rotation of the links, this leads to need to find the relationship between story plastic drift angle and the link plastic rotation. Generally, with the assumption that the frame outside the link is rigid (normally right for RC-MRFs), this relationship can be derived from plastic mechanisms. This is illustrated in Figure 2-24.

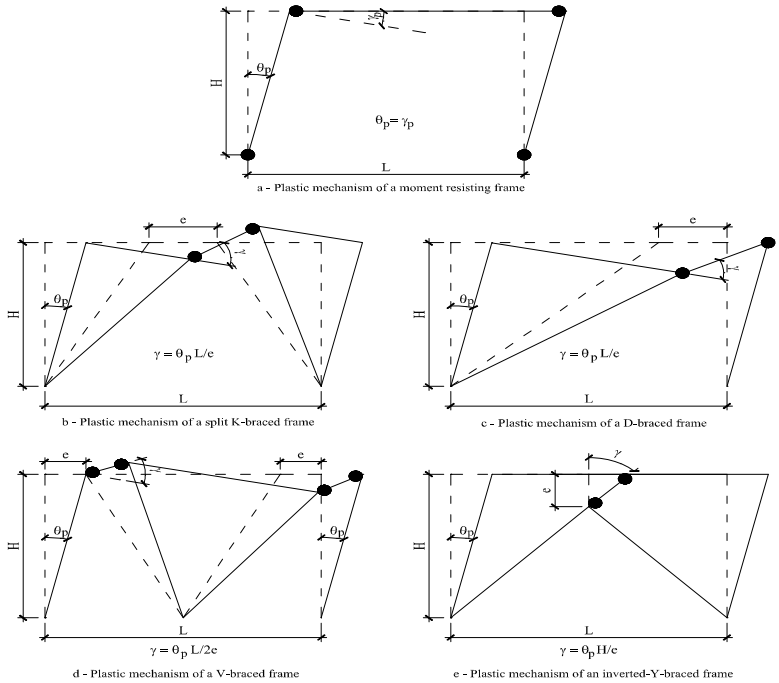

Figure 2-24 – Plastic mechanisms of several EB configurations (Mazzolani et al. 2006)

2.5.4. Retrofitting system using Steel Plate Shear Walls (SPSWs)

2.5.4.1. Introduction

Steel plate shear walls, used for the first time in Japan (1970) and then in US (1976) (Robert, 1995), are made by metallic plates, generally forming the infill of the steel frame structures. However, these plates can also be combined with reinforced concrete moment resisting frames (RC-MRFs) by using additional steel frames surrounding these plates to improve the seismic response of the RC-MRFs (Mazzolani, 2006).

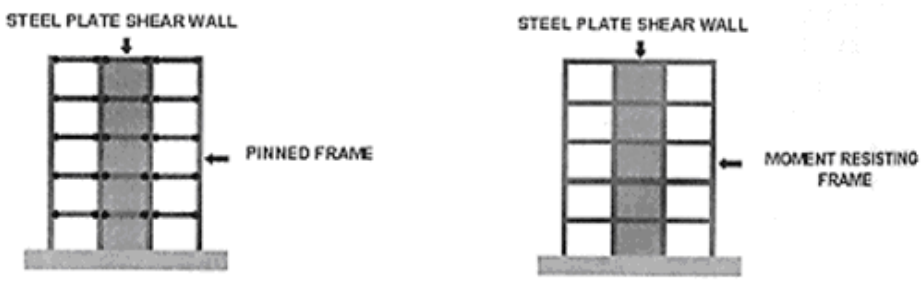

Figure 2-25 – Configuration of steel plate shear walls (Mazzolani, 2006)

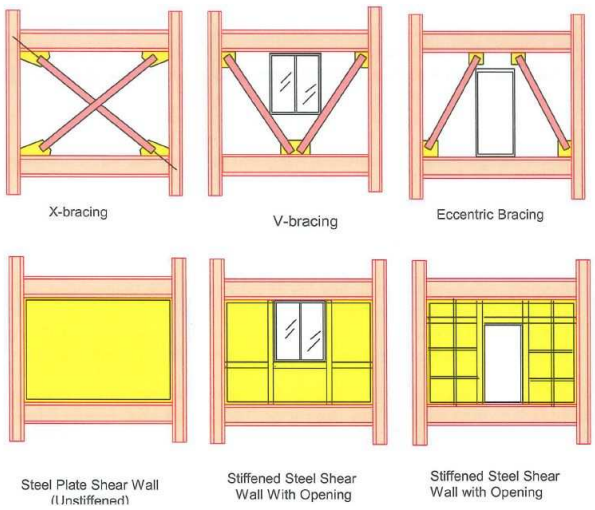

Figure 2-26 – Possibilities of the openings in SPSW and bracing systems (Astaneh-Asl, 2001)

SPSWs, acting as a sort of bracing system, can be considered as two different configurations, as shown in Figure 2-25. These two types are characterised by the role of the frames in carrying seismic forces. The first configuration, known as standard system the left one in Figure 2-25, is the one in which the connections among members are schematised as pin joints: in this case the seismic force is carried by the shear walls, while the remaining parts (frames) will be designed to carry vertical loads only. The second configuration, known as dual systems the right one in Figure 2-25, is a combination of a moment resisting frame and shear walls. The frame, with rigid beam-to-column connection, is designed not only to be capable of carrying both vertical loads but also to combine with shear walls to carry seismic forces (Mazzolani, 2006). A steel shear wall frame consists of column and beam elements augmented by steel infill shear panels, provided over the height of a framing bay. This form is equivalent to a plate girder, with the columns acting as flanges, the beams as stiffeners and the infill panels as the plate girder web. When subjected to lateral loading in the plane of the shear walls, axial loads and a part of lateral forces are resisted through beams and columns, while shear walls will carry the remaining lateral forces by their in-plane shear resistance (Lubell et al., 2000).

Steel walls present a good behaviour under seismic excitations thanks to their consistent capacity of energy dissipation through shear mechanism. In addition, comparing with concrete shear walls, SPSW are much lighter, resulting in a rather low seismic force to the foundation. This leads to the reduction of the costs of the foundation (Robert, 1995). Another advantage of SPSWs comparing with traditional steel ones is its flexibility in realising some openings as shown in the Figure 2-26 (Mazzolani, 2006).

2.5.4.2. Analytical studies of shear walls under shear loading

Up to date, many theoretical and experimental studies have been carried out to characterize the behaviour of slender metal shear walls. These researches are mainly based on the assumptions that SPSW is considered as a web of a stiffened I beam, with the columns and beams of the frames as the flanges and the stiffeners. In the elastic range, the typical stress state of the web is illustrated in Figure 2-27, where principal stress is less than elastically critical stress which makes the web buckle out of plane.

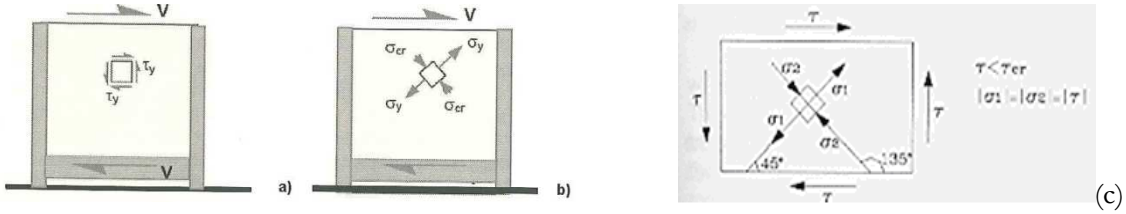

Figure 2-27 – Stress state on the web of a stiffened beam subjected to shear (a) and corresponding principal stresses (b)(c) (Mazzolani et al., 2006)

According to the plate theory, the principal stresses of tension and compression present an inclination of 45º in both directions (Figure 2-27b,c) (Mazzolani, 2006 and Marquoi, 2000). The behaviour of shear panel is linear until the critical stress in the panel is reached and there occurs an out-of-plane buckling of the web. After that the response of the plate is changed: the compression stress cannot increase anymore when the critical stress τ_{cr} in the plate is attained, however the tensile stress still increases up to attaining the yielding strength of the plate material, presenting in the post-buckling stage ((Mazzolani, 2006). Apparently, the ultimate resistance of the plate is constituted by two components: pre-buckling resistance, represented by the critical load and post-buckling resistance. It is illustrated in the following formulae:

$$V_{ultimate} = V_{critical} + V_{post-critical} \qquad \text{Equation 2-1}$$

The critical tangential stress for a rectangular plate subjected to pure shear is determined by following formulae:

$$\tau_{cr} = k \frac{\pi^2 E}{12\left(1-\upsilon^2\right)}\left(\frac{t}{b}\right)^2 \qquad \text{Equation 2-2}$$

where:

- t → thickness of the plate
- b → height of the plate (in reality, the shorter dimensions of the plate)
- E → Young modulus of the material
- υ → Poisson coefficient of the material
- k → plate factor, depending both from the b/d ratio and the boundary conditions, taken as follows:

four sides with simple connections → $k = \begin{cases} 4 + \dfrac{5{,}34}{\alpha^2} & si\ \alpha < 1 \\ 5{,}34 + \dfrac{4}{\alpha^2} & si\ \alpha \geq 1 \end{cases}$

four sides with fixed connections $k = \begin{cases} 4 + \dfrac{5{,}34}{\alpha^2} & si\ \alpha < 1 \\ 5{,}34 + \dfrac{4}{\alpha^2} & si\ \alpha \geq 1 \end{cases}$ with $\alpha = \dfrac{a}{b} = \dfrac{l\,\text{arg}\,er\ side}{shorter\ side}$

Two different approaches are usually used to analyze the behaviour of SPSW subjected shear loading after buckling. The first one is based on the use of simplified model, mainly accounting for the characteristics of the buckled shear panels. The other one focuses on solving the problem on the basis of the nonlinear theory of flexible plates (Mazzolani, 2006). Some studies have proved that two these approaches give the same results and the first one will be presented herein. When shear force is reached to the value of $V_{cr} = \tau_{cr}.b.t$, the web is buckled represented by the presence of showy humps or a sort of wrinkling in the direction of the principal compression stress. After buckling, if the external load is increased the state of stress in the plate will be changed. The increase of the load will cause a redistribution of the initial stresses, characterized by the increase of the tensile stress σ_1, while the compression one σ_2 is unchanged. If the thickness of the web is very small compared to the other dimensions, leading to the very easy out-of-plane buckling of the web, the steel plate will be buckled under a rather low shear force and the stress value σ_2 can be neglected. This allows the application of the following hypotheses:

- the web is not capable of withstanding the loads in the direction normal to the buckling waves

- only the resistant capacity in the direction of the principal tensile stress will be provided, meaning that the stress field is composed by a certain number of tensile diagonals which fully take charge the increase of the external load

The development of the tensile stress field, which is also known as tension field mechanism, is first introduced by Wagner (1931). This theory hypothesized that for a very thin web with very stiff flanges the response of the web is controlled by a series of tension strips having an inclination of an angle ϑ in comparison to the horizontal direction. These strips are illustrated in Figure 2-28.

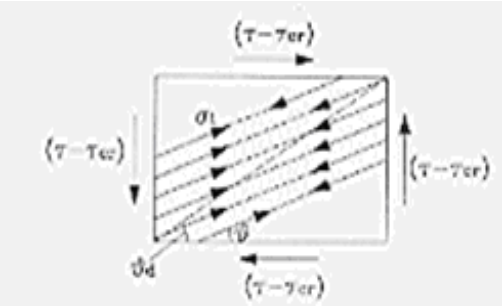

Figure 2-28 – The development of the tensile stresses (Wagner theory)

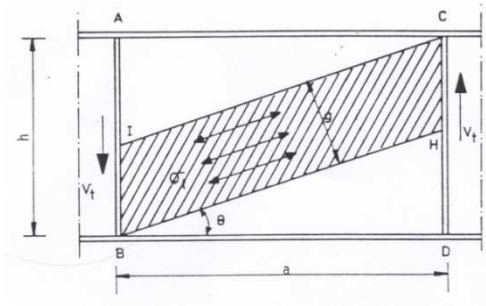

Figure 2-29 – Model of Basler (1960)

Basler-1960 was the first one who proposed the method to predict a good approximation the ultimate capacity of the web panels. In this approach, when the flanges are so flexible to not oppose to the lateral load produced by the tension field, the beams will be collapsed when tension yielding band of the web panel is fully developed, as shown in Figure 2-29. In addition, Basler (1960) also affirmed that the two triangular zones which are adjacent to the yielding zones, the stresses are the same equal to the critical one, τ_{cr}.

From the above two approaches by Wagner and Basler, it is clear that they studied in two opposite situations: the first author considered the web surrounded by rigid flanges, while the second one assumed that the flanges were very flexible and their flexural stiffness would be neglected. When applying these two models for characterizing the behaviour of SPSW, it is necessary to account for the fact that the columns have a significant flexural stiffness, which may affect the inclination of the tension field.

Starting with these two approaches, many studies have been carrying out to exploit the behaviour of SPSWs (University of Alberta, Canada; University of Beckerly, California; Japan). Thorburn et al. (1983) analytically studied the post-buckling behaviour of SPSW under shear loading. Then, at the same year, this analytical study was experimentally verified by Timber and Kulak. The two crucial conclusions from the above studies were formulated (Mazzolani, 2006):

- The buckling strength of shear walls were usually neglected, since visible out-of-plane deflections were observed under a very low shear force even some were buckled before the load application.
- The inclination angle of the tension field with respect to the horizontal direction was different from the one of the web panels of stiffened beams. The stiffness of the columns played an important role in the development of the tension field mechanism.

Thorburn et al.(1983) also proposed two analytical models to determine the stiffness and ultimate resistance of the slender steel panels under the considered load condition. In both of them, the contribution of the panels before buckling was neglected. In addition, the columns were assumed to be continuous over all the height of the wall and the connections between beams and columns were hinges. The first model is known as equivalent diagonal, which considered the thin panel as a single diagonal in each frame field, as shown in Figure 2-30. The panel thickness (t) for a frame having infinitely rigid members could be obtained from the area of the single equivalent diagonal through the following relationship:

$$t = \frac{2.A.\sin\theta\sin(2\theta)}{L.\sin^2(2.\alpha)}$$ Equation 2-3

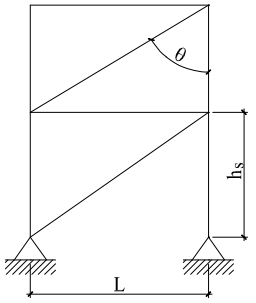

Figure 2-30 – Equivalent diagonal method

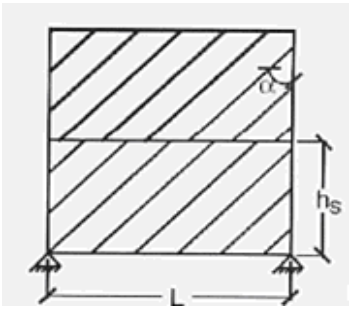

Figure 2-31 – Strip model by Thorburn et al. (1983)

If the frame is very flexible, meaning that the stiffness of the columns is very small, $I_c = 0$, where I_c is their second moment of area, the following formulation is applicable:

$$t = \frac{2.A.\sin(4.\theta)}{L.\tan(\theta)}$$ Equation 2-4

Where:

- A - is the area of the equivalent diagonal member
- L - is the beam length
- θ - is the angle of diagonal to the vertical direction
- α - is the inclination of the generated tension field. This angle, which is considered equal to β for deformable columns, in case of infinitively rigid columns can be obtained from the following relationship:

$$\tan^4 \alpha = \frac{1 + \frac{L.t}{2.A_c}}{1 + \frac{h_s.t}{A_b}}$$ Equation 2-5

- A_b and A_c are the beam and column cross sectional areas, respectively

The second approach, also suggested by Thorburn, is known as strip model. In this approach, the shear wall is represented by a series of inclined strips, hinged to the member ends of the external reaction frame, as illustrated in Figure 2-31. The total transversal section area A_s, equal to the strips width multiplied by the panel thickness, can be computed by:

$$A_S = \frac{L\cos\alpha + h_s \sin\alpha}{n}.t$$ Equation 2-6

Where:

- h_s – is the height of the panel
- n – is the number of the strips
- L – is the length of the panel
- α - is the inclination angle of the strips, determined by the following expression:

$$\tan^4 \alpha = \frac{1 + \frac{L.t}{2.A_c}}{1 + \frac{h_s.t}{A_b} + \frac{h_s^4.t}{360.I_c.L}}$$ Equation 2-7

- t – is the thickness of the panel
- A_b and A_c are the beam and column cross sectional areas, respectively
- I_c – is the second moment of area of the columns

In this study, the columns were only considered in two cases: rigid and flexible ones and moreover, strain hardening of the panel material was neglected. One more important suggestion from the study of Thorburn (1983) is that the number of strips in strip model should be equal to ten.

Based on the strip model theory and using plastic analysis on the panel, ultimate strength of different types of SPSW can be characterised for their preliminary dimensioning. The ultimate resistance of the panel can be computed by the following formulae:

$$V = \frac{1}{2}.f_y.t.L.\sin(2\alpha) \qquad \text{Equation 2-8}$$

Where f_y is the yielding strength of the base material of the plate.

2.5.4.3. Experimental and numerical studies

Up to date, most of the experiments and numerical simulations on SPSW have been implemented in US (University of Beckerly), in Canada (University of Alberta) and in Japan. Some interesting tests are presented hereafter, sorted by countries.

The very first study to exploit the experimental behaviour of slender SPSWs was carried out by Takanashi et al. (1973) and Mimura and Akiyama (1977). These studies not only focused on the behaviour of the panels alone but also accounted for the contribution of the external frames. Takanashi et al. (1973) conducted cyclic tests of 12 one-story and two 2-story specimens. The 12 one-story specimens had about 6'-11" (2.1 m) width and 2'-11" (0.9 m) height. They used steel plates with about 3/32", 1/8" and 3/16" (2.3mm, 3.2mm and 4.5mm) thickness. Compared to typical building dimensions, the specimens could be considered to be ¼–scale of prototype walls. With the exception of one specimen, all specimens had vertical or vertical and horizontal stiffeners welded on one or both sides of the steel plate. The boundary frames were very stiff pin-connected frames. The specimens were loaded along their diagonals to create almost pure shear in the panels. The behaviour of specimens was very ductile and drift angle in some cases exceeded 0.10 radians. The shear strengths of the specimens were predicted well by Von Mises yield criterion given for pure shear as $V_{yspsw} = A_{SPSW}\ (F_{yspsw}/\sqrt{3})$. The researchers concluded that the conventional beam theory could be used to calculate stiffness and strength of stiffened shear walls.

Yamada (1992) reported the results of cyclic tests of steel and composite shear walls. Two specimens were un-stiffened steel plate shear walls. The specimens had a width of 3'-11" (1.2m) and a height of about 2' (0.6 m). The thickness of wall was either 3/64" (1.2mm) or 3/32" (2.3mm). The boundary frames were rigid steel frames encased in rectangular reinforced concrete sections. The specimens were subjected to monotonic loads along their diagonal direction. The failure mode was in the form of fracture of base of boundary rigid frames. The behaviour of specimens was quite ductile and tension field formed along the diagonal.

Sugii and Yamada (1996) have reported the results of cyclic and monotonic tests on 14 steel plates shear walls. The specimens were 1/10 scale model and two stories in height. The boundary frame was rigid composite frame with steel I-shapes encased inside rectangular reinforced concrete sections. Figure 2-32 shows a typical specimen and hysteresis loops. All specimens showed pinching of hysteresis loops due to buckling of compression field.

In the United Kingdom, Sabouri-Ghomi and Roberts (1992) and Roberts (1995) tested 16 steel shear panels under diagonal loading. The specimens in these tests consisted of steel plates placed within a 4-hinged frame and connected to it using bolts and some panels had perforations, as shown in Figure 2-33. The specimens were small-scale with dimensions of steel panels being either 12" x 12" (30.48cm x 30.48cm) or 12" x 18" (30.48cm x 45.72cm). The thickness of steel plate was either 1/32" (8mm) or 3/64" (12mm). The cyclic load was applied along the diagonal axis resulting in steel plate being subjected to pure shear. The tests indicated that all panels possessed adequate ductility and sustained four large

inelastic cycles. Typical hysteresis loops presented in Roberts (1992) shows specimens reaching a ductility of more than seven without any decrease in strength. One of the interesting aspects of this test program was to investigate the effects of perforations in the wall on strength and stiffness. The researchers concluded that the strength and stiffness linearly decreases with the increase in (1-D/d) as shown in Figure 2-33.

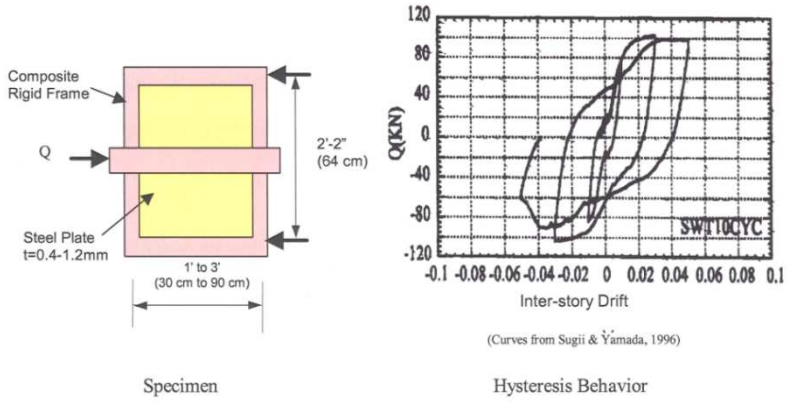

Figure 2-32 – A typical test specimen and typical hysteresis loops for 1mm plate (Sugii and Yamada, 1996)

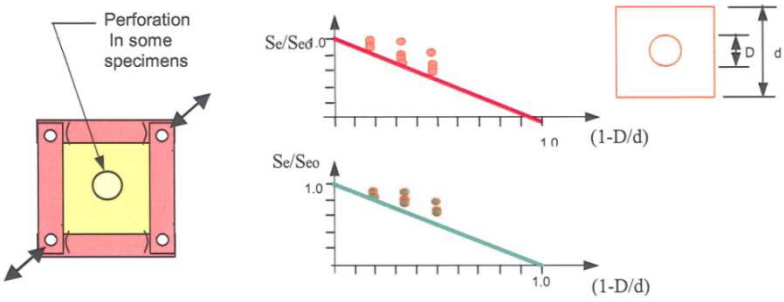

Figure 2-33 – Specimens tested in UK and the effect of perforation on strength and stiffness of steel plate panels (Roberts, 1992)

In the United States, Elgaaly and his research associates (Elgaaly and Caccese, 1993) conducted a number of studies of SPSWs. A series of tests to investigate the effects of the slenderness ratio of the shear plates and of the possible types of beam-to-column connections on the behaviour of SPSWs was conducted by Caccese et al. (1993). They tested five single-bay three-story steel frames, modelled in a length scale ¼, in which 1245mm x 2870mm shear panels, having inter-story heights among sub-panels of 838mm, as shown in Figure 2-34, were inserted. The panels, having different thicknesses as of 0.76mm, 1.9mm and 2.66mm for moment resisting connections and of 0.76mm and 1.9mm for hinged connections, were connected to the external frames by welding. The load was applied on the upper part of the frame and the columns were not axially pre-loaded. The cyclic tests were performed in 24 cycles until the displacements progressively increase up to a maximum value of 50.8mm (2% drift). Then, the load was monotonically increased up to the maximum allowed displacement of the jack. Some main observations and conclusions from these tests are:

- The failure mechanism of the SPSW is dependent on its thickness: while the slenderest panels yielded before the members of the external frame, in panels with higher thickness the failure was governed by column buckling, leading to some negligible effects on the behaviour of SPSW.
- To avoid the buckling phenomena, the columns should be carefully designed with respect to the ultimate capacity of SPSW.
- The employment of rigid instead of hinged beam-to-column connections did not exhibit much different behaviour of SPSW.

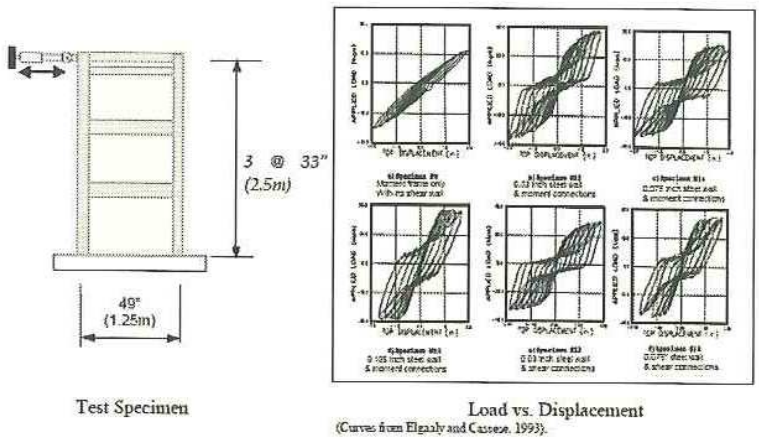

Figure 2-34 – The model tested by Caccese, Elgaaly and Chen-1993

To verify the test results obtained by Caccese et al. (1983), Elgaaly, Caccese and Du (1993) used two approaches, named as finite element model and strip model, to simulate the tests. In the finite element model, nonlinear analyses were adopted using a mesh of 6x6 elements representing the panels in each frame field, while beams and columns were modelled as beam elements. The thickness of the panels used in the modelling was 1.9mm and 2.7mm and it was assumed that the frame was moment resisting one. The results from these simulations showed that the failure loads in both case were determined by the critical loads of the columns, causing their buckling. It was also recognised that the finite element model much overestimated both the strength and the stiffness of the system. This is due to the difficulty in modelling the initial panel imperfections and the out-of-plane deformations of the frame members. In the strip model, the panel with the thickness of 1.9 was adopted to simulate the tests. Twelve strips in each frame field and the inclination angle of the strips of 42.8 degrees were assumed. The result from strip model fit well with those from finite element model. Based on the behaviour of these six specimens, Elgaali et al. (1993) concluded that when an un-stiffened thin plate is used as shear wall, inelastic behaviour commences by yielding of the wall and the strength of the system is governed by plastic hinge formation in the columns. They also concluded that when relatively thick plates are used, the failure mode is governed by column instability and only negligible increase occurs in the strength of the system due to increased thickness of the wall. In general, the researchers recommended the use of thinner, un-stiffened plates such that the yielding of plate occurs before column buckling.

Researchers at the University of Alberta, (Timler and Kulak (1987), Kulak (1991), and Driver et al. (1996) …) have conducted monotonic and cyclic tests of un-stiffened steel plate shear walls. A summary of these tests is given in the following.

In order to verify the analytical model proposed by Thorburn et al. (1983), Timber and Kulak (1983) tested a slender single full-scale steel shear wall. This test was based on the use of two panels with the thickness of 5mm inserted in a steel frame. The frame was constituted by columns and beams having the steel profiles of W310x129 (W12x87) and of W460x144 (W18x97), respectively. The dimensions of the SPSW are 3750x2500mm. It is necessary to note that beams and columns were connected by means of welding to form hinged beam-column connections and moreover no axial force was applied to simulate the presence of gravitational actions. The test procedures were followed by the Canadian code, meaning that the frame would be tested three initial cycles characterized by a maximum drift equal to $h_s/400$, then being pushed until being collapsed. Three main points were concluded as the results of this study:

- Good correlation between predicted and actual web plate stresses was obtained. The inclination angle of the tension field in the central zone of the panel was variable between 44 and 56 degrees.
- The failure of the tests was due to cracking of the welding used to connect the panel to the plates anchored to the frame. The frame showed good ductility when loaded to its ultimate capacity.
- The test results indicate overstrength of more than 2.0 and a ductility of more than 3.5
- Strip model was used to calibrate the tests. It was found that the simulations fit very well to the test results.

Starting with the idea of Timber and Kulak (1983), Tromposch and Kulak (1987) modified some parameters of the former tests. The beams and columns were joined by means of bolted connections. The panel was also reduced to the dimensions of 2750x2200x3.25 mm. The specimen was tested in a horizontal position in a configuration with a deep beam. The axial force present in prototype structure was simulated in the test specimen by two pre-stressing loads per column. The frame was tested in both monotonic and cyclic phases. In cyclic tests, the specimen was subjected to 28 reversible cycles, under maximum value of the applied load equal to the 67% of the system strength. The maximum deflection observed during these loading phases was 17mm (0.8% drift). After this sequence of cycles, the current pre-loading in the columns was eliminated and the specimen was monotonically loaded up to the complete failure. The ultimate displacement was equal to 71mm (3.2% drift). The tests stopped due to the failure by the bolt slip and of the welding between the panel and the gusset plates as in the tests of Timber and Kulak (1983). The hysteretic experimental loops showed a significant pinching effect, but they performed a good and stable energy dissipation capacity. The displacement ductility factor for the last hysteretic curve was between 4 in compression cycle and 7 in tension cycle. In order to simulate the tests, the equivalent strip model was used. It proved a good correlation between the test and the analytical results. Some conclusions were drawn by Tromposch and Kulak (1987):

- The inclined tension bar and strip models can be used to evaluate the strength and ultimate resistance of an un-stiffened SPSW.
- If analytical models for predicting the behaviour of SPSWs are developed based on the assumption that bolted beam-to-column connections are pinned, a conservative estimate of the ultimate strength and stiffness will result.

The hysteretic behaviour of an un-stiffened SPSW is comparable to the hysteretic behaviour of conventional steel braces. All these systems display pinched loop behaviour, causing the degradation of stiffness when the loads are reversal.

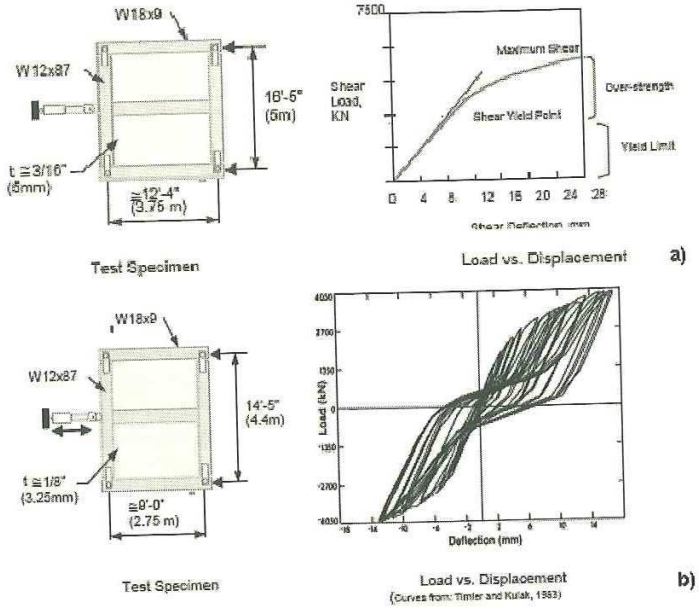

Figure 2-35 – The models tested by Timber and Kulak (1983) and by Tromposch and Kulak (1987)

Driver et al. (1996-1998) have reported the results of cyclic testing of a four-story steel shear wall specimen. The specimen, shown in Figure 2-36, was a ½-scale representation of a dual system with SPSW welded to a special moment-resisting frame. Figure 2-36 shows cyclic response of the first floor steel shear wall panel. The failure mode was fracture of left column at the heat-affected zone of weld connecting the column to the base plate during cycle 20, causing large deformation amplitudes at locally buckled areas of the column flange. Prior to fracture, the specimen behaved in a very ductile manner. Unfortunately, failure mode of this specimen was not directly related to shear neither failure of the wall itself nor the behaviour of the system as a whole. The failure at the base of the column where it was attached to reaction beam was probably due to stress concentration at the base of the specimen where it was connected to the reaction

floor and test set-up. Such stress concentrations are not expected to occur in a real structure. However, even with premature failure of the base of column in this specimen, the cyclic behaviour indicates overstrength of about 1.3 and a ductility of more than 6.0.

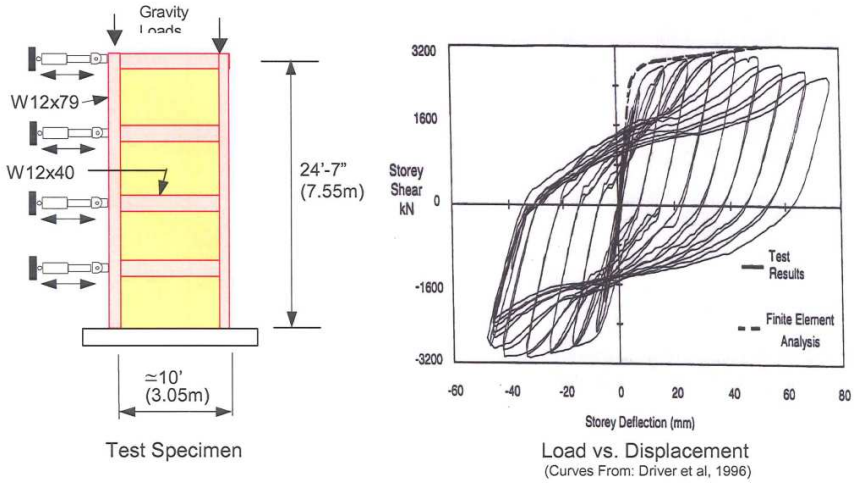

Figure 2-36 – University of Alberta test setup and a sample of hysteresis behaviour

Researchers at the University of British Columbia have completed a series of cyclic and shaking table tests of steel plate shear walls (Lubell, 1997), (Rezai, 1999) and (Rezai et al., 1988 and 2000). In these studies, cyclic shear loads were applied to two single story specimens. Figure 2-37 shows one of the specimens after the test and hysteresis behaviour of the specimen. The boundary frames in the specimens were moment frames resulting in a "dual" structural system. The two specimens differed only in the base gusset plate details and the top beam. For second specimen, stronger base connections and top beam were used. The single story specimens experienced significant inelastic deformations up to ductility of about six. The overstrength was about 1.5. The researchers concluded that the two one story specimens demonstrated that the infill steel plates significantly reduced demand on the moment-resisting frame by producing redundant diagonal story braces that alleviated the rotation demand on the beam-to-column connections. In the shaking table tests of Lubell (1997), a four-story specimen representing 30% scale model of inner core of a residential building was used. Figure 2-38 shows a view of the specimen and the test set-up. The dimensions of each story were almost the same as the one-story specimens. The frame was welded rigid frame making the system a dual system. The members were S3x5.7 (Canadian S75x8). The roof level beam was an S8x23 (Canadian S200x34). In each panel of the specimen, a maximum displacement ductility of 1.5 was achieved prior to a global instability failure propagated by yielding of the columns. The specimen exhibited overstrength of about 1.20. The specimen proved to be somewhat more flexible than the one-story specimens were, as shown in Figure 2-39.

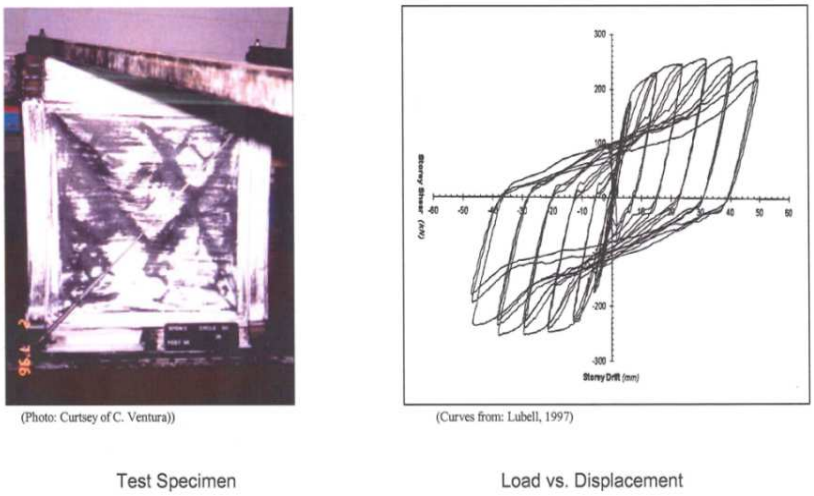

Figure 2-37 – One of the two University of British Columbia specimens with its hysteresis loops

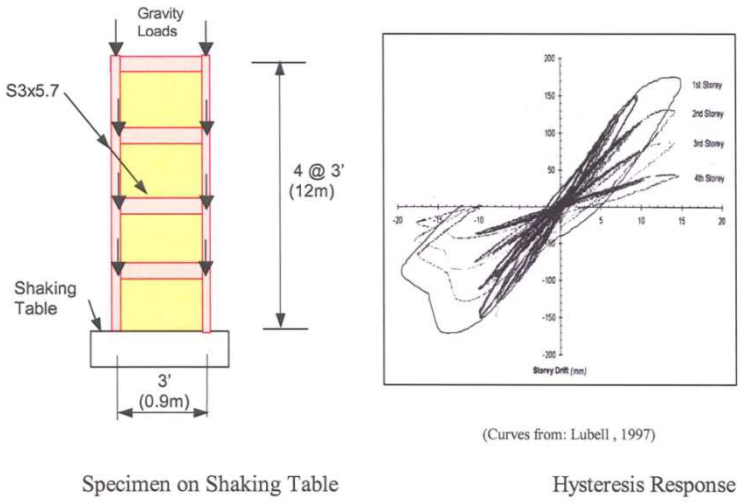

Figure 2-38 – The specimen tested at the Uni. British Columbia and its response

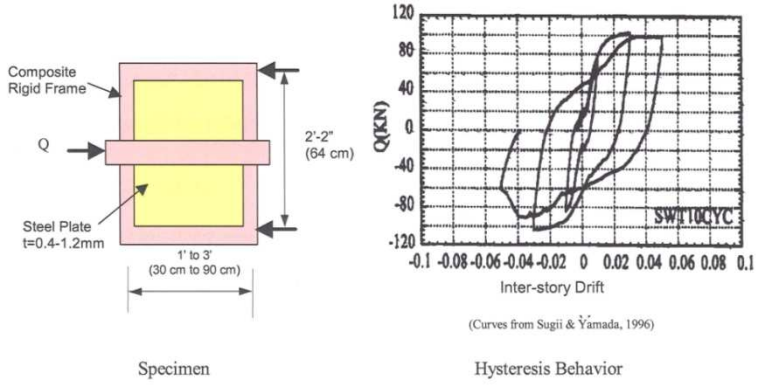

Figure 2-39 – A typical test specimen and typical hysteresis loops for 1mm plate

2.5.4.4. Contribution of the external frame to the overall resistance of SPSWs

It is evident from the studies mentioned above that the external frame not only plays a very role on the behaviour of SPSWs but also contributes significant effects on the overall resistance of the SPSW system. In order to exploit the contribution of the external frame, plastic analysis of SPSWs is usually used with the application of strip model or equivalent tension bar model for predicting the behaviour of the shear wall. Jeffrey Berman revised a procedure for designing and analyzing the SPSWs using plastic analysis, taking into account the effects of the frames on the total response of the SPSWs system. In this study, three types of frames, namely as single story with simple beam-to-column connections, single story with rigid beam-to-column connections and multi-story frames were examined. For the frame with simple beam-to-column connections and inclined strips representing the response of the shear wall, if the beams and columns are assumed remaining elastic (reasonable for most cases in the reality) their contribution to the internal work may be neglected when compared to the internal work done by the shear wall. By equating the external work done by base shear and internal one done by shear wall, the resulting base shear relationship is: $V = \frac{1}{2}.f_y.t.L.\sin(2\alpha)$ as presented in the previous section.

Regarding to the frame with rigid beam-to-column connections, plastic hinges also need to form in the boundary frame to produce a collapse mechanism. The internal work is the sum of two components: work done by the shear wall and done by the external frame, which is equal to $4.M_p.\theta$, where $\theta = \Delta/h_s$ is the story displacement over story height as shown in Figure and M_p is the smaller of the plastic moment capacity of the beams (M_{pb}) or columns (M_{pc}). In most single-story frames, if the beams have sufficient strength and stiffness to anchor the tension field, plastic hinges will form at the top and the bottom of the

columns and not in the beams. The ultimate resistance of a single-story SPSW in a moment resisting frame with plastic hinges in the columns is:

$$V = \frac{1}{2}.f_y.t.L.\sin(2\alpha) + \frac{4.M_{pc}}{h_s} \qquad \text{Equation 2-9}$$

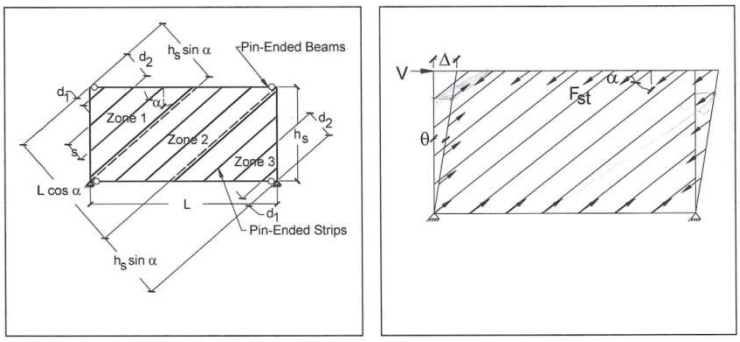

Figure 2-40 – Strip model of single story wall and single story collapse mechanism

For multi-story SPSWs, plastic analysis can also be used to predict its ultimate capacity. Several collapse mechanisms such as the soft-story or the uniform yielding of the shear walls over every story can be the possible failures under seismic forces.

In soft-story mechanisms shown in Figure 2-41, the plastic hinges would form in the columns at the mechanism level called as soft story. Equating the internal and external work done by shear walls, columns and base shear, the following expression could be used for soft-story i in which all flexural hinges developed in columns:

$$\sum_{j=1}^{n_s} V_j = \frac{1}{2}.f_y.t_i.L.\sin(2\alpha) + \frac{M_{pci}}{h_{si}} \qquad \text{Equation 2-10}$$

Where:

- V_j – are the applied lateral forces above the sof-story i
- t_i – is the plate thickness at the soft-story
- M_{pci} – is the total plastic moment capacity of the columns at the soft-story
- h_{si} – is the height of the soft-story
- n_s – is the total number of stories

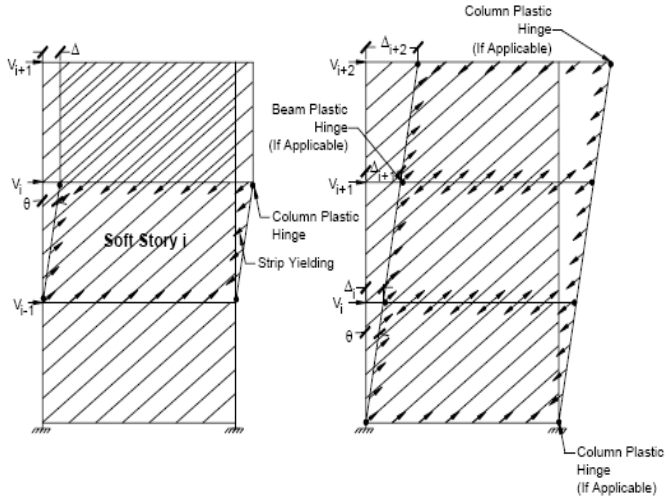

Figure 2-41 – Soft-story and uniform yielding mechanisms of multi-story SPSW

It is necessary to note that the applied lateral forces above the soft-story do external work and they are all displaced by the same lateral displacement (Δ) and the internal work is done by the strips and by the plastic moments of the columns on the soft-story.

The more desirable failure mechanism is the uniform yielding of the shear walls over every story (Figure 2-41). In this type of failure, external work done by each story lateral force, V_i, is calculated by $V_i.\theta.h_i$, where $\Delta_i=\theta.h_i$ is the lateral displacement of the story i due to V_i and θ is the plastic rotation of the frame. The internal work is done by the tension strips of each yielding story. It is necessary to emphasize that the total internal work at any story i is the sum of the work done by the strip yield forces along the bottom and the top of the beam at that story, but they have opposite signs. Therefore, the general equation for ultimate strength of a multi-story is:

$$\sum_{i=1}^{n_S} V_i.h_i = \frac{1}{2}.f_y.(t_i - t_j).L.h_i.\sin(2\alpha) + 2.\sum_{i=1}^{n_S} M_{pl,beam,i} + 2.M_{pl,bottomcolumn} \qquad \text{Equation 2-11}$$

where:

- V_j – are the applied lateral forces above the sof-story i
- t_i – is the plate thickness at the story i
- $M_{pl,beam,i}$ – is the plastic moment capacity of the beams at the story i
- $M_{pl,bottomcolumn}$ – is the plastic moment capacity of the columns at the base
- h_{si} – is the height of the story i
- n_s – is the total number of stories

2.5.4.5. Hysteretic behaviour of SPSW

Following the development of shear walls on the use of resisting the seismic excitations, they have been subdivided into two main typologies, depending on their response under shear forces. The first typology is based on the application of compact plates, which are characterized by the use of low yield point metallic materials and opportune flexural stiffeners in order to avoid buckling of the shear plates. This type of shear wall, which was first proposed and used in Japan, offers high stiffness and resistance to the main structures, limiting the inter-story drifts and absorbing large amount of seismic energy by means of pure shear mechanism. The hysteretic behaviour of this shear wall is shown in Figure 2-42.

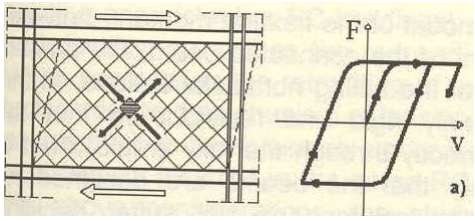

Figure 2-42 – Hysteretic behaviour of a stiffened shear wall

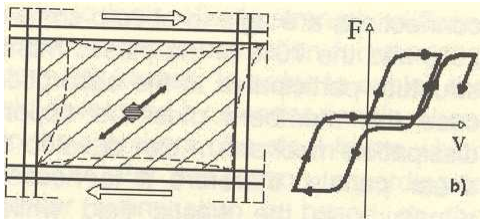

Figure 2-43 – Typically hysteretic behaviour of a slender shear wall

The second type of shear wall is well known as Steel Plate Shear Walls, which is based on the employment of slender steel plates to increase the strength and stiffness of the main structure. In this type of shear walls, due to the very high slenderness, premature shear buckling in the elastic field easily occurs and the overall resistant capacity of the shear walls is contributed by the development of diagonal tension field action after buckling, called as post-buckling resistance. The typically hysteretic behaviour of this type is shown in Figure 2-43. The results from cyclic tests on SPSWs (University of Alberta, University of Berkeley...) have shown that its hysteretic behaviour is pinched but very ductile and stable (Timber et Kulak (1983), Tromposch et al. (1987), Astaneh-Asl et al. (2001)…). Pinching effects, resulting in a degradation of stiffness of the shear walls as illustrated in Figure 2-44, are caused by out-of-plane buckling of the SPSWs during the reversal of shear loading.

An analytical model was proposed by Tromposch et al. (1987) for predicting the shear cyclic behaviour of SPSW. As presented in Figure 2-45, when shear load is applied to the structure, the response is similar to that in monotonic curve, meaning that depending on the magnitude of load the curve may pass the elastic ranges to an arbitrary load at point B. If the structure is unloaded from this point, the curve will be parallel to OA to point C. If the load is reversed in the opposite direction, a tension field will be developed in the panels but this field will be in opposite direction to the previous one. The deflection, which is required for the tension field to develop, is CD' (following by a deviation due to the pinching effect). During this stage of re-buckling, the stiffness of the overall structure is equal to the stiffness of the external frame only. The opposite tension field will be formed from point D and it is assumed that there is a linear transition from D to E, representing the yielding strength in opposite sense. The hysteretic loops are now the same as the previous processes, yielding to point F, unloading to point G, reforming a tension field at point H, and a linear transition back to the previous maximum in tension B.

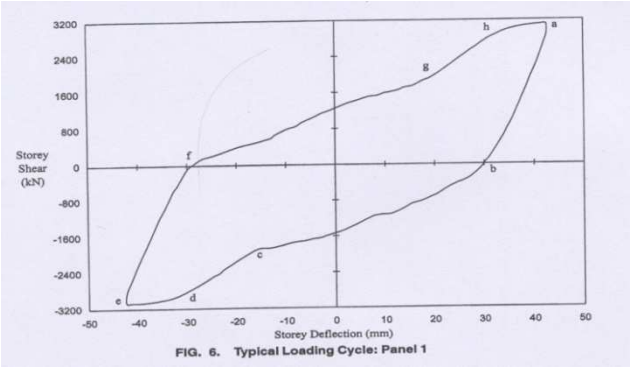

Figure 2-44 – Pinching effect on hysteretic behaviour of SPSW

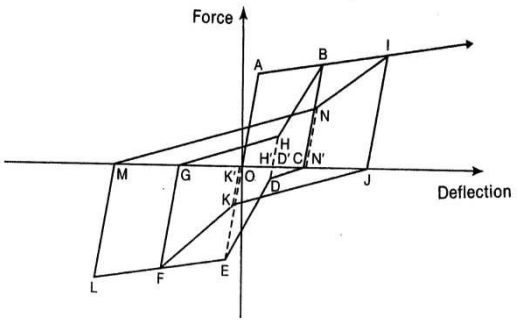

Figure 2-45 – Hysteretic behaviour of the slender SPSWs (Tromposch and G. L. Kulak, 1987)

2.5.4.6. Seismic Design of SPSWs

The seismic design of SPSWs has been regulated in some codes such as US and Canadian Codes. Generally, seismic forces acting to the SPSW systems are determined based on the application of the equivalent lateral force method. SPSW is then designed to carry these seismic forces and expecting failure of SPSW system is based on plastic analysis. The design procedures briefly are presented hereafter:

- Determine the type of Steel Shear Wall Systems: One of two existing type of SPSW system, known as standard and dual systems, should be chosen for the structure.
- Determine the behaviour of SPSW under applied shear: Depending on the slenderness of a shear wall, it can be categorized as Compact, Non-Compact and Slender as shown in Figure 2-46 and explained as follows (Astaneh-Asl (2001)):

If the plate has $\frac{h}{t} < \lambda_p = 1.1.\sqrt{\frac{k_v E}{F_{yw}}}$, it is categorized as Compact Plate which deforms plastically by shear before out-of-plane buckling.

If the plate has $\lambda_p = 1.1.\sqrt{\frac{k_v E}{F_{yw}}} \le \frac{h}{t} < \lambda_r = 1.37.\sqrt{\frac{k_v E}{F_{yw}}}$, it is categorized as Non-Compact Plate. It is expected that the walls in this category are expected to be buckled while some yielding has already taken place.

If the plate has $\lambda_r = 1.37.\sqrt{\frac{k_v E}{F_{yw}}} \le \frac{h}{t}$, it is categorized as Slender Plate. It is expected that the walls in this category are expected to be buckled while almost elastic.

- Calculate the base shear and distribute it along the height of the building as mentioned in the applicable code.

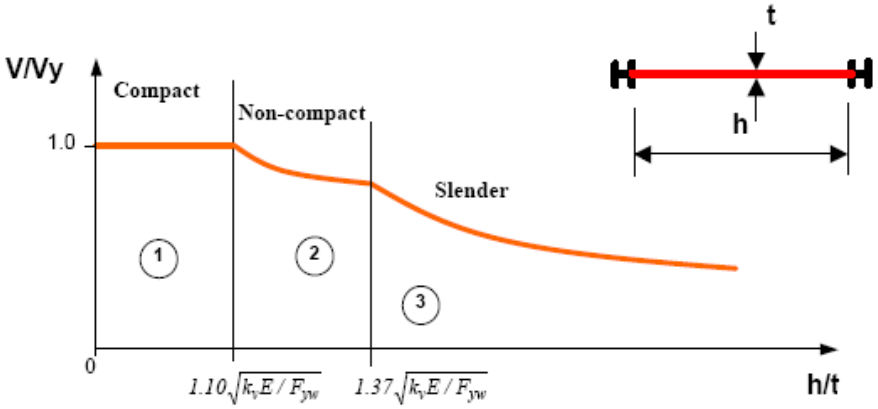

Figure 2-46 – Three regions of behaviour of SPSW

- Determine the thickness of the shear walls to carry the seismic force found in the previous step. For a slender SPSW, this thickness may be calculated based on the minimum plate thickness required for each story by using the following formulas:

$$t = \frac{2.V_s.\Omega_s}{f_y.L.\sin(2\alpha)}$$ (proposed by Jeffrey Bernan) Equation 2-12

where:

Ω_s – the system overstrength factor (described in FEMA 369 or in the US code)

V_s – the design shear story found by equivalent lateral force method

L – the horizontal dimension of the panel

α - the inclined angle of the tensile strips developed in the panel.

or $t = \frac{2.A.\Omega_s.\sin(\theta)}{L.\sin(2\alpha)}$ (proposed by ANSI, AISC 341-05, 2005) Equation 2-13

where:

Ω_s =1.2 – the system overstrength factor

L – the horizontal distance between axes of columns

α - the inclined angle of the tensile strips developed in the panel.

θ - the angle between the vertical axis and the equivalent diagonal of the panel.

A – the sectional area of the equivalent diagonal band.

- Develop the strip model or equivalent diagonal model for computer model to determine the angle of inclination of the strips.
- Characterize the failure modes of the structure in order to re-determine the properties of SPSW.
- Design beams and columns according to Capacity Design principles

- Check the drifts and the failure of the structure
- Design for the connections

2.5.4.7. Behaviour or Response Modification factors of SPSWs

The EC8 has not considered yet the use of SPSWs in both designing the new structures and retrofitting the existing structures. Some analytical and experimental studies were carried out in Italy and UK, however there is no parameter study examining the behaviour factors for this type of structure. The behaviour factor, used in EC8, in some contexts, coincides with the concept of the 'Response Modification Factor', R, used in US and Canada...

Currently, the National Building Code of Canada (CBFFC, 1995), in its 'non-mandatory' Appendix M, specifies the values of R in the provisions on 'Design Requirements' for un-stiffened steel plate shear walls. It provides a value of R equal to 4.0 for SPSW within a special moment frame. This value becomes to 8 when converting to the US code. Astanaeh-Asl (2001) proposed the values of Response Modification Factor, R, of SPSWs in different structures, as in Table 2-5.

Table 2-5 – R values for SPSW proposed by Astanaeh-Asl

Structural Systems	Proposed R
Un-stiffened SPSW inside a gravity carrying steel frame with simple beam-to-column connections	6,5
Stiffened SPSW inside a gravity carrying steel frame with simple beam-to-column connections	7
Dual system with special steel moment frames and un-stiffened SPSW	8
Dual system with special steel moment frames and stiffened SPSW	8,5

2.5.4.8. Connections between SPSW and the boundary frames

There exist several possibilities of connecting SPSW to the boundary frames. The two systems, which are commonly used, are based on the use of bolts and the other, on the use of weld. In both systems in reality, SPSW are not directly connected to the frames. Some plates, running along the heights and the lengths of columns and beams by means of weld, play as the intermediate role to connect the boundary frames with the SPSW. The panels are then welded or bolted to these plates, as illustrated in Figure 2-47, Figure 2-48 and Figure 2-49 (Astanaeh-Asl, 2001). The design of connections is followed by Capacity Design procedures.

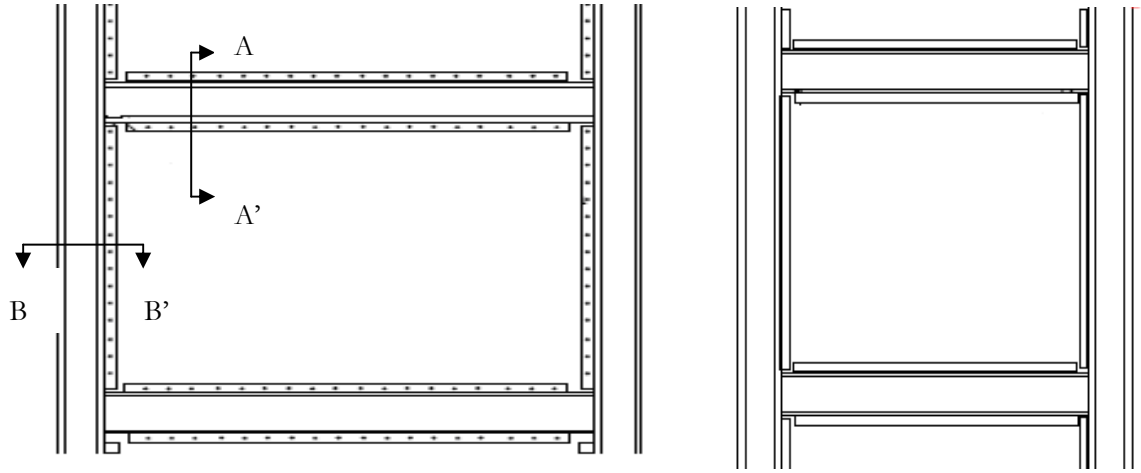

Figure 2-47 – Two possibilities to connect SPSW to the frame: bolted and welded

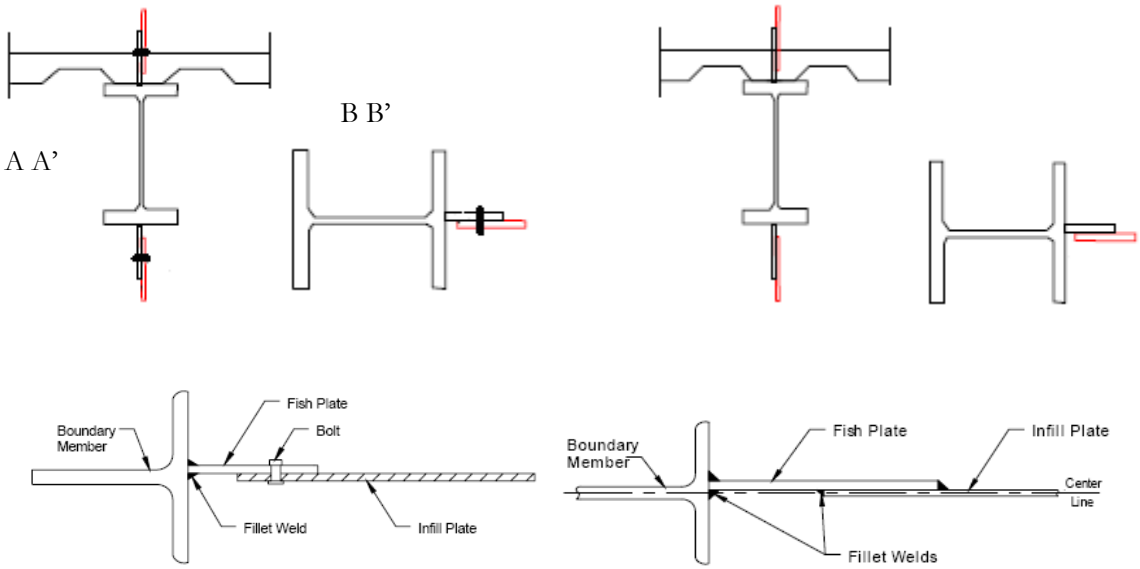

Figure 2-48 – Details of welded connections

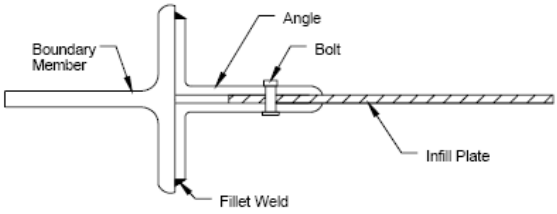

Figure 2-49 – Details of bolted connections

2.5.5. Retrofitting system using Low Yield Steel Shear Walls (LYSWs)

2.5.5.1. Introduction

The use of the SPSWs to resist lateral forces like earthquakes or wind recently becomes more and more broadly. Many benefits exploited from this type of structure are improvement of structural energy dissipation capacity and increase of building lateral stiffness. In addition, this system also takes advantage over others such as concrete shear walls… thanks to steel savings, speed of erection, reduced foundation cost and increased usable space in buildings. However some obstacles still exist that may impede the application of this system. For instance, using yield stress for available steel material, the calculated panel thickness under a given seismic situation may often be much thinner than the available one existed in reality from steel mills. In this case, it is evident that the minimum thickness of the steel must be chosen and it would result in a large difference in panel forces from that required by calculations. Moreover, the traditional walls can not develop their dissipative behaviour in situations of moderate to large earthquake. Indeed, plastic strains occur only for stresses above the yield strength of steel plates, therefore with grades of typical steel it commonly involves large displacements of the ground (Nakashima et al., 1994). To alleviate this problem, there have been many attempts to consider the use of other type of materials which have a lower yield strength such as aluminium or low yield steel (LYS). These systems may play a role as either the primary or the secondary lateral load resisting system of the building, giving rise to promising new trends for the design of steel structures (G. De Matteis et al., 2002). Due to low yield strength, the required thickness of this steel plate obtained from calculations is always much greater than that of the plate made of the normal steel. With the greater thickness, the out-of-plane buckling phenomenon of the LYS plate could be limited, leading to more stable hysteretic behaviour of LYS plates compared to the plates made of the normal steel. This can be explained as follows: If we consider two panels, one made of the common steel and the other made of LYS, dimensioned to carry the same plastic shear resistance V_{Ed}, the panel of LYS will be buckled with the critical shear load much higher than that in the panel of common steel, as illustrated in the following figure (it is supposed that the plate is perfectly flat)

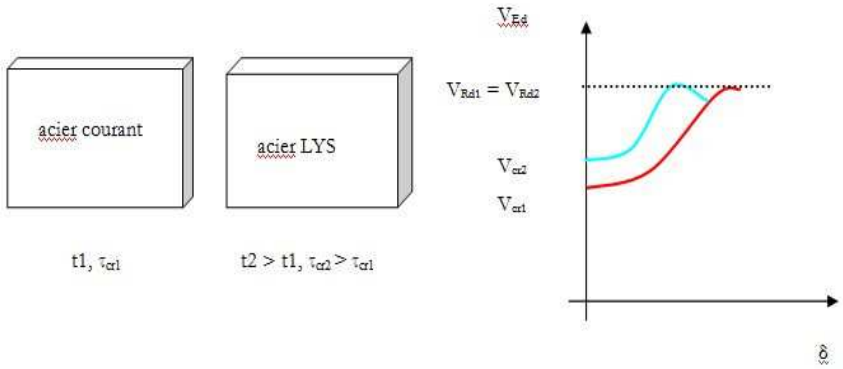

Figure 2-50 – Comparison of the buckling loads of the plates made of common steel or LYS

Apparently, due to the greater critical load, the LYS plate will be buckled much later than the common steel plate if they are loaded in shear at the same time. This leads to the larger area of the hysteretic curves of the LYS plate and more stable cyclic behaviour. In addition, thanks to the high elongation with a conspicuous strain-hardening under load-reversals and with limit strength and stiffness degradation arising after plate buckling (see next section), the LYS panel could absorb a very large energy from the seismic excitations.

In reality, some applications based on the use of stiffened plates made of special low yield strength steels have been introduced in Japan (Tanaka et al., 1998). In this case, because of their exceptional hysteretic behaviour and their capability to early undergo plastic deformations, shear panels are usually conceived as hysteretic dampers. Therefore, they are usually treated as the structural passive control devices. In order to improve both the ultimate resisting capacity of the structure and reduce the damage of main structural members under earthquake loading, shear panels should be designed in such a way to avoid any buckling phenomenon and the capacity of the shear panel should be completely exploited (Nakagawa S. 1996).

2.5.5.2. Mechanical characteristics of the LYS

The chemical composition and mechanical properties of low-yield point steel have been summarized in Table 2-6 and Table 2-7. Due to very low carbon and alloying elements, the nominal yield stress, f_{yLYS}, of low-yield point steel is about 80 – 120 MPa. It has the same Young's modulus as conventional steel and a nominal elongation over 50% (Nakagawa, 1996). This could ensure the LYS panel acting as hysteretic damper to undergo a very large inelastic deformation thus enhancing the energy dissipation capacity of the whole system. Figure 2-51 shows a comparison between low-yield strength steel and conventional steel (Nakashima et al., 1994).It can be seen from the stress-strain relationship of the LYS that its strain hardening is quite high with large elongation until fracture however, the yield plateau of LYS is not clear.

Table 2-6 – Chemical composition of LYS (Nippon Steel Corp. standard) (Yamaguchi et al., 1998)

Steel type		C	Si	Mn	P	S
BT-LYP100	Nippon Steel Standard	≤0.020	≤0.020	≤0.020	≤0.030	≤0.015
	Actual Example	0.001	0.010	0.080	0.008	0.005
BT-LYP235	Nippon Steel Standard	≤0.010	≤0.350	≤1.400	≤0.030	≤0.015
	Actual Example	0.017	0.008	0.380	0.017	0.006

Table 2-7 – Mechanical properties of LYS (Nippon Steel Corp. standard) (Yamaguchi et al., 1998)

Steel type	Yield point (N/mm2)	0.2% offset proof stress (N/mm2)	Tensile (N/mm2)	Elongation at fracture (%)
BT-LYP100	-	80-120	200-300	≥50%
BT-LYP235	215-245	-	300-400	≥50%

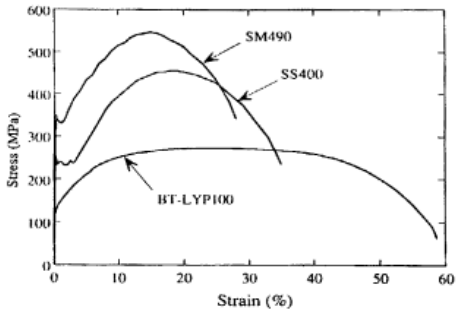

Figure 2-51 – Comparison of stress – strain relationship between LYS and conventional steel

2.5.5.3. Experimental and numerical studies of LYSWs

There have been not many tests and numerical studies of LYSWs under seismic excitations. Some of them were carried out in Japan, some in Italy and in US. The analytical approach for studying LYSW is based on the theory of SPSWs. In general, under an earthquake, the steel walls in low yield dissipate energy permanently through plastic deformations. Their operating principle is identical to that of the steel walls of classic steel. However, as already mentioned, the energy dissipation begins earlier under lower loads due to the lower yield stress however global buckling is delayed because of the thicker panels. Some of studies are discussed hereafter.

De Matteis et al. (2003) conducted a parametric study on shear panels to determine the dominant factors influencing the response of the steel portal frames under earthquakes. The study was conducted by constantly setting the characteristics of portal frames and changing the mechanical properties of the LYS panels. The authors concluded that the low yield strength steels significantly improve the performance of portal frames. The results depended strongly on the stiffness of the panel and the respective portal frames and suggested that LYS panels characterized by low relative strength would allow a significant improvement of seismic performance. The authors also concluded that degradation effects of the hysteretic behaviour of the LYS panels might produce a reduction of panel structural contribution, especially for large frame story deflection.

Another study (Nakashima et al., 1994) focused on the behaviour of three different configurations of panels making of the LYS characterized by a conventional elastic limit at 0.2% with $f_{0,2\%} = 120\,MPa$. The cases differ in the use and position of vertical and horizontal stiffeners (no stiffener, only vertical stiffeners, both vertical and horizontal stiffeners). Panels have the same dimensions in each case, 1200mm x 1200mm x 6mm and are loaded by cycles of imposed displacements. Curves force/displacement of individual cases are given in Figure 2-52. The authors concluded that the LYSWs using vertical and horizontal stiffeners exhibited the most stably hysteretic behaviour among all cases studied. Despite the onset of local buckling in a sub-panels defined by the stiffeners, no significant deterioration in strength was observed. The phenomenon of "pinching" occurred, but remained relatively small compared to the case of conventional steels. Once the stiffeners partially or completely abolished the behavioural signs of deteriorating were faster (respectively, the energy dissipation being only worth about 70 and 40% of the amount completely dissipated by stiffened panels) and the curves were more increasingly affected by the "pinching" effect.

Vian and Bruneau (2004) have tested three specific configurations of LYSWs. A total of three single bay, single story LYSW specimens were designed by the researchers at University of Buffalo, fabricated in Taiwan, and subjected to quasi-static cyclic testing in the NCREE laboratory at NTU. The frames measured 4000mm wide and 2000mm high between member centrelines, and consisted of 345MPa steel members. The infill panels produced by China Steel were 2.6mm thick, LYS plates with an initial yield stress of 165MPa, and ultimate strength of 300MPa. All specimens also have a beam-to-column connection detail that includes reduced beam sections (RBS) at each end (RBS "Reduced Beam Section (Plumier, 1997). This detail was designed to ensure all inelastic beam action would occur at these locations, with the intention of efficient anchoring of infill panel tension field forces, as required at the extremes (roof and basement level beams) of a multi-story SPSW-retrofitted/designed steel frame. A solid panel specimen is shown schematically in Figure 2-53. Subject to cyclic imposed displacements, the panel

examined showed a stable behaviour, with little "pinching" at least until the large displacement. Problems associated with loading structures have led to stop testing earlier than planned, at a shear strain $\psi = 3\%$ (as shown in Figure 2-54).

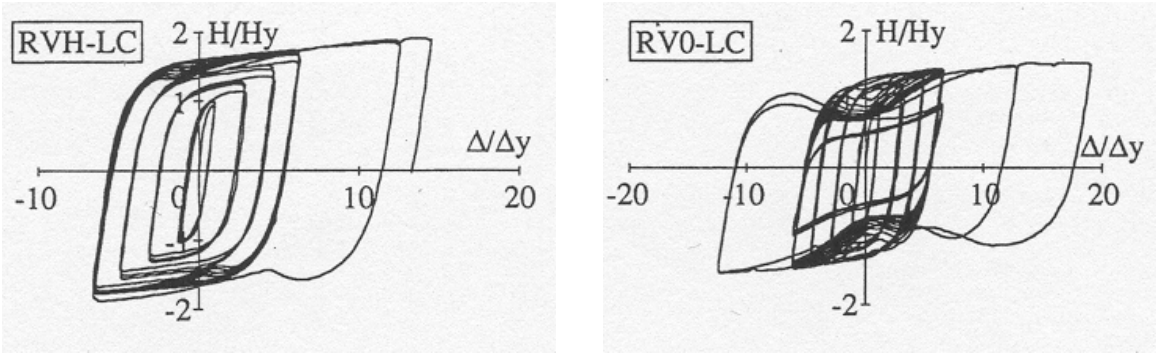

Figure 2-52 – The hysteretic behaviour of LYS panels (left) with horizontal and vertical stiffeners and (right) with vertical horizontal only

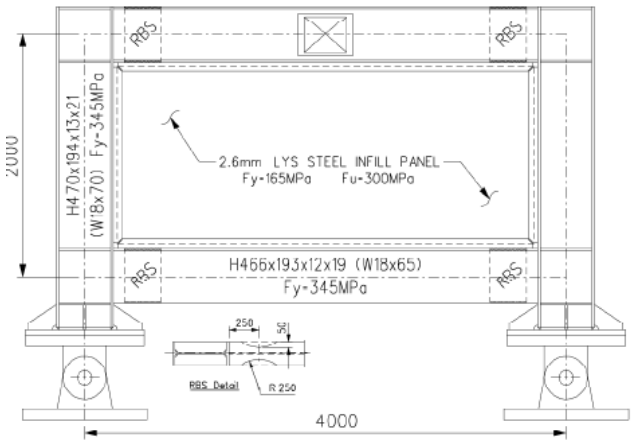

Figure 2-53 – Typical specimen dimensions (Vian and Bruneau, 2004)

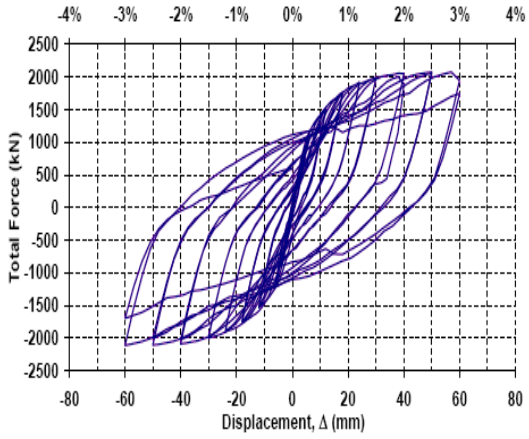

Figure 2-54 – Hysteresis behaviour of the test specimens (Vian and Bruneau, 2004)

2.5.6. Retrofitting system using Aluminium Shear Walls (ASWs)

2.5.6.1. Introduction

The use of aluminium panels as a system of lateral resistance of buildings is justified in case of identical SPSWs or LYS panels. Actually, owning to not easy availability of LYS, the use of pure aluminium as metal material to build shear wall has been introduced (De Matteis et al., 2003). This material is characterized by a very high ductility and by a yield stress level even lower than LYS. Thus, in the case of small earthquakes for relatively low loads, the energy dissipation capacity of the panels is still active (due to the low yield stress the plastic deformations occur for low load levels) and the primary structure undergoes only elastic deformation. In the case of moderate to major earthquakes, the panels are activated earlier than conventional steel panels and energy dissipation through plastic deformation play a very important role. Another advantage on the use of aluminium is that the aluminium industry provides a wide variety of products. It is therefore relatively easy to manufacture aluminium panels unlike the case of LYS panels.

2.5.6.2. Mechanical properties of Aluminium

In case of using aluminium material as shear panels, amongst other things having a low value of yield stress (in the case of aluminium, it is called conventional yield at the strain of 0.2%), only the pure aluminium will be adopted to realise passive seismic protection devices. Indeed, there are various

aluminium alloys containing higher or lower amounts of copper, manganese, ... having yield strengths higher than pure aluminium (type EN-AW 1050A with 99.5% purity) as indicated in the Figure 2-55 for different aluminium alloys (and other metals). Chemical composition and mechanical properties of pure aluminium alloy EN-AW 1050A is presented in Table 2-8.

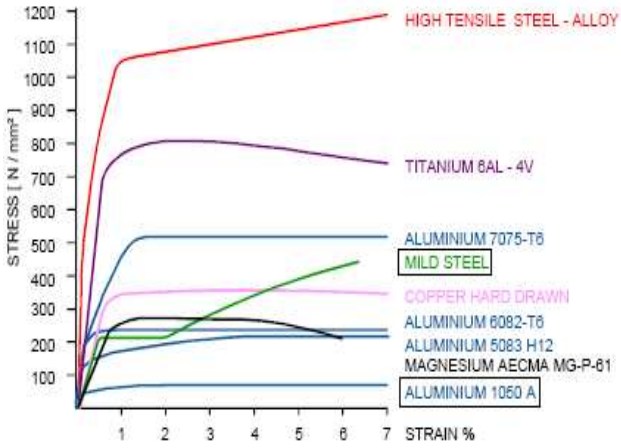

Figure 2-55 – Stress-strain relationships of different alloys

Table 2-8 – Chemical composition and mechanical properties of EN-AW 1050A (De Matteis et al., 2005)

Chemical composition		Mechanical properties			
Commercial denomination	Impurities	Tensile strength (MPa)	Yield strength (0.2% offset, MPa)	Elongation on 5cm (%)	Young Mudulus (MPa)
Aluminium 99,5%	0.02%Cu, 0.40%Fe, 0.31%Si, 0.07%Zn, 0.02%Ti, 0.02% other	70-100	30-70	20-40	70000

2.5.6.3. Experimental and numerical studies of ASWs

Up to date, the use of aluminium panels as a lateral resistant system still remains a theoretical application. Indeed, until now, no existing building makes use of this system. Moreover, the tests are rather few compared to the case of SPSWs and LYSWs.

De Matteis et al. (2005) conducted a numerical study on seismic behaviour of several frame configurations making of stiffened aluminium panels (alloy EN AW-1050A). Three types of frames have been tested: standard multi-storied frames (meaning that the frames carrying the gravity forces and the shear walls acting as the main lateral resistant system); dual multi-storied frames (meaning that lateral force being carried by the two systems); and finally multi-storied frames without panel dimensioned at SLS (earthquake at serviceability). Moreover, two types of frames with the panels were considered: complete filling and partial filling. Before carrying out numerical study, some tests were performed on several panels (1500mm x 1000mm x 5mm) (position and number of different stiffeners). Figure 2-56 shows a view of specimens and their hysteretic behaviour. It is worth noting that some technical treatments (heat treatment) had been used to increase the seismic performance of the panels (increasing the ductility and reducing the low yield stress). The results have indicated that the most dissipative solution is the one in which the number of stiffeners is large and where the use of weld is excluded. Indeed, in this case, the observed behaviour is more stable and more efficient in terms of low cycle strength. As for numerical analysis, they highlighted the beneficial effect of the panels that provide additional stiffness, a significant contribution to the dissipation of energy in even a small earthquake and important contribution to the overall behaviour of the structure to ultimate limit states. In addition, the panels create a global mechanism of dissipative collapse characterized by the deterioration of the panels followed by the formation of plastic hinges in beams. The authors also concluded that the behaviour factors, established at the end of the study, range between 10 and 16 (particularly high values).

Roberts (1992) studied the behaviour of small-sized un-stiffened aluminium panels (300mm x 300mm x 0.54mm and 300mm x 450mm x 0.54mm). Cyclic loading curves exhibit a behaviour strongly affected by the pinching and resistances are relatively low, as seen in Figure 2-57.

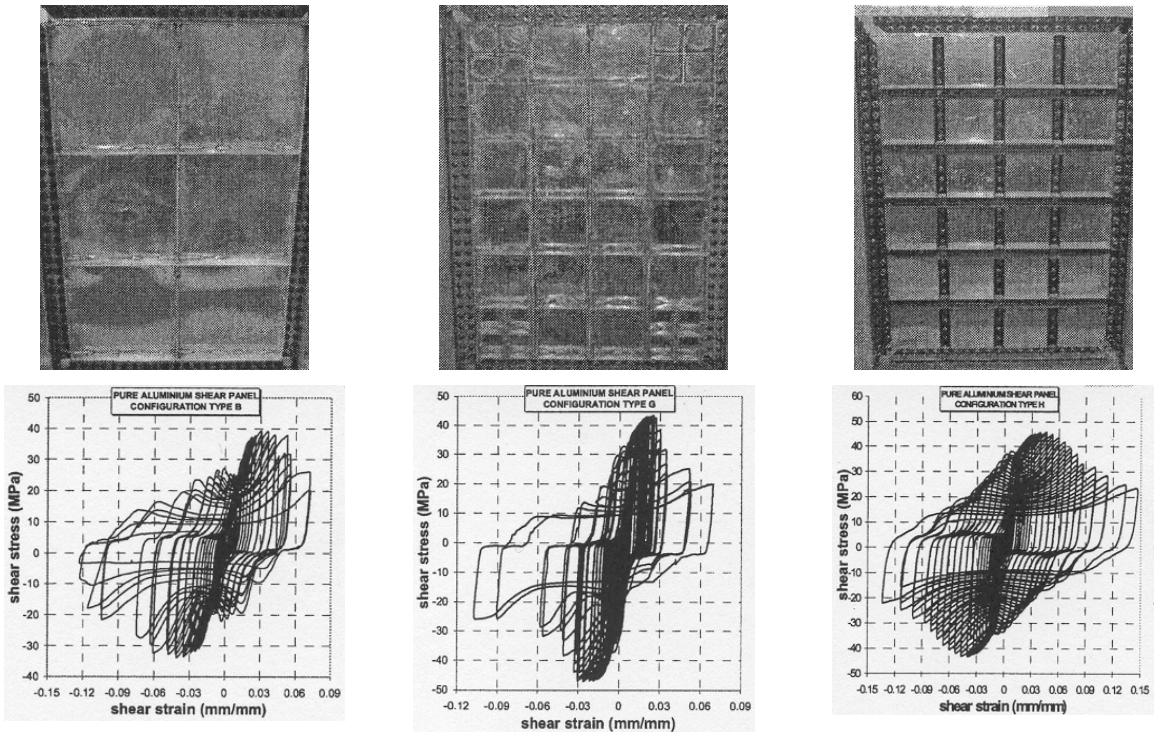

Figure 2-56 – Results of numerical studies of De Matteis et al. (2005) on shear walls made of aluminium

Several aluminium panels were also tested in the context of strengthening structures (reinforced concrete frames, as presented in Figure 2-58) (Mazzolani et al., 2006). The study included a two-storied frame for a total height of 6.81 m and plan dimensions of 6.3m x 5.9 m. Strengthening was achieved by fixing the frame by stiffened aluminium panels inserted in a framework of UPN 180 and 240. The panels have a thickness of 1.5 mm, presented in Figure 2-58. The results of cyclic tests performed on the structure indicate a marked improvement in strength and stiffness of the strengthened frame relative to the frame without aluminium panels. The force-displacement diagram shows in the Figure 2-59. The experimental curve is the envelope curve of the cyclic tests. The difference in stiffness between these two curves is mainly due to the buckling occurring in some panels, buckling not considered in numerical analysis. The ultimate strength of the structure increased from approximately 83.09kN to 300kN for strengthened one.

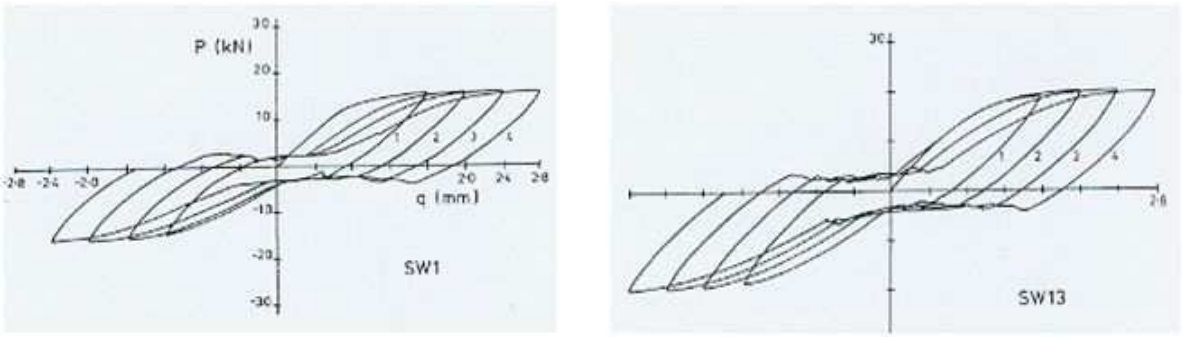

Figure 2-57 - Curve load/displacement of aluminium panels (SW1: 300x300 mm; SW2: 300x450 mm) (Roberts et al., 1992)

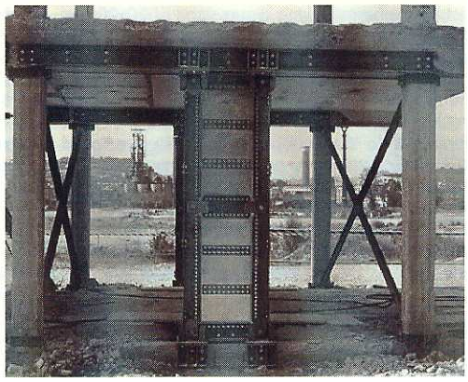

Figure 2-58 – The tested frame and aluminium panels (Mazzolani et al., 2006)

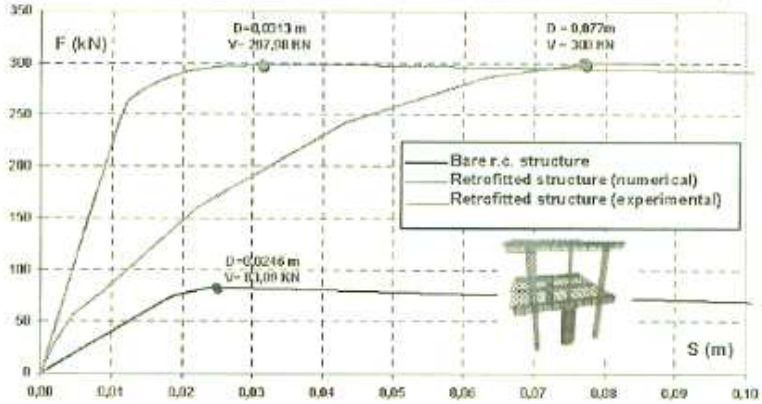

Figure 2-59 – Pushover curve of the studied frame with and without panels (Mazzolani et al., 2006)

2.5.7. Retrofitting system using Perforated Shear Walls (PSWs)

Introduction

Using steel walls (common or LYS) or aluminium is an advantageous solution for the structure to be against the horizontal forces generated by an earthquake. In the vast majority of cases, the use of solid steel plates is mainly exploited for the buildings. However, in some cases it may be necessary to have one or more openings on the steel plates in order to make it possible for various pipes, for example electrical ones, being through the shear walls.

The perforations on the panels generate a reduction in strength and stiffness of those compared to solid plates of the same dimensions (same width, height and thickness). Identically to the case of LYS steel or aluminium, this disadvantage could be overcome by an increase of thickness of the panels. Tests have shown that thin perforated panels exhibited behaviour under cyclic loading more acceptable despite the inevitable buckling (Vian et al., 2004). Due to the fact that the stiffness and strength of the perforated plates are reduced because of the holes, they are able to be yielded with low shear forces, leading to the possibility of prematurely absorbing the seismic energy and of reducing the internal forces generated in the panels to the external frame. This point may be a critical advantage in strengthening existing frames. It is already mentioned above the positive effect of the introduction of panels in frames is to increase their stiffness and to reduce their sensitivity to second order effects. However, this increase in stiffness causes a change in the fundamental period of the structure, leading to the higher seismic forces. This change is not always beneficial.

Experimental studies of PSWs

A series of tests were performed (Roberts and Sabour-Ghomi, 1995) on steel panels with one central circular opening. Different diameters of the hole and panel sizes were considered. The results under cyclic loading indicate a reduction in ultimate load of the panels and their stiffness compared to non-perforated panels. According to the authors, it is possible to obtain strength and stiffness of those conservatively,

reducing by a factor of (1-d/h) of strength and stiffness of the full panel of the same size (h - height of the plate and d – diameter of the hole). For other geometries of openings, the results still remain valid at the condition of working with an equivalent diameter. Figure 2-60 provides curves for some different configurations of the panels (300mm x 300mm x 0.83mm). It can be observed that because the thicknesses of the panels are relatively low compared to other dimensions, buckling occurs in each panel and there is a "pinching" for rather low loading levels. A decrease in ultimate load is also observed with increasing the diameter of the hole in the panel.

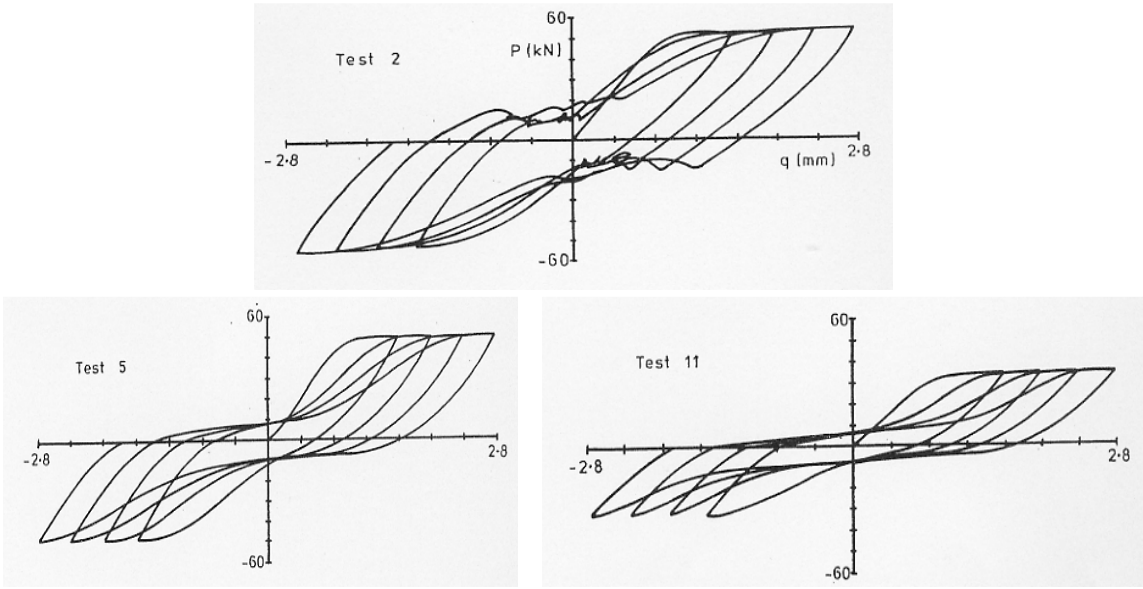

Figure 2-60 – Non perforated panel curve/ Perforated panel curve with a circular hole d = 60 mm/ Perforated panel curve with a circular hole d = 150 mm (Roberts and Sabour-Ghomi, 1995)

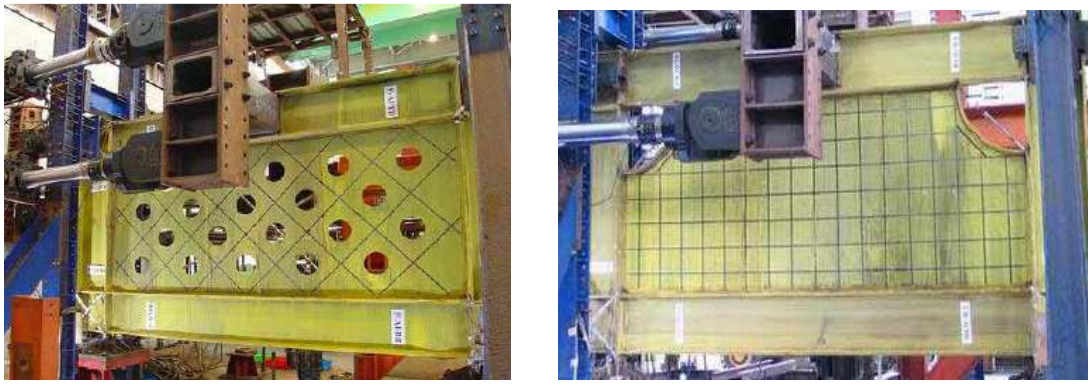

Figure 2-61 – Experiments by Vian and Bruneau (2004)

Vian and Bruneau (2004) tested two types of perforated steel panels LYS. In this study, with the intention of making the plastic hinges on beams, the beam sections were reduced their ends (RBS "Reduced Beam Section"). The panels (4000mm x 2000mm x 2.6mm) have yield strength f_y of 165MPa and ultimate strength f_u of 300MPa. Both configurations are tested respectively using a perforated plate with 20 holes of 200mm diameter and a perforated plate with holes at only two corners as shown in Figure 2-61. Under cyclic imposed displacements, the panels showed stable behaviour, with very little "pinching" at the state of large displacements (Figure 2-62). In the particular case of perforated plates, plastic strains affect the entire panel but remain concentrated in narrow zones around the holes. This solution also reduces noise resulting buckling.

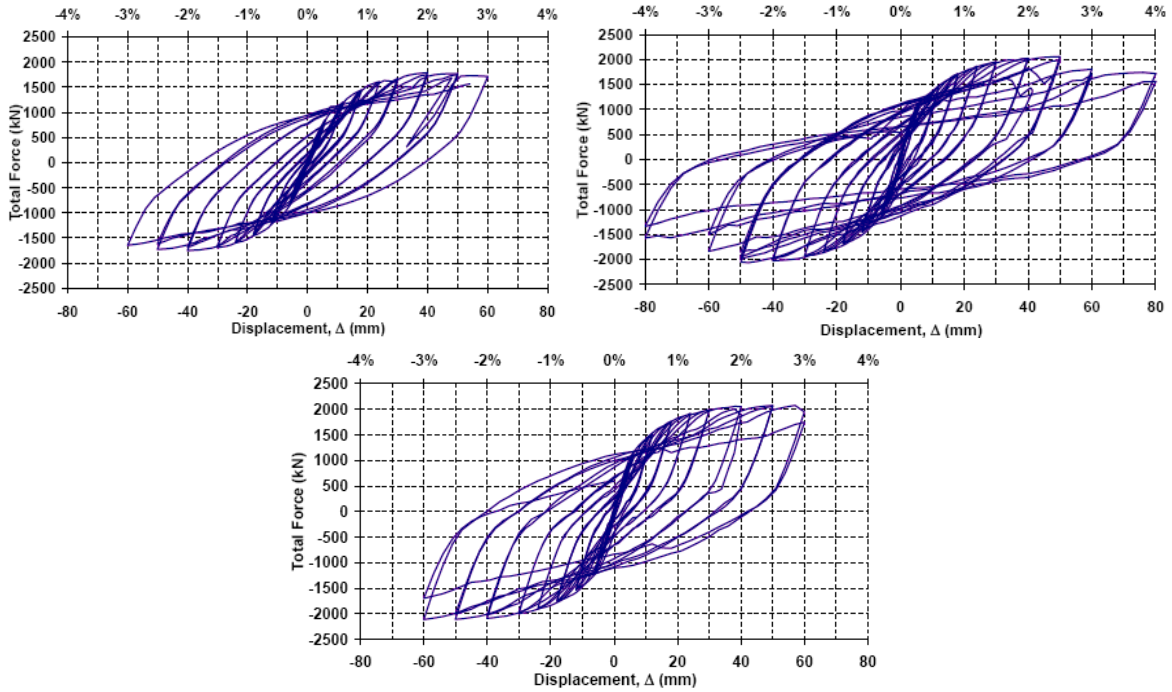

Figure 2-62 – Hysteretic behaviour of the panels by Vian and Bruneau (2004)

2.5.8. Retrofitting system using Reinforced Concrete Shear Walls (RCSWs)

2.5.8.1. Introduction

According to EC8, a wall is a structural element supporting other elements and having an elongated cross section characterized by a length to width ratio greater than 4. Two fundamental types of reinforced concrete walls may be considered as: ductile walls and large lightly reinforced walls.

A ductile wall is attached to the base so that the relative rotation of its base from the rest of the structural system is prevented. It is sized and designed to dissipate energy in a plastic zone or plastic hinge in bending with no opening or perforation above its base with the height being approximately the width of the wall. The behaviour factor of this structure varies between 3 and 4.4 (EC8).

A large lightly reinforced wall is characterized by a large transverse dimension (with the width at least 4m or 2/3 of its height) through which it is supposed to develop a limited crack under a seismic situation. It transforms the seismic energy into potential energy by lifting the masses and energy dissipated in the soil by rigid body rotation. Unlike the first type, the large lightly reinforced wall is unable to dissipate energy in a plastic hinge at base. Therefore, the behaviour factor that can be used is lower and the maximum value equal 3.

The use of reinforced concrete walls (ductile or large lightly reinforced) as the main component to resist lateral forces for new designed buildings has become more and more widespread all over the World. For new designed structures, the RCSWs are able to make them stiff, reducing P-delta effects and precluding some undesired vibration modes such as torsion, therefore the structures can be able to resist large seismic excitations. However, taking advantage of this and making it used in retrofitting the existing reinforced concrete buildings are not an easy task. This is because the fact that the walls generally carry lateral forces mainly in elastic range, and therefore in most cases they have rather large dimensions resulting in very large shear forces at the base of the walls, which will cause more complicated tasks for designing foundation systems, especially in cases of retrofitting.

There is a very few study on RCSWs in retrofitting the existing RC-MRFs to date and the application of RCSW in this field has been still based on the criteria as the same in designing the new structures. Therefore, this retrofitting system will be shortly introduced based on criteria for the new buildings.

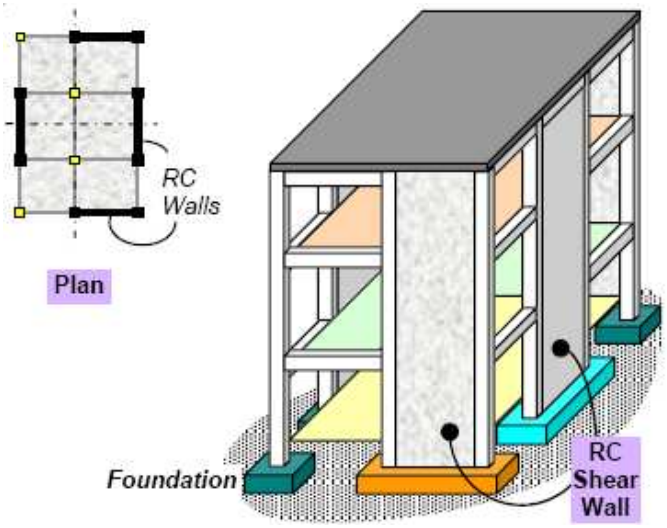

Figure 2-63 – An example of configurations of RC wall systems

2.5.8.2. Capacity design of the walls

The principle of capacity design mentioned above requires the formation of a dissipative mechanism and overall knowledge of local ductile mechanisms (i.e. dissipative) or non-ductile mechanisms (i.e. non-dissipative). In reinforced concrete walls, a single mechanism can be described as ductile. This is the plastic bending obtained by yielding steel reinforcement in tension and plastic deformations of concrete in compression. However, strain at fracture of steel and concrete are significantly different (5% and 0.35%, respectively), it is necessary to provide confinement for the concrete (through so-called confining transverse reinforcement) for increasing its compressive strength but also its elongation at break of a factor of 2 to 4. Without this measure, the ductility and energy dissipation capacity in critical areas would be insufficient because the fracture of the concrete would occur before obtaining significant deformation or yielding of the reinforcement. To get the desired behaviour for the concrete, confinement transverse reinforcement must meet the following criteria (Plumier, 2010):

- closed-loop stirrup
- anchored hooks bent at 135 ° terminated by a straight portion of length 10Φ
- Non-dissipative phenomena affecting a reinforced concrete wall are explained briefly below. There are several brittle failures of the RCSWs, much more than the single phenomenon of the ductile failure in bending (Plumier, 2010):
- shear → cause diagonal tension or slipping
- Alternated shear (in a wall with openings) → cause the damage resulting from alternating inclined cracks which disintegrate concrete.
- Slip the plastic hinge (at the foot of the wall)
- Bond failure
- Buckling of a single element → occurs in a very compressed area if the element is insufficiently maintained transverse stirrups in relevant spaces.
- Localization of plastic deformation in a restricted area

2.5.8.3. Ductile walls

Behaviour factors

The exact determination of the behaviour factor for RCSWs is performed using the following formulae (EC8): $q = q_0 k_w \geq 1,5$

- q_0 base value of the behaviour factor depending on the type of structural system and regularity in elevation
- k_w coefficient reflecting the prevailing failure mode in structural systems of walls given by the formula $k_w = (1+\alpha_0)/3 \le 1 \; et \ge 0{,}5$ where α_0 is the prevailing aspect ratio of the walls of the structural system defined as the ratio h_w / l_w of the height of the wall along the length of its cross section

Depending on the chosen ductility class, the behaviour factor values vary between 3.0 for a class DCM and $4.0\frac{\alpha_u}{\alpha_1}$ for a class DCH and must be reduced by 20% if the buildings are not regular in elevation (α_1 defined as the value with which the seismic force is multiplied to reach for the first time the bending resistance of an element (first yield at any where in the structure), α_u is defined as the value with which the seismic force is multiplied to reach for the formation of plastic hinges in a number of sections enough to develop a global plastic mechanism of the structure). An approximate value of α_u / α_1 for buildings with regular plan walls can be taken equal to 1.1.

Conditions of local ductility

It has been reported previously that the mechanism for the desired plastic walls consists of a flexural plastic hinge at the wall base. It is therefore essential that this area has an adequate plastic rotation capacity. This requirement is translated into a criterion according to the curvature ductility factor defined as the ratio between the curvature reached when the bending moment is equal to 85% of its value reached in the resistant phase of decline post-peak and the curve corresponding to the yield strength. This criterion is defined as follows (EC8):

$$\mu_{\phi réalisé} \ge \mu_\phi = \begin{cases} 2q_0 \dfrac{M_{Ed}}{M_{Rd}} - 1 & si\ T_1 \ge T_c \\ 1 + 2(q_0 \dfrac{M_{Ed}}{M_{Rd}} - 1) T_c / T_1 & si\ T_1 < T_c \end{cases}$$

- q_0 defined as above
- M_{Ed} / M_{Rd} (at the base of the wall in the seismic situation) with M_{Ed} bending moment from the analysis and M_{Rd} flexural resistance
- T_1 fundamental building period in the vertical plane in which bending occurs
- T_c period at the upper limit of the zone of constant acceleration spectrum

Furthermore, the height of the critical zone above the base of the wall can be estimated using the formula: $h_{cr} = \max(l_w; H_w/6)$ (Plumier, 2010) while complying with the following condition $h_{cr} \le \begin{cases} 2l_w \\ h_s \quad pour\ n \le 6\ niveaux \\ 2h_s \quad pour\ n \ge 7\ niveaux \end{cases}$ (with h_s free height of each level, l_w length of the cross section of the wall, H_w the wall height).

In plan, the area to be confined over a length l_c measured from the extreme compression fibre of the wall to the point where the unconfined concrete can attain fracture due to significant compressive strain (i.e. $\varepsilon \ge 0{,}0035$).

Seismic Forces

The walls shall be dimensioned according to the principle of capacity design explained above. To this end, it is necessary to determine the stresses on the critical sections of the wall (through obtained bending moment and shear force). EC8 allows us to determine the envelope of these stresses. Regarding the flexure, the bending moment diagram for calculating the height of the wall is given by an envelope of the moment diagram from the analysis and moved vertically (to take into account that the maximum moment is obtained only base of the wall but on the critical height). Moreover, taking into account the plastic deformation capacity if the structure, it is possible to redistribute the moment with the amount of 30% from the elastic calculation. The shear force is evaluated based on the actual value of the resistance of the plastic hinge base of the wall chosen as the dissipative mechanism. In addition, the shear load should be increased by 50% compared to shear forces from the analysis.

Experimental behaviour of RCSWs

There are several tests on RCSWs. The results are nearly the same. The typical one is presented. Riva et al. (2003) have achieved full-scale study of behaviour under cyclic loading of a reinforced concrete wall designed according to the EC8 by considering an area with moderate seismicity (PGA = 0.2g) and a medium ductility class (DCM) with a behaviour factor q equal to 3.0. The wall, characterized by a height of 16m and a cross combined section of 2800mm x 300 mm (except in its lower part where the dimensions of that section are higher at 2800mm x 400 mm), was tested in a horizontal position. However, the loading was made so that the diagrams of bending moments and shear forces are identical to those of the real situation. In contrast, no axial force is present. Before attaining substantial plastic deformations, the behaviour of the wall was stable and almost elastic as indicated Figure 2-64.

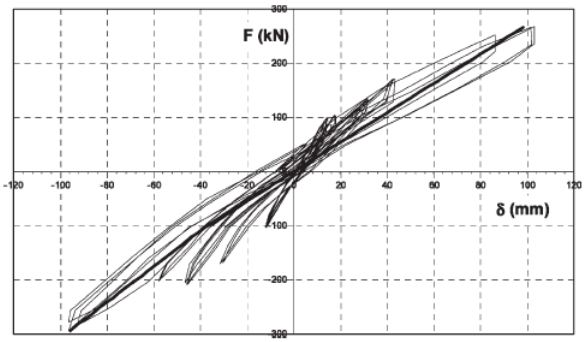

Figure 2-64 - Load displacement diagram of the wall before attaining large plastic deformations

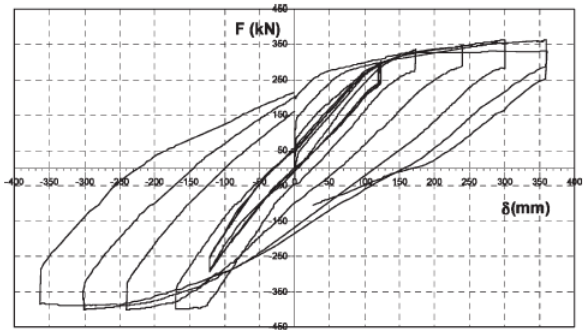

Figure 2-65 - Load displacement diagram of the wall after attaining large plastic deformations

The amount of energy dissipated is relatively small but nevertheless increasing over the loading cycles. The degradations of the strength and stiffness remain low. More precisely, cracks, appearing in the critical section of the wall, indicate (by their low inclination) that bending dominates the behaviour of the wall. Beyond the load causes substantial plastic deformation, the behaviour of the wall remains stable until its collapse. The dissipated energy increases significantly (compared to previous loading cycles), as shown in Figure 2-65 (the lack of symmetry of the diagram as well as sudden drops in the curves at each end of the cycle can be explained by the testing devices). It should be noted that the ruin of the wall (for which the ductility is important) has not occurred by bending but by shear because of a core wall too poorly reinforced (including problems related to the absence of axial).

2.5.8.4. Large lightly reinforced walls

The behaviour of this type of wall is completely different from the classic walls. Indeed, as already mentioned above, a large wall does not form a critical zone at its base. The design aims to promote a global mechanism characterized by limited plastic deformations.

Behaviour factors

The formula described above for walls may also be used in the case of large walls with the same definitions. However, here, the ductility class DCH can be considered. For class DCM, it is 3.0.

Conditions of ductility

Energy dissipation does not take place at a plastic hinge. Ductility criteria do more on the coefficient of curvature ductility. By contrasts, transversal reinforcements are still required in the edge elements of the wall on a length l_c less than or equal to $l_c \le \max \begin{cases} b_w \\ 3 b_w \sigma_{cm} / f_{cd} \end{cases}$ (Plumier, 2010) (with b_w the thickness of the wall, σ_{cm} the average stress of concrete in the compression zone at the ultimate limit state in bending resistance of composite and f_{cd} design compressive concrete). The dimensions of these transversal and vertical bars must meet some specific criteria.

Seismic Forces

In this case, the envelope of bending moments is not allowed to be redistributed. To ensure that the plastic bending precedes the formation of the ultimate limit state in shear, the shear force from the analysis must be increased according to the concept of capacity design. At each level of the wall, the shear force to consider is given by $V_{Ed} = V'_{Ed} \frac{q+1}{2}$ (Plumier, 2010). Also note that due to the uprising of the wall from the ground or the opening and closing of horizontal cracks, additional dynamic normal forces must be taken into account for the verification of flexion.

2.5.8.5. Prefabricated walls

Like their counterparts cast in place, prefabricated structures must dissipate energy through plastic rotations in critical areas. Nevertheless, these structures can also dissipate energy through mechanisms of plastic shear along the joints.

Behaviour factors

It is determined using the following formula: $q_p = k_p k_w q_0$ (EC8). Values k_w and q_0 are determined identically to the case of walls. As for k_p, this is a reduction factor depending on the energy dissipation capacity of prefabricated structures. Its value is set equal to unity when the assemblies of prefabricated components meet the criteria defined by EC8. Otherwise, it is 0.5.

Conditions of ductility

Ductility conditions are identical to the case of reinforced concrete walls. Provisions should also be taken at assemblies according to their position relative to critical areas and depending on their orientation (horizontal or vertical).

2.5.9. Retrofitting system using Composite Shear Walls (CSWs)

Introduction

The composite shear walls (CSWs) discussed here consist of a steel plate shear wall with reinforced concrete walls attached to one side or both sides of the steel plate using mechanical connectors such as shear studs or bolts, as defined in EC8. The composite shear walls have been used in buildings in recent years although not as frequently as the other lateral load resisting systems. This section attempts to provide general information on the basic characteristics of composite shear walls, tests on CSW and some main provisions of current code. Some advantages of the CSW are drawn hereafter:

- Compared to a reinforced concrete shear wall, a composite wall with the same shear capacity, and most likely larger shear stiffness, will have smaller thickness and less weight, leading to more useable floor space particularly in tall buildings and smaller foundations as well as smaller seismic forces.
- A CSW can have cast in place or pre-cast walls. Since steel plate shear walls can provide stiffness and stability during erection, the construction of reinforced concrete walls can be taken out of the critical path of field construction and done independent of fabrication and erection of steel structure.

In a steel shear wall, the story shear is carried by tension field action of the steel plate after buckling of diagonal compression. In a CSW, the concrete wall restrains the steel plate and prevents its buckling

before it yields. As a result, the steel plate resists the story shear by yielding in shears. The shear yield capacity of steel plate can be significantly greater than its capacity to resist shear in yielding of diagonal tension field. In addition, the reinforced concrete wall provides sound and temperature insulation as well as fire proofing to steel shear walls.

General configuration of a CSW is shown in Figure 2-66. It includes steel plate shear walls, reinforced concrete walls, shear connectors and boundary frames.

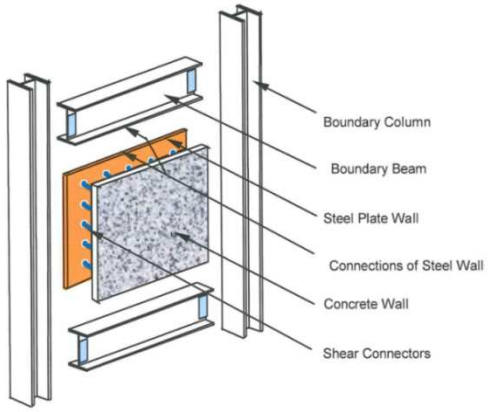

Figure 2-66 – Main components of the typical CSWs (Astaneh, 2002)

Experimental and numerical studies of CSWs

Astaneh and Zhao (1998-2000) conducted the tests on composite shear walls. The main objective of this study was to conduct cyclic testing of a traditional and an innovative composite shear wall and to develop the design and modelling recommendations. The results from studies of an innovative version of the traditional composite shear wall systems showed a significant potential for this innovative system to become a very efficient and high performance lateral load resisting system. Figure 2-67 shows the basic attributes of traditional and innovative composite shear walls tested. Both traditional and innovative composite shear walls studies were "dual" systems with composite shear walls placed within a moment frame, Figure 2-67 (a). The only difference between the two these systems proposed in that study is that in the innovative system there is a gap between the concrete wall and the boundary columns and beams, Figure 2-67 (b). In the traditional composite shear wall there is no gap, and concrete is directly bearing against boundary columns and beams, Figure 2-67(c). This simple difference resulted in significant improvements in the performance as well as increase in ductility and reduction in damage (Astaneh, 2002). The test specimens were ½-scale three stories, one-bay structures. Figure 2-68 shows a typical test specimen. The specimens have identical properties except for a 1.25" (3.2mm) gap provided between the concrete wall and the steel columns and beams in Specimen 1 representing the innovative composite shear wall. Table 2-9 shows the properties of test specimens. The steel plate used in the specimen was A36. The beams and columns were A572 Grade 50 steel. The concrete wall in the specimens was a pre-cast concrete wall connected to the steel plate using ½ inch diameter A325 bolts. The concrete used in the specimens was specified to have f'_c of 4,000 psi (27.6 MPa). The beam-to-column connections in the specimens were moment connections. The loading sequence was developed using the sequence suggested in the AISC Seismic Provisions (AISC, 1997). The loading sequence is set in terms of the total drift of the specimens calculated by dividing the horizontal displacement of the top of the specimen, measured by the actuator, by the total height of specimen. The actual inter-story drift was calculated later by dividing inter-story horizontal displacement by the story height. One of the important results obtained from these tests was shear force drift plot for the specimens. These plots, shown in Figure 2-69, provide valuable information on stiffness, strength, ductility and energy dissipation capacity of the system, all parameters very important in design and analysis of structures. Both specimens were able to reach inter-story drifts of more than 4% without reduction in their strength and both were able to reach inter-story drift of at least 5% when their strength had dropped to about 80% of maximum strength attained during the tests. The authors concluded that the maximum strength of the traditional wall (without any gap around the concrete wall) was slightly higher than the strength of the specimen with the gap and the stiffness of specimen without the gap around the concrete was slightly higher than the stiffness of the specimen with a gap. In both specimens, the strength dropped when the steel plate walls started fracturing through their corner where

there was a ½ inch by 2-inch gap between the wall and the moment connection. Learning from these tests, they suggested avoiding such discontinuities. It was also observed that in both specimens, concrete walls were able to brace the steel wall and prevent their buckling before yielding. During late cycles, steel plates buckled over the free length between the bolts connecting the steel plates to concrete walls. Continuation of cyclic loading beyond this point in both specimens caused tension fracture and punching shear failure of bolts through the steel plate.

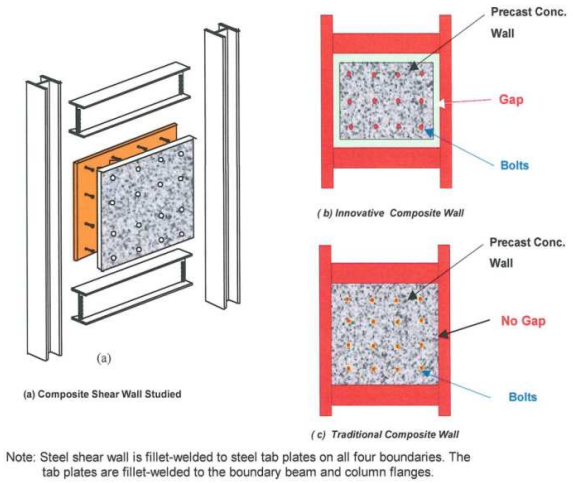

Figure 2-67 – View of traditional and "Innovative" CSWs (Astaneh, 2002)

Figure 2-68 – Test specimens of Zhao and Astaneh (1998-2000)

The most important difference between the behaviours of these two specimens was the behaviour of the concrete wall. In specimen without the wall, during relatively early cycles, the entire edge of the wall developed cracks and spall as seen in Figure 2-70 (left). However, the specimen with a gap around the concrete wall did not show any such damage for the same level of drift applications, Figure 2-70 (right). During later cycles, the damage to the concrete wall of the traditional composite wall was very extensive with almost all of the concrete turned into rubble with reinforcement grid entirely being freed. However, in Innovative specimen with gap around the wall, the damage to concrete wall was relatively limited, Figure 2-70 (left).

Table 2-9 – Properties of the test specimens (Astaneh, 2000)

Spec No.	Columns	Beams	Steel plate thickness	Concrete wall		
				Type of concrete wall	Thickness of concrete wall	Reinf. ρ in each direction
Innovative	W12 x 120	W12 x 26	3/16 in. (4.8mm)	Pre-cast	3 in. (75mm)	0.92%
Traditional	W12 x 120	W12 x 26	3/16 in. (4.8mm)	Pre-cast	3 in. (75mm)	0.92%

In summary, the behaviour of traditional and innovative composite shear walls that were tested indicated that both are excellent systems for lateral load resisting capable of exceeding inter-story drift values of 4% without reduction in their shear strength. In addition, both specimens were able to reach inter-story drifts of more than 5% and still maintain at least 80% of their maximum strength reached during the tests. In the innovative composite shear wall, the concrete wall remained essentially undamaged up to inter-story drift values of about 3% while bracing the steel plate wall, preventing it from buckling and enabling it to reach yielding.

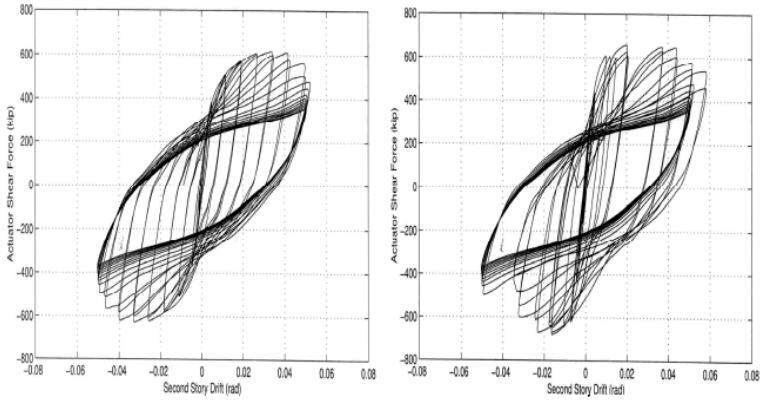

Figure 2-69 – Shear force drift behaviour of Specimens (Astaneh-Asl, 2002)

Behaviour factors

Unlike steel walls, EC8 provides the values of the coefficient of q of composite walls. Thus, according to the ductility class considered (DCM or DCH), the behaviour factor is given by $3\alpha_u/\alpha_1$ or $4\alpha_u/\alpha_1$ with $\alpha_u/\alpha_1 = 1.2$ as a default. As a reminder, this ratio is 1.1 for concrete walls. In other words, the composite walls are considered a bit more dissipative than concrete walls. However, the coefficient values of α_1 and α_u and can be determined on the basis of pushover analysis and the higher value of α_u/α_1 could then be obtained for the composite walls.

In some other codes, such as US, the value of the coefficient R varies between 5 and 8. These codes therefore consider that the composite walls may be very dissipative in some cases.

Failure mechanisms

The capacity design requires knowledge of various possible failure modes of the structure studied and whether they are dissipative (ductile) or non-dissipative (fragile). The elements of the structure can then be sized according to some hierarchy of failure mechanisms (the more ductile than brittle). The possibly ductile failure modes of the CSWs have been suggested by Astaneh-Asl (2002) including:

- sliding bolts connecting the plate to the concrete (and possibly the post and beam framing)
- buckling of the panel (if it does not occur in the elastic range)
- plasticity of panel (shear)

Figure 2-70 – Comparison of Damage to Concrete Wall in Innovative and Traditional

Among the non-dissipative phenomena failures to be avoided, there are tears of steel plates, break the connectors between the concrete and plate, fractures of the steel panel connections at the frame and the destruction of concrete by excessive strain in compression.

2.6. Conclusions

This chapter has presented general points of how to seismically retrofit existing reinforced concrete moment resist frames, including introducing methods to assess their capacity and deficiencies, mentioning about technical strategies and characterizing available retrofitting systems to date. The introduction of evaluation methods and technical strategies mentioned above is based on some modern codes such as EC8 and some recent reference documents such as FEMA 356 (2000), ATC 40 (1997) …

Generally, design processes to retrofit an existing structure under seismic actions are quite clear. The analysis of the structures in retrofitting process is usually based on Displacement-Based approach than traditional approach, i.e. Force-Based, used for designing a new structure. The most difficult issue encountered when seismically retrofitting reinforced concrete moment resisting frames is to select the suitable retrofitting systems. As introduced, up to present, there are not many official guidelines for engineers to choose a reasonable retrofitting system for RC-MRFs. In addition, selecting the retrofitting system for RC-MRFs is still mainly based on the studies on steel structures.

All buildings must be able to withstand the horizontal forces caused by an earthquake. Several systems for the return of these efforts are possible, which include braces (concentric, eccentric and buckling restrained ones) shear walls that it was proposed to study the different variants: concrete walls, solid steel and perforated steel LYS low yield, aluminium, mixed.

In these systems, the concept of energy dissipation is crucial. Indeed, the aim is to dissipate seismic energy in some parts of the structure by large deformations while preserving the other structural elements in the elastic range. This is the principle of capacity design. It requires knowledge of dissipative mechanisms (ductile) and non-dissipative (brittle) of the structural components that may significantly affect the seismic behaviour of the structure.

In order to seismically retrofit or design the structure with the use of structural systems mentioned above, each structure can be characterized by a coefficient called q behaviour factor (or "Response Modification Factor R in the U.S., Canada), which characterizes the ability of the structure to deform plastically.

Based on the large capacity of the structural components in deforming plastically, these factors are used to reduce the seismic actions in order to use linear analysis instead of performing the nonlinear ones. Thanks to that the sections of structural elements and, therefore, costs are also reduced.

A list of the values of the behaviour factors, q used in Europe, or reduction factor, R in US or Canada, valid for the different systems has been given in the following table. No code has specified either these values to the walls made of low yield strength steel, aluminium walls and perforated walls or design concept of these system types.

Table 2-10 – A comparison of R and q factors in US and Europe

	Conventional Concentric Braces	Buckling Restrained Braces	Reinfoced concrete walls	Steel plate shear walls	Composite shear walls
q	1.5-4	No value in EC8	3 to 4.4	No value in EC8	3.6 to 4.8
R	2-6	8	4 to 6	6.5 to 8.5	5 to 8

As already mentioned, the one of the most important factors that makes the advantage of retrofit systems is the energy dissipation capacity. The mechanisms of energy dissipation depend on the material forming the walls. Thus, ductile concrete walls dissipate energy by bending at their base (formation of a plastic hinge) while the steel walls (elastic limit current or lower) and aluminium are the development of plastic shear or tensile plastic on several levels.

For the walls, if the phenomenon of buckling is avoided by using stiffeners, a coating of concrete or thicknesses of plates adapted, the panels can develop their full plastic shear strength without much decrease of strength, stiffness, and therefore, it is possible to obtain a stable hysteretic behaviour. In contrast, the energy dissipation is no longer provided by the shear bands but by diagonal tension field mechanism. Indeed, within the constraints of the plates are being reorganized and we are witnessing the

development of a diagonal tension field that changes the hysteretic behaviour of the plates. Curves load/displacement are characterized by a narrowing or pinching called "pinching" reducing the amount of energy dissipated.

The advantages of steel walls are not confined to a large capacity of energy dissipation. Indeed, compared to concrete walls, the use of steel reduces the thickness of walls required to resist forces of shear. The weight decreases as the seismic actions (depending on the seismic mass of the structure studied) also decrease, leading to the smaller solicitations to foundations. This thickness reduction is also accompanied by a significant space saving. Moreover, assembly of steel plates is faster and easier than the erection of concrete walls (most often cast in place) and the steel walls are able to adapt for both new construction and for the strengthening of existing structures.

Clearly, the steel walls are not free of defects. From the point of view in acoustic sound, it is best to consider concrete walls. The steel plates must also have adequate protection in a fire. In addition, reducing the thickness of the walls in the case of the use of steel does not show that benefit. Indeed, very thin steel plates can be enough to withstand shear forces because of the values of yield strengths of steels used and transverse dimensions of the plates. In other words, high resistance plastics can be obtained with thin plates. However, in some cases these layers, too weak, are not technically feasible. On the other hand, too thin plates lead to buckling and therefore a reduction in the amount of energy dissipated. The solution is obviously to increase the thicknesses (the stiffening is also possible but it is often expensive), but once the plastic resistance mentioned above becomes particularly important and plate works in the elastic range under most earthquakes and therefore the advantage of the plastic work is lost.
To fix the situation, steels with low yield strength (LYS "Low Yield Strength") have been developed. Indeed, to obtain the same strength plastic steel plates with the current low limits (on the order of 100 MPa), an increase of thickness is essential. Buckling is the same time delayed or even cancelled.

The use of aluminium is also planned for the same reasons. Its yield was even lower (about 25 MPa) leads to even higher thicknesses.

Besides, the perforated plates (steel or different alloys) form a third solution to the problem of thicknesses.

In addition, plates are too thin and are not able to significantly reduce the P-Δ effects and drifts between floors at which they are inserted. By contrast, thicker panels stiffen the structure and reduce the sensitivity to displacement and second order effects.

The mixed system of walls, combining steel plates to concrete walls, was also introduced. Concrete can be present in one or both sides of the steel plate and the connection is secured by studs or bolts. The size of these walls is based solely on the shear strength of steel plates, concrete playing a supporting role to prevent warping. The energy dissipation capacity of this system is quite important. In addition, sound insulation and soundproofing walls mixed remains correct as fire resistance (concrete provides protection to the plate).

Finally, it appears from the summary of all possible retrofit systems that the use of steel plates with or without concrete walls appears as an advantageous solution for the resumption of shear stresses generated by an earthquake. However, the current trend is to develop and use materials other than conventional steels. These materials generally have a reduced yield in order to dissipate a greater amount of shear energy (by increasing the thickness of plates so as to delay their buckling) for very low load levels. Materials (or configurations) not too steep using aluminium or perforated panels are also proving positive. They reduce the movements of a structure by a stiffening sufficient but not excessive so as not to over edit the values of periods and increase seismic. The door remains open to any new innovation that meets these criteria and, therefore, the use of expanded metal panels is justified.

3. INTRODUCTION ABOUT EXPANDED METAL PANELS (EMP) AND PREVIOUS STUDY ON EMP

3.1. Introduction about EMP

3.1.1. Introduction

A standard expanded metal (EM) sheet is a truss produced by expansively pressing and simultaneously slitting (steps 1-4 in Figure 3-1) a steel plate made from micro-foam without loss of material. There is neither interlacing nor welding. This truss is a three-dimensional structure but it can be flattened by passing through a cold-roll reducing mill (the lower pictures in Figure 3-1) to obtain another type of EM. Expanded metal panels (EMP) can be finally obtained by cutting the EM sheets with fixed dimensions.

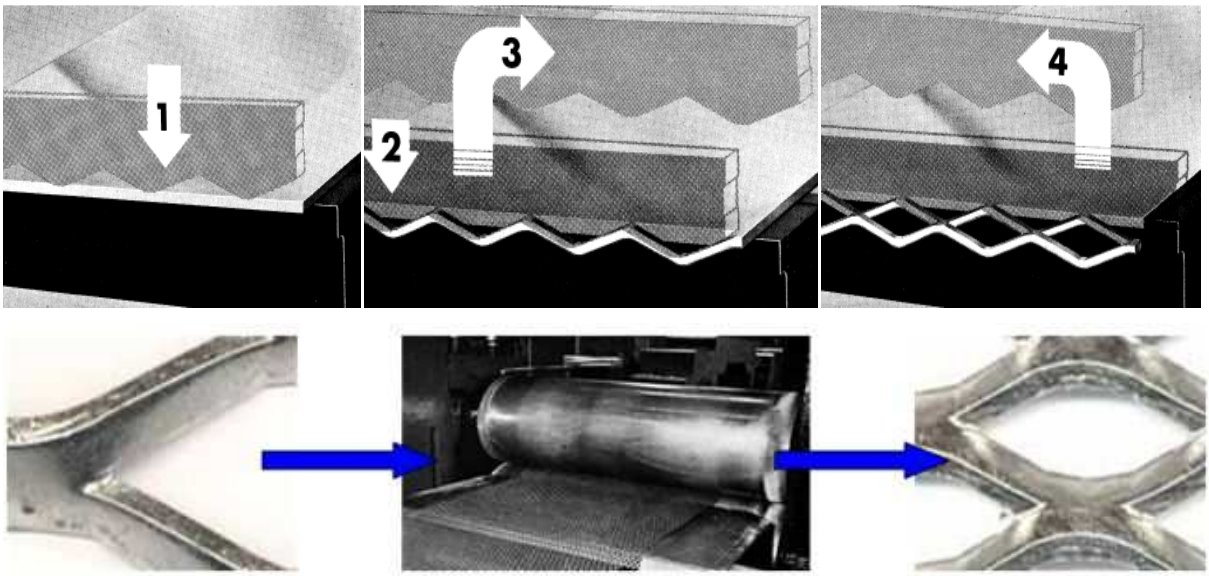

Figure 3-1 – Producing process of EMP

There are a lot of rhomb shaped stitches in an EMP, having nearly the same dimensions. Geometrically, it is constituted by four bars, nearly constantly rectangular sections and characterised by the two diagonals lengths of rhomb-shape mesh, by the width (A) and by the thickness of the bars (B) . These dimensions are illustrated in Figure 3-2. The regular dimensions of an EMP are of about ±1.25m in width and ±2.5m in height. However, the height of the EMP can be increased according to the requirements of the customers (Métal Déployé Belge-MDB, 2003).

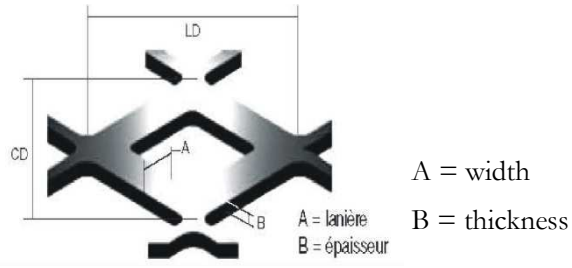

Figure 3-2 –Geometry of a rhomb shaped stitch

Some additional considerations are worth mentioning when working with expanded metal. The manufacture of expanded metal truss is not a "refined" technique: tolerances, due to cuttings and cold stretching, are sometimes very large: manufacturers indicate up to 10% variation on diagonals and bars dimensions. In the same order of ideas, bars are not always perfectly with rectangular sections and, when expanded metal trusses are loaded, some stress concentrations surely occur at the ends of the cuttings. In

some cases, tolerances up to 50% of width of the bars have been measured on the section of the bars between the profile catalogue and the real section (MDB, 2003; EMMA, 1999).

3.1.2. Types of EMP and current applications

The basic types of EM products are standard (regular, normal or raised), flattened, grating architectural (or decorative) meshes and fine meshes (MDB (2003), EMMA (1999)). These products are quite different in geometry, in mechanical properties.

The normal type is produced with high rigidity and light weight in a variety of sizes and weights. Geometrically, as shown in Figure 3-3, there are overlaps at the ends of bars between rhomb shaped stitches in the normal type panels. The light weight and strength of this type make it possible to use in a wide variety of commercial and industrial security application. Some popular applications of this type are storefront protectors, stairway, warehouse enclosures, workers' or equipments' protectors...

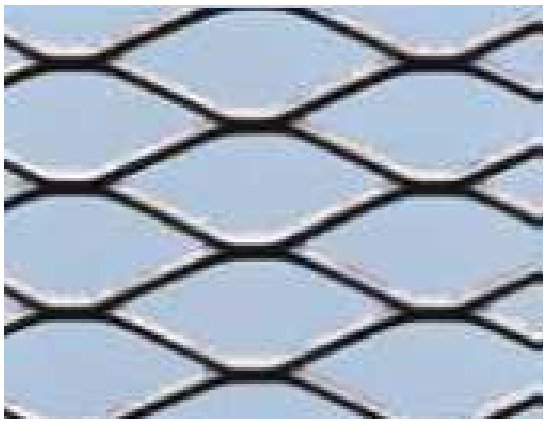

Figure 3-3 – Normal type of EMP

Figure 3-4 – Flattened type of EMP

The flattened type of EMP is manufactured by passing the standard EM sheets through a cold-roll reducing mill. It results in a smooth, flat and level sheet (see Figure 3-4). Flattened type is used in variety of speciality applications, such as book and storage shelves, lamps and lamp shades, folding screen, room dividers and air filtration filters. Two these EMP are also characterized by the dimensions of the rhomb shaped stitches and these dimensions are named as for the EMP. To distinguish these two products by their names, the letter A is added for flattened type, as shown in Table 3-1.

Figure 3-5 – EMP used as front protector

Figure 3-6 – EMP as a fence

Table 3-1 – Distinction between the name of normal and flattened types of EMP

Name	LD(mm)	CD(mm)	A(mm)	B(mm)	EM type
A51.27.35.30	51	27	3.5	3.0	Flatten
A86.46.43.30	86	46	4.3	3.0	Flatten
51.23.32.30	51	23	3.2	3.0	Normal
86.40.32.30	86	40	3.2	3.0	Normal

The ordinary EMP have 1.25m width and 2.00 to 2.50m length. The width of the EMP is usually fixed. The length of the EMP is more flexible and it is possible obtain longer EMP, meaning that the length of EMP can reach 3m or more. Out of these two main products, there are some more special types of EM, such as Grating or Architectural or Decorative meshes, as seen in Figure 3-5 and Figure 3-6.

3.1.3. Mechanical properties of EMP

Up to date, the mechanical properties of EMP are not the primary concerns of the manufacturer. The only important point is to have enough ductility for the manufacturing process. The ductility of the material of EMP is not constant, as one can see in the tests of bars presented in the next chapter.

3.1.4. Conclusions

EMP is currently used in five principal areas: enclosures, protection, support, decoration and filtration. Since EMP is seldom applied for structural applications, mechanical properties of the used steel are not an important point for the manufacturer. Therefore, for further industrial research, it should be important to work on these geometrical and mechanical aspects to obtain a more constant product.

Geometrically, EMP look like plates made from steel or other metals with many voids. These voids have caused the lower weight for this product and leading to the lower cost compared with other metal plates. The metal plates have been used in structural applications for the last decades, mostly in the field of earthquake resistance, playing as the parts of lateral resistance of the structures. It has been explained in Chapter 2 that it was interesting to use low yield strength steel for full plates, steel plates with holes or aluminium plates in order to obtain adequate force-displacement characteristics. EMP could have similar characteristics, which may fulfil the idea to aware its possibilities in retrofitting and upgrading structures for earthquake resistance.

3.2. Previous studies on EMP

As it is rarely used in structural application, there are a very few studies about the mechanical properties of this material to date. A study on EMP has been underway at University of Liege within MacroMousse Projects (MacroMousse, 2010). One part of the overall study was carried out by PECQUET (2005-2008). That study on monotonic behaviour of EMP with small dimensions (the edge being less than 1000mm) showed that under shear forces EMP behave like a tension band (Pecquet E., 2005); (Pecquet E., Cescotto S., 2006). In that study, two approaches analytical and numerical analyses were used to determine plane shear behaviour, global instabilities and ultimate resistances of square EMP under purely monotonic shear loading. The three main parts of that study are summarized hereafter.

3.2.1. Pure plane shear behaviour

The main idea is to obtain global behaviour of an EMP without out of plane deformations of both individual bars of a rhomb-shaped stitch and the panel. This can only be obtained if the dimensions of the EMP are very short and without initial out of plane deformations, or with the use of stiffeners.

Some more hypotheses are made to analyse the plane shear behaviour. Due to having nearly the same geometrical dimensions in all stitches, only one bar of a truss is studied. The overall shear behaviour of the EMP is obtained by assembling the behaviour of all bars in series or in parallel.

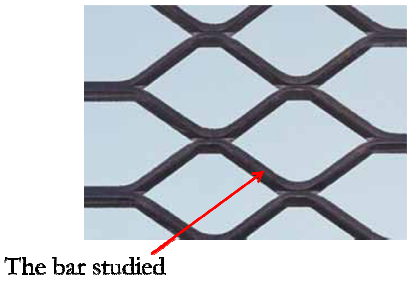

Figure 3-7 – Bar studied in pure plane shear behaviour

Based on the assumption that the material of the bar is elastic perfectly plastic without out of plane instability of either EMP or of bars and large displacements of bars, the elastic behaviour of an individual bar was studied. Three main calculations were performed: the determination of the elastic stiffness by equilibrium in the deformed configuration, the section resistance taking into account the interaction between axial force and bending moment, and the reduction of resistance of compressed bars due to the in plane buckling.

Then, by linearly assembling all tensile bars together and checking the influence of the buckling of the compressed bars, global behaviour of an EMP was determined.

Finally, in one rhomb-shape stitch of an EMP loaded in shear, there are always two bars subjected to tension forces and the other two subjected to compression forces. For these latter ones, buckling can occur. So, this phenomenon is taken into account, reducing the plastic resistance according to the European buckling curves.

The result from the study mentioned above is an analytical model, which is able to determine the elastic stiffness and the ultimate resistance of an expanded metal sheet loaded in shear and for which all out of plane instabilities are prevented.

3.2.2. Complete 3D analytical model of EMP under shear loading

The goal of this part is to characterize elastic buckling of an EMP loaded in shear by comparison between elastic buckling analyses of solid plates by using unstiffened plate theory subjected to pure shear (Pecquet E., 2005; Pecquet E., Cescotto S., 2006) and determination of critical loads in compression by numerical simulation (Pecquet E., Cescotto S., 2006).

For solid plates, a critical stress corresponding to the plate instability can be calculated by Equation 3-1 (Dubas and Gheri, 1986). This concept was initially developed for compressed plates and then extended to cases of shear or combined compression and bending.

$$\sigma_{cr} = \frac{\pi^2 . D_{pl}}{b^2 . t} . k_{cpl} \qquad \text{Equation 3-1}$$

In this equation giving the critical stress, k_{cpl} is a generalized parameter depending on the aspect ratio of the sheet (length divided by width), the number of half waves of buckling and the loading mode (compression, shear …); b is the width (perpendicular to the direction of load) and t is the thickness of the sheet; D_{pl} represents the flexural stiffness of the sheet, calculated by Equation 3-2 (Dubas and Gheri, 1986); E is Young's modulus of the material and ν is Poisson's ratio.

$$D_{pl} = \frac{E . t^3}{12 . \left(1 - \nu^2\right)} \qquad \text{Equation 3-2}$$

Theoretically, the critical stress σ_{cr} is applied uniformly on a side of the boundary of the plate. Therefore, the critical force on one whole side is simply obtained by multiplying the side length and the thickness of the plate:

$$\sigma_{cr} . b . t = P_{cr} = \frac{\pi^2 . D_{pl}}{b} . k_{cpl} \qquad \text{Equation 3-3}$$

If we take the logarithm of Equation 3-3 to the base e; we obtain:

$$\ln\left(P_{cr}\right) = \ln\left(\pi^2 . D_{pl} . k_{cpl}\right) - \ln\left(b\right) = Cte - \ln\left(b\right) \qquad \text{Equation 3-4}$$

Equation 3-4 is a linear equation between the logarithm of P_{cr} and b. This means that, if an EMP behaves like a solid plate, a linear relation between the critical load and the sheet dimensions should be obtained when these quantities are plotted in logarithmic scales.

To study this problem, numerical calculations were used as references for the analytical model. Each bar of a rhomb shape stitch in an EMP was modelled as a 3D beam element. This spatial beam element has

seven degrees of freedom per node (three translations, three rotations and the warping). The finite element program, FINELG, used to do numerical simulation, is a nonlinear code in which all nonlinearities are accounted for. A lot of analyses were performed to determine the critical loads of the square EMP.

Some different trials were made to plot the critical loads of the EMP in function of the critical loads of the full plates. An analytical formula was introduced to correlate the flexural stiffness of an EMP and the flexural stiffness of a solid plate with the same dimensions in thickness, height and length as the EMP.

$$k_{eEMP}\,(or\,D_{EMP}) = D_{pl}\left(\frac{A}{l_{bar}}\right) \qquad \text{Equation 3-5}$$

Where: $k_{e,EMP}$ or D_{EMP} is the flexural stiffness of EMP

D_{pl} is the flexural stiffness of solid plate having the same thickness as EMP (B-dimension)

A is the width of a bar is the dimension A of a rhomb shape stitch

$l_{bar} = \sqrt{\frac{LD^2 + CD^2}{4}}$ is the length of a bar in a rhomb shape stitch.

3.2.3. Ultimate behaviour of square EMP loaded in shear:

With the aim of understanding the ultimate behaviour of EMP loaded in shear and obtaining a simple analytical model to predict their ultimate resistances, two approaches were used: Cardiff plate theory model and numerical simulations. In Cardiff plate theory model the ultimate resistance of a beam web is obtained by three components: critical resistance, tension resistance and plastic resistance of the beam flanges, as seen in Equation 3-6 and Figure 3-8.

$$V_u = V_{cr} + V_t + V_f \qquad \text{Equation 3-6}$$

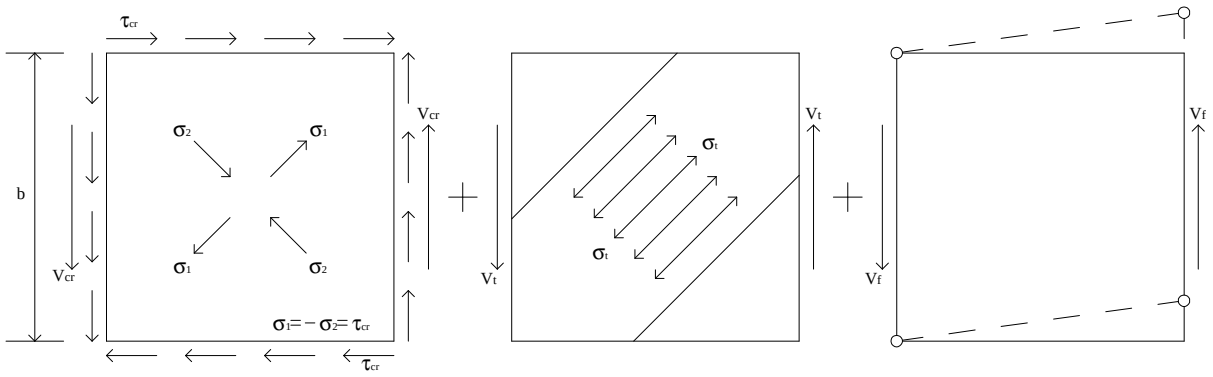

Figure 3-8 – Three components contributed to the resistance of the beam web

The first component is the contribution of the web resistance before out of plane buckling. Because the thickness of bars, which is also the thickness of the square EMP, is very small in comparison to the dimension of the sheet, the square EMP is always globally buckled under a low shear force. Due to early global buckling and moreover because with the same thickness, the elastic stiffness of an EMP is much lower than that of a solid plate, the compression effects on either the overall behaviour of the EMP or the local behaviour of bars can be neglected.

The last component is the contribution of the beam flanges when forming plastic mechanisms. Due to only focusing on pure shear behaviour of the square EMP, no interaction between EMP and boundary elements is taken into account here.

Finally, the second component is the main contribution to the shear resistance of the web. This tensile mechanism, called diagonal tension field, is formed after buckling of the plate (Dubas and Gheri, 1986). The square EMP equivalently works as one tension band developed in post-buckled stages.

Assuming that the square EMP only works in the post-buckled stages, monotonic numerical simulations have been performed on different small square sizes of sheets, the largest dimension being 1000mm, with different commercial expanded metal profiles. Results are presented in terms of loads summarised for all commercial profiles by a linear relation. Results are also expressed in function of dimensions of the diagonal tension band.

3.2.4. Some concluding remarks of the study by Pecquet (Pecquet, 2005)

Some conclusions can be drawn from the study by Pecquet on square EMP having dimensions less than 1000mm:

- If it is possible to preclude the out-of-plane deformations of the EMP by using stiffeners or other solutions, the pure shear behaviour of EMP is similar to that of full plates, depending on the voids of the EMP. Flexural stiffness of the completely plane EMP could be obtained in function of flexural stiffness of the plate having the same thickness, mechanical properties, boundary condition and of the fractional of width of the bars (A) and length of the bars (l_{bar}) of the stitches.
- The critical behaviour of the EMP, loaded in shear, is also like that of the unstiffened full plate. Starting with the critical behaviour of the unstiffened plates mentioned in literature (Dubas and Gheri, 1986), it was concluded that the shear critical behaviour of the EMP is similar that to that of the plate.
- Nonlinear analyses performed to compute the ultimate shear resistance of small square EMP concluded that EMP works as one tension band and the shear resistance is a function of the dimensions of the EMP, the properties of the stitch and the mechanical characteristics of the EMP.

Pecquet E. has introduced a useful idea to study the behaviour of EMP loaded in shear, but there are still some shortcomings about the approaches to describe the overall behaviour of the EMP under shear. They are:

- First, concerning the pure shear behaviour of the EMP, it is quite apparently that the slenderness of the EMP is very large, many times larger than the full plates having the same thickness and dimensions. In addition, fabricating process by using pressing, expanding and slitting provide non-completely flatten sheets. Due to that, it is unrealistic to preclude the out of flatness of the EMP. Therefore, studying the pure shear behaviour of the EMP without taking into account its out-of-plane deformation makes no sense.
- Second, it could be observed from the study of Pecquet in assessing the critical loads of the unstiffened EMP that when the dimensions of the square EMP are increased to the maximum in the study (1000mm) the critical loads of all EMP decrease a lot. This implies that the contribution of the EMP before buckling could completely be neglected and this was also the conclusion of the final part in that study. Therefore the comparison of critical behaviour between the EMP and the full plate becomes useless.
- Third, the nonlinear study of the overall resistance of small square EMP has given a positive input to continue studying the shear behaviour of the EMP. However, that study base on limited dimensions of EMP, which are much less than the dimensions possibly applied in reality. Moreover, the behaviour of the rectangular EMP was not mentioned.
- Finally, it is noteworthy stressing that the analytical model of EMP has not been experimentally examined. To conclude, additional work on EMP including theoretical and experimental development is necessary. It is developed in further sections of this thesis.

4. EXPERIMENTAL STUDY ON EXPANDED METAL PANELS (EMP)

4.1. Introduction

Expanded metal (EM) is not a new construction product, however, there is a very few studies on its mechanical characteristics; therefore, it is seldom used in structural applications. The complete products from EM, as introduced in chapter 3, are rectangular expanded metal panels (EMP) with the approximate dimensions about (±2500mm to 3000mm) x ±1250mm. An EMP includes many rhomb-shape stitches. A rhomb-shape stitch of an EMP is constituted by four bars which have nearly the same geometric dimensions. In order to obtain a larger panel there need to combine several original sheets by using some additional components such as gusset plates with welded, glue or other connection types, etc.

Starting with the idea to apply EMP in structural application, some researches on EMP have been carried out. One of the expected structural applications is to use EMP to retrofit and upgrade existing reinforced concrete frames subjected to seismic excitations. More particularly, it is expected that with the addition of EMP to reinforced concrete moment resisting frames (RC-MRFs), these ones become able to resist shear forces generated by earthquakes.

Until now, the concept of using the EMP as the lateral resisting elements in bracing frames has not been introduced yet. There is even no publication of mechanical properties of the EMP. In order to exploit the EMP to seismically retrofit RC-MRFs, an experimental program has been designed and performed. The final aim is to characterize the behaviour of the EMP subjected to shear loading, which can be similarly regarded as the seismic action.

To experimentally study the overall behaviour of the EMP loaded in shear, mechanical properties of bars forming a rhomb-shape stitch are first determined by doing tensile tests. After that, experiments of EMP in small scale, with the dimensions being less than 1250mm (the originally fabricated dimension of the product), have been performed in monotonic and cyclic shear loading. In practice ordinary spans and story height in RC-MRFs range from (2m x 3m) to (8m x 5m) or even larger. For that reason, it is necessary to combine several EMP to obtain a bigger EMP fitting the real dimensions of the RC-MRFs. Thus, tests of EMP in large scale, which is a combination of several EMP, have been made to realise the monotonic and hysteretic behaviour of EMP loaded in shear and to compare it with the small-scale tests.

Keeping in mind the idea to use EMP in RC-frames to resist lateral forces, the role of EMP will be similar to steel plate shear walls (SPSW) or concentric braces…. Since an EMP geometrically looks like a solid SPSW having a lot of holes causing the large voids or emptiness of the panel, it is expected that EMP work in similar way to SPSW under seismic actions. Therefore, initial approaches to determine the seismic behaviour of EMP have begun with that of SPSW.

As introduced in the previous chapters, the concept of using SPSW as main component against earthquakes has been gained acceptance. A lot of research on SPSW has been carried out in the United States (mostly at University of Berkeley - California), in Japan and in Canada (University of Alberta). Many mid-rise and high-rise structures in several countries have been built using SPSW. According to the development of SPSW in both theory and practice in the 1960s, designers, mainly in Japan, have extensively employed longitudinal and transverse stiffeners of various cross-sections on both sides of SPSW to prevent it from globally buckling. This allows that the yield stress limit of the web material would be reached prior to any lateral buckling of the plates (Timber and Kulak, 1983). The favoured approach of American designers consisted of fewer or no stiffeners. However, a thicker plate was required with the aim to prevent the buckling of the web. Generally, at this stage, all designer tried to exploit the pre-buckling shear resistance of SPSW, and of course, post-buckling resistance of SPSW was always ignored. In 1961, Basler introduced the idea that a thin web can have considerable post-buckling strength. The post-buckling strength depends on the development of a tension field action. In 1980s and 1990s, some studies on post-buckling behaviour of SPSW have been performed at University of Alberta – Canada, at University of Berkeley. A simplified procedure was also proposed for design of SPSW. These

studies have been discussed in detail in Chapter 2. Some essential conclusions can be summarized as follows:

- The contribution of strength of unstiffened SPSW before global buckling can be completely neglected.
- Post-buckling strength of unstiffened SPSW is controlled by the development of tension field action. The angle of inclination of the diagonal tension forces in shear wall web is a function of the column and beam areas, the panel dimensions, and the web thickness.
- Pinching of the force-deformation curve caused by out-of-plane buckling of the steel plate is a typical feature of the hysteretic behaviour of steel plate shear walls.

Based on the results of studies on SPSW, the experiments on EMP have been designed. The dimensions and types of EM are chosen to verify existing expanded metal material. Three parts are presented in this chapter: objectives, design of the experiments and discussions of the results.

4.2. Design Considerations and Objectives of Experiments

The objectives of this experimental investigation are to determine the mechanical characteristics of the EM material, to find the effective types of EM material for structural applications and to examine the performance of the EMP monotonically and cyclically subjected to the shear loading.

In order to reach these objectives, the specimens have to be designed with a number of considerations in mind:

- An EMP is made of a lot of constant rhomb shape stitches, constituted by four rectangular bars. These bars have nearly the same dimensions. The overall mechanical properties of an EMP will be dependent on the properties of the individual bars. Mechanical properties of bars, including elastic modulus, yield stress, ultimate stress, yield strain and ultimate strain, should be characterized by tensile tests.

- There are several types of expanded metal products: normal and flattened types. Amongst all product of EMP, which one can be effective to retrofit and upgrade reinforced concrete moment resisting frames (RC-MRFs)? In order to select suitable types of EMP, the tests in small scale specimens will assess the behaviour and effectiveness of each type of EMP subjected to shear. The test specimens will be chosen so that they will reasonably cover all EMP products. Besides, the test frame has to be designed for many small dimensions of EMP. Moreover, the connection between the specimens and test frame will be considered to choose the connection type for tests in large scale. As the dimensions of a complete EMP are of ±1250mm x ±2500mm, for simplifying the test in small scale, the dimensions of the test frame will be less than the dimensions of an EMP.

- One primary aim of the tests is to determine the ultimate shear resistance of EMP; therefore all components of the tests must be designed in accordance with this ultimate resistance. All mechanical and geometrical properties of all elements of the experiments will be defined by capacity design.

- In order to focus on correctly assessing the only behaviour of the EMP, the test will be designed so that the shear loads from the machine will be entirely transmitted to the EMP.

- The main objective of the experimental studies is to characterize the hysteric behaviour of EMP loaded in shear; therefore tests will be performed in two phases accordingly to ECCS testing procedure (ECCS, 1996): monotonic phase and cyclic phase.

The components of the test setup have been designed. Accounting for all these considerations, the experimental investigation is performed in three stages: (1) tests to determine mechanical properties of EM material; (2) test in small scale specimens and (3) tests in large scale specimens. Figure 4-1 and Figure 4-3 show the overviews of tests in small and large scales.

There are three main components in the tests on EMP, the reaction frame, the force application system (actuator) and measurements. The EMP is connected to the test frames by using gussets called 'intermediate plates'. These plates are connected with the EMP by means of welded or epoxy-glued connections and with test frames by bolt connections.

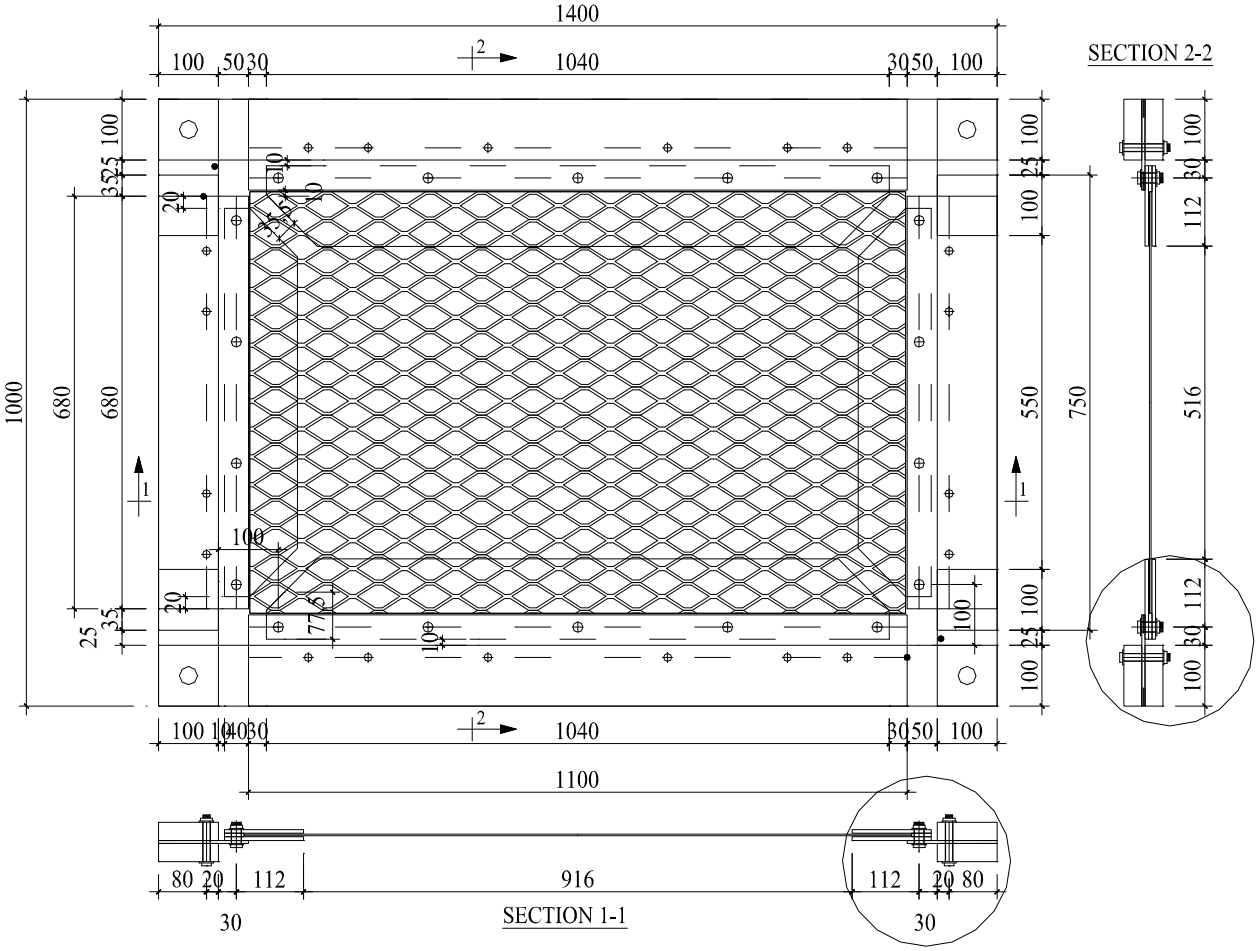

Figure 4-1 – Overview of all components of tests in small scale

4.3. Specimens

As introduced in chapter 3, there are two main types of the EMP, including normal and flatten ones. They are quite different in the geometrical configurations. An EMP has many rhomb-shaped stitches, characterized by four dimensions LD, CD, A and B, as re-shown in Figure 3-2 for the convenience. To distinguish the two types of the EMP, they are labelled according to their geometry. For the flattened type, it is added a letter 'A', representing the 'apati' or flattened EMP. The normal type is named as LD-CD-A-B and ALD-CD-A-B for the flattened type.

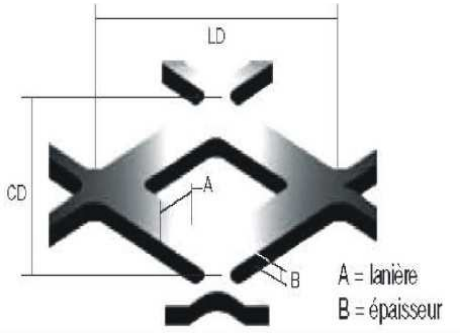

A = width

B = thickness

Figure 4-2 – Geometry of a rhomb shaped stitch

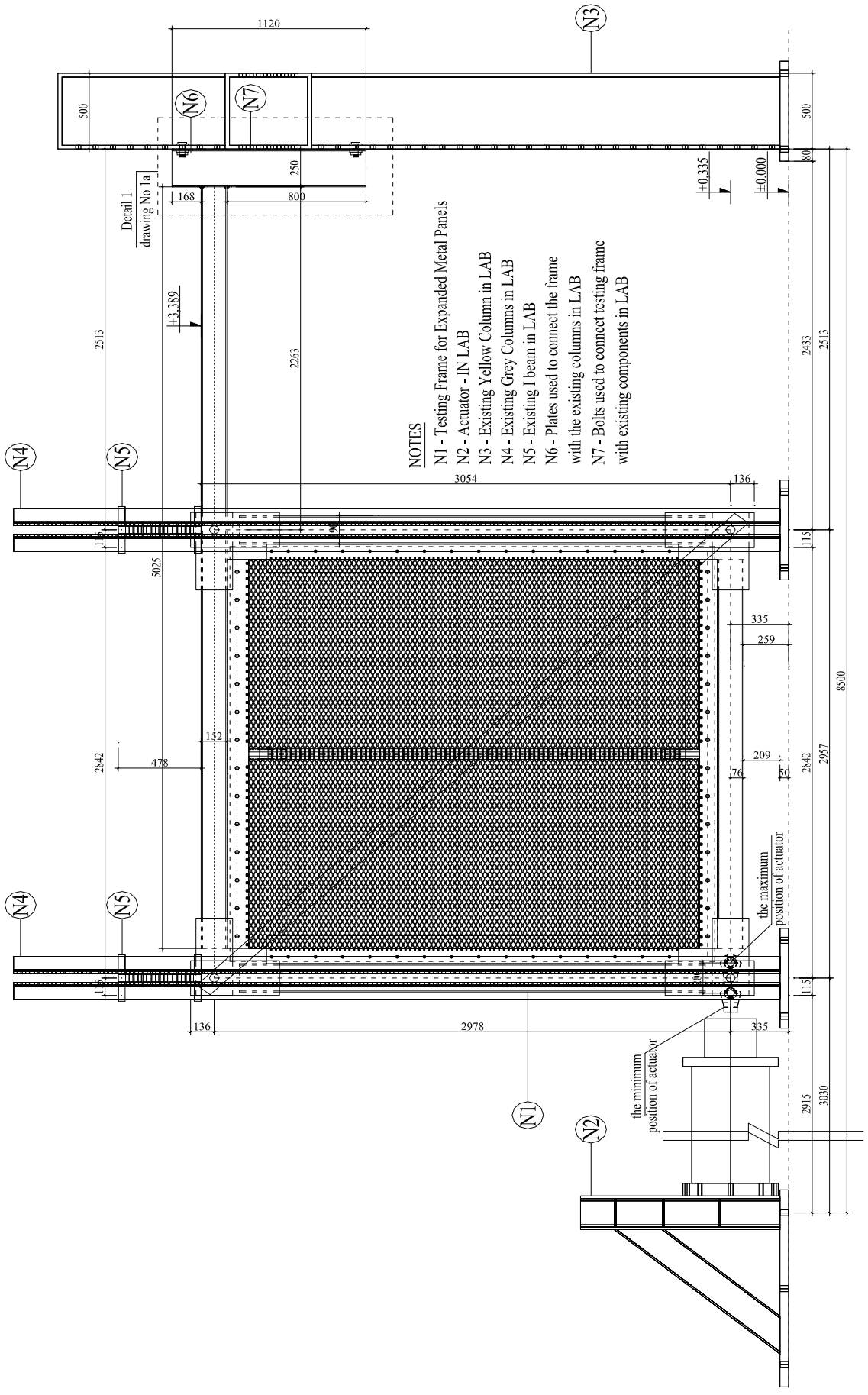

Figure 4-3 – Overview of all components of tests in large scale

4.3.1. Specimens for tensile tests

To do the tests in tension of EMP, 3 rods of each specimen with the length of about 500mm are removed from EMP.

Figure 4-4 shows the specimen prepared for the tensile test.

Figure 4-4 - Specimen for tensile tests

4.3.2. Specimens for shear tests in small scale

In tests in small scale, the largest dimensions are less than the originally fabricated dimensions of EMP, which are of about ±1250mm x ±2500mm or ±3000mm. These tests give flexibility for carrying out a number of preliminary tests to clarify the efficiency of each type of the EMP. They also give an input for assessing the development of overall behaviour of the EMP of the tests in large scale. There are some other considerations when defining test specimens:

- There are many kinds of EMP; therefore specimens should be chosen so that they are easily distinguished and able to represent typical types of the EMP. In addition, in order to compare the behaviour between two types, all specimens should be chosen so that the thicknesses of the bars in all EMP are the same. The EMP specimens of the flattened type include A51-27-35-30 and A86-46-43-30; the specimens of normal type consist of 51-23-32-30 and 86-40-32-30; so in all cases the thickness is 30 x 1/10mm
- As the final objective is to use EMP to seismically retrofit reinforced concrete existing frames, choosing the suitable types of the EMP and types and materials for the connections between the EMP and existing components of the frames is important. Primarily focusing on the pure shear behaviour of the EMP, the connections should be such that they will not fail during the tests. Therefore, the connection should have enough strength, stiffness to resist the ultimate responses generating from the small EMP. Two types of connection material have been studied for test specimens: classical welding and epoxy glue.
- For the tests in small scale, there are two possibilities of connecting the EMP onto the test frame, as shown in Figure 4-5. Particularly, the differences of two directions are the two ways to orient the specimens to the test frame: (1) dimension LD of rhomb shape stitch parallel to the longer dimensions of the frame, (2) dimension LD parallel to the shorter dimensions of the frame. Figure 4-5 presents the two possible directions or orientations.

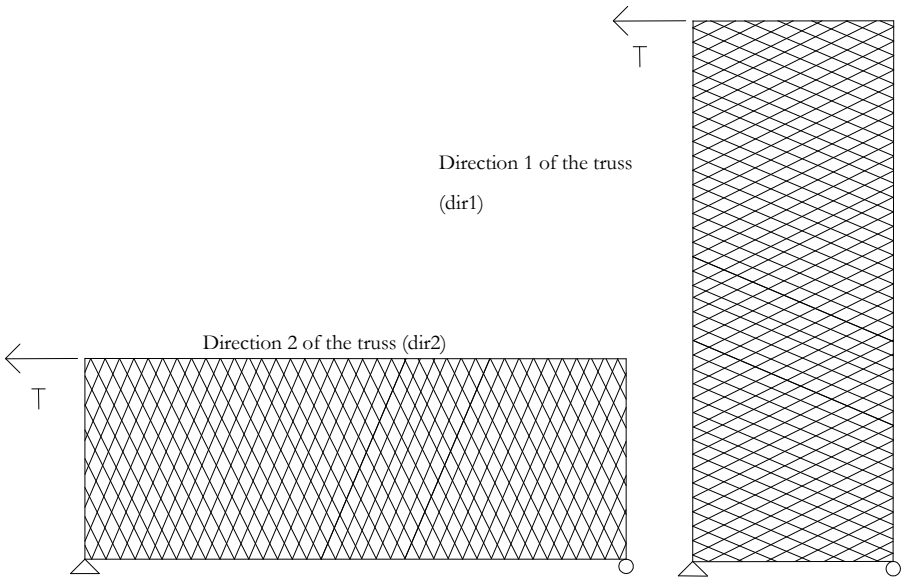

Figure 4-5 – Notions of sheet directions

Taking all considerations into account, the criteria used to clarify test specimens are decided to be the combination of connection types, directions of erecting EMP on test frame and particular name of EMP types. All specimens in small scale tests are summarised in Table 4-1.

Figure 4-6 presents a typical specimen with EMP welded connection before testing. Figure 4-7 and Figure 4-8 show the small EMP with welded and glued connections after connecting the EMP to four gussets.

Figure 4-6 – Overview of specimen A86-46-43-30 dir 1 – welded connections before testing

Table 4-1 – Test specimens in small scale tests

N⁰	Specimens	LD (mm)	CD (mm)	A (mm)	B (mm)	Type of EM	Type of tests	Direction of erection
1	A51-27-35-30 dir1 – welded connections	51	27	3.5	3.0	Flatten	Monotonic + Cyclic	LD // to shorter side of the frame
2	A51-27-35-30 dir2 – welded connections	51	27	3.5	3.0	Flatten	Monotonic + Cyclic	CD // to the shorter side of the frame
3	A86-46-43-30 dir1 – welded connections	86	46	4.3	3.0	Flatten	Monotonic + Cyclic	LD // to the shorter side of the frame
4	A86-46-43-30 dir2 – welded connections	86	46	4.3	3.0	Flatten	Monotonic + Cyclic	CD // to the shorter side of the frame
5	51-23-32-30 dir1 – welded connections	51	23	32	30	Normal	Monotonic + Cyclic	LD // to the shorter side of the frame
6	51-23-32-30 dir2 – welded connections	51	23	3.2	3.0	Normal	Monotonic + Cyclic	CD // to the shorter side of the frame
7	86-40-32-30 dir1 – welded connections	86	40	3.2	3.0	Normal	Monotonic + Cyclic	LD // to the shorter side of the frame
8	86-40-32-30 dir2 – welded connections	86	40	3.2	3.0	Normal	Monotonic + Cyclic	CD // to the shorter side of the frame
9	A51-27-35-30 dir1 – epoxy-glued connection	51	27	3.5	3.0	Flatten	Monotonic + Cyclic	LD // to shorter side of the frame
10	A51-27-35-30 dir2 – epoxy-glued connection	51	27	3.5	3.0	Flatten	Monotonic + Cyclic	LD // to shorter side of the frame
11	A86-46-43-30 dir1 – epoxy-glued connection	86	46	4.3	3.0	Flatten	Monotonic + Cyclic	LD // to the shorter side of the frame
12	A86-46-43-30 dir2 – epoxy-glued connection	86	46	4.3	3.0	Flatten	Monotonic + Cyclic	LD // to the shorter side of the frame
13	51-23-32-30 dir1 – epoxy-glued connection	51	23	3.2	3.0	Normal	Monotonic + Cyclic	LD // to the shorter side of the frame
14	51-23-32-30 dir2 – epoxy-glued connection	51	23	3.2	3.0	Normal	Monotonic + Cyclic	LD // to the shorter side of the frame
15	86-40-32-30 dir1 – epoxy-glued connection	86	40	3.2	3.0	Normal	Monotonic + Cyclic	LD // to the shorter side of the frame
16	86-40-32-30 dir2 – epoxy-glued connection	86	40	3.2	3.0	Normal	Monotonic + Cyclic	LD // to the shorter side of the frame

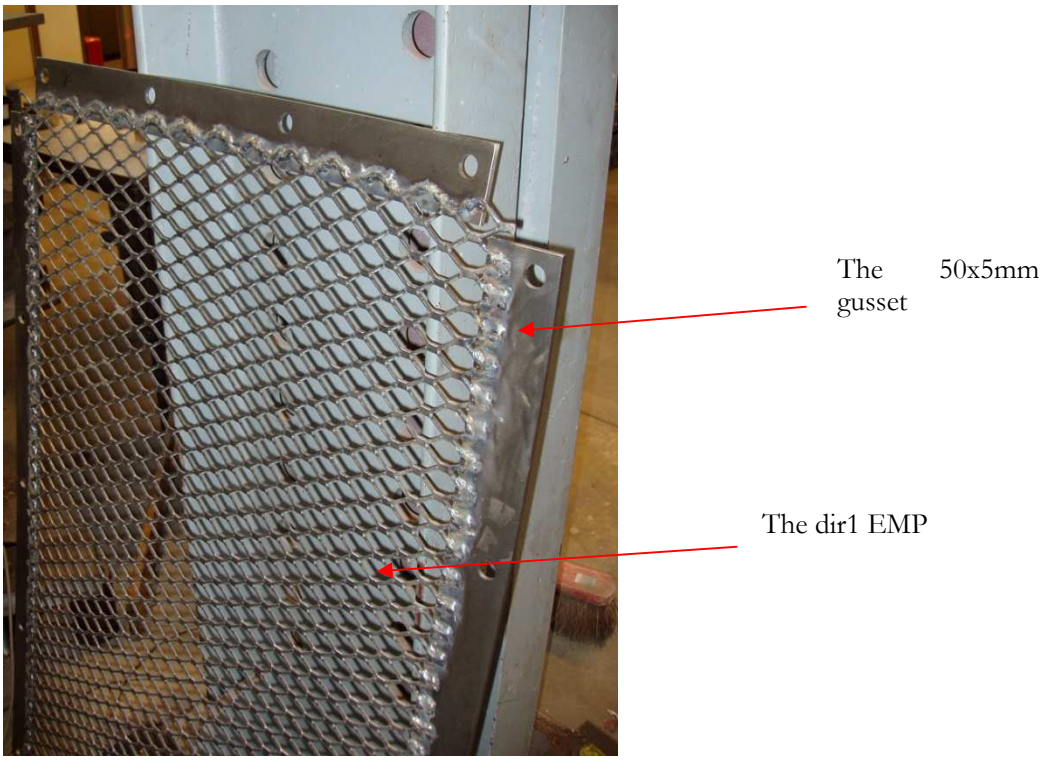

Figure 4-7 – Small EMP specimens – with welded connections

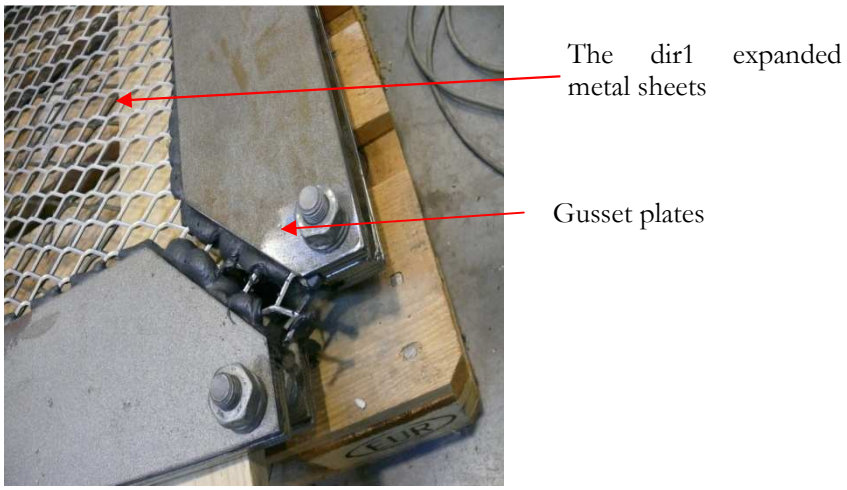

Figure 4-8 – Small EMP specimens – with glued connections

4.3.3. Specimens for shear tests in large scale

The experiments in large scale are carried out after gathering and analysing the data obtained from the results of tests in small scale. Some remarks have been considered when defining the specimens for large scale tests:

- The effective type of EM products to retrofit RC-MRFs: it will be seen later, in both normal and flattened types of EM products, that the flattened type EMP is more suitable for RC-MRFs in terms of strength, stiffness and especially of connections with RC-MRFs than the normal type.

- Overall dimensions of the specimens: the dimensions of an EM sheet are about ±1250mm x ±2500mm (or up to ±3000mm), and the range of dimensions of beam spans and story's heights of RC-MRFs are from (±2000mm x 3000mm) to (±8000mm x 5500mm). It is necessary to combine several EMP to form a complete EMP for real RC-MRFs.

- In accordance with tests in small scale, welded and epoxy-glued connections can effectively be used for connecting EM sheets together and connecting EMP with test frame. However, considering the economical aspects and flexibility to fabricate, welded connections are selected to combine EM sheets together and to connect EMP to the test frame.

- Capacity of testing machine and economical consideration: ultimate shear resistances and ultimate displacements of EMP during the tests are important factors which influence the dimensions and mechanical properties of testing components and the choice of testing machine.

- Connections between specimens and test frame: thanks to the tests in small scale, it can be concluded that welded connections have more advantages than epoxy-glued connections.

Two original EMP are connected together and to test frame by using T-shape steel elements as shown in Figure 4-9 to form a combined EMP. These T-shape steel elements are welded to EMP and bolted to test frame.

It is worth noting that before placing the EMP to test frame, EMP is made to be very stiff by using many additional fish plates. These fish plates are welded to all T-shape steel plates to be sure that there is no initial deformation occurring in EMP because of fabrication or transportation. Test specimens are listed in Table 4-2.

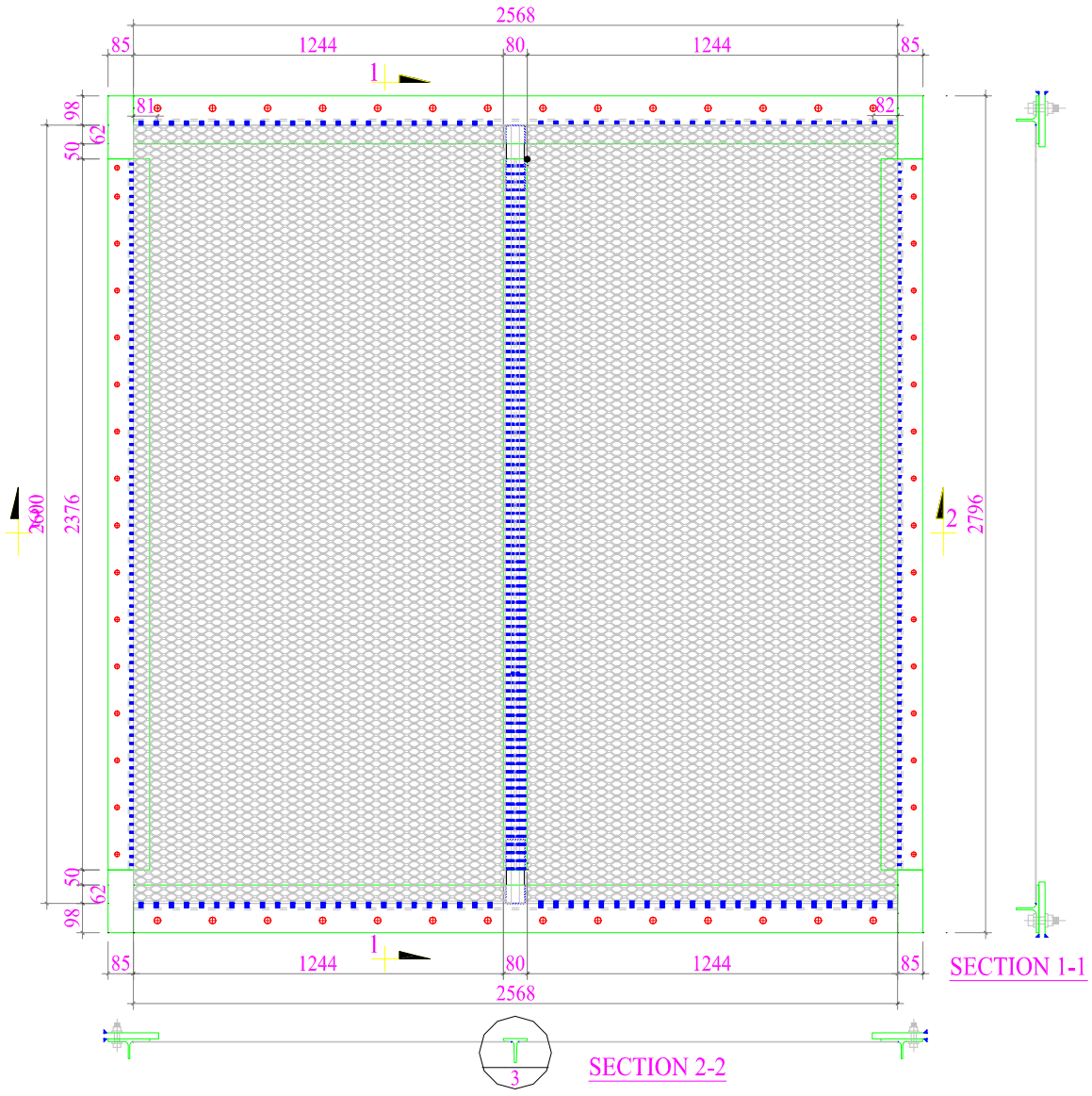

Figure 4-9 – EMP specimen in large scale tests

Table 4-2 – Summary of all specimens in large scale tests

N⁰	Specimens	LD (mm)	CD (mm)	A (mm)	B (mm)	Type of EM	Type of tests	Dimensions of EMP (mm) (width x height)
1	A51-27-35-30 – welded connections	51	27	3.5	3.0	Flatten	Monotonic	2568x2600
2	A86-46-43-30 – welded connections	86	46	4.3	3.0	Flatten	Monotonic	2568x2600
3	A51-27-35-30 – welded connections	51	27	3.5	3.0	Flatten	Cyclic	2568x2600
4	A86-46-43-30 – welded connections	86	46	4.3	3.0	Flatten	Cyclic	2568x2600
5	A51-27-35-30 – welded connections	51	27	3.5	3.0	Flatten	Dynamic	2568x2600
6	A86-46-43-30 – welded connections	86	46	4.3	3.0	Flatten	Dynamic	2568x2600

4.3.4. Test frame

4.3.4.1. Test frame in small scale tests

Only one test frame is used for all specimens of both welded and epoxy-glued connections. The overall dimensions of this frame are constant for all tests. However, because of the differences in the connection materials, the dimensions of EMP specimens of both types are different. This is obvious because the strengths of connection materials are quite different, and it results in a different length of anchorage between EMP and four gussets to be sure that there is no failure in the connection during the tests.

The test frame is defined for stiffness, strength, dimensions, flexibility, suitability for monotonic and cyclic tests, connection between the test frame and EMP.

- The test frame should possess adequate stiffness to resist shear force up to the ultimate load of the biggest commercial EMP without considerable deformations. All the components of the test frame should not deform significantly during all monotonic and cyclic tests so that measured deformations are those of the EMP only.
- Another consideration was the dimensions of the sheared sheets which would influence the dimensions of the test frame. It is good if it is possible to test many various dimensions with different types of small EMP. However, depending on the real largest dimension of EMP which is about ±1.25m width and on the costs of experiments, there were some limitations for choosing sheet dimensions. Additionally, in these testing phases, the focus is on the pure shear behaviour of only the EM sheets without interaction between sheets and frame elements (beams or columns).
- The test frame should be suitable for different types of EM sheets and be convenient for cyclic and monotonic tests. As mentioned above, at this stage, it is not necessary to reproduce true scale tests of building frame, but it is necessary to have enough stitches of the EMP to obtain the global behaviour of the EM sheets, including as well resistance as stability phenomena. Because of that, the test frame must be suitable not only for small rhomb shape stitches but also for the biggest ones. In addition, it is also essential to do tests on squared but also on rectangular sheets with different aspect ratios of EMP.

After assessing many considerations, it has been decided to build a frame with variable dimensions from 400mm x 800mm to 1000mm x 1400mm. Because of construction considerations, dimensions were

variable with a step of 100mm. Figure 4-10 gives a global view of the frame for small scale shear tests in the configuration of the biggest dimensions of specimens.

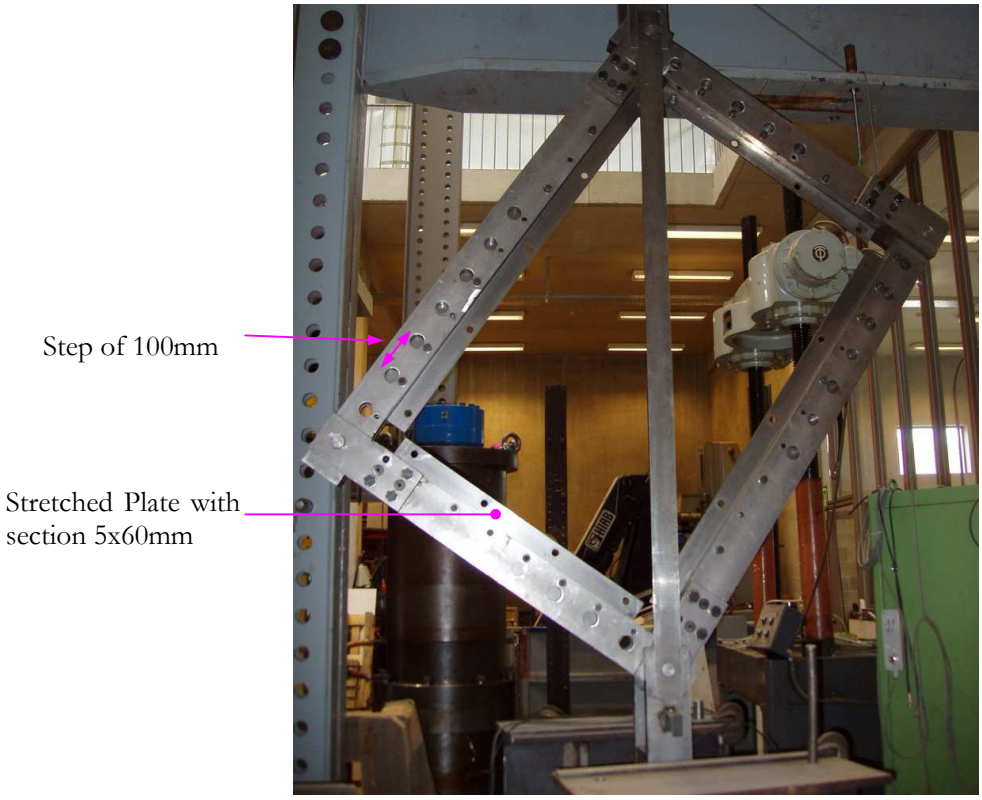

Figure 4-10 - Global view of the test frame for shear tests

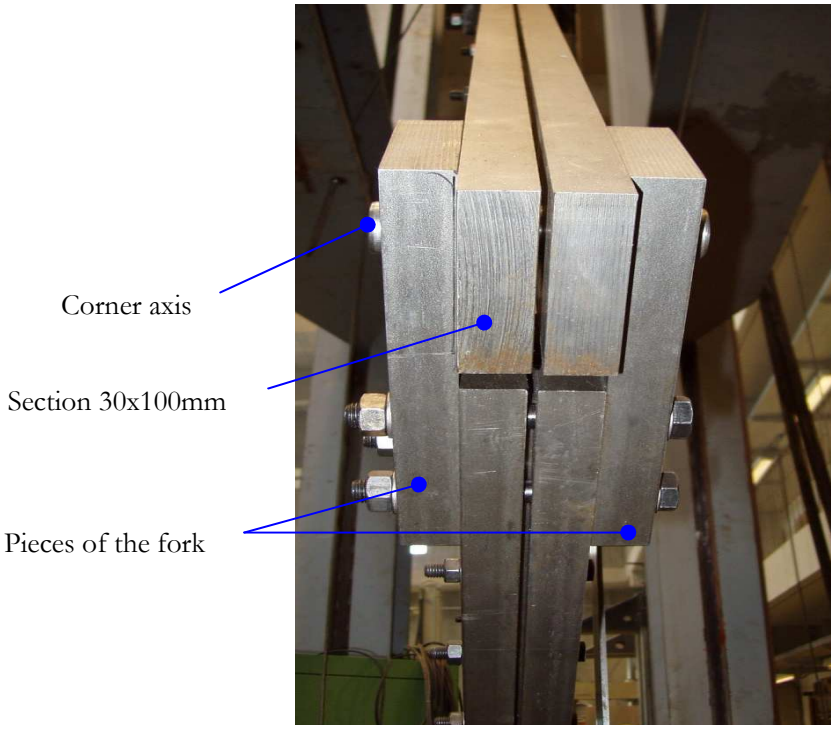

Figure 4-11 – Section of the test frame and joint between two sides of the frame

In the test frame, there are four sides hinged at the corners, and they are connected together by four steel cylindrical axes having a diameter of 30mm. Two forks connect the test frame to the testing machine. To make sure that all hinges rotate freely, four composite rings are placed around the four axes.

Each side of the frame, which consists of two 30x100mm rectangular section bars, is used to stably keep a stretched plate by means of bolts diameter 20mm at 100mm distance. These stretched plates, which have been designed to connect the frame to EMP specimens by bolts diameter 20mm and distances of 250 and 300mm, must be able to resist the same ultimate shear force as the gussets in small EMP specimens. Their section is 50x60mm. With these stretched plates, bolts were used to fix the EMP to the frame without disassembling the whole frame after each test. The diameter and the step of bolts are deliberately determined so that they are stiff enough to sustain the largest shear stresses generated from the sheets. Figure 4-11 presents a view of the loading corners of the frame. It is easy to observe the extremities of the corner axis and the forks that allow superimposing the extremities of two sides to connect them together. The forks also allow changing the frame dimensions flexibly. Additionally, at two of the four corners, which were used to apply the pulling or pushing forces by a jack, additional bigger forks were added around the first forks. They can be observed in Figure 4-12. These additional folks play a very important role in monotonic and cyclic tests, because they not only are used to apply loads but also can prevent the frame from instability when the frame is in compression.

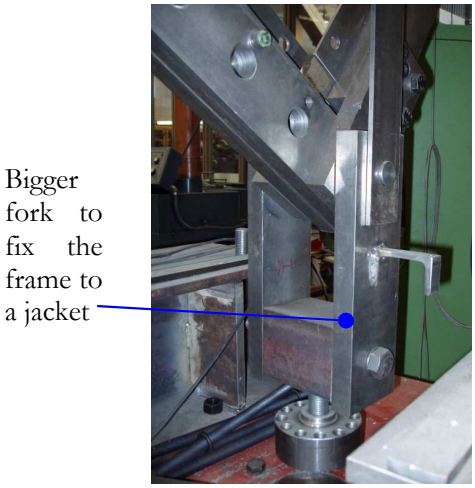

Figure 4-12 – Additional fork for applying force

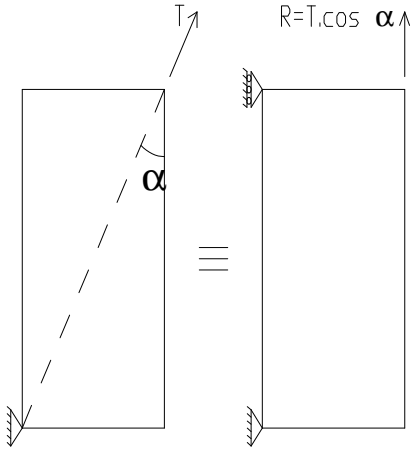

Figure 4-13 – Notions of shear loads acting on the frame

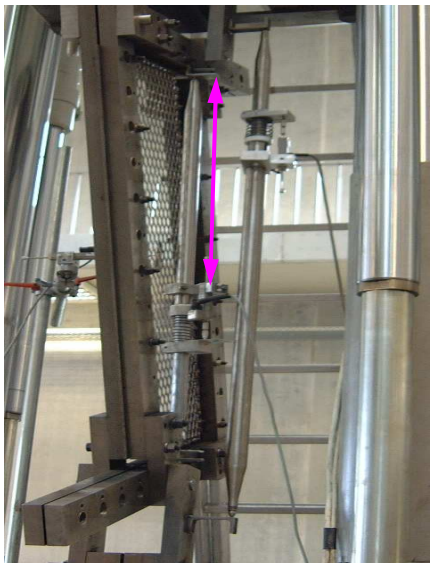

Figure 4-14 – Displacements measurements on an expanded metal sheer test

In order to simplify experiments, the shear forces are applied by a hydraulic jack along just only one diagonal of the frame in both tension and compression directions. In fact, as explained in Figure 4-13, this axial force acting on the diagonal of the frame is equivalent to a direct shear force. With this simplicity, it is easy to achieve both monotonic and cyclic experiments with the fixation of one hinged corner of the frame to the actuator. The opposite hinged corner is pulled only in monotonic tests and pulled/pushed in

cyclic tests. As illustrated on Figure 4-14, the variations of the diagonal length corresponding to each step of increasing force is measured continuously. The applied forces and the displacements in the direction of the diagonal of the frame are recorded at each step. Furthermore, to take into account displacement within the loading system, displacements of the sheet and the jack are simultaneously recorded. The displacements perpendicular to the plane of the sheet at the centre of EMP are not measured because it is not necessary to take into account the out of plane behaviour of the sheets. The testing machine used in the test is SCHENCK 2500kN (the maximum load is 2500 kN).

4.3.4.2. Test frame in large scale tests

Figure 4-15 presents a view of the testing boundary frame with overall dimensions corresponding to the centre lines of the framing members, that is, a bay width of ±2600mm and story height of ±2580mm. These dimensions are chosen to be close to real structural dimensions and account for the real dimensions of EMP while still satisfying the expenses of testing program and constraints imposed by physical space limitations in the laboratory and limitations of testing devices.

The test frame includes two steel columns and two steel beams. The sections of columns and beams are HEA200 and HEA160 respectively. They are hinged to each other by using some additional fish plates and four axes diameters 50mm. Similarly to the tests in small scale, only focusing on pure behaviour of EMP loaded in shear and to be sure that all forces from actuator will be entirely transmitted to EMP, composite rings are placed around all the axes to avoid any friction. Figure 4-16 show the detail of the connection between test specimens and a column of the test frame.

The test frame is constrained laterally by two frames. As shown in Figure 4-15, two frames rigidly fix the test frame so that the top beams are not bent by loads during the tests. The axial forces generated in the columns by vertical components of EMP diagonal tension field are also transmitted to the two frames. The components of the test frame are designed in accordance with EC3 following capacity design referring to the ultimate shear resistance and ultimate displacements of the test EMP. They are also chosen so that they work in the elastic ranges during the tests.

Figure 4-15 – Global view of tests in large scale

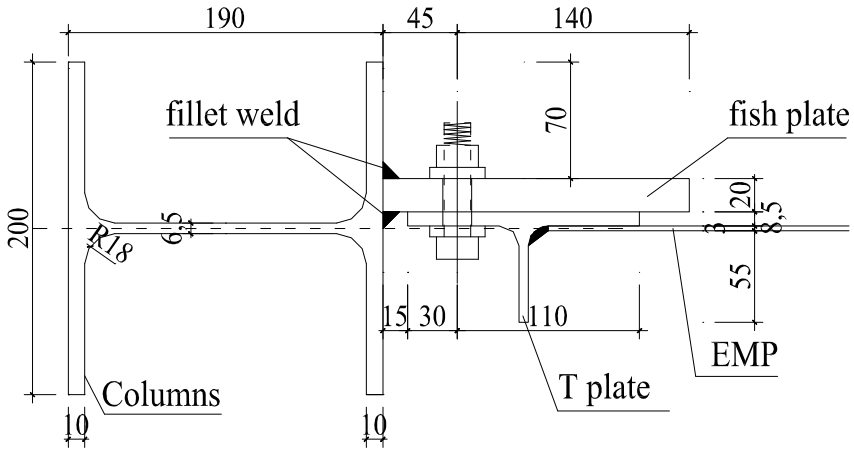

Figure 4-16 – Detail of connection between test frame and test EMP

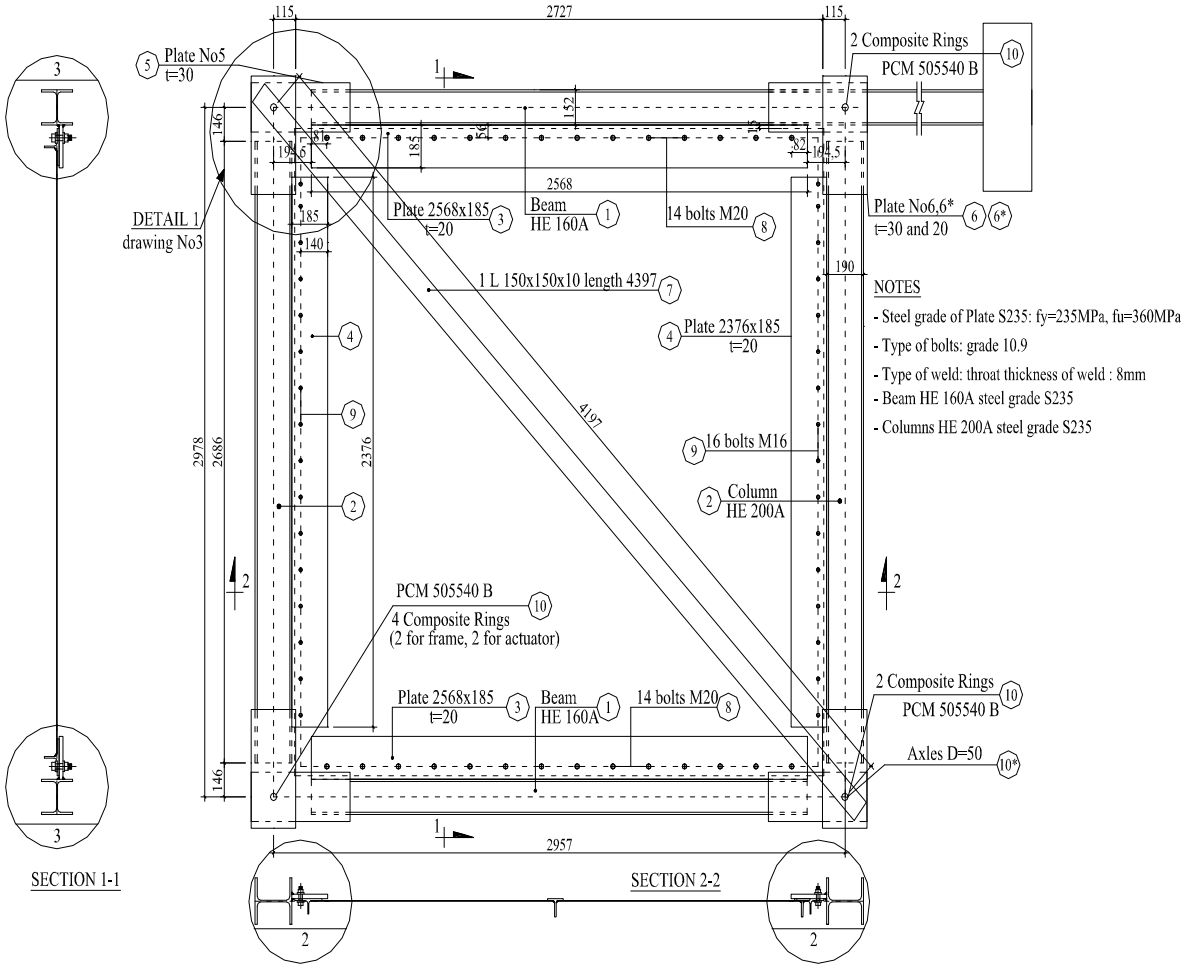

Figure 4-17 – Test frame in large scale tests

4.4. Test procedures

4.4.1. Tensile tests

As presented in the previous sections, tensile tests are used to determine mechanical properties of EM product in general, in particular, initial stiffness and secant stiffness, Young modulus, strain hardening modulus, yield stress, yield strain, ultimate stress, ultimate strain and ductility of the bars in rhomb shape stitches of the EMP are also the primary objectives of tensile tests. All specimens will be pulled until they are completely broken. Force-displacement relationships will be recorded.

4.4.2. Monotonic test phase

Monotonic test mainly aims at determining relationship between shear force and displacement of the EMP. In addition, from the results of monotonic tests, many properties of the EMP specimens will be evaluated to provide data for cyclic test phase such as: monotonic force-displacement curve, conventional limit of elastic range: F_y^+-conventional yielding force and e_y^+-corresponding displacement, and initial stiffness of specimen.

In this phase of experiments, the forces acting on the EMP specimens are monotonically increased until complete failures of the specimens can be clearly observed. The displacements, which correspond to each step of monotonically increasing forces, will be recorded simultaneously. In fact, the monotonic tests should be implemented in two opposite directions: compression and tension. However, because of the symmetry of the expanded metal panels, only the tests of one in two directions will be carried out.

4.4.3. Quasi-static cyclic test phase

The cyclic test procedure is based on the recommendation of ECCS (ECCS, 1996). Cyclic testing phase is divided into two stages. A first stage is a monotonic test used to define the parameters of the cyclic test**.** A second stage is to test the EMP specimens in cyclic loading. First stage procedures are listed in Table 4-3.

Table 4-3 – Exploiting the data from monotonic tests

Step	Descriptions
1	Evaluating the tangent at the origin of the Force-displacement curve; it gives a tangent modulus $E_t^+ = \tan(\alpha_y^+)$
2	Locating the tangent that has a slope of $\frac{E_t^+}{10}$
3	Defining the level of F_y^+ which is the intersection of the two tangents
4	Determining the value of e_y^+ which is the displacement corresponding to that intersection

Second stage could start after having the results from the first stage. In this stage, the EMP specimens will be pulled and pushed successively in many cycles. The tests are run with control displacements. The test procedure of this stage is presented in Table 4-4.

Table 4-4 – Cyclic test procedures

Steps	Applied displacements in tension	Applied displacements in compression	Number of cycles
1	$e_y^+/4$	$e_y^-/4$	1
2	$2*e_y^+/4$	$2*e_y^-/4$	1
3	$3*e_y^+/4$	$3*e_y^-/4$	1
4	e_y^+	$-e_y^+$	1
5	$2*e_y^+$	$-2*e_y^+$	3
>=6	$(2+2n)e_y^+$	$(2+2n)e_y^+$	3

4.5. Test observations

4.5.1. Tensile tests

Figure 4-18 shows the results of six tensile tests of the flattened EMP bars with the length being equal to 500mm. These bars were randomly removed from the original EMP by oxygen cuttings. It should be emphasized that because of the very small dimensions of EMP bars all these tensile tests are not followed by 'standard tests'.

It can be clearly observed on the figure that the mechanical properties of the EMP vary largely including yield stress, yield strain, maximum stress and maximum strain. These variable characteristics of the EMP lead to large differences in its strain and displacement ductility, ranging from 2 to 10. Apparently the EMP is not a constant mechanical product as warned by the fabricators. In addition, an interesting and useful observation in these tensile tests is that there was no failure or fracture at the end of bars. Before fracture, the section of the broken bar has been reduced visibly.

The assumed mechanical properties and stress-strain relationship of an EM bar are shown in Table 4-5.

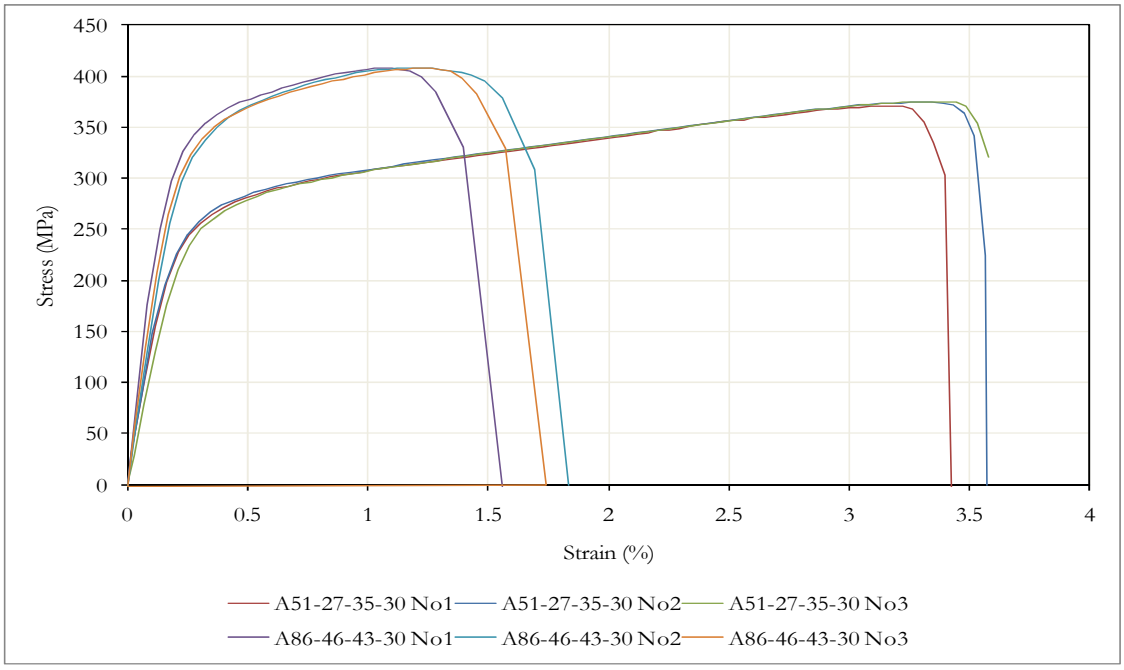

Figure 4-18 – Tensile tests and proposed stress-strain curves for EM products

Table 4-5 – Typical mechanical properties of an EM bar

Elastic Modulus - E_{EM} (MPa)	Yield Stress (MPa)	Yield Strain (%)	Strain Hardening Modulus (E_{strEM}) (MPa)	Ultimate Strain (%)	Ultimate Stress (MPa)
134800	337	0.25	1169	3.5	375
134800	350	0.35	4444	1.7	410

4.5.2. Small scale tests

4.5.2.1. Monotonic loading test phase

General features

It should be noted that there is a series of monotonic tests in small scale. Both welded and glued connection specimens have been tested. The overall dimensions of the rectangular EMP are 660mm x 1056mm.

Under monotonic loading up to the failure, it can be observed that the behaviour of all test specimens can be divided into an elastic stage and a plastic stage. The elastic range starts from the beginning of a test until reaching yield displacement. These yield deformations of all specimens range from 0.85mm (0.12% drift) to 1.17mm (0.18% drift), as shown in Table 4-6. Beyond the elastic range, all the small EMP specimens perform plastic deformations until attaining ultimate displacements. During the plastic deformations the section area of bars reduces and the slope of force-displacement curves decreases considerably.

In all tests, there are four couples of two similar tested EMP in eight test specimens. In a couple, the expanded metal profile is the same. They are different in the way of placing them into the test frame, as shown in Table 4-1 and re-explained in Figure 4-19. Because of this difference, the values of yield displacements, yield force, ultimate displacements and ultimate shear force of each specimen in each couple are slightly different.

Figure 4-19 – Two possibilities of placing the EMP into the test frame: Direction 1 – Left; Direction 2 – Right

In all the specimens, there are visible out-of-plane deformations. These initial buckling deformations are different in each specimen. They become much clearer after rather low shear forces are applied. The shapes of buckling waves, as shown in Figure 4-20, are nearly the same for all testing small EMP specimens. Although the sheets are prone to global buckling, there is no buckle of individual bar observed from the beginning to the end of the test.

The first broken bars observed in all tests are located at the diagonal corners. The section areas of these bars are clearly decreased before being broken. In spite of the fact that some bars are broken, the sheets keep carrying shear forces. It is also observed that after each bar is broken the shear force is suddenly reduced and then increased until the sheets are completely broken. The broken bars first appear at the corners of the test frame and then spread gradually to the centre of the sheets.

All the tests are stopped because small EMP specimens have been largely deformed. There is no failure either at the weld connections between the expanded metal panels and the plates or at the bolt connections between sheet-plates and intermediate-plates.

Particular features:

The normal type of tested specimens buckles more rapidly than the flattened type. The shear forces causing buckling in normal type specimens are lower than in flattened types. In each expanded metal type, the ultimate shear forces are proportional to the section area of bars and inversely proportional to the voids of the sheets. The initial stiffness of normal types is much lower than that of flattened types.

Although ultimate shear forces in normal type specimens are less than those in flattened types, the corresponding displacements in normal types are much greater than that in flattened types. Apparently, normal type specimens are more ductile than flattened type specimens. Ductility factors of normal types are twice greater than those of flattened types.

Figure 4-20 – Buckling shapes after testing of specimens

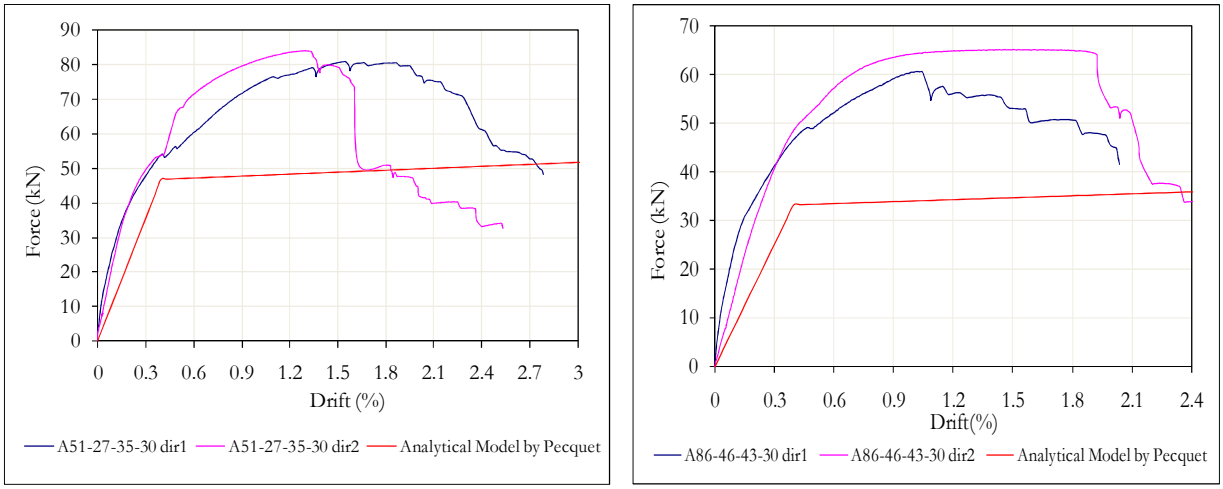

Figure 4-21 – Force–drift curve in monotonic tests of flattened types and analytical model by Pecquet (2005)

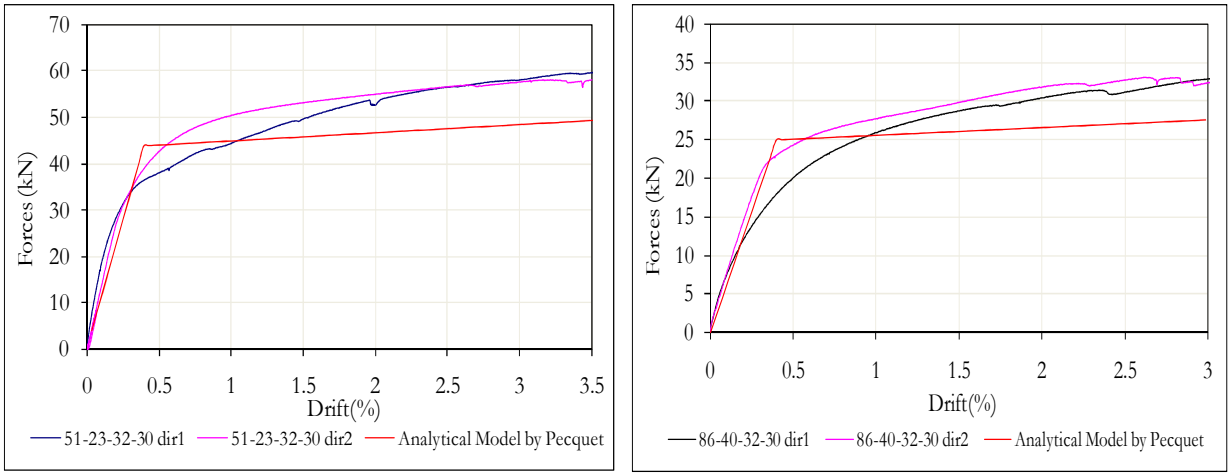

Figure 4-22 – Force–drift curves in monotonic tests of normal types and analytical model

Table 4-6 – Monotonic test results in small scale – weld specimens

Specimens	Yield force (kN)	Yield displacement (mm)	Yield Drift (%)	Initial Stiffness (kN/mm)	Ultimate shear force (kN)	Ultimate displacement (mm)	Ultimate Drift (%)
1	33.4	1.00	0.14	33.4	78.9	09.4	1.35
2	32.2	1.00	0.14	32.2	83.7	08.7	1.25
3	27.9	0.85	0.12	32.8	60.8	07.1	1.02
4	25.9	1.17	0.17	22.1	65.0	08.3	1.2
5	27.3	1.30	0.18	21.0	60.6	25.7	3.7
6	18.0	0.90	0.13	20.0	57.5	20.3	2.9
7	09.3	0.93	0.13	10.0	31.3	15.6	2.24
8	10.2	0.93	0.13	11.0	32.3	15.7	2.26

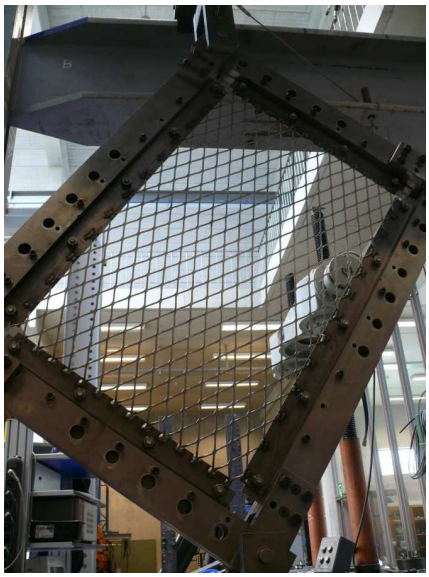

Figure 4-23 – Global view of the specimen A86-46-43-30 dir2 before testing

Figure 4-24 – Broken bars appeared in the monotonic test of specimen A51-27-35-30 – direction 2

4.5.2.2. Cyclic test phase

It should be recalled that there are two series of cyclic tests in small scale, which are distinguished by the differences of the connections between EMP and the intermediate plates to form test specimens, as explained in the previous sections. The first tests have welded connections with the overall dimensions of EMP about 695mm x 1095mm but the effective dimensions of rectangular EMP only about 660mm x 1056mm. The others have epoxy-glued connections with the bounding dimensions of EMP about 695mm x 1095mm but the effective dimensions of rectangular EMP only about 516mm x 916mm.

The effectively working dimensions of the specimens have been reduced because of the connection lengths, which must be long enough to resist the tensile and compressive axial forces generated in the bars of the EMP during the test. Thus, although two series of tests share the same test frame, which has the dimensions of 1000mm x 1400mm, and have the same overall dimensions of small EMP, the effective dimensions of EMP in welded connections and glue connections are 660mm x 1056mm and 516mm x 916mm, respectively. There are eight specimens for a series of tests. The main characteristics of tests are given from Table 4-7 through Table 4-11.

General features

There are several common features observed rather clearly in cyclic tests of the two series of specimens: weld and epoxy-glued specimens. They are discussed in detail hereafter.

First, all specimens in both series of tests behave elastically in the first four cycles until reaching a yield displacement which is also nearly the same as the yield displacements in monotonic tests. In the elastic range, the behaviour of all specimens looks not completely symmetric. The reasons for this physical phenomenon are the initial deformations of small EMP specimens leading to some initial stress and the very small displacements of EMP in this stage. Displacements of the jacks and of the EMP are much different. Beyond the elastic range when the displacements become larger, the hysteric loops are more symmetric, as seen in Figure 4-26 and Figure 4-27.

Second, initial out of plane deformations are observed in most of EMP specimens before testing. These deformations are unavoidable because of very thin sheets. In addition, it is impossible to constantly keep EMP specimens absolutely flat during fabricating processes, especially on specimens of welded connections. In some specimens, these phenomena become clearer after low shear forces are applied to the sheets, like in the monotonic tests. Out of plane deflections of the sheets become larger and larger in successive cycles.

Third, in all monotonic tests, there is no instability of individual bar. The same states of the bars are also observed in first four cycles in quasi-static cyclic tests. However, when reaching yield displacements and up to the occurrences of first broken bars, instability phenomena of bars are clearly observed in most of welded specimens. This phenomenon is also observed in the tests of epoxy specimens, but much later, mostly at the stage of near failure of the specimen. The buckled bars are located close to the connections between the EMP and the gusset plates. In addition, the section areas of all the buckled bars are visibly reduced.

Fourth, likewise monotonic tests, all first broken bars, as shown in Figure 4-25, are located at four corners of the test frame, and before being broken their section areas are considerably reduced. It is also observed that the crack directions in all cyclic tests start at four corners and then progress to the centre of the sheets to form four crack lines. It is worth noting that, in almost all cyclic tests, the maximum shear force is attained on the cycle in which the first broken bars have appeared.

Fifth, during first four cycles of both test series, the behaviour of the small EMP specimens is linear. From fifth cycle to the end of the tests the shapes of hysteretic behaviour of the small EMP specimens are stable S-shapes. Hysteretic loops in all specimens are characterized by strong pinching. Pinching effects are due to the global instabilities of the small EMP specimens, which cause large degradation in both stiffness and strength of the sheets. Like in monotonic tests, tension bands are developed in sheets in every cycle. In addition, before redeveloping new tension band the stiffness of the sheets is approximately equal to zero in the other diagonal, which results in the pinching observed in diagrams.

Sixth, as observed in monotonic tests, if two specimens have the same profiles but are different in the way of setting up to the test frame, their behaviour is not much different. In cyclic tests, their behaviour is very similar in the first four cycles. It means that in these cycles, the sheets are in the elastic range. However, in the plastic range, the hysteretic curves are slightly different, particularly when reaching the ultimate displacements. The values of ultimate characteristics and number of hysteretic cycles are similar in these couples of specimens. This means that the numbers of rhomb-shaped stitches in EMP play a crucial role in its ultimate responses.

Seventh, one significant feature of hysteretic response of the EMP, which is observed in all tests, is the strong pinching effect. This is caused by the easy out-of-plane deformation of the EMP due to very small value in thickness and low yield stress. The imminent buckling and low yield point could lead to the very limited elastic stiffness and in most of cases the resistance before buckling has no meaning to the overall resistance of the EMP. In addition, in cyclic tests, when the loads are reversed, the EMP can immediately buckle in the opposite directions, compared to the previous loading. This is the reason of decreasing both stiffness and strength.

Finally, from the beginning to the end of the tests, there has been no failure either at the welded connections or epoxy-glued connections between the expanded metal panels and the test frame. Furthermore, it is also observed that there is no failure on the test frame.

Particular features

There are also some particular features depending on each type of specimens and on connections used to link the test frame and the specimens. They are debated as follows.

First of all, it is clearly observed in all tests that the ultimate characteristics (force and displacement) of the specimens are completely dependent on the geometrical configurations of the specimens. Having the same dimensions of EMP, however, due to the use of different connection material leading to the different connection lengths (to be sure that EMP has been firmly connected to the test frame) and to the differently effective dimensions of the EMP, the maximum loads of the epoxy-glued specimens are less than that of specimens using weld connections.

Table 4-7 – First four cycle results of specimens with welded connections

Specimens	Monotonic yield force (kN)	Monotonic yield displacement (mm)	Monotonic yield Drift (%)	Forces at fourth cycle (kN)	Displacements at fourth cycle (mm)	Drift at fourth cycle (%)
1	33.4	1.0	0.14	30.4	1.01	0.15
2	32.2	1.0	0.14	31.1	1.02	0.15
3	27.9	0.85	0.12	20.2	0.88	0.13
4	25.9	1.17	0.17	24	1.10	0.15
5	27.3	1.3	0.18	23.4	1.01	0.15
6	18.0	0.9	0.13	19.0	1.00	0.15
7	9.3	0.93	0.13	10.1	1.20	0.17
8	10.2	0.93	0.13	11.0	1.29	0.19

Table 4-8 – Cyclic test results at displacements corresponding to maximum resistance in monotonic tests – welded specimens

Spe.s	Mono. Max. shear resistance (kN)	Corres. Disp. (mm)	Corres. drift (%)	Corresponding shear force (kN)	Disp. at relatively corresponding to monotonic test (mm)	Corres. drift (%)	No. of cycles (cycles)
1	78.9	9.4	1.35	56.0	9.8	1.41	23
2	83.7	8.7	1.25	74.0	9.7	1.40	14
3	60.8	7.1	1.02	42.5	8.7	1.30	20
4	65.0	8.3	1.2	43.3	9.3	1.34	11
5	60.6	25.7	3.7	15.5	20.9	3.0	32
6	57.5	20.3	2.9	40.5	20.4	3.0	12
7	31.3	15.6	2.24	23.2	14.5	2.1	11
8	32.3	15.7	2.26	28.9	14.5	2.1	14

Another important point is that the buckled bars in the tests using the welded connection has appeared much sooner that that using the epoxy-glue connection. Moreover, in the epoxy-glued specimens this phenomenon has been observed when these bars have been performed high plastic deformations. These buckled bars, only observed in welded specimens, are located almost at the boundary of the specimens, close to connections. On the other hand, they are scattered largely in tests of epoxy-glued specimens. This could be explained by the stress concentration and greater residual strains at the connection due to welding.

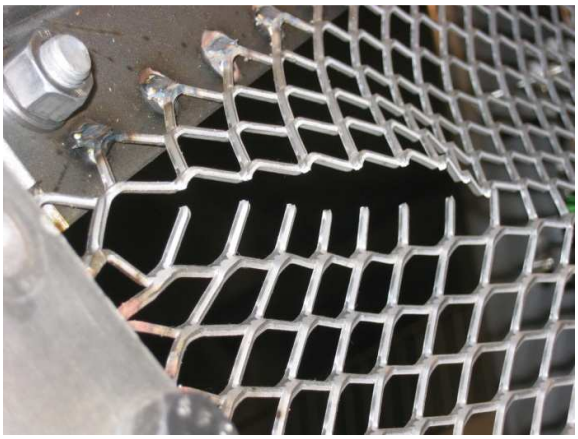

Figure 4-25 – Crack line and broken bars

Table 4-9 – Maximum shear resistance in cyclic tests and corresponding displacements – welded specimens

Specimens	Cyclic maximum shear resistance (kN)	Cyclic corresponding displacements (mm)	Cyclic corresponding drifts (%)	Number of cycles (cycles)
1	71.6	08.3	1.20	20
2	-75.6	-16.9	2.40	16
3	-48.2	-20.2	2.90	26
4	-49.3	-14.8	2.10	13
5	-48.0	-07.3	1.10	14
6	-45.0	-07.0	1.00	10
7	27.0	09.3	1.33	8
8	-28.0	-10.8	1.56	12

Table 4-10 – First four cycle results of specimens with epoxy-glued connections

Specimens	Forces at fourth cycle (kN)	Displacements at fourth cycle (mm)	Drift at fourth cycle (%)
9 – glue connections	39.4	0.80	0.15
10 – glue connections	36.0	1.10	0.22
11 – glue connections	49.0	0.80	0.15
12 – glue connections	43.9	1.20	0.22
13 – glue connections	42.7	1.20	0.22
14 – glue connections	24.0	1.76	0.34
15 – glue connections	20.2	1.40	0.31

Comparing the responses of two types of EMP, as shown in Table 4-8 and Table 4-9, the number of cycles in hysteretic behaviour of flattened expanded metal types and the energy which is dissipated are greater than that of normal types. It is also observed that out of plane deformations at failure of normal type specimens are much greater than those of flattened specimens, leading to the lower ultimate strength of that EMP. As shown in Figure 4-26 and Figure 4-27, pinching is larger in the flattened type than in the normal type specimens.

Another significant feature is that the maximum loads of the flattened EMP are on average 25% higher than that of the normal EMP. Besides, it has been much easier to connect the flattened type to the test frame by using weld connection than the normal type. These two features could make the advantage of the flattened type over the normal type.

Table 4-11 – Cyclic testing results at displacements corresponding to maximum resistance in monotonic tests – epoxy-glued specimens

Specimens	Cyclic maximum shear resistance (kN)	Cyclic corresponding displacements (mm)	Cyclic corresponding drifts (%)	Number of cycles (cycles)
9 – glue connections	77.2	4.5	0.80	11
10 – glue connections	90.5	5.7	1.10	11
11 – glue connections	66.2	4.2	0.99	11
12 – glue connections	54.4	7.1	1.40	11
13 – glue connections	51.0	6.1	1.14	8
14 – glue connections	30.7	8.3	1.60	8
15 – glue connections	31.1	6.0	1.20	8

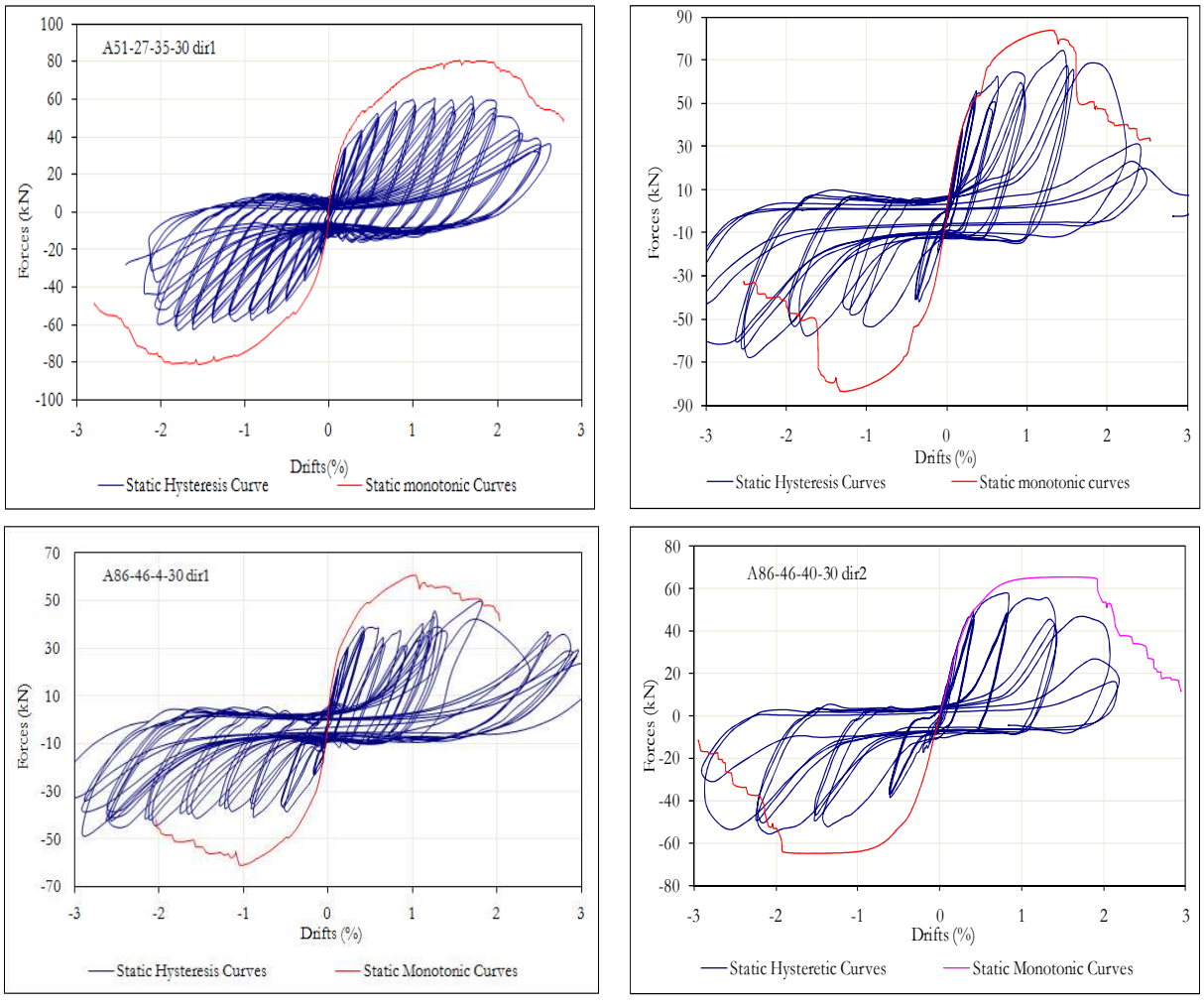

Figure 4-26 – Hysteretic behaviour of flattened type specimens

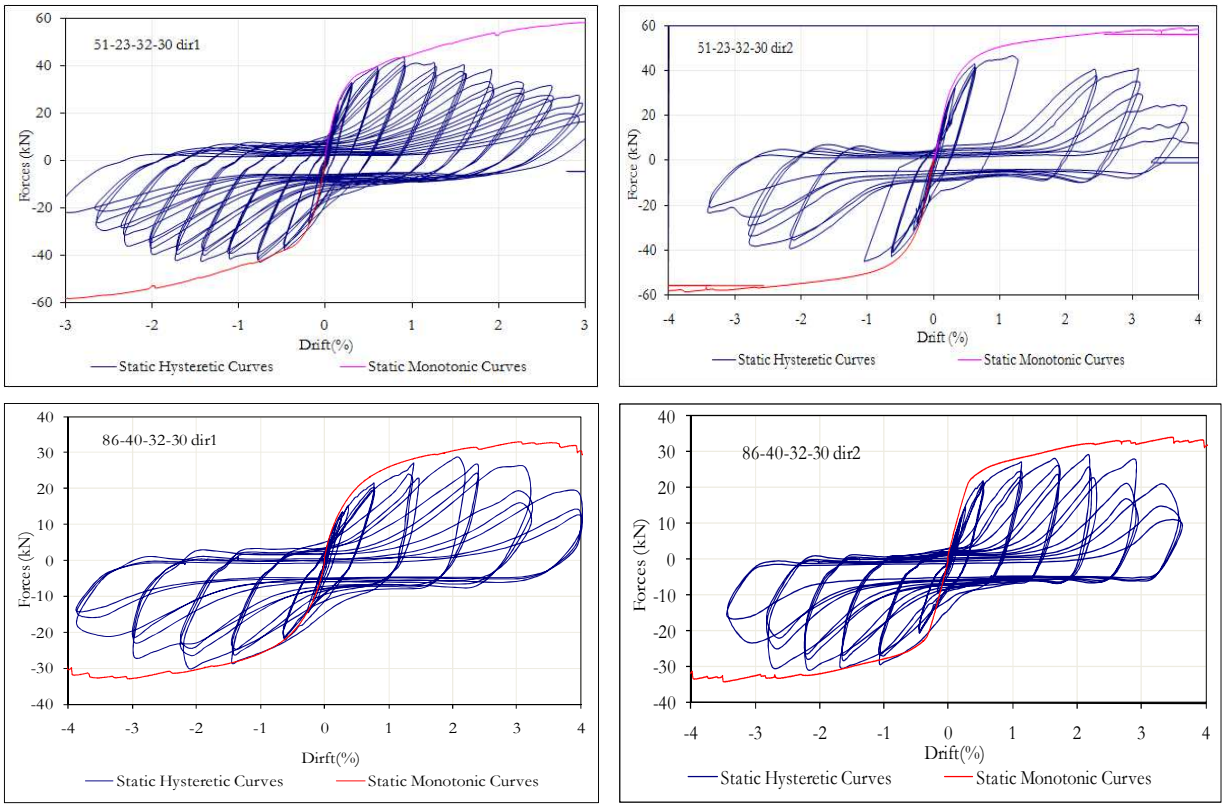

Figure 4-27 – Hysteretic behaviour of normal type specimens – weld connection

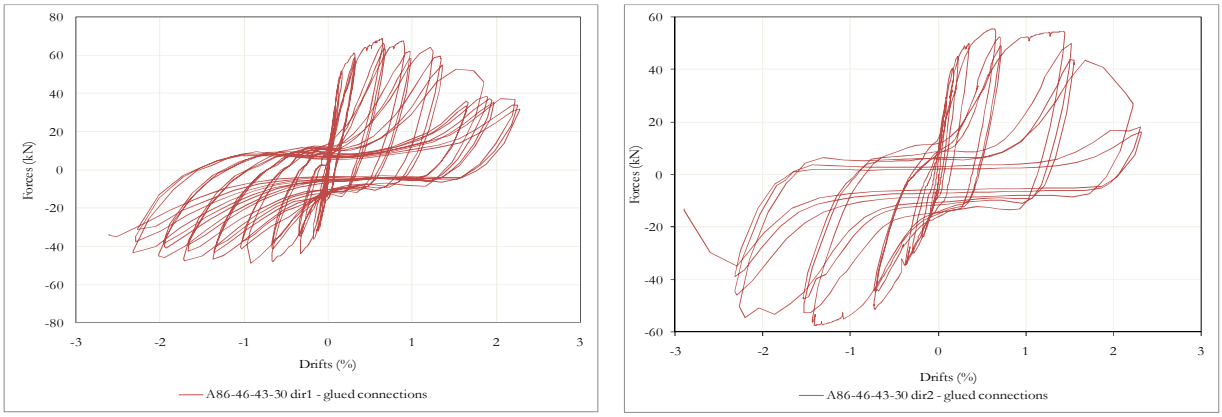

Figure 4-28 – Hysteretic behaviour of flattened type specimens – glue connections

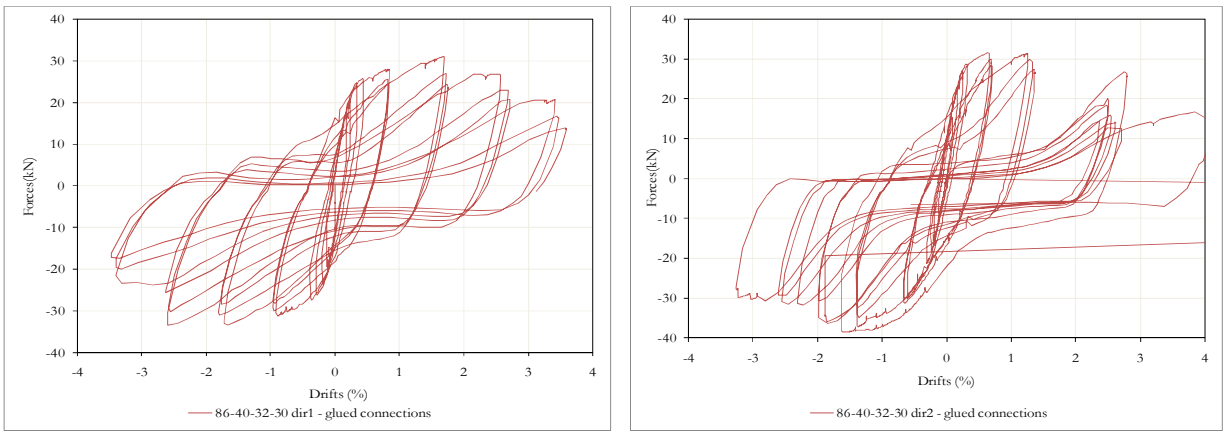

Figure 4-29 – Hysteretic behaviour of normal type specimens – glued connections

4.5.3. Tests in large scale

4.5.3.1. Monotonic loading phase

Like in the tests in small scale, monotonic tests in large scale have been carried out with the aims at determining the parameters for quasi-static cyclic and dynamic tests, at assessing the ductility of the EMP and at comparing with numerical simulations of test specimens. As mentioned, there are two tests in monotonic phases corresponding to two products of the flattened EMP: A51-27-35-30 and A86-46-43-30. This type of EMP has been chosen thanks to its advantage over the normal type such as higher stiffness and strength, and more importantly easier in connecting the EM sheets and the intermediate plates to form the complete EMP. The results of the tests are shown in Table 4-12, Figure 4-30 and Figure 4-31.

General features

In general, the overall behaviour of the specimens in large scale tests is somehow similar to those of small scale tests. However, there has been a rather large difference in ductility. The ductility of the material and of the EMP in large scale tests is lower than in small ones. In tensile tests of bars removed from the commercial profiles prepared for small scale tests, the strain ductility has been about 6 to 10. Nevertheless, in the bulk of EMP profiles for tests in large scale, the strain ductility has been about 2 to 5. This is, of course, not much surprising because, as mentioned before, EMP is not a material having the constant mechanical properties and the panels delivered for large scale tests are different from those delivered for small scale tests.

Some common features of the tests in large scale are discussed hereafter in comparison with the results from the tests in small scale.

A first general point, which has been easily seen, is that in both type of specimens, the out of plane deformations are clearly observed before testing. The initial out of plane deflection of the specimen A86-46-43-30 is greater than that of the specimen A51-27-35-30. One can deduce that the larger the voids of EMP, the bigger the out of plane deformations are. Furthermore, these deformations become much clearer when applying very low shear loads. All of these physical phenomena are similar to those of tests in small scale. However, the buckling shapes of EMP in large scale tests are quite different from the small ones, as clearly observed in Figure 4-20 and Figure 4-30. It can be explained that because two sheets of EMP panels are connected together by using a stiff T-shape steel element at the middle of EMP, as shown in Figure 4-9, the latter more or less prevent EMP from buckling. Therefore, two sheets of EMP will be buckled with two separate shapes.

The second feature, as observed from the beginning to the end of all tests, is that the behaviour of the specimens is similar to one in monotonic tests of small scale. It can also be divided into two ranges: nonlinear elastic and nonlinear plastic ranges. The yielding points of the tests cannot be clearly defined. Based on the instruction of ECCS (1986), two stiffness tangents of load-displacement relationships are located, and conventional yielding displacements and yielding loads are approximately determined. It is worth noting that both elastic and plastic behaviour of the specimens are nonlinear. Table 4-12 summarises all considering properties of the tests. The yield forces of two tests of A51-27-35-30 and A86-46-43-30 are 140kN and 90kN in order. The yield displacements of these two tests are 23.0mm (0.9%) and 23.6mm (0.99%), respectively.

Table 4-12 – Monotonic test results in large scale

Specimens	Yield force (kN)	Yield displacement (mm)	Yield Drift (%)	Initial Stiffness (kN/mm)	Maximum shear resistance (kN)	Ultimate displacement (mm)	Ultimate Drift (%)
1 – A51-27-35-30	140	23.0	0.90	6.1	190.4	47.8	1.9
2 – A86-46-43-30	90	23.6	0.99	3.8	111.1	35.3	1.5

Although yielding properties of tested EMP are not easily determined, maximum shear loads and corresponding transversal displacements of EMP are easier observed. After reaching maximum shear forces, it can be seen that the stiffness and strength of the specimens decrease a lot. Regardless of the large degradation in stiffness and strength, the displacements of the EMP are still increased until reaching maximum displacements, which are about three to five times greater than yielding displacements. The shear loads, which correspond to maximum displacements, are about 65% of ultimate loads.

Likewise the tests in small scale, the first broken bars observed in all monotonic tests are located at the two corners of the two sheets of test EMP, which are right-lower corner of the specimen A51-27-35-30 and left-upper corner of the specimen A86-46-43-30. In addition, the section areas of these bars, which are in tension, are clearly decreased before being broken. In spite of the fact that some bars are broken, the test EMP keeps carrying shear forces until failure. It is also observed that after each bar is broken the shear force is suddenly reduced and then increased until the sheets are completely broken. On the other hand, not like in small scale when the broken bars first appear at the corners of the test EMP and then spread gradually to the centre of the sheets, in large scale test all broken bars have been mostly located at the boundary of the EMP, as seen in Figure 4-31. As in small monotonic tests, though the EMP is prone to global buckling, no buckling of individual bar is observed.

Finally, all the tests are stopped because the small EMP specimens have been largely deformed, and tensile strips are broken. At failures, large out of plane deformations in both specimens are clearly observed. There is no failure either at the weld connections between the expanded metal panels and the plates or at the bolt connections between sheet-plates and intermediate-plates.

Figure 4-30 – Global buckling shapes of two sheets of the EMP panel

Figure 4-31 – Broken bars in monotonic large scale tests

Particular features

The initial out of plane deformations of the specimen A51-27-35-30 are much less than those of the specimen A86-46-43-30. It is obviously because with the same thickness of the EMP, the voids of A86-46-43-30 are much greater than the voids of A51-27-35-30. This leads to the greater numbers of rhomb-shape stitches in the specimen A86-46-43-30 and to the greater stiffness of A51-27-35-30 despite having the same thickness.

As seen in Table 4-12, the maximum shear forces and maximum displacements of EMP are inversely corresponding to the voids of EMP. The voids of the specimen A86-46-43-30 are greater than that of A51-27-35-30, whilst the maximum shear forces and displacements are in contrary.

Specimen 1 - A51-27-35-30

Before setting up the specimen into the test frame, it is easy to observe that there are some out of plane deformations. These deformations are present on the sheet because of welding connections between expanded metal sheet and the gussets. At the beginning of the test, corresponding to the very small values of displacements and shear forces (less than 23,0mm – 0.9% drift and 140kN), the behaviour of the specimen is mainly elastic. Moreover, at this initial part of the test, it is clearly observed that global instability of the sheet has appeared with buckling waves. These waves are parallel to tension diagonal. After global buckling, the applied forces and displacements are increased and the sheet develops a visible tension diagonal field until the specimen is completely broken. There are some broken bars which can be seen at the diagonal corner opposite to the tension field. The section areas of these bars are clearly decreased before being broken. After each bar is broken, the shear force is suddenly reduced. Although there are some discrete broken bars appeared at the opposite corners of tension field, however, at the ultimate load, the sheet is completely broken with the cracks along the diagonal. The EMP is totally ruptured at the force of 190.4kN and the displacement of 47.8mm (1.9% drift). As expected, there is no rupture neither at the welding between the sheet and the gussets nor at the bolt connections between the sheet and the frame. Figure 4-32 shows a view of the EMP after the test. Figure 4-33 shows the static relationship between force and drift of the specimen.

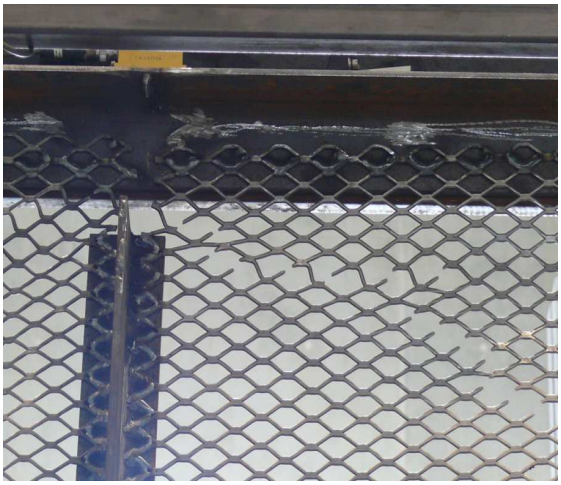

Figure 4-32 – Broken bars of EMP at failures of the large scale tests

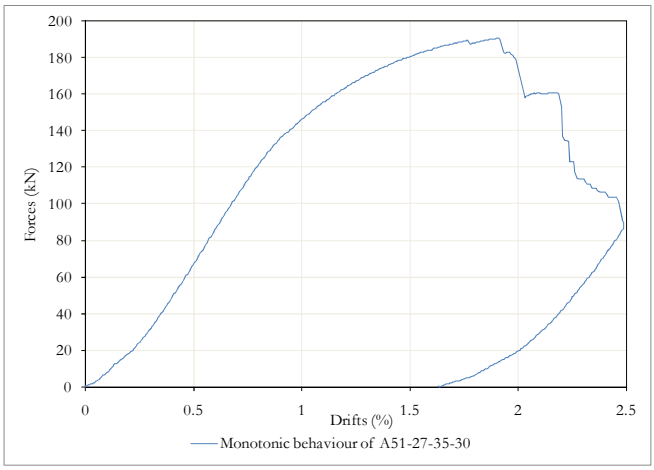

Figure 4-33 – Monotonic behaviour of specimen 1 – A51-27-35-30

Specimen2 – A86-46-43-30

Because the voids of this specimen sheet are large, one can easily observe the out of plane deformation of the sheet before erecting the sheet to the test frame. These initial deformations of the specimen are discretely distributed because of welding between the sheet and gussets. Up to the displacement value of 23.6mm (0.99% drift), the sheet behaved almost elastically and the corresponding force was of 90kN. Furthermore, the EMP is globally buckled at very low shear force. The buckling waves are along the diagonal at which force applied. At the end of the test, a large out of plane deformation is observed. Before the EMP is completely broken, many broken bars are observed and their sectional areas are largely reduced. The ultimate shear force and displacement are 111.1kN and 35.3mm (1.5% drift), respectively.

The test is stopped because of large degradation in strength of the specimen. Test is terminated when the drift approximately reached to 2% and the shear force is reduced to 60kN. Figure 4-34 shows global instability of specimen. Figure 4-35 shows relationship between force and drift of the specimen.

Figure 4-34 – Global instability of the specimen in large scale tests

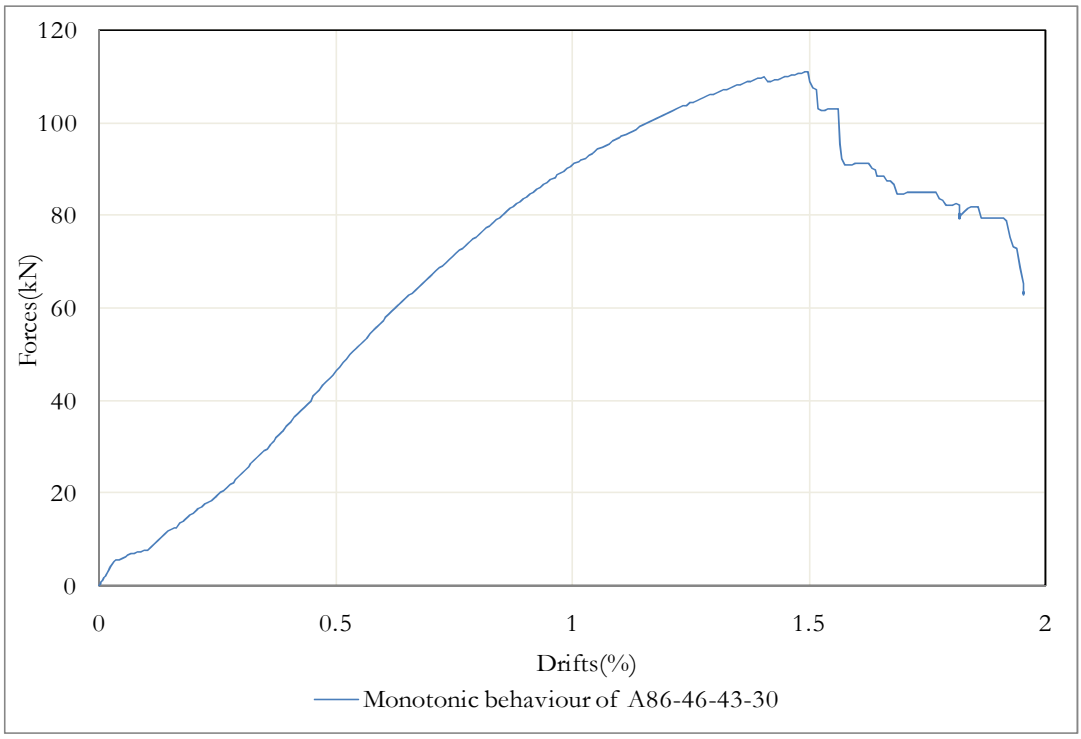

Figure 4-35 – Monotonic behaviour in large scale tests

4.5.3.2. Cyclic loading phase

General features

All specimens in both tests behave elastically in the first four cycles until reaching a yield displacement which is also nearly the same as the yield displacements in monotonic tests. In the elastic range, the behaviour of all specimens is not completely symmetric. The reasons for this physical phenomenon are that there always exist initial deformations of small EMP specimens leading to some initial stress. Beyond elastic ranges when the displacements become larger, the hysteric loops are more symmetric.

Initial out of plane deformations are visible in most of EMP specimens before testing. These deformations are unavoidable because of very thin sheets. In addition, it is impossible to constantly keep EMP specimens absolutely flat during fabricating processes, especially in specimens with welded connections. In specimen 1, A51-27-35-30, this phenomenon becomes clearer after low shear forces are applied to the sheets. Out of plane deflections of the sheets are larger in successive cycles.

In all monotonic tests, there is no instability of individual bar. The same states of the bars are also observed in first four cycles in quasi-static cyclic tests. However, when reaching yield displacements and up to the appearances of first broken bars, some bars have been locally buckled. In addition, the section areas of all the buckled bars are reduced visibly. It is noteworthy stressing that all these bars are located very close to the boundary of the test frame, where weld connections have been used to connect EMP to the gusset plates.

Like in monotonic tests, all first broken bars, as shown in Figure 4-36, are located at four corners of the test frame, and before being broken their section areas are considerably reduced. It is also observed that the crack directions in all cyclic tests start at four corners and then progress to the centre of the sheets to form four crack lines. It is worth noting that, in almost all cyclic tests, the maximum shear force is attained in the cycle in which the first broken bars have appeared.

Figure 4-36 – Broken bars of the sheets in large scale EMP specimen

Table 4-13 – First four cycle results of specimens with welded connections

Specimens	Monotonic yield force (kN)	Monotonic yield displacement (mm)	Monotonic yield Drift (%)	Forces at yielding (kN)	Displacements at yielding (mm)	Drift at yield cycle (%)
1 – welded connections	140.0	23.0	0.90	140.7	22.4	0.89
2 – welded connections	090.0	23.6	0.99	93.4	23.1	0.97

During first four cycles of both tests, the behaviour of the EMP specimens is nearly linear. From the fifth cycle to the end of the tests, the shapes of hysteretic behaviour of the EMP specimens are stable S-shapes. Hysteretic loops in all specimens are characterized by strong pinching. Pinching effects are due to the global instabilities of the EMP specimens, which cause large degradation in stiffness of the sheets. Like in monotonic tests, tension bands are developed in sheets in every cycle. In addition, before redeveloping new tension band the stiffness of the sheets is approximately equal to zero in the other diagonal, which correspond to the pinching observed in the diagram. From the beginning to the end of the tests, there has been no failure either at the welded connections between the expanded metal panels and the test frame. It

is also observed that there is no failure on the test frame. Table 4-13 to Table 4-15 present the results of the tests in large scale.

Table 4-14 – Cyclic results at displacements corresponding to ultimate forces in monotonic tests (*Corres. – Corresponding)

Specimens	Monotonic max shear force (kN)	*Corres. displacement (mm)	*Corres. drift (%)	*Corres. shear force (kN)	Disp. at relatively *corres. to monotonic test (mm)	*Corres. drift (%)	Number of cycles (cycles)
1 – weld connection	190.4	47.8	1.9	195	42.4	1.80	8
2 – weld connection	111.1	35.3	1.5	109	35.4	1.51	8

Table 4-15 – Maximum shear forces in cyclic tests and corresponding displacements

Specimens	Cyclic ultimate shear forces (kN)	Cyclic corresponding displacements (mm)	Cyclic corresponding drifts (%)	Number of cycles (cycles)
1 – welded connections	195	42.4	1.80	8
2 – welded connections	109	35.4	1.51	8

Particular features

Specimen 3 - A51-27-35-3

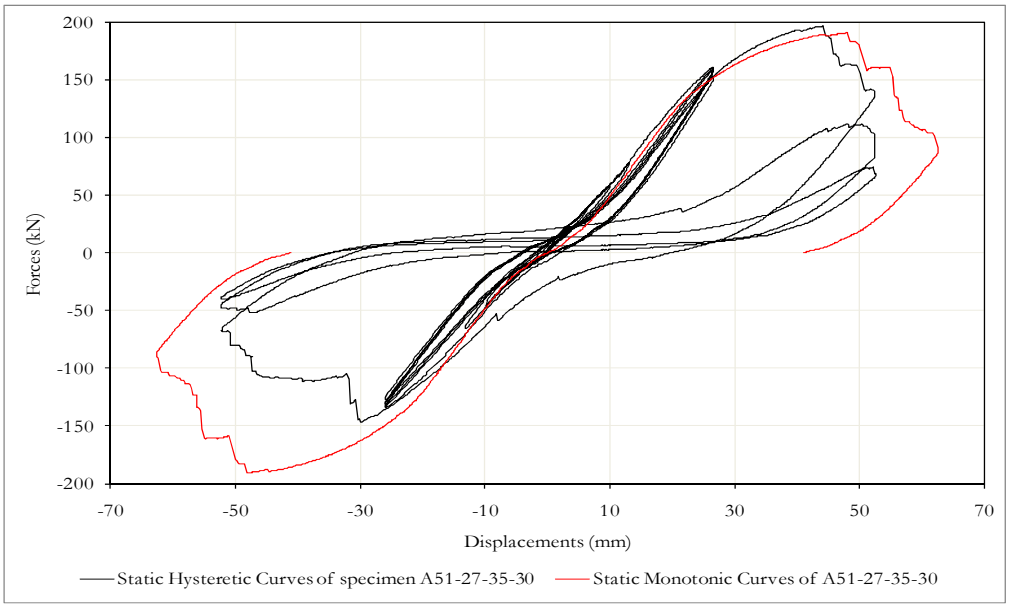

Figure 4-37 – Hysteretic behaviour of the specimen A51-27-35-30

The behaviour of this specimen in first four cycles appears elastic. It is easy to observe that force-displacement relationship at these cycles is not symmetric. At first haft of fourth cycle, when the displacement is up to -3.45mm (0.14% drift) the corresponding shear force was of 23.4kN, but when the displacement is +3.2mm (0.13% drift), the corresponding shear force is just only of 12.3kN. In next cycles, the loops became more symmetric. From the fifth cycle, within a group of three successive cycles without changing in target displacements, one can clearly observe the stiffness degradations. After first

four cycles, global instabilities of the specimen become clearer. And when the sheet is completely broken, the out of plane deformations are much larger than in monotonic test.

The first broken bar is at the down-left corner of the EMP. After that the forces acting on the sheet still increase in next cycles until reaching the maximum values. It is also observed that before being broken, the section of the bar is reduced and that bar is apparently buckled. It is worth noticing that the cracks of the sheet until complete failure almost develop in four corners. In addition, from the fifth cycle, before changing the directions of loading, one can observe the rapid increasing of displacement, and the stiffness of the EMP is approximately equal to zero. Figure 4-37 shows the hysteretic curves of the EMP in large scale tests in comparison with corresponding monotonic curve.

Specimen 4 – A86-46-43-30

Specimen 4 exhibits linear behaviour during the first four cycles. Global buckling begins to occur from the beginning of the test and progresses in subsequent cycles. At the first haft of cycle 5, the magnitude of the buckling waves becomes more visible. The first broken bar is locally buckled. After this cycle, the global deformations increase quickly. Besides global instability can be easily observed, local buckling of some bars is also observed. Until having reached complete failure, it is clearly observed that the fractures of the sheet are developed along the diagonals. The specimen is successfully tested up to 64.0mm ($4e_y$, 2.5% drift). The maximum shear force in tension was of 111.1kN which occurred at $2e_y$ – 1.25% drift. The test was stopped at cycle 8 because the force is reduced to 30.0kN and corresponding displacement is 72.0mm. Figure 4-38 shows the relationship between forces and drifts of hysteretic and monotonic behaviour.

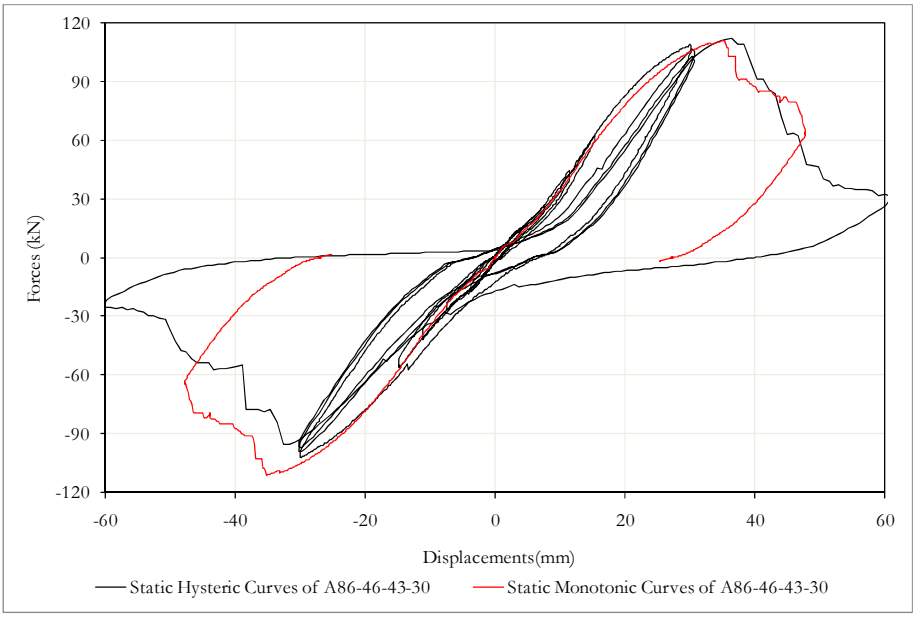

Figure 4-38 – Hysteretic behaviour of the specimen A86-46-43-30

4.6. Summary of observations

An experimental test program has been carried out on small scale and large scale of unstiffened expanded metal sheet test specimens. The main objectives of the tests is to calibrate the simple analytical model for monotonic shear loading that has been proposed by Pecquet (2005) and to study the hysteretic behaviour of expanded metal sheets subjected to shear. The correlation between the analytical model (Pecquet (2005)) and monotonic tests varies largely. In some cases, the analytical model much underestimates the real behaviour of the small EMP specimens. It may be that only one tension band for the monotonic behaviour of the sheets is not enough. The sheets might work in more than one tension band or the numerical parametric study only on square EMP is not enough for assessing its real behaviour with rectangular shapes.

Observing the shear behaviour of EMP, some conclusions have been drawn.

First, because under rather low shear forces the sheets are globally buckled, the contribution of compression diagonal to the resistance of sheets can be completely neglected. In both monotonic and cyclic phases of the tests all sheets have buckled at very low shear forces. Some of the specimens (specimens 7 and 8 in small scale, and specimen 2 in large scale) were globally buckled before testing. Furthermore it was observed that normal types of small EMP specimens, including specimen 5, 6, 7 and 8 (profiles: 51-23-32-30 and 86-40-32-30), buckle more easily than flattened types, which are specimens 1, 2, 3 and 4 (profiles: A51-27-35-30 and A86-46-43-30).

Second, the first broken bars observed in both monotonic and cyclic phases of tests are located near one of four corners, and the crack lines then develop to the centre of the sheets. Besides there is no bar being locally buckled in monotonic tests. However, in all cyclic tests, many bars have been buckled before being broken. Moreover, in almost all cyclic tests, the maximum shear forces have been attained on the cycle on which first broken bar has been observed.

Third, the maximum shear forces of small EMP specimens in monotonic tests are dependent on the voids of the sheets. With nearly the same voids, ultimate shear forces of flattened type specimens are much greater than those of normal types. Nevertheless, it is observed that maximum displacements of flattened types are much less than those of normal types and the ductility of normal types are greater than that of flattened types.

Fourth, the hysteretic loops of all specimens are S-shaped with pinching effects, but they are stable. The displacement ductility of all specimens is largely different, ranging from 4 to 13. Pinching effects on all specimens due to yielding in tension and to buckling in compression caused the degradation of stiffness of the sheets. In cyclic tests, pinching effects are clear in successive cycles beyond the elastic range. In addition, the magnitude of the buckling deformations and deterioration in stiffness of sheets are increased correspondingly.

Fifth, the degradation in stiffness of the sheets due to pinching effects results in a smaller enclosed area under the hysteretic curve and, therefore, a lower amount of energy absorbed by the system during successive cycles. In addition, in all specimens in cyclic test phases, the stiffness of the sheets is approximately equal to zero during the inversion of force. The deflection required to redevelop the tension field is based on the yielding displacements experienced by the sheets on the previous cycles.

Sixth, the ductility of panels is related to the ductility of the base material itself, which is not at present subject to special control. For sure, if seismic applications of EMP go in to practice, a control of the steel material characteristics should be imposed.

Another important point is that to connect the EMP with the boundary frame, the use of welding in the flattened type EMP is much easier than in the normal type. This advantage of the flattened type over the normal one is due to the flatness in plane of the geometry.

Finally, to conclude, EMP seems to be suitable for the use in retrofitting structures subjected to in-plane shear thanks to some advantages such as strength and ductility. However, it is important for fabricator to produce a much more constantly mechanical product. In addition, some more parametric study should be made to obtain a better analytical model of EMP subjected to shear in both monotonic and cyclic loading.

5. SIMULATIONS OF THE TESTS AND PARAMETRIC STUDY OF EMP SUBJECTED TO SHEAR LOADING BY NUMERICAL APPROACH

5.1. Introduction

A series of experiments of the EMP in small and large scales has been performed to examine the behaviour of such lateral resisting systems under severe monotonic and quasi-static cyclic shear loading. Parallel to conducting the experimental investigations, it is necessary to use a method of analysis in order to be able to predict the behaviour of test specimens so that all the components of the tests can be designed properly. Besides, using the model, it can be possible to predict the required hydraulic jack capacities, strokes and the movements of measuring devices. In addition, based on the comparison between the test data and results of the numerical analyses, the numerical model can be calibrated and refined as necessary. More importantly, using the refined model, a parametric study can be performed to address the analytical simplified models of the EMP under shear. These models will be the essential tool used in the next steps of this study.

Two main parts will be presented in this Chapter. First, numerical simulations of the tests will be introduced, including a detailed description of the model of the EMP in the test, differences between the model and the experiments and comparison and assessment of the results. Second, a parametric study on EMP under shear by the numerical approach will be next performed. In this part, the elements, the material properties, the initial deformations and the solution strategy are all mentioned in general aspects. The analytical models, developed from the parametric study, will be presented as well. Concerning the numerical code, the numerical model is analyzed by using FINELG (1999), a fully nonlinear code developed at University of Liege.

5.2. Numerical simulations of the tests

5.2.1. Description of the model

5.2.1.1. Modelling of the components of the test

When modelling the experimental test it has been recognized that the most difficult problem is how to make the modelling as much like the tests. This, of course, could not be fulfilled in many cases. Minor differences, for example in connection conditions of the structure, can significantly influence the behaviour of specimens. When modelling the test specimens, the connections and boundary conditions are very hard to define. In addition, complicating the problem is the effect of residual stresses induced by panel welding. Therefore, as mentioned in the previous sections, some factors are simplified in the model and some adjustments are made to make the modelling as close to the tests as possible.

As described in detail in Chapter 4, there are two independent series of tests, in small and large scales, being conducted. The configurations of these tests are different in specimens (dimensions, connections and number of experiments) and in manner of performing the tests. However, both tests have three main components including test specimens, test frames and test devices. The configurations of these two tests will be briefly recalled for convenience for the modelling of the tests by numerical simulations.

In small scale, the specimens consist of small EMP having the largest dimensions of 1095mm being less than the originally fabricated EMP and gusset plates or 'intermediate plates', which are used to connect the EMP with the test frame by means of bolts. The EMP is connected with the gusset plates by using weld or glue materials. Obviously, these materials are selected depending on the ultimate capacity of the EMP which is estimated based on the behaviour of SPSW. The test frame is constituted by rectangular bars and some additional gusset plates. They are hinged together to be sure that the forces from the machine are entirely transferred to the test specimens.

In large scale, the test specimens include two originally fabricated EMP, connected together by welding them with an additional T (see Chapter 4). The combined EMP is then welded to the gusset plates to form the test specimens. The test frame consists of two beams and two columns, made from HEA160 and 200. They are connected by using four composite rings, which are able to make them freely rotate. The specimens are linked to the test frame by means of bolts. Obviously, all components of the tests are considered in the numerical model. They are discussed in detail hereafter.

First of all, an EMP consists of many identical rhomb-shaped stitches, formed by four EM bars having constant cross sections. Each bar of a rhomb shape stitch is like a beam with constant rectangular section. In the normal type of EM product, as number 1 and 2 in Figure 5-2, there are overlaps at the ends of bars causing the increase of their cross sections. Because of these overlaps, there are a little inclination and increase of the thickness at the ends of each bar. It means that two bars do not lie in plane. Differently from the normal type, in the flattened type of EM products, as number 1, 2, 3 in Figure 5-2, there is no overlap at the ends of bars. However there is still some increase of the cross sections at the ends of each bar. All bars are consecutively linked together in one plane to form a flattened sheet. Apparently, the stiffness at the ends of bars is nearly doubled, so it is possible to assume that a bar is fixed at both ends, and additionally the fixed points or the clamps of bars can freely move in and out of plane. However, the increase of the section at the ends of bars is neglected in the numerical models. So, it has been chosen to use 3D beam elements to model the bars of the expanded metal rhomb-shaped stitch. This spatial beam element has seven degrees of freedom per node (three translations, three rotations and the warping).

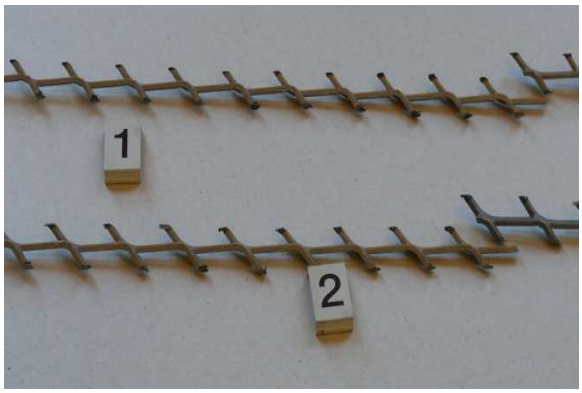

Figure 5-1 – Bars of normal types of EM bars

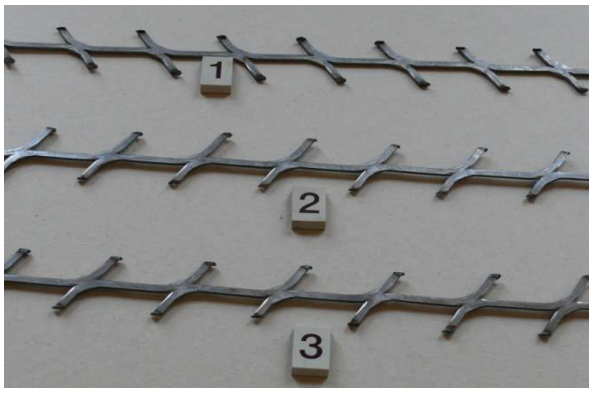

Figure 5-2 – Bars of flattened types of EM bars

Second, a crucial point is that how many finite elements to use for each bar. The final goal is to obtain the global behaviour of the EMP, in plane and out of plane. In addition, it is also necessary to model sheets of large dimensions. Thus, it is important to limit the number of elements and it has been decided to use only one element for each bar. In this case, the global behaviour of the sheet can be reproduced with global instabilities but the buckling of an individual bar is ignored.

Third, as observed in the description of the test components, the EMP will be connected to a test frame by using some additional fish plates. This test frame consists of four equivalent steel beams, which have rectangular sections of about 100mmx100mm in small scale and I-shape sections of HEA160, HEA200 in large scale, presented in detail in the previous chapter. Four corners of the test frame are hinges. This configuration of the test frame ensures that all forces from the actuator will be entirely transmitted to the EMP and the deformation of test frame under shear will be small enough so that it will not affect to the behaviour of the EMP. Apparently, the forces from the actuator will cause internal forces (M_x, M_y, M_z, Q_x, Q_y) in four components of the test frame. Therefore, these components are modelled as 3D beam elements as the bars of the EMP. However, in the model, the sections of these beams are taken from some trials and decided to be 250x250mm (not 100x100mm as in the tests) in order to be sure that there is no influence of test frame to the behaviour of the EMP.

Fourth, the presence of the connection tabs, or 'fish plates', used to connect two originally fabricated EMP or to link the EMP with the boundary beams and columns, are not represented in the finite element model. Rather, the infill EMP is considered to be connected directly to the beams and columns, as shown in Figure 5-3 and Figure 5-4. In order to take into account the eccentricity of the forces because of these plates, an outrigger element is added in the model as shown in Figure 5-3 and Figure 5-4

Finally, the finite element code used for this study, FINELG, is a nonlinear code, in which geometrical and mechanical nonlinearities are taken into account, and phenomena of plasticity and instability are covered. For easy simulations, an automatic mesh generator has been developed in Visual Basic language with Excel interface. The complete data file is then generated for FINELG.

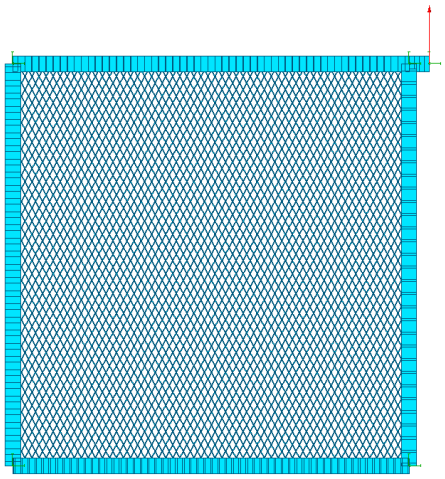

Figure 5-3 – Model of tests in large scale used in FINELG

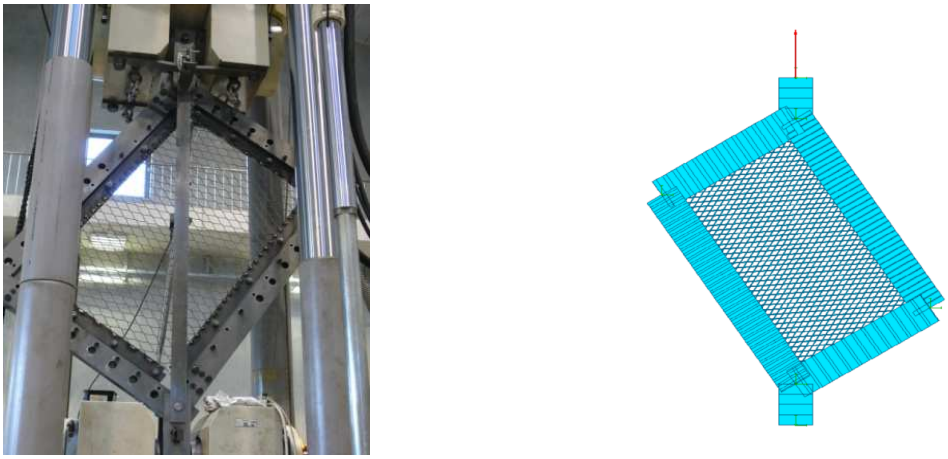

Figure 5-4 – Model of tests in small scale used in FINELG (left: in the test; right: numerical simulation)

5.2.1.2. Material properties

In order to correctly model the experiments in numerical simulations, one needs to know the real mechanical properties of each component in the modelling. There are two kinds of material used in the model: one representing the EMP and the rest representing the other components such as the boundary frame, fish plates…

Based on the studies on thin steel plate shear walls working in shear (Timber and Kulak (1983)…), in order to exploit the behaviour of the steel plate, the four boundary beams of the test frame should work only in elastic range and their deformation should be very small so that they do not effect the deformation of the plate. Thanks to this stiff frame, it is possible to completely exploit the shear ultimate capacity of the steel plate or the EMP under the increasing forces, as observed in the tests of the steel plate and EMP, presented in the previous chapters. Therefore, in the modelling of the tests of EMP, the material of four boundary beams and columns and of the fish plates is assumed to be completely linear elastic with very high value of Young Modulus compared to that of EMP. Linear elastic finite element has been chosen for the components constituted the boundary frame. Young modulus of them has been taken as 200 GPa.

The mechanical properties of each bar in EMP will be determined based on the tensile tests of the bars. In fact, when an EMP is loaded in shear, each bar is simply submitted to tension with limited bending. This

bending could be a factor affecting the behaviour of the bar. Therefore, it is better if the stress-strain relationship of the bar due to the tension force and the bending has been determined. However, it is apparent that doing the test of these very thin and short bars is impractical. Thus, in the present study, the test of mechanical properties has been uniquely carried out with tensile ones.

Each bar of the rhomb shape stitch has a relatively short length, maximum 3 or 4 centimetres. Because of that, it has been decided to test on a line of bars with the length of about 500mm. Such a line after test up to failure is presented in Figure 5-5. It can be seen on Figure 5-5, at the ends of this line of bars, where the specimen was clamped in the test machine, that bars are not perfectly aligned. That is the real shape of the whole line of bars before tensile test. In the centre of this line of bars, because of the tensile test, by tension and some bending, bars are now perfectly aligned. This phenomenon is translated on the mechanical properties by a Young's modulus lower than the usual one for EM. However, in numerical simulations, because modelling is made with perfectly aligned bars, this reduced value of Young's modulus is imposed. On the specimen illustrated here above, necking can also be seen near the failure section (Pecquet, 2005). Results of these tests are presented in detail in chapter 4. Tests have been performed several times with nearly the same results for each batch of product but quite different for different batch of EMP. Each time, initial length, displacements and force were measured. From these measurements and with the cross section of the bars, stress-strain curves can be obtained.

Figure 5-5 – View on a line of bars after failure

EMP material is modelled as an isotropic one with a simple rate-independent multi-linear constitutive behaviour including the effects of both softening and strain hardening. The softening branch is used in the model to predict the ductility of the EMP. The material properties are identical in both tension and compression, with the constitutive parameters being based on the results from measured tensile tests, as summarized in Table 4-5 and Figure 4-18. The Von Mises yield surface is supposed for the yield criterion.

A last important point to be considered is that this determination of mechanical properties has to be performed on each batch of expanded metal. Currently, manufacturers are not able to warrant the constant mechanical properties of Expanded Material! Differences are often non negligible! This is the worst disadvantage of this material, but it could easily be improved by imposing requirements on the base steel characteristics, if practical application like seismic retrofitting requires constant material quality.

5.2.1.3. Initial conditions

The behaviour of very thin EMP in real RC frames subjected to in-plane membrane forces (shear forces) can be significantly affected by initial out-of-plane deformations and it must be accounted for in the numerical model. The elastic stiffness of a perfectly flat plate or EMP is very high under in-plane shear stresses. Nevertheless, if there is a slightly initial out-of-plane deformation, the in-plane shear stiffness of EMP will be substantially decreased.

Before testing, the geometry of un-stiffened EMP is such that some out-of-flatness, caused by effects such as distortion due to welding, beam deflections, and the eccentric fish plate connections, is obvious to occur prior to the application of in-plane shear loading. Due to that, the initial imperfections of EMP must be taken into account before the strength analysis. There are several solutions to determine initial out-of-plane deformations. They can be obtained from the measurement of the actual initial conditions in similar structures. Alternatively, the first global buckling mode of EMP may be used, obtained from an eigenvalue buckling analysis of EMP systems, with the loading applied in the same manner as for the subsequent strength analysis. The latter approach is used in this study. FINELG code gives the normalised critical displacements: the biggest displacement is equal to one. It has been chosen to multiply the displacement field by 1/200 of the sheet dimension to give the initial deformation state. And in addition, the importance of these initial imperfections may play an important role on the global non linear

behaviour of the EMP loaded in shear. It is necessary to notice that residual stresses are not included in the modelling because these quantities are not measured in this research programme.

5.2.1.4. Solution strategies

Concerning the different types of analyses, linear elastic analysis is first used to obtain the elastic stiffness in shear. After that, the critical behaviour is examined, with a linear elastic material law. This analysis gives several critical loads corresponding to different instability modes; only the first one, corresponding to the lowest instability load, is examined in this study. This mode is then used to give the shape of the initial deformations in the fully nonlinear analysis to determine overall behaviour of EMP subjected to in-plane shear loading.

For instability analysis, FINELG computes the eigenvalues and the corresponding eigenvectors of either linear instability problem, or the so-called nonlinear of incremental instability problem (Manual of FINELG, 1999). It is of interest to examine the overall behaviour of the EMP, therefore the linear instability approach, based on EULER stability criterion and on computational technique of the secant method, is adopted in the current study for predicting the global buckling modes of the EMP.

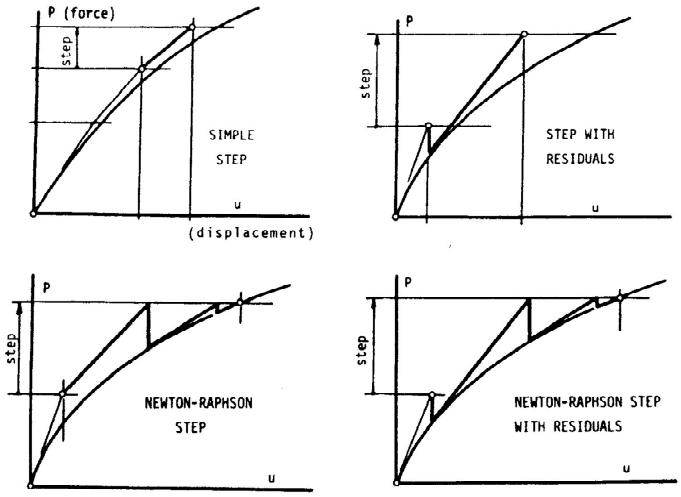

Figure 5-6 – Iterative procedures available in FINELG

For fully nonlinear strength analysis, there are several numerical techniques available in FINELG which enable one to follow the behaviour of a structure under increasing external loading up to collapse or instability. Post-critical behaviour may be interesting to study in order to better understand the collapse mechanism of the structure. There are also some loading methods such as imposed load, imposed displacement or arc-length used in FINELG in order to overcome the limit points of the structures. In the current study, imposed displacement approach is adopted in order to follow the experimental steps. Nonlinear geometrical effects are dealt with through the finite elements using either the total or the up-dated or the co-rotational lagrangian formulation. Nonlinear material effects are treated via the incremental plasticity theory (small strains); usual constitutive laws, such as elastic-perfectly plastic, bilinear, tri-linear, multi-linear, Ramberg-Osgood, etc..., are included in the program. For computational technique to solve nonlinear algebraic equations, FINELG uses step by step approach with six different kinds of steps being able to be performed (see Figure 5-6), including:

a - simple step;

b - simple step taking into account the residuals of the previous step;

c - NEWTON-RAPHSON step, i.e. with equilibrium corrections;

d - NEWTON-RAPHSON step taking into account the residual of the previous step;

e - NEWTON-RAPHSON step, without computing a new tangent matrix at the first iteration of the step if the previous ones is converged (if not, same as c.);

f - NEWTON-RAPHSON step without computing a new tangent matrix at the first iteration of the step if the previous ones is converged (if not, same as d.).

5.2.2. Comparison of numerical analysis and experimental studies of EMP under monotonic shear loading

Like the experiments, the imposition of displacements is used to control the numerical step analyses. The displacements are monotonically increased until reaching the ultimate response of the EMP. The load vs. panel deflection responses for both the test and numerical simulations are presented in Figure 5-7 for small scale tests and Figure 5-8 for large scale tests.

Figure 5-9 presents the buckling waves of the specimens in the tests and in numerical simulations at the same stage of loading and failure stages of the specimen A86-46-43-30 in the tests and in the numerical analyses are illustrated in Figure 5-10 and Figure 5-11. Table 5-1 to Table 5-4 give the results of the tests and numerical simulations of the tests of some typical specimens in small and large scales.

Observing the responses of the specimens between tests and numerical simulations has indicated that there have been some very common and different points from the beginning to the end of the overall behaviour: elastic buckling, ultimate responses.

First, the elastic buckling of the EMP has not been clearly seen in both the tests and the modelling of small scale at the very beginning of the tests, especially for the specimens of the flatten type. However, in large scale, this phenomenon is clearly observed, represented by sudden changes of the slopes on the force-displacement curves. This means that due to this imminent elastic global buckling, stiffness of the EMP is suddenly decreased and its capacity beyond buckling has been activated and the tension field has been formed on the EMP at the very soon stage, especially when the dimensions of the EMP are close to the dimensions of the RC-MRF in reality.

Second, it can be easily observed that although the results from modelling defer slightly from the test in both small and large scales at the beginning, however, the modelling shows a trend towards the same ultimate capacity as in the tests, as presented in Table 5-2 and in Figure 5-7 and Figure 5-8. There are several reasons that further refinements to the model of the analyses are not made. This might lead to those differences between tests and numerical results. First of all, the increase of the section at the end of bars of the rhomb-shaped stitch is not taken into account in the model, which may cause a smaller initial stiffness and strength of the model compared to the tests. Second, due to the manufacturing and test fabrication processes there must be some stress concentration on somewhere of the test specimens, but that is not taken into account in the model. Finally, as discussed in 5.2.1.3, the residual stresses on the test specimens are not measured. They must be present on the EMP before testing and they are also not accounted for in the numerical simulations.

Third, as being seen in Figure 5-9, the buckling waves in numerical simulation fit rather well to the buckling waves in the tests. It is also observed in Figure 5-10 that the broken bars in the tests are corresponding to the bars in the numerical modelling. These bars are almost fully red in Figure 5-11.

Another interesting point observed on Figure 5-7 is that with the same profiles of EM but different in the erection direction their behaviour is not the same. This discrepancy is considered to occur for the reason that the number of bars or of rhomb shape stitches of A51-27-35-30 dir2 specimen is fewer than those of A51-27-35-30 dir1 specimen.

Fifth, as observed on the results of tests and the numerical analyses, their yield displacements are approximately equal. Furthermore, the results for all EMP and for overall EMP behaviour show that finite element model predicts the ultimate load relatively accurately.

Finally, a much different parameter is the maximum displacement of the test of A51-27-35-30 dir1 when the shear load is reduced to 40% of strength capacity of the EMP specimen. In the other specimens, these differences are not considerable. The reasons explaining for these physical phenomena are that the buckling of individual bars is not modelled on the analysis and the broken bars are not excluded from the model when they attain ultimate strains. Another different point is that on the test curves there are some points, which can be easily observed, having "jumps" on the test curves. These points represent the sudden reductions in stiffness and strength of EMP. This is because, as explained in Chapter 4, many bars

forming the strips of EMP are suddenly broken causing the degradation of stiffness and strength of EMP. These phenomena cannot be clearly seen in the numerical simulations.

Table 5-1 – Monotonic test results in small scale

Specimens	Yield force (kN)	Yield displacement (mm)	Yield Drift (%)	Initial Stiffness (kN/mm)	Maximum shear force (kN)	Maximum displacement (mm)	Maximum Drift (%)
1 – A51-27-35-30 dir1	33.4	1.00	0.14	33.4	78.9	09.4	1.35
2 – A51-27-35-30 dir2	32.2	1.00	0.14	32.2	83.7	08.7	1.25
3 – A86-46-43-30 dir1	27.9	0.85	0.12	32.8	60.8	07.1	1.02
4 – A86-46-43-30 dir2	25.9	1.17	0.17	22.1	65.0	08.3	1.2

Table 5-2 - Monotonic results of numerical simulations in small scale

Specimens	Yield force (kN)	Yield displacement (mm)	Yield Drift (%)	Initial Stiffness (kN/mm)	Maximum shear force (kN)	Maximum displacement (mm)	Maximum Drift (%)
1 – A51-27-35-30 dir1	45.0	1.7	0.26	26.5	98.1	11.2	1.70
2 – A51-27-35-30 dir2	40.2	1.6	0.25	25.1	93.4	12.4	1.88
3 – A86-46-43-30 dir1	35.8	1.03	0.14	39.6	73.4	08.6	1.10
4 – A86-46-43-30 dir2	34.5	1.02	0.13	33.1	75.0	10.1	1.30

Table 5-3 – Monotonic test results in large scale

Specimens	Yield force (kN)	Yield displacement (mm)	Yield Drift (%)	Initial Stiffness (kN/mm)	Max. shear force (kN)	Max. displacement (mm)	Max. Drift (%)
1 – A51-27-35-30	140	23.0	0.90	6.1	190.4	47.8	1.9
2 – A86-46-43-30	90	23.6	0.99	3.8	111.1	35.3	1.5

Table 5-4 – Numerical results of monotonic loading in large scale

Specimens	Yield force (kN)	Yield displacement (mm)	Yield Drift (%)	Initial Stiffness (kN/mm)	Max. shear force (kN)	Max. displacement (mm)	Max. Drift (%)
1–A51-27-35-30	160	25.0	0.98	6.60	210.0	49.8	1.98
2–A86-46-43-30	98	24.2	1.00	3.84	126.0	38.0	1.60

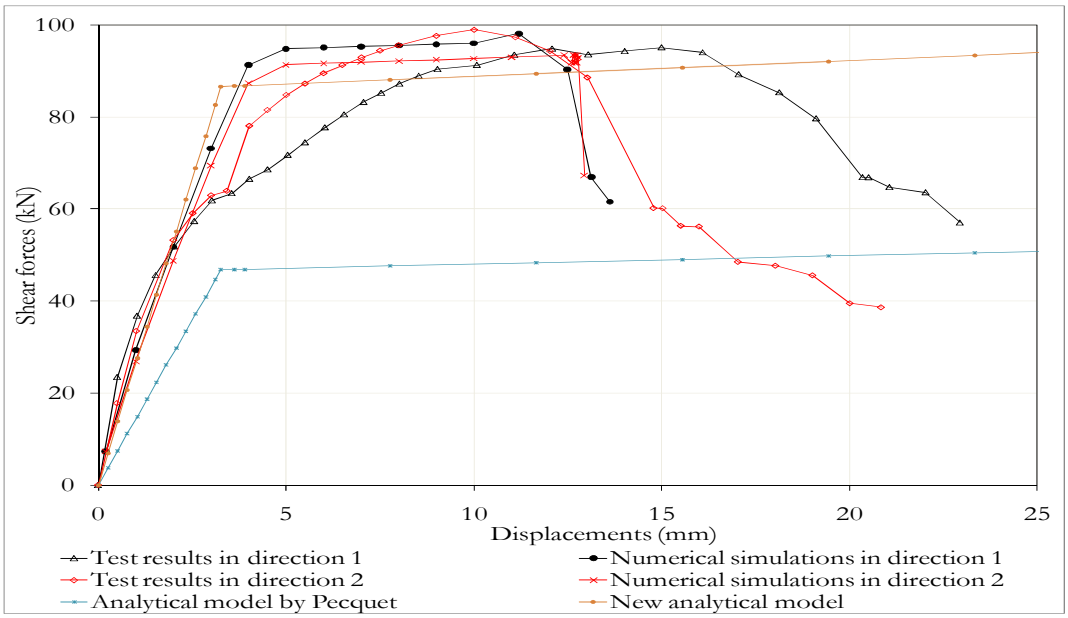

Figure 5-7 – Load vs. deflection curves of the monotonic tests and the numerical simulations of A51-27-35-30 dir1 and A51-27-35-30 dir2- small scale tests

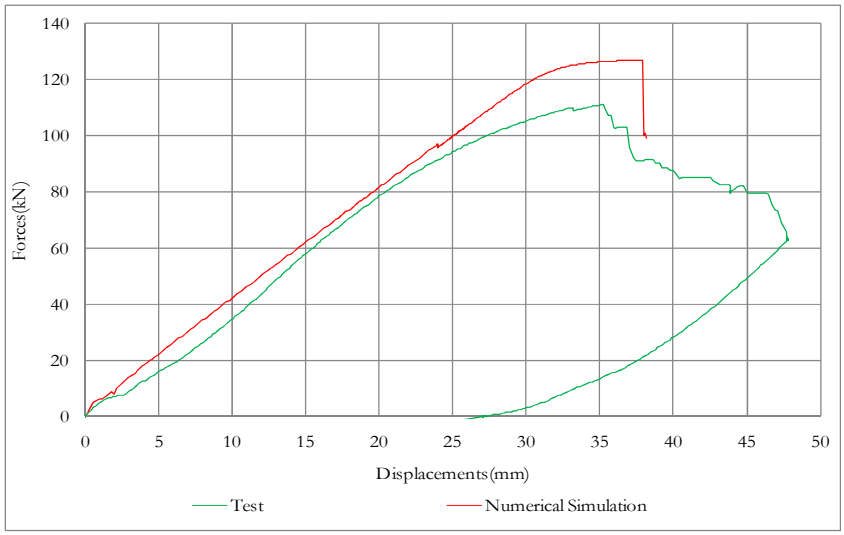

Figure 5-8 – Load vs. deflection curves of the tests and the models of A86-46-43-30 in large scale tests

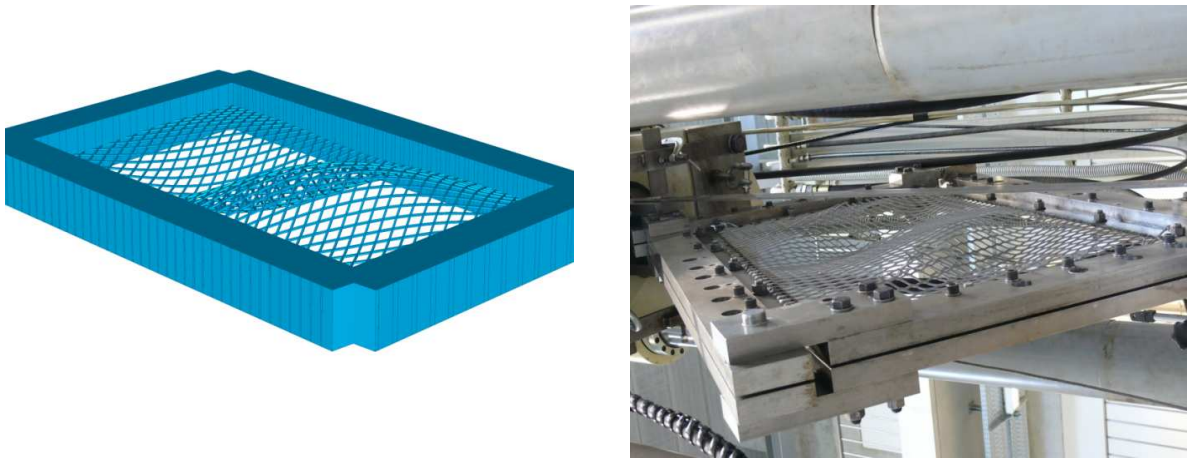

Figure 5-9 – Out-of-plane deformations in the tests and in the numerical simulation during loading of A51-27-35-30 in large scale tests

Figure 5-10 – Deformations of the EMP at the test of A86-46-43-30 dir2 in small scale

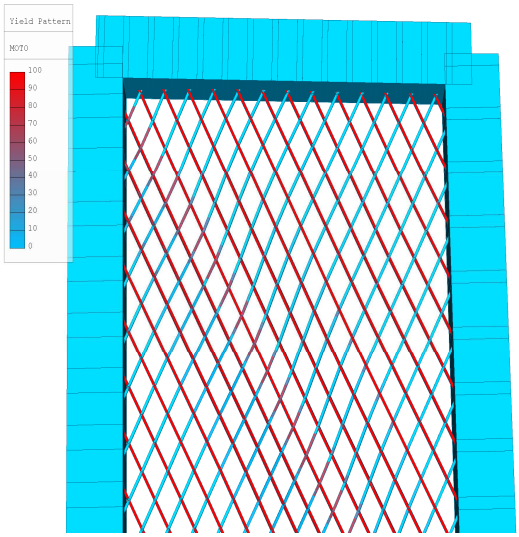

Figure 5-11 – Fully yield bars (very large deformations – considered as failure) at the failure of the EMP A86-46-43-30 dir2 in small scale by the numerical simulation.

5.2.3. Comparison of numerical analysis and experimental studies of EMP under cyclic shear loading

The monotonic loading analyses provide a means of determining the envelope of the cyclic response up to the ultimate capacity. However, it is clear that the monotonic response cannot represent the behaviour of the EMP under the situation of the earthquake, in which the shear loading is alternate, especially the real energy dissipated by the EMP. Hence, in order to be fully aware of the hysteretic behaviour of EMP and to develop a simplified model for its use in modelling with real structures, the numerical model should be able to predict the unloading and reloading responses with acceptable accuracy. A cyclic analysis has been performed on EMP with loading sequences similar to those of quasi-static cyclic experiments. The nonlinear geometric effects are included in the analyses and as stated previously a kinematic hardening rule is used to model Baushinger effects during load reversals. Table 5-5 to Table 5-8 present the results of the numerical simulations in comparison with those of the tests. Some important features have been drawn from this comparison. They are discussed hereafter.

At the beginning of the loading sequence (within first four cycles), the specimens in modelling is a little stiffer than those in the tests. This is the same as in monotonic phase. The shift of stiffness from elastic range to post-buckling range has not been well observed in the tests of small scale and it has been much clearer in the large scale tests. On the other hand, these phenomena are well predicted in the numerical modelling. The global buckling of the EMP at rather low shear load is marked by abruptly changing the global stiffness and by the increase of out-of-plane deformation. At the intermediate loading level, there is a little discrepancy of stiffness between the models and the tests. This is considered to be mainly due to the differences between the model and the tests, such as, for instance, the increase at the end of each bar, which is not covered in the model...

A very crucial feature of the hysteretic behaviour that is well predicted by the finite element models is the pinching effects of hysteresis curves. As clearly observed in the experiments, the test specimen exhibits substantially reduced stiffness during the very early reloading phases, as shown in Figure 5-12 . This occurs prior to the full development of the new diagonal tension field in EMP. The reduced stiffness is also present on numerical simulations. This pinching effect is primarily due to the degradation of the stiffness and strength of the specimens, which is mainly caused by the out-of-plane instability of EMP during the loading reversals and by the stiffness degradation of the material after yielding. It is noteworthy stressing that, although pinching effects have been well predicted in numerical simulations in comparison with those in the tests, however numerical modelling seem to over-predict these phenomena. It can be

very clearly observed that at the beginning of each new three-cycle loading the behaviour between tests and numerical ones fit really well, including stiffness, strength and the degradation of them when the load is reversed. Nevertheless, at the successive cycles, the behaviour obtained from numerical simulations is much more pinched than that from the tests. The results from the tests are more stable than that of numerical ones.

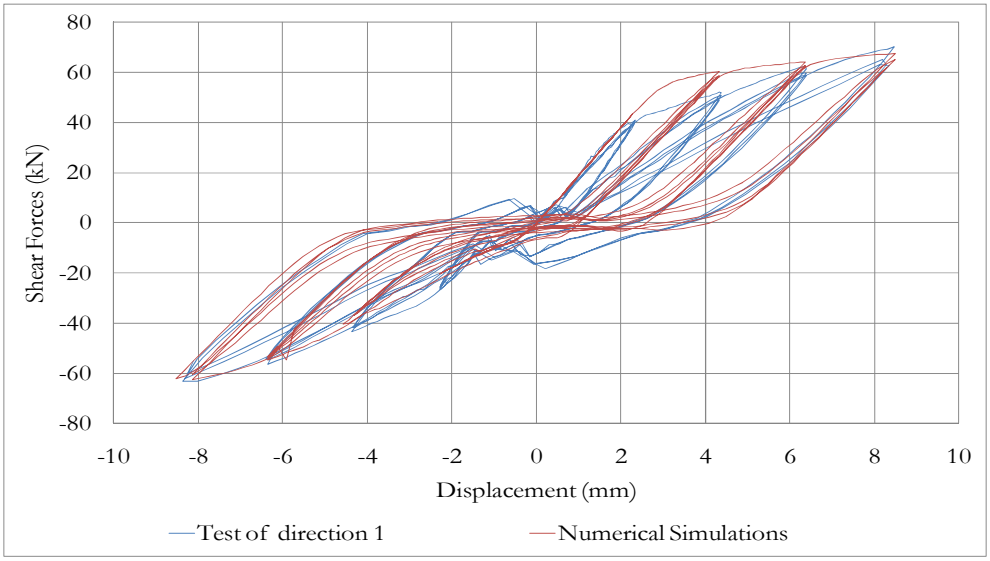

Figure 5-12 – Hysteretic curves of the cyclic tests and numerical simulations of the A51-27-35-30 dir1 - small scale tests

Some other significant features are the ultimate properties, ductility and tension field of the EMP. As shown from Table 5-5 to Table 5-8, the ultimate results between tests and numerical are not largely different. The numerical simulations little over-estimate the maximum responses of the specimens, including shear forces, displacements and number of cycles. As observed in the tests, the tension field of EMP has been developed cycle by cycle along two diagonals. This phenomenon has been also observed in the numerical modelling.

To conclude, the numerical modelling exhibits a rather good tool for predicting the responses of EMP working under shear.

Table 5-5 – First four cycle results of the tests – small scale specimens

Specimens	Yield forces		Yield displacements		Yield drifts	
	Monotonic	Cyclic	Monotonic	Cyclic	Monotonic	Cyclic
1	33.4	30.4	1.00	1.01	0.14	0.15
2	32.2	31.1	1.00	1.02	0.14	0.15
3	27.9	20.2	0.85	0.88	0.12	0.13
4	25.9	24.0	1.17	1.10	0.17	0.15

Table 5-6 – First four cycle results of the numerical simulations – small scale specimens

Specimens	Yield forces		Yield displacements		Yield drifts	
	Monotonic	Cyclic	Monotonic	Cyclic	Monotonic	Cyclic
1	45.0	44.0	1.70	1.69	0.26	0.26
2	40.2	39.0	1.58	1.57	0.24	0.23
3	35.0	34.8	1.65	1.64	0.25	0.25
4	32.3	32.1	1.58	1.56	0.22	0.22

Table 5-7 – Maximum shear forces in cyclic tests and corresponding displacements – small scale specimens

Specimens	Cyclic ultimate shear forces (kN)	Cyclic corresponding displacements (mm)	Cyclic corresponding drifts (%)	Number of cycles (cycles)
1	71.6	8.3	1.2	20
2	-75.6	-16.9	2.4	16
3	-48.2	-20.2	2.9	26
4	-49.3	-14.8	2.1	13

Table 5-8 – Maximum shear forces in cyclic numerical simulations and corresponding displacements – small scale specimens

Specimens	Cyclic ultimate shear forces (kN)	Cyclic corresponding displacements (mm)	Cyclic corresponding drifts (%)	Number of cycles (cycles)
1	75.0	10.4	1.5	24
2	-80.5	-18.6	2.6	20
3	-52.5	-22.4	3.2	28
4	-55.4	-16.4	2.4	16

5.2.4. Summary and conclusions

The finite element model gave a somewhat slightly different representation of the load vs. panel deflection curve of the conducted tests. Although there are still some differences, the numerical approach is very useful to predict the behaviour of the EMP loaded in shear. It is possible to use FINELG as an acceptable tool to develop a parametric study with the aims at determining a more simplified behaviour of the EMP under shear loading which is able to be used in the next step of this study. Besides, there are some important points needed to be concerned when performing numerical analyses of EMP.

First, the material properties of the EMP bars play a crucial role on the overall behaviour, and they must be represented in the model as accurately as possible. Despite having to be modelled in the numerical simulations, the manner to represent initial imperfections is of considerably less importance. The absence of the gusset or fish plates used to connect the EMP and the test frame in the modelling of the finite element mesh does not have a significant effect on the panel behaviour. The reason may be that the gusset plates and the test frame work together and not being deformed and give no effect on the overall behaviour of the EMP.

Second, the properties of boundary frame also play an un-negligible role in the numerical modelling. The deformation of this frame significantly affects the behaviour of the EMP, therefore its stiffness and material properties should be chosen so that its deformation is small enough to not causing the behaviour of the EMP.

5.3. Parametric study on EMP loaded in shear

5.3.1. Introduction

Previous section has presented numerical simulations on the tests. It is clear that there has been a good correlation between the results of the tests and of the numerical simulations. The numerical code, FINELG, is capable of predicting the shear behaviour of the EMP. The final aim of this study is to exploit the EMP in seismic retrofitting and upgrading existing reinforced concrete moment resisting frame structures (RC-MRF). Therefore, in order to model the EMP in RC-MRF in practical point of view, it is better to develop a more simplified model which is able to represent the behaviour of the EMP under shear loading. The results from tests have provided useful information; however, they are not enough to

represent the shear behaviour for all types of EMP and it is unable to find a simplified model of EMP from the test results. The best way is to again use numerical simulations to test different types and dimensions of the EMP in order to find an acceptably simplified model for the EMP under shear.

5.3.2. Description of the typical test model in the parametric study

5.3.2.1. Components of the model

Figure 5-13 shows the overview of the typical test model in numerical simulations. The two basic components consist of the EMP and the boundary frame. There are many kinds of flattened EMP. They are all examined from small to big dimensions in order to see the development of the pure behaviour of the EMP subjected to shear loads. To fulfil the objective of addressing the simplified model of the EMP under shear, based on the previous studies on steel plates working under shear, the mechanical properties of these two components are discussed in detail in next sections. These are the geometrical characteristics of the EMP, type of finite elements that can be used for modelling the EMP, properties of the boundary frames, initial deformations, residual stress, solution strategy…

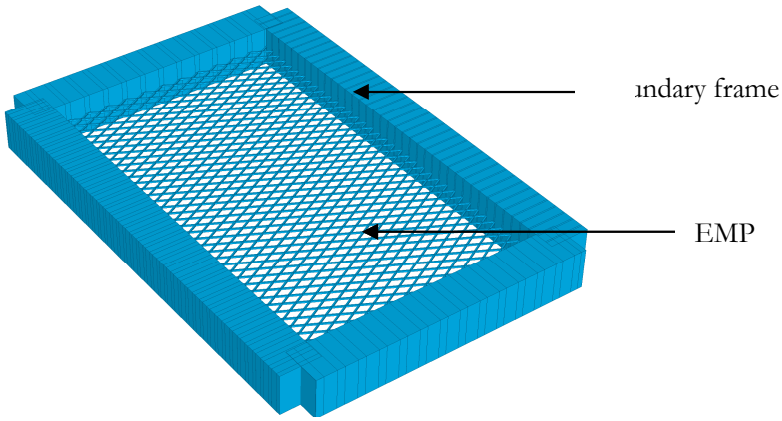

Figure 5-13 – Overview of typical finite element model for the parametric study

5.3.2.2. Finite elements

In order to correctly model EMP by using the finite element method, the most important point is what type of finite elements is suitable for the components in the model. An EMP includes many rhomb shape stitches formed by four nearly constant rectangular section bars. In reality, there are some tolerances between each stitch and each bar of a stitch. However, to make it possible to be use more easily in numerical study, all bars in each stitch of the EMP are assumed as having the same dimensions. In addition, despite practically having bigger dimensions at the end of each bar, it will be neglected in the model of study. It can lead to underestimate the ultimate response of EMP. However it is acceptable if a factor which is used to take into account this difference by comparison of theoretical and experimental results is used. With the increases of dimensions at the end of each bar, it is supposed that all bars are connected together by rigid joints. These joints can move vertically, horizontally and rotationally in and out of plane. With these assumptions, each bar of an EMP is modelled as a 3D beam with constant rectangular section, shown in Figure 5-14. A 3D spatial beam element has seven degrees of freedom.

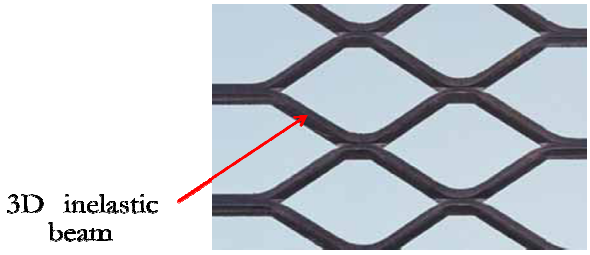

Figure 5-14 – Finite elements used in numerical simulations

One more important point is how many finite elements to use for each bar. As explained in the previous section, one finite element is adopted for each bar. In addition, the global behaviour of the sheet is examined and the buckling of an individual bar is ignored. As being seen in the experimental investigations that for EMP without stiffeners preventing out of plane instabilities global instabilities occur, however buckling of an individual bar is never observed. Therefore, the present numerical model is efficient enough. The finite element code used for the analysis, FINELG, is a fully non-linear program, in which all nonlinearities are accounted for.

5.3.2.3. Material characteristics of bars

Material properties of the bars in numerical simulations are exploited from tensile tests. These characteristic values are not constant in all types of EMP, including elastic stiffness, maximum stress and strain... In addition, the ductility of bars is not consistent either, varying rapidly between types of EMP and between batch products of EMP. Therefore, the average values will be taken for the ideal stress-strain relationship for 3D inelastic beam.

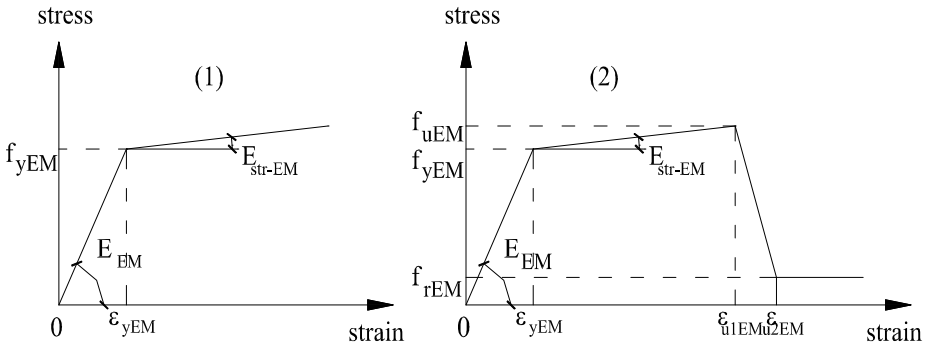

Figure 5-15 – Material law for bars of EMP: (1) for determining the ultimate resistance; (2) for determining the ductility

Where:

E_{EM} is the elastic modulus of EM
E_{strEM} is the strain hardening modulus of EM
f_{yEM} is yield stress of EM
f_{uEM} is ultimate stress of EM
f_{rEM} is assumed remaining stress of EM (1% of f_u)
ε_{yEM} is yield strain of EM
ε_{u1EM} is ultimate strain of EM
ε_{u2EM} is assumed strain of EM corresponding to the f_r.

Figure 5-15 shows the material law used for numerical simulations. It is very important to note that there are two models being assumed: (1) is used to determine the ultimate shear resistance of the EMP and the other multi-linear law is selected with descending part representing the degradation of the strength and softening of the material to assess the ductility of the EMP. To avoid non-converging problem due to the failure of an EMP bar, the strain of the bar is assumed as unlimited, however in the second model (2) the remaining stress of the bar after reaching to the maximum strain is assumed to be very little. This gives two advantages: (1) not affecting the results of ultimate resistance of the EMP by the numerical analysis and (2) being able to predict the ductility of the EMP. Table 5-9 shows the characteristic values used for the numerical tests of the EMP.

Table 5-9 – Material properties of EM bars

E_{EM} (MPa)	E_{strEM} (MPa)	f_{yEM} (MPa)	f_{uEM} (MPa)	f_{rEM} (MPa)	ε_{yEM}	ε_{u1EM}	ε_{u2EM}
134000	1169	337	375	4	0.0025	0.035	0.045

5.3.2.4. Characteristics of the boundary frames

Many studies on steel plate shear walls have examined the effects of the properties of the boundary frame on the shear behaviour of the infill panel. It was found that the frame rigidity influences the lateral rigidity of an inner panel in two distinct ways, caused by the lateral deflection of the frame itself and the bending deformation of the frame components. The lateral deflection of the frame is a component of the total panel deflection. However, the bending deformation of the boundary frame components (columns and beams) causes a redistribution of the forces in the tension field developed in the panel. These studies also proposed that the shear strength and lateral stiffness of the infill plate should be entirely exploited as a contribution to the overall strength and stiffness of the structure. To obtain this, it is necessary to limit the bending deformation of the individual component of the frame and the boundary frame should be stiff enough to avoid this deformation. In the current study, the EMP will be used in RC-MRFs, in which the beams and columns have a rather large lateral stiffness compared to the thin EMP, so the EMP will be able to attain its ultimate capacity. Therefore, in order to determine the shear behaviour of the EMP, the boundary frame components should be stiff enough and have sufficient cross-sectional dimensions not influencing on the deformation of the EMP due to their own deformation under shear.

To obtain suitable dimensions of the boundary frame, many trials with varying dimensions and Young modulus have been examined for each type of the EMP by numerical simulations. Depending on the size and properties of tested EMP, there exists a minimum value of the boundary dimensions that not affect the shear behaviour of the EMP.

5.3.2.5. Initial conditions

The behaviour of the very thin EMP in real structures subjected to in-plane membrane forces can be significantly influenced by initial out-of-plane deformations. These deformations must be taken into account in the numerical simulations. It is quite clear that the stiffness of a perfectly flat plate is very high under in-plane shear stresses. Nevertheless, only with the presence of a very small out-of-plane deformation, it will significantly reduce the in-plane shear stiffness (P.Dubas et al, 1986).

The geometry of the EMP is such that some out-of-flatness, caused by some effects such as distortion due to welding, deflections of the floor or eccentric fish plate connections, is right to occur prior to the application of the shear stresses. The initial out-of-flatness deformations must be taken into account before doing the strength analysis. These deformations may be obtained from measurement of the actual initial conditions in similar structures. Alternatively, the first buckling mode with an assumed out-of-plane deformation may be used. These deformations can be obtained by the products of the normalized deformations from an eigenvalue buckling analysis of the EMP system, which is subjected to the shear loading in the same manner as for subsequent strength analysis and an assumed ratio, taken into account the possibly real deformations. Due to some limitations of measuring the initial deformations, the latter approach is used in all analyses conducted in this study.

The FINELG code gives the normalised critical displacements: the biggest displacement is equal to one. It has been chosen to multiply the displacement field by 1/200 of the sheet dimension to give the initial deformation state. These are small values, surely lower than in reality, but, as it will be seen hereafter, it allows seeing the critical behaviour on force displacement curves. And in addition, the importance of these initial imperfections plays a negligible role on the global nonlinear behaviour of the sheet loaded in shear.

5.3.2.6. Residual stress

Residual stresses are not included in the modelling of the EMP in this parametric study.

5.3.2.7. Steps of analyses and solution strategy

The analyses are performed from small to large dimensions with different kinds of the EMP and different ratios between the width and the height, including 1/1; 1/2; 2/1; 1/3; 3/1. The purposes of those are to see the development of the shear behaviour of the EMP from small to large scale and able to find out the

rules of development. The analyses with different ratios mentioned above aim at covering the possibly real dimensions of the EMP, which is used in reality afterward.

For one EMP, three types of analyses are performed step by step. First, linear analysis is first used to determine the elastic stiffness of the panels. Critical analysis is the next step of the analyzing process. This analysis, as explained in section 5.2, gives several global buckling modes of the EMP. The first mode shape is used as the shape of initial imperfection for the next step. Fully nonlinear analysis is then used to see the complete behaviour of the EMP loaded in shear. To reduce the problem of divergences, imposed displacement method is used for the last step of the analyses.

5.3.3. Behaviour of the EMP under monotonic shear loading

The monotonic behaviour of EMP loaded in shear is examined based on that of un-stiffened plates. According to the theory of an un-stiffened plate subjected to shear (Dubas, P. and Gehri, 1986), its monotonic behaviour is divided into 2 stages: prior to buckling and post-buckling. Prior to buckling, a web plate subjected to pure shear stresses resists load by so-called 'beam-action' (Thorburn et al, 1983); Tromposh et al, 1987). The stress at this stage is a combination of two principal stresses of equal magnitude, diagonal tensile and compressive components.

When the shear load increases, the values of two components are increased correspondingly until the shear buckling stress of the plate has been exceeded. When the shear load reaches to critical resistance of the plate, elastic instability is marked by out-of-plane deformations presented by the formation of inclined buckled waves in the direction of the diagonal tension. Once critical buckling has occurred the global behaviour of the plate is changed because the compressive principal stress cannot increase any further. After buckling the resisting mechanism which is developed in the plate is still stable because the loading is resisted by an increase in the pure diagonal tensile component. However, stable tensile field will uniformly develop if the boundary elements are infinitely stiff (Dubas, P. and Gehri, 1986). If the plate is a part of a plate girder structure the flanges may contribute substantially to shear carrying capacity of the girder. Briefly, the ultimate resistance of a plate under subjected to monotonic shear loading is the sum of three components: prior to buckling, tension field and flange mechanisms, as shown in Figure 5-16.

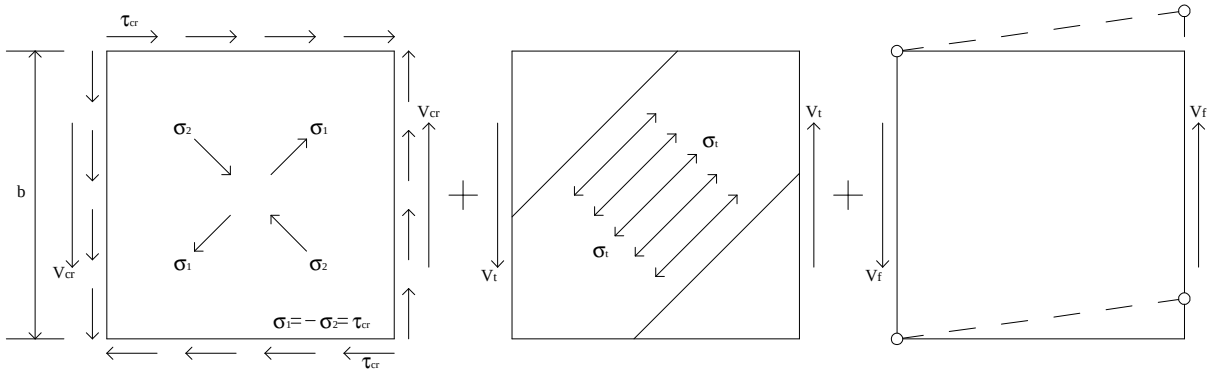

Figure 5-16 – Plate model for a beam web

Following the vicinity of plate theory, in present section, shear resistance of the EMP will be studied by using numerical simulations. There is a difference between analysis of the EMP and the plates at this stage, that is, the contribution of flange mechanisms of boundary elements is not taken into account in the study of the EMP. Many tests and studies on the steel plates (as presented in Chapter 2) have proved that in order to develop the full tensile mechanisms for the inner plate the boundary frame must be stiff enough so that its deformation by shear will be very little in elastic range and not affect the deformation of the steel plate. The influence of each component will be discussed in detail hereafter.

5.3.3.1. Prior-to-buckling shear resistance of EMP

There are two distinct criteria being usually used to characterize the failure load of an element or a member under compressive load. The first one is the load causing the local stresses somewhere on the

cross-section of the element to reach the yield stress of the material. The other one is that load which causes the in instability of the member, resulting in a premature failure of the member. The presence of very thin plate loaded in shear immediately reminds of stability problem and the elastic instability commonly occurs before the stresses reach the yield stress. As well known in plate theory that when subjected to a shearing force in excess of that which will cause buckling, a tension zone will develop in the plate and the plate is still capable of resisting additional shear up until the tension yield stress of the material is attained. For stocky plates or plates with stiffeners (like plates in girder structures) the critical loads are significantly large and their contribution to the total shear strength of the plate is significant. However, for very thin plates in comparison with the boundary dimensions the slenderness is very high (up to 300-400 and even up to 1000) and it is clear that the thin plates are almost immediately buckled when being loaded. Therefore, the shear resistance that is attributed to the ultimate shear strength of the plate before buckling will almost be dropped (Thorburn et al, 1983).

The question imposed here is that what are the differences between the behaviour of the EMP and the un-stiffened plate? Before the instability occurs it is necessary to know how large the contribution of the resistance of EMP before buckling to its ultimate shear resistance is. In addition, the fabricated EMP will have initial out-of-straightness that puts it very easy to incipient buckling. Therefore, is it possible to neglect the shear resistance of the EMP before buckling like the un-stiffened plate? Similarly to the behaviour of un-stiffened plates, the prior-to-buckling shear resistance of the EMP is dominated by elastic resistance. The larger elastic critical loads of the EMP are the larger contribution to ultimate resistance of the EMP is. On the contrary, if the critical loads or instability loads of the EMP are very low the contribution to ultimate resistance of the EMP is very small. And if they buckle immediately when the shear load applies there will be little contribution to ultimate shear resistance of the EMP.

A lot of numerical simulations are performed to determine critical loads of various types of EMP loaded in shear. First, critical analysis of the square EMP with different profiles is executed and then different ratios length/width of the EMP which are 1/2, 1/3, 2/1, 3/1… are the subjects of the next analyses. For rectangular EMP with the same ratio of length/width, there are two ways to erect the EMP, that is, the dimension LD of stitches will be parallel to the length direction or to height direction. Because of these differences the critical loads of EMP may be different regardless of the same ratio. Figure 5-17 shows the differences between two directions of erection. Figure 5-18 to Figure 5-20 show the critical loads of square and rectangular EMP with different ratio dimensions and profiles.

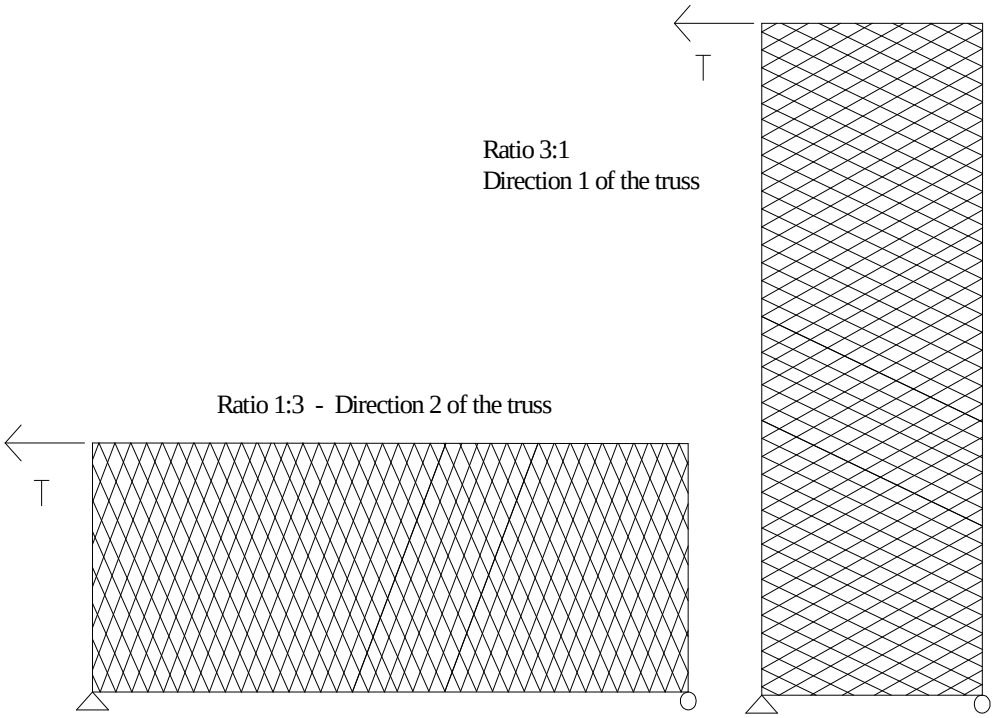

Figure 5-17 – Two directions of EMP loaded in shear

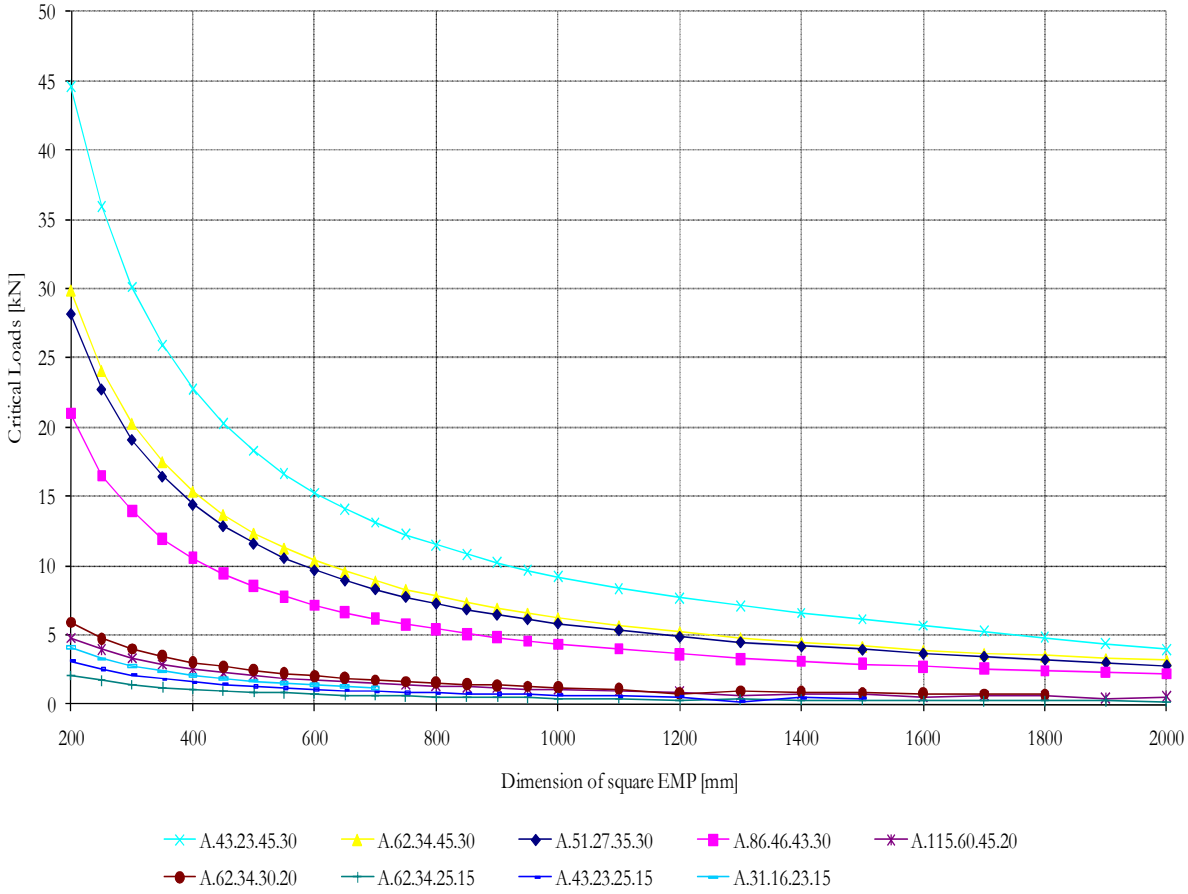

Figure 5-18 – Critical loads of different square EMP with different profiles subjected to shear.

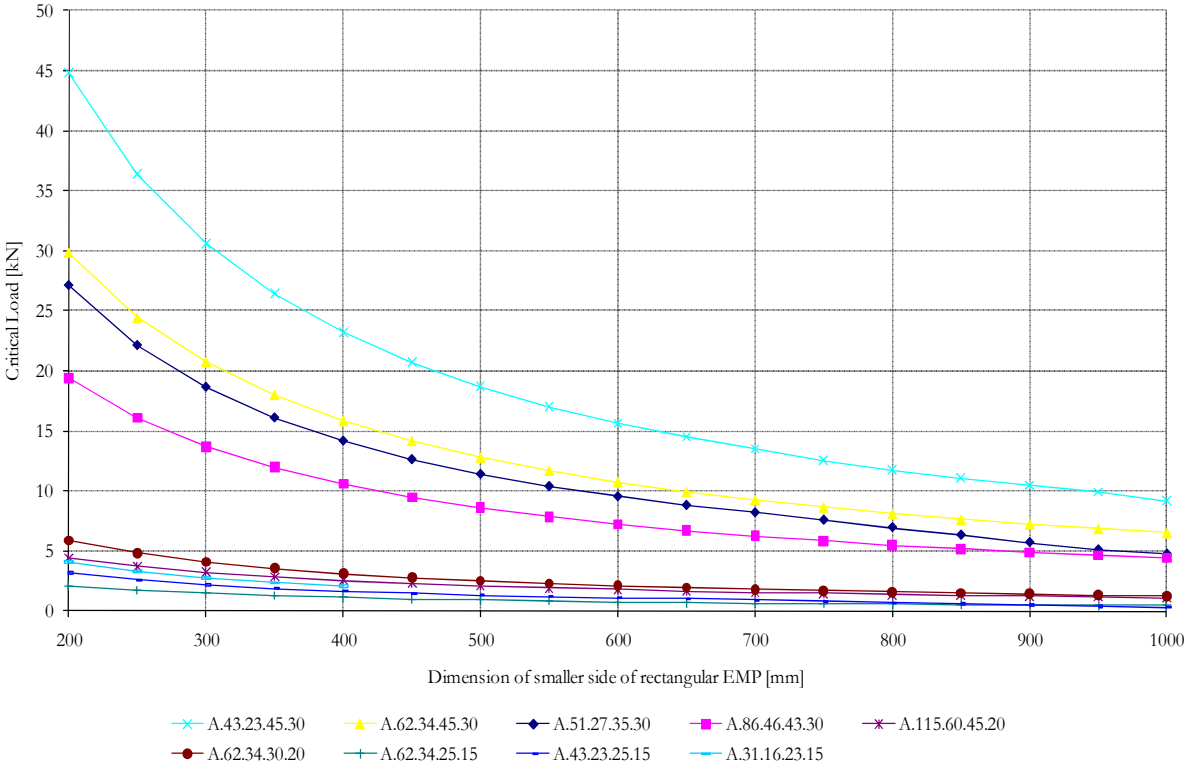

Figure 5-19 – Critical loads of rectangular EMP with ratio 1x2 direction 1 subjected to shear

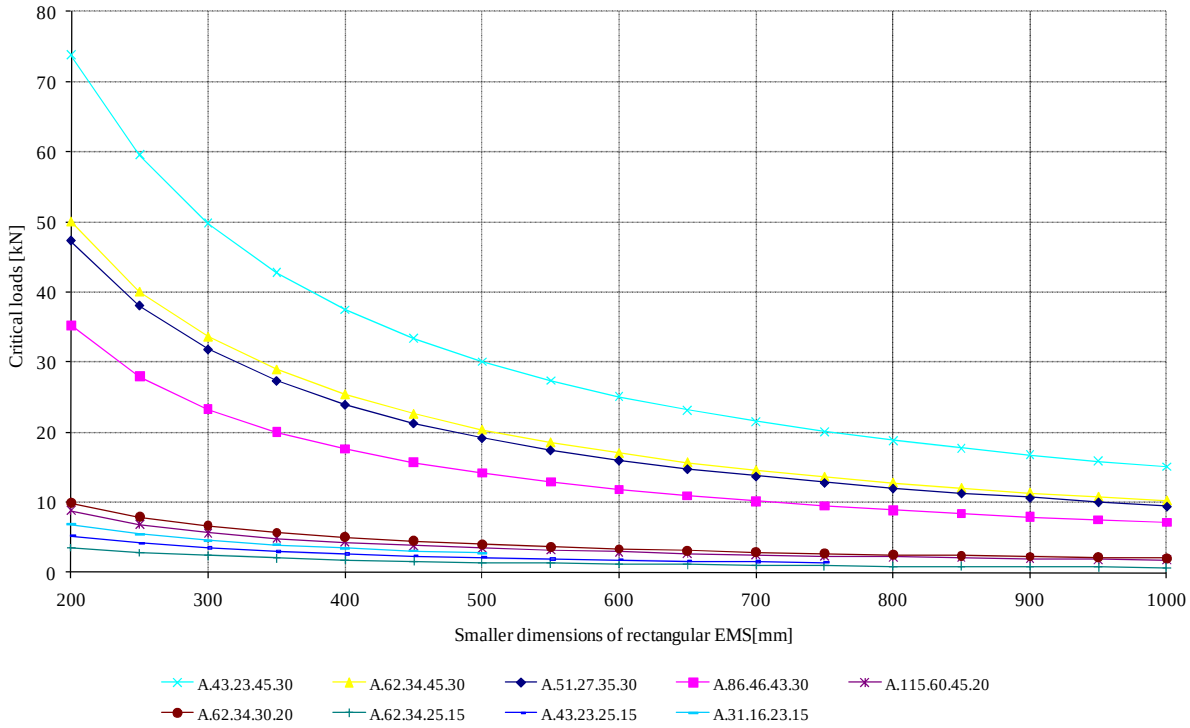

Figure 5-20 – Critical loads of rectangular EMP with ratio 1x2 direction 2 subjected to shear.

As expected, the critical loads decrease rapidly when the dimensions of EMP increase. For many profiles of EMP with the small values in thickness (such as A115x60x45x20, A62x34x25x15…) the critical loads are approximately equal to zero. This means that under very low shear loads the EMP buckle and some EMP are immediately buckled at the beginning of presence of loads. Therefore, it is possible to neglect the contribution of the shear resistance of the EMP before buckling to its total shear resistance.

To conclude, the effects of out of plane deformation and residual stress are neglected in order to determine the contribution of elastic resistance of an EMP before buckling. These assumptions are acceptable because of the very low critical loads of the EMP.

5.3.3.2. Effects of initial deformations or imperfections on ultimate resistance of the EMP

All the real EMP almost has some initial lack of flatness caused by manufacturing processes. The important effect of initial deformations or initial geometric imperfections is to produce out-of-plane deformations from the onset of loading.

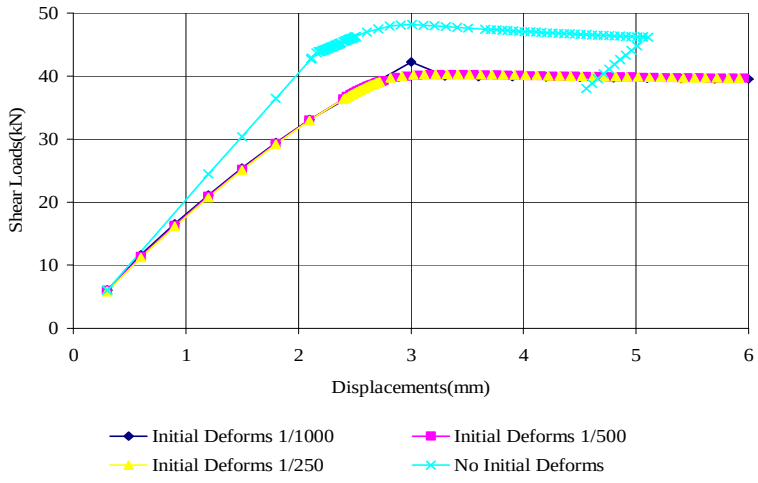

Figure 5-21 – Shear behaviour of square EMP B=500mm MD51-27-35-30 with different imperfections

Initial imperfections could have an effect on the buckling of EMP. However, the effect on the collapse load or maximum load of EMP is much less important because the tensile component of load resistance dominate the behaviour of EMP. The tensile component, which is insensitive to the imperfections, reduces the sensitivity of shear EMP strength to imperfection level. Many numerical simulations are done with different initial deformations and different profiles and dimensions to estimate the effect of imperfections on ultimate strength of EMP. Figure 5-21 shows the behaviour of a square EMP B=500mm with profile A51-27-35-30 with different imperfections.

As clearly observed in all cases, the imperfections only slightly reduce the initial or elastic stiffness of the EMP. However, they don't much affect the maximum shear resistance.

5.3.3.3. Maximum or post-buckling shear resistance of the single EMP and equivalent models

The main objective of this part is to study the ultimate behaviour of the EMP subjected to shear. As mentioned above, the ultimate shear resistance of a very thin EMP is dependent on the tension field action which develops after the EMP globally buckles. Due to early global buckling and the dominance of tension field the EMP is insensitive with initial deformations and the contribution of shear resistance of the EMP before global instability is negligible. With the aids of the numerical simulations ultimate shear resistance of the EMP will be determined. Analytical models to estimate the properties of the tension field of EMP will be developed.

As introduced in previous parts, in the numerical simulation each bar of a stitch in the EMP will be modelled by a spatial beam finite element. The EM material used for determining the ultimate resistance of the EMP is modelled by bilinear law with the strain hardening.

Knowing that initial deformations are always present in EMP, imperfections which are related to the first instability mode are imposed on EMP onset of loading with the value of 1/1000 dimension of the sheets. These imperfections are, of course, much smaller than in reality, however, as proven previously, the imperfections have very little effect on the ultimate behaviour of EMP.

A very large number of numerical simulations (approximately 2500 cases) have been performed to determine ultimate shear strength of many EMP which are different in material profiles, in dimensions, and in directions of loading. Figure 5-22 presents typical force displacement relationships for simulations on different square EMP made from commercial profile A51-27-35-30.

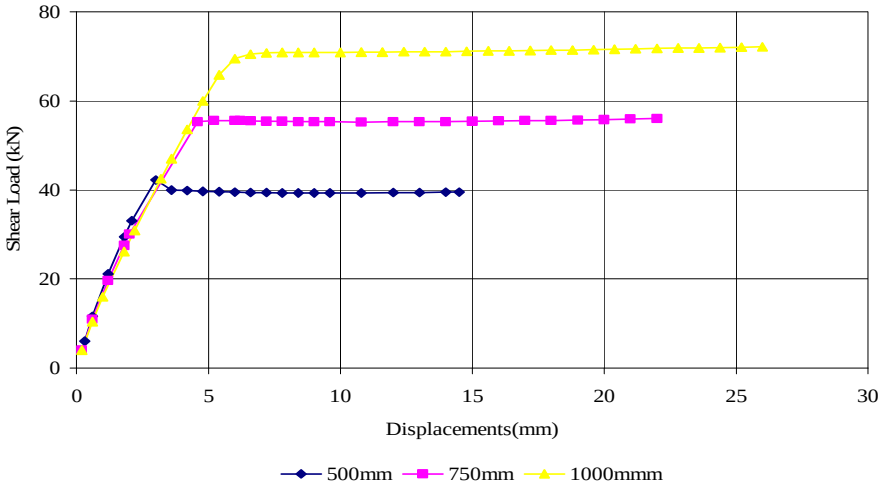

Figure 5-22 – Shear behaviour of three square EMP: type of A51-27-35-30

Figure 5-22 presents the typical force displacement curves of rectangular EMP with ratio 1:2 and direction 1 which are made from commercial profile A51-27-35-30.

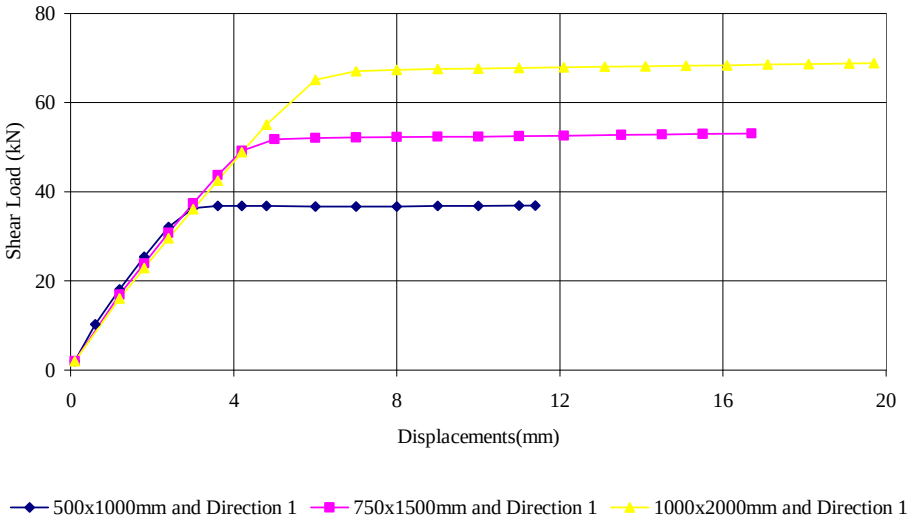

Figure 5-23 – Behaviour of rectangular EMP with ratio 1:2 and direction 1 subjected to shear

It is clearly observed that the elastic stiffness in shear is nearly the same for different sizes of the square and rectangular EMP. If the dimensions of EMP increase, the number of stitches and the ultimate resistance increase accordingly. When plasticity of EMP occurs, the global stiffness of EMP decreases substantially and the global displacements increase under constant or even decreasing load.

Having assessed that the ultimate shear resistance of the EMP is controlled by a tension band, it gives an idea to find the parameters which affect this tension band. Some numerical tests are made to determine the properties of the tension band. The first trial is to plot the ultimate loads in functions of sizes of the EMP. Figure 5-24 to Figure 5-26 show the values of plastic resistance and corresponding dimensions of the square and rectangular EMP with different ratios and directions of erection (as explained in 5.3.3.1)

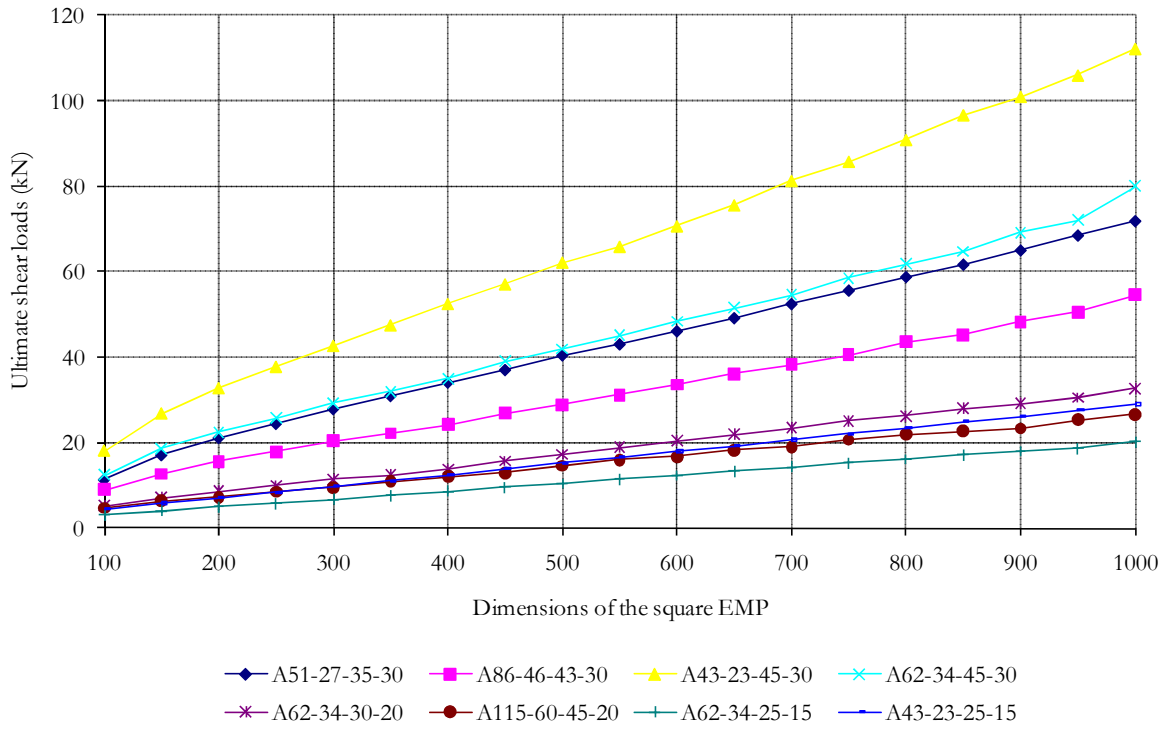

Figure 5-24 – Plastic resistance in function of the dimensions of square EMP subjected to shear

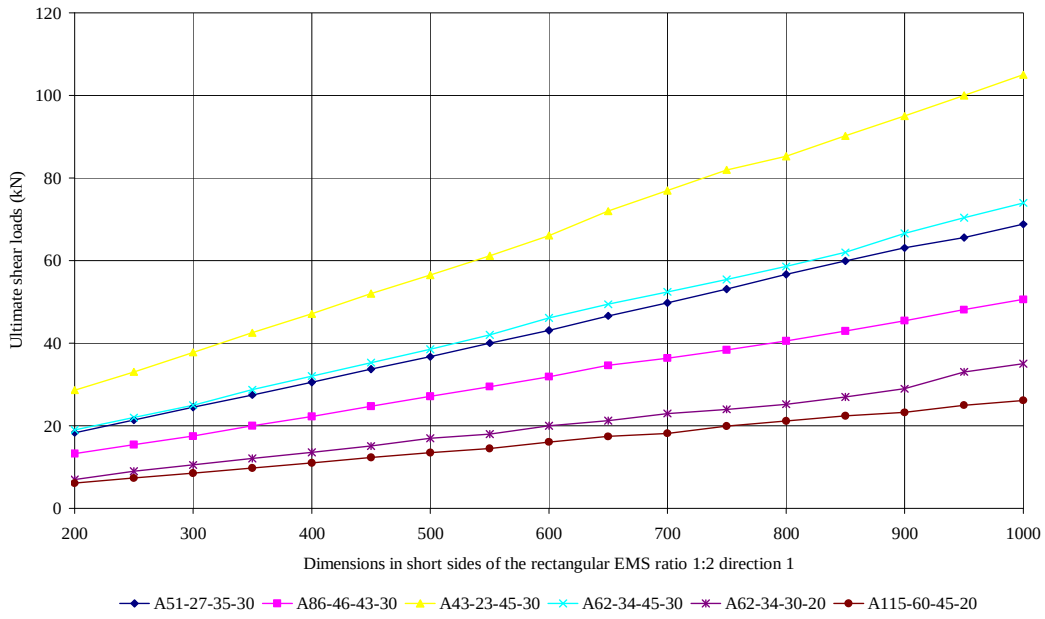

Figure 5-25 – Plastic resistance in function of the dimensions of rectangular EMP ratio 1:2 and direction 1 subjected to shear

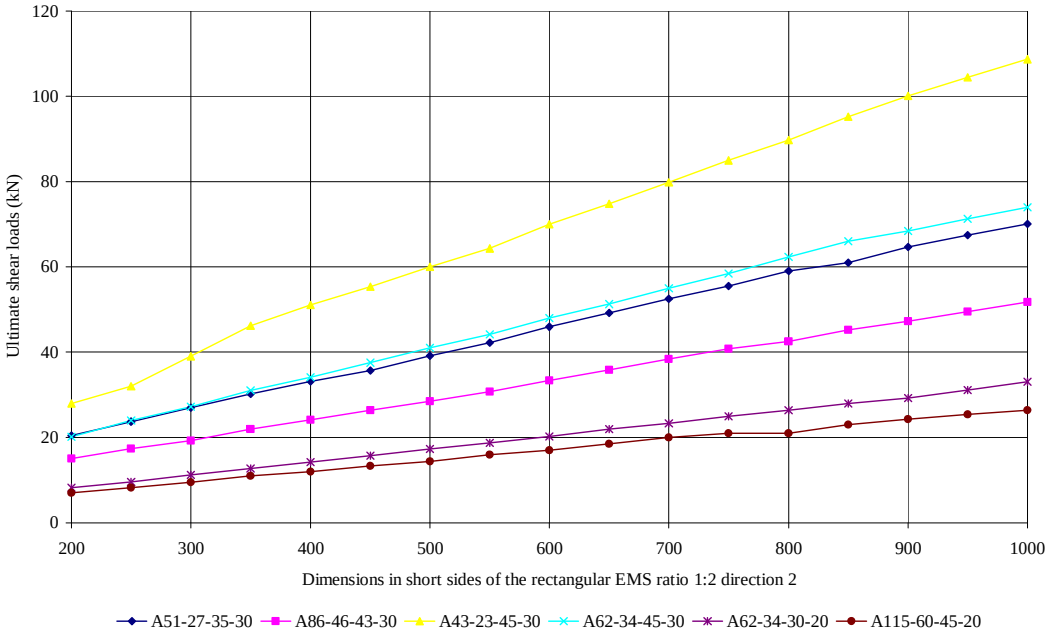

Figure 5-26 – Plastic resistance in function of the dimensions of rectangular EMP ratio 1:2 and direction 2 subjected to shear

Nearly perfectly linear relationships are clearly observed. This implies that there is a constant development of the effective width of the diagonal band in tension with the dimension of the EMP. It can also be seen that the loads and their slopes are dependent on the thickness and the void of the EMP (higher for commercial profiles with big thickness or/and small void percentage). These considerations give the idea to plot, in function of the dimension of the sheets, the plastic resistance divided by the thickness of the sheet and by the ratio between the width (A) and the length of the bars (l_{bar}). These dimensions are explained in Figure 5-30 and in Chapter 3. Results are plotted in Figure 5-27.

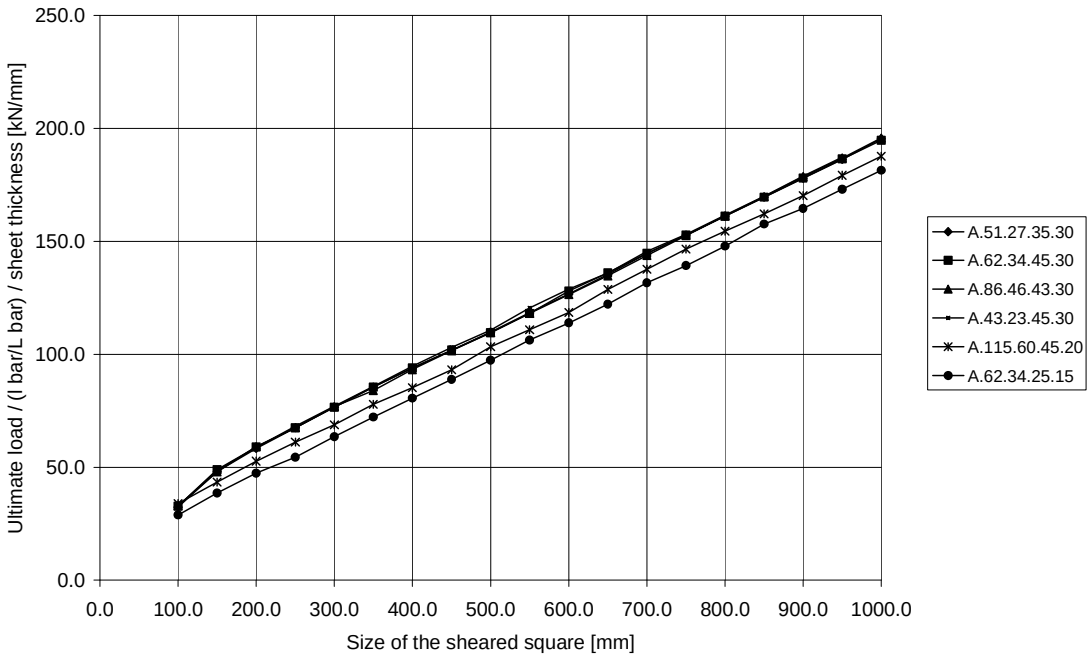

Figure 5-27 – Plastic resistance characterised by a single linear relation for all the commercial profiles

It is clear that all curves have almost the same slope for all the commercial profiles. This indicates that the effective width of the equivalent band increased proportionally to the sizes of the EMP. It gives an idea to plot plastic resistance divided by the thickness of the sheet, B, by the ratio between the width and the length of the bars (A and l_{bar}), by the diagonal length (l_{dia}) and by the ultimate stress generated in the band (f_u), in functions of the sizes of the EMP. These curves are plotted in Figure 5-28 and Figure 5-29. The symbols A, B, f, l_{bar} and l_{dia} are graphically explained in Figure 5-30.

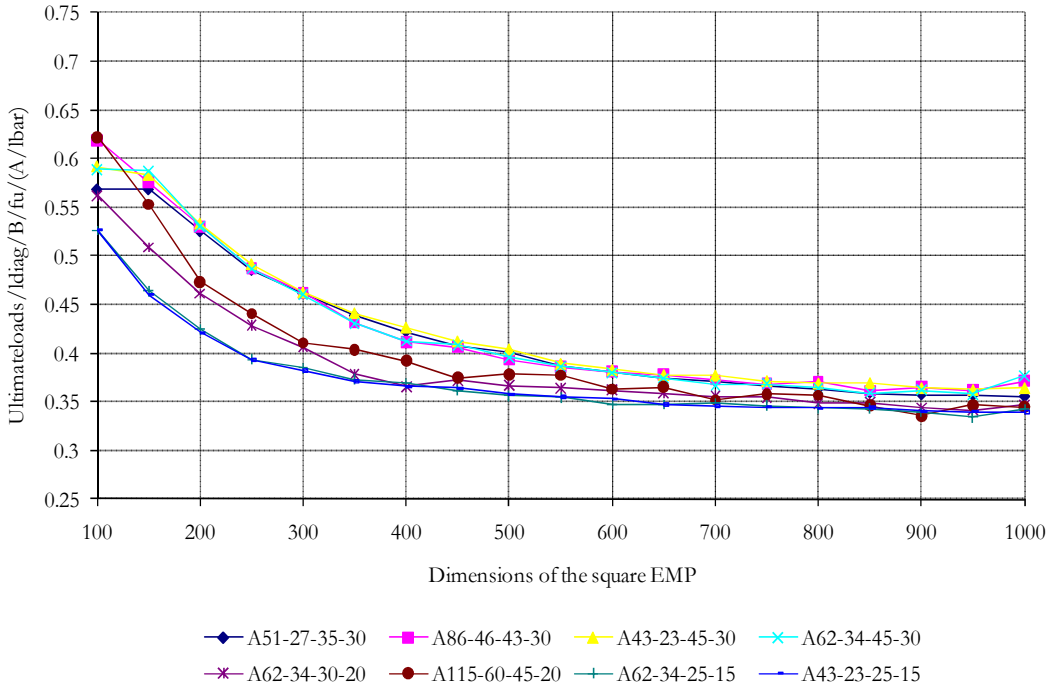

Figure 5-28 – Relationship between dimensions of ratio of square EMP and their plastic resistance divided by the product of diagonal length (l_{dia}), thickness (B), ultimate stress (f_u)and ratio of width to length of bars (A/l_{bar})

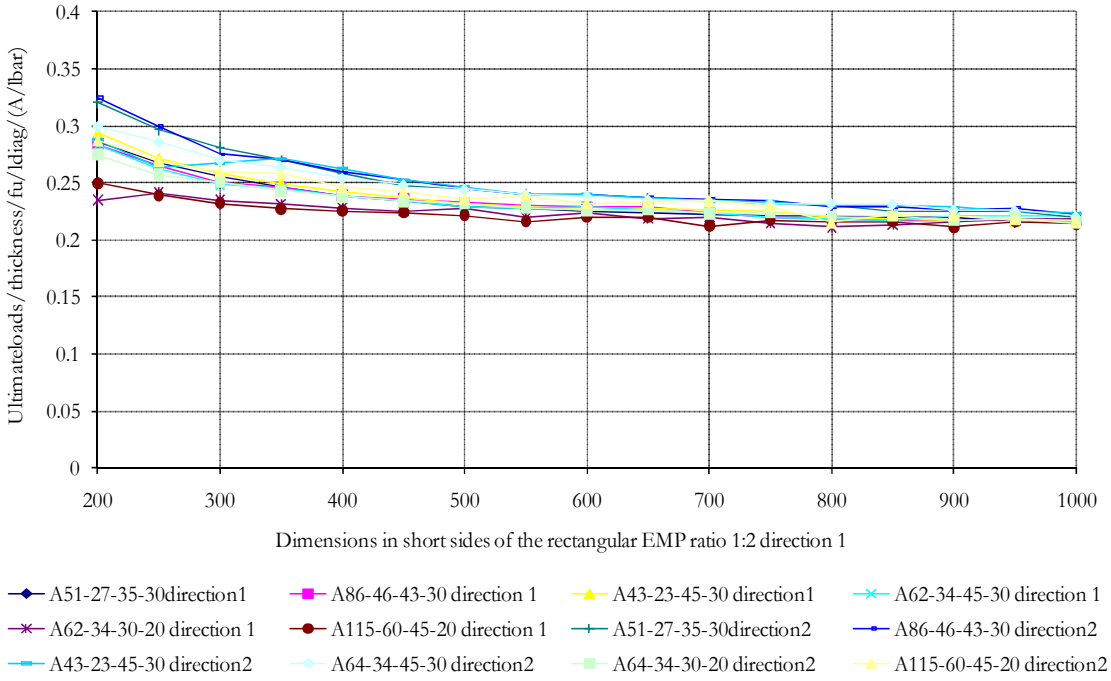

Figure 5-29 – Relationship between dimensions of ratio of rectangular EMP ratio 2:1 direction 1 and their ultimate resistance divided by the product of diagonal length (l_{dia}), thickness (B), ultimate stress (f_u) and ratio of width to length of bars (A/l_{bar})

An interesting result observed from pictures above is the convergence of all curves when the sizes of the EMP are large enough. For any commercial profile, depending on the ratio between the width and height of the EMP, all the curves have an asymptote. This asymptote is approximately at a level equal to 0.35, 0.27 and 0.18 for square EMP, rectangular EMP with ratio 2/1 and rectangular EMP with ratio 3/1, respectively. This can be very useful to determine the ultimate strength of the EMP to reinforce buildings frames against earthquakes.

In conclusion, considering the ultimate shear resistance, EMP works equivalently to a diagonal band in tension. The tension behaviour of the band can represent the shear behaviour of the EMP. In short, the shear resistance of an EMP can be expressed by following expression:

$$V = \gamma.\alpha.l_{dia}.B.f = W.B.f \qquad \text{Equation 5-1}$$

Where: l_{dia}, B, f are explained in Figure 5-30

$V = \gamma.\alpha.l_{dia}.B.f = W.B.f$

$\alpha = A/l_{bar}$;

γ is the factor depending on the ratio between width/height of the EMP.

$\gamma = 0.35$ for square EMP

$\gamma = 0.23$ for rectangular EMP with ratio 2/1

$\gamma = 0.18$ for rectangular EMP with ratio 3/1

$W = \gamma.\alpha.l_{dia}$ is the effective width of the EMP

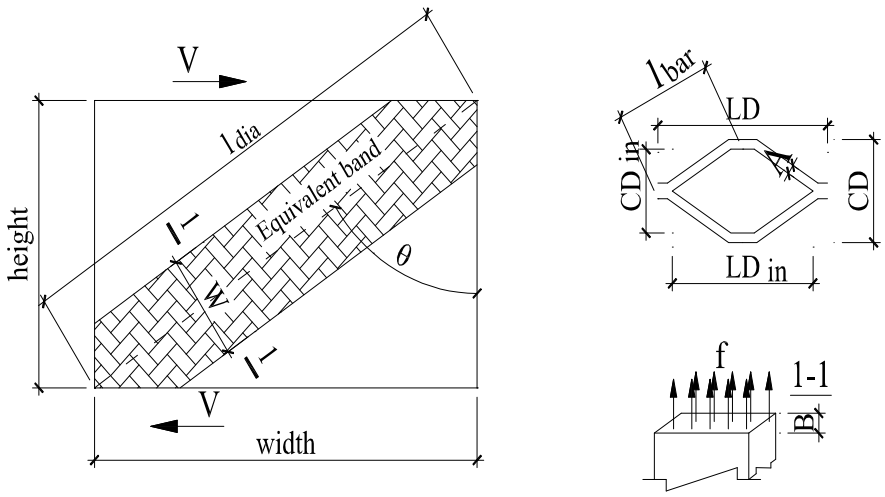

Figure 5-30 – The equivalent band of the EMP

5.3.3.4. Shear resistance of a combined EMP

It is necessary to stress that the simplified shear behaviour of the EMP, presented in the previous section, is applicable for the single EMP. This means that for the EMP having the widths less than the fabricated width (±1,25m), it is possible to predict its shear behaviour by Equation 5.1. However, in reality, in order to apply the EMP to the real RC-MRF with the dimensions of width x height about (4-8 m) x (2.5-4 m), the combination between two, three or more EMP is quite evident, as mentioned in experimental study (Chapter 4). Therefore, it is necessary to examine the shear behaviour of a combination of EMP. There are some possibilities which can be used to connect several EMP to obtain larger EMP. Two EMP will be connected together thanks to the use of an intermediate gusset plate by using either weld connection or glue connection (Chapter 4). Figure 5-31 presents a combined EMP by using weld connection.

Figure 5-31 – Combination of two EMP A51-27-35-30

A very crucial point raised here is that what are the suitable characteristics of the intermediate plate? As explained explicitly in section 5.3.2.4, in order to exploit the ultimate shear strength and stiffness of the EMP, it is necessary to have a boundary frame stiff enough. If the intermediate plate is very stiff and it is connected to the boundary frame of the EMP, the behaviour of a combined EMP will be divided into two different equivalent bands. Figure 5-32 shows a view of these two bands.

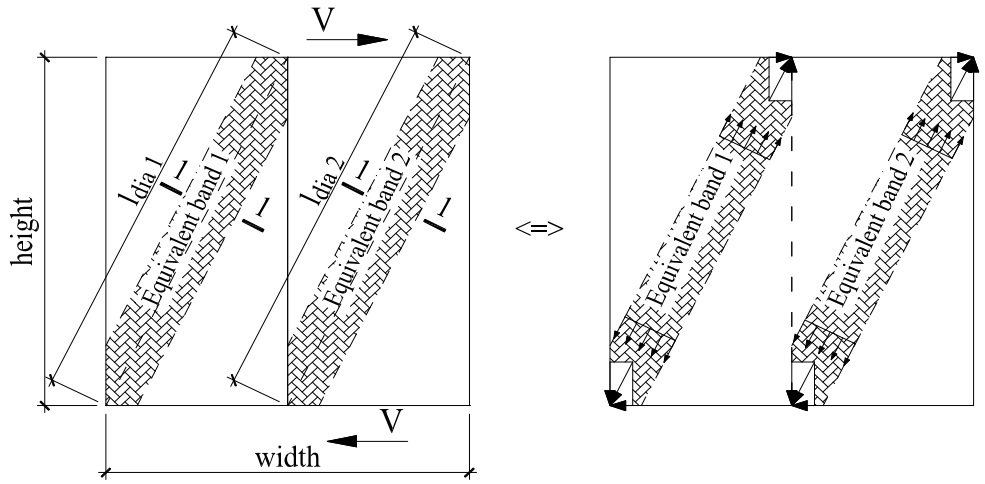

Figure 5-32 – The simplified model of a combined EMP with stiff intermediate gusset

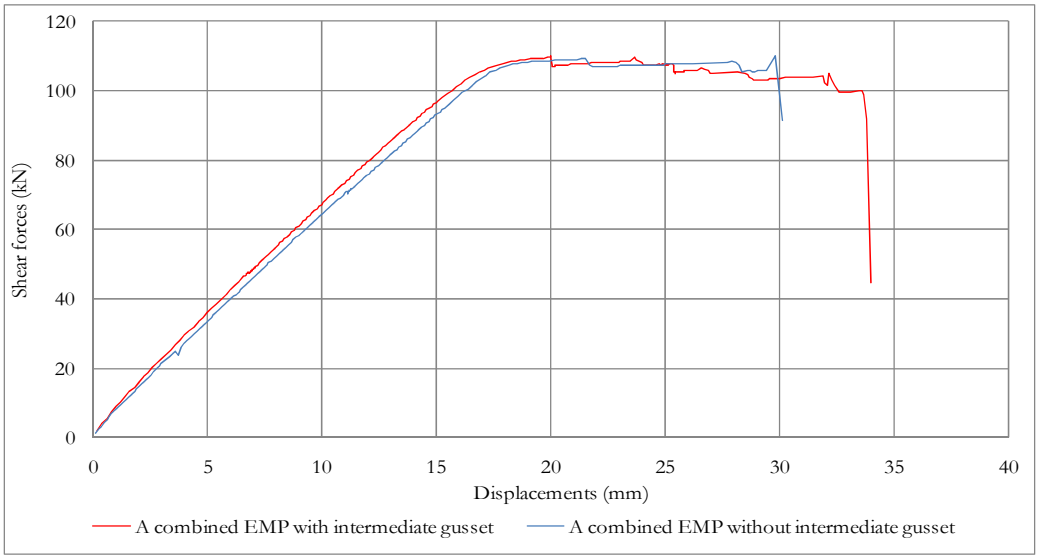

Figure 5-33 – Influence of gusset plate on the shear behaviour of a combined EMP

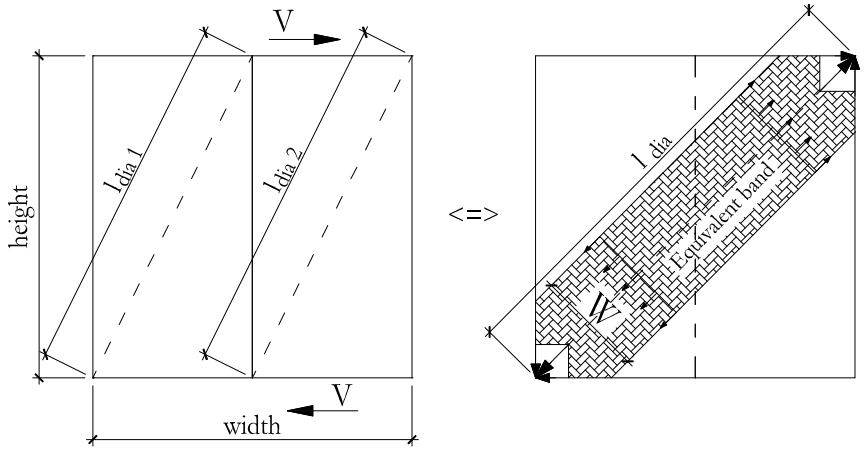

Figure 5-34 – The simplified model of a combined EMP with non-stiff intermediate gusset

On the contrary, if the intermediate plate is not stiff enough and not connected to the boundary frame, it may only play a role to link two different EMP forming a combined EMP and may not contribute much to the behaviour of the combined EMP. This implies that two single EMP with the intermediate gusset will create a new combined EMP which may be equivalent to a single EMP having dimension twice larger than the original ones. A number of numerical tests have been performed to see the influence of non-stiff

gusset plates on the shear behaviour of a combined EMP. Figure 5-33 presents the shear behaviour of the combined EMP with and without the intermediate gusset plate. There is only a light difference observed in these two curves. It is necessary to note that the cross-section dimension of the gusset plate is selected in these tests as the minimum value based on the capacity of the individual EMP. Apparently, the shear behaviour of a combined EMP is almost similar to that of a single EMP with the same dimension without the gusset plate. This is graphically explained in Figure 5-34.

5.3.3.5. Drifts and Ductility of the EMP

Ductility is an important parameter of a structure to help it minimize the major damage when subjected to a severe earthquake without much degrading its strength. The larger ductility has the structure the more input energy it can dissipate and the more its ability to sustain large deformations when working in inelastic ranges during the earthquake.

There are different levels of ductility: the ductility of a material, of a structure or a structure's component. The ductility of a system is usually defined as ductility factor. This factor can be defined as either the maximum strain, rotation or displacement divided by the yield strain, rotation or displacement (Popov, 1980). The ductility of material is usually defined by strain ductility. Regarding EM, based on the tensile tests of bars presented in Chapter 4, strain ductility of EM can be expressed as the following equation:

$$\mu_{\varepsilon EM} = \frac{\varepsilon_{uEM}}{\varepsilon_{yEM}} or = \frac{\Delta_{uEMP}}{\Delta_{yEMP}} \qquad \text{Equation 5-2}$$

Because the EM material is a non-constant mechanical product to date, so the ultimate and yield strains of different EM bars in different batch products are largely different. Therefore, its strain ductility also varies largely. However, in order to simply calibrate the ductility of the EMP, the stress-strain relationship of the bars of the rhomb shaped stitches is assumed to be constant and have the values indicated in Table 5-9. These are the average values deduced from a lot of tensile tests.

For a member and/or a structure, the ductility is classified based on their deformation (curvature ductility, displacement ductility etc…). For a structure subjected to seismic actions, the ductility is usually defined based on its lateral displacement. The displacement ductility is calculated by the ratio between maximum and yield displacements. The yield deformation of a structure is determined at the deformation at which a plastic hinge first appears at anywhere. The maximum deformation is defined by several different criteria, such as the deformation at which the global mechanism is formed or at which there is a local failure or much degradation of the strength compared to the ultimate strength… Therefore, ductility of the EMP can be calculated by the ratio between maximum and yield lateral displacements, as the following formulae:

$$\mu_{dEMP} = \frac{d_{uEMP}}{d_{yEMP}} \qquad \text{Equation 5-3}$$

The yield displacement, d_{yEMP}, is determined as the displacement at which the first hinge is formed any where at any bar of the EMP. The maximum displacement, d_{uEMP}, is taken as the value at which the strength of EMP is reduced significantly or equal to the value of 20% of the maximum shear force.

In order to determine its yield and maximum displacements by a numerical approach, the modelling of the EMP is calibrated to provide the same ultimate shear resistances as the EMP (see the previous sections). The only difference is that material properties of 3D bars of rhomb shaped stitches are assumed as multi-linear with both strain hardening and softening of the material, as mentioned in 5.3.2.3, with the aim at determining the maximum displacements of the EMP. In addition, based on this determination of ductility, it is also possible to calculate the yield and ultimate drifts of the EMP under shear.

A lot of numerical simulations have been performed based on the assumptions of material law mentioned above. Figure 5-35 shows examples displacement ductility of the square EMP A86-46-43-30 determined by numerical simulations.

In conclusion, the displacement ductility of the EMP, established by numerical simulations, ranges from 4 to 13.3. The yield drifts based on these calculations are varied from 0.12% to 0.4% and the ultimate drifts

are from 3.0% to 3.5%. It is worth noting that these values are within the values obtained from the tests in both monotonic and cyclic phases of small scale.

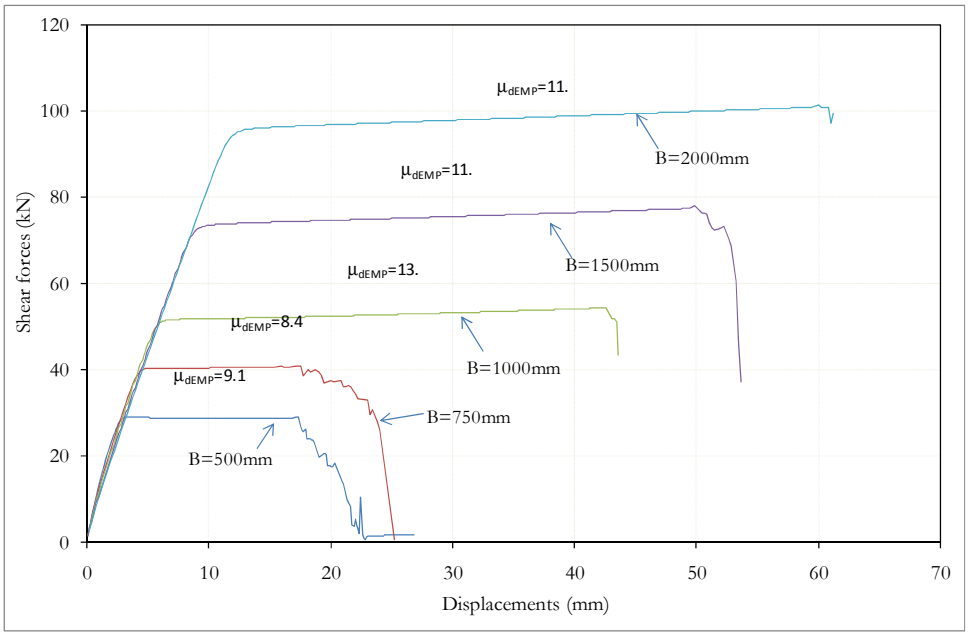

Figure 5-35 – Monotonic behaviour and displacement ductility of square EMP of A86-46-43-30

5.3.4. Simplified behaviour of the EMP under cyclic shear loading

5.3.4.1. Cyclic shear loading behaviour of common structural systems

In order to address the cyclic loading response of the EMP, a comparison with other commonly used systems will be useful. As presentation in detail in chapter 2, there are many different retrofitting systems which are effective to seismically retrofit or upgrade RC-MRFs. This section will re-introduce in very brief their hysteresis behaviour under cyclic loading with aims at assessing the differences between them and the hysteresis behaviour of the EMP. Up to date, there are two main categories of structures used to resist lateral forces: frames and shear walls. For frames, three types of structural systems are commonly used as lateral load resistance: moment resisting frame, simply supported frame with steel bracing or vertical shear walls. The hysteresis behaviour of a moment resisting frame is shown in Figure 5-36. This curve was obtained from a structural assemblage comprised of two half columns and two beams (Popov E.P, 1980). It shows a very good ductility, with the ductility factor in excess of ten. The failure of this system is usually due to the contribution of second order effects in large lateral displacements.

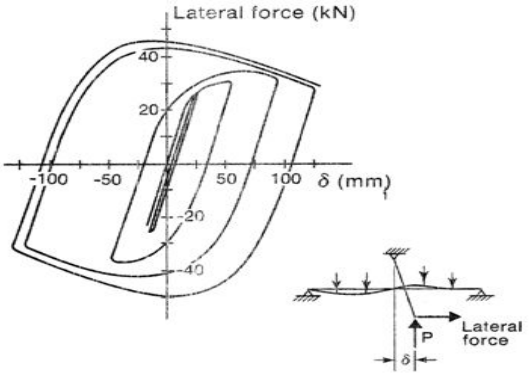

Figure 5-36 – Hysteresis behaviour of a Moment Resisting Frame (Popov E.P, 1980)

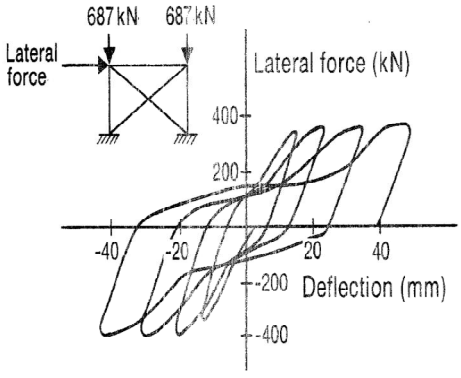

Figure 5-37 – Hysteresis behaviour of a Diagonally Braced Frame (Popov E.P, 1980)

For the frame systems using diagonal braces, the hysteresis behaviour is quite different from one to the others. It is much dependent on the type of braces used in the structures. The systems from two typical configurations, K and X-bracing (conventional braces), generally exhibit a degenerating pinched loop behaviour when subjected to cyclic loads. The hysteresis behaviour of X-bracing system is presented in Figure 5-37. The pinched effect is the result of the buckling of one diagonal in the brace (Tromposch and Kulak, 1997). Recently, Buckling Restrained Braces have been introduced to improve the disadvantage of the behaviour of bracings.

Another advanced type of the frame systems commonly used to date is eccentrically brace frame. This system is designed so that the short link yields before the yielding of buckling members (Popov E.P, 1980).

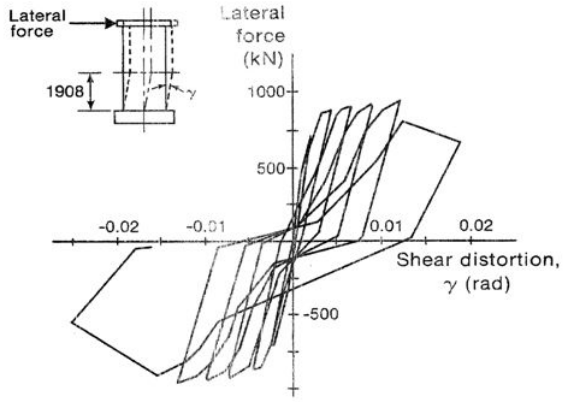

Figure 5-38 – Hysteresis behaviour of a Reinforced Concrete Shear Wall (Oesterle, R.G, 1978)

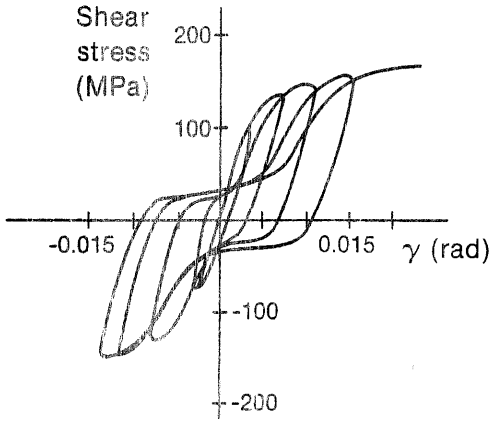

Figure 5-39 – Hysteresis behaviour of an un-stiffened steel plate shear wall (Takahashi Y., Takeda, 1973)

Shear walls are also commonly used as the lateral force resisting system. There are two typical types of shear walls: reinforced concrete shear walls and shear walls made from metal. The hysteretic loops of the reinforced concrete shear walls vary greatly, mainly depending on the configurations and the detail of the longitudinal and transversal reinforcements. Hysteresis loops of a simple reinforced concrete shear wall are illustrated in Figure 5-38. The pinching in the diagram is the result of reinforcement yielding and concrete cracking.

The shear walls made from metal, especially from steel have been gained recently acceptance. There are several configurations of this type of structures. They are discussed in chapter 2. Two typical hysteretic loops of two different configurations, which are un-stiffened steel plate shear walls and heavily stiffened steel plate shear walls, are presented in Figure 5-39 and Figure 5-40.

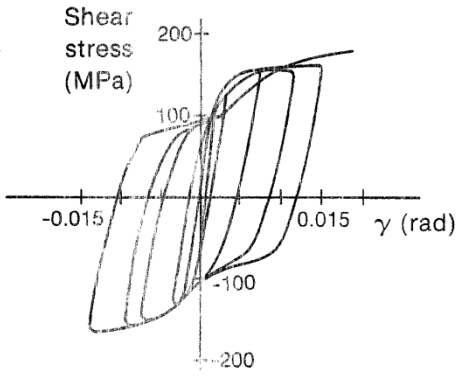

Figure 5-40 – Hysteresis behaviour of a heavily stiffened steel plate shear wall panel (Takahashi Y., Takeda, 1973)

5.3.4.2. Comparison of the hysteresis behaviours

When assessing the hysteresis behaviour of any structural system, it is necessary to compare with what is considered as ideal hysteretic behaviour. The ideal hysteresis behaviour can be considered as one that maximizes the enclosed area for a final given deflection. The loops of the ideal hysteresis behaviour should be stable and non-degenerating in strength of the system. It simply means that these loops should continue to trace approximately the same load versus deformation path for each subsequent cycle.

In most of structure systems, hysteretic response of a steel moment resisting frame, as presented in 5.3.4.1 and Figure 5-36, rather resembles the ideal one that is previously described. The energy dissipated by this system is rather large based on a big amount of area enclosed by the hysteretic loops. In addition, this behaviour is very stable, following nearly the same path for each of the higher loading cycles. This also leads to a stable energy dissipated in the system cycle by cycle. This ideal hysteretic behaviour is also more or less observed in eccentrically braced frames, concentrically buckling restrained braced frames and in heavily stiffened steel plate shear walls.

For a steel plate shear wall, the hysteresis behaviour is almost dependent on its critical resistance. If the steel plate shear wall buckles prior to yielding, this will lead to the degradation of both stiffness and strength of the system, and of course some pinching effects of the loops will be observed. The pinched hysteretic loops are the characteristic responses of structures that have members buckling under compressive loads. This behaviour is clearly observed in conventional steel brace system, as seen in Figure 5-37; the members which are yielded in tension cannot carry any compressive load without buckling. A disadvantage of this system is that it must perform a larger deformation to absorb the same amount of energy than a system displaying the same back-bone curve but having fully developed hysteretic loops.

Pinching is a typical characteristic of the hysteresis behaviour of reinforced concrete shear wall and more or less of reinforced concrete beams and columns. The amount of pinching and stability of the loops are essentially related to the configurations of structure and details of the reinforcement. The pinching in this system is not caused by buckling of any member, as in other systems mentioned above, but is the result of the change in stiffness and strength due to the cracking of the concrete and yielding of the reinforcement.

Pinched hysteretic loops are also the typical behaviour of an un-stiffened steel plate shear wall. Due to the very low elastic buckling resistance, the un-stiffened steel plate shear wall is always buckled before yielding, leading to much degradation of stiffness when shear load is reversed.

It is apparent that the observed hysteresis behaviour of the un-stiffened EMP is independent of the resistance of the panel before buckling because the elastic resistance of the panel to buckling is very small. The panel always buckles when the shear load applies and this leads to very pinched effects of the hysteresis loops. This behaviour is somewhat similar to conventional steel cross bracing, un-stiffened steel plate shear walls and reinforced concrete elements. However, the behaviour of the EMP is more pinched than the others, leading to the smaller enclosed area of the loops and lower energy dissipated in the system.

5.3.4.3. General steps to analyse EMP under quasi-static cyclic shear loading

Under a seismic excitation the structure behaves dynamically. This behaviour is dependent on many factors such as the properties of the structure, the characteristics of the earthquake itself and the soil conditions, all having an effect on its dynamic response. Theoretically, in order to understand the real response of a structure under seismic excitations, it is necessary to perform nonlinear dynamic analysis. Some essential information are used as input in this type of analysis, such as material properties, structural properties (plastic resistance, damping…) and hysteretic curves of members or materials…

Generally, a hysteretic curve of a frame member is experimentally or numerically developed by applying a dynamic load or a quasi-static cyclic load in alternate directions. The area enclosed by hysteretic loops is equal to the energy absorbed by the system. If a structure in general or a member of the structure in particular absorbs a large amount of energy and exhibits sound and stable hysteretic loops, that structure behaved well in earthquakes (Tromposch and G. L. Kulak, 1987).

The monotonic loading analyses of a frame member provide an effective means of estimating the envelope of the cyclic response up to the ultimate capacity of the EMP. However, in order to fully

describe the cyclic behaviour, the finite element model must be able to trace the loading and unloading responses with acceptable accuracy. The goal of this section is to develop a simplified hysteretic behaviour of EMP subjected to quasi-static cyclic shear loading by using numerical analyses. The code, FINELG again, is used. Some assumptions have been made, the same as in monotonic simulations, such as initial deformations, mechanical properties of boundary frames, finite elements of the EMP. In addition, the effects of all nonlinearities have been taken into account. A kinematic rule was used to simulate the Bauschinger effect during the load reversals. Many EMP with different dimensions, profiles and directions of erecting the EMP to the testing boundary frames were analyzed to see the development of hysteretic behaviour of the EMS and to address the simplified model. Concerning the analysis of load-deformation curves, the ECCS testing procedure will be followed. It has been summarised in 4.4.2 and 4.4.3.

5.3.4.4. Description of hysteretic behaviour of EMP loaded in shear by numerical simulations

Based on the results from numerical analyses under monotonic loading, conventional yield displacements and the corresponding loads are determined with the assumption that the yield displacements of the EMP will be equal to the displacements at which the first yield at anywhere in the EMP occurs. As in the physical tests, F_y^+, F_y^-, e_y^- and e_y^+ are the yield forces and the yield displacements of the EMP in tension and compression, respectively. Figure 5-41 shows the picture of cyclic loading in numerical simulations.

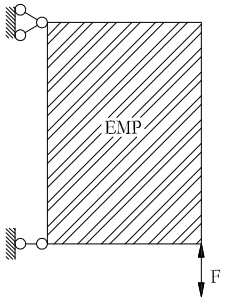

Figure 5-41 – Cyclic loading on EMP in numerical simulations

Many numerical tests have been performed to see the development of the hysteretic behaviour of different profiles and dimensions of the EMP. It has been found that the hysteretic loops of the EMP are similar to those of SPSWs. The difference is that the EMP exhibit much more pinching than SPSWs. Some characteristic properties of hysteretic behaviour of the EMP will be explained by the numerical tests of some EMP hereafter. Table 5-10 gives an example of numerically established of yield loads, maximum loads and corresponding yield and ultimate displacements of square EMP A51-27-35-30 and different dimensions under monotonic shear loading. Table 5-11 gives the controlling displacements in cyclic analyses of different square EMP with the profile A51-27-35-30.

Table 5-10 – Summary of yield and ultimate values of loads and displacements of different square EMP made with A51-27-35-30

Number of order	Dimension of square EMP (mm)	Monotonic yield displacements $e_y^{+,-}$ (mm)	Monotonic yield loads $F_y^{+,-}$ (kN)	Monotonic ultimate displacements $e_u^{+,-}$ (mm)	Monotonic maximum loads $F_u^{+,-}$ (kN)
1	500	1.8	29.4	18.4	40.4
2	750	5.1	054.9	17.9	055.6
3	1000	7.1	070.9	19.1	071.8
4	1250	9.3	086.0	22.5	087.6
5	1500	11	101.2	40.0	105.5
6	1750	12.6	116.2	42.3	121.2

Table 5-11 – Some controlling parameters for cyclic analyses of different square EMP A51-27-35-30

Square EMP B=500mm		Square EMP B=750mm		Square EMP B=1000mm		Square EMP B=1250mm		Square EMP B=1500mm	
Disp. (mm)	No of Cycles	Disp. (mm)	No of Cycles	Disp. (mm)	No of Cycles	Disp. (mm)	No of Cycles	Disp. (mm)	No of Cycles
0.7	1	1.28	1	1.78	1	2.33	1	2.75	1
1.4	1	2.55	1	3.55	1	4.65	1	5.50	1
2.1	1	3.83	1	5.33	1	6.98	1	8.25	1
2.8	1	5.10	1	7.10	1	9.30	1	11.0	1
5.6	3	10.20	3	14.20	3	18.6	3	22.0	3
11.2	3	20.40	3	28.40	3	37.2	3	44.0	3
16.8	3	40.80	3	56.80	3	74.4	3	88.0	3

Following the controlling parameters, cyclic analyses are carried out by gradually increasing the lateral displacements. The typical hysteretic behaviour of an EMP from the numerical simulations can be divided into two stages and explained as follows:

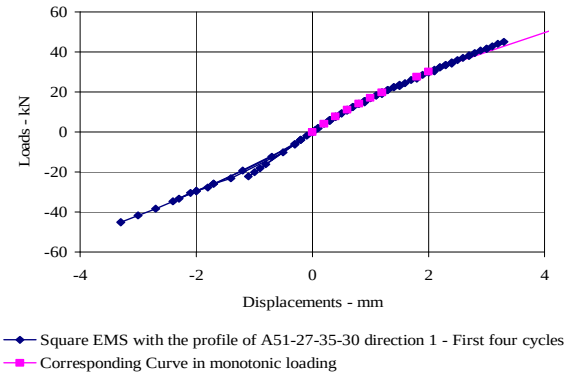

Figure 5-42 – First four cycle behaviour of 750mm square EMP with the profile of A51-27-35-30 direction 1 under shear loading

Elastic stage: the EMP behaves elastically in the first four cycles until reaching the yield displacement, which is nearly the same as in monotonic loading. As clearly observed in Figure 5-42 and Figure 5-43, the initial stiffness of the EMP in monotonic loading and cyclic loading in the first four cycles is almost the same in two directions of loading. It is also observed in the numerical simulation that the out-of-plane waves are quite visible at the beginning of this stage for EMP in large dimensions (>1000mm). This is due to the fact that the critical load of the EMP is rather low and as shown in the figures below there is not much change in the stiffness of the studied EMP due to global buckling. This also means that the tension band has been developed.

Post-buckling stage: After attaining the yield displacement in one direction, the EMP behaves plastically with a quick change in lateral stiffness of the panel, as seen in Figure 5-45. At this stage, the panel will be loaded by groups of three successive cycles with the same target displacement, as explained in 4.4.3. At the first cycle of the first group, when the displacement of the panel reaches $2e_y$, it is easy to see the tension field developed in the panel and it is then unloaded until reaching the displacement of $-2e_y$ with the slope of unloading branch parallel to that of the elastic stage. When the panel is completely unloaded, there still exists a residual displacement due to the plastic deformation. Then the panel is loaded in the opposite direction. At the beginning of this phase, the stiffness of the panel is relatively low, almost equal to zero. As about half of the residual displacement is recovered, the stiffness of the panel is considerably increased until the yield displacement is attained. The panel is then loaded up to the displacement of $-2e_y$. The curve from $-e_y$ to $-2e_y$ is the same as in positive

displacements and tension field development is also observed. The panel is again unloaded when reaching to the displacement of $-2e_y$. The unloading branch is somewhat similar to that in opposite loading. The residual displacement can also be seen clearly. The panel is then reloaded until reaching the displacement of $2e_y$. The increase of lateral stiffness of the panel is observed at the displacement of one half of the residual displacement. When the displacement of the panel reaches to the value of $2e_y$, the corresponding lateral force is somewhat less than that in the previous cycle. In the next two cycles in this group of loading, the hysteretic behaviour of the panel is similar. The degradation of the stiffness and of the strength of the panel is also observed. The next cycles of loading in other groups also give the same phenomenon. It is necessary to stress that the global out-of-plane buckling of the panel is seen in each cycle. This phenomenon causes the pinching in the force-displacement diagram of the panel and smaller energy dissipation in the system. It is also important to note that the backbone curve of the hysteretic behaviour of the EMP is completely coincident with the curve under monotonic loading. Figure 5-45 and Figure 5-46 show the typical hysteretic loops obtained from numerical analyses of the square EMP A51-27-35-30 with dimensions of 500mm and 750mm respectively.

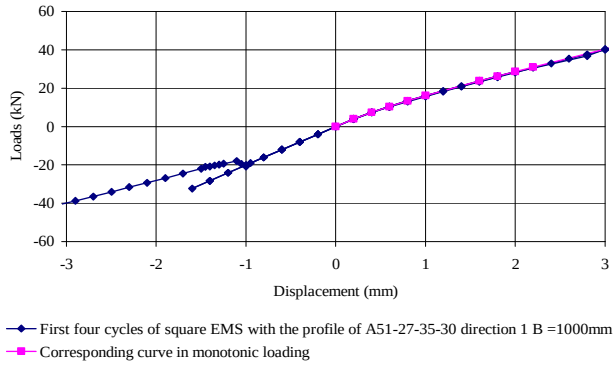

Figure 5-43 – First four cycle behaviour of 1000mm square EMP with the profile of A51-27-35-30 under shear loading

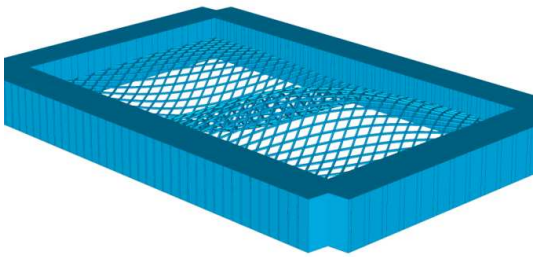

Figure 5-44 – Elastic buckling of the EMP

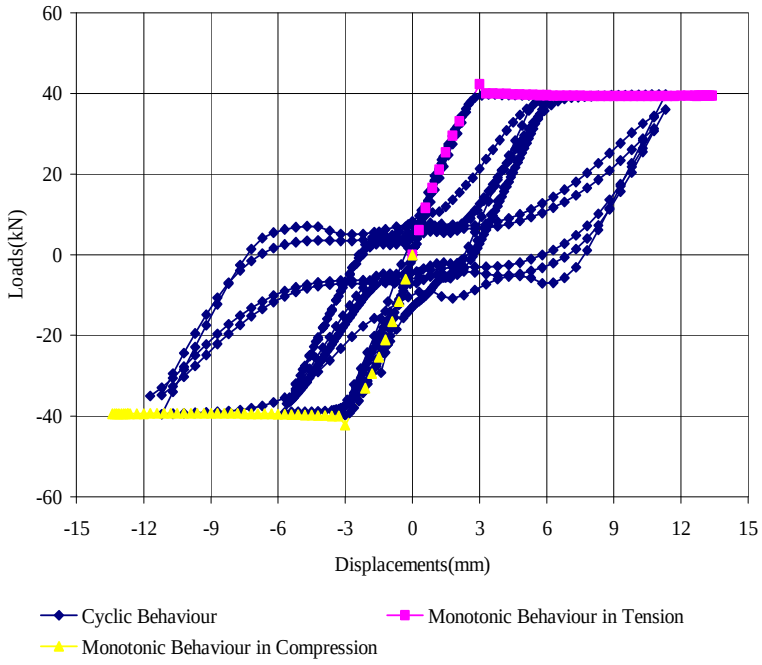

Figure 5-45 – Hysteretic behaviour of 500mm square EMP with the profile of A51-27-35-30 subjected to shear loading

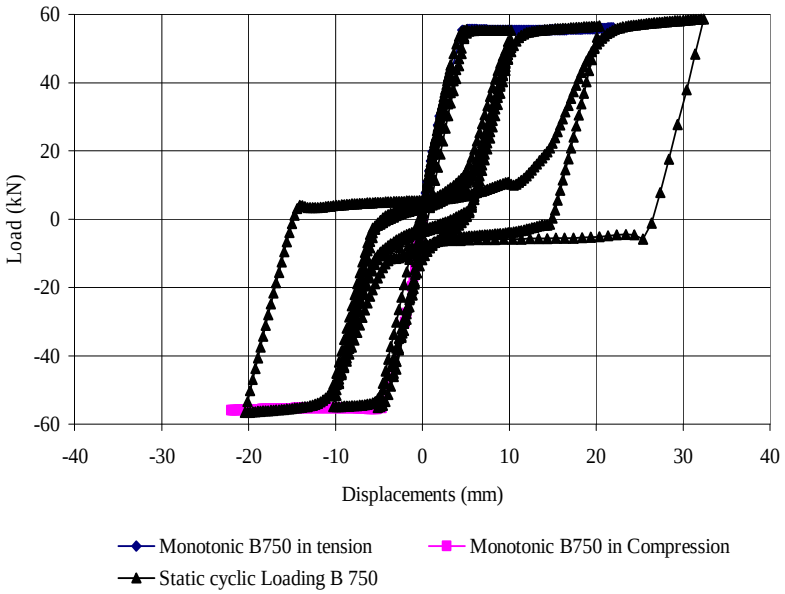

Figure 5-46 – Hysteretic behaviour of 750mm square EMP with the profile of A51-27-35-30 subjected to shear loading

5.3.4.5. Simplified analytical model for hysteretic behaviour of EMP loaded in shear

Based on more than 200 numerical simulations for different profiles and dimensions of EMP cyclically loaded in shear, an approximate bilinear model for hysteretic loops of the EMP has been calibrated. It is valid for EMP surrounded by a very rigid, pin jointed frame as illustrated in Figure 5-47 and described herein. V_{cr}, V_y and V_u are the critical, yield and ultimate shear forces of the EMP, and Δ_y, Δ_p, Δ_u are the yield, plastic and the ultimate displacements, respectively. From points O to A the response is elastic and linear. In fact, at this stage there is a shift of stiffness of the EMP due to buckling. However, the critical load V_{cr} is approximately equal to zero. Therefore, the resistance before global buckling is negligible. After buckling an inclined tension field develops and the EMP yields when the shear load equals V_y. From A to B_1, the EMP strains plastically and from B_1 to C_1 it unloads elastically with the line B_1C_1 parallel to OA. The length OC_1 is proportional to the plastic elongation of the tensile diagonal. At the beginning of load reversal, there is a residual displacement of the EMP due to the plasticity. The plastic contraction of the opposite diagonal occurs. The stiffness of the EMP at this stage is equal to zero. The OD_1 is proportional to the corresponding plastic contraction of this diagonal and it can be computed by:

$$OD_1=\beta OC_1. \qquad \text{Equation 5-4}$$

The ratio β, is taken as 0.5 obtained based on the plastic theory of thin plates (Dubas and Gehri, 1986). The opposite tension field behaviour continues from D_1 to E_1. Contribution of compressive band, when loads are reversed, is also negligible. A new inclined tension field, corresponding to the line D_1E_1, will develop in the opposite diagonal when compressive stresses in this diagonal are fully recovered. At the point E_1 the shear load is equal to $-V_y$. From E_1 to F_1, the EMP strains plastically in the opposite direction and it unloads from F_1 to G_1, parallel to OA. The plastic elongation of the panel diagonal D-D during the second half of the cycle is proportional to the length G_1D_1. Hence the length C_1H_1 is given by:

$$C_1H_1=\beta G_1D_1. \qquad \text{Equation 5-5}$$

At H_1, the EMP buckles and from H_1 to B_1 an inclined tension field develops again. From B_1, the second cycle is similar to the first one. The length of G_1D_2 and C_2H_2 are given by:

$$G_1D_2=\beta H_1C_2 \text{ and } C_2H_2=\beta G_2D_2. \qquad \text{Equation 5-6}$$

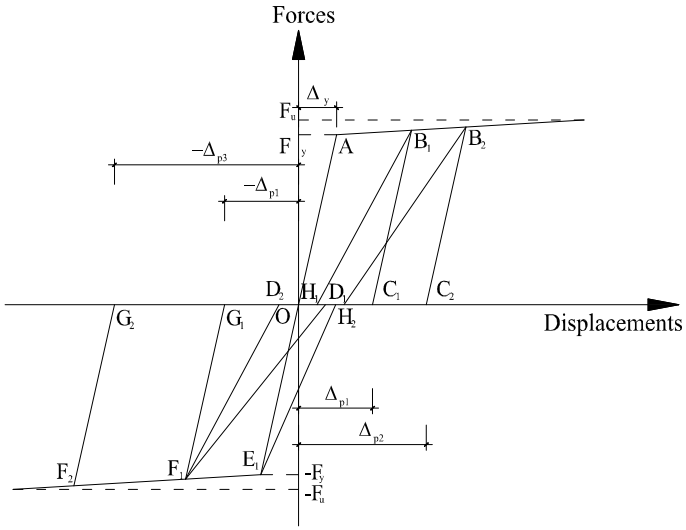

Figure 5-47 – The simplified hysteretic behaviour of EMP

A comparison between the results of the analytical model and of the numerical simulations in first 7 cycles of a test on a square EMP A57-23-35-30 with the dimensions of 500mm is shown in Figure 5-48.

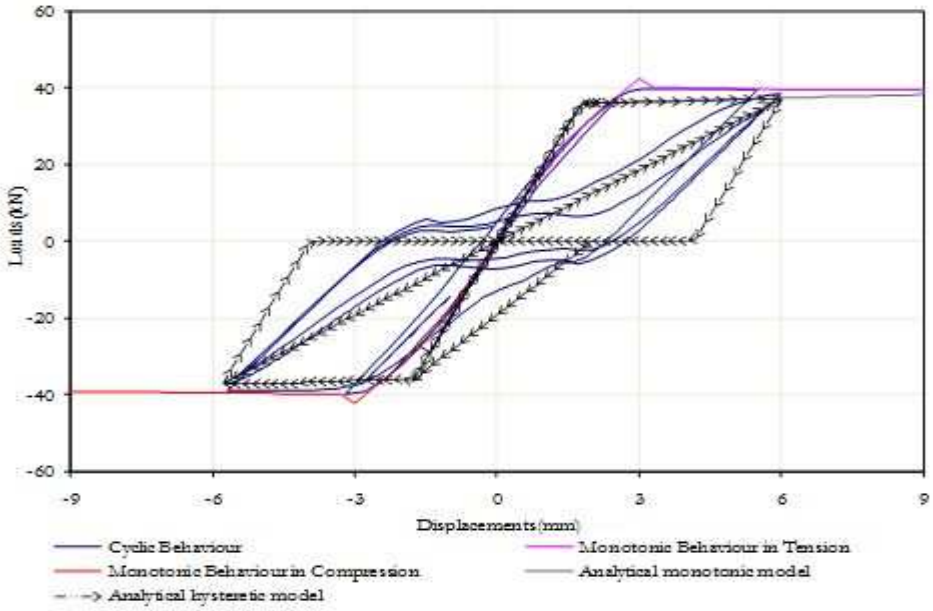

Figure 5-48 – Comparison of hysteretic behaviour of analytical model and numerical model for a square EMP A51-27-35-30 with the dimension of 500mm

5.4. Conclusions

Numerical models making of finite elements have been developed and calibrated on the physical experiments on EMP loaded in shear described in Chapter 4. These numerical models have been used to make a parametric study with the aim of developing a simplified model able to represent the shear behaviour of EMP. The following conclusions have been made based on the comparisons between the tests and the numerical simulations and on the parametric study.

1. There is a good correlation between the results obtained from the experiments and numerical simulations using finite elements. Finelg, the code used for modelling the tests, is capable of predicting both monotonic and hysteretic responses of the EMP subjected to shear.
2. The "one inclined tension bar model" can be used with acceptable accuracy to evaluate the response of the EMP under shear loading. The characteristics of this tension bar is dependent on the

geometrical and mechanical properties of the EMP, on the boundary dimensions of the frame and on some fixed ratios which are related to the ratio between the length and the height of the boundary frame.

3. The hysteresis and monotonic behaviour of EMP loaded in shear can be predicted with reasonable accuracy by the analytical model developed in this chapter.
4. If it is assumed that the EMP is fabricated with steel having constant mechanical properties, the ductility of EMP under shear is in the range from 4 to 13.
5. The ultimate drifts of the EMP can be about 3% to 3.5% and the yield drifts about 0.12% to 0.4%.
6. The hysteresis behaviour of un-stiffened EMP is comparable to the hysteresis behaviour displayed by conventional steel concentric braces, by un-stiffened steel plate shear walls or by reinforced concrete shear walls. Some existing hysteretic models used to represent these three systems can be used to model EMP input in real structures.

6. DESIGN OF REINFORCED CONCRETE MOMENT RESISTING FRAMES (RC-MRFs)

6.1. Introduction

The studies on EMP introduced in the previous chapters have indicated a potential for application of EMP in structural field that is, retrofitting the buildings to improve their resistance to seismic actions. The structural type of buildings chosen for this application is the reinforced concrete moment resisting frames (RC-MRFs). The reasons of choosing this type are:

- first, many moment resisting reinforced concrete structures have been built over the last years in many parts of the World as the main lateral resisting systems, ignoring the seismic situations. Of course, these structures may be located in low seismicity regions. Many of them have not been designed under the situations of earthquake due to the fact that there is no development of modern congruent codes in the countries of those buildings. This may lead to the requirements of seismically retrofitting or even rebuilding for the future uses.
- second, the use of RC-MRFs as the main resisting structural component is now still increasing rather fast thanks to some advantages over other type of structures: (1) cost of building used this structural type being relatively low; (2) construction time being short; (3) allowance for architectural decorations and (4) long-time using.
- third, as already discussed in the previous chapter, in order to activate the capacity of EMP, it should be applied on stiffening components to rather flexible type of structures to enable the development of the tensile mechanism in the EMP. If the EMP is well connected with the beams and columns of RC-MRFs, it will be activated thanks to the large stiffness of the beams and columns.

The main purpose of this chapter is to present the basic design processes and configurations of two groups of RC-MRFs: (1) RC-MRFs in accordance with EC2 and (2) RC-MRFs in accordance with both EC2 and EC8. They will be considered as the existing RC-MRFs as above said. The first group represents the existing reinforced concrete structures designed without taking into account the seismic situations. The latter one is related to structures designed and detailed based on modern seismic code but needing an upgrade for some reasons. For instant, this can occur in a region when the climate change or the observation of higher seismic activities causes the increase of design actions. The increase of PGA in seismic zone activities can lead to the conclusion that there is a lack of resistance of the existing structure.

Designing RC frames is the subject of the next sections of the present study. Clearly, the results of the final seismic retrofit or upgrade and the effectiveness of the EMP on the retrofit solution are significantly influenced by the choices and interpretation of the codes presented in this chapter. Therefore, the main principles and essential criteria of design according to EC2 and EC8 and detail configurations of the general RC-MRFs are first introduced. Then, the studied frames will be described in detail. Some limitations on the cases of RC-MRFs in the current study are also discussed.

6.2. General criteria and design steps pf RC-MRFs according to EC2

6.2.1. Preliminary design

The design of RC-MRFs is an iterative process, starting with the preliminary choice of dimensions of the frame components. This choice is dependent on functionalities, the architectural requirements of the buildings and on the requirements from codes (such as the conditions for normal uses of the occupants leading to some limitations of the dimensions of beams and columns...). Choosing the dimensions, material types and design properties is the next step in preliminary design. A quick linear analysis is then carried out to preliminarily check the deflections of the member and the overall behaviour of the structure.

Generally, choosing the dimensions of the frame components much depends on the experience of the engineers. Many publications (Mosley et al (2007); Nilson et al (2004); Park et Paulay (1974)…) are available to help one select the structural dimensions in the safe side to avoid re-selecting these dimensions. However, this usually leads to much overstrength of the members in particular and of the structure in general.

In the present study, the dimensions will be almost selected based on checking the serviceability limit state required by codes with the aim at obtaining the lower bound values of the dimensions. Concrete and steel grades are assumed to be similar for the all studied buildings: C25/30 and S500 grades. In principle, the grades of the concrete and steel can be changed if the structures are designed with too high over strength or don't meet some essential requirements from codes after trying all other possibilities (such as increasing the dimensions of the structural components...).

6.2.2. Limit states

The overall goal of design is to obtain acceptable probabilities that the structures will perform as the intended behaviour. It means that during the expected life time the structures are not allowed to pass their limit states. According to EC2, limit states include two basic groups which are defined as states beyond which the structure violate an agreed performance criterion. They are (a) ultimate limit states and (b) serviceability limit states.

Ultimate limit states are those related with collapse or failure including loss of equilibrium or stability of the structure or components, and generally govern their strength. This requires that the structure has to be able to withstand the external actions for which it is designed so that it ensures the safety of the building's occupants.

Serviceability limit states are generally corresponding to conditions of the structure in use. Generally, the most important serviceability limit states are:

- Deflections – the appearance or efficiency of any part of the structure or the comfort of occupants should not be adversely affected by the deflections of frame members
- Cracking – local failure due to cracking and spall of the concrete should not cause discomfort to the occupants of buildings or failures of the structure
- Durability – this must be met with the design purpose
- Other criteria such as excessive vibration, fatigue, fire resistance and special requirements in special circumstances

Depending on the properties and importance of the buildings, the importance of each limit state might vary. In the context of this study, the two first serviceability limits will be considered for the initial member sizing of the designed frames.

6.2.3. Material properties

6.2.3.1. Concrete

The selection of the concrete grade is usually governed by the minimum strength that depends on the intensity of loading and the form and size of the structural components. To make it simpler for the design process, as mentioned in the previous section, the concrete grade of all studied frames is taken as C25/30. For the design of cross-sections, the simplified stress-strain relationship of the concrete is presented in Figure 6-1. The values of the characteristic strength, elastic modulus, yield strain and ultimate strain of the C25/30 concrete are taken from Table 3.1 of EC2 and showed in the following table.

Table 6-1 – Material properties of the concrete C25/30

Grade of the concrete	f_{ck}(MPa)	f_{cm}(MPa)	E (GPa)	ε_{c3}	ε_{cu3}
C25/30	25	33	31	0.00175	0.0035

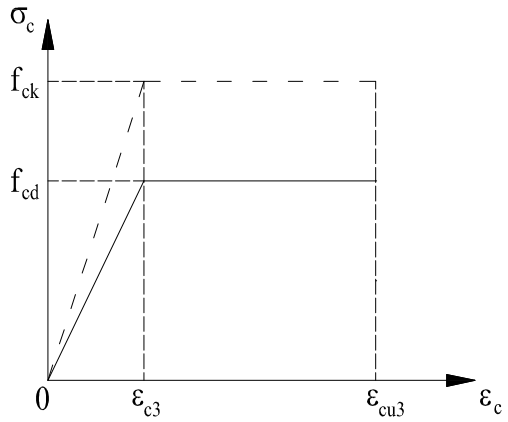

Figure 6-1 – Bilinear stress-strain relation of concrete for the design of cross-sections – EC2

The value of the design compressive strength is defined as

$$f_{cd} = \frac{\alpha_{cc} f_{ck}}{\gamma_c} \qquad \text{(Equation 6-1)}$$

where

$\alpha_{cc} = 1$ – is the coefficient taking into account the long term effects on the compressive strength.

γ_c – is the material partial factor (presented in the following sections)

6.2.3.2. Steel

The modulus of elasticity of the steel is also assumed those suggested in EC2, taken as 200GPa. The characteristic yield strength of the steel used for design calculations is assumed to be equal to the nominal value. The steel grade S500 will be used in the present study. The nominal values of yield and ultimate tensile strengths are those tabulated in EC2 in accordance with EN10080, see Table 6-2.

Table 6-2 – Properties of reinforcement

Grade	Class	Characteristic yield strength f_{yk} (MPa)	Ultimate tensile strength f_t (MPa)	Characteristic strain at maximum force, ε_{uk}	Mean value of density
S500	B	500	$>1.08f_{yk}$	5%	7850 kG/m^3

The stress-strain relationship of the reinforcing steel used for design is also taken from EC2; it is shown in Figure 6-2. The maximum design strain of the steel is usually assumed to be equal to $0.9\varepsilon_{uk}$.

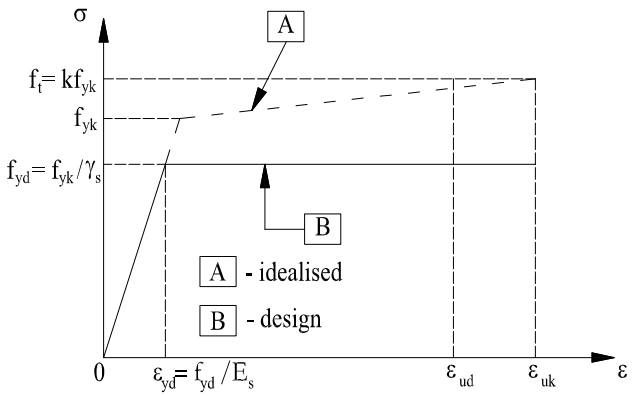

Figure 6-2 – Idealised and design stress-strain diagrams for reinforcing steel (for tension and compression)

6.2.4. Design situations

EN 1990 (2002) has classified the design situations as persistent, transient, accidental and seismic ones. These situations account for all possible working conditions of the buildings from constructional periods to their life time.

In the current study, the persistent situations that correspond to the normal use, in which wind and snow are included, are regarded as the unique design situation of the studied buildings. The influence in the final design and structural member proportioning of the transient and accidental situations (i.e., execution or repair, fire, explosion, impact ...) are neglected.

6.2.5. Partial factors of safety

Partial factors are the parameters taking into account the uncertainties of the buildings during the construction process and their life working time. EC2 defines two types of safety partial factors as those of material and of actions depending on the limit states of the design consideration.

6.2.5.1. Partial factors of materials (γ_m)

EN1991-1 (2002) has proposed the partial factors of materials based on the uncertainties of the strength of the material in actual members and on the severity of the limit state being considered. Recommended values for γ_m of concrete and reinforcing steel from EN1991-1 (2002) are given in Table 6-3. These values will be used in persistent and transient design situations.

Table 6-3 – Partial factors of safety applied to the material (γ_m)

Limit state	Persistent and transient design situations	
	Concrete	Reinforcing steel
Ultimate		
Flexure	1.5	1.15
Shear	1.5	1.15
Bond	1.5	1.15
Serviceability	1.0	1.0

6.2.5.2. Partial factors of actions (γ_f)

Taking into account possible errors and inaccuracies due to some causes such as inaccuracy of calculation, unforeseen stress redistributions or constructional inaccuracies, the design value of action in EN1991-1 (2002) is determined by the product of characteristic actions and the partial factors of safety (γ_f).

The values of these factors are dependent on the importance of the limit state under consideration, on the types of actions and on the probability of particular combinations of actions occurring during the life time of the structures.

Actions are divided into permanent and variable ones. Permanent actions are those related to weights of the buildings and variable ones are those concerning about non-persistent loads. Variable actions are categorized as leading (the predominant variable action on the structure, denoted as $Q_{k,1}$) and accompanying (secondary variable actions – denoted by $Q_{k,i}$).

In addition, in some cases, the presence of the actions may cause some advantages for the structure; therefore, referring the effects of the actions on the design situations, actions are also divided into favourable and unfavourable ones.

Table 6-4 and Table 6-5 give the recommended values of partial safety factors of actions according to different categorisations of actions.

Table 6-4 – Partial safety factors of the actions at the ultimate limit state (non seismic situations)

Persistent or transient design situation	Permanent actions (G_k)- γ_G		Leading variable action ($Q_{k,1}$) - γ_Q		Accompanying variable actions ($Q_{k,i}$) - γ_Q	
	Unfavourable	favourable	Unfavourable	favourable	Unfavourable	Favourable
a. For checking the static equilibrium of a structure	1,10	0,90	1,50	0	1,50	0
b. For the design of structural members	1,35	1.00	1,50	0	1,50	0
c. As an alternative to (a) and (b) above to design for both situations with one set of calculations	1,35	1,15	1,50	0	1,50	0

Table 6-5 – Partial safety factors of the actions at the serviceability limit state (non seismic situations)

Design situations	Permanent actions	Variable actions
All	1.0	1.0

6.2.6. Actions

Actions on the structures are usually known as permanent and variable ones. Their classifications for common design are given in Table 6-6 (EN1991-1 (2002)).

Table 6-6 Classification of actions

Permanent actions	Variable actions
a – self weight of structures, fitting and fixed equipment	a – imposed floor loads b – snow loads c – wind loads

Permanent actions include the weight of the structure itself and all architectural configurations. These weights will be calculated based on the some assumed architects' drawings, including partitions, cladding, ceilings and screeds... For the buildings within the categories A and B (EN 1990 (2002) – 2002 [R6.1]), no special equipment or static machines are taken into account as parts of permanent actions.

Variable actions are those related to the non-constant loads, such as wind, snow or weights of the buildings' occupants. These actions are difficult to determine accurately. EN1991-1 (2002) has proposed some characteristic values for variable actions.

6.2.6.1. Characteristic values of actions

Two categories of the buildings, office and residence, are examined in this study. Permanent loads, accounting for the floors, claddings and partitions, will be simplified to be a uniformly distributed load per meter square. The brick walls in residential buildings will be taken into account as the distributed load directly acting on beams. The distribution on the beam of permanent and variable actions in the gravity direction is dependent on: (a) the position of the frame (interior or exterior), (b) detailing and working conditions of the slabs (transferring forces from the slabs to the beam).

Gravity variable loads are dependent on the particular conditions of the buildings. To make it simpler for the study, the characteristic values of uniformly imposed loads are taken from EN1991-1 (2002) and given in Table 6-7. The value of uniform snow load is set to be equal to 0.4kN/m².

Table 6-7 – Imposed loads on the studied buildings

Types of buildings	Intermediate floors	Roof floors
Office	3kN/m²	2kN/m²
Residence	2kN/m²	2kN/m²

The wind forces for the whole structure will be determined by calculating forces using force coefficients as defined in EN 1991-1-4.

$$F_w = c_s.c_d . \sum_{elements} c_f . q_p(z_e).A_{ref} \qquad \text{Equation 6-2}$$

Where:

$c_s c_d$ is the structural factor (section 6 - EN 1991-1-4 (2002))

c_f is the force coefficient for the structure (section 7 - EN 1991-1-4 (2002))

$q_p(z_e)$ is the peak velocity pressure at reference height z_e (section 7 - EN 1991-1-4 (2002))

A_{ref} is the reference area of the structure (section 7 - EN 1991-1-4 (2002))

6.2.6.2. Load combinations at ultimate limit states:

EN 1990 (2002) permits the simplified combinations as an alternative to persistent and transient design situations. They are summarized as follows:

a – Design situations with one variable action only: $1.35\sum G_{k,j} + 1.5Q_{k,1}$ (j>=1)

b – Design situations with two or more variable actions: $1.35\sum G_{k,j} + 1.5Q_{k,1} + 1.05\sum Q_{k,i}$ (j>=1; i>=2)

6.2.6.3. Load combinations at serviceability limit states

The simplified verification of EN 1990 (2002) will be used for the serviceability limit states under persistent and transient design situations. They are given hereafter:

a – Design situations with one variable action only: $1.0\sum G_{k,j} + 1.0Q_{k,1}$ (j>=1)

b – Design situations with two or more variable actions: $1.0\sum G_{k,j} + 0.9Q_{k,i}$ (j>=1; i>=1)

6.2.7. Analysis of internal forces of RC-MRFs

6.2.7.1. Modelling and idealisation of the frames

The purpose of analysis is to verify the overall stability and determination of internal forces of the structures' members (the distribution of internal forces and moments). Some classical simplifications are supposed to idealize the frames for the analysis such as: (1) beams and columns being represented by a simple line diagram, based dimensionally on the centreline distances between columns and between floor beams; (2) all the members are prismatic, with constant moment of inertia between centrelines; (3) some simplified behaviour of materials, as mentioned in previous sections, are assumed …

It is evident that the usual assumption applied in analyzing the frame that the members are prismatic, with constant moment of inertia between centrelines, is not strictly correct. A beam connecting a column may be prismatic up to the column face. However, from that point to the column centreline, it has largely

increased depth, with a very great second moment of area which could be assumed to be infinite compared with that of the remainder of the span. This is also valid for the columns when having infinite stiffness at joint compared with the rests. Therefore, in order to model the beams and columns strictly correctly, this variation should be considered in the analysis. This means that a beam or a column will be constituted by three parts: two different parts at two ends and a span part. Two parts at two ends of beams and columns will form very rigid joints. This leads to the effective length of beams and column being less than the original lengths. However this is usually neglected in elastic analysis.

Another important consideration when performing the analysis of RC-MRFs is about the moments of inertia of the reinforced concrete members. This is due to the fact of the differences between global linear analysis of the frame and the design of sections of the members. Generally, the design of beams and columns is based on cracked section theory, i.e. on the supposition that tension concrete is ineffective. It might seem more reasonable if moments of inertia of the frame members are calculated in that way in order to determine the internal forces and deformations of the members. However, this would make the design become much more complicated and time consuming. Due to that, it is not considered in the current study.

All slabs of the buildings are casted in place with the frame components. In order to take into account the contributions of the slab to the stiffness and strength of the frames, beams in frames are usually considered as T-sections. Effective flange width of the beams is taken based on some parameters as the web dimensions, the span, the support conditions…

In general, all structures should be analyzed in complete 3-D models. However, if all the studied frames are regular in both plan and elevation, it is allowed to use planar models: one in x and one in y directions to analyze the structures (EC2, EC8).

6.2.7.2. Structural Analysis

According to EC2, there are several methods which can be used to analyze the internal forces and displacements of the frames. They include linear or nonlinear ones such as linear elastic analysis, linear elastic analysis with limit moment redistribution, plastic analysis or fully non-linear analysis. In present study, linear analysis is adopted for determining the bending moments, shear and axial forces of the frame members. No moment redistribution is made. The computer code, used for the analysis, is SAP2000 (nonlinear version 14).

6.2.7.3. Second order effects

It has been learnt that in many cases the second order effect has an influence on the internal forces and structural deformations. EC2 allows neglecting the effects of second order on the bracing frame if it meets some conditions:

- The effects of the second order are less than 10% of the first order.
- Torsion instability is not governing, i.e. the building is reasonably symmetrical.
- Global shear deformations are negligible.
- Bracing members are rigidly fixed at base.
- The stiffness of the bracing members is reasonably constant along the height.
- The total vertical load increases by approximately the same amount per story.

As an alternative to the conditions above, the global second order effects in buildings may be ignored if:

$$F_{V,Ed} \le k_1 . \frac{n_s}{n_s + 1.6} . \frac{\sum E_{cd} I_c}{L^2} \quad \text{(EC2)} \qquad \text{Equation 6-3}$$

Where:

- $F_{V,Ed}$ – is the total vertical loads on bracing members
- n_s – is the number of stories

- L – is the total height of the building above level of moment restraint
- E_{cd} – is the design value of the modulus of elasticity of concrete
- I_c – is the second moment of area (un-cracked concrete section) of bracing members
- k_1 – is coefficient (taken as 0.31)

6.2.8. Analysis of the sections at ultimate limit states

The configurations and detailing of the frames' components from the preliminary design process will be checked and finalised by analyzing their cross-sections. The material properties used for design of sections are presented in the previous sections.

Design of sections due to bending and axial forces

To determine the flexural reinforcing contents of beams, distribution of strains and stresses across the sections in bending is assumed that (a) the concrete will crack in the regions of tensile strains and that, after cracking, all the tension is carried by the reinforcement and (b) that plane sections of a structural member remain plane after straining, meaning that the distribution of the strains across the sections is linear. Figure 6-3 shows the cross-section of a member subjected to bending and the resultant strain diagram together with the equivalent rectangular stress block.

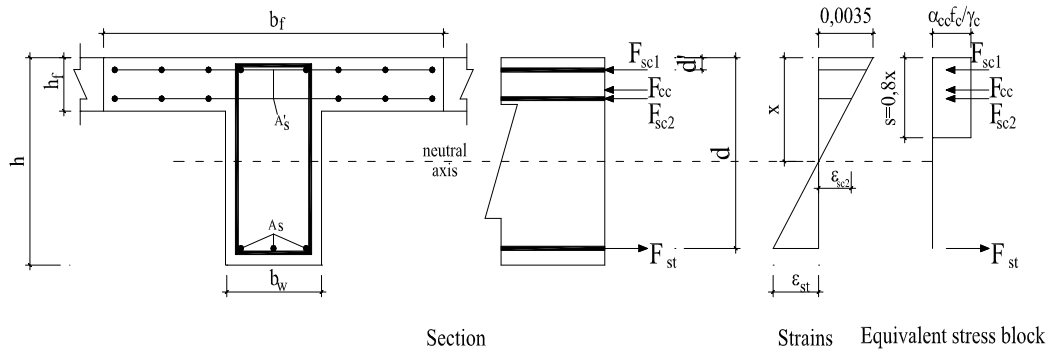

Figure 6-3 – Beam section with the strain diagram and the stress block

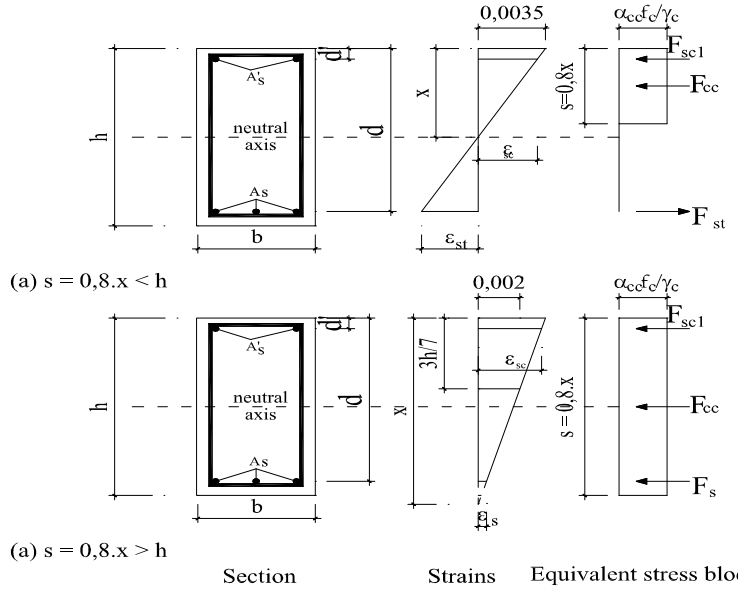

Figure 6-4 – Bending plus axial load with varying position of neutral axis in a column

For design of reinforcements of columns, in which the cross-section is subjected to a moment M and an axial compressive force N, distribution of the strains and stresses of a section will be dependent on the eccentricity of that section (ratio between M and N). Figure 6-4 represents the cross-section of a column with typical strain and stress distributions for varying eccentricities, similarly to the different distances of

neutral axes, as defined in EC2. If there is any tension in the section the limiting concrete strain is taken as 0.0035. If there is no tension in the section the limiting strain is taken as a value 0,002 at the level of 3/7 of the depth of the section height. For a given section with particular distribution of reinforcing steels, the flexural resistance of that section is dependent on the value of axial force acting on the section. To design the reinforcements of the column, M-N interaction curves are usually used. These curves represent the flexural resistance of a section and can be constructed by applying the basic equilibrium and strain compatibility equations with the gradually varying the neutral distances in the stress-strain relations. Some excel sheets have been established to make it easier for design of sections of beams and columns.

Design of section for shear resistance:

Shear resistance of a section is realised by the concrete, the longitudinal reinforcements and the transversal or inclined reinforcements.

In the present study, it is assumed that in all cases the failure due to shear will never occur anywhere in the structures. Therefore, design of section due to shear will not be presented.

6.2.9. Check for serviceability limit states

It is well known that the performance of structures at service load is an important design consideration; therefore all codes require that member performance in normal use must be satisfactory, when loads are those actually expected to act, i.e., when the load factors are 1.0. The deformations of the structure or members under service loads may be excessively large, or long-term deflections due to sustained loads may cause damage. This may affect the functionalities of the buildings.

In EC2, the reinforced concrete structures should be designed with the considerations of deflections and crack at service loads. In addition, in some special cases, vibrations and fatigue of the members or structures should be checked. The aim of design should be to ensure an adequate margin of safety against collapse and against the possibility that the structure will become unfit for use at service loads.

Analysis of the structure at serviceability limit states is usually carried out based on elastic theory, with stresses in both concrete and steel assumed to be proportional to strain.

6.3. Design of RC-MRFs according to EC2 and EC8

6.3.1. General introduction about seismic design

The ultimate aim of designing the structures under a seismic excitation is to provide them adequate capacity to be able to resist lateral forces generated by the earthquake. When a structure is subjected to a ground motion of an earthquake, it responds dynamically in a vibratory fashion.

When the structure is behaving elastically, the maximum response acceleration will depend on the structure's natural period of vibration and the magnitude of the damping present. In inelastic ranges, the dynamic responses of the structure under seismic actions become more complicated and rather difficult to know correctly. Therefore, although the seismic analysis and design of RC-structures have rapidly developed for last two decades, essential requirements in most codes to determine seismic forces are still based on linear elastic responses of the structures.

Some new trends to do this difficult work are trying to model the structures as similarly as possible in the same situations as they would be in the reality. Force-based design approach has been gradually substituted by displacement-based design approach. The displacement-based method is the most advanced one to date to model the real behaviour of the structures under seismic actions. The application of displacement-based design in practice is more and more in favour quite certainly due to many problems of the force-based design method.

A fundamental problem with force-based design, especially when applied to reinforced concrete and masonry structures is the selection of appropriate member stiffness (Priestley, 2007). Generally, in the procedures used in seismic design based on forces, some assumptions must be made about the member sizes before the design seismic forces are determined, as commonly used in most codes. These forces are then distributed between members based on their assumed stiffness. It is clear that the calculated design

forces will no longer be valid if there is a need to modify the member sizes from the initial selections. Theoretically, it requires the recalculation of the design seismic forces and distribution of these forces is necessary. However, these iteration steps are not always made in practice because of very time consuming work.

Another important obstacle of force-based design approach used for reinforced concrete or masonry structure is the way in which member stiffness is calculated. In forced-based approach, linear elastic analysis is usually adopted. This requires using the gross-section stiffness of the members. In seismic situations, many codes require the reduced stiffness of the members to represent the influence of cracking of the concrete or masonry. A common assumption is 50% of the gross-section stiffness (EC8 or ATC 312). In some codes (New Zealand, EC8…), the reduced stiffness of the members is regulated depending on the member types, for example 35% of the gross-section stiffness for beams. Clearly the value of stiffness assumed will significantly affect the design seismic forces.

A more important consideration in force-based approach is that regardless of what assumption for the stiffness of the members is made, the member stiffness is traditionally supposed to be independent of the strength for a given member section. It is not reasonable in many cases, especially for reinforced concrete structures where the stiffness is dependent on the detailed configurations of the reinforcements.

In addition, there has been a long debate about using concept of ductility and its relation to force-reduction or behaviour factors in the force-based design approach. Despite of the fact that some definitions are quite clear for the use of behaviour factors (q-factors) in EC8 or force –reduction factors in US or other codes, there are some problems in realistically modelling the structures. For example, it has long been realized that the equal-displacement approximation is inappropriate for both very short-period and very long-period structure. And it is also of doubtful validity for medium period structures when they undergo large inelastic deformations (Priestley, 2007).

Although there are still some problems with force-based design, this method has been improving and is being commonly used in practice due to its simplicity and acceptability from a safety point of view. All RC frames, which have been designed in relevance with EC2 in the previous section, will be next designed in accordance with both EC2 and EC8. These frames are the subjects of the seismically upgrading study based on the use of EMP. The resulting frames from this part will significantly affect the effectiveness of use EMP after upgrading. Therefore, some efforts have been made to be able to examine the effectiveness of EMP, such as reducing the dimensions of beams and columns as small as possible to avoid their overstrength. Force-based design approach with energy dissipation and ductility is used to dimension the frames' components.

This section will present the general rules for designing RC-MRFs in accordance with EC8. Some limitations of the frames studied will be also introduced in general aspects that affect the resulting frames. The detailed requirements depending on Ductility Class of the structures that affect the resulting frames are presented as well.

6.3.2. Design concepts, limitations of the studied RC-frames in accordance with EC8

EC8 provides guidance on the basic principles for good seismic design of buildings. These principles can be applied to all types of buildings; they are not mandatory. One of the most important goals in modern codes like EC8 is to design the RC-structures with the aim of ensuring stable, reliable dissipative performance in predefined 'critical regions', limiting the inertial forces in other parts of the structures. The design and detailing rules are regulated in these 'critical regions' so that under the design seismic excitations they would perform intended behaviour in large inelastic deformations. This is related to the capacity of the structures in general or of the members in particular in absorbing the energy thanks to intended plasticity of the predefined members. Ductility of the members or the structures is one of the key factors that ensure their stable plastic behaviour to prevent them from the brittle failure modes such as shear or compression failures in concrete or buckling of the reinforcement steel. Three ductility classes are introduced in EC8, that is:

- Low (ductility class low (DCL)) in which no hysteretic ductility is intended and the resistance to earthquake loading is achieved through the strength of the structure rather than ductility.

- Medium (DCM) where rather high levels of plasticity are permitted and corresponding design and detailing requirement are necessary.
- High (DCH) in which very large deformations are permitted accompanied by even more strict and onerous design and detailing requirements.

In this study, all RC-MRFs are designed corresponding to Low and Medium Ductility Classes (DCL and DCM). These kinds of Ductility Class are likely to form the most commonly used group in practice of building reinforced concrete structures. The rules in EC8 for designing DCM RC-structures aim at providing the capacity to withstand non-linear load cycles without significant strength degradation, precluding the brittle failures of the structural components and improving the ability of predefined critical regions to undergo large inelastic deformations. Generally, this includes:

- Ensuring flexural yielding prior to shear failure.
- Providing stronger columns than beams to obtain a more efficient beam side way mode of response and avoid soft story failure.
- Retention of an intact concrete core within confining links.
- Prevention of buckling of longitudinal reinforcement.
- Limiting the flexural tension reinforcement to suppress concrete crushing in the compression zone.

RC-MRFs, as defined in EC8, have to be designed to carry at least 65% of the total base shear force. In the present study, the base shear forces generated from seismic actions will be completely carried by the frames. Moreover, they are regular in both elevation and plane. This allows simplifying the analysis of the frames, as recalled in Table 6-8. Behaviour factor, q, mentioned in Table 6-8, is an essential factor used in EC8 to ensure the structure to be designed correspondingly to the desired ductility class. It is applied as a global reduction factor of the internal forces that would develop in the fictitious representation of the structure as elastic with 5% damping (Fardis, 2009). With the application of the behaviour factor, the internal forces for which the members of the structure are dimensioned can be determined through linear elastic analysis.

Table 6-8 – Simplification of analysis of structures (Table 4.1 – EC8)

Regularity		Allowed Simplifications		Behaviour factor
Plan	Elevation	Model	Linear-elastic Analysis	(for linear analysis)
Yes	Yes	Planar	Lateral force*	Reference value
Yes	No	Planar	Modal	Decreased value
No	Yes	Spatial**	Lateral force*	Reference value
No	No	Spatial	Modal	Decreased value
* If the condition of **4.3.3.2.1(2)** a) is also met; ** Under the specific conditions given in **4.3.3.1(8)** a separate planar model may be used in each horizontal direction, in accordance with **4.3.3.1(8)**.				

6.3.3. General criteria of the design process

6.3.3.1. Design situations

According to EN 1990 (2002), there are three design situations classified as persistent, transient and accidental. For simplification, only two of them will be taken into account, that is:

- Persistent situations that correspond to conditions of normal use, in which wind and snow actions are excluded.
- An accidental situation which is corresponding to a seismic event.

The influence on the final design of transient situations and of other accidental situations (such as fire, explosion or impact) is neglected.

6.3.3.2. Materials

Materials of the frames designed in accordance with EC8 are selected the same as for the frames designed according to EC2.

6.3.3.3. Partial factors of safety

Partial factors of materials and of actions used for design of the frames according to both EC2 and EC8 should be distinguished. Partial factors are dependent on the design situations. For the persistent and transient design situations, these factors are presented in the previous section. The partial factors used in seismic design situations are presented hereafter.

6.3.3.3.1. Partial factors of materials (γ_m)

The values of partial factors γ_c and γ_s adopted for the accidental design situation are applied as recommendation of EC8, given in Table 6-9.

Table 6-9 – Partial factors of safety applied to the material (γ_m)

Limit state	Seismic design situations	
	Concrete (γ_c)	Reinforcing steel (γ_s)
Ultimate		
Flexure	1.5	1.0
Shear	1.5	1.0
Bond	1.5	1.0
Serviceability	1.0	1.0

6.3.3.3.2. Partial factors of actions (γ_f)

Table 6-10 and Table 6-11 give the recommended values of partial safety factors of actions according to different categorisations of actions.

Table 6-10 – Partial safety factors of the actions at the ultimate limit state

Persistent or transient design situation	Permanent actions (G_k) - ψ_G		Accompanying variable actions ($Q_{k,i}$) - ψ_{2i}	
	Unfavourable	favourable	Unfavourable	favourable
b. For the design of structural members	1.00	1.00	0.30	0

Table 6-11 – Partial safety factors of the actions at the serviceability limit state

Design situations	Permanent actions	Variable actions
All	1.0	1.0

6.3.4. Actions

6.3.4.1. Actions in cases of persistent design situations

Permanent actions due to self-weight and variable actions due to imposed, snow loads and wind forces are all taken into account in the design of frames under persistent situations. The characteristic values of the persistent design situations at different limit states are exactly the same as the values used in the design of frames designed according to EC2.

6.3.4.2. Actions in cases of seismic design situations

6.3.4.2.1. Ultimate limit states and no-collapse requirements (NCR)

According to 4.3.3.5.2 EC 8, vertical component of the seismic action will be taken into account in the cases of structures which are listed below:

- For horizontal or nearly horizontal structural members spanning 20m or more; for horizontal or nearly horizontal cantilever components longer than 5;
- For beams supporting columns;

In the present study, all RC-MRFs are regular in plan and elevation. There is neither member spanning 20m or more nor beams supporting columns. In these cases, vertical component of the seismic action can be neglected irrespectively of the vertical design PGA. There is only horizontal component of the seismic action accounted for. From now on, it is important to note that seismic action will be understood as only the horizontal component of the seismic action. EC8 requires the structure that it should be well designed with the ultimate limit state or No-collapse performance level. This will entail protection of life under rare seismic action, through prevention of collapse of any structural member and retention of structural integrity and residual load capacity after the event (Fardis, 2009).

6.3.4.2.1.1. Design peak ground acceleration (PGA)

The basis of the seismic design of the new structures in EC8 is to design the structures under the "design seismic action" so that the no collapse takes place. The "design seismic action" is usually specified through the "design ground acceleration" in the horizontal direction, a_g, being equal to the product of "reference peak ground acceleration" on rock from national zone maps (a_{gR}) and importance factor (γ_I) of the building; the studied structures belong to the ordinary category corresponding to the value of γ_I equal to 1 (EC8). The "reference PGA" corresponds to the reference return period, T_{NCR}, of the "design seismic action" for structures of ordinary importance. The reference return period is dependent on the seismic hazard and limit state of the design process. Each country decides the level of seismic protection that its society can assume. EC8 recommends the default value T_{NCR} = 475 years, corresponding to a probability of exceedance in 50 years for the no-collapse requirement, equal to 0.1, P_{NCR} = 0.1.

6.3.4.2.1.2. Elastic spectra of the horizontal components in EC8

The elastic response spectral acceleration for the horizontal components of the seismic action defined in EC8 is of the Newmark type and is given in the following expressions:

$$0 \le T \le T_B : \; S_e(T) = a_g \cdot S \cdot \left[1 + \frac{T}{T_B} \cdot (\eta \cdot 2{,}5 - 1)\right] \qquad \text{Equation 6-4}$$

$$T_B \le T \le T_C : \; S_e(T) = a_g \cdot S \cdot \eta \cdot 2{,}5 \qquad \text{Equation 6-5}$$

$$T_C \le T \le T_D : \; S_e(T) = a_g \cdot S \cdot \eta \cdot 2{,}5 \left[\frac{T_C}{T}\right] \qquad \text{Equation 6-6}$$

$$T_D \le T \le 4\text{s} : \; S_e(T) = a_g \cdot S \cdot \eta \cdot 2{,}5 \left[\frac{T_C T_D}{T^2}\right] \qquad \text{Equation 6-7}$$

Where :

- Se(T) is the elastic response spectrum;
- T is the vibration period of a linear single-degree-of-freedom system;

- a_g is the design ground acceleration on type A ground ($a_g = \gamma_I.a_{gR}$);
- a_{gR} is the reference peak ground acceleration on type A ground;
- T_B is the lower limit of the period of the constant spectral acceleration branch;
- T_C is the upper limit of the period of the constant spectral acceleration branch;
- T_D is the value defining the beginning of the constant displacement response range of the spectrum;
- η is the damping correction factor with a reference value of $\eta=1$ for 5% viscous damping; $\eta = \sqrt{10/(5+\xi)} \geq 0{,}55$; where ξ is the damping ratio factor (%)
- S is the soil factor, depending on the ground types and type of spectra. Two different spectrum shapes, type 1 and type 2, are defined in EC8 for a given ground type, as illustrated in Figure 6-5.

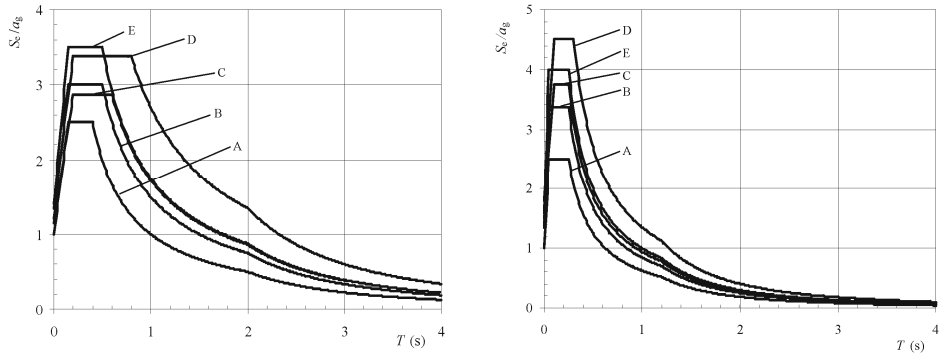

Figure 6-5 – Recommended elastic response spectra for type 1 (left) and type 2 (right)

In the present study, some hypotheses are made for the design of frames: the design spectrum shape type 1 is used and the damping ratio is assumed to be equal to the default value and thus $\eta=1$. Table 6-12 presents the values of parameters used for defining the elastic response spectrum.

Table 6-12 – EC8 values of parameters S, T_B, T_C and T_D defining the elastic response spectrum Type 1

	Type 1 Earthquake			
Soil	S	T_B(s)	T_C(s)	T_D(s)
A Rock or rock-like formation, including at most 5 m of weaker material at the surface.	1.0	0,15	0,4	2,0
B Deposits of very dense sand, gravel, or very stiff clay, several tens of metres in thickness, gradual increase of mechanical properties with depth.	1,2	0,15	0,5	2,0
C Deep deposits of dense or medium-dense sand, gravel or stiff clay with thickness from several tens to many hundreds of metres.	1,15	0,20	0,6	2,0
D Deposits of loose-to-medium cohesion-less soil or of predominantly soft-to-firm cohesive soil.	1,35	0,20	0,8	2,0
E A surface alluvium layer of soil similar to C or D with thickness varying between about 5 m and 20 m, underlain by stiffer material	1,4	0,15	0,5	2,0

6.3.4.2.1.3. Design spectrum for elastic analysis

Depending on the type and the ductility class chosen for the structure, the elastic spectrum will be scaled down by a behaviour factor (q). This results in the reduction of the seismic forces used for design of the structure and apparently it also results in smaller dimensions of the components of the structures, however, the structure is still capable of reaching the desired displacements caused by earthquake thanks to its ductility and overstrength. This reduction is a 'trick' of the code to account for the capacity of the structure working in the inelastic range under seismic actions. This also allows analyzing the structure

linearly elastically and avoiding a nonlinear analysis. The design spectrum defined in EC8 is given in the following expressions:

$$0 \le T \le T_B : S_d(T) = a_g \cdot S \cdot \left[\frac{2}{3} + \frac{T}{T_B} \cdot \left(\frac{2,5}{q} - \frac{2}{3} \right) \right] \quad \text{Equation 6-8}$$

$$T_B \le T \le T_C : S_d(T) = a_g \cdot S \cdot \frac{2,5}{q} \quad \text{Equation 6-9}$$

$$T_C \le T \le T_D : S_d(T) = \begin{cases} a_g \cdot S \cdot \eta \cdot \frac{2,5}{q} \cdot \left[\frac{T_C}{T} \right] \\ \ge \beta . a_g \end{cases} \quad \text{Equation 6-10}$$

$$T_D \le T \le 4s : S_d(T) = \begin{cases} a_g \cdot S \cdot \eta \cdot \frac{2,5}{q} \left[\frac{T_C T_D}{T^2} \right] \\ \ge \beta . a_g \end{cases} \quad \text{Equation 6-11}$$

Factor β gives a lower bound for the horizontal design spectrum, acting as a safeguard against excessive reduction of the design forces due to the flexibility of the system. The recommended value in EC8 is 0.2.

6.3.5. Ground types

Seven ground types are explicitly defined in EC8. In the current study, all the buildings will be designed according to the ground type C. This type is characterized by average shear wave velocities higher than 180 and lower than 360 m/s, with a number of blows N_{SPT} = 15-50 blows/30cm and shear strength from c_u = 70-250 kPa. Typically, this corresponds to deep deposits of dense or medium dense sand, gravel or stiff clay with thickness from several tens to many hundreds of meters.

6.3.6. Methods of analysis

As all buildings are regular in both plan and elevation, the buildings can be analyzed as planar frames, as explicitly defined in EC8. The linear elastic methods used to design the frames at different limit states can be the equivalent lateral force method or modal response spectrum one depending on the modal properties of the frames. These linear methods of analyses use design response spectrum, determined from elastic response spectrum with 5% damping of linearly elastic structure divided by behaviour factor q. The use of a linear method of analyses does not imply that the structure will respond elastically; it is simply a tool for the simplification of practical design in accordance with force-based approach in seismic design with the elastic spectrum divided by the behaviour factor.

The lateral force method of analysis

The equivalent lateral force method is applicable in the limits of Table 6-8 and when the fundamental period T_1 of the structure is less than $4.T_c$ and 2.0s, with T_C, as explained, is the upper limit of the period of the constant spectral acceleration branch.

The seismic force acting on the structure is derived separately in the two horizontal directions based on the first translational mode in that horizontal direction:

$$F_b = \lambda m S_d(T_1) \quad \text{Equation 6-12}$$

Where:

- $S_d(T_1)$ is the value of the design spectrum at the fundamental period T_1 in the horizontal direction considered

- λm is the effective modal mass of the fundamental mode. The coefficient λ mentions about the contribution of the total mass to the first mode vibration of the structure. The first period can be determined by several ways such as empirical formulas or Rayleigh quotient or modal analysis … $m = \sum G + \sum \psi_{E,i} Q_{k,i} = \sum G + \sum \psi_{2iQ} \varphi Q_{k,i}$

The base shear is then translated into a set of lateral inertia forces in the same direction applied to the degrees of freedom, i, of the structure by assuming a distribution with height, z, of the peak lateral drifts, $\Phi(z)$. Then, when a single mode of vibration of the peak lateral inertia force is proportional to $\Phi(z_i)m_i$, where m_i is the mass associated with that degree of freedom, the base shear is distributed to the degrees of freedom by:

$$F_i = F_b \frac{\phi_i m_i}{\sum \phi_j m_j} \qquad \text{Equation 6-13}$$

The modal response spectrum analysis

The modal response spectrum analysis is a real linear dynamic method based on the design response spectrum with 5% damping. In this method, the structure is analyzed separately in each mode of vibration and then they are combined together by using some rules such as SRSS (Square root of the sum of the squares) and CQC (complete quadratic combination) (EN 1998-1 (2004), Fardis (2009)…). The modal response spectrum method is not limited for any type of structures.

Torsion effects

According to EC8, if the lateral stiffness and mass are symmetrically distributed in plan and unless the accidental eccentricity is taken into account by a more exact method, the accidental torsion effects may be accounted for by multiplying the action effects in the individual load resisting elements by a factor δ given by:

$$\delta = 1 + 0.6 * \frac{x}{L_e} \qquad \text{Equation 6-14}$$

where $x = \frac{L_e}{2}$ and L_e=15m, meaning $\delta = 1.3$

If the building is distributed symmetrically in plan and elevation, it can be divided into 2 plane models and the factor δ may be determined by:

$$\delta = 1 + 1.2 * \frac{x}{L_e} \qquad \text{Equation 6-15}$$

where $x = \frac{L_e}{2}$ and L_e=15m, meaning $\delta = 1.6$

However, based on the development in Plumier (2010), it can be shown that those reference values are too high in the type of buildings studied here, so that a value of $\delta = 1.2$ is chosen to take torsion into account.

6.3.7. Simplified modelling of the frames for linear analysis

Modelling of beams and columns:

The goal of modelling and analysis is to provide data for the phase of detailed design, including design of ultimate and serviceability limit states. According to Section 4 of EN 1998-1, the model of building structure for linear analysis should represent well the distribution of stiffness and mass all over the building; therefore, modelling the structure in 3D is the best way to fulfil the requirements from the code. However, in many cases, this becomes unnecessary and time consuming for analysis because the structure

is not too much complex. For the framed buildings, regular in both plans and elevations, EN 1998-1 allows analyzing the internal forces and deformations in two planar frames, as mentioned in previous parts.

Beams and columns are modelled as prismatic 2D beam elements, characterized by their cross-sectional area, A, moment of inertia, I_y , with respect to the principal axe y, shear area A_y along this local axis. All beams in the models have T-section shapes, accounting for the contributions of the slabs to the stiffness of the beams and the frames. Due to the flanges, the centroidal axes will be moved towards the flanges, leading to the height of the stories in the models being change slightly. Nevertheless, this is not taken into account in the model. Masses of beams and columns are assumed to be lumped at the nodal points and associated in general with all degree of freedom there.

In accordance with EC8, the structural model should also account for the contribution of joint regions (e.g. end zones in beams and columns of frames) to the deformability of the structure. The stiffness of the beams and columns at joints may become infinitive compared to the other remaining parts and the effective lengths of beams and columns are slightly changed. Thus, the beam element falling into the physical region of a joint with another member is often considered as rigid. However, if this is done for all members that frame into a joint, the overall stiffness of the structure is much overestimated. Therefore, it is supposed in EC8 that only the part within the physical joint of the less stiff elements, usually of the beams, is assumed to be rigid. There are two possibilities of modelling the rigid ends of the beam, mentioned in EC8, comprising (1) using the clear length of the beam as the real elastic length and (2) inserting a fictitious short elements between the real ends of the elastic member. The first approach is adopted in this study, with assumption that clear length is determined by the distances between centrelines of columns.

Cracked stiffness of the concrete

In order to design the structure for energy dissipation and ductility, the purpose of EN 1998-1 is to lead the structure into inelastic range with overall bilinear behaviour. The elastic stiffness used to determine the internal forces and deformations of the structure should be corresponding to the stiffness of the elastic branch of that behaviour. Clearly, the use of the full elastic stiffness of un-cracked concrete is inappropriate. Therefore, section 4 of EN 1998-1 requires that the analysis of reinforced concrete structures should be based on member stiffness taking into account the effect of cracking, corresponding to the initiation of yielding of the reinforcement. It is also permitted to take that stiffness as equal to 50% of the corresponding stiffness of the un-cracked members, not accounting for the presence of the reinforcement. If not more accurate modelling the cracked member is needed to be performed. Actually, the value of 50% of the un-cracked stiffness, as mentioned in EN 1998-1, is over-conservative because many experiments have shown that the secant stiffness of typical reinforce concrete members at incipient yield is on average about 50% or less of that of un-cracked gross concrete sections (Panagiotakos, T.B and Fardis, 2001). This may lead to an increase in the deformations of the structure. However, with the reduction of the stiffness, the period of the structure will increase leading to smaller spectral accelerations and lower seismic forces on the structure.

Second order effects

EN 1998-1 requires accounting for the second order effects in case of vertical members of the story having the second-order moment exceeding 10% of the first-order moment in aggregate. This may be represented by the value of the ratio:

$$\theta = \frac{P_{tot} d_r}{V_{tot} h} \qquad \text{Equation 6-16}$$

Where:

- θ – is the inter-story drift sensitivity coefficient.
- P_{tot} – is the total gravity load at and above the story considered in the seismic design situation.
- $d_r = d_{s_i} - d_{s_{i-1}}$ - is design inter-story drift, evaluated as the difference of the average lateral displacements d_s at the top and the bottom of the story under consideration.

- V_{tot} – is the total seismic shear at the considered level.

6.3.8. Combinations of actions

According to Eurocode 8, in the case of seismic design situation, the following load combination must be taken in order to compute the mass of inertia that is fully coupled with the structural system:

$$\sum G_{k,j} + \psi_{E,i} \sum Q_{k,i} \qquad \text{Equation 6-17}$$

Where:

- $\psi_{E,i}$: combination coefficient.
- $\psi_{E,I}$ is determined by $\psi_{E,i} = \varphi \psi_{2,i}$. The value of φ is to be from EC8

  $\varphi = 1.0 \rightarrow$ for the top story; $\varphi = 0.8 \rightarrow$ for the correlated occupancies;

  $\varphi = 0.5 \rightarrow$ for the independent occupancies
- $\psi_{2,i}$: combination coefficients given in Table 6-10 (from the Annex A1:1990 (2002), table A.1.1)

$\psi_{2,i} = 0.3 \rightarrow$ for the occupancy (category A).

$\psi_{2,i} = 0 \rightarrow$ for the snow and wind loads.

In EN1990, the load combination under the design situation of a seismic event is defined as:

$$G_{k,j} + \psi_{E,i} Q_{k,i} + A_{Ed} \qquad \text{Equation 6-18}$$

Where: A_{Ed} is the earthquake action.

6.3.8.1. Serviceability limit states – damage limitation state

In accordance with EC8, the serviceability limit states or damage limitation states are associated with damage occurrence, corresponding to states beyond which specified service requirement are no longer met. For the buildings having non-structural elements of ductile materials attached to the structure, the following limits shall be observed:

$$d_r \nu \leq 0.01 h \qquad \text{Equation 6-19}$$

Where:

- h: is the story height
- ν: is the reduction factor to take into account the lower return period of the seismic action associated with the damage limitation requirement. The value of ν also depends on the important class of the building. The value of d_s must be smaller than the value derived from the elastic spectrum.
- d_r: is design inter-story drift; $d_r = d_{s_i} - d_{s_{i-1}}$, evaluated as the difference of the average lateral displacements d_s at the top and bottom of the story under consideration.

To determine the displacement, if linear analysis is performed the displacements induced by the design seismic action shall be calculated on the elastic deformations of the structural system by means of the following simplified expression:

$$d_s = q_d * d_e \qquad \text{Equation 6-20}$$

Where:

- d_s: is the displacement of a point of the structural system induced by the seismic action.

- d_e: is the displacement of the same point of the structural system, as determined by a linear analysis based on the design response spectrum.
- q_d: is the displacement behaviour factor, assumed equal to q unless otherwise specified.

It is necessary to note that when determining d_e, the torsion effects of the seismic actions shall be accounted for and elastic modulus of the concrete should be reduced 50% to take into account the concrete cracking.

6.3.9. Capacity design for longitudinal reinforcements of columns and transverse reinforcements of beams and columns

It is very necessary to emphasize that the desired failure mode of seismic design is the beam-sway plastic mechanism, in which the plastic hinges will develop at two ends of beams and at the base of first-story columns (EC8, Priestley (2007), Fardis (2009), Park and Paulay (1974)). It implies that the formation of plastic hinges in columns (except the ones at the base) should be avoided if possible. There are several reasons for avoiding or at least delaying column plastic hinges. First of all, column sideway mechanisms usually require the very large curvature ductility demand for columns and, obviously, this often leads to very large dimensions of columns and complicated configurations of longitudinal and transverse steel. Second, a failure at columns often leads to much more serious consequences than the failure at beams. Furthermore, column yielding in all columns of a story will cause the permanent misalignment of the structure and leading to the larger P-delta effect. Also, hinges developed in all columns of a story will make large inter-story sway, causing problems of instability. This may reduce the gravity-carrying capacity of the structure.

For the design of the column in seismic situation, estimation of moment and concurrent axial loads is not an easy task. Generally, this may be completely done by performing full nonlinear time history analysis. However, this type of calculation is not usually applied in a design office due to its complication and time-consumption. Compression load, most commonly present in columns, may increase the bending capacity but also reduces the curvature ductility.

The failure due to shear of all reinforced concrete structural components is always non-ductile or brittle. Under seismic excitations, if shear failure occurs before appearing of plastic hinges due to bending at beams or columns of a frame structure, the capacity of that component in dissipating earthquake input energy through inelastic deformations will be much significantly reduced. In many cases, the local failures due to shear may cause some un-predicted overall failures of the structure.

Due to the disadvantage of forming plastic hinges in column and the brittle failure due to shear, as the discussion above, most modern seismic codes suggest the 'capacity design method' for designing longitudinal reinforcements for columns and transverse reinforcements for both beams and columns.

Generally, the principle of capacity design is simple. The bending moments, used for designing longitudinal reinforcements of a column, will be determined based on the bending resistances of the all beams framing to that column to form the beam-column joint and some overstrength factors. Similarly, for designing transverse reinforcement in beams and columns, shear forces will be calculated with the assumption that plastic hinges will appear at two ends of that beams or columns. For practical application, EC8 has proposed some recommendations for applications of Capacity Design of columns in bending and of both beams and columns in shear. Some main rules are extracted hereafter. For the capacity design of columns in bending in seismic situations, the following condition should be satisfied at all joints of primary seismic beams with primary seismic columns:

$$\Sigma M_{Rc} \geq 1.3\Sigma M_{Rb} \qquad \text{Equation 6-21}$$

Where

- ΣM_{Rc} is the sum of the design values of the moments of resistance of the columns framing the joint. The minimum value of column moments of resistance within the range of column axial forces produced by the seismic design situation should be used in expression Equation 6-21; and

- ΣM_{Rb} is the sum of the design values of the moments of resistance of the beams framing the joint. When partial strength connections are used, the moments of resistance of these connections are taken into account in the calculation of ΣM_{Rb}.

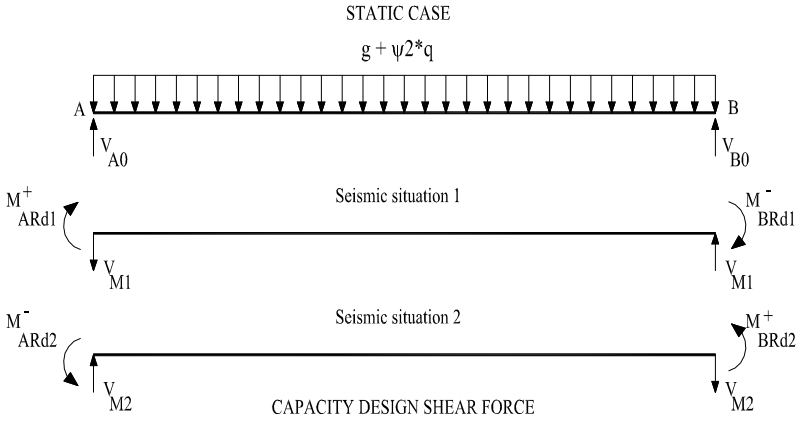

Figure 6-6 – Capacity design for the shear force in primary beams

For capacity design of beams in shear in seismic situations, the design shear forces shall be determined on the basis of the equilibrium of the beam EC8 under: a) the transverse load acting on it in the seismic design situation and b) end moments $M_{i,d}$ (with i=1,2 denoting the end sections of the beam), corresponding to plastic hinge formation for positive and negative directions of seismic loading. The plastic hinges should be taken to form at the ends of the beams or (if they form there first) in the vertical elements connected to the joints into which the beam ends frame. The end moments, $M_{i,d}$, should be calculated with some considerations taken into account as follows:

- At end section i, two values of the acting shear force should be calculated, i.e. the maximum $V_{Ed,max,i}$ and the minimum $V_{Ed,min,i}$ corresponding to the maximum positive and the maximum negative end moments Mi,d that can develop at ends 1 and 2 of the beam (see Figure 6-6).
- End moments $M_{i,d}$ should be determined as the following formulae

$$M_{i,d} = \gamma_{Rd} M_{Rb,i} \min(1, \frac{\sum M_{Rc}}{\sum M_{Rb}}) \qquad \text{Equation 6-22}$$

where

+ γ_{Rd} is the factor accounting for possible overstrength due to steel strain hardening, which in the case of DCM beams may be taken as being equal to 1.0;

+ $M_{Rb,i}$ is the design value of the beam moment of resistance at end i in the sense of the seismic bending moment under the considered sense of the seismic action;

+ ΣM_{Rc} and ΣM_{Rb} are the sum of the design values of the moments of resistance of the columns and the sum of the design values of the moments of resistance of the beams framing into the joint. The value of ΣM_{Rc} should correspond to the column axial force(s) in the seismic design situation for the considered sense of the seismic action.

- At a beam end where the beam is supported indirectly by another beam, instead of framing into a vertical member, the beam end moment $M_{i,d}$ there may be taken as being equal to the acting moment at the beam end section in the seismic design situation.

For capacity design in shear of primary seismic columns, the design values of shear forces shall be determined on the basis of the equilibrium of the column under end moments $M_{i,d}$ (with i=1,2 denoting the end sections of the column), corresponding to plastic hinge formation for positive and negative directions of seismic loading. The plastic hinges should be taken to form at the ends of the beams connected to the joints into which the column end frames, or (if they form there first) at the ends of the columns. End moments $M_{i,d}$ may be determined from the following expression:

$$M_{i,d} = \gamma_{Rd} M_{Rc,i} \min(1, \frac{\sum M_{Rb}}{\sum M_{Rc}})$$ Equation 6-23

where

+ γ_{Rd} is the factor accounting for overstrength due to steel strain hardening and confinement of the concrete of the compression zone of the section, taken as being equal to 1.1;

+ $M_{Rc,i}$ is the design value of the column moment of resistance at end i in the sense of the seismic bending moment under the considered sense of the seismic action;

+ ΣM_{Rc} and ΣM_{Rb} are the sum of the design values of the moments of resistance of the columns and the sum of the design values of the moments of resistance of the beams framing into the joint. The value of ΣM_{Rc} should correspond to the column axial force(s) in the seismic design situation for the considered sense of the seismic action.

6.3.10. Detailing requirements

There are many strict requirements in EC8 for different type of Ductility Class. Table 6-13 to 6-16 (summarised by Fardis, 2009) present essential criteria related to beams and columns.

Table 6-13 – EC8 rules for detailing and dimensioning of primary beams (secondary beams: as in DCL) (Fardis, 2009)

	DCH	DCM	DCL
Critical region length	1.5 h_w	h_w	h_w
Longitudinal bars			
ρ_{min}, tension side	$0.5 f_{ctm} / f_{yk}$	$0.5 f_{ctm} / f_{yk}$	$0.26 f_{ctm} / f_{yk}$;0.13%
ρ_{max}, critical regions	$\rho' + 0.0018 \frac{f_{cd}}{\mu_\phi \varepsilon_{sy,d} f_{yd}}$	$\rho' + 0.0018 \frac{f_{cd}}{\mu_\phi \varepsilon_{sy,d} f_{yd}}$	0.04
$A_{s,min}$, top and bottom	2Φ14 (308mm²)	-	-
$A_{s,min}$, top-span	$A_{s,top\text{-}supports}/4$	-	-
$A_{s,min}$, critical regions bottom	0.5 $A_{s,top}$	0.5 $A_{s,top}$	-
$A_{s,min}$, support bottom		$A_{s,bottom\text{-}span}/4$	
Shear design			
d_{bL}/h_c – bar crossing interior joint	$\le \frac{6.25(1+0.8\upsilon_d)}{\left(1+0.75\frac{\rho'}{\rho_{max}}\right)} \frac{f_{ctm}}{f_{yd}}$	$\le \frac{7.5(1+0.8\upsilon_d)}{\left(1+0.75\frac{\rho'}{\rho_{max}}\right)} \frac{f_{ctm}}{f_{yd}}$	-
d_{bL}/h_c – bar anchored at exterior joint	$\le 6.25(1+0.8\upsilon_d) \frac{f_{ctm}}{f_{yd}}$	$\le 7.5(1+0.8\upsilon_d) \frac{f_{ctm}}{f_{yd}}$	-
Transverse bar			
(i) Outside critical regions			
Spacing $s_w \le$	0.75d	0.75d	0.75d

$\rho_w \geq$	$0.08\sqrt{\frac{f_{ck}(MPa)}{f_{yk}(MPa)}}$	$0.08\sqrt{\frac{f_{ck}(MPa)}{f_{yk}(MPa)}}$	$0.08\sqrt{\frac{f_{ck}(MPa)}{f_{yk}(MPa)}}$

Table 6-14 – EC8 rules for detailing and dimensioning of primary beams (secondary beams: as in DCL) (Fardis, 2009) (continue)

	DCH	DCM	DCL
(ii) In critical regions			
d_{bw}	6mm	6mm	6mm
Spacing $s_w \leq$	$\frac{h_w}{4}$, $6d_{bL}$, $24d_{bw}$, 175mm	$\frac{h_w}{4}$, $8d_{bL}$, $24d_{bw}$, 225mm	-
Shear design			
V_{Ed}, seismic	$1.2\frac{\sum M_{Rb}}{l_{cl}} \pm V_{o,g+\psi_2 q}$	$1.0\frac{\sum M_{Rb}}{l_{cl}} \pm V_{o,g+\psi_2 q}$	From analysis for seismic design action plus gravity
$V_{Rd,max}$, seismic	As in EC2: $V_{Rd,\max} = 0.3\frac{(1-f_{ck}(MPa))}{250} b_{wo} z f_{cd} \sin(2\delta)$; $1 \leq \cot\delta \leq 2.5$		
$V_{Rd,s}$, outside critical regions	As in EC2: $V_{Rd,s} = b_w z \rho_w f_{ywd} \cot(\delta)$; $1 \leq \cot\delta \leq 2.5$		
$V_{Rd,s}$, critical regions	$V_{Rd,s} = b_w z \rho_w f_{ywd} (\delta = 45^0)$	As in EC2: $V_{Rd,s} = b_w z \rho_w f_{ywd} \cot(\delta)$; $1 \leq \cot\delta \leq 2.5$	

(1)NDP (Nationally Determined Parameter) according to EC2; The Table 6-13 gives the value recommended in EC2.

(2) μ_φ is the value of the curvature ductility factor that corresponds to the basic value, q_0, of the behaviour factor used in the design: $\mu_\varphi = \begin{cases} 2q_0 - 1 (T_1 < T_C) \\ 1 + 2(q_0 - 1)\frac{T_C}{T_1} \end{cases}$;

(3) The minimum area of bottom steel, $A_{s,min}$, is in addition to any compression steel that may be needed for the verification of the end section for the ULS in bending under the (absolutely) maximum negative (hogging) moment from the analysis for the design seismic action plus concurrent gravity, M_{Ed}.

(4) h_c is the column depth in the direction of the bar, $\nu_d = N_{Ed}/A_c f_{cd}$ is the column axial load ratio, for the algebraically minimum value of the axial load due to the design seismic action plus concurrent gravity (compression: positive).

(5) At a member end where the moment capacities around the joint satisfy: $\sum M_{Rb} > \sum M_{Rc}$, M_{Rb} is replaced in the calculation of the design shear force, V_{Ed}, by $M_{Rb} (\sum M_{Rb} > \sum M_{Rc})$.

(6) z is the internal lever arm, taken equal to 0.9d or to the distance between the tension and the compression reinforcement, $d–d_1$.

Table 6-15 – EC8 rules for detailing and dimensioning of primary columns (secondary columns: as in DCL) (Fardis, 2009)

	DCH	DCM	DCL
Cross section sides, h_c, b_c ≥	0.25m;h_v/10 if $\theta = \frac{P\delta}{Vh} > 0.1$ (1)	-	-
Critical region length(1) ≥	1.5 h_c, 1.5 b_c, 0.6m, l_c/5	1.0 h_c, 1.0 b_c, 0.45m, l_c/5	h_c, b_c
Longitudinal bars (L)			
ρ_{min}	1%		$0.1\frac{N_d}{A_c} f_{dy}$;0.2% (2)
ρ_{max}	4%		4%(2)
d_{bL} ≥	8mm		
Bars per side	3		2
Distance between restrained bars	≤ 150mm	≤200m	-
Distance of unrestrained bar from the nearest restrained bar	150mm		
Transverse bar			
(i) Outside critical regions			
d_{bw} ≥	6mm, d_{bL}/4		
Spacing s_w ≤	20d_{bL}, h_c, b_c, 400mm		12d_{bL}, 0.6h_c, 0.6b_c, 240mm
At lap splices, if b_{bL}>14mm, s_w ≤	12d_{bL}, 0.6h_c, 0.6b_c, 240mm		
(ii) In critical regions			
d_{bw} ≥(4)	$6\text{mm}, 0.4\left(\frac{f_{yd}}{f_{ywd}}\right)^{1/2} d_{bL}$	6mm, d_{bL}/4	
Spacing s_w ≤(4), (5)	6d_{bL}, b_0/3, 125mm	8d_{bL}, b_0/2, 175mm	-
ω_{wd} ≥(6)	0.08	-	-
aω_{wd} ≥(5)(6)(7)(8)	30$\mu_\Phi^*\nu_d\varepsilon_{sy,d}b_c/b_0$-0.035	-	-
In critical regions at column base			
ω_{wd} ≥	0.12	0.08	-
aω_{wd} ≥(5)(6)(7)(8)(9)(10)	30$\mu_\Phi\nu_d\varepsilon_{sy,d}b_c/b_0$-0.035		-

Capacity design at beam-column joints (11)	$1.3\sum M_{Rd} \le \sum M_{Rc}$ No moment in transverse direction of column		
Axial load ratio $\nu_d = \frac{N_{Ed}}{A_c f_{cd}}$	≤0.55	≤0.65	-

Table 6-16 – EC8 rules for detailing and dimensioning of primary columns (secondary columns: as in DCL) (Fardis, 2009) (continued)

	DCH	DCM	DCL
Shear design			
V_{Ed}, seismic(12)	$1.3\frac{\sum M_{Rc}^{ends(12)}}{l_{cl}}$	$1.1\frac{\sum M_{Rc}^{ends(11)}}{l_{cl}}$	From analysis for seismic design action plus gravity
$V_{Rd,max}$, seismic(13)	As in EC2: $V_{Rd,\max} = 0.3\frac{(1-f_{ck}(MPa))}{250} b_{wo} z f_{cd} \sin(2\delta)$; $1 \le \cot\delta \le 2.5$		
$V_{Rd,s}$, seismic (13)(14)(15)	As in EC2: $V_{Rd,s} = b_w z \rho_w f_{ywd} \cot(\delta) + N_{Ed}\frac{h-x}{l_{cl}}$; $1 \le \cot\delta \le 2.5$		

(1) h_v is the distance of the inflection point to the column end further away, for bending within a plane parallel to the side of interest; l_c is the column clear length.

(2) Note (1) of Table 6-13 applies.

(3)For DCM: if a value of q not greater than 2 is used for the design, the transverse reinforcement in critical regions of columns with axial load ratio ν_d not greater than 0.2 may just follow the rules applying to DCL columns.

(4) For DCH: In the two lower storeys of the building, the requirements on dbw, sw apply over a distance from the end section not less than 1.5 times the critical region length.

(5) Index c denotes the full concrete section and index '0' the confined core to the centreline of the perimeter hoop; b_0 is the smaller side of this core.

(6) ω_{wd} is the ratio of the volume of confining hoops to that of the confined core to the centreline of the perimeter hoop, times f_{yd}/f_{cd}.

(7) a is the "confinement effectiveness" factor, computed as $a = a_s a_n$; where: $a_s = (1-s/2b_0)(1-s/2h_0)$ for hoops; $a_n = 1-\{b_0/((n_h-1)h_0)+h_0/((n_b-1)b_0)\}/3$ for rectangular hoops with n_b legs parallel to the side of the core with length b_0 and n_h legs parallel to the one with length h_0.

(8) For DCH: at column ends protected from plastic hinging through the capacity design check at beam-column joints, $\mu_\varphi*$ is the value of the curvature ductility factor that corresponds to 2/3 of the basic value, q_0, of the behaviour factor used in the design; at the ends of columns where plastic hinging is not prevented because of the exemptions listed in Note (11) below, $\mu_\varphi*$ is taken equal to μ_φ defined in Note (2) of Table 6-13 (see also Note (10) below); $\varepsilon_{sy,d} = f_{yd}/E_s$.

(9) Note (2) of Table 6-13 applies.

(10) For DCH: The requirement applies also in the critical regions at the ends of columns where plastic hinging is not prevented, as falling within the exemptions in Note (11) below.

(11) The capacity design check does not need to be fulfilled at beam-column joints: (a) of the top floor, (b) of the ground storey in two-storey buildings with axial load ratio νd not greater than 0.3 in all columns, (c) if shear walls resist at least 50% of the base shear parallel to the plane of the frame (wall buildings or wall-equivalent dual buildings), and (d) in one-out-of-four columns of plane frames with columns of similar size.

(12) At a member end where the moment capacities around the joint satisfy: $\sum M_{Rb} < \sum M_{Rc}$ M_{Rc} is replaced in the calculation of the design shear force, V_{Ed}, by M_{Rc} ($\sum M_{Rb} > \sum M_{Rc}$).

(13) z is the internal lever arm, taken equal to 0.9d or to the distance between the tension and the compression reinforcement, $d–d_1$.

(14) The axial load, N_{Ed}, and its normalised value, ν_d, are taken with their most unfavourable values for the shear verification under the design seismic action plus concurrent gravity (considering both the demand, V_{Ed}, and the capacity, V_{Rd}).

(15) x is the neutral axis depth at the end section in the ULS of bending with axial load.

6.4. Case study structures

6.4.1. Description of case study RC-MRFs

This study is limited to two categories of buildings referring to the domestic or residential and office buildings, categorised as A and B in EN 1990 (2002). Moment resisting frames are chosen as the main structural resistance elements of the buildings. These types of frames are also well known as bracing or un-braced frames, meaning that all actions including gravity and lateral ones are carried only by the frames. The buildings in this study are also limited to rectangular plans. In this study only the short edge frames are analysed.

Up to present, these types of structures are widely used in many countries such as Viet Nam, Laos, Algeria ... They may be designed (or may be not) taking into account seismic design situations. Thus, two groups of RC-MRFs, one being designed according to EC2 and the other one in accordance with both EC2 and EC8, are the subjects of this study. The plan and elevation of four configurations of case study frames are presented in Figure 6-7.

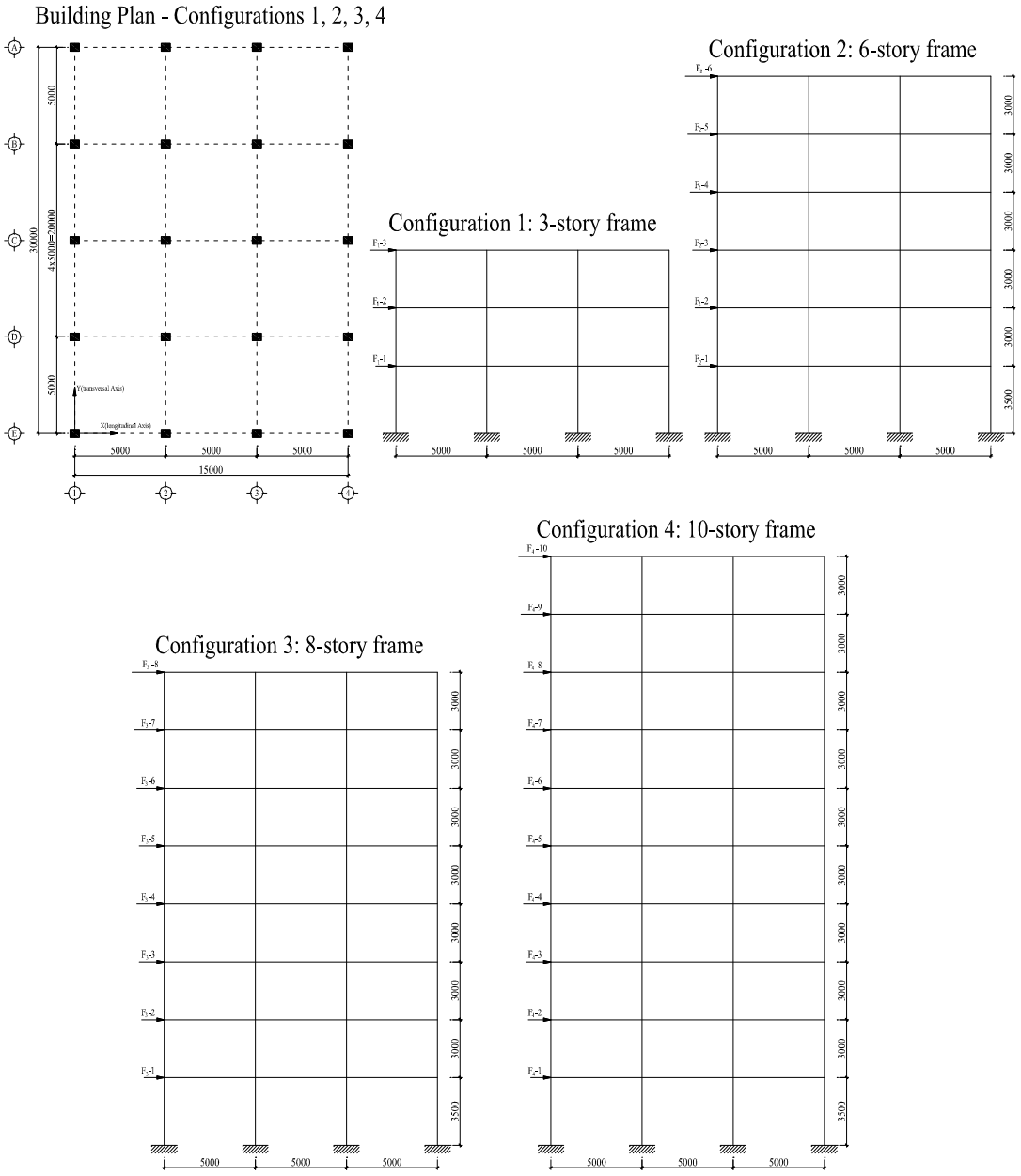

Figure 6-7 – Case study structures: Configurations 1, 2, 3, 4 (dimensions in meters)

The studied frames are located in three seismic zones, having PGA of 0.05, 0.15g and 0.3g respectively, representing the low, medium and high seismicity regions. As mentioned, these buildings are first designed in accordance with EC2 and ignoring seismic actions, the resulting frames called 'EC2-0.05g , EC2-0.15g or EC2-0.3g' representing the zones in which they are located. These frames are referred to 'EC2-group'.

Then, they are also designed according to both EC2 and EC8, named 'EC8-DCL or DCM-0.05g , 0.15g or 0.3g' under three types of seismicity with PGA of 0.05g , 0.15g and 0.3g. These frames are grouped in 'EC8-group'. To distinguish the studied frames between each geometrical configuration, their names are added the term 'Configuration No' at the beginning, with configuration defined in Figure 6-7.

All buildings have some common geometrical features: (1) they have a rectangular plan and are regular in elevation; (2) the first story height of all buildings is assumed to be the same and equal to 3.5m and the height of other stories is equal to 3.0m; (3) the dead loads and the live loads are assumed to be constant for all buildings; and (4) all buildings are assumed to be located on soil C, as defined in EC8.

The first feature might allow that the structural analysis of the buildings can be divided into two planar frames. As mentioned, the present work is limited to the frames in shorter dimensions.

At the first thought, it is intended to design all the frames in the EC2-group with the purpose of limiting the overstrength of the structures as much as possible. To do it, it is necessary to determine the dimensions of the frame components as small as possible. This will permit easier examining the effectiveness of the retrofitting system using EMP in this group. However, in the next step of the study, these frames are then designed in accordance with EC8 with different target ductility classes. There are many refinements in seismically designing the frames to ensure their energy dissipated capacity corresponding to the chosen ductility class such as limitations of story drifts…. This leads to somewhat largely changing the dimensions of the frame components of the same frame configuration in different ductility class.

It is difficult to compare the different design of that configuration, especially the reinforcing steel contents, when they are designed for different seismic action and ductility classes. Therefore, aiming at an easier comparison of the design and of the details of frames, the dimensions of the frame members are chosen based on the minimum requirements from EC8. This leads to changing the numbers of frames studied in EC2-group, as seen in Table 6-17 and 18. It means that having the same plan and story dimensions but located in different seismic zones (PGA of 0.05g, 15g and 0.3g), the cross-sections of the elements will be different. Thus, in this case, the sections corresponding to EC8-group with PGA of 0.05g or 0.15g, which are designed according to EC2, are those called EC2-0.05g or EC2-0.15g frames. On the other hand, the frames, which are located in regions with PGA of 0.3g, are first designed in accordance with EC2 and called EC2-0.3g frames. The details of geometrical configurations of the frames studied are presented in Tables 6-18 to 21. The detail of hypothesis for concrete sections and steel reinforcement and the goal of design are given in Table 6-17.

According to EC8, the minimum dimensions of the frame components are dependent on several critical requirements, such as the ductility class chosen for the designed structure, the behaviour of non-structural components in the building and damage limitations for the structure at the serviceability limit state. Due to that, in many cases the dimensions of the components are mainly governed by the serviceability limit state, especially for the structure designed under a large seismic excitation. This sometimes leads to a rather high overstrength of the structure.

Pairs of frames in each configuration (one designed to EC2 and one to EC8) have the same geometrical spans. All of the slabs are made of a reinforced concrete and act as diaphragms, being rigid in plane. It is also supposed that the slab of that pair is the same although it is designed in accordance with two different codes, EC2 and EC8. The slab thickness varies from 120mm to 150mm depending on the dimensions of the plan. Figure 6-8 shows the typical reinforcement configurations of the floors, regardless of their thickness.

As required in EC2 and EC8, to account for the contribution of slabs to the stiffness of studied frames, some parts of the floors is taken into account as parts of the frame. The slab is considered as the flanges of the beams with a width equal to an "effective width". The effective width of the flanges is dependent on parameters such as the slab thickness, span of the beams and distance between two planar frames. The

reinforcement of the slabs within the effective width of the beams is regarded as one part of total reinforcement area of beams ($b_{eff}=b_w+4h_f$ (5.4.3.1.1-EC8)).

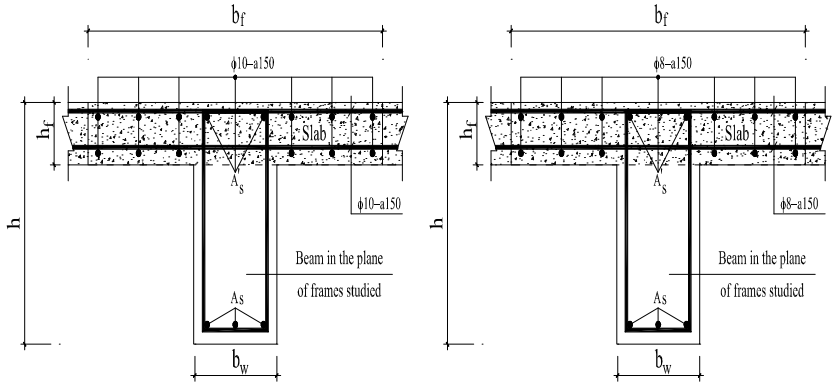

Figure 6-8 – Reinforcement configurations of the slab

Table 6-17 – Hypothesis and motivation for defining different design in each Configuration

Name	Hypothesis for defining concrete sections	Hypothesis for defining steel reinforcement	Motivation
EC2-0.05g	Design to EC2 for gravity, service, wind, snow Located in the seismic zone PGA=a_{gR}=0.05g	Minimum in an EC2 design for gravity, service, wind and snow	To know how a structure designed to EC2 behaves if zonation becomes a_{gR}=0.05g To be able to compare steel content of an EC2 design with steel content of an EC2+EC8 design for a_{gR}=0.05g
EC2-0.15g	Concrete sections are those of design to EC8 for PGA=a_{gR}=0.15g Design to EC2 for gravity, service, wind, snow	Minimum in an EC2 design for gravity, service, wind and snow	To know how a structure designed to EC2 behaves if zonation becomes a_{gR}=0.15g To be able to compare steel content of an EC2 design with steel content of an EC2+EC8 design for a_{gR}=0.15g. However, the concrete sections are not minimum.
EC2-0.3g	Concrete sections are those of design to EC8 for PGA=a_{gR}=0.3g Design to EC2 for gravity, service, wind, snow	Minimum in an EC2 design for gravity, service, wind and snow	To know how a structure designed to EC2 behaves if zonation becomes a_{gR}=0.3g To be able to compare steel content of an EC2 design with steel content of an EC2+EC8 design for a_{gR}=0.3g. The concrete sections are not minimum.
EC8-0.05g-L	Design to EC2 for gravity, service, wind Design to EC8 for earthquake in seismic zone PGA=a_{gR}=0.05g and low ductility class. Design includes checks of drift limitation.	Minimum in an EC2+EC8 design	For comparison to EC2-0.05g and to EC8-0.05M in steel content For comparison in Pushover and NLTH behaviour For comparison of a factors deduced from Pushover

Table 6-18 – Hypothesis and motivation for defining different design in each Configuration (continued)

Name	Hypothesis for defining concrete sections	Hypothesis for defining steel reinforcement	Motivation
EC8-0.05g-M	Like EC8-0.05g-L but EC8 design is ductility class DCM.	Minimum in an EC2+EC8 design	For comparison to EC2-0.05g and to EC8-0.05L in steel content For comparison in Pushover and NLTH behaviour For comparison of a factors deduced from Pushover
EC8-0.15g-L	Design to EC2 for gravity, service, wind Design to EC8 for earthquake in seismic zone PGA=a_{gR}=0.15g and low ductility class. Design includes checks of drift limitation.	Minimum in an EC2+EC8 design	For comparison to EC2-0.05g and to EC8-0.05L in steel content For comparison in Pushover and NLTH behaviour For comparison of a factors deduced from Pushover
EC8-0.15g-M	Like EC8-0.15g-L but EC8 design is ductility class DCM.	Minimum in an EC2+EC8 design	For comparison to EC2-0.05g and to EC8-0.05L in steel content For comparison in Pushover and NLTH behaviour For comparison of a factors deduced from Pushover
EC8-0.3g-M	Like EC8-0.15g-DCM but for earthquake in seismic zone PGA=a_{gR}=0.3g	Minimum in an EC2+EC8 design	For comparison to EC2-0.05g and to EC8-0.05L in steel content For comparison in Pushover and NLTH behaviour For comparison of a factors deduced from Pushover

Table 6-19 – List of case study RC-MRFs

Case study	Design Code	Location zone
EC2-0.05g	EC2	PGA of 0.05g
EC2-0.15g	EC2	PGA of 0.15g
EC2-0.3g	EC2	PGA of 0.3g
EC8-0.05g-L	EC2+EC8	PGA of 0.05g
EC8-0.05g-M	EC2+EC8	PGA of 0.05g
EC8-0.15g-L	EC2+EC8	PGA of 0.15g
EC8-0.15g-M	EC2+EC8	PGA of 0.15g
EC8-0.3g-M	EC2+EC8	PGA of 0.3g

Table 6-20 – Geometrical dimensions of the components of frames studied (in meters)

Config. studied	Case study	Number of stories/spans	Span length			Story height	
			Span 1	Span 2	Span 3	Floor 1	Others
1	EC2-0.05g EC2-0.15g EC2-0.3g EC8-0.05g-L EC8-0.05g-M EC8-0.15g-L EC8-0.15g-M EC8-0.3g-M	3/3	5	5	5	3.5	3.0
2	as above	6/3	5	5	5	3.5	3.0
3	as above	8/3	5	5	5	3.5	3.0
4	as above	10/3	5	5	5	3.5	3.0

Table 6-21 – Cross-sectional dimensions of the components of frames studied (in meters)

Config. studied	Case study	Number of stories	Columns		Beams			Slab
			Internal	External	Width	Height	Flange width	
1	EC2-0.05g EC2-0.15g EC2-0.3g EC8-0.05g-L EC8-0.05g-M EC8-0.15g-L EC8-0.15g-M EC8-0.3g-M	3	0.30x0.30 0.35x0.35 0.50x0.50 0.30x0.30 0.30x0.30 0.35x0.35 0.35x0.35 0.50x0.50	0.30x0.30 0.35x0.35 0.50x0.50 0.30x0.30 0.30x0.30 0.35x0.35 0.35x0.35 0.50x0.50	0.25	0.35	0.60 ; 0.85 ; 1.10	0.15
2	EC2-0.05g EC2-0.15g EC2-0.3g EC8-0.05g-L EC8-0.05g-M EC8-0.15g-L EC8-0.15g-M EC8-0.3g-M	6	0.35x0.35 0.35x0.35 0.60x0.60 0.35x0.35 0.50x0.50 0.35x0.35 0.50x0.50 0.60x0.60	0.35x0.35 0.35x0.35 0.60x0.60 0.35x0.35 0.50x0.50 0.35x0.35 0.50x0.50 0.60x0.60	0.25	0.35	0.85 ; 1.1 ; 1.2	0.15
3	EC2-0.05g EC2-0.15g EC2-0.3g EC8-0.05g-L EC8-0.05g-M EC8-0.15g-L EC8-0.15g-M EC8-0.3g-M	8	0.60x0.60	0.50x0.50	0.25	0.4	1.10 ; 1.20	0.15

Table 6-22 – Cross-sectional dimensions of the components of frames studied (in meters) (continued)

Config. studied	Case study	Number of stories	Columns		Beams			Slab
			From 1-4 (1-5)	From 5-8 (6-10)	Width	Height	Flange width	
4	EC2-0.05g	10	0.60x0.60	0.50x0.50	0.25	0.4	1.10; 1.20; 1.30; 1.40	0.15
	EC2-0.15g		0.60x0.60	0.50x0.50				
	EC2-0.3g		0.80x0.80	0.70x0.70				
	EC8-0.05g-L		0.60x0.60	0.50x0.50				
	EC8-0.05g-M		0.80x0.80	0.70x0.70				
	EC8-0.15g-L		0.60x0.60	0.50x0.50				
	EC8-0.15g-M		0.80x0.80	0.70x0.70				
	EC8-0.3g-M		0.80x0.80	0.70x0.70				

Concerning the material properties of the studied frames, they are assumed to be identical for all structures having: (a) concrete cubic characteristic strength, f_{ck}=25MPa and (b) steel characteristic yielding strength, f_{yk}=500MPa.

For all buildings, a distributed permanent load of 5.67kN/m² represents finishing and partitions at all floors. A distributed live load equivalent to a weight of 3kN/m² is considered for occupancy at inter-story floors, and a live load of 2kN/m² is supposed for roof. All frames are subjected to a wind load of 0.67kN/m² on pressure surfaces.

Table 6-23 and 24 summarises the total seismic masses ($G+\psi_{Ei}Q$) participating in the vibration of the whole buildings and of such studied frames.

Table 6-23 – Total seismic masses of buildings and studied frames

Config. Studied	Case study	Total mass G (ton)		Total mass Q (ton)		Seismic total mass ($G+\psi_{Ei}Q$) (ton)	
		Whole building	Studied frame	Whole building	Studied frame	Whole building	Studied frame
1	EC2-0.05g	633.2	158.3	256.8	64.2	694.8	173.7
	EC2-0.15g	640.4	160.1	256.8	64.2	702.0	175.5
	EC2-0.3g	668.0	167.0	256.8	64.2	739.6	182.4
	EC8-0.05g-L	633.2	158.3	256.8	64.2	694.8	173.7
	EC8-0.05g-M	633.2	158.3	256.8	64.2	694.8	173.7
	EC8-0.15g-L	640.4	160.1	256.8	64.2	702.0	175.5
	EC8-0.15g-M	640.4	160.1	256.8	64.2	702.0	175.5
	EC8-0.3g-M	668.0	167.0	256.8	64.2	739.6	182.4
2	EC2-0.05g	1294.0	323.5	532.0	133.0	1421.6	355.4
	EC2-0.15g	1294.0	323.5	532.0	133.0	1421.6	355.4
	EC2-0.3g	1422.0	355.5	532.0	133.0	1550.0	387.5
	EC8-0.05g-L	1294.0	323.5	532.0	133.0	1421.6	355.4
	EC8-0.05g-M	1349.2	337.3	532.0	133.0	1476.8	369.2
	EC8-0.15g-L	1294.0	323.5	532.0	133.0	1421.6	355.4
	EC8-0.15g-M	1349.2	337.3	532.0	133.0	1476.8	369.2
	EC8-0.3g-M	1422.0	355.5	532.0	133.0	1550.0	387.5

Table 6-24 – Total seismic masses of buildings and studied frames (in ton) (continued)

Config. Studied	Case study	Total mass G (t)		Total mass Q (t)		Seismic total mass ($G+\psi_{Ei}Q$) (t)	
		Whole building	Studied frame	Whole building	Studied frame	Whole building	Studied frame
3	EC2-0.05g	1893.2	473.3	716.0	179.0	2064.8	516.2
	EC2-0.15g	1893.2	473.3	716.0	179.0	2064.8	516.2
	EC2-0.3g	1893.2	473.3	716.0	179.0	2064.8	516.2
	EC8-0.05g-L	1893.2	473.3	716.0	179.0	2064.8	516.2
	EC8-0.05g-M	1893.2	473.3	716.0	179.0	2064.8	516.2
	EC8-0.15g-L	1893.2	473.3	716.0	179.0	2064.8	516.2
	EC8-0.15g-M	1893.2	473.3	716.0	179.0	2064.8	516.2
	EC8-0.3g-M	1893.2	473.3	716.0	179.0	2064.8	516.2
4	EC2-0.05g	2376.0	594.0	898.4	224.6	2591.6	647.9
	EC2-0.15g	2376.0	594.0	898.4	224.6	2591.6	647.9
	EC2-0.3g	2622.0	655.5	898.4	224.6	2837.6	709.4
	EC8-0.05g-L	2376.0	594.0	898.4	224.6	2591.6	647.9
	EC8-0.05g-M	2622.0	655.5	898.4	224.6	2837.6	709.4
	EC8-0.15g-L	2376.0	594.0	898.4	224.6	2591.6	647.9
	EC8-0.15g-M	2622.0	655.5	898.4	224.6	2837.6	709.4
	EC8-0.3g-M	2622.0	655.5	898.4	224.6	2837.6	709.4

6.4.2. RC-MRFs designed according to both EC2 and EC8

EC8 recommends that structures should be designed as a whole. This means that the buildings should be analysed in 3-D models. However, all buildings in this study are regular in both elevation and plan; therefore it is possible to divide the 3-D structures into 2 planar frames in two perpendicular directions. To limit the number of frames studied, only the frames in shorter dimensions are taken into account. They are studied independently of the frames in the other direction of the buildings.

Twenty case study frames in four configurations of the EC8-group are designed under three peak ground accelerations of a_{gR}=0.05g, 0.15g and 0.3g, earthquake of type 1. Buildings are all supposed to be on a ground type C, which are deep deposits of dense or medium-dense sand, gravel or stiff clay with thickness from several centimetres to many hundred of meters. All of them are designed according to two ductility classes, namely Low and Medium classes (DCL and DCM). For convenience, Table 6-25 recalls design parameters of the frames under studied in this group.

Table 6-25 – Design parameters of the frames in EC8-groups

Configurations	Group and zone of PGA for case study	a_g (g)	DC	q
1 to 4	EC8-0.05g	0.05	DCL/DCM	1.5/3.9
1 to 4	EC8-0.15g	0.15	DCL/DCM	1.5/3.9
1 to 4	EC8-0.3g	0.30	DCM	3.9

Member cross-sectional dimensions of the studied frames in this group are given in Table 6-21 and 22. These dimensions were selected based on the maximum limitations of story drifts required by EC8 and to support the idea of comparing the differences of results of designed frames caused by different Ductility Classes (for frames in EC8-group with PGA of 0.05g and 0.15g). It is necessary to stress that in order to avoid significant overstrength of the frame, much effort was done to choose the dimensions and

reinforcement content of the frame components to be as small as possible. In most of cases, this selection could be done by choosing these dimensions with respects of the limits set by the inter-story drift control limitations, by the desire to reduce second-order effect and by the maximum allowable reinforcement steel ratios.

Due to the fact that all the buildings are symmetrical in plan and elevation with respect to two orthogonal axes and there is either discontinuity or abrupt change in the dimensions and stiffness of adjacent stories, only accidental torsion effects are taken into account (EC8). As suggested by EC8, internal forces from the analysis with seismic situations will be multiplied by a factor δ. In addition, for the frames designed in accordance with EC8, taking the cracking of concrete into account, flexural stiffness of beams and columns are assigned to be one-half of the corresponding un-crack ones.

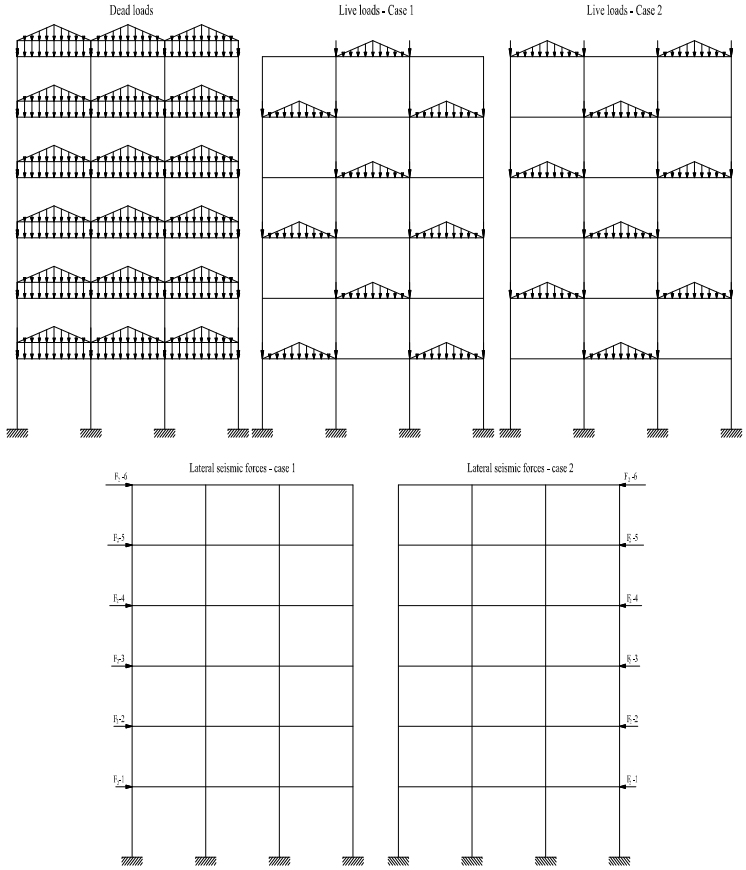

Figure 6-9 – Cases of gravity loads and seismic forces on the studied frames for all limit states

Figure 6-9 shows all load cases in the seismic design situation of all frames. The seismic force cases in the figure only represent the loading directions of the seismic excitations. Table 6-26 to Table 6-27 present the partial factors of the loads in some main combinations of loads in seismic situations according to EC8 and EN1990. Table 6-28 shows the partial factors of loads for calculating the efficient seismic weight of the frames according to EC8. SAP 2000 is used to do the first check of the cross-sectional dimensions of all members, to determine the combinations of internal forces and inter-story drifts of all frames and to calculate detail longitudinal and transversal rebar of the structural elements.

Table 6-26 – Partial factors of main combinations of loads according to EC8 and EN1990 at the ultimate limit state of seismic situations

Combinations	Dead load	Live load1 (ψ_{Ei})	Live load2 (ψ_{Ei})	Seismic load – Case1	Seismic load – Case 2
1	1.0	0.3	0.3	1.0	-
2	1.0	0.3	0.3	-	1.0

Table 6-27 – Partial factors of main combinations of loads according to EC8 and EN1990 at the serviceability limit state of seismic situations

Combinations	Dead load	Live load1 (ψ_{Ei})	Live load2 (ψ_{Ei})	Seismic load – Case1	Seismic load – Case 2
1	1.0	1.0	1.0	1.0	-
2	1.0	1.0	1.0	-	1.0

Table 6-28 – Partial factors of loads for calculating effective seismic mass participating into the vibration modes of the frames according to EC8

Dead load	Live load1 (ψ_{Ei})	Live load2 (ψ_{Ei})
1.0	0.24	0.24

6.4.2.1. Global design results

The data and some results for the frames designed to EC2 and EC8 are summarized in Table 6-29, Table 6-30 and from Figure 6-10 to Figure 6-13. The elastic periods of the frames were determined by eigenvalue analysis of SAP 2000 (CSI, 2009). Table 6-29 also reports the effective mass participation ratios of the first modes and the fundamental periods of the structures in respect with crack of the concrete being taken into account. The design base shears of the 12 cases are shown in Table 6-30.

The design base shear coefficients, V_b/W, and the maximum 'sensitivity coefficient' θ in all stories, which is equal to the ratio of second-order to first-order seismic moments, $N\delta/Vh$, are shown in Figure 6-10 and Figure 6-11.

Figure 6.12 and Figure 6-13 depict the top and maximum inter-story drift ratio, δ/h. It is noteworthy stressing that these global response results were computed on the basis of the cracked stiffness of the member. In addition, based on the comparison of the computed values of θ with EC8 requirements, in some cases, internal forces in the frames are multiplied by $1/(1-\theta)$ due to P-delta effects when $0.1<\theta<0.2$. As seen in Figure 6-13, the maximum value of θ in all frames is less than 20%; therefore second order effect is just considered by the factor $1/(1-\theta)$.

Table 6-29 – Global results of the EC8 group

Confi-Group	a_g (g) - DC	q-factor	$T_{1,crack}$ (s)	μ_Φ	% Effective Mass – 1st mode	Confi-Group	a_g (g) - DC	q-factor	$T_{1,crack}$ (s)	μ_Φ	% Effective Mass - 1st mode
1-EC8	0.05-L	1.5	1.15	6	91.8	2-EC8	0.05-L	1.5	1.84	8.1	86.0
	0.05-M	3.9	1.15	15	91.8		0.05-M	3.9	1.73	9	84.0
	0.15-L	1.5	0.95	7	90.3		0.15-L	1.5	1.84	8.1	86.0
	0.15-M	3.9	0.95	16	90.3		0.15-M	3.9	1.73	9	84.0
	0.3-M	3.9	0.8	13	85.0		0.3-M	3.9	1.32	12	80.0
3-EC8	0.05-L	1.5	1.57	6.7	79.0	4-EC8	0.05-L	1.5	2.02	6.7	79.0
	0.05-M	3.9	1.57	13	79.0		0.05-M	3.9	1.83	12	76.0
	0.15-L	1.5	1.57	6.7	79.0		0.15-L	1.5	2.02	6.7	79.0
	0.15-M	3.9	1.57	13	79.0		0.15-M	3.9	1.83	12	76.0
	0.3-M	3.9	1.57	9	79.0		0.3-M	3.9	1.83	12	76.0

Table 6-30 – The values of design base shear and local ductility required

Confi-Group	a_g (g)-DC	Base shear (kN)	$\mu_{\Phi,required}$	Confi-Group	a_g(g)-DC	Base shear (kN)	$\mu_{\Phi,required}$
1-EC8	0.05-L	111.4	2.0	2-EC8	0.05-L	119.4	2.0
	0.05-M	43.2	6.8		0.05-M	58.0	6.8
	0.15-L	341.0	2.0		0.15-L	358.4	2.0
	0.15-M	131.0	6.8		0.15-M	134.0	6.8
	0.3-M	262.0	6.8		0.3-M	388.8	6.8
3-EC8	0.05-L	188.2	2.0	4-EC8	0.05-L	188.6	2.0
	0.05-M	72.7	6.8		0.05-M	116.6	6.8
	0.15-L	559.0	2.0		0.15-L	566.0	2.0
	0.15-M	216.0	6.8		0.15-M	218.0	6.8
	0.3-M	431.0	6.8		0.3-M	695.7	6.8

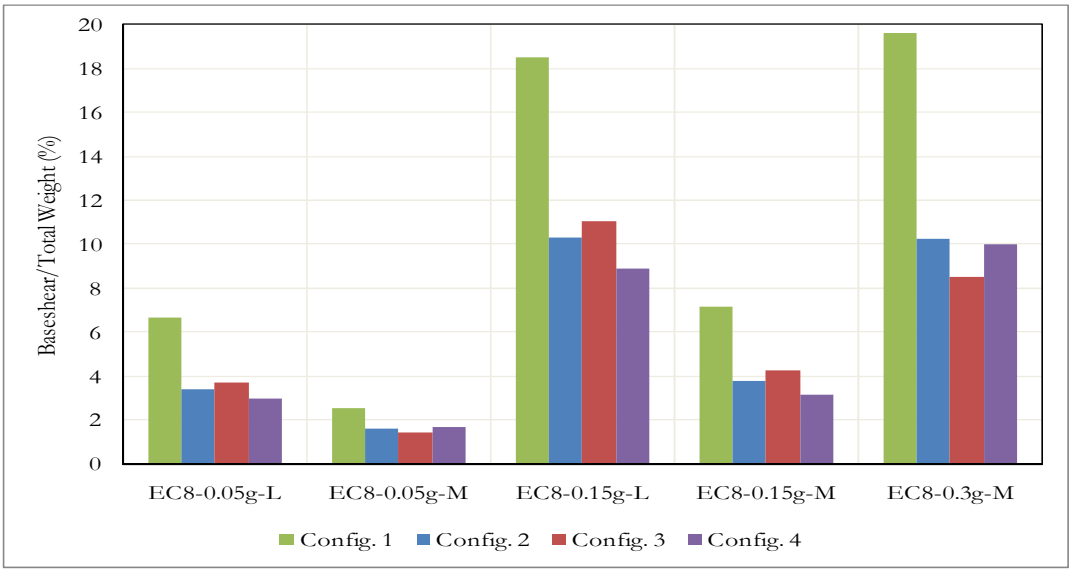

Figure 6-10 – Design base shear coefficient (V_b/W)

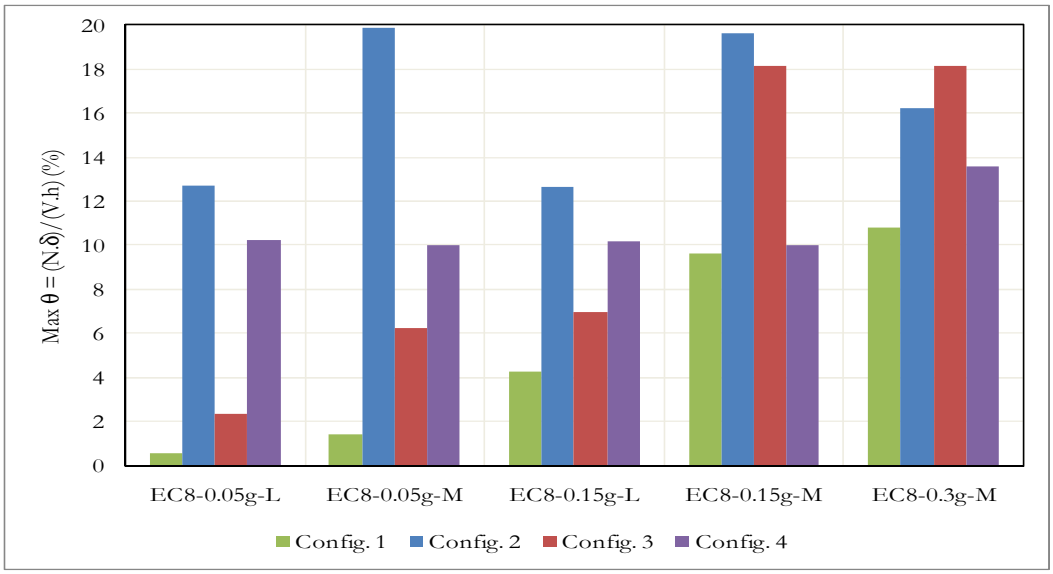

Figure 6-11 – Maximum sensitivity coefficient in all stories (Max $\theta = N.\delta/V.h$)

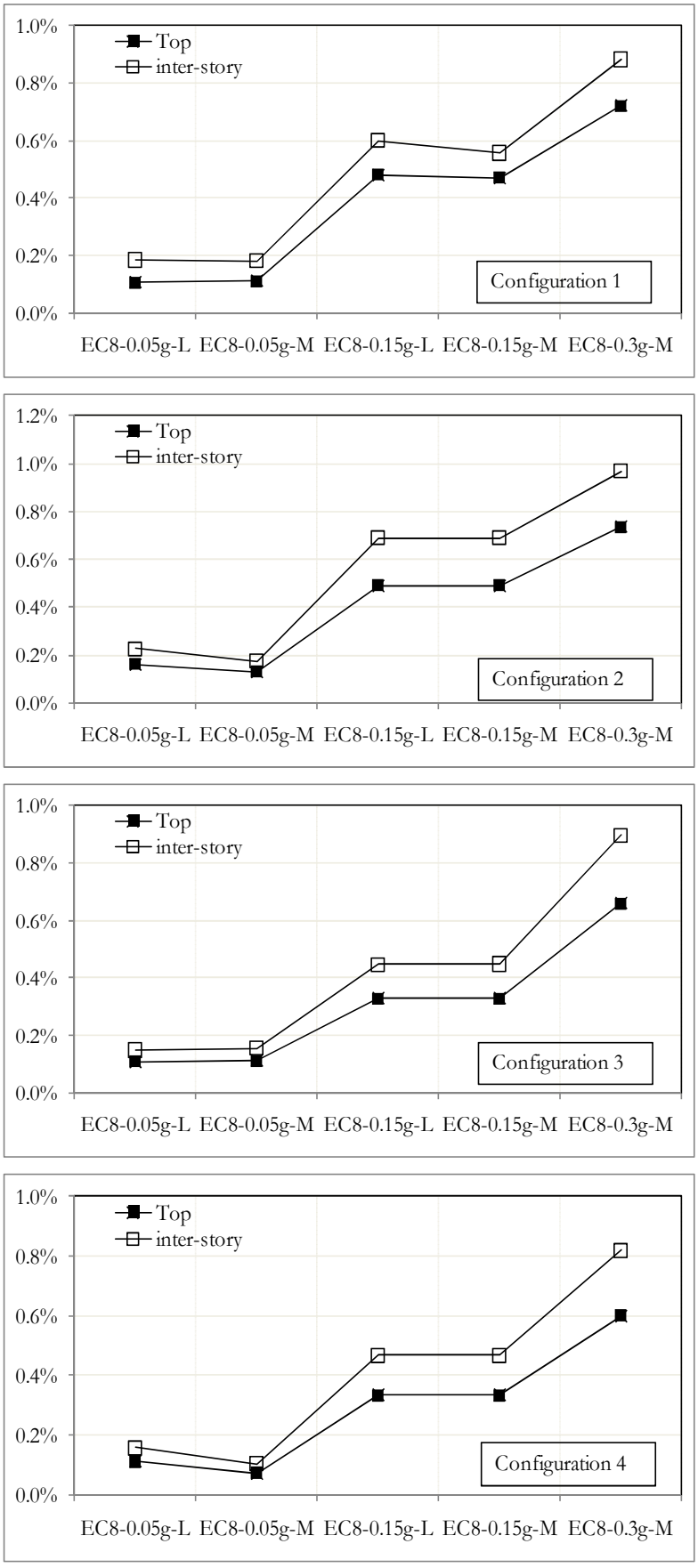

Figure 6-12 – Top and maximum inter-story drift ratio (δ/h) for the four studied configurations

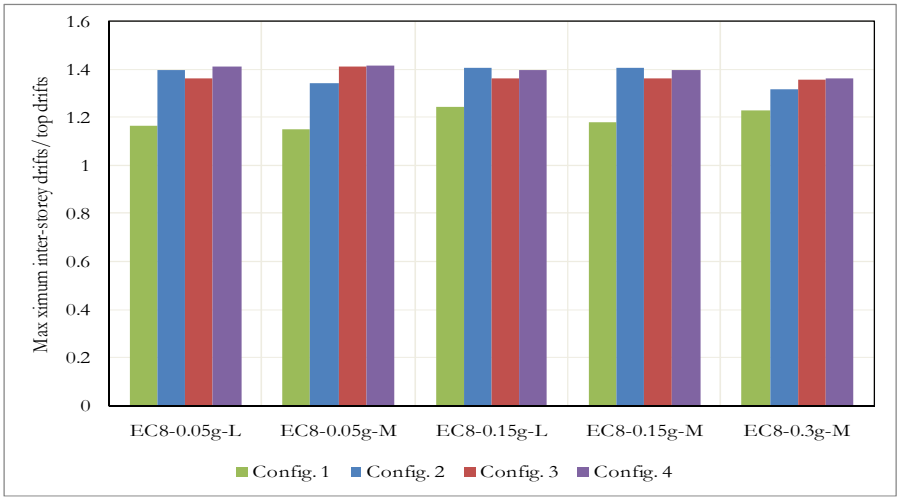

Figure 6-13 – Ratio of maximum inter-story drift to top drift for the studied frames

6.4.2.2. Longitudinal reinforcement configurations of the RC-MRFs studied

The required longitudinal steel contents in beams have been calculated from SAP 2000 and checked by RESPONSE 2000 (Evan C.Bentz, 2000) and by CUBIA (Montejo and Kowalsky, 2007). Based on that and considering some detail requirements mentioned in Table 6-13 and Table 6-15 for local ductility at node and critical regions, the reinforcement configurations of beams have been chosen. Table 6-31 shows the design moments and the resisting moments of some selected components in all studied frames. Table 6-32 to Table 6-33 shows the steel configurations and steel contents of the beams and columns in all studied cases from the analyses and the steel configurations selected.

Table 6-31 – Maximum design and resisting moments of beams and columns (kNm)

Configuration/ Case	Beams				Columns	
	Design moments		Resisting moments		Design moments	Resisting moments
	M^{+}_{Ed}	M^{-}_{Ed}	M^{+}_{Rd}	M^{-}_{Rd}	M_{Ed}	M_{Rd}
1/EC8-0.05g-L	68.5	-121	91	-129	57.4	120
1/EC8-0.05g-M	68.5	-121	110	-129	57.4	120
1/EC8-0.15g-L	89	-189	139	-191	190	322.2
1/EC8-0.15g-M	45	-104.2	116	-136	72.5	228.7
1/EC8-0.3g-M	60	-123	116	-136	146	397.2
2/EC8-0.05g-L	64	-129	97	-135	70.7	162
2/EC8-0.05g-M	53	-110	90	-121	91.0	459.7
2/EC8-0.15g-L	140	-217	163	-231	203	356.1
2/EC8-0.15g-M	53	-116	90	-121	132	459.7
2/EC8-0.3g-M	132	-140	163	-192	363	818
3/EC8-0.05g-L	53	-125.4	108	-163	160	753
3/EC8-0.05g-M	53	-125.4	108	-163	145	753
3/EC8-0.15g-L	171	-270	233	-281	483	894.1
3/EC8-0.15g-M	55	-134	102	-141	186	894.1
3/EC8-0.3g-M	125	-199	157	-209	372	894.1

Table 6-32 – Maximum design and resisting moments of beams and columns (kNm) (continued)

Configuration/ Case	Beams				Columns	
	Design moments		Resisting moments		Design moments	Resisting moments
	M^{+}_{Ed}	M^{-}_{Ed}	M^{+}_{Rd}	M^{-}_{Rd}	M_{Ed}	M_{Rd}
4/EC8-0.05g-L	57	-145.6	109	-173	200	817.4
4/EC8-0.05g-M	53	-133	125	-145	286	1520.6
4/EC8-0.15g-L	176	-273	233	-281	481	963
4/EC8-0.15g-M	54	-172	157	-209	201	1468
4/EC8-0.3g-M	123	-220	186	-259	371	1468

It is worth noting that in some cases, especially for Medium Ductility Class, the reinforcement of the beams has been governed by the requirements from the code in the critical regions, such as maximum and minimum steel content and reinforcement ratio in comparison between top and bottom.

Besides, longitudinal reinforcement of the columns in order to ascertain the favourable mechanisms of the structures at ultimate, the response is governed by the capacity design, not only by the design moments. In most of the cases, especially for the frames located in the region of PGA of 0.3g, the reinforcement of columns has been selected corresponding to the minimum steel content required by the code (ρ=1%). This is due to the fact that the dimensions of columns have been selected based on damage limitations leading to overstrength of the structures.

Table 6-33 – Reinforcement in all studied frames

Config./ Case	Story	Beams (mm^2)				Column (mm^2)	
		From analysis		Chosen		Chosen by Capacity design	
		Top	Bot.	Top	Bottom	Exterior	Interior
1/EC8-0.05g-L	1	1002	460	12Φ8+2Φ16(1005)	3Φ14(462)	8Φ16(1609)	8Φ20(2513)
	2	826	445	12Φ8+2Φ16(1005)	3Φ14(462)	8Φ16(1609)	8Φ20(2513)
	Roof	773	327	12Φ8+2Φ12(829)	3Φ14(462)	8Φ16(1609)	8Φ20(2513)
1/EC8-0.05g-M	1	1002	460	12Φ8+2Φ16(1005)	3Φ16(603)	8Φ16(1609)	12Φ18(3054)
	2	826	445	12Φ8+2Φ16(1005)	3Φ16(603)	8Φ16(1609)	12Φ18(3054)
	Roof	772	462	12Φ8+2Φ12(829)	3Φ14(462)	8Φ16(1609)	12Φ18(3054)
1/EC8-0.15g-L	1	1332	750	12Φ10+3Φ16(1546)	3Φ18(763)	8Φ25(3927)	8Φ25(3927)
	2	1332	750	12Φ10+3Φ16(1546)	3Φ18(763)	8Φ25(3927)	8Φ25(3927)
	Roof	679	378	12Φ8+2Φ12(829)	3Φ14(462)	8Φ18(2035)	8Φ18(2035)
1/EC8-0.15g-M	1	748	368	12Φ8+2Φ10(760)	3Φ14(462)	8Φ20(2513)	8Φ25(3927)
	2	748	368	12Φ8+2Φ10(760)	3Φ14(462)	8Φ20(2513)	8Φ25(3927)
	Roof	648	378	12Φ8+2Φ8(703)	3Φ14(462)	8Φ20(2513)	8Φ25(3927)
1/EC8-0.3g-M	1-2	1092	409	12Φ10+3Φ14(1404)	3Φ18(763)	12Φ16(2413)	12Φ16(2413)
	Roof	792	378	12Φ8+2Φ12(830)	3Φ14(462)	12Φ16(2413)	12Φ16(2413)

Table 6-34 – Reinforcement in all studied frames

Config./ Case	Story	Beams (mm²)				Column (mm²)	
		From analysis		Chosen		Chosen by Capacity design	
		Top	Bot.	Top	Bottom	Exterior	Interior
2/EC8-0.05g-L	1-5	1060	448	12Φ10+2Φ10(1100)	3Φ14(462)	8Φ14(1232)	8Φ18(2034)
	Roof	575	430	12Φ10+2Φ10(1100)	3Φ14(462)	8Φ14(1232)	8Φ18(2034)
2/EC8-0.05g-M	1-5	915	375	12Φ8+3Φ12(944)	3Φ14(462)	12Φ16(2413)	12Φ16(2413)
	Roof	597	364	12Φ8+2Φ8(703)	3Φ14(462)	12Φ16(2413)	12Φ16(2413)
2/EC8-0.15g-L	1-5	1474	887	12Φ10+3Φ20(1885)	3Φ20(942)	8Φ20(2513)	8Φ25(3927)
	Roof	551	374	12Φ10+2Φ10(1100)	3Φ14(462)	8Φ16(1609)	8Φ14(1232)
2/EC8-0.15g-M	1-5	922	390	12Φ8+3Φ12(943)	3Φ14(462)	12Φ16(2413)	12Φ16(2413)
	Roof	551	374	12Φ8+2Φ8(703)	3Φ14(462)	12Φ16(2413)	12Φ16(2413)
2/EC8-0.3g-M	1-5	1083	383	12Φ10+2Φ10(1100)	3Φ16(603)	12Φ20(3770)	12Φ20(3770)
	Roof	580	374	12Φ8+2Φ12 (830)	3Φ14(462)	12Φ20(3770)	12Φ20(3770)
3/EC8-0.05g-L	1-4	881	322	12Φ10+2Φ10(1100)	3Φ14(462)	12Φ20(3770)	12Φ20(3770)
	5-7	881	322	12Φ10+2Φ10(1100)	3Φ14(462)	12Φ16(2413)	12Φ16(2413)
	Roof	447	328	12Φ8+2Φ8(703)	3Φ12(339)	12Φ16(2413)	12Φ16(2413)
3/EC8-0.05g-M	1-4	881	320	12Φ10+2Φ10(1100)	3Φ16(603)	12Φ20(3770)	12Φ20(3770)
	5-7	881	320	12Φ10+2Φ10(1100)	3Φ16(603)	12Φ16(2413)	12Φ16(2413)
	Roof	447	328	12Φ8+2Φ8(703)	3Φ14(462)	12Φ16(2413)	12Φ16(2413)
3/EC8-0.15g-L	1-4	1600	945	12Φ10+3Φ20(1884)	4Φ20(1257)	12Φ20(3770)	12Φ20(3770)
	5-7	1600	945	12Φ10+3Φ20(1884)	4Φ20(1257)	12Φ20(3770)	12Φ20(3770)
	Roof	617	374	12Φ8+2Φ8(703)	3Φ14(462)	12Φ20(3770)	12Φ20(3770)
3/EC8-0.15g-M	1-4	896	374	12Φ8+4Φ10(917)	3Φ14(462)	12Φ20(3770)	12Φ20(3770)
	5-7	896	374	12Φ8+4Φ10(917)	3Φ14(462)	12Φ16(2413)	12Φ16(2413)
	Roof	551	374	12Φ8+2Φ8(703)	3Φ14(462)	12Φ16(2413)	12Φ16(2413)
3/EC8-0.3g-M	1-4	1324	675	12Φ10+3Φ14(1404)	3Φ18(763)	12Φ20(3770)	12Φ20(3770)
	5-7	1324	675	12Φ10+3Φ14(1404)	3Φ18(763)	12Φ16(2413)	12Φ16(2413)
	Roof	530	374	12Φ8+2Φ8 (703)	3Φ14(462)	12Φ16(2413)	12Φ16(2413)
4/EC8-0.05g-L	1-5	1065	351	12Φ10+2Φ12(1169)	3Φ14(462)	12Φ20(3770)	12Φ20(3770)
	6-9	1065	351	12Φ10+2Φ12(1169)	3Φ14(462)	12Φ16(2413)	12Φ16(2413)
	Roof	390	331	12Φ8+2Φ8(703)	3Φ12(339)	12Φ16(2413)	12Φ16(2413)

Table 6-35 – Reinforcement in all studied frames (continued)

Config./ Case	Story	Beams (mm²)				Column (mm²)	
		From analysis		Chosen		Chosen by Capacity design	
		Top	Bot.	Top	Bottom	Exterior	Interior
4/EC8-0.15g-L	1-5	1655	953	12Φ10+3Φ20(1884)	4Φ20(1257)	12Φ20(3770)	12Φ20(3770)
	6-9	1655	953	12Φ10+3Φ20(1884)	4Φ20(1257)	12Φ16(2413)	12Φ16(2413)
	Roof	570	374	12Φ8+2Φ8(703)	3Φ14(462)	12Φ16(2413)	12Φ16(2413)
4/EC8-0.05g-M	1-5	739	273	12Φ8+3Φ12(942)	3Φ16(603)	20Φ20(6283)	20Φ20(6283)
	6-9	739	273	12Φ8+3Φ12(942)	3Φ16(603)	20Φ18(5089)	20Φ18(5089)
	Roof	414	263	12Φ8+2Φ8(703)	3Φ14(462)	20Φ18(5089)	20Φ18(5089)
4/EC8-0.15g-M	1-5	1073	374	12Φ10+3Φ14(1404)	3Φ18(763)	20Φ20(6283)	20Φ20(6283)
	6-9	1073	374	12Φ10+3Φ14(1404)	3Φ18(763)	20Φ18(5089)	20Φ18(5089)
	Roof	563	374	12Φ8+2Φ8(703)	3Φ14(462)	20Φ18(5089)	20Φ18(5089)
4./EC8-0.3g/M	1-5	1732	1111	12Φ10+4Φ16(1747)	3Φ20(942)	20Φ20(6283)	20Φ20(6283)
	6-9	1732	1111	12Φ10+3Φ14(1747)	3Φ20(942)	20Φ18(5089)	20Φ18(5089)
	Roof	824	374	12Φ8+2Φ12(830)	3Φ14 (462)	20Φ18(5089)	20Φ18(5089)

Table 6-36 – Reinforcement contents (ρ, %) in comparison with criteria from EC8

Config./ Case	Story	Beams				Columns			
		ρ_{Chosen}		ρ_{max} (EC8)		ρ_{Chosen}		ρ_{min} and ρ_{max} (EC8)	
		ρ_{Top}	$\rho_{Bot.}$	ρ_{maxTop}	$\rho_{maxbot.}$	Exterior	Interior	ρ_{min}	ρ_{max}
1/EC8-0.05g-L	1	0.57	0.26	4.0	4.0	1.79	2.79	0.2	4
	2	0.57	0.26	4.0	4.0	1.79	2.79	0.2	4
	Roof	0.47	0.26	4.0	4.0	1.79	2.79	0.2	4
1/EC8-0.05g-M	1	0.57	0.34	0.78	1.01	1.79	3.39	1.0	4
	2	0.57	0.34	0.78	1.01	1.79	3.39	1.0	4
	Roof	0.47	0.26	0.70	0.91	1.79	3.39	1.0	4
1/EC8-0.15g-L	1	0.9	0.43	4.0	4.0	3.21	3.21	0.2	4
	2	0.9	0.43	4.0	4.0	3.21	3.21	0.2	4
	Roof	0.50	0.26	4.0	4.0	1.66	1.66	0.2	4
1/EC8-0.15g-M	1	0.43	0.26	0.7	0.87	2.05	3.21	1.0	4
	2	0.43	0.26	0.7	0.87	2.05	3.21	1.0	4
	Roof	0.40	0.26	0.7	0.87	2.05	3.21	1.0	4
1/EC8-0.3g-M	1-2	0.79	0.43	0.87	1.23	1.00	1.00	1.0	4
	Roof	0.47	0.26	0.7	0.91	1.00	1.00	1.0	4

Table 6-37 – Reinforcement contents (ρ, %) in comparison with criteria from EC8

Config./ Case	Story	Beams				Columns			
		ρ_{Chosen}		ρ_{max} (EC8)		ρ_{Chosen}		ρ_{min} and ρ_{max} (EC8)	
		ρ_{Top}	$\rho_{Bot.}$	ρ_{maxTop}	$\rho_{maxbot.}$	Exterior	Interior	ρ_{min}	ρ_{max}
2/EC8-0.05g-L	1-5	0.62	0.26	4.0	4.0	1.00	1.66	0.2	4
	Roof	0.62	0.26	4.0	4.0	1.00	1.66	0.2	4
2/EC8-0.05g-M	1-5	0.50	0.24	0.68	0.94	1.00	1.00	1.0	4
	Roof	0.37	0.24	0.68	0.81	1.00	1.00	1.0	4
2/EC8-0.15g-L	1-5	1.13	0.53	4.0	4.0	2.05	3.21	0.2	4
	Roof	0.62	0.26	4.0	4.0	1.31	1.00	0.2	4
2/EC8-0.15g-M	1-5	0.53	0.26	0.7	0.97	1.00	1.00	1.0	4
	Roof	0.40	0.26	0.7	0.84	1.00	1.00	1.0	4
2/EC8-0.3g-M	1-5	0.62	0.34	0.80	1.06	1.33	1.33	1.0	4
	Roof	0.47	0.26	0.70	0.91	1.33	1.33	1.0	4
3/EC8-0.05g-L	1-4	0.58	0.24	4.0	4.0	1.00	1.00	0.2	4
	5-7	0.58	0.24	4.0	4.0	1.00	1.00	0.2	4
	Roof	0.37	0.18	4.0	4.0	1.00	1.00	0.2	4
3/EC8-0.05g-M	1-4	0.58	0.24	0.68	1.02	1.00	1.00	1.0	4
	5-7	0.58	0.24	0.68	1.02	1.00	1.00	1.0	4
	Roof	0.37	0.24	0.68	0.81	1.00	1.00	1.0	4
3/EC8-0.15g-L	1-4	0.99	0.66	4.0	4.0	1.33	1.33	0.2	4
	5-7	0.99	0.66	4.0	4.0	1.33	1.33	0.2	4
	Roof	0.37	0.24	4.0	4.0	1.33	1.33	0.2	4
3/EC8-0.15g-M	1-4	0.48	0.24	0.68	0.88	1.33	1.33	1.0	4
	5-7	0.48	0.24	0.68	0.88	1.00	1.00	1.0	4
	Roof	0.37	0.24	0.68	0.81	1.00	1.00	1.0	4
3/EC8-0.3g-M	1-4	0.74	0.40	0.84	1.18	1.33	1.33	1.0	4
	5-7	0.74	0.40	0.84	1.18	1.00	1.00	1.0	4
	Roof	0.37	0.24	0.68	0.81	1.00	1.00	1.0	4
4/EC8-0.05g-L	1-5	0.62	0.24	4.0	4.0	1.00	1.00	0.2	4
	6-9	0.62	0.24	4.0	4.0	1.00	1.00	0.2	4
	Roof	0.37	0.24	4.0	4.0	1.00	1.00	0.2	4
4/EC8-0.05g-M	1-5	0.50	0.32	0.76	0.94	1.00	1.00	1.0	4
	6-9	0.50	0.32	0.76	0.94	1.00	1.00	1.0	4
	Roof	0.37	0.24	0.68	0.81	1.00	1.00	1.0	4

Table 6-38 – Reinforcement contents (ρ, %) in comparison with criteria from EC8

Config./ Case	Story	Beams				Columns			
		ρ_{Chosen}		ρ_{max} (EC8)		ρ_{Chosen}		ρ_{min} and ρ_{max} (EC8)	
		ρ_{Top}	$\rho_{Bot.}$	ρ_{maxTop}	$\rho_{maxbot.}$	Exterior	Interior	ρ_{min}	ρ_{max}
4/EC8-0.15g-L	1-5	0.99	0.66	4.0	4.0	1.33	1.33	0.2	4
	6-9	0.99	0.66	4.0	4.0	1.00	1.00	0.2	4
	Roof	0.37	0.24	4.0	4.0	1.00	1.00	0.2	4
4/EC8-0.15g-M	1-5	0.48	0.24	0.68	0.88	1.00	1.00	1.0	4
	6-9	0.48	0.24	0.68	0.88	1.00	1.00	1.0	4
	Roof	0.37	0.24	0.68	0.81	1.00	1.00	1.0	4
4./EC8-0.3g-M	1-5	0.92	0.50	0.94	1.36	1.00	1.00	1.0	4
	6-9	0.92	0.50	0.94	1.36	1.00	1.00	1.0	4
	Roof	0.44	0.24	0.68	0.88	1.00	1.00	1.0	4

6.4.2.3. Capacity design for transversal reinforcements of beams and columns

Following the rules of capacity design of shear forces on beams and columns of EC2, all beams and columns are designed. For beams, stirrups having diameter of 10mm with number of legs depending on the longitudinal reinforcements, which range from 2 to 4, are used. For columns, stirrups with 10mm in diameter, having 4 to 8 legs, are adopted. Table 6-39 and Table 6-40 show the maximum shear forces that can be generated during seismic excitations and shear resistance of typical beams and columns in all studied frames. It is clear that the shear resistance of all components are rather big to ascertain that plastic hinges will be formed due to bending only.

Table 6-39 – Maximum design and resisting shears of beams and columns (kN)

Configuration/ Case	Beams				Columns	
	From Gravity	From seismic	Sum	Resistance	From seismic	Resistance
	$V_{(g+\psi 2q)}$	$\gamma_{Rd} \sum M_{i,d} / l_{cl}$	$V_{Ed,max,i}$	max ($V_{Rd,s}$; $V_{Rd,max}$)	$\gamma_{Rd} \sum M_{i,d} / l_{cl}$	max ($V_{Rd,s}$; $V_{Rd,max}$)
1/EC8-0.05g-L	50	44	94	191	75.4	381.0
1/EC8-0.05g-M	50	47.8	97.8	191	75.4	565.5
1/EC8-0.15g-L	50	66.0	106.0	191	202.4	381.0
1/EC8-0.15g-M	50	50.4	100.4	191	107.0	565.5
1/EC8-0.3g-M	48.4	50.4	98.8	191	249.7	381.0
2/EC8-0.05g-L	51.0	46.4	97.4	191	102.0	381.0
2/EC8-0.05g-M	50.0	42.2	92.2	191	224.0	565.5
2/EC8-0.15g-L	51.0	78.8	129.8	191	224.0	381.0
2/EC8-0.15g-M	50.0	42.2	92.2	191	288.5	565.5
2/EC8-0.3g-M	50.0	73.2	123.2	191	562.0	661.0
3/EC8-0.05g-L	50.0	54.2	104.2	221.8	473	661.0

Table 6-40 – Maximum design and resisting shears of beams and columns (kN) (continued)

Configuration/ Case	Beams				Columns	
	From Gravity	From seismic	Sum	Resistance	From seismic	Resistance
	$V_{(g+\psi 2q)}$	$\sum M_{i,d} / l_{cl}$	$V_{Ed,max,i}$	max ($V_{Rd,s}$; $V_{Rd,max}$)	$\sum M_{i,d} / l_{cl}$	max ($V_{Rd,s}$; $V_{Rd,max}$)
3/EC8-0.05g-M	50.0	54.2	104.2	221.8	473	661.0
3/EC8-0.15g-L	50.0	102.8	152.8	221.8	562.0	661.0
3/EC8-0.15g-M	50.0	48.6	98.6	221.8	562.0	661.0
3/EC8-0.3g-M	50.0	73.2	123.2	221.8	562.0	661.0
4/EC8-0.05g-L	50.0	56.4	106.4	221.8	514.0	661.0
4/EC8-0.05g-M	50.0	54.0	104.0	221.8	956.0	1196.0
4/EC8-0.15g-L	50.0	102.8	152.8	221.8	605.3	661.0
4/EC8-0.15g-M	50.0	73.2	123.2	221.8	923.9	1196.0
4/EC8-0.3g-M	50.0	89.0	149.0	221.8	923.9	1196.0

6.4.3. Some concluding remarks on the reinforcement configurations between DCL and DCM design of RC-MRFs in EC8-group

When observing the steel contents from the analyses, it is clear that for a given ground acceleration the Ductility Class has not much influence on the quantities of steel. For different ductility classes, on the average, DCM has a little advantage over DCL on the quantities of steel under a given ground motion. Regarding the distribution of the steel in the framed structures, it is clear that the increase of Ductility Class shifts steel from beams to columns. This is because increase of ductility class resulting from the increase of behaviour factors decreases the design base shears, which in turn directly reduce the design bending moments in beams. Nevertheless, such reduction of the design actions is not directly reflected in columns because the steels of the columns are controlled by Capacity Design rules; therefore they are more independent of the Ductility Class.

In many cases, especially in the DCM frames, due to the damage limitations and minimum reinforcement contents required by the code, the reinforcement configuration of the beam is not close to the calculated steel area obtained from the analysis. In addition, the reinforcement of the column, in most of the cases, is controlled by Capacity Design. However, it must be recalled that DCL design is not recommended for moderate and high seismicity zones (a_{gR}>0.1g) because of the uncertainties on action and because a DCL design does not provide any safety margin in case the seismic action is greater than expected.

6.4.4. RC-MRFs designed according to EC2

6.4.4.1. Frame analysis

As already discussed, the dimensions of the components of all frames in this group are chosen the same as in the DCL frames in EC8-group. They are presented in Table 6-21. According to EC2, these planar frames will be designed under gravity, wind and snow loads. Gravity loads include dead loads or self weights of the structure and live loads due to the habitants in the buildings. The value of live loads is assumed constant for all buildings, as mention in 6.4.1. The dead loads are calculated based on the geometrical configurations of the frames neglecting the presence of the reinforcements. Wind and snow loads are determined based on EN 1991 (2002). Simplified combinations, as permitted in EN 1990 (2002), are used as an alternative to persistent and transient design situations. The partial factors used in different combinations of actions are summarized in Table 6-41 and Figure 6-14. To determine the unfavourable positive moments of beams, live loads are divided in two cases, as explained in Figure 6-14. For obtaining

the unfavourable negative moments of the beams at the joints, two cases of the live loads are taken into account in one combination. In order to determine the internal forces in the frame at ultimate limit state, linear elastic analysis is performed using SAP 2000, version 14.1.0 (SAP2000, 2009). In the modelling, some assumptions have been made to simplify the analysis. Gross-section stiffness without taking into account the presence of the reinforcement is assumed for beams and columns. Beams and columns are modelled as linear beam finite elements based on the Bernoulli beam element. Due to not too large lateral deformations, second-order effects are not accounted for in the structural analyses. No moment redistribution is carried out in the current study.

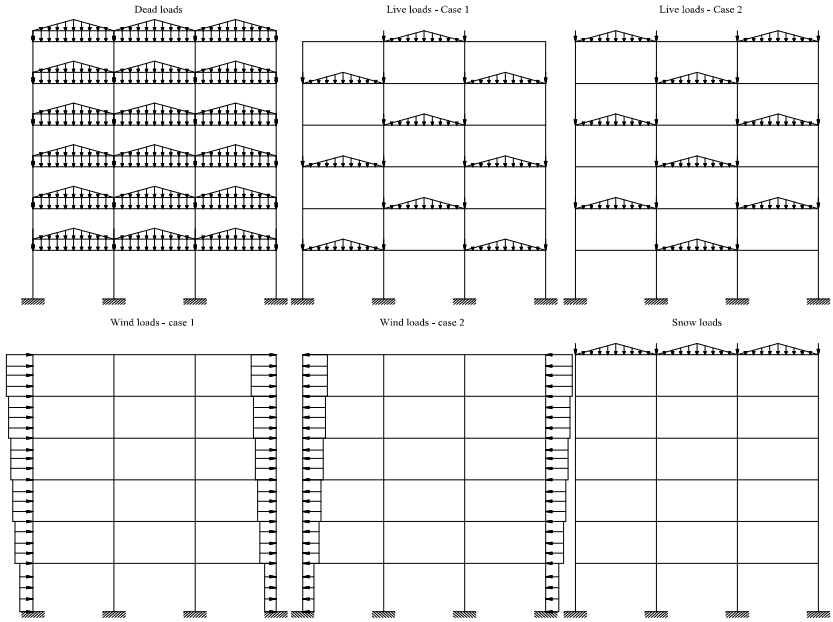

Figure 6-14 – Gravity, wind and snow load cases on the studied frames for all limit states

Table 6-41 – Partial factors of some main combinations of loads according to EC2 and EN1990 at the ultimate limit state

Combinations	Dead load	Live load1	Live load2	Wind load1	Wind load2	Snow load
1	1.35	-	-	1.5	-	-
2	1.35	-	-	-	1.5	-
3	1.35	1.5	-	-	-	-
4	1.35	-	1.5	-	-	-
5	1.35	1.5	1.5	-	-	-
6	1.35	1.5	1.5	1.05	-	1.05
7	1.35	1.5	-	1.05	-	1.05
8	1.35	-	1.5	1.05	-	1.05
9	1.35	1.5	1.5	-	1.05	1.05
10	1.35	1.5	-	-	1.05	1.05
11	1.35	-	1.5	-	1.05	1.05
12	1.35	1.05	1.05	1.5	-	1.05
13	1.35	1.05	1.05	-	1.5	1.05
14	1.35	1.05	1.05	1.05	-	1.50
15	1.35	1.05	1.05	-	1.05	1.50

The sections are then designed to have ultimate capacities that at least equal the bending moment and forces from such an analysis. The reinforcement content of the sections is also calculated by SAP2000. It seems incongruous that although the sections are designed by strength method, accounting for the inelastic behaviour of the materials, while the bending moments, shear and axial forces at the ultimate response are calculated assuming linear elastic behaviour of the members.

Nevertheless, this method is still valid because the distribution of inertial forces always satisfies the conditions of static equilibrium and the boundary conditions. Such a design might be considered as a valid lower-bound solution, as well-known in limit analysis (Park and Paulay, 1974).

Another important consideration, as required by EC2, is to check the frames at the serviceability limit state. There are some changes of partial factors at this limit state. In all cases, the deformations of the structures are satisfactory at serviceability limit state as required by the code.

6.4.4.2. Longitudinal reinforcement configurations of the beams and columns of studied frames

Table 6-42 presents some typical values of maximum design and resisting moments of beams and columns in this group.

The reinforcements have been first obtained from SAP2000 and then checked by RESPONSE 2000 (Evan C.Bentz, 2000), by CUBIA (Montejo and Kowalsky, 2007) and by some excel sheets with detailing rules extracted from EC2.

It should re-emphasize that the longitudinal reinforcements are chosen to be as small as possible. In some sections, they are equal to the minimum values required in the code. This allows better seeing the advantages of the EMP in capacity of seismically retrofitting the frames designed. This is going to be discussed in detail in next chapters.

The reinforcement contents of the case study frames in this EC2-group are given from Table 6-43 and Table 6-44.

Table 6-42 – Maximum design and resisting moments of beams and columns (unit: kNm)

Configuration/ Case	Beams				Columns	
	From analysis		Chosen		From analysis	Chosen
	M^{+}_{Ed}	M^{-}_{Ed}	M^{+}_{Rd}	M^{-}_{Rd}	M_{Ed}	M_{Rd}
1/EC2-0.05g	68.5	-121	91	-129	57	102.5
1/EC2-0.15g	60	-104	97	-135	33	111.0
1/EC2-0.3g	52	-93	97	-135	44.5	236.4
2/EC2-0.05g	60	-123	97	-135	63	244.5
2/EC2-0.15g	60	-123	97	-135	63	244.5
2/EC2-0.3g	51	-106	116	-136	115	508.5
3/EC2-0.05g	54	-138	108	-163	139	605.4
3/EC2-0.15g	54	-138	108	-163	139	605.4
3/EC2-0.3g	54	-138	108	-163	139	605.4
4/EC2-0.05g	56	-158	108	-163	195	691
4/EC2-0.15g	56	-158	108	-163	195	691
4/EC2-0.3g	55	-143	108	-163	277	1197

Table 6-43 – Reinforcement Area from the analyses and chosen steel configurations of the frames in the EC2-group

Confi. /Case	Sto.	Beams (mm^2)				Column (mm^2)			
		From analysis		Chosen		From analysis		Chosen	
		Top	Bottom	Top	Bottom	Exterior	Interior	Exterior	Interior
1/ EC2-0.05g	1-2	1003	485	12Φ8+2 Φ16 (1005)	3Φ14 (462)	772	1249	8Φ14 (1232)	8Φ16 (1609)
	Roof	772	477	12Φ8+2 Φ12 (829)	3Φ14 (462)	967	270	8Φ14 (1232)	8Φ16 (1609)
1/ EC2-0.15g	1-2	860	423	12Φ10+2 Φ10 (1100)	3Φ14 (462)	368	368	8Φ8 (402)	8Φ8 (402)
	Roof	745	434	12Φ10+2 Φ10 (1100)	3Φ14 (462)	1017	368	8Φ14 (1232)	8Φ8 (402)
1/ EC2-0.3g	1-2	770	375	12Φ10+2 Φ10 (1100)	3Φ14 (462)	750	750	8Φ12 (905)	8Φ12 (905)
	Roof	729	377	12Φ10+2 Φ10 (1100)	3Φ14 (462)	911	750	8Φ14 (1232)	8Φ12 (905)
2/ EC2-0.05g and 0.15g	1	1060	446	12Φ10+2 Φ10 (1100)	3Φ14 (462)	739	2089	8Φ12 (905)	8Φ22 (3041)
	2	1060	446	12Φ10+2 Φ10 (1100)	3Φ14 (462)	368	1579	8Φ8 (402)	8Φ16 (1609)
	3	1060	446	12Φ10+2 Φ10 (1100)	3Φ14 (462)	368	462	8Φ8 (402)	8Φ10 (628)
	4-5	1060	446	12Φ10+2 Φ10 (1100)	3Φ14 (462)	368	368	8Φ8 (402)	8Φ8 (402)
	Roof	633	430	12Φ10+2 Φ10 (1100)	3Φ14 (462)	1062	368	8Φ14 (1232)	8Φ8 (402)
2- EC2-0.3g	1-5	889	365	12Φ10+2 Φ10 (1100)	3Φ14 (462)	1080	1080	12Φ12 (1357)	12Φ12 (1357)
	Roof	688	348	12Φ10+2 Φ10 (1100)	3Φ14 (462)	1080	1080	12Φ12 (1357)	12Φ12 (1357)
3- EC2-0.05g-0.15g and 0.3g	1-4	1030	333	12Φ10+2 Φ10 (1100)	3Φ14 (462)	1080	1080	12Φ12 (1357)	12Φ12 (1357)
	5-7	1030	333	12Φ10+2 Φ10 (1100)	3Φ14 (462)	750	750	12Φ10 (943)	12Φ10 (943)
	Roof	574	328	12Φ10+2 Φ10 (1100)	3Φ14 (462)	750	750	12Φ10 (943)	12Φ10 (943)

Table 6-44 – Reinforcement Area from the analyses and chosen steel configurations of the frames in the EC2-group (continued)

Confi. /Case	Sto.	Beams (mm^2)				Column (mm^2)			
		From analysis		Chosen		From analysis		Chosen	
		Top	Bottom	Top	Bottom	Exterior	Interior	Exterior	Interior
4-EC2-0.05g	1-5	987	360	12Φ10+2Φ10 (1100)	3Φ14 (462)	1080	1080	12Φ12 (1357)	12Φ12 (1357)
	6-9	987	360	12Φ10+2Φ10 (1100)	3Φ14 (462)	750	750	12Φ10 (943)	12Φ10 (943)
	Roof	647	323	12Φ10+2Φ10 (1100)	3Φ14 (462)	750	750	12Φ10 (943)	12Φ10 (943)
4-EC2-0.15g	1-5	987	360	12Φ10+2Φ10 (1100)	3Φ14 (462)	1080	1080	12Φ12 (1357)	12Φ12 (1357)
	6-9	987	360	12Φ10+2Φ10 (1100)	3Φ14 (462)	750	750	12Φ10 (943)	12Φ10 (943)
	Roof	647	323	12Φ10+2Φ10 (1100)	3Φ14 (462)	750	750	12Φ10 (943)	12Φ10 (943)
4-EC2-0.3g	1-5	1080	365	12Φ10+2Φ10 (1100)	3Φ14 (462)	1080	1080	20Φ12 (2262)	20Φ12 (2262)
	6-9	1080	365	12Φ10+2Φ10 (1100)	3Φ14 (462)	750	750	20Φ10 (1571)	20Φ10 (1571)
	Roof	647	323	12Φ10+2Φ10 (1100)	3Φ14 (462)	750	750	20Φ10 (1571)	20Φ10 (1571)

6.4.4.3. Transversal reinforcement Configuration and Limitations of the studied RC-MRFs

It has been recognized for a long time that transverse reinforcement plays a very important role on the behaviour of a beam-column element. Especially in reinforced concrete beams or columns, the configurations of transverse reinforcement has significant influence on mechanical properties of the concrete, on the development of the crack of the elements, on the strain of the steel, on the moment-curvature relationship, and therefore on the ductility of the sections and the overall element.

If a RC-MRF structure is designed in accordance with a seismic modern code, the stirrups of structural components have to be designed with the strict application of Capacity Design rules. This will ascertain that brittle failure due to shear will never occur or never occur before the failure due to flexural bending. To succeed that, the shear force, used for designing stirrup, is usually determined based the moment resistance at two ends of the components. However, for the RC-MRFs designed in accordance with EC2, the transverse reinforcements are not designed following 'Capacity Design' rules. The design shear force is determined based on the analysis under gravity and lateral forces such as wind.

Under the ordinary condition (for instance under serviceability load) the structure will work in elastic range. If the structure is subjected to an earthquake, it may be loaded into inelastic range. The failure of that structure under this condition will significantly depend on the failure of component due to shear or due to bending. The failure due to shear usually leads to brittle collapse of the structural components. Thus it should be avoided.

Stirrups of beams and columns have diameter of 10mm and 2 to 6 legs, depending on the configurations of the longitudinal reinforcements. Table 6-45 shows the maximum shear forces that can be generated during a seismic excitation and shear resistance of some typical elements. Observing from Table 6-45, it

can be seen that shear resistance of beams and columns in all studied frames is much larger than the values possibly occurring during the earthquake. This ensures that failure should not take place in beam due to shear. But the beam column node is another weak point, for which no stirrup is present. This negative effect is assessed in Chapter 7.

Table 6-45 – Maximum shear forces generated during earthquake and shear resistance of beams and columns (kN)

Configuration/ Case	Beams				Columns	
	From Gravity	From seismic	Sum	Resistance	From seismic	Resistance
	$V_{(g+\psi 2q)}$	$\gamma_{Rd} \sum M_{i,d} / l_{cl}$	$V_{Ed,max,i}$	max ($V_{Rd,s}$; $V_{Rd,max}$)	$\gamma_{Rd} \sum M_{i,d} / l_{cl}$	max ($V_{Rd,s}$; $V_{Rd,max}$)
1/EC2-0.05g	50	44.0	94.0	191.0	69.7	381.0
1/EC2-0.15g	50	46.4	96.4	191.0	69.7	381.0
1/EC2-0.3g	51	46.4	97.4	191.0	148.6	381.0
2/EC2-0.05g	50	46.4	96.4	191.0	153.7	381.0
2/EC2-0.15g	50	46.4	96.4	191.0	153.7	381.0
2/EC2-0.3g	50	50.4	100.4	191.0	319.7	661.0
3/EC2-0.05g	50	54.2	104.2	221.8	380.5	661.0
3/EC2-0.15g	50	54.2	104.2	221.8	380.5	661.0
3/EC2-0.3g	50	54.2	104.2	221.8	380.5	661.0
4/EC2-0.15g	50	54.2	104.2	221.8	434.5	661.0
4/EC2-0.15g	50	54.2	104.2	221.8	434.5	661.0
4/EC2-0.3g	50	54.2	104.2	221.8	434.5	1196.0

6.5. Summary

A set of thirty two RC-MRFs has been designed in accordance with two codes EC2 and EC8. They are divided into two groups, EC2 and EC2+EC8 groups, depending on the code considered in the design. These two groups consist of 4 configurations with different geometrical dimensions, representing the main structural resisting components for the buildings. The buildings in each configuration have similar dimensions in plan and elevation. They are located in three zones with soil C (defined by EC8), having the PGAs of 0.05g, 0.15g and 0.3g. The RC-MRFs in the same configuration and seismicity zone have similar cross-sectional dimensions of the concrete. In the zone having PGA of 0.15g, three frames have been considered: one designed without taking into account seismic actions and the other two designed with seismic actions accounted for with two different Ductility Classes: Medium and Low. In the remaining zone, two frames have been designed corresponding to (1) one followed by EC2 and (2) one followed by EC8 with Medium Ductility Class. The cross-sectional dimensions of frames studied have been selected as small as possible; therefore they are chosen based on the damage limitations from EC8. This permits observing the influence of ductility class on the steel contents of beams and columns and reducing the overstrength of the frames in order to assess the effectiveness of the EMP in retrofitting existing frames in the next steps of the present study. Comparing the resulting frames between two groups and within the group, obtained from the design, some concluding remarks have been drawn:

- The cross-sectional dimensions of frame components have significant effects on their steel content. This is not only because of changed internal forces due to the changes of cross-sectional dimensions, but also because minimum steel contents required by the codes for the frames belonging to the EC8-group, lead to changes of the overall stiffness and strength of the frames.

- The steel contents of columns in EC2-group are dependent on the design moment only. In the EC8-group, the steel in columns is influenced by the Capacity Design rules 'strong columns – weak beams'. For the low-rise buildings in EC2-group, the steels of columns are usually governed by gravity loads and lateral forces (wind); however, for the medium and high-rise frames, due to much larger cross-sectional dimensions, the steel contents of the columns are usually obtained from minimum imposed by the codes.
- In general, the steel contents of beams of the frames in the EC2-group are less than that of the frames in EC8-group. This is because the frames designed to EC8 must meet the requirements from EC2 as well.
- For the frames in EC8-group, different Ductility Class results in some changes of steel contents of beams and columns. Observing the results of reinforcements from analysis, it is clear that an increase of the Ductility Class usually shifts the steel contents from beams to columns. This will ascertain the increase of ductility of the structures, forming plastic hinges sooner in beams and also leading to higher behaviour factor.
- Finally, the slab has played a very significant role on both cross-sectional dimensions and steel contents of the components of the RC-MRFs. This is reflected through the effective width and reinforcements within this width of the slab contributing to both the stiffness and bending resistance of the beams.

7. SEISMIC EVALUATION OF EXISTING RC-MRFs

7.1. Introduction

In order to seismically retrofit an existing building, as introduced in Chapter 2, one of prime concern is to determine the deficiencies of that building. The knowledge of the deficiencies will help engineers suitably select the corresponding retrofit strategy and retrofitting system. In order to find the deficiencies of the existing structure, besides collecting data on site such as testing material properties, checking the dimensions of the components…, it is necessary to know the performance of the structure under design and severe earthquakes. This can only be done by doing the experiments and/or performing analysis on models of the structure.

EC8 provides six methods for determining the seismic performance of an existing structure, including linear elastic ones (lateral force, modal and static dynamic analyses) and nonlinear ones (nonlinear static, q-factor, nonlinear dynamic analyses). There are some refinements, which have been developing recently such as incremental nonlinear dynamic and pushover adaptive analyses. If the structure performs elastically, the results from nonlinear and linear analyses will be nearly the same. If the structure performs beyond elastic range, which is likely under severe earthquakes, the results from linear methods are no longer satisfactory. Therefore, in the present study, as mentioned in the Chapter 6, the linear methods have been used to design the RC-MRFs and nonlinear ones will be next used in evaluating the capacity of the designed frames. More particularly, in order to evaluate the capacity of the designed frames, nonlinear static analysis (also well known as Pushover analysis) is first performed and then fully nonlinear dynamic analysis is carried out to check the results obtained by Pushover analysis.

In this chapter, steps, general models and methods for evaluating the seismic performance of the RC-MRFs are going to be first introduced. Then, the detailed description of selected ones, used to seismically assess the existing RC-MRFs designed in the previous chapter, is discussed. The deficiencies, shortcomings and detailed seismic behaviour of the existing structures studied are also presented.

7.2. Steps for seismic evaluation of the existing RC-MRFs

Figure 7-1 shows five steps for seismic evaluation of the existing RC-MRFs. The first step is about collecting the data for evaluation process, including determining the geometrical configurations, properties of material on site and at laboratory… Steps 2 to 4 are related to the analysis of the sections and the overall behaviour of the frames. Each part in these steps is discussed in the following sections. The final step is to assess the seismic performance of the existing frames. Generally, the behaviour of the structures will be compared with criteria from codes or official documents and its failure will be assessed, based on various criteria: local failure, global failure. Deficiencies and shortcomings of the structures will be concluded in this step.

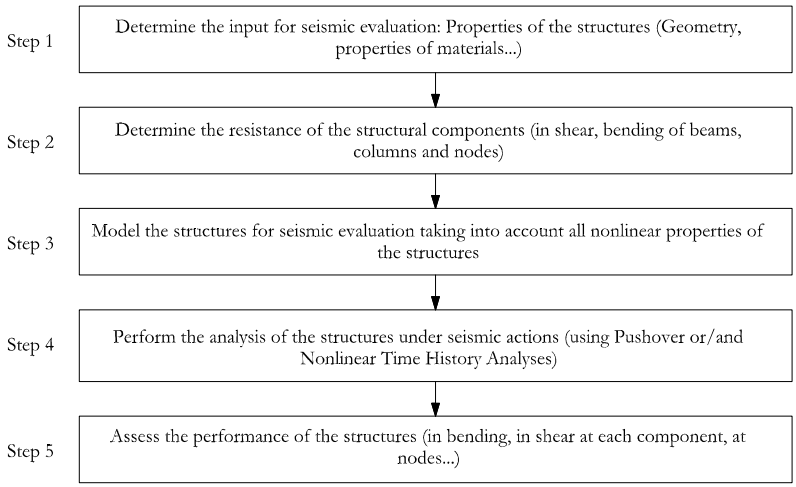

Figure 7-1 – Steps for seismic evaluation of the existing RC-MRFs

7.3. General models of RC-MRFs for seismic evaluation

7.3.1. Introduction

When a RC-MRF is subjected to severe seismic excitations, the behaviour of members in particular and of the structure in general, especially in the lower part of the building, is controlled by lateral displacements. Since it is not economically feasible to design the RC-MRF to remain elastic during severe earthquake ground motions, the frames are likely to exceed the yield moment of the cross-section in critical regions of the structure and lead to inelastic deformations. In lower stories, critical regions are usually located at the ends of girders and columns and at beam-column joints. In upper stories inelastic deformations can also take place in some more regions such as near the mid-span of the girders. Critical regions can be classified according to the actions governing their behaviour. Since the seismic response of the entire structure depends on the hysteretic behaviour of these regions, accurate models of such behaviour need to be characterized. Idealising these models should be based on an accurate representation of the material behaviour of reinforcing steel and concrete and take into account the controlling states of stress and strain in order to identify the main parameters influencing the hysteretic behaviour of each critical region. In addition, the problems arising from the transfer of stresses between reinforcing steel and surrounding concrete under cyclic load reversals also need to be addressed.

When modelling the structure in nonlinear range, a balance between precision, complexity of the modelling and running time spent in the analysis should be considered. Moreover, it should stress that the final goal is to retrofit the RC-MRFs in accordance with EC8, thus the modelling should always remain congruent with that code. Due to the fact that the present study is limited to planar moment resisting frames, the following fundamental elements are needed for determining the nonlinear responses of such structures subjected to cyclic deformation reversals: a girder element, a column element, a beam-column joint and a foundation element. The girder element should also include the effect of the slab, making it become T- or L-beam elements. Shear wall or infill panel elements are not dealt with in this study because all attention is focused on the behaviour of moment frames. It is assumed that floor diaphragms are infinitely rigid so that a single degree of freedom represents the lateral displacements of an entire story.

Since the beam-column joint element proposed in this study describes deformations arising at the beam-column interface and its stiffness is assumed to be infinitely compared with other parts framing to it, therefore, in this case the RC-MRFs consists of only three types of elements: (a) a beam element, (b) a column element and (c) a foundation element. This subdivision implies that the beam-column joint panel zone remains rigid. The frame is assumed to be fixed at base with very rigid foundation. This means that foundation is considered to move exactly the same as the movement of the ground when earthquake happens. Thus, it is precluded in the modelling of the studied frames. The modelling of beams and columns are presented in detail hereafter.

7.3.2. Modelling of beams and columns

When subjected to severe earthquake excitations, inelastic deformations of a RC-MRF are expected to take place at the ends or at mid-span of beams or columns, as clearly observed in both tests and real performance during and after the earthquakes. The behaviour of those critical regions in girders is governed by flexure, shear and the transfer of stresses between reinforcing steel and concrete. On the other hand, axial forces play a crucial role on the seismic performance of the columns. When these regions are subjected to cyclic deformation reversals, considerable stiffness deterioration is always observed. This is due to several factors and the most important of which are:

(1) concrete cracking and splitting along reinforcing bars;

(2) cyclic deterioration of bond between reinforcing steel and surrounding concrete;

(3) shear sliding in regions with cracks running through the entire depth of the member;

(4) crushing and spall of concrete;

(5) Bauschinger effect of reinforcing steel;

These factors are also the reasons inducing the stiffness deterioration observed in interior and exterior beam-column joints. In this case, the hysteretic behaviour is governed by the large change in bending moments from one face of the joint to the other which causes a combination of high shear and bond stresses. Large bending moments at the girder ends induce yielding of the reinforcement, which, combined with the diagonal cracks induced by shear, leads to slippage of reinforcing bars in the joint. This manifests itself as bar pull-out at the beam-column interface and results in concentrated rotations known as fixed-end rotations at the beam ends (Filip C.Filipou, 1998). Therefore, in order to represent as correctly as possible the different phenomena mentioned above, it is necessary to model precisely the hysteretic behaviour of critical regions in RC beams and columns. There are several possibilities to decompose a beam element into sub-elements, as shown in Figure 7-2:

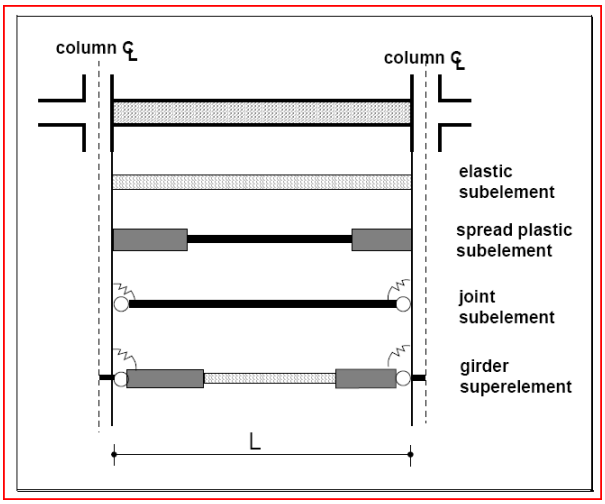

Figure 7-2 – Possibilities of decomposition of the beam to sub-elements

(1) an elastic beam sub-element representing the behaviour of the beam before yielding of the reinforcement

(2) a plastic beam sub-element with lumped plastic hinges or plastic zones at the ends representing the behaviour of the beam in the post-yielding range; the length of the plastic zones is called as critical regions and is a function of the loading history, dimensions of the element…;

(3) a joint sub-element accounting for the fixed-end rotations and the sliding due to shear at the beam-column interface.

Figure 7-2 also shows that the beam-column joint panel zone is considered as infinitely rigid. In addition, as also noted in Chapter 6, it is assumed in this study that shear deformations are neglected. Obviously, this is a limitation of the present work.

7.3.2.1. Linear elastic beam element

The linear elastic beam sub-element represents the behaviour of the girder before yielding of the reinforcement. Its length is equal to the clear span L of the girder. In addition, it is assumed to have the constant section stiffness EI along the span. This assumption is obviously an approximation. In general, reinforcement layout typically varies along the length of the girder with different amounts of reinforcement at the top and bottom of the cross section. When the negative bending moments act such that the top of the section is subjected to tension including the slab, the shape of compression zone is rectangular having a width equal to the width of the web. Part of the slab reinforcement contributes to the tensile force thus significantly increasing the yield strength of the section, but not affecting much the stiffness before yielding. When the bending moments act reversely such that the bottom of the section is subjected to tension, the compression zone is either rectangular or often T-shaped. Clearly the effective slab width in tension and compression needs to be determined because it may much contribute to the strength and stiffness of the girder element.

The elastic section stiffness EI, used in the current study, is assumed to be equal to the average of the positive (tension at the bottom) and negative (tension at the top) section stiffness at the two girder ends.

The elastic section stiffness is determined as the secant stiffness of the moment curvature relation at yielding of the tension reinforcement. In EC8 the secant stiffness is assumed to be equal to one half of the un-cracked gross section stiffness.

The effect of slab has been included in determining the strength and stiffness of the girder based on the effective width specified in EC8 and EC2. It should be noted that girders spanning between interior columns typically have a symmetric arrangement of reinforcement with respect to the girder mid-span. By contrast, exterior girders are likely to have different amounts of reinforcement at each end. In the latter case the average stiffness is determined from the positive and negative section stiffness at each end. The approximation of the constant average section stiffness is certainly unsatisfactory, if it is desired to study the response of the structure under service loads. However, in evaluating process, attention is focused on predicting the behaviour of the structure under large deformation reversals. Such response is not much affected by the stiffness of the structure before yielding.

7.3.2.2. Inelastic beam element

The inelastic beam sub-element accounts for the inelastic deformations of the girder after yielding of the reinforcement. There are three general ways of modelling this sub-element, which are also relevant to EC8:

(a) In the first model, all inelastic deformations are assumed to be concentrated in a hinge of zero length located at each end of the girder. The two hinges are connected by an elastic bar to form the concentrated plastic beam sub-element.

(b) The second model accounts for the gradual spread of inelastic deformations into the girder as a function of loading history. In this an inelastic zone of gradually increasing length is located at each end of the girder. The two inelastic zones are connected by an elastic bar to form the inelastic beam sub-element.

(c) The third model is based on distributed inelasticity and fibre modelling approach. The beam-column element is divided into several sections based on the Navier-Bernoulli beam element.

Bond and shear effect are neglected in the present study. The first and the third one are adopted for modelling flexural behaviour of the beam element in the current study. They are discussed in more detail hereafter.

Concentrated plastic beam element

In the concentrated plastic sub-element, the inelastic deformations taking place at the girder ends after yielding of the reinforcement are represented by a rigid-plastic, as in Figure 7-20, or bilinear-plastic hinge, as in Figure 7-19. The hinge, which is depicted as a nonlinear spring in Figure 7-3, is only activated when the moments at the girder ends first exceed yielding. Since all inelastic deformations are lumped at the plastic hinges at the two ends of the girder, the remaining part of the concentrated plastic sub-element used to connect the two hinges is the linear elastic one.

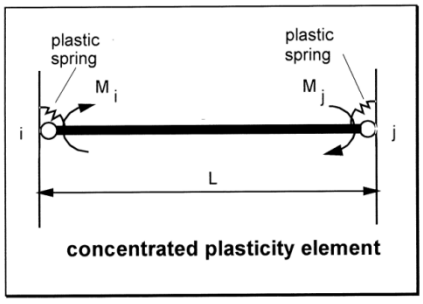

Figure 7-3 – Concentrated plasticity beam sub-elements

With this model, it is necessary to introduce the parameters for the hinges of such an element, saying capacity of the beams or columns. To do that there needs to evaluate the moment-curvature or moment-rotation relationships of the plastic hinge at the critical regions. The ultimate capacity of plastic hinges (yield and ultimate strength and deformations) is then given in the model to determine its seismic

performance. This requires analysing the cross-sectional behaviour of the beam or column taking into account the ultimate strengths and deformations of the concrete and reinforcement.

Hysteresis laws of critical regions in flexure of RC members for nonlinear dynamic analysis:

- **Bilinear Model**

Elastic-perfectly plastic hysteretic models have been used by many researchers due to its simplicity. The first application of this model was by Veletsos and Newmark (1960) when determining the maximum displacement of an elasto-plastic simple system, in which the initial period was practically the same as that of an elastic system and longer than 0.5s (Otani, 1979).

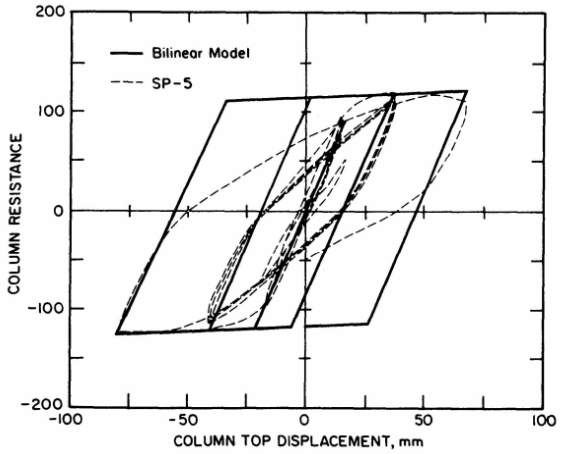

Figure 7-4 – Bilinear hysteresis model

In this model, a finite positive slope was assigned to the post yield stiffness to account for the strain-hardening characteristic, called a bilinear model. The bilinear model does not represent the degradation of loading and unloading stiffness with increasing displacement amplitude reversals (Figure 7-4) and the model is not suited for a refined nonlinear analysis of a reinforced concrete structure.

- **Clough 's Degrading Stiffness Model**

An effective model for the reinforced concrete members was first introduced by Clough (Otani, 1980), who introduced the stiffness degradation in the elasto-plastic model, saying the response point during unloading or re-loading moved toward the previous maximum response point of the previous cycles. The unloading slope remained parallel to the initial elastic slope. This change was able to simulate the flexural behaviour of the reinforced concrete members.

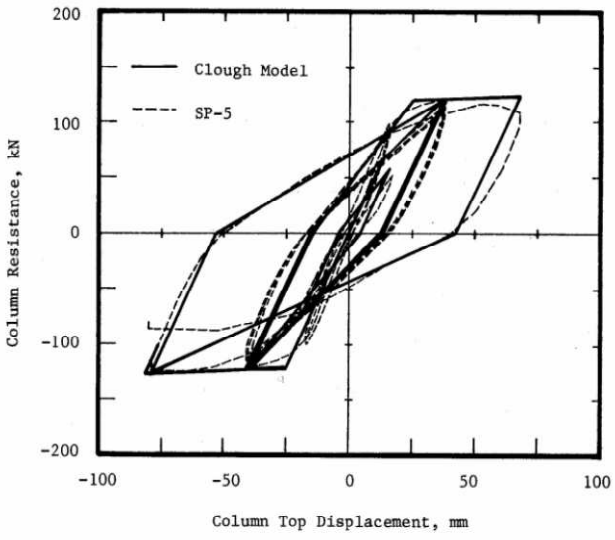

Figure 7-5 – Clough's degrading stiffness model

- **Takeda's Degrading Stiffness Model**

Based on the experimental observations, a more refined and sophisticated hysteresis model was developed by Takeda et al. (l970). This model included stiffness changes at flexural cracking and yielding and also strain-hardening characteristics. The unloading stiffness was reduced by an exponential function of the previous maximum deformation. Takeda et al. also prepared a set of rules for load reversals within the outermost hysteresis loop. These are major improvements over the Clough (1966) model. Failure or extensive damage caused by shear or bond deterioration was not considered in the model. The Takeda model, similar to the Clough model, simulates dominantly flexural behaviour (Figure 7-6). Simplified Takeda hysteresis models were proposed by Otani and Sozen (1972) and by Powell (1975), using a bilinear backbone curve.

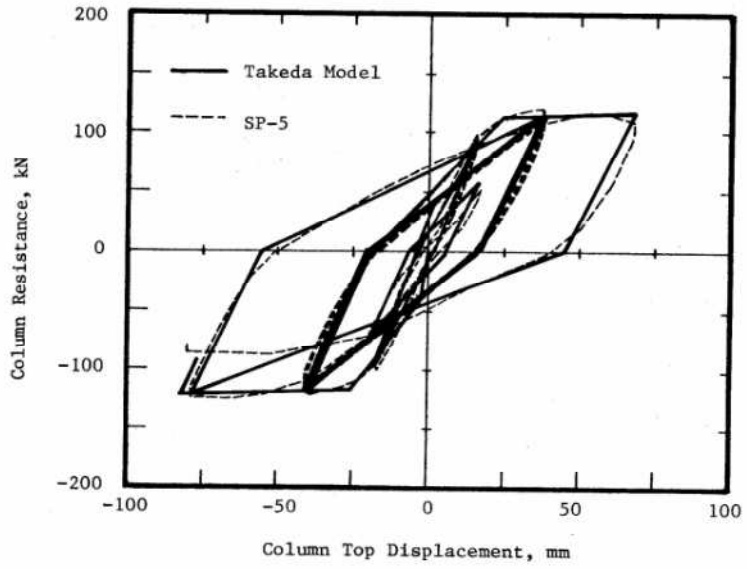

Figure 7-6 – Takeda's degrading stiffness models

When compared with the elasto-plastic model, less energy is absorbed per cycle beyond yielding by Clough's degrading model. Resulting from the response analysis of a series of single-degree-of-freedom systems, Clough, 1966 concluded that the degrading stiffness model did not cause any significant change in the ductility demand of long-period structures (period longer than 0.6s) compared with the elasto-plastic model; on the other hand, the degrading stiffness model required significantly larger ductility from short-period structures than the corresponding elasto-plastic systems and the response waveform of a degrading stiffness model was distinctly different from that of an ordinary elasto-plastic model. The model is relatively simple, and has been used extensively in nonlinear analysis with the inclusion of strain-hardening characteristics (Figure 7-5).

- **Takeda-Takayanagi Models**

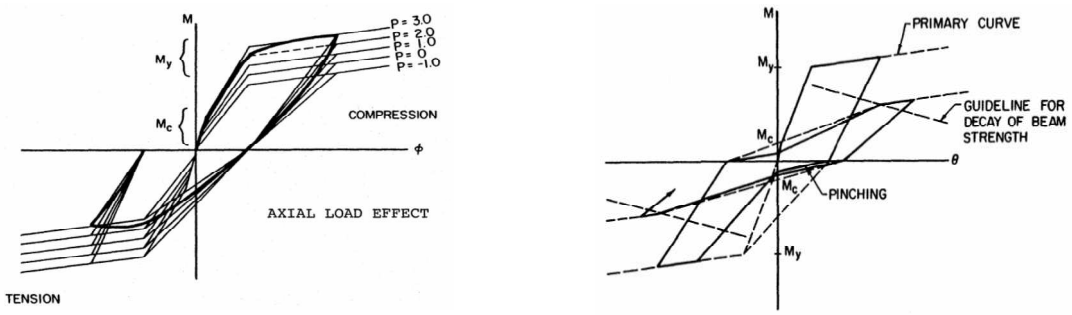

(a) axial force variation (b) pinching and strength decay

Figure 7-7 – Takeda-Takayanagi models (Takayanagi and Schnobrich, 1976):

Takayanagi and Schnobrich (1976) incorporated the effect of axial force variation in the Takeda model by preparing various backbone curves at different axial load levels (Figure 7-7a).

A pinching action and strength decay are inevitable in a short and deep member due to pullout of the reinforcement and deterioration in shear resistance. Takayanagi and Schnobrich introduced a pinching action and strength decay in the Takeda model (Figure 7-7b). Whenever a response point was located in the positive rotation-negative moment range or the negative rotation-positive moment range, the pinching was introduced. After the moment exceeded the yield level, the strength degradation was included.

- **Degrading Tri-linear Hysteresis Model**

A model simulating dominantly flexural stiffness characteristics was developed in Japan by Fukada in 1969 (Otani, 1980). The backbone curve is a tri-linear shape with stiffness changes at cracking and yielding. Up to yielding, the model behaves in the same way as the bilinear model. Once deformation exceeds the yield point, the model behaves as a perfectly plastic system. Upon unloading, the unloading point is treated as a new "yield" point, and unloading stiffness corresponding to pre- and post cracking are reduced proportionately so that the behaviour becomes of the bilinear type in a range between the positive and the negative yield points (Figure 7-8).

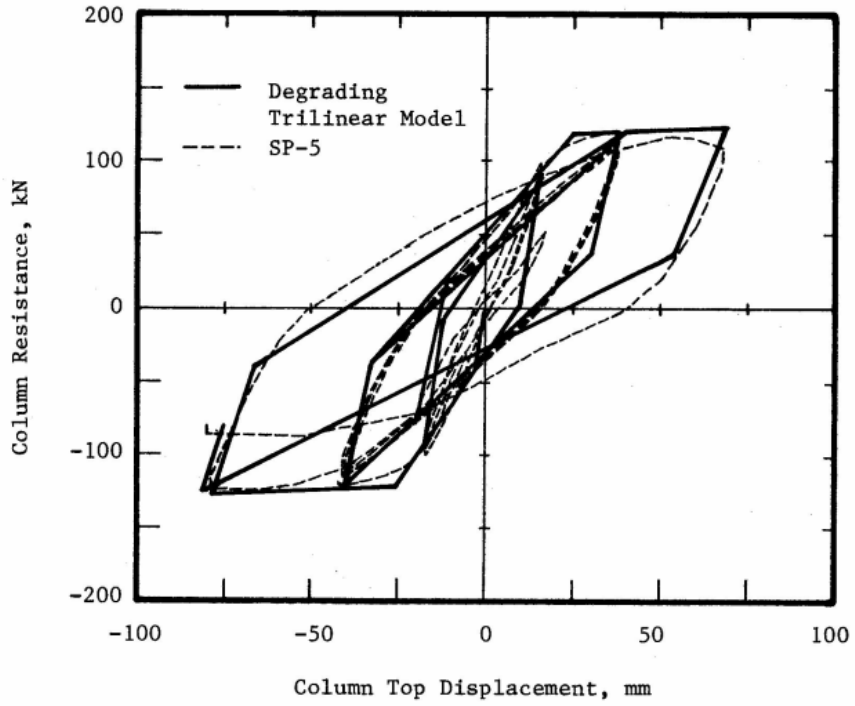

Figure 7-8 – Degrading tri-linear model

Strain-hardening characteristics can be easily included in the degrading tri-linear model. The hysteresis energy dissipation per cycle beyond the initial yielding is proportional to the displacement, and the equivalent viscous damping factor becomes constant. The fatness of a hysteresis loop is sensitive to the choice of a cracking point.

- **Pivot hysteresis model (Dowell et al, 1998)**

This model is first introduced by Dowell et al (1998). It is somewhat similar to Takeda model but has some additional parameters to control degrading hysteresis loop (Figure 7-9). This model is governed by three simple rules and has the ability to capture the dominant nonlinear characteristics of reinforced concrete elements under cyclic load. The backbone curve used for positive and negative loading is shown in Figure 7-9. The first and second branches of the strength envelope represent cracked-section stiffness and strain hardening stiffness, respectively. Strength degradation from shear failure or confinement failure is also represented by the third branch. The final branch allows for a linearly decreasing residual strength. Primary pivot points P_1 through P_4 control the amount of softening expected with increasing displacement, using parameters α_1, α_2 as shown in Figure 7-9. Pinching pivot points PP_2 and PP_4 fix the

degree of pinching following a load reversal, through parameters β_1^*,β_2^*. The response follows the strength envelope as long as no displacement reversal occurs. Once the yield displacement is exceeded in either direction, a modified strength envelope is defined by the lines joining PP_4 to S_1 and PP_2 to S_2, as illustrated in Figure 7-9. The pinching pivot points start moving toward the origin of the force-deformation relation, once strength degradation occurs. The pinching parameters, β_1^*,β_2^*, are given by the following equations:

$$\beta_u^* = \beta_i ; d_{i\max} \le d_{t_i} \qquad \text{Equation 7-1}$$

$$\beta_u^* = \frac{F_{i\max}}{F_{t_i}} \beta_i ; d_{i\max} > d_{t_i} \qquad \text{Equation 7-2}$$

Where β_1 and β_2 define the degree of pinching for a ductile flexural response before strength degradation occurs. Displacements d_{imax} and d_{ti} represent the maximum displacement and strength degradation displacement, respectively, in the ith direction of loading. F_{imax} and F_{ti} represent the force levels corresponding to d_{imax} and d_{ti}. The primary advantage of the pivot hysteresis model when compared to the other models is its ability to represent effects of cyclic axial load due to frame action, unsymmetrical sections, and strength degradation. Cyclic actual load effects are achieved with predefined parameters, and the more general variation in axial load due to vertical accelerations is not included. Unlike other models, the pivot model recognizes that yielding in one direction does not soften the member in the opposite loading direction.

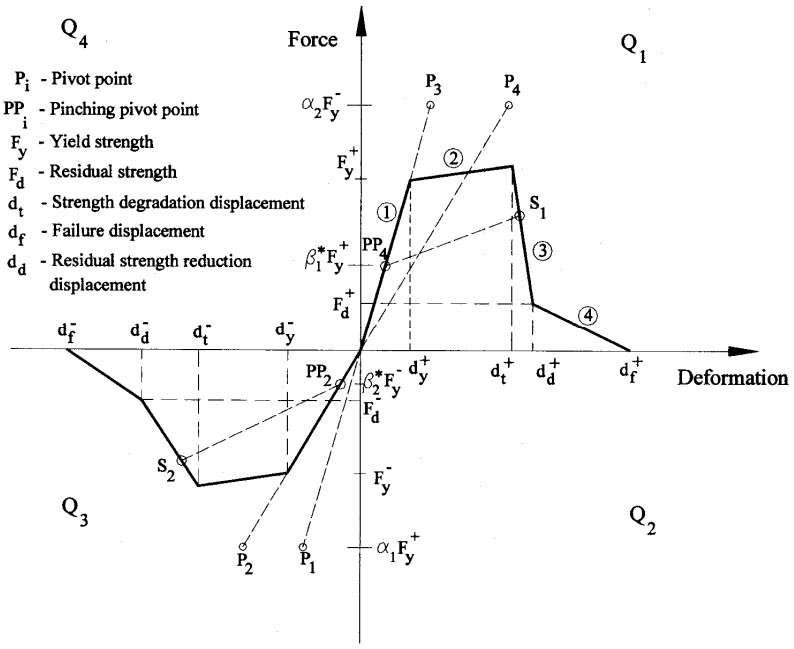

Figure 7-9 – Pivot hysteresis loops (Dowell et al, 1998)

Distributed plasticity and fibre modelling beam element

In this model, the so-called fibre approach is used to represent the cross-section behaviour, where each fibre is defined by a uniaxial stress-strain relationship. The beam-column element is divided into a number of segments, with each segment represented by fibre elements. Each of the fibre elements is constituted by areas of concrete (confined and unconfined) and areas of longitudinal bars, as presented in Figure 7-11.

They are given appropriate material properties to model reverse loading (i.e. arbitrary tension/compression histories). Generally, laws of materials of the sections are defined separately for unconfined cover concrete, confined core concrete and reinforcement. The sectional stress-strain state of beam elements is then obtained through the integration of the nonlinear uniaxial stress-strain response of the individual fibres (typically 300-400 fibres) in which the section has been subdivided as in Figure 7-10 and based on Navier-Bernoulli approximation that the sections remain plane after being deformed. Material stress is assumed constant between integration points along the fibre element.

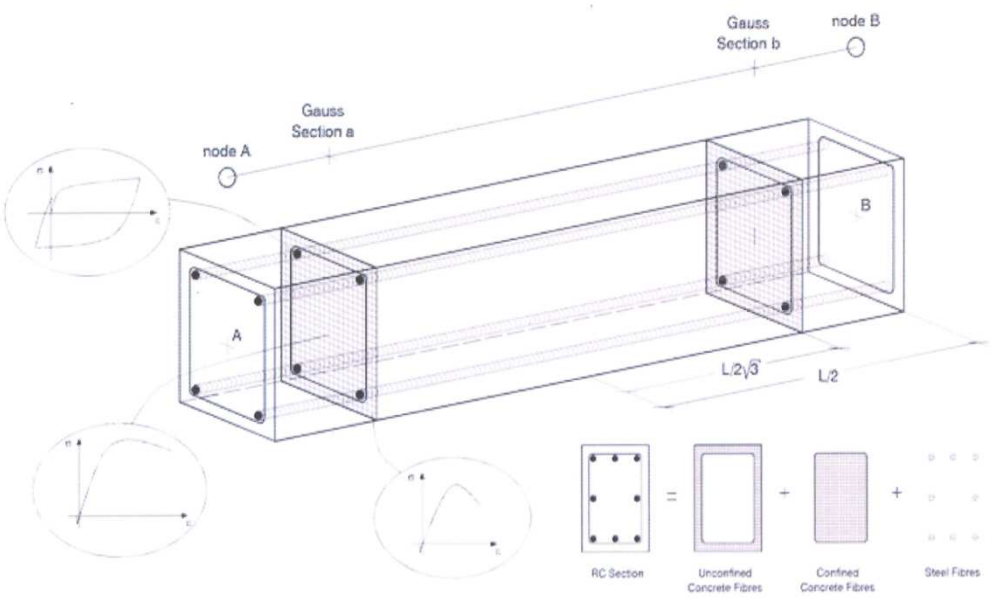

Figure 7-10 – Distributed inelasticity

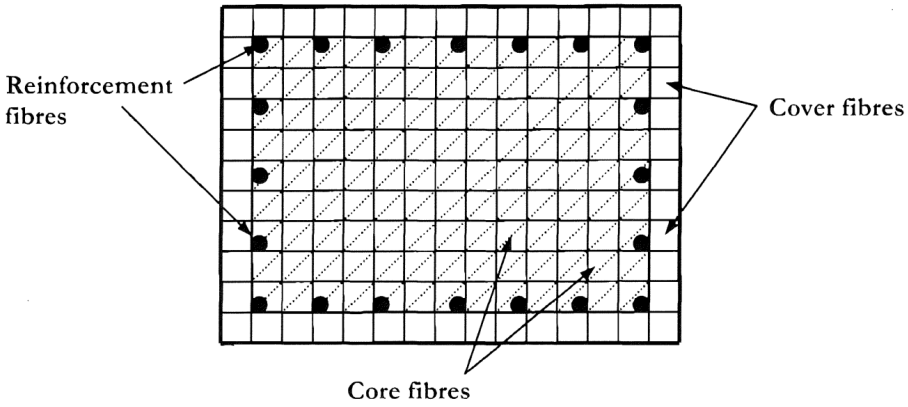

Figure 7-11 – Section Modelling with Fibres

Such models are quite different from the two mentioned above and the advantages of this are (SeismoStruct Manual, 2010 and Pinho, 2006):

- No requirement of a prior moment-curvature analysis of members as in lumped plastic hinge;
- No need to introduce any element hysteretic response (since it is implicitly defined by the material constitutive models);
- The influence of varying axial force on strength and stiffness is modelled directly;
- Straightforward representation of biaxial loading, and interaction between flexural strength in orthogonal directions.
- Member post-peak strength reduction resulting from the softening or failure of the materials can be directly calculated.

However, there are also some draw-backs when using fibre-elements to model beam-column elements, that is:

- Fibre elements are able to model only flexural behaviour of the beams and columns. Shear strength and shear deformation are generally out of ability.
- Shear deformations at anywhere in the structure must be modelled by special non-fibre elements

- Because of the very large number of fibre elements need to completely model a complex structure, computer time for such a complicated analysis like the nonlinear dynamic one can be very large. This is not suited for practical design in the office if 3-D response of the structure is needed.

It is clear that all disadvantages of the fibre element approach are related to the shear deformations of the beams and column, which are out of scope in the present study. Therefore, it is acceptable to adopt this fibre-element in modelling RC-MRF in the nonlinear range.

The adopted stiffness-based element cubic formulation then allows both the representation of the spread of inelasticity along the member length as well as the implicit incorporation of interaction between axial force and transverse deformation of the element. The use of a sufficient number of elements per structural member permits the reproduction of plastic hinge (in their full length), typical of members subjected to high levels of material inelasticity. The spread of inelasticity across the section and along the member length is thus achieved without requiring expertise calibration of any lumped plasticity element.

7.3.3. Damping

Sources of damping mechanisms in structural systems include viscous, hysteretic and friction damping. The latter has very less influence on the response of the structure, thus it is neglected in the present study. The other two are discussed in more detail hereafter.

If the response of the structure is entirely elastic, all codes require that nonlinear and linear dynamic analysis should give the same results. For a SDOF, linear dynamic analysis produces the same peak response as given by the elastic response spectrum, associated in EC8 with viscous damping ratio 5% of critical. Therefore, for obtaining the consistency between methods, nonlinear dynamic analysis should have a built-in 5% viscous damping ratio associated with elastic response. It should be recalled that in a design context the upper limit of the elastic regime is defined by yielding of members. So, the 5% viscous damping ratio is considered to encompass all sources of damping up to member yielding, including any structural damping of hysteretic nature, e.g., due to cracking of concrete members and energy dissipation during pre-yield cycles (Fardis, 2009). After member yielding, hysteretic damping is the criterion to represent the energy dissipation capacity of the structure and should be reflected just by the nonlinear force-deformation laws describing the post-yield behaviour of members in cyclic loading. There are possibilities to define the hysteretic damping for the structure. Having known that the forces due to viscous damping enter in the equations of motion as $C\dot{U}$, so for convenience of the numerical integration of the nonlinear equations of motion, the damping matrix, C, is typically taken to be of the Rayleigh type,

$$C = \alpha_0 M + \alpha_1 K \qquad \text{Equation 7-3}$$

Rayleigh damping gives a viscous damping ratio ζ at a circular frequency ω equal to:

$$\zeta = \frac{1}{2}\left(\frac{\alpha_0}{\omega} + \alpha_1 \omega\right) \qquad \text{Equation 7-4}$$

It means that the mass-proportional part damps out lower-frequency components and the stiffness-proportional part for high-frequency ones. To achieve values of the damping ratio as close as possible to the target value $\zeta = \zeta_0 = 0.05$ within the predominant frequency range of the response, it is possible to specify $\zeta = \zeta_0$ at two circular frequencies, ω_1 and ω_2. Thus, α_0 and α_1 can be obtained from:

$$\begin{Bmatrix} \alpha_0 \\ \alpha_1 \end{Bmatrix} = \frac{2\zeta}{\omega_1 + \omega_2} \begin{Bmatrix} \omega_1 \omega_2 \\ 1 \end{Bmatrix} \qquad \text{Equation 7-5}$$

For analysis under a single component of the seismic action, meaning only horizontal or vertical, a good choice for ω_1 and ω_2 is the circular frequency of the modes with the two highest modal base shears in the elastic structure (Fardis, 2009).

7.4. Seismic actions

According to EC8, there are several possibilities of evaluating earthquake input for different hazard levels used to seismically analyze the structure. For seismic designing purposes, zonation map-based procedures and site-specific studies are used to determine the seismic actions. The first one is usually adopted for defining the seismic actions for general structures. It is based on the use of the PGA maps to define the seismic input at one or different hazard levels under different site conditions. The results from these procedures are elastic response spectra or design spectra for a given zone corresponding to a PGA. This seismic input is also used for assessing the designed or existing structures by Pushover analysis. The response spectrum is introduced in Chapter 6.

Other alternative representations of the seismic action for evaluating or assessing the inelastic responses of the structure based on advanced analysis are natural records of earthquake known as recorded or simulated accelerograms and artificial accelerograms (Figure 7-12). The artificial accelerograms can be mathematically generated by random vibration theory. They are usually created so that it is possible to develop a signal with a response spectrum matching a target response spectrum with a predefined accuracy (e.g. 3-5% margin of error) (Fardis, 2009). The target response spectrum is often extracted from EC8 with a corresponding PGA. In an artificial accelerogram, both stationary and non-stationary random processes have been suggested like the recorded or simulated accelerograms.

EC8 requires that artificial accelerograms should be generated so as to match the elastic response spectrum given in the code for 5% viscous damping. Moreover, the duration of the accelerograms should be corresponding to the magnitude, frequency and some other seismological features in establishing the ground accelerations. A minimum number of three accelerograms should be generated with the stationary part possessing a minimum duration of 10 seconds.

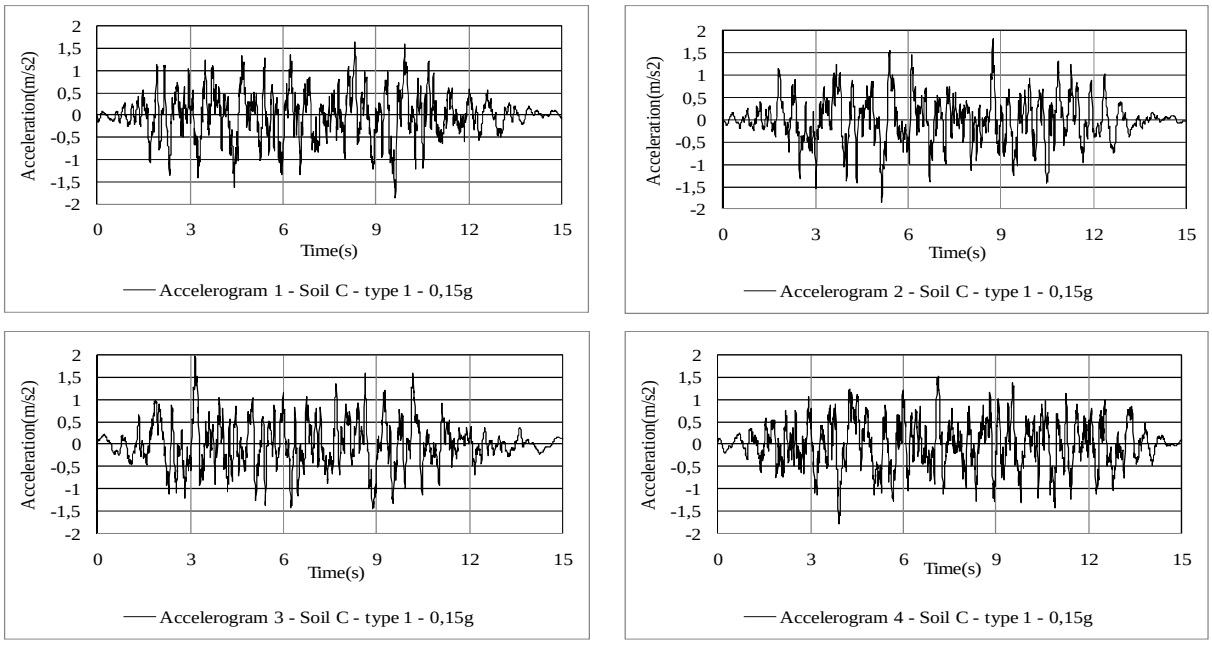

Figure 7-12 – Accelerograms for Nonlinear Dynamic Analyses

Figure 7-12 shows the example seismic excitations, used in the current study, which comprise a set of four artificial accelerograms, corresponding to PGA=0.15g, and obtained from basic normalised series of accelerations, generated by GOSCA, a software developed at University of Liege, under the following assumptions: Response spectrum consistent with the EC8 for soil profile C, earthquake type 1, PGA of 0.15g and damping ζ=5%; and total duration of 15 seconds (time step 0,007s).

Figure 7-13 shows the elastic response spectrum obtained from EC8 and generalized elastic response spectra obtained from three artificial accelerograms. SEISMOSIGNAL, a free soofware developed by SEISMO Group, was used to determine the elastic response spectra.

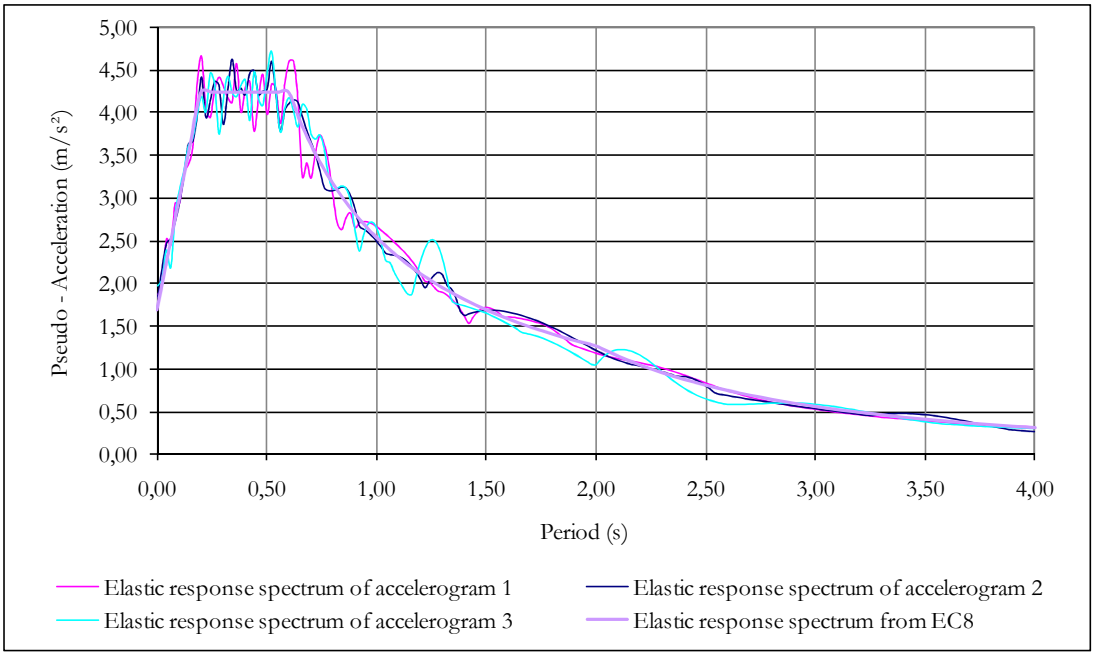

Figure 7-13 – Comparison of elastic response spectra from three accelerograms and EC8 of PGA of 0.15g soil C type 1 Earthquake

7.5. Nonlinear methods of seismic evaluation of RC-MRF

7.5.1. Nonlinear static ('Pushover') analysis

This method of analysis has been developing for several decades. It is completely not a fully dynamic method of analysis. As introduced in Chapter 2, there are several names concerning about this method, such as Capacity Spectrum Method used in ATC 40, or Pushover in EC8. Although the ways to implement the analysis with the use of this method are different, however the fundamental meaning is the same for all. Pushover analysis related to EC8 and EN 1998-3 is adopted and introduced in this study. According to EC8, nonlinear static or pushover analysis has two additional uses:

- To verify the value of the factor α_u/α_1 in cooperated in the basic value q_0 of the behaviour factor to take into account for the overstrength caused by the redundancy of the structure system, as explained in Figure 7-14.
- To design the buildings on basis of a nonlinear static analysis and deformation-based verification of its ductile members, instead of force-based design with linear static analysis and the design spectrum incorporating the behaviour factor q

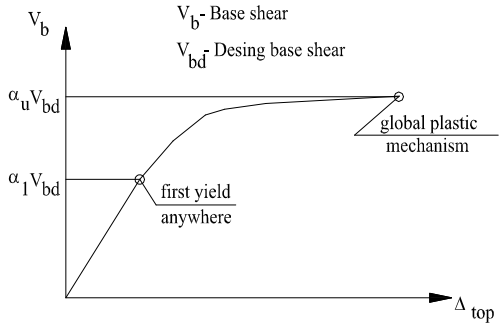

Figure 7-14 – Definition of factor α_u and α_1 on the basis of base shear versus top displacement diagram from pushover analysis

In general, pushover is nonlinear static approach carried out under constant gravity loads and monotonically increasing lateral forces which are applied at the location of the masses in the structural model to simulate the inertia forces generated by a single horizontal component of the seismic action.

Since the applied lateral forces are increased gradually, the method is able to describe the evolution of structural plastic mechanisms from the first yields to the global or local collapse and of stages of structural damage. This evolution is associated with magnitude of the imposed loads and with horizontal displacements. More simply, this method is a development or an extension of the lateral force method of linear analysis into the nonlinear domain.

General steps of seismically assessing the structure using Pushover analysis in correlation with N2 method, proposed by Faijar (2000), are summarised as follows:

STEP 1: DATA

A 3-D or 2-D model of the building structure is used. The floor diaphragms are assumed to be rigid in the horizontal plane. Generally, the number of degrees of freedom is three times the number of storeys N, representing displacements at the storey levels in the horizontal directions x and y, and torsion rotations: $U^T = [U_x^T, U_y^T, U_z^T]$. In addition, the nonlinear force-deformation relationships (usually base shear vice visa top displacements) for structural elements under monotonic loading are also needed. Seismic demand is traditionally defined in the form of an elastic (pseudo)-acceleration spectrum S_{ae} ("pseudo" will be omitted in the following text), in which spectral accelerations are given as a function of the natural period of the structure T. In principle, any spectrum can be used. However, the most convenient is a spectrum of the Newmark-Hall type as defined in EC8. The specified damping coefficient is taken into account in the spectrum.

STEP 2: SEISMIC DEMAND IN AD FORMAT

Starting from the traditional acceleration spectrum (acceleration versus period), inelastic spectra in acceleration–displacement (AD) format will be determined. To convert from traditional elastic response spectrum to AD format for an elastic SDOF system, the following relation will be applied:

$$S_{de} = \frac{T^2}{4\pi^2} S_{ae}$$ Equation 7-6

where S_{ae} and S_{de} are the values in the elastic acceleration and displacement spectrum, respectively, corresponding to the period T and a fixed viscous damping ratio. For an inelastic SDOF system with a bilinear force – deformation relationship, the acceleration spectrum (S_a) and the displacement spectrum (S_d) can be determined as:

$$S_a = \frac{S_{ae}}{R_\mu}$$ Equation 7-7

$$S_d = \frac{\mu}{R_\mu} S_{de} = \frac{\mu}{R_\mu} \frac{T^2}{4\pi^2} S_{ae} = \frac{\mu}{R_\mu} \frac{T^2}{4\pi^2} S_a R_\mu = \mu \frac{T^2}{4\pi^2} S_a$$

Equation 7-8

where μ is the ductility factor defined as the ratio between the maximum displacement and the yield displacement, and R_μ is the reduction factor due to ductility, i.e., due to the hysteretic energy dissipation of ductile structures. Note that R_μ is not equivalent to the reduction factor R used in seismic codes. The code reduction factor R, which is in EC 8 called behaviour factor q, takes into account both energy dissipation and the so-called overstrength R_s. It can be defined as $R = R_\mu R_s$. Several proposals have been made for the reduction factor R_μ. In the N2 method, it is made use of a bilinear spectrum for the reduction factor R_μ

$$R_\mu = (\mu - 1)\frac{T}{T_C} + 1 \qquad T < T_C$$ Equation 7-9

$$R_\mu = \mu \qquad T \geq T_C$$ Equation 7-10

where T_C is the characteristic period of the ground motion. EC8 has defined T_C as the transition period where the constant acceleration segment of the response spectrum (the short-period range) passes to the constant velocity segment of the spectrum (the medium-period range). Equation 7-9 and Equation 7-10 suggest that, in the medium – and long-period ranges, the equal displacement rule applies, i.e., the displacement of the inelastic system is equal to the displacement of the corresponding elastic system with the same period. Starting from the elastic design spectrum, and using Equation 7-6 to Equation 7-10, the demand spectra for the constant ductility factors μ in AD format can be obtained. They represent the inelastic demand spectra.

STEP 3: PUSHOVER ANALYSIS

Using a pushover analysis, a characteristic nonlinear force–displacement relationship of the MDOF system can be determined. Usually, base shear and roof (top) displacement are used as representative of force and displacement, respectively. The selection of an appropriate lateral load distribution is an important step within the pushover analysis. One practical possibility, as supposed by EC8, is to use two different displacement shapes (load patterns) and to envelope the results. Lateral loads are applied in mass centres of different stories. The vector of the lateral loads P, which generally consists of components in three directions (forces in the x and y direction and torsion moments), is determined as:

$$P = p\Psi = pM\Phi \qquad \text{Equation 7-11}$$

where M is the mass matrix. The magnitude of the lateral loads is controlled by p. The distribution of lateral loads Ψ is related to the assumed displacement shape, Φ. The procedure can start either by assuming displacement shape Φ and determining lateral load distribution Ψ according to Equation 7-11, or by assuming lateral load distribution Ψ and determining displacement shape Φ from Equation 7-11. Generally, Φ can consist of non-zero components in three directions (two horizontal directions and of torsional rotation). In such a case (coupled displacement shape) lateral loads also consist of components in three directions. The procedure can be substantially simplified if lateral loads are applied in one direction only. This is a special case that requires that also the assumed displacement shape has non-zero components in one direction only, e.g.

$$\Phi^T = [\Phi_x^T, 0^T, 0^T] \qquad \text{Equation 7-12}$$

This special case is used in the proposed extended version of the N2 method. From Equation 7-11 and Equation 7-12 it follows that the lateral force in the x-direction at the ith level is proportional to the component $\Phi_{x,i}$ of the assumed displacement shape Φ_x, weighted by the storey mass m_i

$$P_{x,i} = pm_i\Phi_{x,i} \qquad \text{Equation 7-13}$$

It is necessary to not that in the proposed method, lateral loading, determined according to Equation 7-11 and Equation 7-12, is applied independently in two horizontal directions, in each direction with + and – sign.

STEP 4: EQUIVALENT SDOF MODEL AND CAPACITY CURVE

In the N2 method, seismic demand is determined by using response spectra. Inelastic behaviour is taken into account explicitly. Consequently, the structure should be modelled as a SDOF system. Different procedures have been used to determine the characteristics of an equivalent SDOF system. In the N2 method, the starting point is the equation of motion of a 3D structural model (with 3N degrees of freedom) representing a multi-storey building (damping is not taken into account because it will be included in the spectrum)

$$M\ddot{U} + R = -Msa \qquad \text{Equation 7-14}$$

R is a vector representing internal forces, a is the ground acceleration as a function of time, and s is a vector defining the direction of ground motion. In the case of uni-directional ground motion, e.g. in the direction x, the vector s consists of one unit sub-vector and of two sub-vectors equal to 0.

$$s^T = [1^T, 0^T, 0^T] \qquad \text{Equation 7-15}$$

In the N2 method, ground motion is applied independently in two horizontal directions. Consequently, two separate analyses have to be performed with two different s vectors (vector Equation 7-15) and a similar vector that corresponds to the ground excitation in the y-direction). A derivation, presented in (Faijar, 2002) yields the following formulas. The displacement and force of the equivalent SDOF system D^* and F^* are defined as

$$D^* = \frac{D_t}{\Gamma}; F^* = \frac{V}{\Gamma}$$ Equation 7-16

where D_t is the top displacement of the MDOF system and

$$V = p\Phi^T Ms = pm^*$$ Equation 7-17

is the base shear of the MDOF model in the direction of ground motion. m* is the equivalent mass of the SDOF system

$$m^* = \Phi^T Ms$$ Equation 7-18

The constant controls the transformation from the MDOF to the SDOF model and vice–versa. It is defined as

$$\Gamma = \frac{\Phi^T Ms}{\Phi^T M \Phi} = \frac{m^*}{L^*}$$ Equation 7-19

Note that m* depends on the direction of ground motion. Consequently, D* and F* also depend on the direction of ground motion. In the case of ground motion in one (x) direction (Equation 7-15) and assuming a simple uncoupled displacement shape (Equation 7-12), the following equations apply

$$m^* = \sum m_i \Phi_{x,i}$$ Equation 7-20

$$V_x = \sum pm_i \Phi_{x,i} = \sum P_{x,i}$$ Equation 7-21

$$\Gamma = \frac{\sum m_i \Phi_{x,i}}{\sum m_i \Phi_{x,i}^2}$$ Equation 7-22

Equation 7-22 is the same equation as in the case of planar structures. As a result, the transformation from the MDOF to the SDOF system and vice versa is exactly the same as in the case of a planar structure. Γ is usually called the modal participation factor. Note that the assumed displacement shape Φ is normalized – the value at the top is equal to 1 and any reasonable shape can be used for Φ. As a special case, the elastic first mode shape can be assumed. The same constant Γ applies for the transformation of both displacements and forces (Equation 7-16). As a consequence, the force–displacement relationship determined for the MDOF system (the V–D_t diagram) applies also to the equivalent SDOF system (the F^*–D^* diagram), provided that both force and displacement are divided by Γ.

In order to determine a simplified (elastic–perfectly plastic) force–displacement relationship for the equivalent SDOF system, engineering judgement has to be used. In Annex B of EC8 the bilinear idealization is based on the equal energy principle. Note that the displacement demand depends on the equivalent stiffness which, in the case of the equal energy approach, depends on the target displacement. In principle, an iterative approach is needed, in which a target displacement is assumed, the bilinear idealization is made and the target displacement is determined. This value is then used then as the new approximation for target displacement. According to Eurocode 8, the displacement at the formation of plastic mechanism can be used as the initial approximation for target displacement. Iteration is allowed but not required. For the graphical procedure, used in the simple N2 method, it is convenient that the post-yield stiffness is assumed as being equal to zero. This option is used in EC8, also because it yields conservative results (larger target displacement than other idealizations). The elastic period of the idealized bilinear system T* can be determined as

$$T^* = 2\pi\sqrt{\frac{m^* D_y^*}{F_y^*}}$$ Equation 7-23

Where F_y^* and D_y^* are the yield strength and displacement, respectively. Note that, alternatively, first the bilinear idealization of the pushover curve can be made and then the transformation to the equivalent SDOF system can be added. The same equations apply. Finally, the capacity diagram in AD format is obtained by dividing the forces in the force–deformation (F^*-D^*) diagram by the equivalent mass m^*

$$S_a = \frac{F^*}{m^*}$$ Equation 7-24

The procedure is applied for both horizontal directions, in each direction with + and – sign.

STEP 5: SEISMIC DEMAND FOR THE EQUIVALENT SDOF SYSTEM

The determination of the seismic demand for the equivalent SDOF system is illustrated in Figure 7-15 (for medium – and long-period structures, for which the "equal displacement rule" applies. Both the demand spectra and the capacity diagram have been plotted in the same graph. The intersection of the radial line corresponding to the elastic period T^* of the idealized bilinear system with the elastic demand spectrum defines the acceleration demand (strength), required for elastic behaviour S_{ae}, and the corresponding elastic displacement demand S_{de}. Say represents both the acceleration demand and the capacity of the inelastic system expressed in terms of the yield acceleration. The reduction factor R_μ can be determined as the ratio between the accelerations corresponding to the elastic and inelastic systems

$$R_\mu = \frac{S_{ae}(T)}{S_{ay}}$$ Equation 7-25

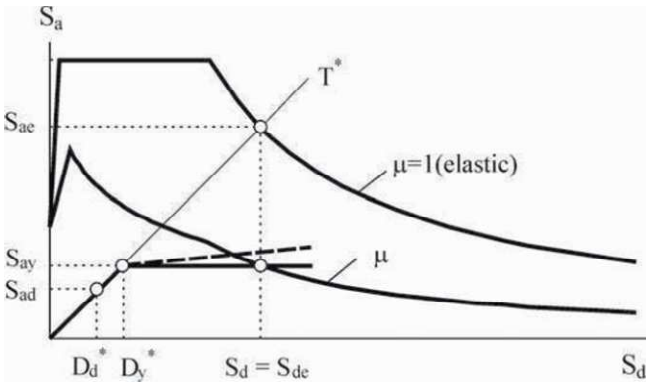

Figure 7-15 – Elastic and inelastic demand spectra versus capacity diagram (Faijar, 2000)

In general, the design acceleration S_{ad} is typically smaller than the yield acceleration S_{ay}. If the elastic period T* is larger than or equal to T_C, the inelastic displacement demand S_d is equal to the elastic displacement demand S_{de}. From triangles in Figure 7-15 it follows that the ductility demand, defined as $\mu = S_d/D_y^*$, is equal to R_μ

$$S_d = S_{de}(T) \qquad T \geq T_C$$ Equation 7-26

$$\mu = R_\mu$$ Equation 7-27

If the elastic period of the system is smaller than T_C, the ductility demand can be calculated from the rearranged as:

$$\mu = (R_\mu - 1)\frac{T_C}{T^*} + 1 \qquad T < T_C$$ Equation 7-28

The displacement demand can be determined either from the definition of ductility as

$$S_d = \mu D_y^* = \frac{S_{de}}{R_\mu}\left(1+\left(R_\mu - 1\right)\frac{T_C}{T^*}\right) \qquad \text{Equation 7-29}$$

In both cases ($T^*<T_C$ and $T\geq T_C$) the inelastic demand in terms of accelerations and displacements corresponds to the intersection point of the capacity diagram with the demand spectrum corresponding to the ductility demand μ, provided that the post-yield stiffness in the capacity diagram is zero. At this point, the ductility factor determined from the capacity diagram and the ductility factor associated with the intersecting demand spectrum are equal. In the case of a post-yield stiffness different from zero, the intersection point is determined with the horizontal line through the yield acceleration rather than with the capacity diagram.

STEP 6: GLOBAL SEISMIC DEMAND FOR THE MDOF MODEL

The displacement demand for the SDOF model S_d is transformed into the maximum top displacement D_t of the MDOF system (target displacement) by using Equation 7-16.

STEP 7: DETERMINATION OF TORSIONAL EFFECTS

Torsional effects are determined by a linear modal analysis of the 3D mathematical model, independently for excitation in two horizontal directions and combining the results according to the SRSS rule.

7.5.2. Nonlinear dynamic (time-history) analysis (NLTH)

The nonlinear time-dependent response of the structures can be obtained through direct numerical integration of its differential equations of motion. The input for NLTH analysis can be artificial or natural ground motions. In the present study, as previously introduced, artificial accelerograms generated by GOSCA code have been used. There are several available methods, which are able to solve the nonlinear differential equations of motion such as Newmark, Wilson, Hilber-Hughes-Taylor methods; the later has been chosen for the present study.

7.6. Seismic performance of the case study RC-MRFs

7.6.1. Introduction

In the current section the seismic performance of the set of buildings designed and presented in the previous chapter to ground motions at the design motion intensity is studied through a series of nonlinear static and dynamic analyses. These analyses have been performed with the purpose of clarifying the nonlinear structural behaviour and its interactions with some main design and detailing parameters. In addition, a comparison of the results obtained from nonlinear static and dynamic analyses is also made. Some basic assumptions, adopted for nonlinearly modelling the existing RC-MRF, are first introduced in detail. Then, the results from the seismic assessment are going to be presented and discussed. Deficiencies of the existing frames are addressed as well.

7.6.2. Basic Assumptions and methodology for nonlinear analyses

7.6.2.1. Methodology

The analysis of twenty frames, designed in Chapter 6, have been performed using a plane structural model developed for the analysis of nonlinear monotonic and hysteretic response of the RC-MRFs studied, subjected to nonlinear static and dynamic loading. All RC frames in six Configurations are first performed by Pushover analysis, following the procedure of N2 method, as mentioned in EC8, with two lateral load models: modal and uniform. Nonlinear Time History Analysis (NLTH) is then adopted for addressing the completely hysteretic response of the structures. The seismic input is represented by means of a series of artificial accelerograms acting at the base of the structures, mentioned in the previous sections. These accelerograms were generated by GOSCA (Denoel V, 2001). Two frame groups in the study has been analysed under eight nominal accelerograms (two sets of four series corresponding to the values of 0.15g

and 0.3g of the design accelerations). The main characteristics of structural model adopted are presented below, as well as the assumptions for idealising the structures.

Finite element model and analysis procedure

The structural members have been modelled as linear elements, in which the nonlinear behaviour is regarded as concentrated inelastic flexural plastic hinges at two ends of the girders and columns, assuming an elastic behaviour in the remaining portion of each element. The properties of plastic hinges have been evaluated on the basis of the moment-curvature diagrams of end sections with constant plastic length of the hinges. The hinges are idealised by a bilinear Takeda hysteretic model, in which the degradation in stiffness of a reinforced concrete element is taken into account. The hysteretic model is established by the linearization of the moment-curvature diagrams of the sections, obtained from CUBIA (Montejo, 2007) and RESPONSE 2000 (Bentz, (2000)). The development of hysteresis response of the members is based on some essential features of the flexural behaviour of reinforced concrete members. Positive and negative bending moments have been separately dealt with, thus allowing the idealization of asymmetrical moment-curvature relationship.

The nonlinear response of the structures studied has been evaluated using the computer code SAP 2000, which is capable of performing both nonlinear static and dynamic analysis of the structures considering the above described structural model.

A preliminary nonlinear static with the full-loaded application, nonlinearities in geometry and material taken into consideration is first carried out with vertical loads corresponding to the total effectively vibrated weight attributed to the structural plane. The weight has been taken as total dead loads and 30% of live loads on the frames, as required by EC8. The results from this analysis will become the initial conditions for the Pushover and nonlinear dynamic analyses.

The Pushover analysis, as already mentioned, has been carried out following N2 method (Faijar, 2000). Some excel sheets have been made to transform the frames of multi degree of freedoms to single degree of freedom frames and to calculate the target displacement and performance point under a given PGA in soil C.

The nonlinear dynamic analysis has been based on the direct integration of incremental equations of motion established in terms of the structural discretization, using the Hilber-Hugges-Taylor integration associated to an iterative process in each time-step. The stiffness and mass matrices have been determined by the direct stiffness method and a Rayleight damping proportional to mass and initial stiffness has been adopted. Regarding the damping matrix, the coefficients influencing mass and stiffness have been chosen in order to achieve the required damping ratio (ξ=5%) in the first and second vibration modes of the structures.

7.6.2.2. Detail modelling assumption and input data

Like in design phase, the properties of the cross sections, i.e. area and moment of inertia, have been calculated assuming T-shaped sections for beams taking into account the contribution of the slab. To evaluate the stiffness of the members before yielding it is assumed that initial stiffness of cracked reinforced concrete elements is equal to 50% of un-cracked stiffness ones, as supposed by EC8. The nonlinear characteristics of the beams and columns are located at two ends, called critical regions. The seismic behaviour of these regions is dependent on their moment-curvature diagrams and plastic hinge lengths. The moment-curvature relationships (M-φ) at the different sections, under monotonic loading, have been calculated by the fibre method (CUBIA (Montejo, 2007) and RESPONSE 2000 (Bentz, 2000), considering the material properties of reinforcing steel and concrete stress-strain relationships. To perform nonlinear analyses of the frames, actual (mean) values of material strengths are considered, instead of the design strength, to reflect the expected real overstrength of the structures: Steel S500 with a stress-strain diagram typical of Tempcore steel (f_y=500MPa; E=200GPa); concrete C25/30 with mean compressive unconfined strength of 33MPa; a uniaxial nonlinear constant confinement model, proposed by Mander et al. (1998), is assumed for nonlinear properties of the concrete. The confinement ratio is taken as 1.2 for the concrete core and as 1.0 for the cover. Mean value for concrete C25/30 according to EC2, i.e. 33MPa, and a strain corresponding to peak strength equal to 0.2% and an ultimate strain equal to 4.0% have been adopted for the analyses. An elastic-perfectly plastic steel stress-strain diagram is assumed,

characterised by a maximum strength equal to 500MPa and a Young modulus equal to 200GPa. Figure 7-16 presents the calculation of plastic resistance of a typical beam in all frames by RESPONSE 2000 (Bentz, 2000). Two values of moment resistance including negative and positive ones are shown. The unit of M-φ curve in Figure 7-16 is kNm-rad/km. Steps of calculating the resisting moment of a column, having dimensions of 350x350mm with longitudinal steel of 8Φ16, is shown in Figure 7-17. It should be stressed that this calculation is based on two computer programs: CUBIA (Montejo, 2007) and RESPONSE 2000 (Bentz, 2000). The moment-curvature curve is determined by CUBIA at certain level of axial forces. The unit of curvature is 1/m.

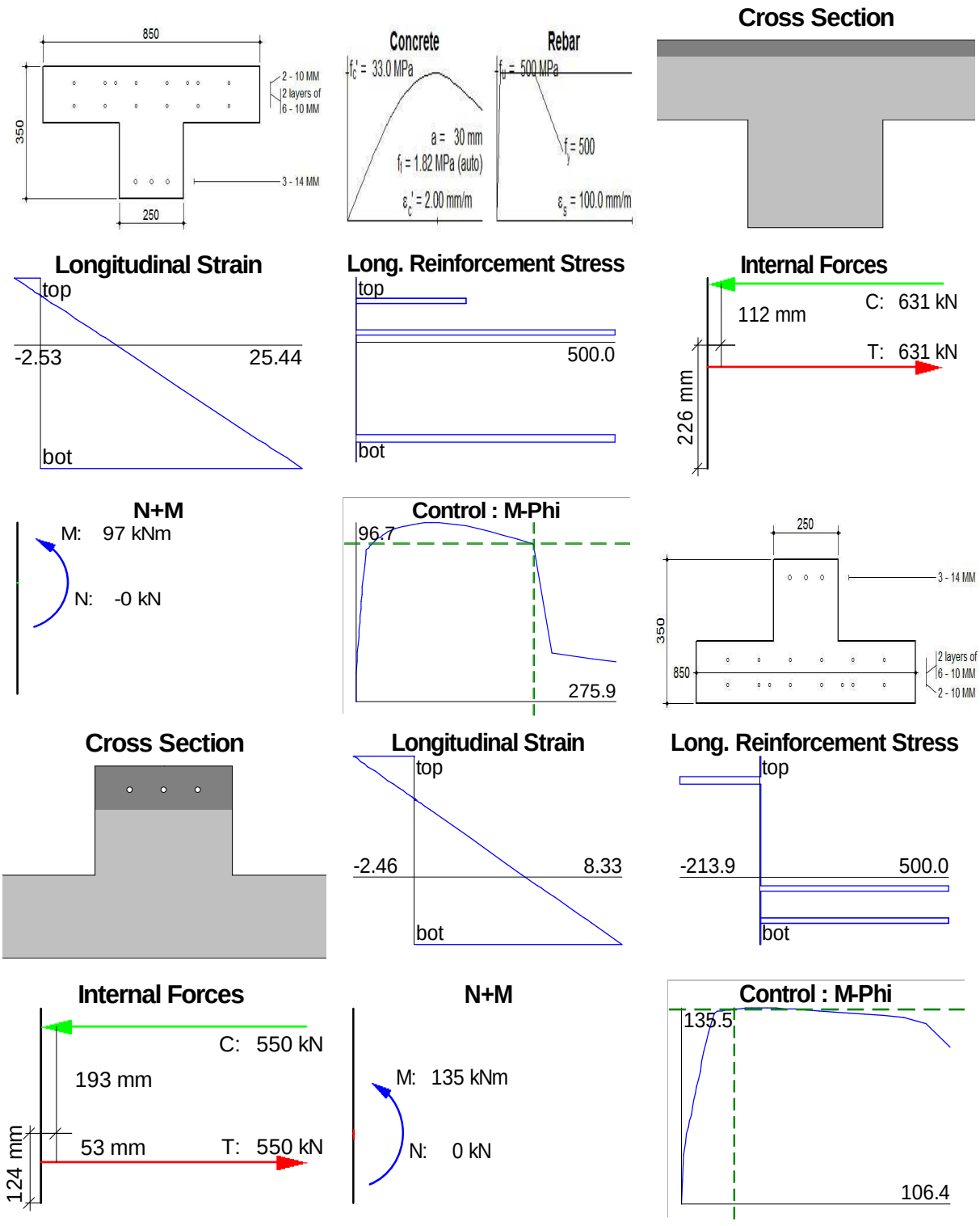

Figure 7-16 – Calculation of resistance of a beam in studied frames

For different types of the M-φ diagrams of the end sections the effects of strength degradation has not been taken into account but pinching effects due to crack of the concrete and yielding of the steel have been accounted for.

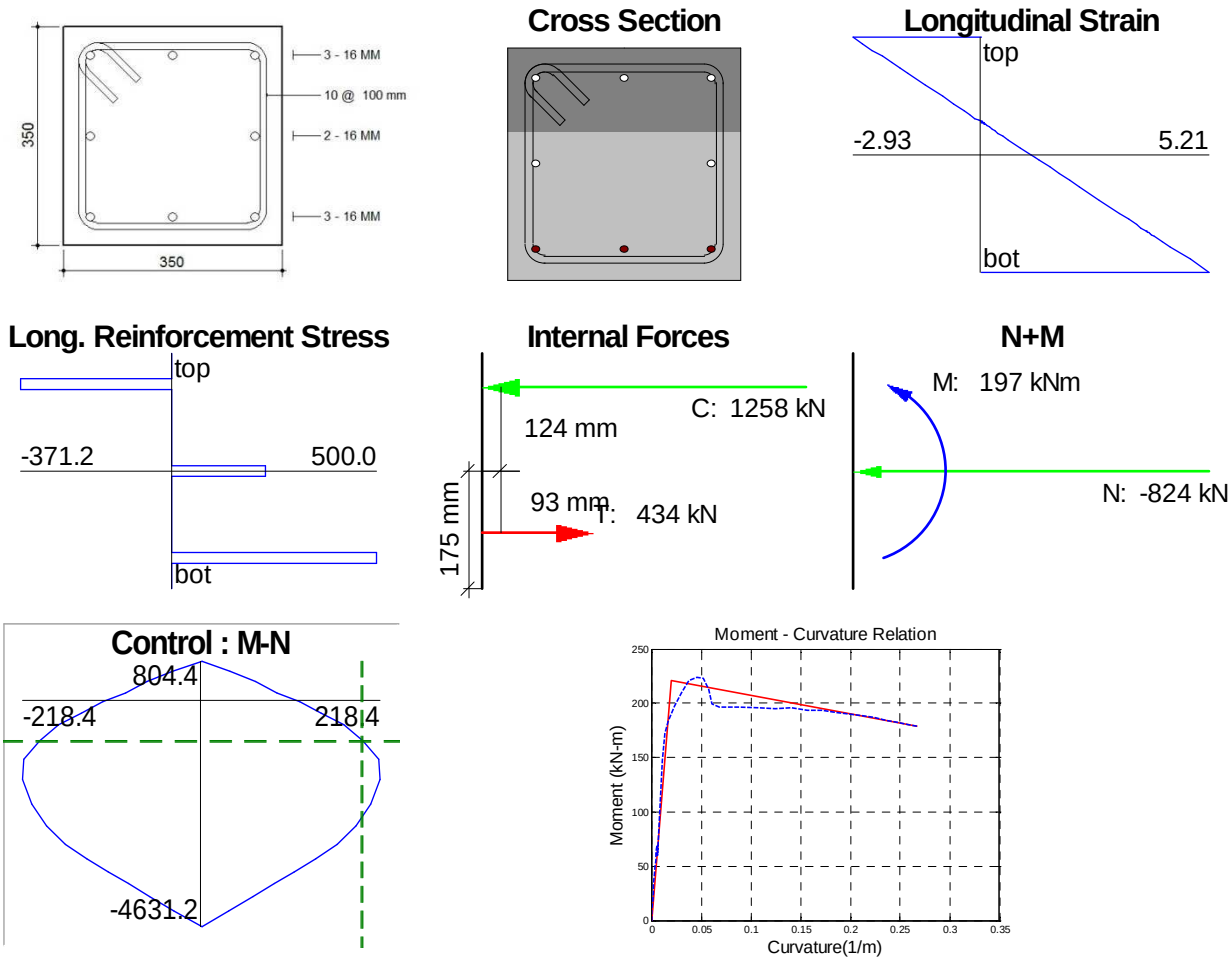

Figure 7-17 – Calculation of resistance of a beam in studied frames

Hysteretic behaviour for critical regions of beams and columns in Nonlinear Time History Analysis

In order to represent the hysteresis behaviour of RC elements, the pivot hysteresis model (Dowell et al, 1998) is adopted. Detailed description of this model has been explained at the beginning of this Chapter. The model is re-illustrated in Figure 7-18. The specification of the properties is identical to that for the Kinematic or Takeda model, with the addition of the following scalar parameters, taken as the suggestions for RC elements in SAP 2000 (CSI, 2009):

• $\alpha 1$, which locates the pivot point for unloading to zero from positive force, taken as 10

• $\alpha 2$, which locates the pivot point for unloading to zero from negative force, taken as 10

• $\beta 1$, which locates the pivot point for reverse loading from zero toward positive force, taken as 0.7, meaning that stiffness of the elements is reduced 30% compared to the elastic stiffness.

• $\beta 2$, which locates the pivot point for reverse loading from zero toward negative force, taken as 0.7, meaning that stiffness of the elements is reduced 30% compared to the elastic stiffness.

• η, which determines the amount of degradation of the elastic slopes after plastic deformation, taken as 0, meaning that unloading slope is equal to elastic slope.

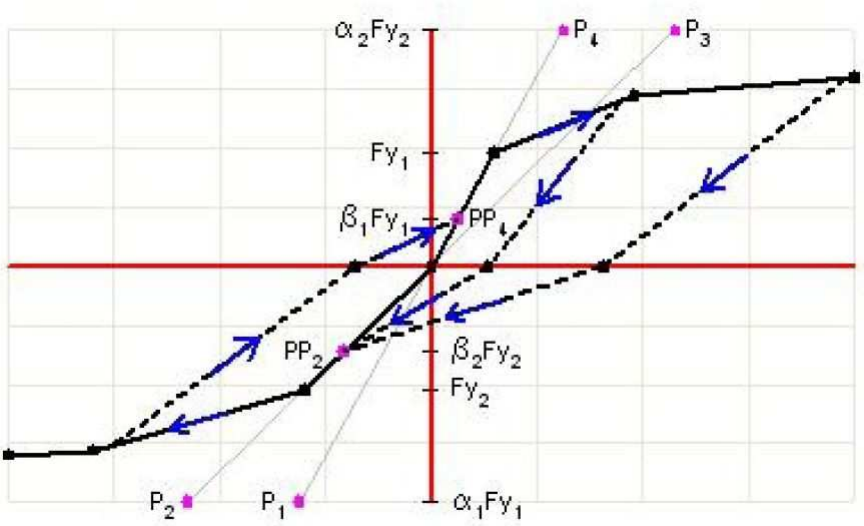

Figure 7-18 – Pivot hysteresis model for RC elements (Dowell et al., 1998)

Seismic performance criteria for beams and columns for nonlinear analysis

As all components in studied frames are modelled as linear finite elements in which nonlinear material properties are governed by plastic hinges concentrated on two ends of beams or columns, the behaviour of these plastic hinges should be characterized to give the input for the nonlinear analysis. As mentioned above, the behaviour of critical regions of beams and columns is determined by the aids of CUBIA and RESPONSE 2000. Besides, the criteria which can be used to address the seismic performance of the critical regions should be adopted. Some existing official documents are available for different types of RC-sections, resulting from experimental and numerical studies. Recommendation of FEMA 356 (2000), as shown in Figure 7-19 and Figure 7-20, is adopted to introduce plastic hinges in beams. Reinforced concrete columns have been modelled using the same models identified for beams, except that axial force variations under the action of earthquake loading are also taken account.

Each plastic hinge represents concentrated post-yield behaviour. The load-deformation relation is described by linear response from A (unloaded component) to an effective yield B. Subsequently, there is linear response, at reduced stiffness, from B to C, with sudden reduction in lateral load resistance to D, response at reduced resistance to E, and final loss of resistance thereafter. The slope from B to C, is taken as equal to 10% of the initial slope. C has an ordinate equal to the strength of the component and an abscissa equal to the deformation at which significant strength degradation begins. FEMA 356 makes a distinction between several kinds of failure modes, depending on the nature of the element (beams, columns). Each kind of failure mode is governed by its specific type of non-elastic behaviour (parameters a, b, c, d, e in Figure 7-19) depending on some relevant parameters. For beams, the following failure modes have to be considered (Table 7-1):

- beams controlled by flexure;
- beams controlled by shear;
- beams controlled by inadequate development or splicing along the span;
- beams controlled by inadequate embedment into beam-column joint;

The following parameters are under consideration for beams:

$$\xi = \frac{\rho - \rho'}{\rho_{bal}} \qquad \text{Equation 7-30}$$

Where ϱ is the ratio of non-prestressed tension reinforcement, ϱ' is the ratio of non pre-stressed compression reinforcement, ϱ_{bal} is the reinforcement ratio producing balanced strain conditions. ξ is a geometrical parameter, related to the symmetry of upper and lower reinforcement, and related to the relative quality of the materials steel and concrete; the parameters a, b and c used to describe the plastic

hinge behaviour have to be computed for positive and negative bending moments, since in general $\rho \neq \rho'$. The 'conformity' of the transverse reinforcement:

$$\frac{V}{b_w d\sqrt{f_c^{'}}} \qquad \text{Equation 7-31}$$

Where V is the design shear force at section, b_w the web width, d is the distance from extreme compression fibre to centroid of tension reinforcement, $f_c^{'}$ is the compressive strength of concrete. This ratio is a parameter related to the shear failure mode (and thus related to the risk of brittle failure).

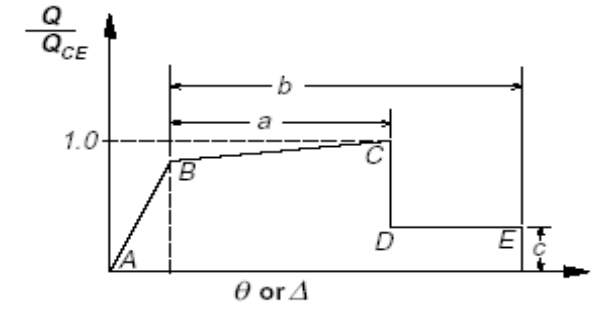

(a) Deformation

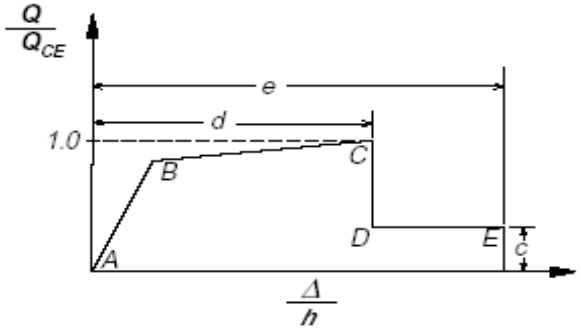

(b) Deformation ratio

Figure 7-19 – Generalized load deformation behaviour in a plastic hinge according to FEMA 356

Based on FEMA356, seismic performance of the reinforced concrete members has been added in the SAP 2000 program, specifying additional deformation measures of the plastic hinges:

- IO: immediate occupancy.
- LS: life safety.
- CP: Collapse prevention.

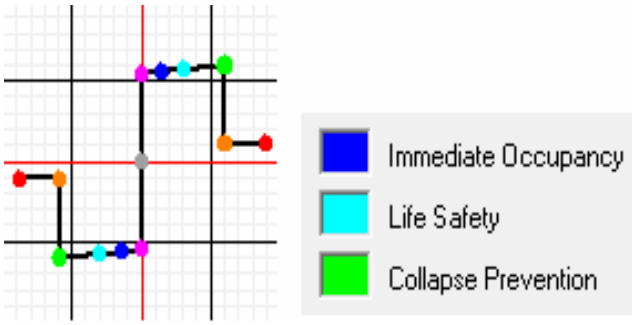

Figure 7-20 – Rigid-plastic beam-column element in SAP 2000 in relevance with FEMA 356

These points are informational measures that are reported in the analysis results and used for performance-based design. They do not have any effect on the behaviour of the structure.

Table 7-1 – Ductility parameters a, b, c for beams according to FEMA 356

Table 6-7 ***Modeling Parameters and Numerical Acceptance Criteria for Nonlinear Procedures—Reinforced Concrete Beams***

			Modeling Parameters[3]			Acceptance Criteria[3]				
						Plastic Rotation Angle, radians				
						Performance Level				
			Plastic Rotation Angle, radians		Residual Strength Ratio		Component Type			
							Primary		Secondary	
Conditions			a	b	c	IO	LS	CP	LS	CP
i. Beams controlled by flexure[1]										
$\frac{\rho - \rho'}{\rho_{bal}}$	Trans. Reinf.[2]	$\frac{V}{b_w d \sqrt{f'_c}}$								
≤ 0.0	C	≤ 3	0.025	0.05	0.2	0.010	0.02	0.025	0.02	0.05
≤ 0.0	C	≥ 6	0.02	0.04	0.2	0.005	0.01	0.02	0.02	0.04
≥ 0.5	C	≤ 3	0.02	0.03	0.2	0.005	0.01	0.02	0.02	0.03
≥ 0.5	C	≥ 6	0.015	0.02	0.2	0.005	0.005	0.015	0.015	0.02
≤ 0.0	NC	≤ 3	0.02	0.03	0.2	0.005	0.01	0.02	0.02	0.03
≤ 0.0	NC	≥ 6	0.01	0.015	0.2	0.0015	0.005	0.01	0.01	0.015
≥ 0.5	NC	≤ 3	0.01	0.015	0.2	0.005	0.01	0.01	0.01	0.015
≥ 0.5	NC	≥ 6	0.005	0.01	0.2	0.0015	0.005	0.005	0.005	0.01

For columns, FEMA 356 has suggested the following failure modes depending on the overwhelming parameters that control the behaviour of the columns (Table 7-2):

Table 7-2 – Ductility parameters a, b, c for columns according to FEMA 326 (2000)

Table 6-8 ***Modeling Parameters and Numerical Acceptance Criteria for Nonlinear Procedures—Reinforced Concrete Columns***

			Modeling Parameters[4]			Acceptance Criteria[4]				
						Plastic Rotation Angle, radians				
						Performance Level				
			Plastic Rotation Angle, radians		Residual Strength Ratio		Component Type			
							Primary		Secondary	
Conditions			a	b	c	IO	LS	CP	LS	CP
i. Columns controlled by flexure[1]										
$\frac{P}{A_g f'_c}$	Trans. Reinf.[2]	$\frac{V}{b_w d \sqrt{f'_c}}$								
≤ 0.1	C	≤ 3	0.02	0.03	0.2	0.005	0.015	0.02	0.02	0.03
≤ 0.1	C	≥ 6	0.016	0.024	0.2	0.005	0.012	0.016	0.016	0.024
≥ 0.4	C	≤ 3	0.015	0.025	0.2	0.003	0.012	0.015	0.018	0.025
≥ 0.4	C	≥ 6	0.012	0.02	0.2	0.003	0.01	0.012	0.013	0.02
≤ 0.1	NC	≤ 3	0.006	0.015	0.2	0.005	0.005	0.006	0.01	0.015
≤ 0.1	NC	≥ 6	0.005	0.012	0.2	0.005	0.004	0.005	0.008	0.012
≥ 0.4	NC	≤ 3	0.003	0.01	0.2	0.002	0.002	0.003	0.006	0.01
≥ 0.4	NC	≥ 6	0.002	0.008	0.2	0.002	0.002	0.002	0.005	0.008

1. When more than one of the conditions i, ii, iii, and iv occurs for a given component, use the minimum appropriate numerical value from the table.
2. "C" and "NC" are abbreviations for conforming and nonconforming transverse reinforcement. A component is conforming if, within the flexural plastic hinge region, hoops are spaced at ≤ $d/3$, and if, for components of moderate and high ductility demand, the strength provided by the hoops (V_s) is at least three-fourths of the design shear. Otherwise, the component is considered nonconforming.
3. To qualify, columns must have transverse reinforcement consisting of hoops. Otherwise, actions shall be treated as force-controlled.
4. Linear interpolation between values listed in the table shall be permitted.

- columns controlled by flexure;
- columns controlled by shear;
- columns controlled by inadequate development or splicing along the clear height;
- columns controlled by axial loads exceeding 0.70P;

Similarly to the beams, there are several parameters which are needed to be taken into consideration to determine the limit values of seismic performance of critical regions of columns. They are recalled here for convenience:

- $\frac{P}{A_g f_c^{'}}$ Equation 7-32
- $\frac{V}{b_w d\sqrt{f_c^{'}}}$ Equation 7-33

Where P is the axial internal forces in earthquake situations acting on columns; A_g is the gross cross-sectional area; $f_c^{'}$ is the compressive strength of concrete; V is the internal shear forces.

7.6.2.3. Responses controlled the seismic performance of the studied RC-MRFs

In general, the seismic performance of an existing frame is dependent on seismic performance of the critical sections and of the beam-column joint.

The behaviour of critical regions is based on their resistance in shear and in bending. For all studied frames, as mentioned in Chapter 6, they are designed with very large shear resistance so that even under severe earthquake there is no failure in beams or column caused by shear. Thus, the critical regions are governed by flexural deformations. It is necessary to stress that all critical sections in studied frames have been checked that they have enough local ductility to be possibly developed the plastic hinges due to bending.

For the beam-column joints, if the frames are designed in accordance with EC8 with DCM class, it is not necessary to verify the failure of node due to plastic hinges formed at two ends of beams because they are designed according to capacity design rules. On the contrary, for the frames designed in accordance with EC2 or EC8 with DCL class, the resistance of compression strut in the beam-column nodes has to be checked because they are not designed accordingly to capacity design rules. In general, there is no stirrup in the joints. The procedure to check the capacity of the joints is presented hereafter.

Figure 7-21 presents a simple way to determine the resistance of a joint under seismic situations. Under the seismic situation, M^{+}_{left} and M^{-}_{right} are the internal forces due to bending. These moments will cause the action effect F_{strut} at the joints. The values of F_{strut} can approximately calculated by:

$$F_{strut} = \frac{\left|M^{+}_{left}\right| + \left|M^{-}_{right}\right|}{h_w}$$ Equation 7-34

Where: h_w is the height of the beam.

The resistance of the joint is dependent on the efficient compression part. This part is dependent on the effective width of the node, $b_{ef,n}$, possibly determined by:

$$b_{ef,n} = 0.2 l_{n,dia} = 0.2\sqrt{h_w^2 + h_c^2}$$ Equation 7-35

Where: $l_{n,dia}$ is the diagonal length of the node; h_c is the height of the column, as expressed in Figure 7-21.

The compression strut resistance can be determined as the following formulae:

$$R_{strut} = \nu f_{cd} b_{ef,n} b_c = 0.5 f_{cd} 0.2\sqrt{h_w^2 + h_c^2} b_c \quad \text{Equation 7-36}$$

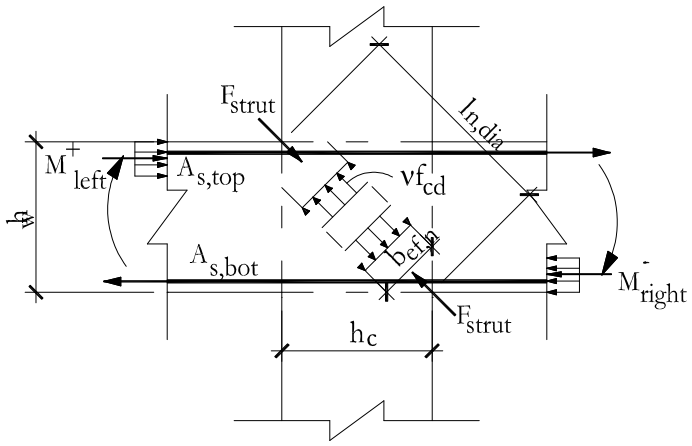

Figure 7-21 – Determination of the resistance of compression strut at joint

7.6.2.4. Definition of ductility and ultimate response for the RC-MRFs

Definition of ductility capacity and ultimate response of the RC-MRFs have long been discussed and there has still been difficulty in reaching approval with the research community as to the appropriate definition of yield and ultimate displacements of the RC-MRFs. There are several definitions of yield displacement of a RC frame, as explained in Figure 7-22. They are point 1 corresponding to the intersection of the line through the origin with initial stiffness and the nominal strength, point 2 corresponding to the displacement at the first yield and point 3 referring to the intersection of the line through the origin with secant stiffness through first yield and the nominal strength. There is also a wide diversity of defining ultimate response of the structures, including response at peak strength, response corresponding to 20% or 50% (or some other percentage) degradation from the peak (or nominal) strength, response at initial fracture of transverse reinforcement and response at ultimate inter-story drifts which can be taken as 3% as in most seismic codes.

Due to such variation of defining the yield and capacity of the structure, it is obviously necessary to state a selected definition of ductility capacity. Referring to Figure 7-22, the yield displacement is taken to be defined by point 3 and the ultimate displacement by the lesser of displacement at peak strength or at ultimate drift limitation. There is a reason explained why yield displacement has been chosen at point 3, which is the intersection of the line through origin and secant stiffness through the first yield as discussed in Priesley (2007), that a reinforced concrete structure loaded to first yield, unloaded and then reloaded, will perform linear unloading and reloading, along the line through point 3. Therefore, when cracking occurs, the line from the origin through point 3 may provide the best estimate of elastic stiffness at levels close to yield. From Figure 7-22, it is possible to deduce that:

$$\Delta_y = \frac{V_u}{V_{1,y}} \Delta_{1,y} \quad \text{Equation 7-37}$$

$$\mu = \frac{\Delta_u}{\Delta_y} = \frac{\Delta_u V_{1,y}}{\Delta_{1,y} V_u} \quad \text{Equation 7-38}$$

Where: $\Delta_{1,y}$ is the displacement at first yield of the structure; Δ_y is the equivalent yield displacement of the structure; $V_{1,y}$ is the base shear corresponding to the first yield displacement and V_u is the base shear corresponding to the ultimate response of the structure.

Concerning about the maximum displacement of the structures, the lateral displacement at which the strength is equal to 80% of the maximum strength is regarded as the maximum one.

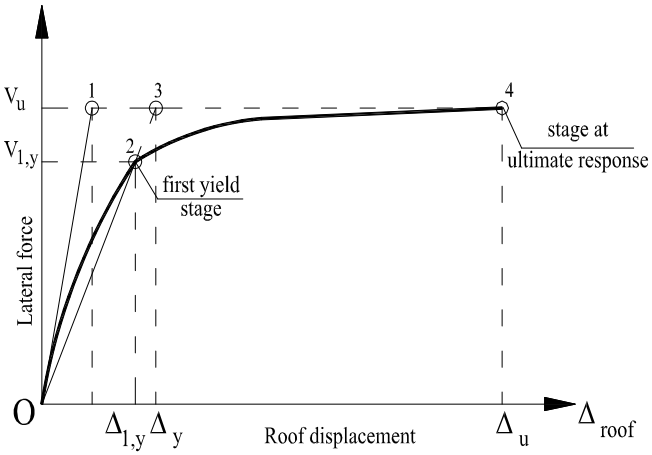

Figure 7-22 – Definition of ductility capacity and ultimate response of the RC-MRFs

7.6.3. Evaluation of response of the RC-MRFs studied

7.6.3.1. Brief re-description of the existing RC-MRFs

Twenty RC-MRFs in four configurations have been designed and detailed as presented in Chapter 6. They will be evaluated based on some basic assumptions and analytical methods mentioned above. The detail configurations of these frames have been described in very detail in chapter 6.

Some essential characteristics, especially in geometrical configurations, have been recalled hereafter for convenience.

Configuration 1

In this configuration, the eight RC-MRFs have been designed. Three of them are belonged to EC2-group (each located at the different region with PGA of 0.05g, 0.15g and 0.3g) and the other five, belonged to EC8-group, are designed and detailed in accordance with both EC2 and EC8 (four designed in zone having PGA of 0.05g and 0.15g with two ductility classes: L and M; and the remaining located in zone with PGA of 0.3g with ductility class of medium (M)).

All frames in this case are the same in number of stories (3 stories), number of spans (3 spans), lengths of spans and height of stories. There are three types of cross-sectional dimensions in these frames. The two frames in the EC8-0.05g group and the EC2-0.05g frame have the same dimensions of columns and beams, which are 0.3m x 0.3m and 0.25m x 0.35m, respectively. The two EC2-0.15g and EC8-0.15g-L frames have the dimensions of columns and beams of 0.35m x 0.35m and 0.25m x 0.35m, respectively. The remaining frames in this group have the dimensions of columns and beams of 0.5m x 0.5m and 0.25m x 0.35m, respectively.

Configuration 2

Eight RC-MRFs in this configuration include three frames designed in accordance with EC2 and the others according to both EC2 and EC8 and they have some common features in geometry, being six stories, three equal spans of 5m, first-story height being 3.5m and the others being 3m. In addition to that, due to the same dimensions in plan and elevation, the thickness of the slab and cross-sectional dimensions of beams have been chosen equally, that is, 0.15m thick of the slab and 0.25m wide x 0.35m high of the beams respectively.

For the dimensions of the columns, they have been divided into two cases, in respect with two groups of RC-MRF studied. For the frames in the EC8-group, because of drift limitations required by the code, the dimensions of column have had to be selected differently depending on the seismicity magnitude of the zones on which the frames are located.

For the zone having PGA of 0.05g and 0.15g, dimensions of rectangular columns are 0.35m x 0.35m and they are 0.5m x 0.5m for the zone of 0.3g. Moreover, in the zone having PGA of 0.05g and 0.15g, two ductility classes, DCL and DCM, have been adopted for the design cases. Only DCM has been adopted for the frame located in the zone having the PGA of 0.3g. At last, these two kinds of frames are then chosen and designed for EC2-group. It should be noted that in order to ensure the limitation of drift under serviceability earthquakes in preliminary design process, the dimensions of columns of EC8-0.05g-M and EC8-0.15g-M frames are increased and greater than those of columns of EC8-0.05g-L and EC8-0.15g-L frames

Configuration 3

In this configuration, there are six frames, having 8 stories. Because the initially chosen dimensions of beams and columns have met the requirement of drift limitations in three seismic zones having PGA of 0.05g, 015g and 0.3g respectively, thus there is only one frame in the EC2-group. Three other frames have been designed with respect to three PGA of 0.05g, 0.15g and 0.3g.

Two ductility classes, DCM and DCL, have been chosen to design the frames, which are located in the zone having PGA of 0.05g and 0.15g. The remaining frame has been designed with medium ductility class and it is located at the zone with PGA of 0.3g. The dimensions of beams are 0.25m in width and 0.35m in height with the slab having the thickness of 0.15m. Sections of columns from story 1 to 4 are squared with the dimensions of 0.6m and from 5-8 having the squared shape with the side of 0.5m.

Configuration 4

This configuration consists of 10-story frames, having the same number and dimension of spans as Configuration 1, 2 and 3. The height of the first floor is 3.5m like three previous cases as well. At the first thought, with the aim to compare the steel content in frames designed with different ductility classes, it was intended to choose all cross-sectional dimensions of columns for the zone with PGA of 0.05g and 0.15g being 0.6m x 0.6m and 0.5m x 0.5m for the stories from 1 to 5 and 6 to 10, respectively. However, due to damage limitation under serviceability earthquakes, the dimensions of columns of EC8-M frames are increased. Similarly to the zone having seismicity of 0.3g, higher dimensions of columns have had to be chosen to satisfy the serviceability limit states. They are 0.8m x 0.8m for the columns from stories 1 to 5 and 0.7m x 0.7m for the remaining stories. Due to the increase of the column dimensions, the cross-sectional dimensions have chosen a little higher than the previous configurations. They have 0.25m in width and 0.4m in height.

Two ductility classes, DCM and DCL, have been adopted for the frames in zone with PGA of 0.05g and 0.15g. Only ductility class DCM has been adopted for the frame in zone with higher seismicity.

7.6.3.2. Linear and nonlinear periods of the studied RC-MRFs

A linear dynamic analysis has first been carried out to evaluate the fundamental periods of the structures. Nonlinear pushover and nonlinear dynamic analyses have been then performed to evaluate the real response of the RC-MRFs studied.

The approximate values of linear and nonlinear periods of the structures are depicted in Table 7-3. The linear and nonlinear periods have been determined from time histories of top displacement as the average of four accelerograms of the ratios t/n, where n is the number of complete cycles of displacement and t the duration of the series from linear and nonlinear dynamic analyses (Cavalho et al., 1997).

Observing the fundamental periods from linear and nonlinear analyses on frames studied it can be observed that for the frames located in zones having low seismicity (PGA of 0.05g), the nonlinear and linear fundamental periods are the similar. It means that the frames in these cases work in elastic range and nonlinearity due to geometry has an inconsiderable influence on the stiffness and response of the structures.

On the other hand, the values of nonlinear periods in cases of the frames located in zones having PGA of 0.15g and 0.3g are greater than the elastic periods obtained by linear analysis. This is due to the decrease of the structural stiffness, caused by nonlinear behaviour in material and in geometry. In addition to that, in most of cases having the same geometrical dimensions, the increase of periods for linear dynamic to nonlinear dynamic analyses in EC2 group is much higher than those in EC8 group. It means that the

frames in EC2 group have been experienced in inelastic range much more than in EC8 group. This also leads to much decrease of the stiffness of the structures and more plastic hinges formed during the attacks of earthquake.

Table 7-3 – Fundamental periods of the RC-MRFs studied from linear and nonlinear dynamic analyses

Config.	Case	Fundamental periods (s)	
		Linear dynamic	Nonlinear dynamic
1	EC2-0.05g	1.25	1.25
	EC2-0.15g	0.96	1.10
	EC2-0.3g	0.84	0.91
	EC8-0.05g/L	1.25	1.25
	EC8-0.05g/M	1.25	1.25
	EC8-0.15g/L	0.96	0.97
	EC8-0.15g/M	0.96	0.99
	EC8-0.3g/M	0.84	0.89
2	EC2-0.05g	1.99	1.99
	EC2-0.15g	2.07	2.11
	EC2-0.3g	1.74	1.80
	EC8-0.05g/L	1.99	1.99
	EC8-0.05g/M	1.54	1.54
	EC8-0.15g/L	2.07	2.09
	EC8-0.15g/M	1.55	1.61
	EC8-0.3g/M	1.74	1.82
3	EC2-0.05g	1.67	1.67
	EC2-0.15g	1.67	1.72
	EC2-0.3g	1.90	2.00
	EC8-0.05g/L	1.67	1.67
	EC8-0.05g/M	1.67	1.67
	EC8-0.15g/L	1.67	1.70
	EC8-0.15g/M	1.67	1.71
	EC8-0.3g/M	1.90	1.95
4	EC2-0.05g	1.84	1.84
	EC2-0.15g	1.84	2.05
	EC2-0.3g	1.79	2.20
	EC8-0.05g/L	1.84	1.84
	EC8-0.05g/M	1.79	1.79
	EC8-0.15g/L	1.84	2.03

	EC8-0.15g/M	1.79	1.93
	EC8-0.3g/M	1.79	2.02

Comparing the structures in EC8-group, it is also observed that the fundamental periods of the structures due to nonlinear response is more significant for the structures designed for an acceleration of 0.3g and for increasing ductility. It can be explained that under severe seismic excitations the structures, therefore, will perform much nonlinear behaviour due to both material and geometrical nonlinearities, causing much decrease of their both stiffness and strength. For the frames located in zone having PGA of 0.15g, the periods of frames designed with DCM are always slightly higher than those designed with DCL. This means that the frames designed with DCM are more ductile than ones with DCL, as expected. The increase of the ground acceleration also has an effect on the nonlinear periods of the structures, as clearly seen in the structures in Configuration 3, in which all frames have the same geometrical configurations but the increase of PGA makes the stiffness of the structures decrease when compared to the ones in the zone of lower PGA.

From the comparison of the periods between the structures in two groups it is clear that in many cases the structures designed with low ductility are much stiffer than the structures not designed according to the seismic code. This can be explained by some strict requirements from the code such as capacity design rules.

7.6.3.3. Nonlinear response of the studied RC-MRFs

Following the five steps presented in Figure 7-1, seismic performance of the studied RC-MRFs is assessed. The results, presented herein, are based on the Pushover and NLTH analyses.

The first check in all frames in EC2-group and the frames designed accordingly to EC8 with DCL class is about the existence of brittle failure of critical regions due to shear and failure at beam-column joints. This can be easily done by Pushover analysis. All these regions have rather high shear resistance compared to bending resistance, as presented in Chapter 6, so that the seismic performance of these regions is governed by flexural deformation. In beam-column joints, the resistance of compression strut and shear resistance are calculated and compared with action effects due to increased seismic forces at each step of loading in Pushover analysis. Figure 7-23 to 26 present the characteristic features of studied frames established by Pushover analysis: failure points, target displacements under design PGA if the frames are well retrofitted… Capacity curves in Figure 7-23 to 26 depict the drifts at top and corresponding base shears of the frames. Some common features can be observed in this figure. The seismic behaviour of all frames in EC2-group and in EC8-group with low ductility (DCL frames), is governed by brittle failure. Because all these frames have been designed with significant shear resistance; there is no failure due to shear. However, all these frames collapse because of failure at beam-column joints. The failure at nodes is marked by triangular symbols in black and in red, representing EC8-DCL and EC2 frames. In general, the failure at nodes has occurred beyond the elastic range. In most of cases, the node failure is coincident with the first plastic hinges occurring in the frames. In some cases (Configuration 2-EC8-DCL, Configuration 4-EC8-DCL), the beam-column joints even collapse in the elastic range when the horizontal seismic loads are not so high. For the remaining frames, failure of nodes has occurred at the stage at which two plastic hinges has formed at beam ends around the nodes.

Clearly, for the earthquakes with PGA of 0.15g, the RC-MRFs should not be designed with Low Ductility Class because the frame cannot reach the performance point, due to brittle failure caused by shear or by crushing of concrete in beam-column joints. On the other hand, for earthquakes with PGA of 0.05g, all frames (even EC2-0.05g ones) are only loaded to elastic range; therefore there is no failure in these frames under design PGA. However, brittle collapse is also observed in EC2-0.05g and EC8-0.05g-L frames under earthquakes with PGA little greater than design PGA.

Figure 7-23 to 26 also shows the theoretical capacity curves of the EC2 and EC8-DCL frames if it is assumed that all nodes have been retrofitted. It is also observed that in each configuration if the frames have the same geometrical configurations but have been designed with different ductility classes and/or different codes, their initial stiffness is the same (same line from the origin to the first yield any where in the frames). The lateral drifts or displacements at the first yield in EC8-DCM frames are always lower than in the frames of the EC2 or EC8-DCL groups. Although the frames designed with EC8-DCM have

smaller quantity of reinforcements, their maximum lateral displacements or drifts are greater than those of the frames in EC8-DCL, if it is assumed that the beam-column joints of the EC8-DCL frames are well retrofitted.

In order to check the ability of EMP to retrofit the existing frames, from now on it is assumed that all beam-column joints in EC2 group and in EC8 group with DCL have been retrofitted by some means to prevent them from being failed under seismic attacks. Based on that, more analyses on these frames can be carried out in order to evaluate the seismic performance of the studied frames.

Figure 7-27 to Figure 7-33 summarise the values of global response of the RC-MRFs studied from Pushover and NLTH analyses of four different accelerograms, in terms of failure mechanisms, top displacements, base shears, inter-story drifts and maximum resistible PGAs. Most of main characteristics of the nonlinear behaviour of the frames studied are presented hereafter.

If it is supposed that all frames in EC2 group and in EC8 group with DCL are not failed because of collapse of the beam-column joints, the diagrams of the overall behaviour of all studied frames show that the structures exhibit strong nonlinear response, both Pushover and NLTH analyses. This is reasonable because all the frames have been designed with many efforts in order to reduce the cross-sectional dimensions. In addition to that, the steel configuration of frame components has been selected so that the steel contents are close to the minimum required one. In all configurations, the frames designed in accordance with medium ductility class are more ductile than the ones in EC2-group or designed according to low ductility class. This is expressed in some aspects, such as lower required base shear, larger drift and target displacements, more plastic hinges formed at designed PGA and at failures. For the RC-MRFs in EC8-group, located in zone having PGA of 0.05g and 0.15g and designed with two DCs: M and L, it is observed that the softening of these structure with increasing ductility is reflected in the maximum values of response, showing on the average a tendency for the reduction of force demands associated with the increase of lateral drifts.

The unfavourable observed failure mechanisms in EC2 group are column-sway ones in one or several stories, leading to large P-delta effects on the columns in lower stories. The column-sway mechanism in one story is well known as soft-story mechanism, as illustrated in Figure 7-27 (top). The column-sway mechanism in several stories is shown in Figure 7-27 (bottom). The plastic failure mechanisms of studied frames in EC8 group are presented in Figure 7-28. They are partial beam-sway (Figure 7-28, left) or full beam-sway (Figure 7-28, right) mechanisms. The favourable failure modes of the frames in EC8 group are the results from capacity design rules in the frames designed in accordance with EC8.

By observing the drifts and corresponding base shears of performance points under design PGA by Pushover and maximum drifts and corresponding base shears by NLTH analyses, it is clear that the results between pushover and NLTH are not consistent, especially for the RC-MRFs having large fundamental periods (Configuration 3 and 4). In most of the structures studied the target displacement established by the Pushover analysis is greater than the maximum displacement established by the NLTH analysis.

For the structures in EC2-group, the distribution of plastic hinges is scattered in both beams and columns. This is observed in both Pushover and NLTH analyses. On the contrary, for the structures in EC8-group, as expected, plastic hinges are concentrated at two ends of beams, at bottom of base columns and at top of top columns. This is resulted from Capacity Design. It is also observed that the number of severely damaged plastic hinges in the structures designed with higher ductility is much higher than in the ones designed for lower ductility.

Figure 7-29 presents the displacements at design PGA at top of all studied frames by Pushover and NLTH analyses with the assumption that there is no failure at beam-column joints for the frames in EC2 group and EC8-DCL frames. It can also be observed that the results of these two methods are not consistent. For the frames located in the zone having PGA of 0.05g and 0.15g, the differences between Pushover and NLTH analyses are about 2-7%. However, for the frames in the zone having higher PGA, namely 0.3g, Pushover analysis much over-estimates the top displacements of the structures compared with the results from NLTH analysis. In some cases, the difference is up to 50%.

Figure 7-30 shows the values of design base shears, maximum base shears generated in the frames under seismic actions from Pushover and NLTH analyses, supposing again no failures at beam-column joints. For the low structures and those designed in accordance with EC8-DCL, the design base shears and

maximum base shears generated during the earthquake are approximately equal with Pushover and NLTH analyses. However, for higher frames and frames designed to EC8-DCM, the design base shears and maximum base shears during the response to seismic actions are different in Pushover and NLTH analyses. In some cases, the difference is about 40%.

The peak base shears response in Pushover and NLTH analyses at the design PGA are not equal. In some cases, they are largely different. From pushover response of the structures in EC8-group, it is clear that in some cases ultimate and peak base shears are coincident, mainly in the low-rise and regular frames. On the other hand, in medium and high rise RC-MRFs, the ultimate and peak base shears are different; this is because the ultimate base shears are chosen in accordance with seismic performance criteria of the members and the structures, such as limitations of inter-story drift, strain hardening of the members after yielding. These "ultimate" values are usually corresponding to the full or partial beam-sway mechanisms of the structures. It is necessary to stress that the peak and "ultimate" base shears are less influenced by the Ductility Class than the design base shears. This is because these base shears represent the real resistance of the structures and they are affected by the various sources of overstrength parameters, supplied by the all components of the structures. Many of these parameters, such as the reinforcement contents controlled by gravity loads or by minimum requirement from the code or cross-sectional dimensions controlled by drift limitations, are independent of the ductility class.

One of the basic overstrength sources is the difference between the mean strengths of steel and concrete, on which the nonlinear analyses have been based, and the design values of these strengths. The ratios of the mean to design strengths are about 1.1 and 2.0 for steel and concrete respectively. The mean strengths are the values possibly developed in real conditions in the structural members. The other important sources of overstrength are from the rounding-up of bars during proportioning of the reinforcement, the minimum steel content and detailing rules by gravity loads or by adjacent cross-sections, the Capacity Design magnification of column moments and the contribution of the slab reinforcement and effective width to the strength and the stiffness of the beam top flange… One more implicit source of overstrength in these cases is from the nonlinear analyses under unidirectional ground motions without taking into account the accidental eccentricity; meanwhile all structures have been designed for the affects of an accidental eccentricity of 5% dimensions of the structure in plan. All sources of overstrengths have contributed to an aggregate overstrength factor ranging in the present cases from about 1.33 to 2.25, as seen in Table 7-4.

Figure 7-31 illustrates the maximum inter-story drifts under the seismic excitations at design PGA as computed by Pushover and NLTH analyses; if it is also assumed that the local failure of beam-column joints is neglected. It is observed that for the frames designed in accordance with EC8 under serviceability earthquakes (with intensity equal to half of the ultimate ones) the maximum inter-story drifts are less than 0.75%, which is the drift limitation for serviceability earthquake in EC8.

Figure 7-32 shows the ratio of maximum to average inter-story drift, deduced from the comparison of the peak inter-story drift to the value at top. This ratio can be used as a measure of the tendency for soft-story mechanism development (Fardis, 1993). This ratio is proportional to the increase of the ductility class, from EC2 to DCM. Moreover, for the structures in EC8 group, although Capacity Design rules against the soft-story mechanism have been applied, the increase in this ratio is larger in DCM than in DCL. This means that the increased inelasticity of the structures due to lower design shear forces and higher ductility inherently tends to develop through soft-story mechanisms rather than global beam-sway ones. Also, the large drift ratios imply significant P-Δ effects, which have been accounted for in nonlinear analysis.

Figure 7-33 shows a comparison of the design PGA and the maximum resistible PGA of all frames studied. For the frames in EC2-group, and EC8-DCL frames, many of them do not have enough strength and ductility to resist the seismic actions at design PGA, expressed by the lower value of maximum resistible PGA compared to the design PGA of zone where the frame is located. It is also observed in the frames at the zone with PGA of 0.05g and 0.15g of EC8-group that although the frames designed with Low Ductility Class have much more quantities of steel contents than the ones designed with Medium Ductility Class, however, the maximum resistible PGA of the latter frames are equal or higher than the ones in Low Ductility Class. This is due to the lack of local detailing at beam-column joints in EC8-DCL frames and larger capacity of energy dissipation in the frames having Medium Ductility.

Table 7-4 also presents some characteristics of the studied frames from Pushover analysis such as: first yield displacement ($\Delta_{1,y}$) and corresponding base shear ($V_b^{1,y}$); ultimate base shear (V_b^u) and the corresponding displacement (Δ_m); energy dissipated in the systems (E) at failure; the failure mechanisms of the systems at ultimate state; the overstrength factors and the q-factor of the systems, computed by $q = \frac{V_b^u}{V_b^{1,y}} \times \frac{\Delta_m}{\Delta_{1,y}}$. These factors have been calculated based on the ductility of the 'equivalent' SDOF structures and overstrength of the original MDOF frames. It is clear that q-factors increase with the increase of the Ductility Class and are rather greater than the ones used in the design phase.

In conclusion, two types of deficiencies of the existing frames have been detected, including in complete load path due to early failure of beam-column joints and soft-story mechanisms. Both of these deficiencies are met in structures designed only to EC2. Incomplete load path is the shortcoming of the EC8-DCL frames. Many of those cannot reach to the performance point under the design PGA. It is clear that in zone having PGA of 0.15g, the frames should not be designed in accordance with Low Ductility Class.

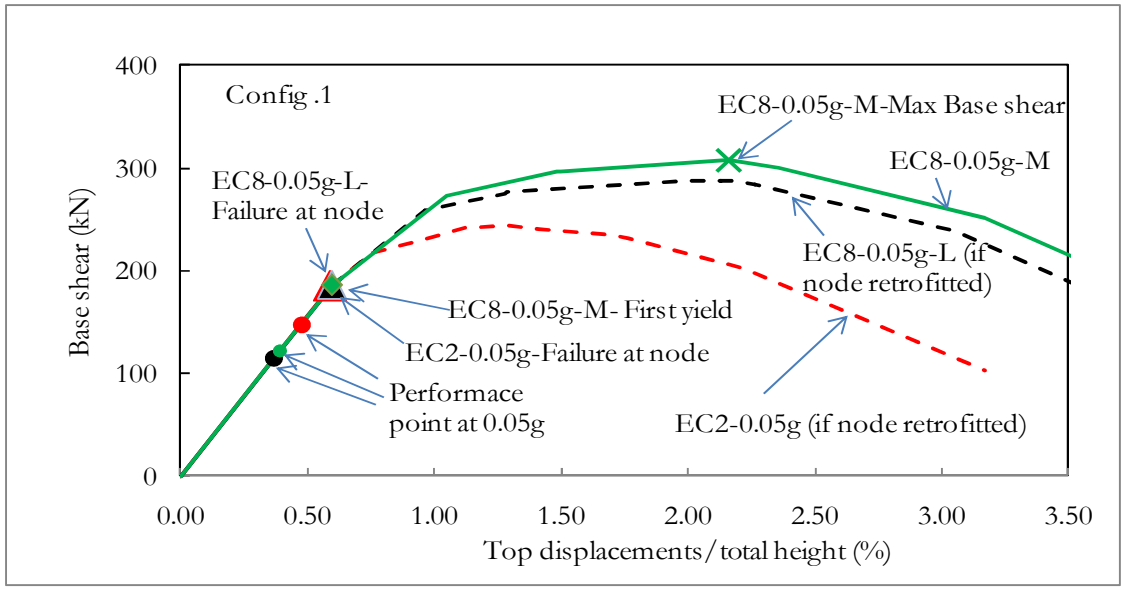

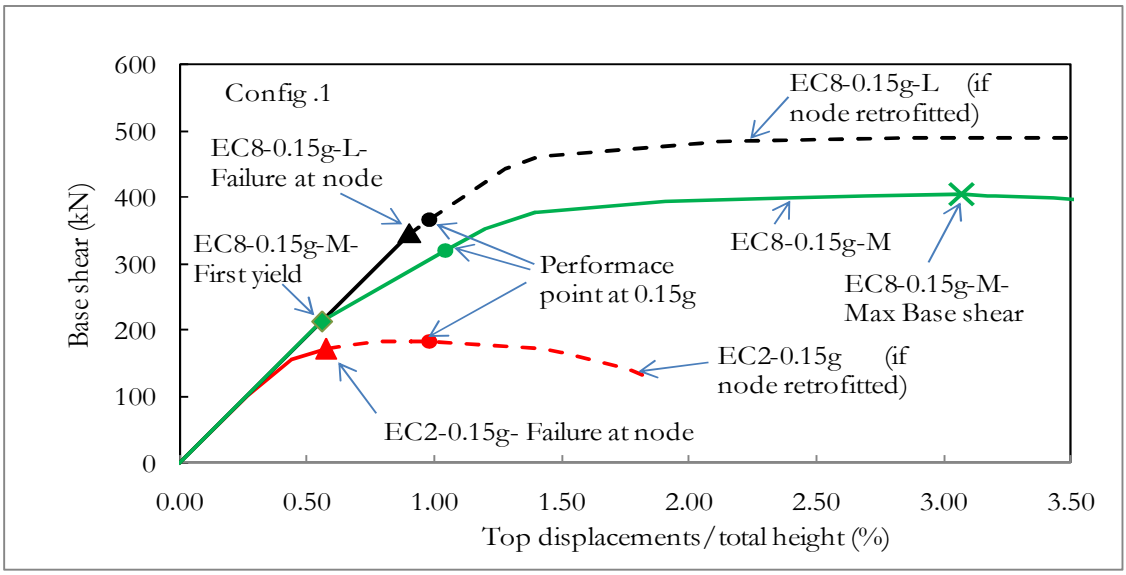

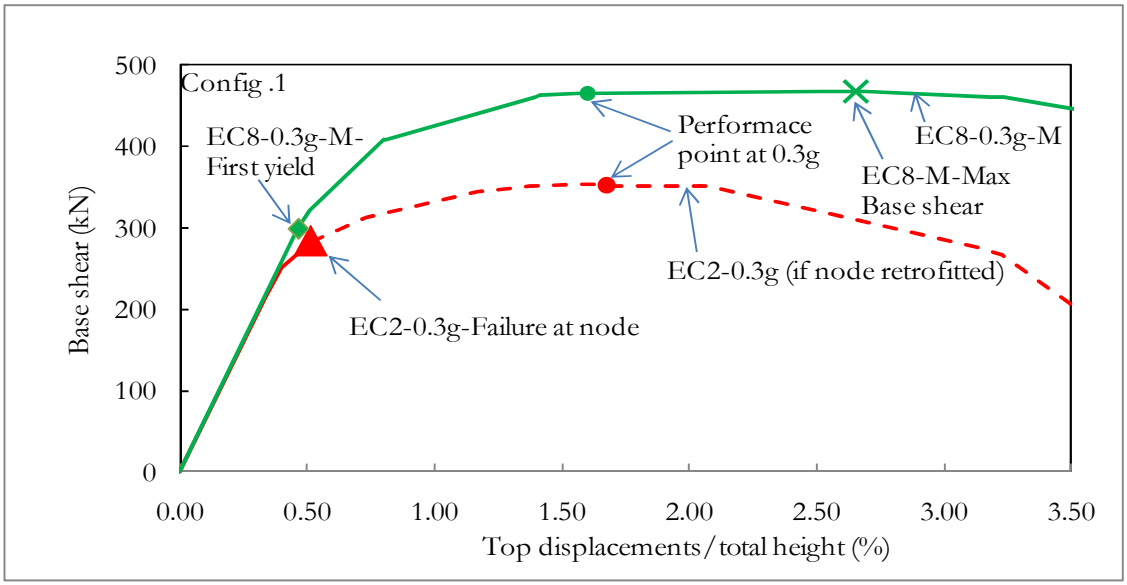

Figure 7-23 – Pushover curves and target drifts at design PGA established by Pushover analysis of RC-MRFs of Configuration 1

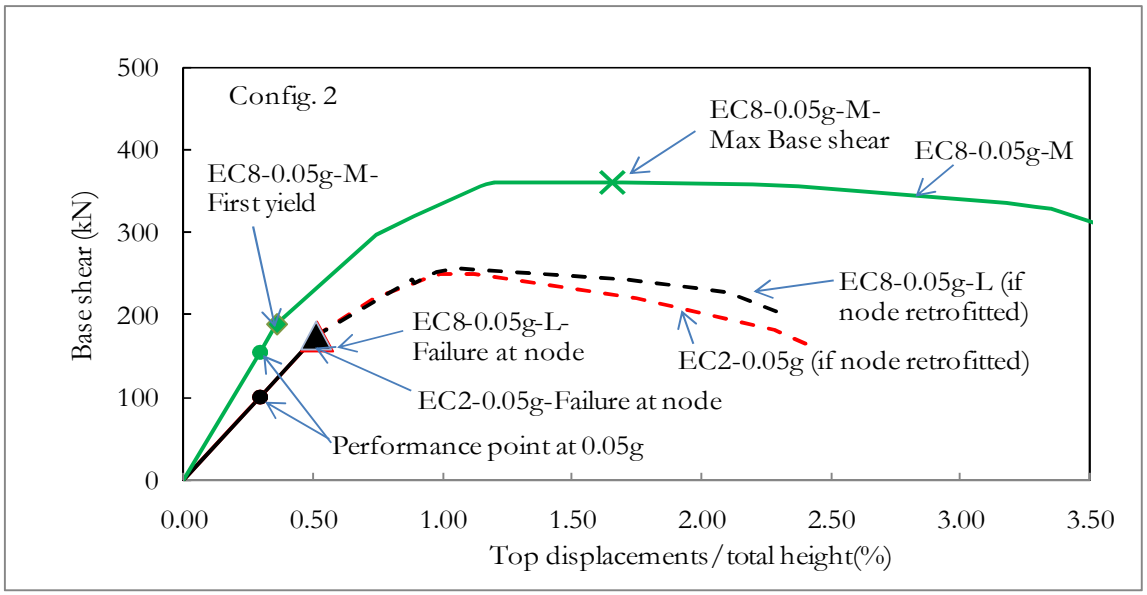

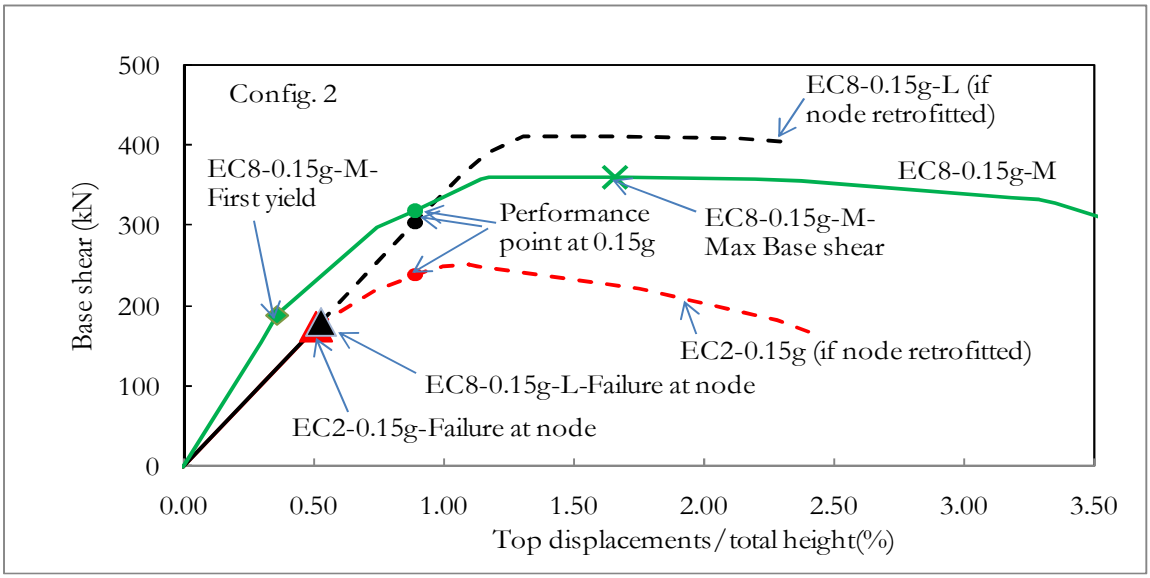

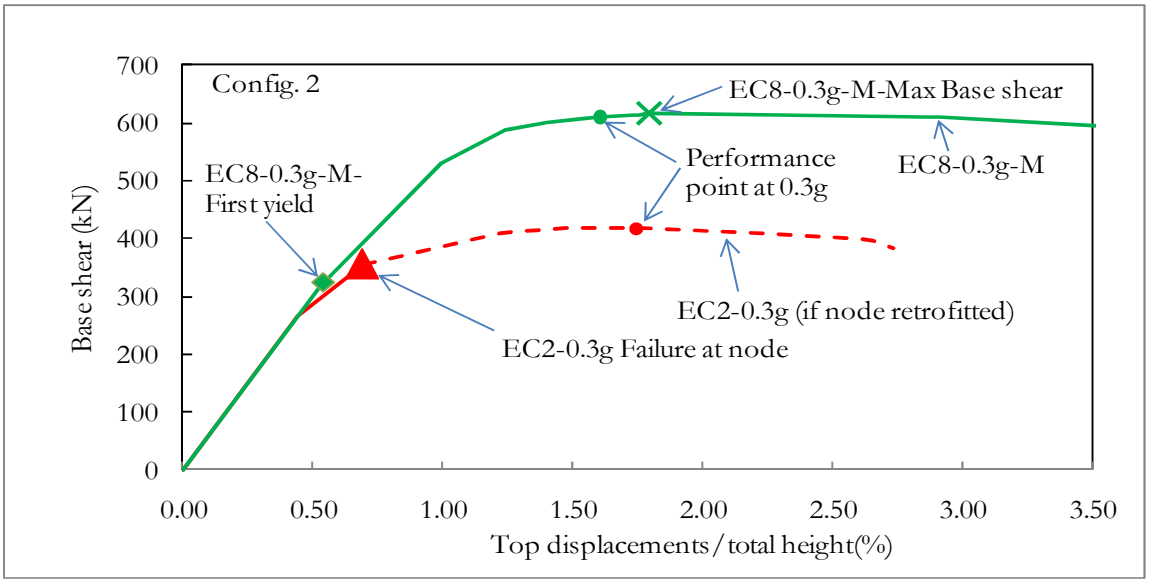

Figure 7-24 – Pushover curves and target drifts at design PGA established by Pushover analysis of RC-MRFs of Configuration 2

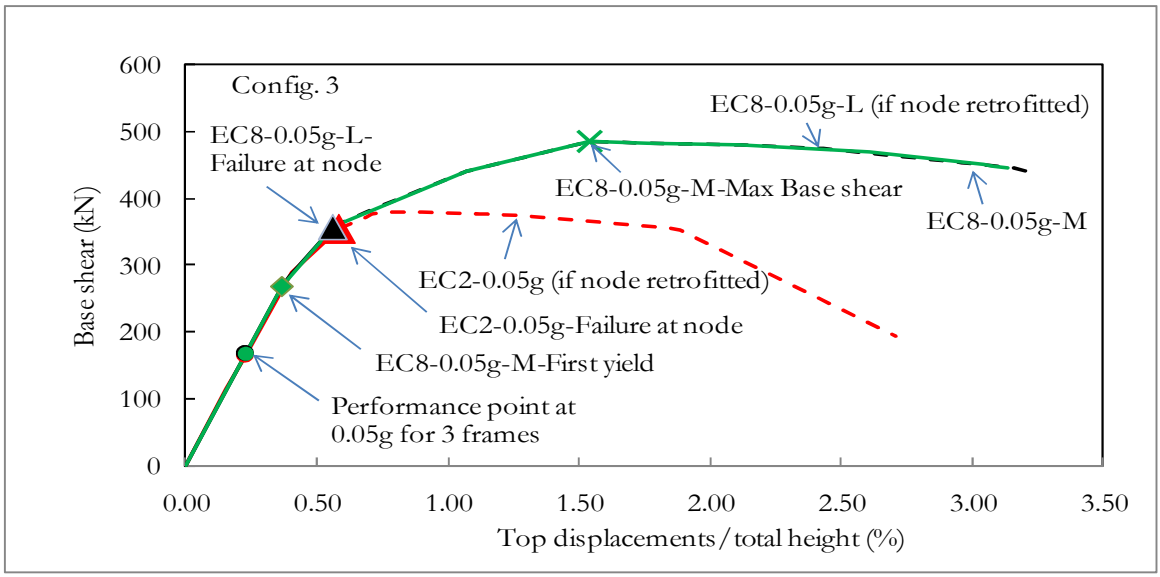

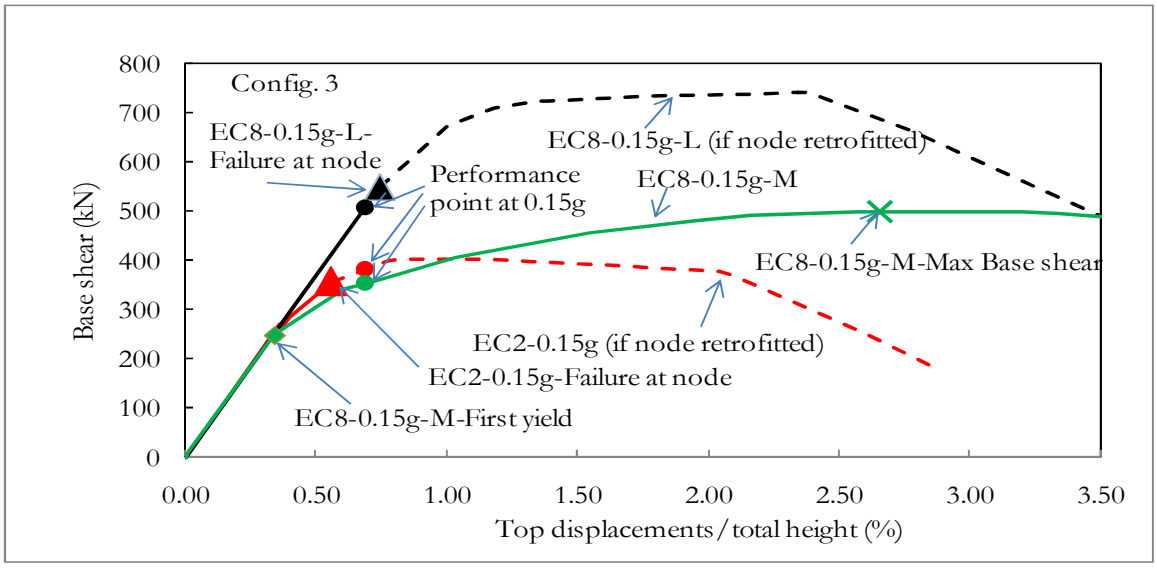

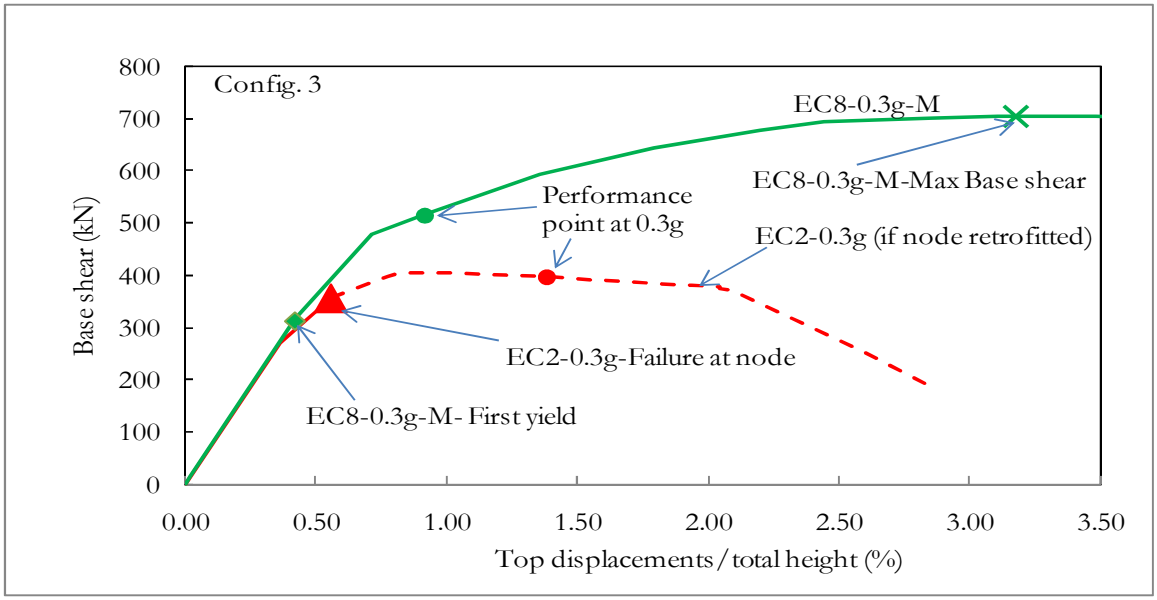

Figure 7-25 – Pushover curves and target drifts at design PGA established by Pushover analysis of RC-MRFs of Configuration 3

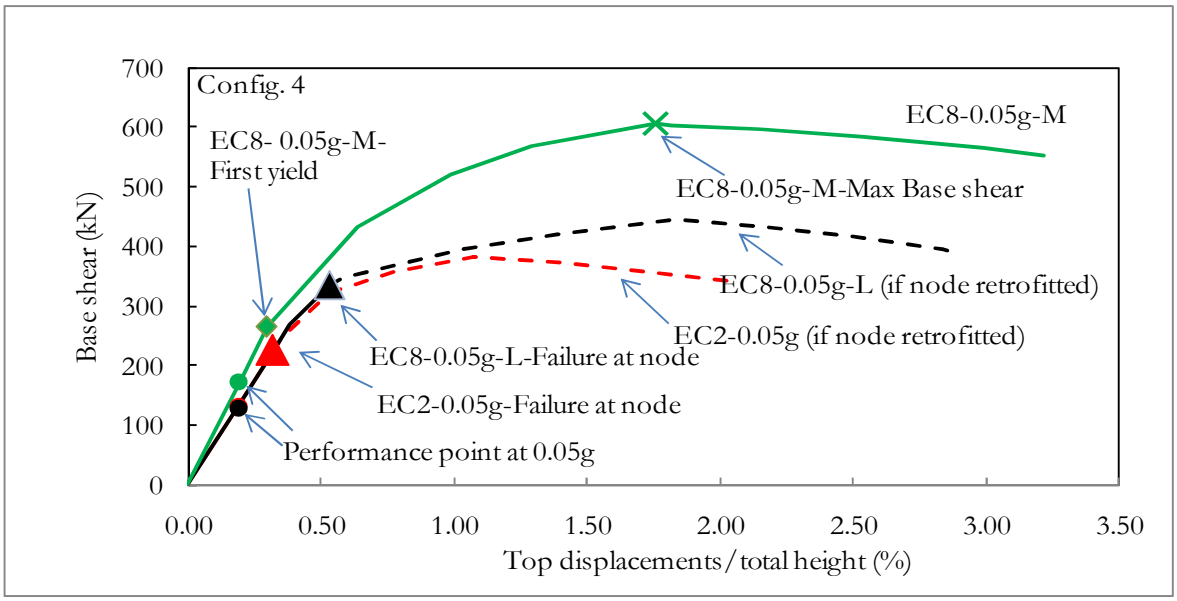

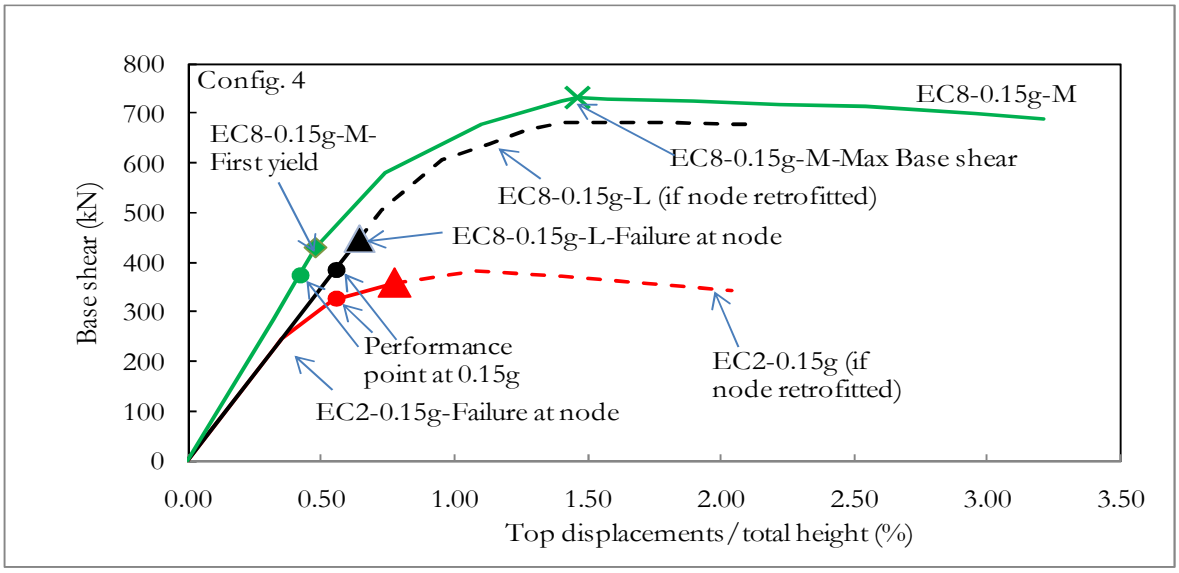

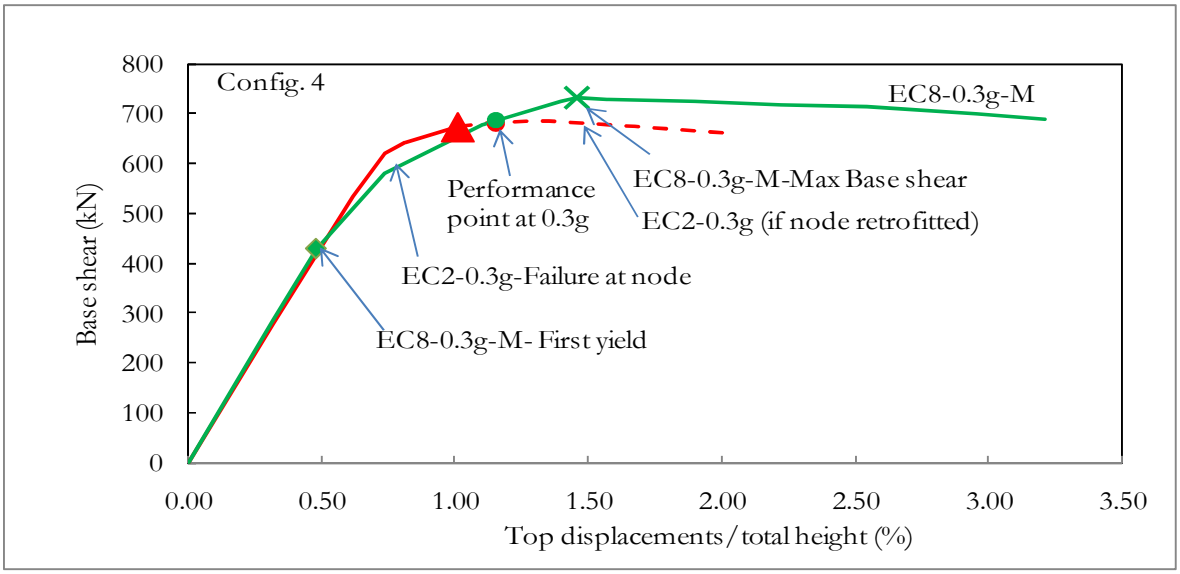

Figure 7-26 – Pushover curves and target drifts at design PGA established by Pushover analysis of RC-MRFs of Configuration 4

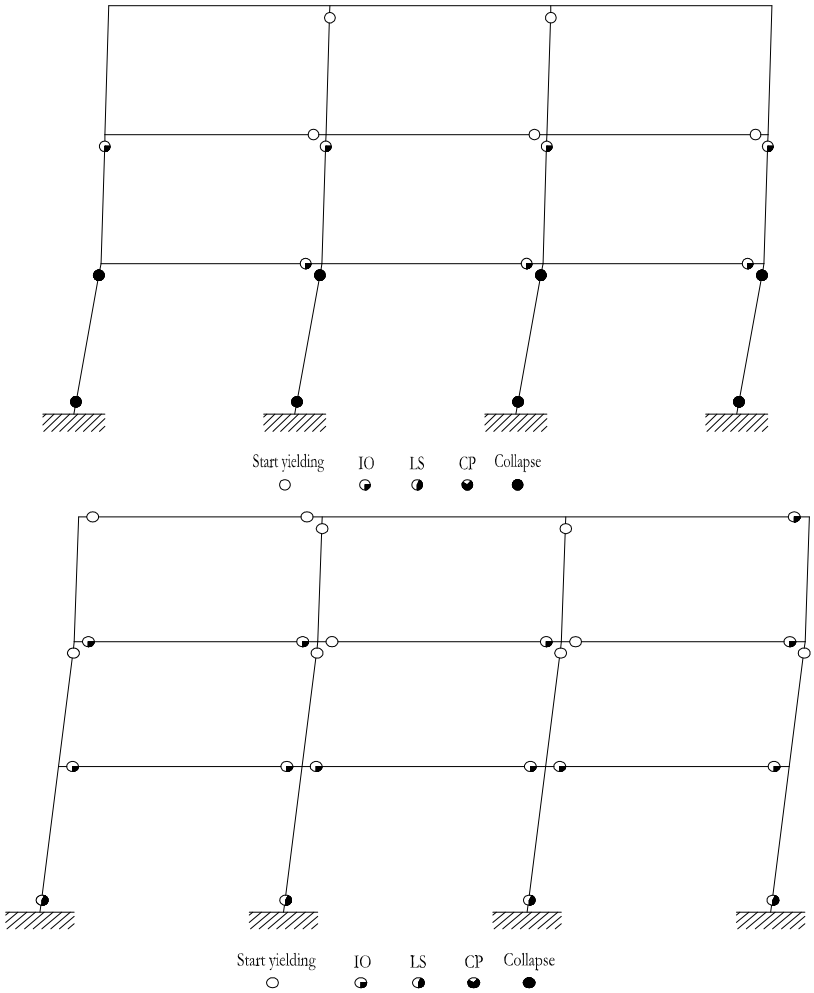

Figure 7-27 – Typical failure mechanisms of the studied frames in EC2 group (if node retrofitted)

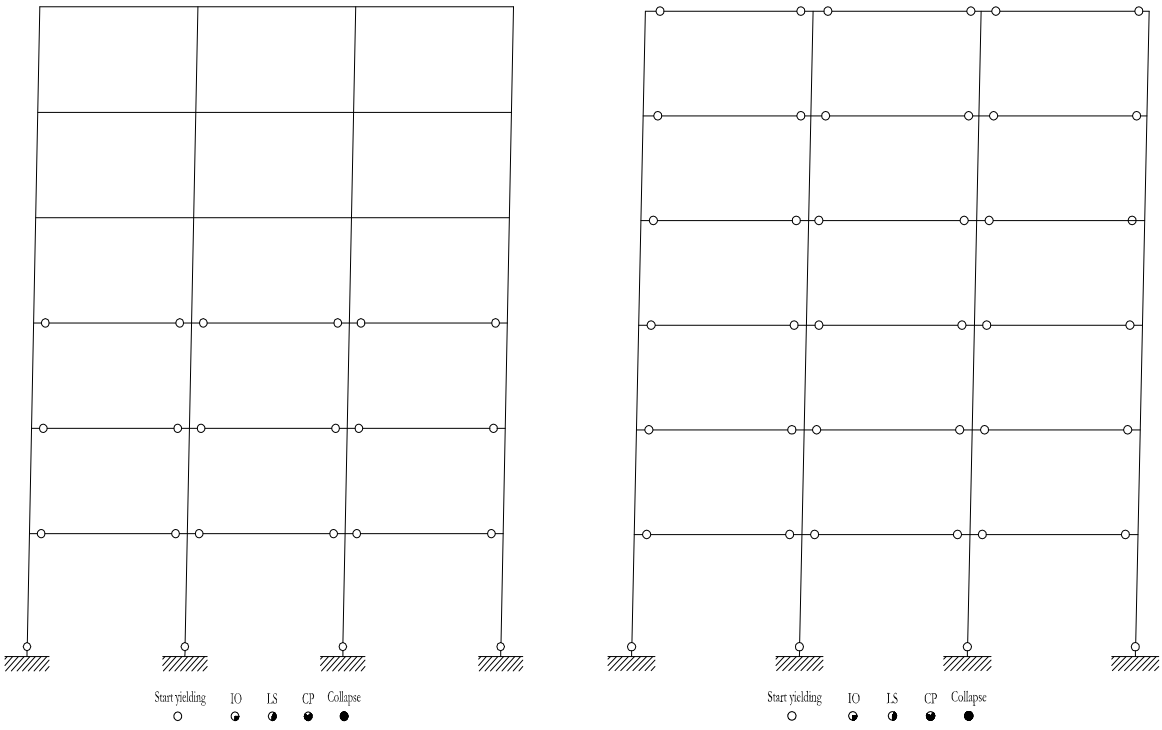

Figure 7-28 – Typical failure mechanisms of the EC8-DCM frames and EC8-DCL if node retrofitted

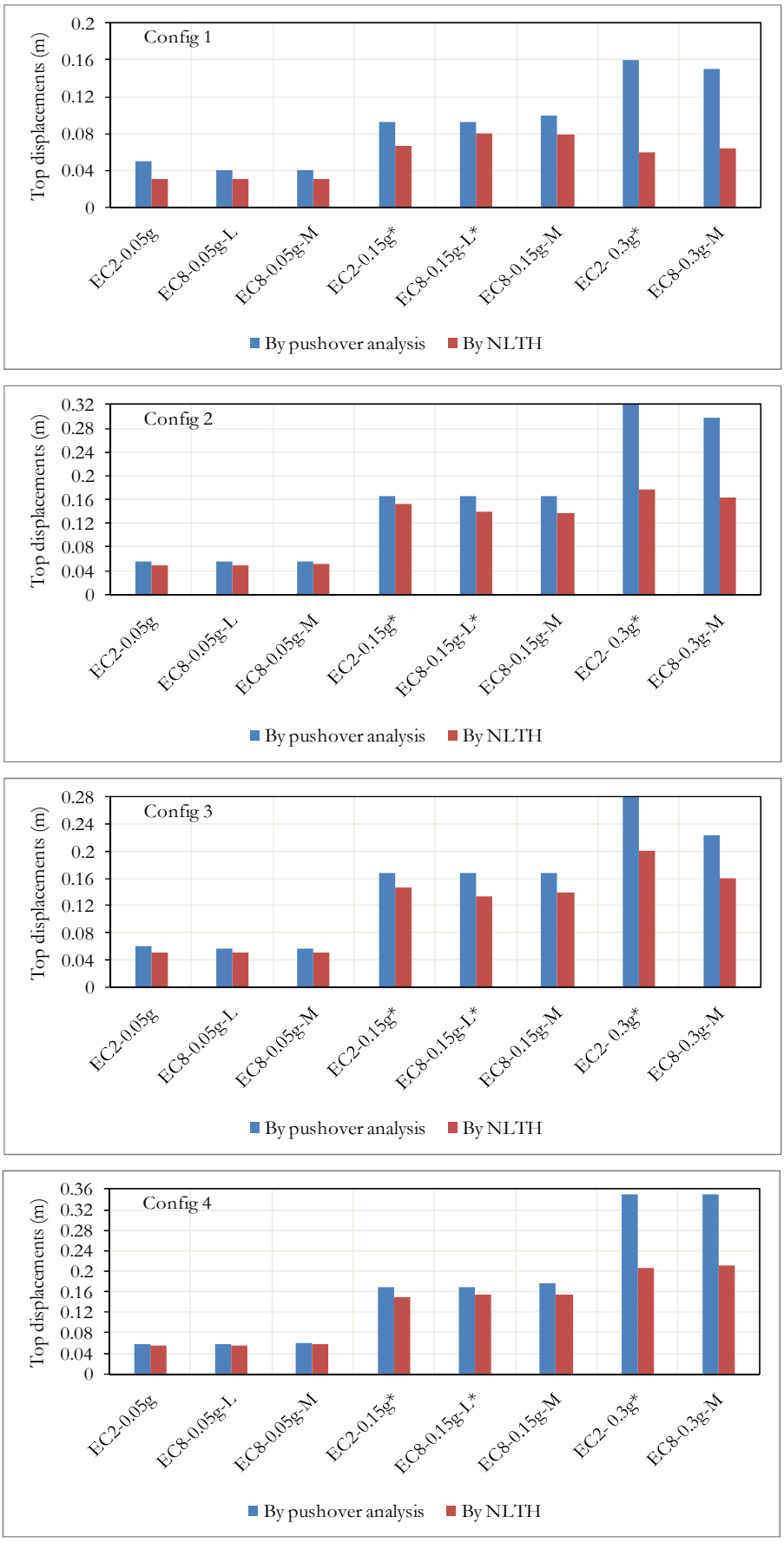

Figure 7-29 – Top target displacements established by Pushover and maximum top displacements established by NLTH of studied RC-MRFs under design PGA (* - frames with node retrofitted)

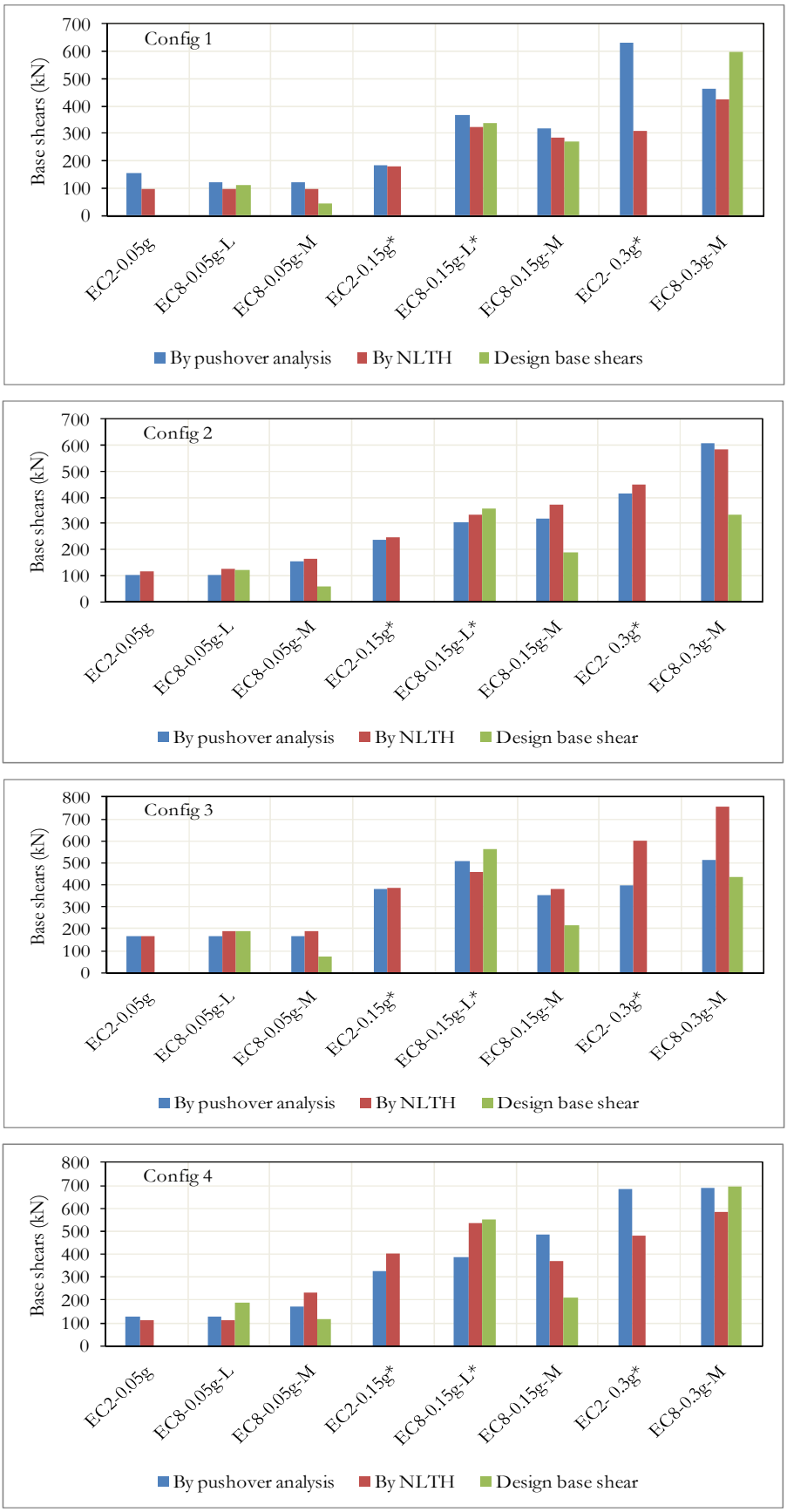

Figure 7-30 – Design base shears, base shears corresponding to target displacements established by Pushover and maximum base shears established by NLTH of studied RC-MRF under design PGA (* - frames with node retrofitted)

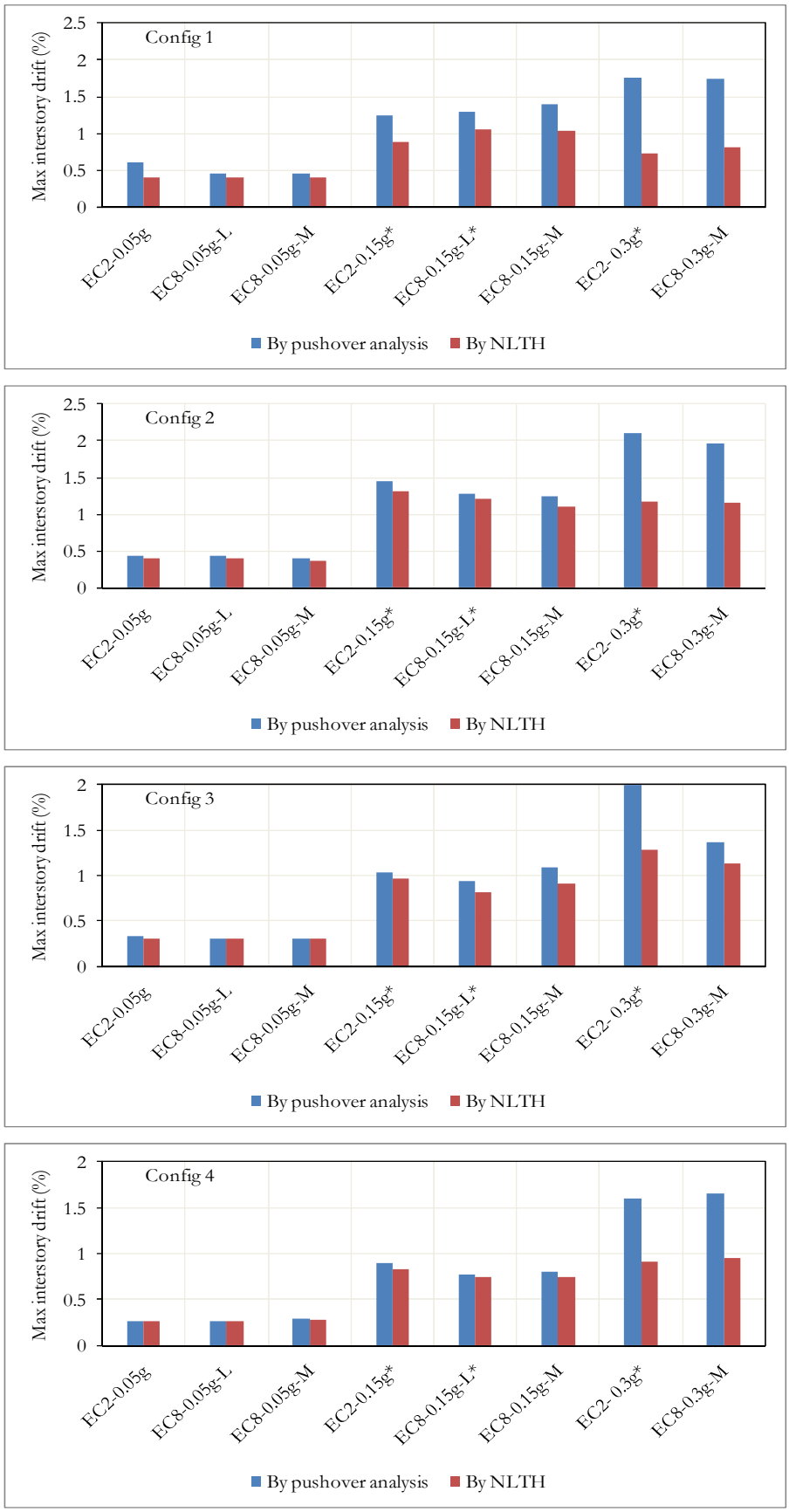

Figure 7-31 – Maximum inter-story drifts at target displacements established by Pushover and maximum inter-story drifts established by NLTH of studied RC-MRFs under design (* - frames with node retrofitted)

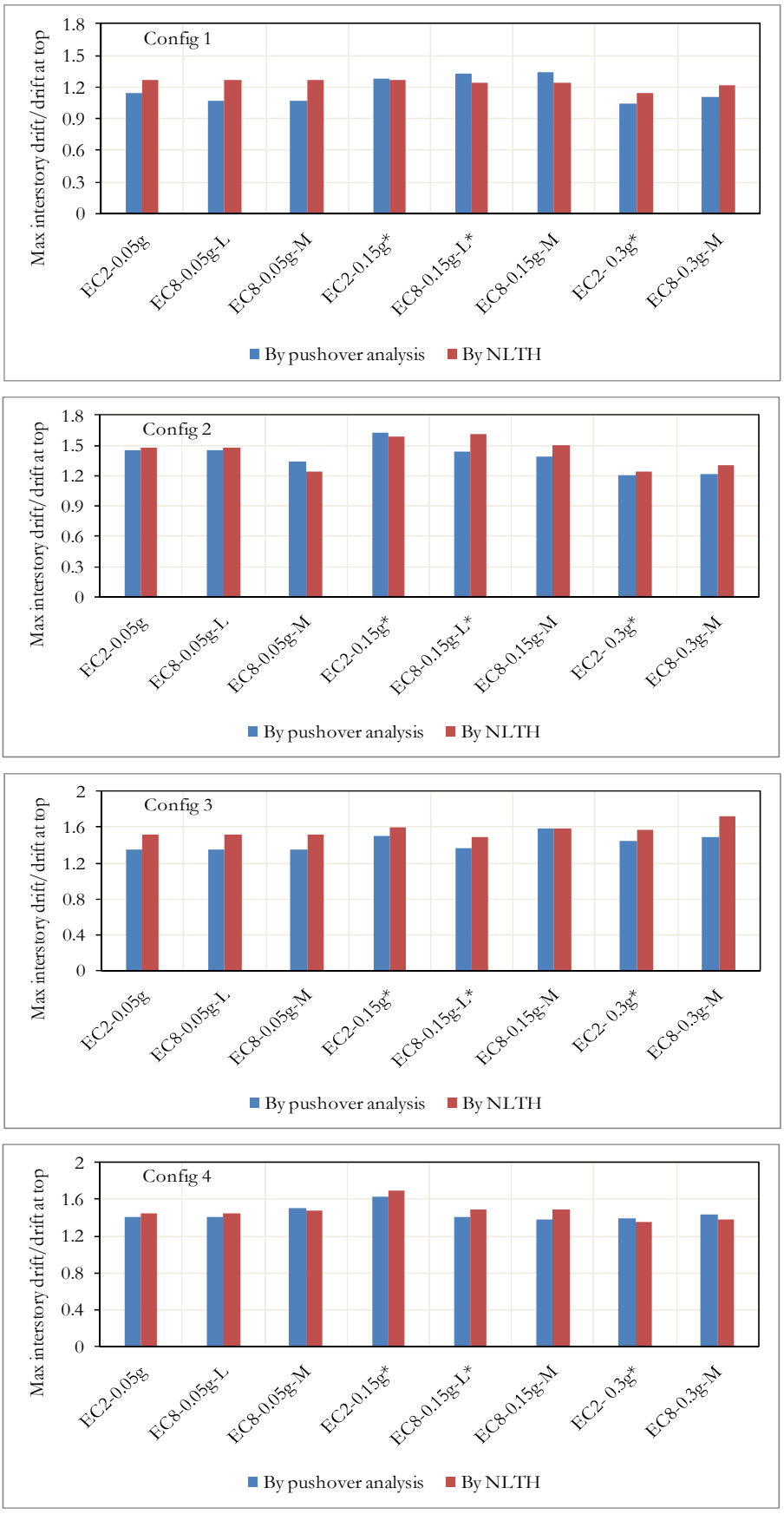

Figure 7-32 – Ratios between maximum inter-story drifts and top drifts at target displacements of studied RC-MRFs under design PGA established by Pushover and NLTH analyses (* - frames with node retrofitted)

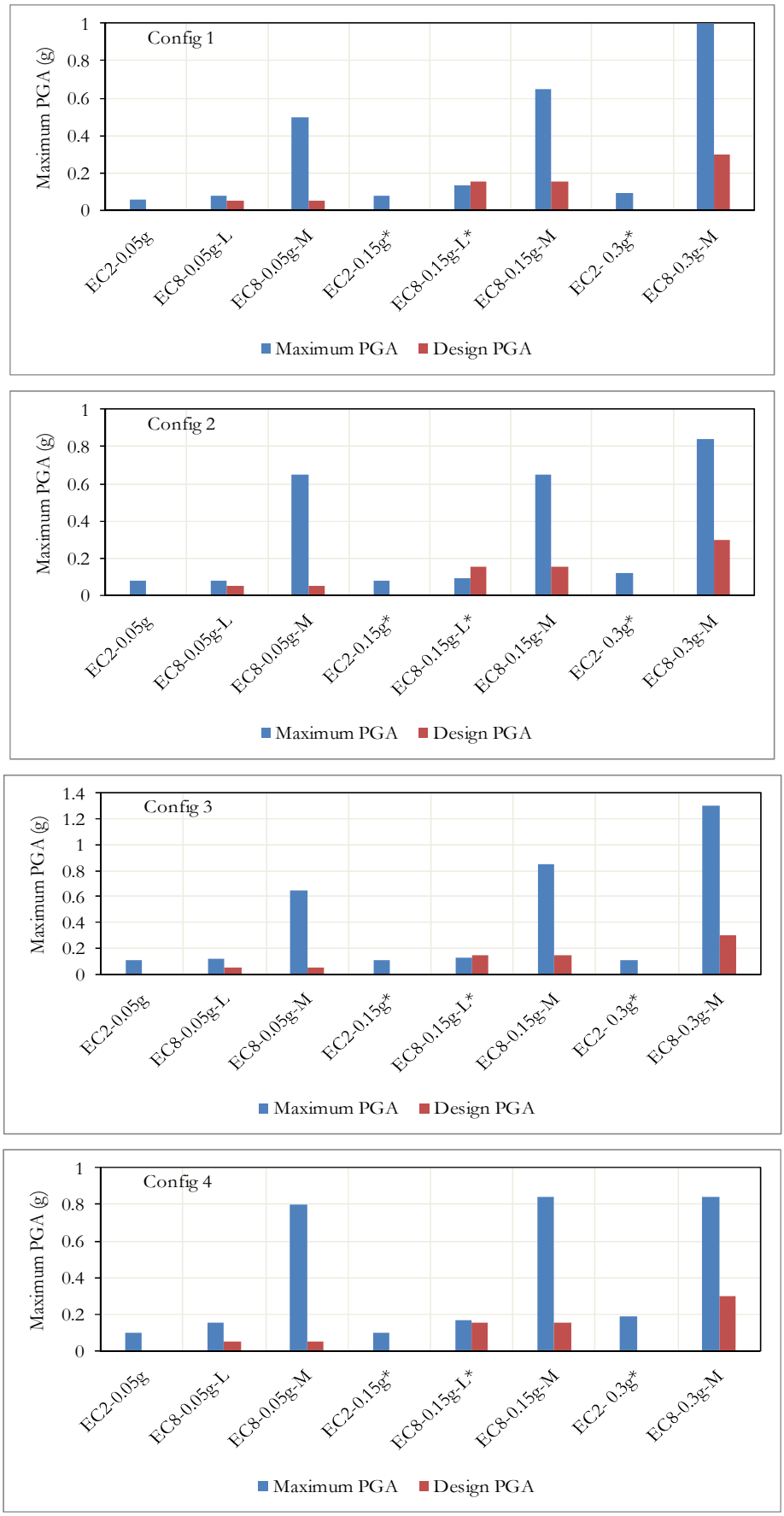

Figure 7-33 – Design and maximum resistible PGA of studied RC-MRFs established by Pushover analysis (* - the frames need node retrofitted)

Table 7-4 – Response of the frames by pushover analysis

Case	Group	$V_b^{1,y}$ (kN)	$\Delta_{1,y}$ (m)	V_b^u (kN)	Δ_u (m)	E (kNm)	Criteria of failure	Overstrength	q
1	EC2-0.05g	184.6	0.056	184.6	0.056	5.18	Node	1.00	-
	EC2-0.15g	100.7	0.03	172.6	0.06	5.52	Node	1.71	-
	EC2-0.3g	213.8	0.03	283.7	0.05	7.73	Node	1.33	-
	EC8-0.05g-L	186.0	0.057	186.0	0.057	5.26	Node	1.00	-
	EC8-0.05g-M	186.0	0.057	307.3	0.21	46.2	Beam sway	1.65	6.1
	EC8-0.15g-L	346.1	0.09	346.1	0.09	31.2	Node	-	-
	EC8-0.15g-M	214.2	0.05	403.9	0.29	92.8	Beam sway	1.89	10.9
	EC8-0.3g-M	298.2	0.04	468.3	0.25	98.3	Beam sway	1.57	9.8
2	EC2-0.05g	174.7	0.10	174.7	0.10	8.29	Node	-	-
	EC2-0.15g	174.7	0.10	174.7	0.10	8.29	Node	-	-
	EC2-0.3g	264.9	0.08	354.7	0.13	25.0	Node	1.34	-
	EC8-0.05g-L	174.7	0.10	174.7	0.10	8.29	Node	1.00	-
	EC8-0.05g-M	188.0	0.07	360.3	0.31	81.8	Beam sway	1.92	8.5
	EC8-0.15g-L	360.9	0.20	180.3	0.10	8.84	Node	-	-
	EC8-0.15g-M	188.0	0.07	360.3	0.31	81.8	Beam sway	1.92	8.5
	EC8-0.3g-M	324.0	0.10	614.9	0.33	140.0	Beam sway	1.90	6.3
3	EC2-0.05g	114.6	0.04	355.1	0.14	28.8	Node	3.10	10.8
	EC2-0.15g	356.5	0.14	356.5	0.14	27.1	Node	-	-
	EC2-0.3g	356.5	0.14	356.5	0.14	27.1	Node	-	-
	EC8-0.05g-L	268.3	0.09	357.2	0.14	27.0	Node	1.33	2.1
	EC8-0.05g-M	268.3	0.09	485.3	0.38	130.0	Beam sway	1.81	7.6
	EC8-0.15g-L	547.4	0.18	294.8	0.10	14.4	Node	-	-
	EC8-0.15g-M	247.3	0.08	500.0	0.65	254.0	Beam sway	2.02	16.4
	EC8-0.3g-M	312.2	0.10	703.0	0.78	427.0	Beam sway	2.25	17.6
4	EC2-0.05g	245.9	0.11	245.9	0.11	13.3	Node	-	-
	EC2-0.15g	245.9	0.11	245.9	0.11	13.3	Node	-	-
	EC2-0.3g	620.2	0.23	620.2	0.23	72.3	Node	-	-
	EC8-0.05g-L	267.8	0.12	333.9	0.16	15.7	Node	1.25	1.7
	EC8-0.05g-M	264.6	0.09	604.8	0.54	234.0	Beam sway	2.29	13.7
	EC8-0.15g-L	504.3	0.22	447.7	0.196	43.9	Node	-	-
	EC8-0.15g-M	428.7	0.15	730.4	0.48	243.0	Beam sway	1.70	5.45
	EC8-0.3g-M	428.7	0.15	730.4	0.48	243.0	Beam sway	1.70	5.45

7.7. Concluding remarks

In this Chapter, general methods and common models used for seismically assess the existing RC-MRFs in relevance with EC8 have been introduced. Amongst those models, the linear beam elements with two concentrated plastic hinges at two ends of beams and columns has been adopted for evaluating the seismic response of the studied RC-MRFs, designed in Chapter 6. Additionally, two nonlinear methods including Pushover and NLTH analyses have been used to analyse the structures. Hysteretic behaviour of the nonlinear plastic hinges of beams and columns are based on pivot models, suggested by Dowell et al. (1988). Performance criteria of the frames are based on FEMA 356 (2000). SAP 2000 has been selected as the code for performing the nonlinear static and nonlinear dynamic analyses. Four accelerograms, generated by GOSCA (Denoel, 2001), has been used as the seismic input for NLTH analysis.

Thirty two RC frames designed in the previous chapter have been seismically assessed in very detail. The seismic performance of the frames in EC8-group, which have been designed in accordance with both EC2 and EC8, are all able to meet the design goal, implying that they can reach the target displacement and develop the desired failure mechanisms. For the frames in EC2-group, there are some deficiencies found such as the incomplete load path or the soft-story failure.

A comparison of the results between Pushover and NLTH analyses has shown that Pushover in conjunction with N2 methods, adopted by EC8, always over-estimates the seismic response of the existing frames: the target displacements imposed by the earthquake are greater in the Pushover evaluation than the one in the NLTH. The results of Pushover analysis for the large-period frames rather largely differ from the results obtained by NLTH analysis.

The failure of studied RC-MRFs, obtained by Pushover, has been considered to take place under three circumstances: local failure, attainment of maximum resistance or too large inter-story drift ratios. The two first criteria are observed in low-story frames (Configurations 1, 2) and the later is observed in the taller structures (Configurations 3 and 4). Frames in EC2-group have exhibited some undesired failure mechanisms such as soft-story or local brittle failure due to crushing of the concrete. In contrast, all frames in EC8-group have developed the favourable mechanisms like full or partial beam-sway mechanisms.

Parallel to predicting the deficiencies of the existing RC-MRFs, their q-factors and maximum seismic capacity has also been evaluated based on Pushover analysis. It is clear that the q-factors obtained from analyses for DCM design are higher times than those from the code by a factor of about 1.5 to 2.

8. ON THE USE OF EMP TO SEISMICALLY RETROFIT OR UPGRADE RC-MRFS

8.1. Introduction

Chapter 6 and 7 have presented general criteria of EC2 and EC8 for designing and seismically evaluating RC-MRFs. A number of typical RC-MRFs, used as the main lateral resisting systems to resist lateral forces, have been introduced. A part of them has been designed according to both EC2 and EC8. The others have been designed only in accordance with EC2. The approach to design RC-MRFs in accordance with EC8 is based on force-based design with two different ductility classes. The seismic performance and deficiencies of the RC-MRF studied have been investigated with aids of Pushover and Nonlinear Time History Analyses. The performance criteria of the frames' components have been based on FEMA 356 (2000).

It has been clear that under a given ground motion there have been some undesired failure modes of the frames, especially for the ones in EC2 group and the ones designed to EC8-DCL. In these frames, failure modes such as the failure of beam-column joints and soft-story mechanism, leading to incomplete load path deficiency of the existing frames, have been detected. For the other ones, designed in relevance with Medium ductility class (DCM), it has been observed that partial or full beam sway failure modes have dominated seismic behaviour of the frames at the ultimate state.

The basic idea of this chapter is first to present the application of the EMP in seismically retrofitting and/or upgrading the existing RC-MRFs. The final aim is to develop a design procedure that can be used to design and select the properties of EMP in order to seismically retrofit or upgrade the RC-MRFs. The Direct Displacement-Based Design (DDBD) method is chosen to carry out the process.

For convenience, characteristics of different types of EMP under shear such as geometrical configurations, ultimate resistances, displacements and ductility, are first recalled at the beginning sections. The need of using DDBD to seismically design the structure with EMP is then introduced. Fundamental background of DDBD is summarized as well. The EMP will be preliminarily designed to carry all or a part of seismic forces generated by the earthquake. Their influences on overall and local behaviour of the frames after retrofitting will be examined as well. Advantages and disadvantages of the EMP for this application will be discussed in detail in the final section.

8.2. Summary of geometrical characteristics and seismic behaviour of EMP under shear

8.2.1. Summary of typically geometrical configurations of EMP

Out of two types of EMP, as studied in Chapter 4 and 5, the flatten type of EMP is more efficient for the use of seismically retrofitting RC-MRF. The advantage of the flatten type over the normal type comes from three main points: geometrical configuration, strength and stiffness. Thanks to its flatness without overlap between the stitches, the flatten type is easier to connect to the boundary frames than the normal type if welding is used. For the same geometrical configuration, the flatten type has greater strength and stiffness than the normal type. Table 4-1 and 8-2 summarise all the available flatten type profiles of EMP to date. Symbols LD, CD, LD_{in}, CD_{in}, A, B are defined at Figure 5-30.

Table 8-1 – Typical available EMP profiles

Type of EMP	LD (mm)	CD (mm)	interior LD (mm)	interior CD (mm)	A (mm)	B (mm)	$\alpha = \frac{A}{length_{bar}}$
A115.60.45.20	115	60	100	55	4.5	1.8	0.074
A86.46.43.30	86	46	74	37	4.3	2.7	0.095
A.62.34.25.15	62	34	50	30	2.5	1.4	0.078

Table 8-2 – Typical available EMP profiles (continued)

Type of EMP	LD (mm)	CD (mm)	interior LD (mm)	interior CD (mm)	A (mm)	B (mm)	$\alpha = \frac{A}{length_{bar}}$
A62.34.30.20	62	34	50	28	3	1.8	0.094
A62.34.45.30	62	34	45	25	4.5	2.8	0.147
A51.27.35.30	51	27	41	20	3.5	2.7	0.136
A43.23.25.15	43	23	33	18	2.5	1.4	0.116
A43.23.45.30	43	23	30	15	4.5	2.8	0.219
A31.16.23.15	31	16	26	12	2.3	1.3	0.145
A28.15.25.10	28	15	20	11	2.5	0.9	0.183
A28.15.25.15	28	15	20	11	2.5	1.4	0.183
A21.12.17.15	21	12	16	9	1.7	1.3	0.160
A16.7.10.06	16	7	10	4	1	0.5	0.142
A16.7.18.10	16	7	10	3	1.8	0.9	0.259
A10.6.10.06	10	6	6	3	1	0.5	0.218
A10.5.12.10	10	5	6	3	1.2	0.9	0.268

8.2.2. Summary of seismic behaviour of EMP under shear

The complete study on EMP under shear loading has been presented in Chapter 3, 4 and 5. The main results related to the seismic performance of EMP are recalled herein.

Monotonic loading

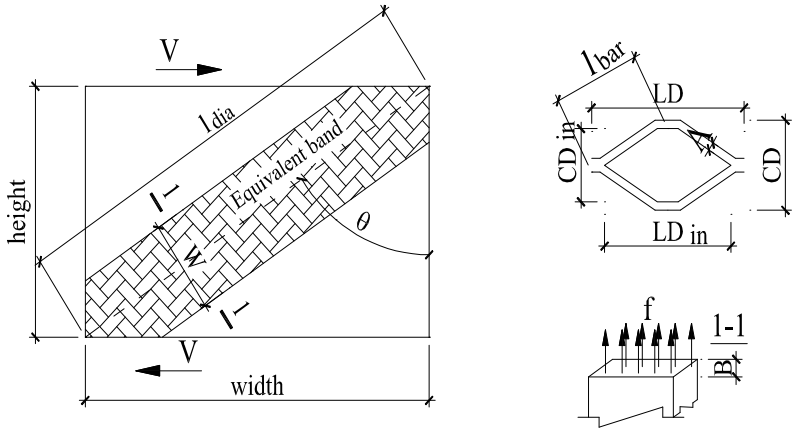

Figure 8-1 – The equivalent band of the EMP

When an EMP is subjected to a monotonic shear load, it will similarly work as one diagonal band in tension. The tension behaviour of the band can represent the shear behaviour of the EMP. In short, the shear resistance of an EMP can be expressed as following expression:

$$V = \gamma.\alpha.l_{dia}.B.f = W.B.f \qquad \text{Equation 8-1}$$

Where: l_{dia}, B, f are explained in Figure 5-30; $\alpha = A/l_{bar}$;

γ is the factor depending on the ratio between width/height of the EMP.

γ = 0.35 for square EMP; γ = 0.23 for rectangular EMP with ratio 2/1;

γ = 0.18 for rectangular EMP with ratio 3/1

$W = \gamma.\alpha.l_{dia}$ is the effective width of the EMP

Cyclic loading

Based on the results of over 200 numerical simulations for different profiles and dimensions of EMP cyclically loaded in shear, an approximate bilinear model for hysteretic loops of the EMP, surrounded by a very rigid, pin jointed frame is re-illustrated in Figure 5-47 and re-described herein. V_{cr}, V_y and V_u are the critical, yield and ultimate shear forces of the EMP, and Δ_y, Δ_p, Δ_u are the yield, plastic and the ultimate displacements, respectively. From points O to A the response is elastic and linear. In fact, at this stage there is a shift of stiffness of the EMP due to buckling. However, the critical load V_{cr} approximately equals zero. Therefore, the behaviour before global buckle is negligible. After buckling an inclined tension field develops, and the EMP yields when the shear load equals V_y. From A to B_1, the EMP strains plastically and from B_1 to C_1 it unloads elastically with the line B_1C_1 parallel to OA. The length OC_1 is proportional to the plastic elongation of the tensile diagonal. At the beginning of load reversal, there is a residual displacement of the EMP due to the plasticity. The plastic contraction of the opposite diagonal occurs. The stiffness of the EMP at this stage is equal to zero. The length OD_1 is proportional to the corresponding plastic contraction of this diagonal, and is computed by:

$OD_1=\beta OC_1$. Equation 8-2

The ratio β, taken as 0.5, is obtained based on the plastic theory of a thin plate. The opposite tension field behaviour continues from D_1 to E_1. Contribution of compressive band, when loads are reversed, is also negligible. A new inclined tension field, corresponding to the line D_1E_1, will develop in the opposite diagonal when compressive stresses in this diagonal are fully recovered. At the point E_1 the shear load is equal to $-V_y$. From E_1 to F_1 the EMP strains plastically in the opposite direction, and it unloads from F_1 to G_1, parallel to OA. The plastic elongation of the panel diagonal D-D during the second half of the cycle is proportional to the length G_1D_1. Hence the length C_1H_1 is given by:

$C_1H_1=\beta G_1D_1$. Equation 8-3

At H_1, the EMP buckles and from H_1 to B_1 an inclined tension field develops again. From B_1, the second cycle is similar to the first one. The length of G_1D_2 and C_2H_2 are given by:

$G_1D_2=\beta H_1C_2$ and $C_2H_2=\beta G_2D_2$. Equation 8-4

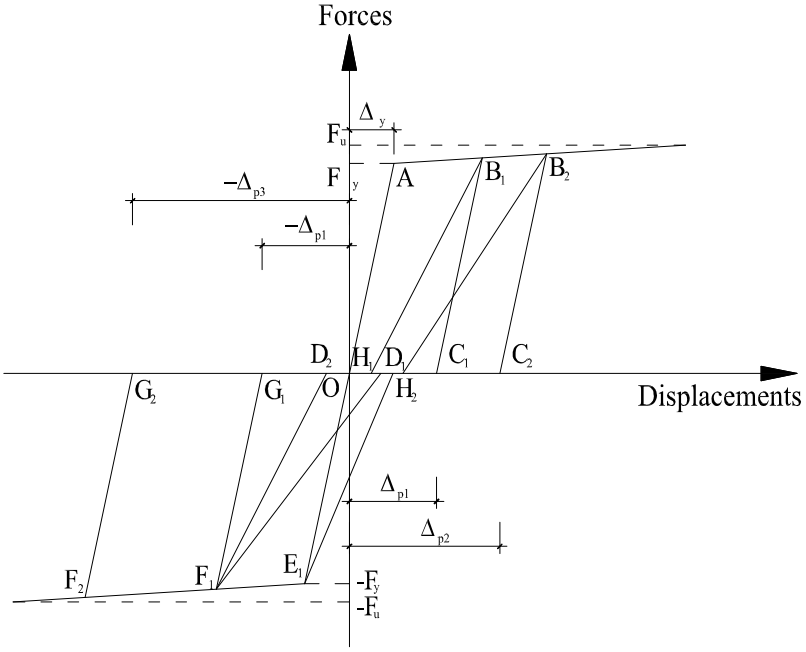

Figure 8-2 – The simplified hysteretic behaviour of EMP

8.3. Background of Direct Displacement-Based Design (DDBD)

8.3.1. The need of Direct Displacement-Based Seismic Design approach for retrofitting RC-MRFs by using EMP

In the last years, the importance of displacements generated in the structure by the seismic excitations has been recognised. Methods based on displacements which allow designing the structures to meet much closer the requirements of Performance-Based Design are becoming accepted throughout the engineering community. One method is known as Direct Displacement-Based Design (DDBD) (Priestley, 2007).

Some main shortcomings of Force-Based Design have been briefly introduced in chapter 6. This section will discuss some essential reasons why DDBD has been selected to seismically design the EMP in order to retrofit or upgrade the existing RC-MRFs. In particular, the need of using DDBD rather than Force-Based Design in seismic design or retrofitting of structures is explained as follows.

First, it has also long been realised that for design or retrofitting of structures based on forces, the results are not well suited to Performance-Based Design because the performance criteria are usually checked as the final design step. Moreover, especially for retrofitting work where the behaviour of the structure to be retrofitted is already known, it is much easier for the designers to know the performance states of the structure if it is designed to meet a target displacement. Thanks to allowing designing to a specific performance level, DDBD is more flexible than force based design in accuracy of the design objective.

Second, interdependency of strength and stiffness in Force-Based Design makes it not correctly model the structures, especially for RC ones, in seismic situations where some degradation of stiffness due to concrete cracking has to be taken into account. The degradation of stiffness in Force-Based Design is usually assumed to be 30 to 60 per cent of the gross stiffness without cracking. This value of stiffness is taken to calculate the periods of the structure and then to determine the base shear that is generated by the seismic action. Based on this base shear, internal forces of the structure will be determined and the strengths or resistances of the structural components will be determined afterwards. The cross-sectional dimensions at the preliminary steps have significant effects on the reinforcement at the final stage of the design process which decides the strength of the structure; and the strength (depending on the reinforcement configuration), in turn, will more or less change the stiffness of the structural members. Therefore, the overall stiffness of the structure will be changed leading the changes of periods and base shear. This change will have influence on the inertial forces of the structure and therefore on the strength again. Thus, iterative process is always needed to get more exact results. However, this work is rarely implemented in Force-Based Design.

Third, based on the assessment of the existing frames, their deficiencies have been detected. The retrofit work should be able to improve the seismic performance of the existing frames. Therefore, under a given earthquake the retrofitted frames have to be deflected to a certain drift or displacement at which the target performance is met. It is very difficult to fulfil this task with Force Based Design in which the strength is the primary concern.

Finally, retrofitting with the use of Force-Based Design, it is well known that a ductility class (DC) must be selected at preliminary design for the structures. This DC is represented by a q factor, which is used to determine the base shear and member forces and to design the sections. In most cases, the base shears and the design ones are not consistent when the structure is re-checked by Pushover or NLTH analyses. Therefore, choosing DC for a new design of a RC-MRF is somehow affected by feeling and experience. In addition, for the retrofitting work using a combination of EMP and RC-MRFs, the q factor representing the DC of this new system cannot be predicted correctly at the beginning of retrofitting process. Therefore, Force-Based Design in this context may be not suitable.

8.3.2. Background of Direct Displacement-Based Design (DDBD) for RC-MRFs

A complete work on figuring out the procedures of DDBD in designing and retrofitting structures under seismic actions has been proposed by Priestley et al. (2007) and Calvi (2009). The following section is mostly based on these books.

8.3.2.1. General background of DDBD

In the DDBD, the most important point for designing or retrofitting a multi-degree of freedom (MDOF) structure is to determine the characteristics of the equivalent single-degree-of-freedom (SDOF) structure (representation of performance at ultimate displacement response) based on energy dissipated equivalence and inelastic displacement profiles of the MDOF. This equivalent "SDOF-substitute" structure is simply characterized by the secant stiffness k_e at maximum or desired displacement Δ_d or Δ_u and by a level of an equivalent viscous damping (EVD) ξ_{eq} representing the combined effect of viscous and hysteretic dissipation of the structure. The peak displacement response of the system is selected based on deformation limit states corresponding to the desired performance level of structural or non-structural elements. The key parameters of the equivalent SDOF structure are presented in Figure 8-3a, where k_i stands for the initial elastic stiffness, r is the ratio of post-yield to initial stiffness, Δ_y is the yield displacement, μ is the displacement ductility, F_u and F_y are the maximum force and yield force, respectively.

At this stage, knowledge of the yield displacement of the structure is required in order to calculate the system displacement ductility at the peak response and allow an estimation of the EVD of the system. It was concluded by some studies (Priestley, 2007; Maley, 2010…) that the yield displacement can be found independently of the strength within the system.

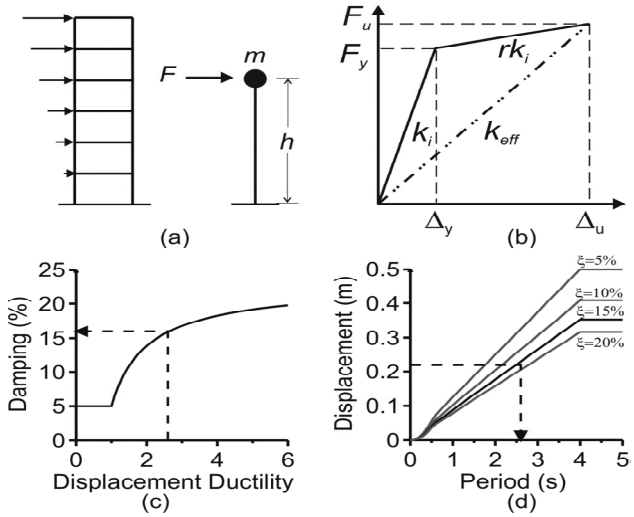

Figure 8-3 – Key steps of DDBD for MDOF system (Maley, 2010)

In order to estimate the EVD from the ductility of the system at maximum response, an appropriate damping-ductility relationship calibrated for the expected hysteretic response of the system is required. This is illustrated in Figure 8-3c. The EVD represents the combined effects of elastic and hysteretic energy dissipation within the system. Having known the EVD and the design displacement of the system, the required secant or effective period of the system is obtained from the reduced design displacement response spectrum as shown in Figure 8-3d. Therefore, the design base shear of the system is given directly by simple calculation from Equation 8-5 and Equation 8-6. Then, the design base shear obtained from the SDOF structure is distributed as equivalent inertia lateral forces in the MDOF structure. Afterwards, the design moments at potential plastic hinges locations are determined as well as the design moments and shears for all the others critical structural sections throughout the structure.

$$k_e = \frac{4\pi^2 m_e}{T_e^2} \qquad \text{Equation 8-5}$$

$$V_{base} = k_e \Delta_d \qquad \text{Equation 8-6}$$

8.3.2.2. The main governing steps of DDBD for designing or retrofitting a frame structure

The procedure for designing or retrofitting a frame structure based on DDBD is summarised as follows.

Step 1: Determination of the characteristics of the equivalent SDOF substitute structure

The inelastic first-mode shape of the MDOF structure at the limit state displacement or drift of the most critical member, based on performance level considerations (material strain or drift limits of structural or non-structural components), is required to define the effective mass, the effective height, and the design displacement of the equivalent SDOF substitute structure. This is introduced in Figure 8-4.

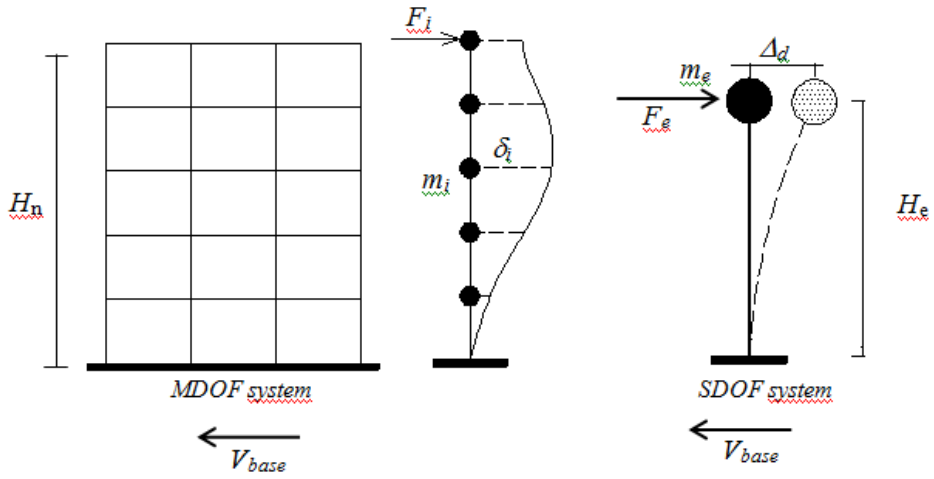

Figure 8-4 – Simplified model of a multi-storey building

Where:

m_i are the masses at each significant level i
δ_i are the design displacements
m_e is the equivalent mass of the SDOF
H_i is the height of each floor
H_n are the total height of the building
H_e is the equivalent height
Δ_d is the design displacement

Inelastic Displacement Profile:

As already mentioned, the design displacement profile of a MDOF system at the ultimate response of the system is fundamental to characterize the "substitute SDOF" system for DDBD. For design or retrofit purposes, approximate design profiles are available for standard structural forms including RC-MRF (Priestley et al., 2007). The design displacement profile of the MDOF RC-MRF, δ_i, could be obtained in accordance with the height and number of stories, introduced by Priestley (2007), as:

$$for\ n \le 4: \quad \delta_i = \frac{H_i}{H_n} \qquad \text{Equation 8-7}$$

$$for\ n > 4: \quad \delta_i = \frac{4}{3} \cdot \left(\frac{H_i}{H_n}\right) \cdot \left(1 - \frac{H_i}{4H_n}\right) \qquad \text{Equation 8-8}$$

The design displacement at story i, Δ_i, are found by using the inelastic shape vector, δ_i, scaled with respect to the critical storey displacement, Δ_c, and to the corresponding mode shape at the critical storey level δ_c.. The design displacements of the individual masses at story, i, are obtained from:

$$\Delta_i = \delta_i \cdot \left(\frac{\Delta_c}{\delta_c}\right) \qquad \text{Equation 8-9}$$

Design Displacement of the SDOF structure

The design displacement of the equivalent SDOF structure can be given by:

$$\Delta_d = \sum_{i=1}^{n}\left(m_i \Delta_i^2\right) / \sum_{i=1}^{n}\left(m_i \Delta_i\right) \qquad \text{Equation 8-10}$$

Equivalent Mass of the SDOF structure

The mass of the substitute structure is given by the following equation:

$$m_e = \sum_{i=1}^{n} m_i \left(\frac{\Delta_i}{\Delta_d} \right) = \frac{\sum_{i=1}^{n} m_i \Delta_i}{\Delta_d}$$

Equation 8-11

Equivalent Height of the SDOF structure

The equivalent height of the "SDOF substitute structure" is given by:

$$H_e = \sum_{i=1}^{n} \left(m_i \Delta_i H_i \right) / \sum_{i=1}^{n} \left(m_i \Delta_i \right)$$

Equation 8-12

Step 2: Estimation of the level of equivalent viscous damping ξeq

To obtain the EVD, ξ_{eq}, the displacement ductility μ must be known. The displacement ductility is the ratio between the design displacement Δ_d and the yield displacement Δ_y. The yield displacement is estimated according to the considered properties of the structural elements, for example through the use of approximated equations proposed by Priestley et al. (2007) based on the yield curvature of the section.

Displacement ductility of the SDOF structure

The design ductility displacement of the equivalent SDOF system at the design displacement is given by:

$$\mu_\Delta = \frac{\Delta_d}{\Delta_y}$$

Equation 8-13

Yield displacement for RC frames

The yield displacement is given by the following equation:

$$\Delta_y = \theta_y H_e$$

Equation 8-14

where θ_y is the yield drift and for reinforced concrete frames is given by:

$$\theta_y = 0.5 \varepsilon_y L_b / h_b \text{ (Priestley, 2007)}$$

Equation 8-15

ε_y is the yield strain of steel, L_b is the beam length and h_b is the beam section depth.

Equivalent viscous damping

To take into account the inelastic behaviour of the real structure, hysteretic damping (ξ_{hyst}) is combined with elastic viscous damping (ξ_0) and an equivalent viscous damping is defined as:

$$\xi_{eq} = \xi_0 + \xi_{hyst}$$

Equation 8-16

Where: ξ_0 is the critical damping

ξ_{hyst} is the hysteretic damping

Step 3: Determination of the effective period Te of the SDOF structure

The effective period at peak displacement response, T_e, is found from the design displacement spectra, the latter is defined for the equivalent viscous damping ξ_{eq}, as shown in Figure 8-5. The displacement spectra for other different levels of ξ than 5% can be found using the formulation defined in EC8, Equation 8-17, or by another appropriate method, Equation 8-18 (Priestley, 2007).

$$S_{D,\xi} = S_{D,5\%} \left(\frac{10}{5+\xi} \right)^{1/2}$$

Equation 8-17

$$S_{D,\xi} = S_{D,5\%} \left(\frac{7}{2+\xi} \right)^{1/2}$$

Equation 8-18

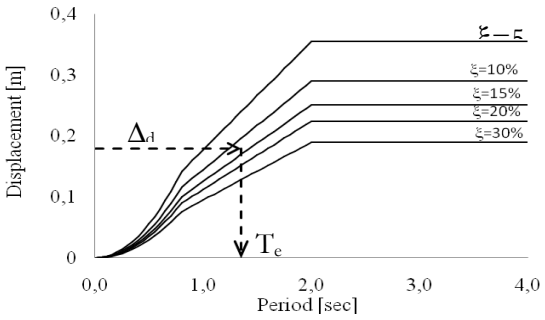

Figure 8-5 – Design displacement spectra

Step 4: Determination of the base shear and story shear forces due to seismic actions

Based on the effective mass and period of the "equivalent SDOF substitute structure" determined from the previous steps, the effective stiffness k_e of the "substitute SDOF structure" can be obtained by:

$$k_e = \frac{4\pi^2 m_e}{T_e^2} \qquad \text{Equation 8-19}$$

For the SDOF system, the design base shear is computed as the product of the effective stiffness by the design displacement.

$$V_{base} = k_e \Delta_d \qquad \text{Equation 8-20}$$

Step 5: Distribution of the design base shear vertically and horizontally to the structural elements of the lateral load resisting system.

The base shear force is distributed to the floor levels as Equation 8-21 (Priestley, 2007):

$$F_i = F_t + 0.9V_{base}\frac{(m_i\Delta_i)}{\sum_{i=1}^{n}(m_i\Delta_i)} \qquad \text{Equation 8-21}$$

Where: $F_t = 0.1V_{base}$ at roof level, and $F_t = 0$ at all other levels.

8.4. Application of DDBD for seismically retrofitting RC-MRFs by using EMP

8.4.1. General introduction

In this section, we will develop a way for designing EMP to seismically upgrade or retrofit the existing RC-MRFs based on the fundamental approach of the DDBD. It is well known that amongst the factors affecting the design procedures of DDBD, the three most important ones are the selection of the target displacement profiles, the target lateral drifts or displacements and the equivalent viscous damping of the structure. Thus, these three factors, accounting for the combination of RC-MRFs and EMP (called herein dual systems or retrofitted systems) are first discussed. For final completeness, a chart of the retrofit process is then given.

8.4.2. Target displacements or target drifts for the retrofitted RC-MRFs and maximum shear resistance of the RC-MRFs

Based on the assessment of Pushover analysis (see Chapter 7), one can see that the seismic performance of the existing frames is different. For the frames in EC2 group and frames designed with EC8-DCL, brittle failure due to crushing of concrete at beam-column joints dominates their seismic performance. Some of those frames can reach the first yield due to bending before that failure. The others fail in the elastic range, at low base shears. For the remaining frames, which are designed in accordance with EC8-DCM, the seismic performance is favourable with partial or beam-sway mechanisms.

Clearly, the retrofit work using EMP should ensure that the unfavourable failure will not occur under a given seismic action. This means that under a given earthquake, the retrofitted structures should reach target displacements or target drifts, at which there is no brittle failure due to crushing of concrete at beam-column joints of frames in EC2 and EC8-L groups or not too large lateral drifts leading to the severe damage of non-structural components of frames in EC8-M group. Based on the results of assessment of the existing frames by Pushover analysis, their deficiencies are known; therefore the limit drifts or displacements can be readily defined. These drifts or displacements are usually at the top of the existing frames. They are usually chosen to be equal or less than the drifts at which the brittle failure occurs in the EC2 and EC8-L frames or at which EC8-M frames have too large displacements. In addition, at the selected target displacements, the maximum base shear resistance of the existing frames can be easily determined from Pushover curves. This is graphically explained in Figure 8-6. In this figure, the left one presents the EC2 and EC8-L frames in which brittle failure due to node governs the seismic behaviour. The maximum displacement of the retrofitted frame must be targeted in the dashed region in Figure 8-6. This will ensure that under a designed earthquake brittle failure will not occur. The right one of Figure 8-6 introduces a selected point for an EC8-M frame. This point is chosen based on the limit of drift or of displacement at a performance point targeted for the retrofitted frames. In addition, it should be stressed that the selected point on Pushover curve for the existing frames must be selected so that the base shear generated in the existing frames should not be greater than their capacity. In many cases, it is necessary to iterate to obtain the appropriate target displacement. This will be discussed in more detail in the following sections and in case study examples.

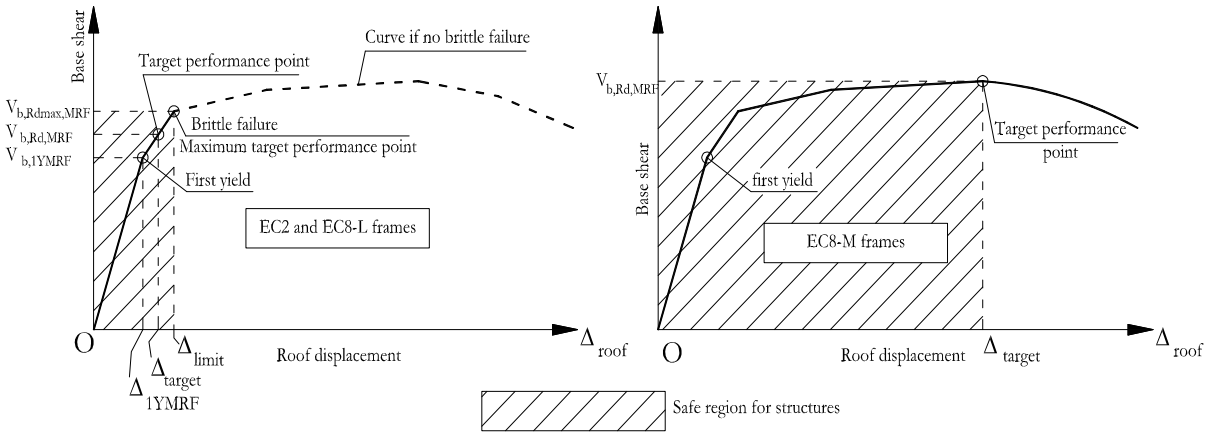

Figure 8-6 – Description of the selected displacement of the existing frames

8.4.3. Target displacement profiles for the retrofitted RC-MRFs

Having selected the target displacements for the retrofitted frames, in accordance with DDBD, it is necessary to predict the deflected shapes or displacement profiles of the frames under seismic actions. The assumed displacement shape at the first stage is one of the key factors essentially affecting the results of design or retrofitting work. Generally, the choice of the target displacement profiles is dependent on the desired performance of the structure under the attack of the earthquake. Based on evaluating the nonlinear seismic response of RC-MRFs (Fardis, 1993; Pettinga, 2005; Paulay 2002…), it was found that there are several failure modes of RC-MRFs under seismic actions. They are soft-story mechanisms (in 1, or 2 or 3… stories), local failures caused by shear or collapse of beam-column joints and partial or full beam-sway mechanisms. For the frames designed in accordance with modern seismic codes, the latter failure mechanisms are always observed thanks to Capacity Design rules. On the other hand, in the RC-MRFs which are not designed according to any seismic codes or with Low Ductility Class, the first two failure modes are usually observed, especially for the low- and medium-rise structures where the advantage of axial force in increasing the moment resistance of the columns is very small. The desired mechanism involves the formation of flexural plastic hinges at the ends of beams in the intermediate floors, except or not at the roof level, and in combination with the plastic hinges developed at the base of first-story columns.

For RC-MRFs with slab casted in place, there have been some studies focusing on their inelastic mode shape due to seismic actions (Pettinga and Priestley, 2005; Paulay, 2002…) with the aim to find the inelastic displacement shapes corresponding to the desired failure modes. From moment curvature analyses of many types of RC-MRFs with different ratios between member length and section height, as reported in Priestley (2007) and Priestley (1998), it was found that for a given structural type or structural member type and size, stiffness and strength are effectively proportional, and therefore the yield curvature or yield displacement is the independent parameter. Having had the same assessment, Paulay (2002) developed the idea of controlling the behaviour of a RC structural system during seismic response through the assignment of strength distribution. Observing that the yield displacement of RC-MRFs is essentially independent of strength and that member stiffness is proportional to the strength assigned, therefore the distribution of stiffness and hence the displaced shape may be dictated by the strength distribution within the system. Thus, by defining the strength distribution during preliminary design, the behaviour of the structure can be manipulated to the designer's benefit to promote a desired design displacement profile. With the similar approach, Priestley et al. (2007) proposed the approximate displacement profiles for the DDBD of RC-MRFs, based on the height and number of stories, are given Equation 8-7 and Equation 8-8. They are recalled here for convenience.

$$for\ n \le 4:\ \delta_i = \frac{H_i}{H_n} \qquad \text{Equation 8-22}$$

$$for\ n > 4:\ \delta_i = \frac{4}{3}\cdot\left(\frac{H_i}{H_n}\right)\cdot\left(1-\frac{H_i}{4H_n}\right) \qquad \text{Equation 8-23}$$

In fact, these profiles have been taken from the work of Pettinga and Priestley (2005), in which RC-MRF were empirically studied to see their dynamic behaviour in accordance with DDBD approach. These approximations are based on the formation of a beam-sway mechanism. Further, they have no dependence on the level of seismic response, making no distinction between elastic and inelastic displaced shapes, which are regarded as sufficiently similar for regular frames provided they exhibit beam-sway behaviour, the desired mechanism (Pettinga and Priestley, 2005).

8.4.4. Equivalent Viscous Damping of RC-MRF with EMP

Differently from force-based design approach, in order to construct the design displacement spectra, DDBD uses an equivalent viscous damping (EVD), which is coupled with an equivalent linear SDOF system to represent the elastic and inelastic energy dissipation of a nonlinear system during seismic loading (Priestley, 2007; Maley et al., 2010). The EVD is defined as a function of the viscous damping of the "substitute SDOF" structure, ξ_0, and inviscous damping, ξ_{hyst}, related to the hysteretic behaviour and the system ductility at the design displacement of the nonlinear system, as expressed in the following equation.

$$\xi_{eq} = \xi_0 + \xi_{hyst} \qquad \text{Equation 8-24}$$

ξ_0 is the damping used to determine the elastic response of a SDOF system by NLTH. The value of ξ_0 is mainly dependent on the material of the structure, usually taken as 5% for reinforced concrete structure. This damping is the crucial element in determining elastic response spectra for designing structure in force-based approach. Hysteretic damping, ξ_{hyst}, is related to energy dissipated in the structure due to its inelastic behaviour. The value of this factor is usually calibrated based on the analyses of a substitute structure (i.e. analyses using secant stiffness, rather than initial stiffness and equivalent damping to represent the hysteretic damping) and on equating the energy absorbed by hysteretic steady-state cyclic response to a given displacement level to the one absorbed by the substitute structure with the equivalent damping. There have been several studies concerning development of the EVD-ductility relationships taking into account the hysteretic damping of the structures for DDBD. Most of them have been summarised in Priestley (2007). Several functions have been introduced in that book. A very important point in these functions is that the secant stiffness has been adopted instead of the initial stiffness to characterize the equivalent linear system.

The EVD of the substitute structure in DDBD is related to displacement ductility and hysteretic shape of the system. These two factors are dependent on the structural layout considered, types of structural

materials and corresponding yield and ultimate displacements. For a dual system, the EVD must be a combination of the all individual components. More particularly, the EVD of the RC-MRF with EMP is the combination of EVD of the RC-MRF and of the EMP itself.

Having determined the EVD of the system, the design displacement spectrum can be obtain by scaling the elastic displacement design spectrum with a reduction factor, R_ξ, obtained from an equation such as Equation 8-25, as also supposed by EC8.

$$R_\xi = \left(\frac{0.1}{0.05 + \xi_{EVD}} \right)^{0.5} \qquad \text{Equation 8-25}$$

8.4.4.1. EVD of the reinforced concrete frames

There have been several studies in calibrating the EVD of RC-MRF to date. Most of them have been discussed in Priestley et al. (2007). Priestley et al. (2007) have introduced an EVD-ductility relationship, as Equation 8-26, for use with RC-frames that are based on the Takeda Fat hysteretic rule and may be used to characterize the nonlinear behaviour of RC-structures.

$$\xi_{MRF} = 0.05 + 0.565\left(\frac{\mu_{MRF} - 1}{\mu_{MRF}\pi} \right) \qquad \text{Equation 8-26}$$

Where: $\xi_{RC\text{-}MRF}$ is the equivalent viscous damping at a frame ductility demand of μ. The equivalent viscous damping expression of Equation 8-26 was calibrated for a viscous damping level of 5% by Grant and Priestley (Priestley, 2007).

In order to determine the EVD of the existing RC frame, it is necessary to calculate its displacement ductility, which is the ratio between target displacement and yield displacement. The target displacement has been chosen based on the failure mode of the frames from Pushover analysis, as presented in previous sections. The yield displacement of the existing frames is also determined from the results of Pushover analysis. This will be explained in more detail hereafter.

Yield displacements of the RC-MRFs

For designing a new RC-MRF based on DDBD, there exist some formulas which can be used to estimate the yield displacement of the frame depending only on the preliminary selection of the cross-sectional dimensions and geometrical configuration of the frame. These formulas have been introduced in Priestley (2007) based on many calculations on different types of RC-MRFs. However, in the present study, all RC-MRFs have been designed and evaluated by Pushover and NLTH analyses. Therefore, their yield properties are known. The work needed to be done here is to determine the yield displacements of equivalent SDOF structures corresponding to each existing frame. As defined in section 7.5.2.3, the yield displacement of an existing RC-MRF can be determined from Pushover curve as the following figure:

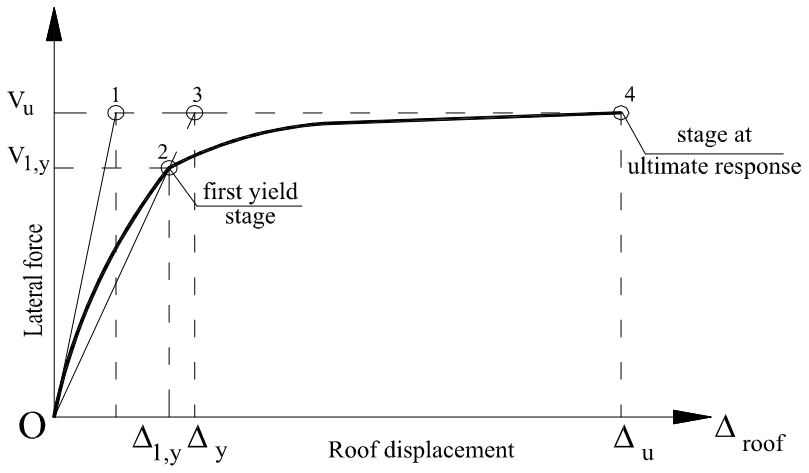

Figure 8-7 – Definition of ductility capacity and ultimate response of the RC-MRFs

8.4.4.2. EVD of the EMP

Similarly to all other structural types, EVD of the EMP consists of two damping components, including elastic and hysteretic ones. Viscous damping, as mentioned in the section above, is taken as 5%. To determine the appropriate level of EVD hysteretic damping of the "substitute structure" in DDBD, it is necessary to perform NLTH for both real and "substitute" structures. Then, by equating the total energy absorbed by the hysteretic behaviour of the both systems subjected to specific accelerograms, different levels of EVD corresponding to different hysteresis behaviour will be addressed. Priestley (2007) introduced several studies on determining EVD of the structures (Grant et al, 2005; Jacobsen, 1960…), in which some of them had calibrated the EVD for different hysteresis rules to give the same peak displacements as the hysteretic response, using inelastic time-history analysis. Most of hysteretic behaviour of different structural types has been covered. A set of formulas, which is correct for tangent-stiffness viscous damping of 5% and corresponding to different types of hysteresis behaviour, was introduced in Priestley (2007). However, there is another simple way to obtain the EVD of the system with EMP by comparing the hysteresis behaviour of the EMP with the hysteresis behaviour of other systems. As already explained in detail in Chapter 4 and 5, the hysteretic response of EMP is pinched, representing the degradation of the stiffness when the lateral load is reverse. A typical behaviour of EMP is represented in Figure 5-48. Its behaviour is like the model of Takeda Thin (1970), as presented in Figure 8-9.

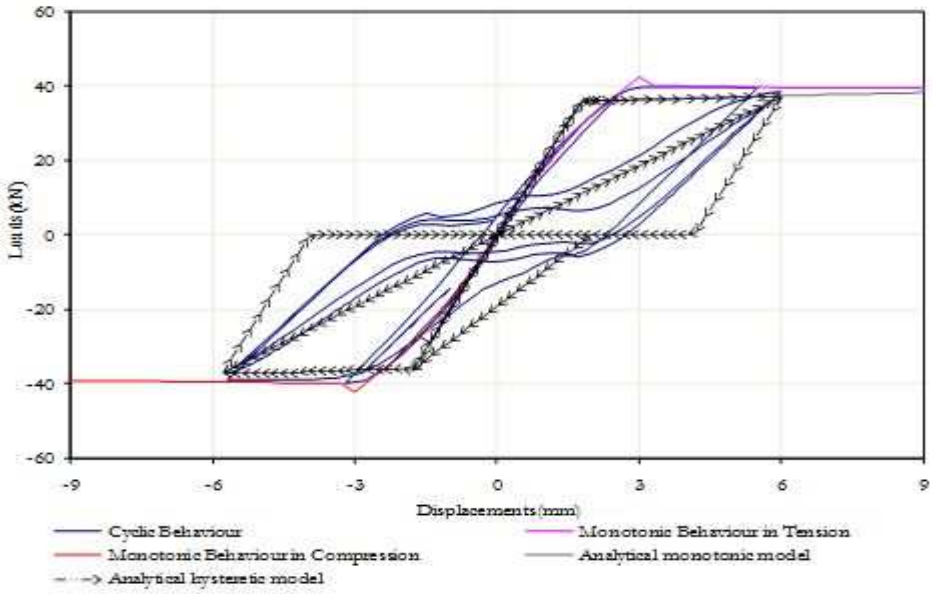

Figure 8-8 – A typical hysteretic behaviour of a square EMP A51-27-35-30 with the dimension of 500mm

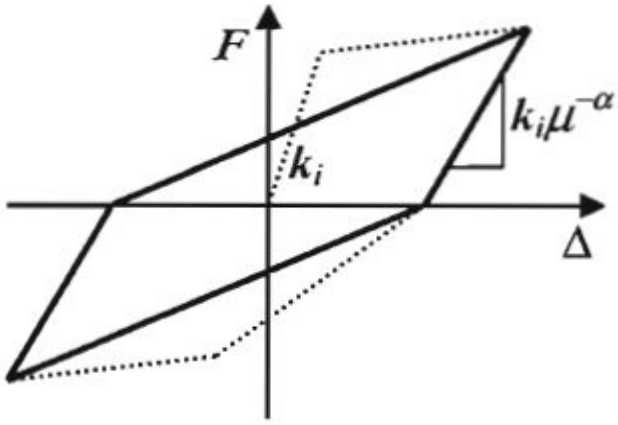

Figure 8-9 – Takeda Thin hysteresis rule (Priestley, 2007)

Therefore, it may be possible to adopt the EVD of Takeda thin model, as reported in Priestley (2007), for the EMP. This formula is given in Equation 8-27.

$$\xi_{EMP} = 0.05 + 0.444\left(\frac{\mu_{dEMP} - 1}{\mu_{dEMP}\pi}\right)$$ Equation 8-27

Determination of the ductility of the EMP system through Strength Assignment

Depending on the structural layout considered and corresponding yield profiles, the displacement ductility at design response in DDBD will often vary up the height of a MDOF structure. In addition, the variation in ductility over the height of the structure is still based on the differences between its elastic and inelastic first-mode shapes. Consequently, the global ductility is finally dependent on the variation of local ductility and corresponding inelastic first-mode shape of the structure. This allows estimating the system global ductility, μ_{dEMP}, by weighting the various ductility contributions in proportion to the work done by each system, respectively (Maley, 2010). For frame-type structure, the following equation, supposed in Priestley (2007), may be used to do this where the ductility at each level, $\mu_{dEMP,i}$, is weighted by the corresponding story shear, V_i, acting on EMP at story i and story drift, θ_i.

$$\mu_{dEMP} = \frac{\sum V_{EMP,i}\theta_{EMP,i}\mu_{dEMP,i}}{\sum V_{EMP,i}\theta_{EMP,i}}$$ Equation 8-28

The ductility at each level of EMP, $\mu_{dEMP,i}$, is determined by the ratio between target displacement or drift of the EMP (the same as of the retrofitted frame at each story) and the yield displacement or yield drift of the EMP. The target displacement or drift of the EMP at each story is determined based on the target displacement and target displacement profile of the retrofitted frame, as presented in 8.4.3. The yield displacement of EMP at each story can be calculated from the yield drift of EMP at that story. The average yield drift of EMP at each story is dependent on the type and properties of chosen EMP at each story. As presented in Chapter 4 and 5, these values range from 0.12% to 0.4%. The corresponding story shear, V_i, acting on EMP at each story of the retrofitted frame is dependent on the stiffness of the RC-MRF and the EMP system itself.

It is clear that in order to calculate both ductility and shear story on EMP it is necessary to know the properties of EMP at each story, which are still unknown at this stage of design process. However, there is still another approach which can help determine the system ductility of the system based on strength assignment proposed by Paulay (2002). The concept of controlling the behaviour of a reinforced concrete structural system under seismic actions by using the assignment of strength distribution has been used in several studies (Maley, 2010; Paulay, 2002…). The reason for using this in reinforced concrete structure is due to the independence of the yield displacements and the strength (Paulay, 2002).

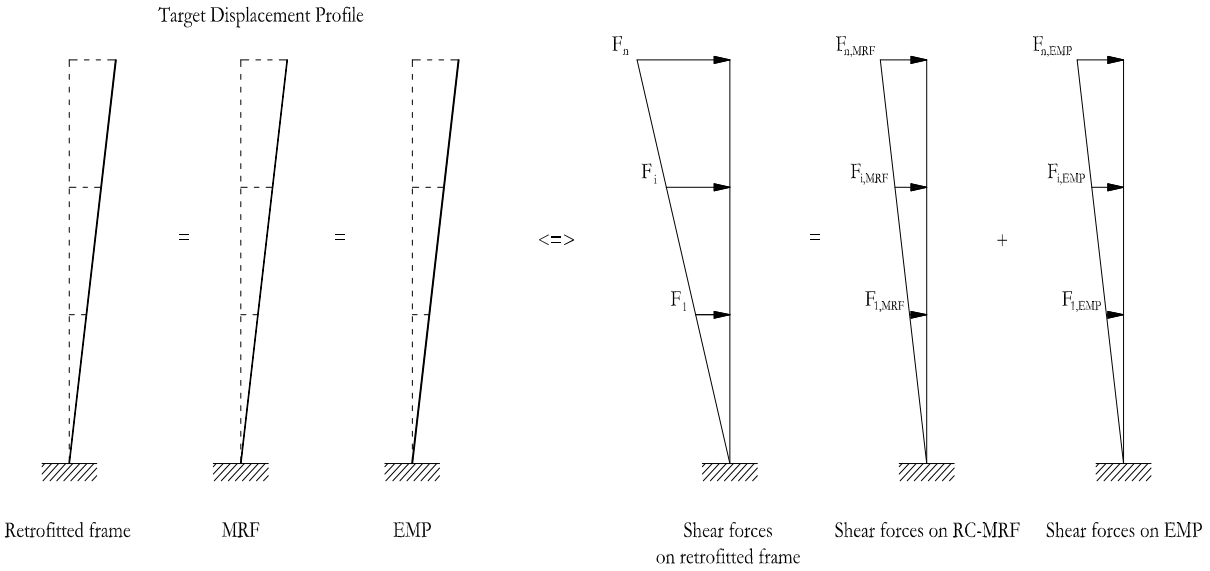

Figure 8-10 – Strength assignment to determine the shear story and ductility of the EMP system

Thus, the member stiffness is proportional to the strength assigned and the distribution of stiffness and resulting displacement shape may be obtained by the strength distribution within the system. As a result,

by defining the strength distribution over the height of the structure during the preliminary design, the seismic behaviour with a desired design displacement profile of the structure can be anticipated. We will assume that this concept may be used for the retrofitted system comprising of the RC-MRF and the EMP to help dictate the ductility and shear story of the system. As explained in Figure 8-10, the shear force acting on EMP at each story can be determined from the subtraction of total shear force of the retrofitted system and the shear force acting on that story of the RC-MRF.

8.4.4.3. EVD of the retrofitted RC-MRFs with EMP

As mentioned, the best way to generate the EVD of either a dual or a single structure is to perform NLTH of both origin "MDOF" and "substitute SDOF" ones and then equating the hysteretic energy dissipated by both systems at a specific displacement. However, this is a very time-consuming and not an easy work. For a dual structure, if the EVD of individual components of the structure are known, there exists another simpler solution to determine the overall EVD of the system. This is done by using the similar way as calibrating the system ductility.

In a similar manner to the individual system ductility demands, the dual-system EVD may be found by weighting the contributions of EVD of the individual systems. In order to best represent the lateral resistance offered to the system it is recommended that each contribution be weighted in proportion to the overturning moment resisted as in Equation 8-29 (Sullivan et al., 2006).

$$\xi_{sys} = \frac{M_{OTM,MRF}\xi_{MRF} + M_{OTM,EMP}\xi_{EMP}}{M_{OTM,MRF} + M_{OTM,EMP}} \qquad \text{Equation 8-29}$$

where ξ_{SYS} is the dual system EVD, $M_{OTM,MRF}$ and ξ_{MRF} and $M_{OTM,EMP}$ and ξ_{EMP} are the overturning moments and EVD of the MRF and EMP systems, respectively.

8.4.5. Design, selection and distribution of EMP for the RC-MRFs

The principle of designing EMP system for retrofitting the existing frame is presented in Figure 8-11 and Figure 8-12 of the section 8.4.6. One of the most important and difficult work is to find the suitable distributions and characteristics of the EMP for the existing RC-MRFs to improve its seismic behaviour. It is very necessary to note that whatever the design approach for the retrofit is chosen the final performance of the 'retrofitted' frames must be congruent with the requirements from the EN-1998-1 (2004) and EN-1998-3 (2004). Based on the results of evaluation, the deficiencies of the existing frames have been detected at their ultimate limit states. They are related to some typical performance of the overall structure or the structural components such as the soft-story mechanism, local failures, excess of interstory drifts or the global failure.... These failures are corresponding to two main types: Strong Beam/Weak Column and Incomplete Load Path. This is a hint for selecting the target displacement for the retrofitted frame mentioned in Figure 8-11 and Figure 8-12.

Figure 8-11 presents three main cases for designing EMP in retrofitted frames. For the case (a) in Figure 8-11, it is used when target displacement of the retrofitted frame is less than the yield displacement of the EMP and the yield displacement of the RC frame is less than the selected target displacement. Thus, EMP will only contribute to elastic stiffness and resistance of the dual system. Capacity of EMP in absorbing seismic energy through hysteresis behaviour will not be activated. Because the yield displacement of the RC frames is lower that that of retrofitted frame the capacity of absorbing seismic energy under design earthquake of the RC frame is activated. In case (b) in Figure 8-11, all ductility, secant stiffness and ultimate strength of the EMP are activated to resist seismic actions. It is used when target displacement of the retrofitted frame is greater than yield displacements of EMP and RC frame. Capacity of both individual systems in absorbing seismic energy through hysteresis behaviour will be activated. Figure 8-11c mentions about the case when the retrofitted frame will only work in elastic range. This is used as the target displacement is small, meaning that the brittle failure occurs at a rather low displacement.

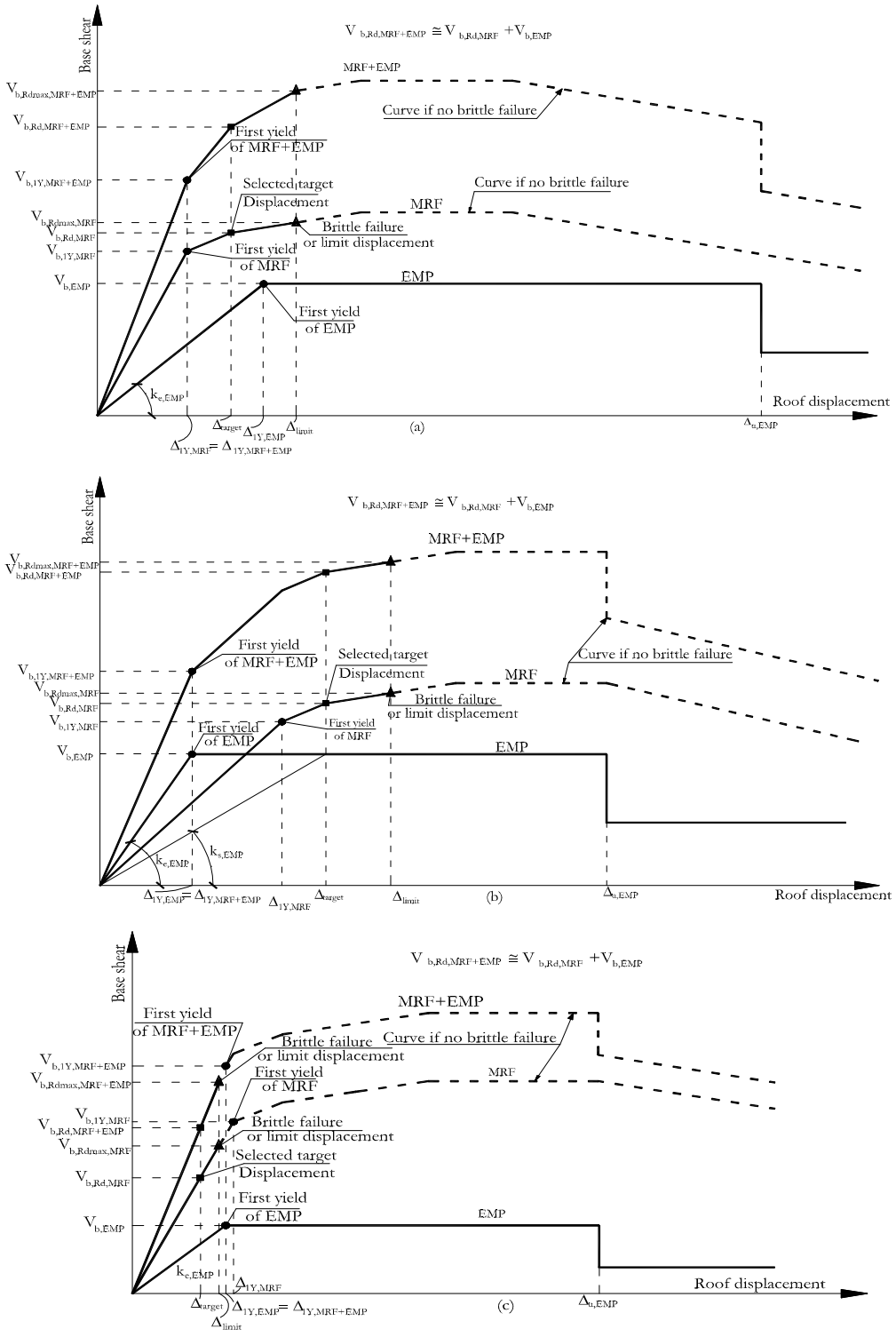

Figure 8-11 – Principle of designing EMP

Figure 8-12 of the section 8.4.6 presents a complete procedure for designing EMP in the dual system. In order to select and distribute EMP on the RC-MRFs with the use of DDBD, it is necessary to determine shear forces induced by the design earthquake on the individual components of the retrofitted system. To do that there needs to determine and distribute these lateral forces to each system. For new design of a dual system, it is possible to fix a percentage of total lateral force to one system and the remaining one has to carry the rest of total lateral force. However, in the current case, the retrofitted frame consists of an existing system and a new one, EMP. Thus, the selection of EMP is significantly influenced by the selection of the capacity of the existing frame contributing to the overall resistance of the dual system. The

selected capacity is corresponding to a selected target displacement and an equivalent shear force, $F_{b,Rd,MRF}$ of the existing frame, as presented in step 1 in Figure 8-12. It should be noted that the selected target displacement should be less than the maximum displacement, Δ_{limit} in Figure 8-11, of the existing frame. At this limit deformation, the frame is considered to fail due to crushing of the concrete at beam-column joints or to the shear failure at beams or columns or too large lateral drifts… Distributing this shear force on each story level allows calculating the shear capacity of each story, $F_{b,MRF,i}$ that contribute to the shear resistance of the retrofitted frame at each story. Based on the selected target displacement, following the steps in DDBD, one can determine all properties of the SDOF equivalent system. Besides, with the aid of Pushover analysis of the existing frame, presented in Chapter 7, ductility of the RC frame at selected target displacement is calculated, therefore, EVD of the RC frame is determined as Equation 8-26. This is illustrated in step 2 in Figure 8-12. Steps from 3 to 6 illustrate the way to determine total base shear acting on SDOF equivalent system at design PGA. The total seismic base shear force acting on the retrofitted RC-MRFs is determined by DDBD approach. It is dependent on the desired displacement profiles, on the effective stiffness of the SDOF equivalent system and on the design displacement. The effective stiffness is related to intersection of the design displacement and inelastic displacement spectrum of a seismic action. If the total base shear at ultimate or target response of the retrofitted structure is known, it is possible to determine the remaining shear forces that will be carried by the EMP system by subtracting the target story shears of the retrofitted system to the capacity story shears carried by the frame. Based on the shear forces acting on EMP, all characteristics of the EMP system can be found such as types, system ductility and system EVD of the EMP. However, these parameters, in turn, will influence on the total equivalent viscous damping of the dual and the SDOF system, leading to the change of the seismic demand on the structure. Therefore, the effective stiffness of the substitute structure will be changed causing the variation of the total target base shear. This, in turn, will change the shear force acting on the EMP and a reselection of the EMP is necessary. Obviously, determination of the base shear and selection of EMP for the existing frame are an iterative process. After obtaining the total base shears acting on dual system, the shear forces in each story can be determined using Equation 8-21 and shear forces at each story acting on EMP can also be calculated based on the assumed portion of the base shear made in previous steps. From this, it is possible to choose EMP at each story corresponding to the calculated shear forces and yield drifts at step 4. Step 8 in Figure 8-12 is an important one. This step makes sure that the selection of EMP, target displacement of the retrofitted system is appropriate or not. This is done by making an elastic analysis under lateral distributed forces in step 7 with some assumptions for the retrofitted frame in congruence with DDBD such as stiffness of EMP taken as secant one and modulus of concrete taken as 50% of uncracked one. In this step, the top displacement of the retrofitted frame and the total base shear acting on RC frame under lateral forces should be compared with the selected target displacement and capacity base shear of the existing frame determined in step 1. If they are much different it is necessary to reassume the target displacement from step 1 or reselect the yield properties of EMP from steps 3 and 4 in order to change the properties of the retrofitted system to change the base shear. This is explained in Figure 8-12 of next section and in more detail in the design examples presented in section 8.5.

Concerning the positions of selected EMP on each story, because all the studied frames are symmetrical in plan the EMP will be put on the middle bays of the frames.

8.4.6. Chart for design of EMP to seismically retrofit the frames

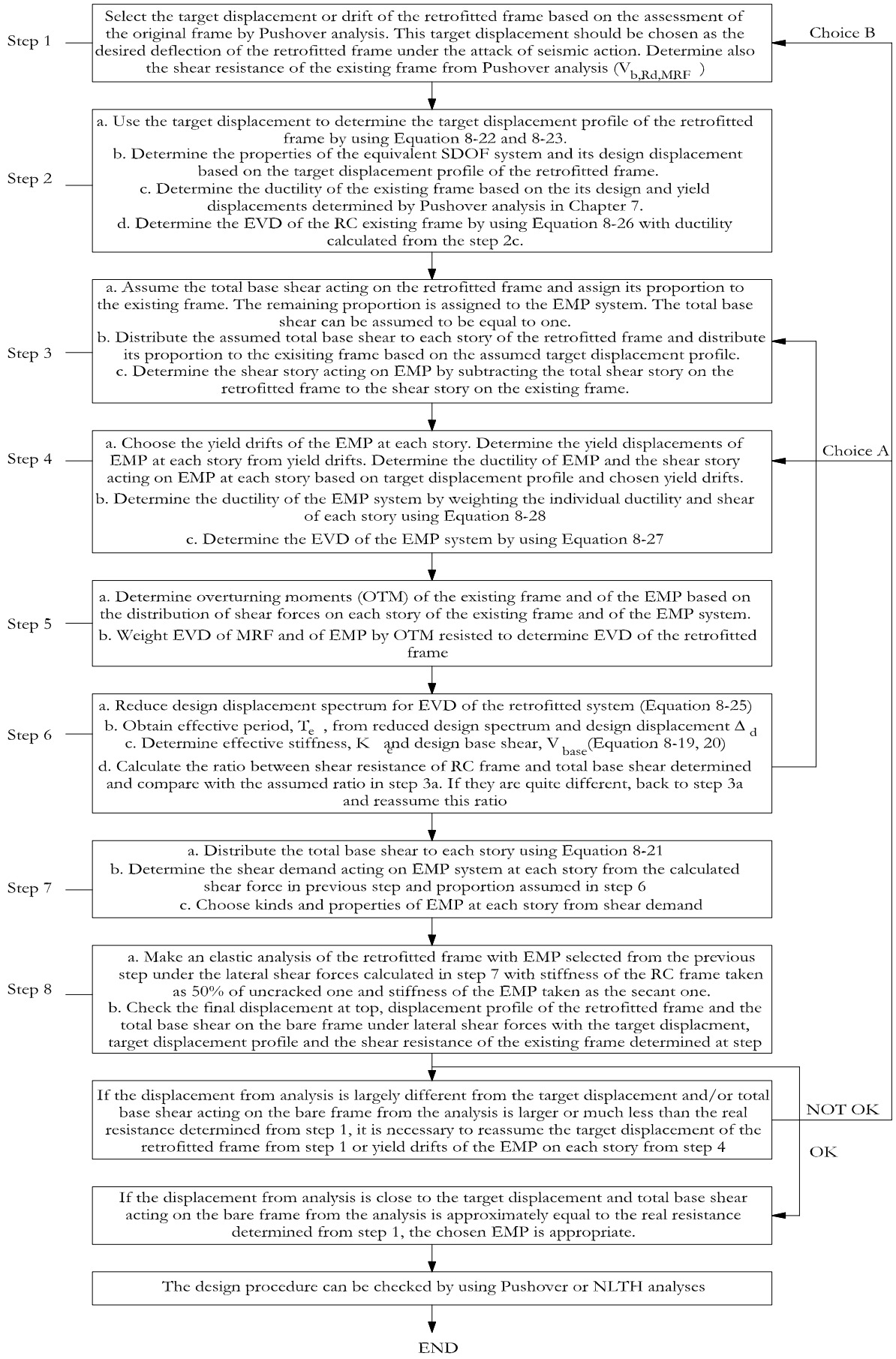

Figure 8-12 – Design procedures of EMP

8.5. Design of EMP retrofitting in case study RC-MRFs using DDBD method

This section will introduce the application of EMP in retrofitting and upgrading the seismic performance of the case study RC-MRFs, which have been designed and evaluated in Chapter 6 and 7. The design procedure is based on DDBD as discussed in detail in the previous sections. More particularly, in the following sections, two particular examples are first presented in detail as the sample examples. Some hypotheses are made in order to facilitate the design. These design examples are developed in section 8.5.1 and 8.5.2 then assessed using Pushover and NLTH evaluation in section 8.5.3. General results in the retrofitting process of all retrofitted frames are also presented at the end of this section.

8.5.1. Case study example 1

The following is the first design example of retrofitting a three-story case study building (Configuration 1, Case study EC2-0.3g), in which the retrofitted system is based on the elastic stiffness and strength of the EMP system. The frame will be designed using EMP under the seismicity with PGA of 0.3g. All the design process is presented in detail hereafter. This example is corresponding to Figure 8-11(a).

Step 1: Selecting the target displacement of the retrofitted frame

The pushover curve of the existing frame is shown in Figure 8-13. The curve consists of two parts: the continuous line from origin to the brittle failure of the frame due to crushing of concrete at the beam-column joint and the dashed line from the node failure point to ultimate behaviour of the frame if it is assumed that node is retrofitted. The failure of node of this frame is shown by the triangular symbol. The performance point corresponding to the magnitude of earthquake having PGA of 0.3g is also presented in the figure. It is clear that under the PGA of 0.3g the frame will fail before reaching the target displacement due to premature failure at the beam-column joint. In order to ensure that after being retrofitted the frame can reach the target displacement or drift under the seismicity with PGA of 0.3g the retrofitted frame should not exceed the displacement or drift at which the collapse of beam-column joint occurs. Therefore, the target drift or displacement at the top of retrofitted frame should be less than that value. For the current frame, the drift at failure due to node is 0.513% corresponding to a top displacement of 0.049m. The first choice of target drift or displacement at top of the retrofitted frame is 0.4% or 0.038m. Also, the maximum resistance of the existing frame is found to be 283.7 kN corresponding to the drift of 0.513% and the shear resistance of the RC frame at 0.4% drift is found to be 250.5 kN. The first yield displacement of the frame is 0.032m (0.33% drift).

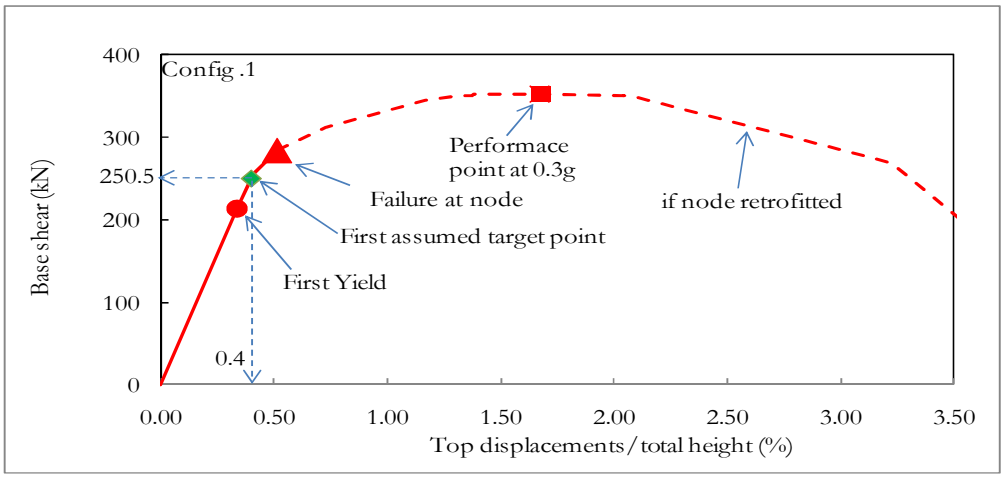

Figure 8-13 – Pushover curve of the existing frame and selected target drift (Case study EC2-0.05g)

Step 2: Target displacement profile, equivalent Single Degree of Freedom Properties of the retrofitted frame and determination of the ductility and Equivalent Viscous Damping (EVD) of the existing frame

Based on the target drift of 0.4%, the target design displacement profile is defined using Equation 8-22 and 8-23. This enables to calculate the properties of the new retrofitted system and of its equivalent SDOF system. They procedure of this calculation is given in Table 8-3.

Table 8-3 – Calculation of design properties of 6-story frame based on DDBD (Config. 1/Case EC2-0.3g)

Story, i	H_i, m	m_i, t	Δ_i, m	$m_i\Delta_i$, tm	$m_i\Delta_i^2$, tm²	$m_i\Delta_i H_i$, tm²
3	9.5	55.6	0.038	2.11	0.080	20.06
2	6.5	62.1	0.026	1.62	0.042	10.50
1	3.5	62.1	0.014	0.87	0.012	3.04

From these properties, the design displacement, Δ_d, the effective mass, m_e, the effective height, H_e, of the equivalent SDOF system are defined as follows:

$$\Delta_d = \sum_{i=1}^{n}\left(m_i\Delta_i^2\right)/\sum_{i=1}^{n}\left(m_i\Delta_i\right) = \frac{0.134}{4.596} = 0.029m$$

$$m_e = \sum_{i=1}^{n} m_i\left(\frac{\Delta_i}{\Delta_d}\right) = \frac{\sum_{i=1}^{n} m_i\Delta_i}{\Delta_d} = \frac{4.596}{0.029} = 157.2t$$

$$H_e = \sum_{i=1}^{n}\left(m_i\Delta_i H_i\right)/\sum_{i=1}^{n}\left(m_i\Delta_i\right) = \frac{33.60}{4.496} = 7.31m$$

Also based on the assessment of the existing frame by Pushover analysis, as in Figure 8-13, the yield drift of the existing frame is already known. Therefore, the ductility of the existing frame can be readily determined from ratio between the target drift and the yield drift of the existing frame. In this example, the ductility of the existing frame is found to be 1.19. The damping ratio of the RC-MRF is

$$\xi_{MRF} = 0.05 + 0.465\left(\frac{\mu_{MRF} - 1}{\mu_{MRF}\pi}\right) = 0.0784 = 7.84\%$$

Step 3: Assuming the unit base shear acting on the retrofitted frame; proportioning this base shear to the RC frame and to the EMP system; determining the shear story on EMP system

In order to calculate the EVD of the EMP system, it is necessary to know the shears and the ductility of EMP at each story. This can be done by using strength assignment to the RC frame and the EMP system. This is based on the approach proposed by Paulay (2002). Assuming that the total base shear acting on retrofitted system is equal to one with 50 percent of the base shear assigned to the existing frame, the remaining will be assigned to the EMP system. Based on the target displacement profile calculated in step 2, the shear story on the RC frame and on the EMP system can be distributed as in Table 8-4.

Table 8-4 – Distributing the total base shear to the RC frame and to the EMP system and calculation of the shear story on the RC frame and on the EMP (Config. 1/Case EC2-0.3g)

Story, i	$F_{i,total}$	$V_{i,total}$	$F_{i,MRF}$	$V_{i,MRF}$	$F_{i,EMP}$	$V_{i,EMP}$
3	0.459	0.459	0.230	0.230	0.230	0.230
2	0.351	0.810	0.176	0.405	0.176	0.405
1	0.189	1.000	0.094	0.500	0.094	0.500
SUM	1.000	4.147	0.500	1.135	0.500	1.135

Step 4: Choosing the yield drifts for the EMP; determining ductility of EMP system and EVD of the EMP system

The global ductility of EMP system is dependent on the local ductility at each story, which is in turn dependent on the target and yield drifts of EMP on that story. The target drifts over the height of the retrofitted frame is already determined. The yield drifts of EMP on each story can be chosen from 0.12% to 0.4% as presented in Chapter 4 and 5. In the current example, EMP yield drifts for all stories have first been chosen to be equal to 0.3%. From this drift and the shear story on EMP system, one can calculate the yield displacements as well as the ductility of EMP on each story. The global ductility of the EMP

system is then determined by weighting the ductility and shear story on each story. This is presented in Table 8-5.

Table 8-5 – EMP design ductility demand calculation summary (Config. 1/Case EC2-0.3g)

Story, i	Story height	$\theta_{y,EMP}$ (rad)	$\mu_{i,EMP}$	$\Delta_{y,EMP}$ (m)	$V_{i,EMP}$	$V_{i,EMP}\theta_{i,EMP}$	$V_{i,EMP}\theta_{i,EMP}\mu_{i,EMP}$
3	3	0.003	1.00	0.009	0.230	0.0007	0.0007
2	3	0.003	1.00	0.009	0.405	0.0012	0.0012
1	3.5	0.003	1.00	0.0105	0.500	0.0015	0.0015
					Σ	0.0034	0.0034

The overall ductility of the EMP system is (Equation 8-28):

$$\mu_{dEMP,sys} = \frac{\sum V_{EMP,i}\theta_{EMP,i}\mu_{EMP,i}}{\sum V_{EMP,i}\theta_{EMP,i}} = \frac{0.0034}{0.0034} = 1.00$$

The EVD of the EMP system is then calculated analogously to that of the MRF, following Equation 8-27:

$$\xi_{EMP} = 0.05 + 0.444\left(\frac{\mu_{dEMP}-1}{\mu_{dEMP}\pi}\right) = 0.05 = 5\%$$

Step 5: Determining OTM of both EMP and existing frame and calculating the Equivalent Viscous Damping of the retrofitted RC-MRF with EMP

The EVD of the dual system will be calculated based on the EVD of the individual systems by weighting their EVD and OTM corresponding to the shear story of each system, as in Equation 8-29. The proportions of overturning moment resisted by each system is determined using statics, together with Equation 8-21 for the distribution of the equivalent lateral force acting on the dual system, as presented in Table 8-6, the EVD of the dual system can be obtained by weighting the values of EVD of the individual system:

$$\xi_{sys} = \frac{M_{OTM,MRF}\xi_{MRF} + M_{OTM,EMP}\xi_{EMP}}{M_{OTM,MRF} + M_{OTM,EMP}} = \frac{3.665\times 7.84\% + 3.665\times 5\%}{3.665 + 3.665} = 6.42\%$$

Table 8-6 – Overturning moment calculation from equivalent force profiles (Config. 1/Case EC2-0.3g)

Story, i	Story height	H_s	F_{total}	M_{total}	F_{MRF}	M_{MRF}	F_{EMP}	M_{EMP}
3	3	9.5	0.459	4.364	0.230	2.182	0.230	2.182
2	3	6.5	0.351	2.284	0.176	1.142	0.176	1.142
1	3.5	3.5	0.190	0.662	0.084	0.331	0.084	0.331
		Σ	1.000	7.310	0.500	3.655	0.500	3.655

Step 6: Inelastic design spectra and DDBD design base shear

From the dual-system EVD, the spectrum reduction factor, R_ξ, is determined:

$$R_\xi = \left(\frac{0.10}{0.05+\xi_{EVD}}\right)^{0.5} = \left(\frac{0.10}{0.05+0.0642}\right)^{0.5} = 0.94$$

Using this reduction factor to reduce the design spectrum, the effective period, T_{eff}, can be found from the design displacement, Δ_d, and the reduced spectrum as demonstrated in Figure 8-14. The effective, K_e, and subsequently the design base shear are then calculated:

$$K_e = \frac{4\pi^2 m_e^2}{T_e^2} = \frac{4\pi^2 \times 157186}{0.38^2} = 42974109\,N/m$$

$$V_{base} = K_e \Delta_d = 1256605\,N = 1256.6\,kN$$

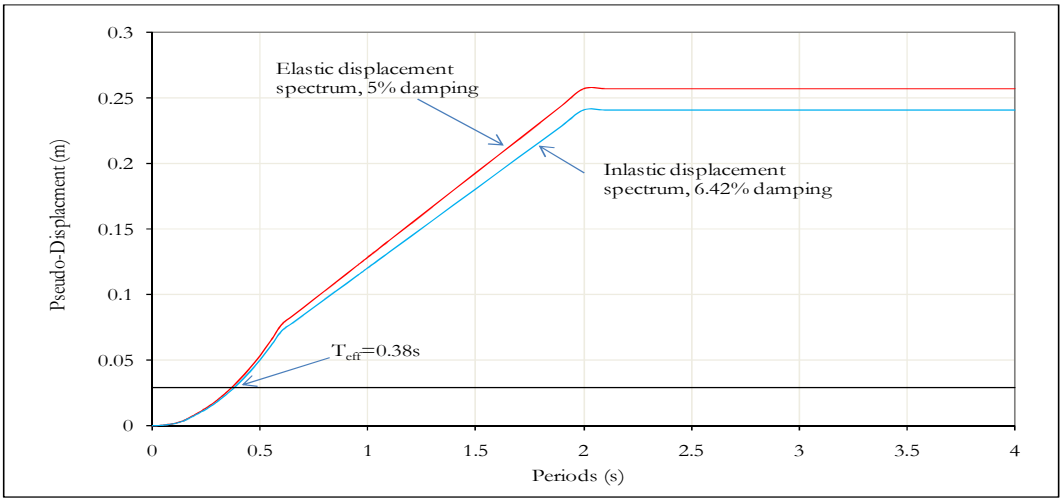

Figure 8-14 – Obtaining effective period, T_{eff}, from design displacement, Δ_d, and reduced displacement design spectrum

Comparing the shear resistance of the RC frame, chosen in step 1, with the total base shear acting to the dual system, calculated above, we can see that the RC frame contributes about 19.9% of the resistance to the dual system, not 50% as already assumed (250.5/1256.6 = 19.9%). Therefore, it is necessary to reassume the contribution of the RC frame to the retrofitted system (back to step 3a). After two iterative steps, the shear resistance of the RC frame contributing to the total shear resistance of the retrofitted frame is found to be 19%. The damping of the dual system is 5.54% and the effective period of the substituted SDOF system is 0.37s, as shown in Figure 8-15. The effective stiffness and design base shear are found to be 45328425 N/m and 1325.5kN, respectively.

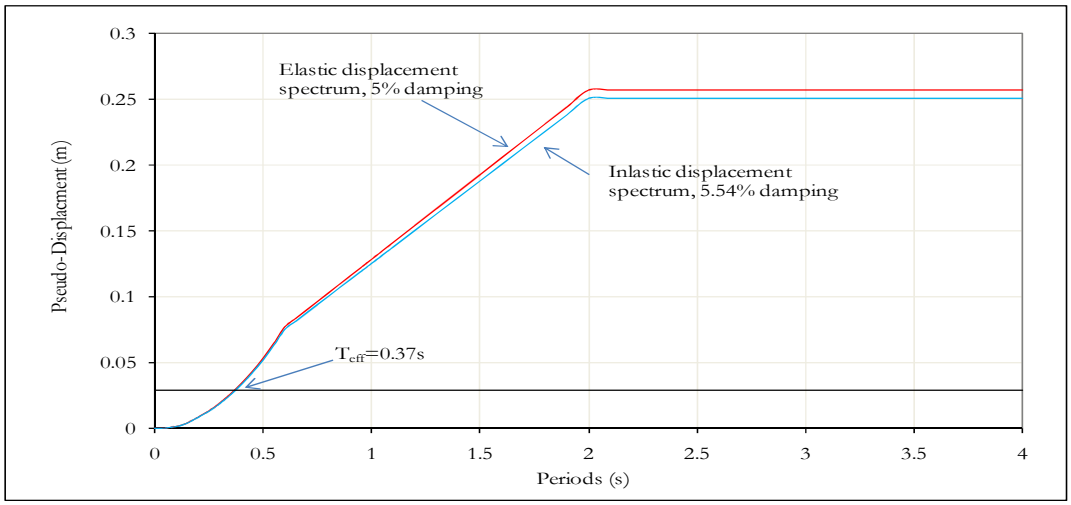

Figure 8-15 – Obtaining effective period, T_{eff}, from design displacement, Δ_d, and reduced displacement design spectrum

Step 7: Distributing the total base shear to each story and selecting and distributing the EMP throughout the structure

Having obtained the total base shear acting on structure, the shear forces acting on each story over the height of the case study frame can be determined by using Equation 8-21. Based on these shear forces, the shear story acting on EMP system can be calculated based on shear proportions to EMP assumed in step 3. The types of EMP in each story can be selected with the help of Table 4-1. Due to the symmetry in

geometry, EMP shall be put at the middle span of the frame. Table 8-7 shows the selected EMP and their properties for each story in the current example.

Table 8-7 – Selection of EMP through out the frame (Config. 1/Case EC2-0.3g)

Story	$F_{i,total}$ (kN)	$V_{Ed,total}$ (kN)	$V_{Ed,EMP}$ (kN)	Type of EMP	$V_{Rd,EMP}$ (kN)
3	680.5	680.5	551.2	5A21-12-17-15	551.2
2	419.2	1099.7	890.8	8A21-12-17-15	890.8
1	225.7	1325.5	1073.6	5A62-34-45-30	1145.0

Step 8: Making an elastic analysis of the retrofitted frame and comparing the properties of the retrofitted frame with the design criteria

According to the proposed procedure in retrofitting the existing frame using EMP, the retrofitted frame will be elastically analysed under a set of shear forces determined from the previous steps. It should be noted that the stiffness of beam and column elements is reduced by 50% taking into account the cracking of the concrete, as required by EC8. In addition, in accordance with DDBD, the stiffness of EMP will be taken as the secant stiffness, corresponding to the target displacement or target drift of the retrofitted frame. The values of initial stiffness and secant stiffness of EMP at each story are given in Table 8-8.

Table 8-8 – Stiffness of EMP through out the retrofitted frame (Config. 1/Case EC2-0.3g)

Story	Type of EMP	$V_{Rd,EMP}$ (kN)	Yield displacement (m)	$\mu_{dEMP,i}$	Initial stiffness (kN/m)	Secant stiffness (kN/m)
3	5A21-12-17-15	551.2	0.009	1.00	61244.4	61244.4
2	8A21-12-17-15	890.8	0.009	1.00	98997.8	98997.8
1	5A62-34-45-30	1145.0	0.009	1.00	127222.2	127222.2

Under lateral shear forces determined, by performing the linear analysis of the retrofitted frame using SAP2000 with EMP modelled as linear link elements with elastic stiffness taken as secant stiffness given in Table 8-8, the top displacement of the retrofitted structure is found to be 0.0383 m and the total base shear acting on the RC-MRF is found to be 341.5 kN. It is clear that the top displacement under designed PGA is not much different from the selected target displacement. However, the total base shear acting on the RC frame is much larger than the shear resistance of the existing frame, which is equal to 250.5 kN. In addition, the ratio of this base shear and the total base shear on retrofitted frame is found to be 25%, different from 19% assumed in the preliminary design process. Clearly, it is necessary to reassume the target displacement at top and the yield drifts of EMP of the retrofitted frame. It is worth stressing that the total base shear on the retrofitted frame is more sensitive to the effective period of the equivalent SDOF system than the target displacement. This effective period is dependent on the ductility of the EMP system and of the existing frame, which is, in turn, related to chosen yield drifts of the EMP and the target drift of the retrofitted frame. Because of that in some cases, many iterative steps have been performed to obtain a reasonable target drift of the retrofitted frame and the yield drifts of the EMP system.

Table 8-9 – Profiles, shear resistance and secant stiffness of selected EMP through out the retrofitted frame (Config. 2/Case EC2-0.05g)

Story	Type of EMP	$V_{Rd,EMP}$ (kN)	Yield displacement (m)	$\mu_{dEMP,i}$	Initial stiffness (kN/m)	Secant stiffness (kN/m)
3	3A51-27-35-30	582.3	0.0045	1.00	129400.0	129400.0
2	3A43-23-45-30	975.0	0.0045	1.00	216666.7	216666.7
1	6A51-27-35-30	1218.0	0.00525	1.00	232000.0	232000.0

In the current example, the final target drift is found to be 0.35% and the yield drifts of the EMP are taken as 0.15%. The profiles and effective secant stiffness of selected EMP used to retrofit the existing

frame are given in Table 8-9. The final displacement of the retrofitted frame from linear analysis is equal to 0.026m (0.28% drift) and the total base shear acting on the RC frame is found to be 232 kN, which is lower than the shear resistance of the existing frame. The RC frame contributes about 15% of the total base shear acting on the retrofitted system.

8.5.2. Case study example 2

In this section another design example of retrofitting a six-story case study building (Configuration 2, Case study EC2-0.05g), in which the ductility of EMP system is activated, is presented. It corresponds to Figure 8-11(b). The frame will be designed using EMP under a new seismicity with PGA of 0.15g.

Step 1: Selecting the target displacement of the retrofitted frame

The pushover curve of the existing frame is shown in Figure 8-16. There are two parts in the curve: the continuous one from origin to the brittle failure of the frame due to crushing of concrete at the beam-column joint and the other, represented by the dashed line, from the node failure point to ultimate behaviour of the frame if it is assumed that node is retrofitted. The failure of node of this frame is coincident with the first hinge occurring on the beam. This is shown by the triangular symbol. Two performance points corresponding to two magnitudes of earthquake having PGAs of 0.05g and 0.15g are also presented in the figure. It is clear that under the earthquake with PGA of 0.05g the frame can reach the target displacement, however, under the PGA of 0.15g the frame will fail before reaching the target displacement due to premature failure at the beam-column joint. In order to ensure that after being retrofitted the frame can reach the target displacement or drift under the seismicity with PGA of 0.15g the retrofitted frame should not exceed the displacement or drift at which the collapse of beam-column joint occurs. Therefore, the target drift or displacement at the top of retrofitted frame should be less than that value. For the studied frame, the drift at failure due to node is 0.514% corresponding to a top displacement of 0.095m. The first choice of target drift or displacement of the retrofitted frame is 0.5%. The maximum resistance of the existing frame is found to be 174.7 kN corresponding to the drift of 0.514% and the shear resistance of the RC frame at 0.5% drift is found to be 170 kN.

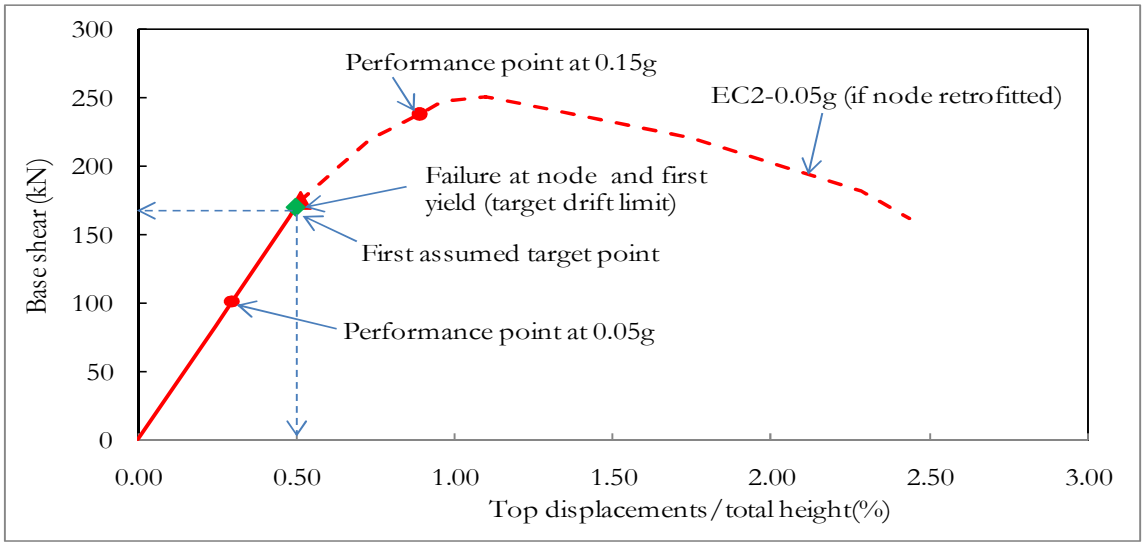

Figure 8-16 – Pushover curve of the existing frame and selected target drift (Case study EC2-0.05g)

Step 2: Target displacement profile, equivalent Single Degree of Freedom Properties of the retrofitted frame and determination of the ductility and Equivalent Viscous Damping (EVD) of the existing frame

Based on the target drift of 0.5%, the target design displacement profile is defined using Equation 8-22 and 8-23. This enables to calculate the properties of the new retrofitted system and of its equivalent SDOF system. They are shown in Table 8-10.

From these properties, the design displacement, Δ_d, the effective mass, m_e, the effective height, H_e, of the equivalent SDOF system are defined as follows:

$$\Delta_d = \sum_{i=1}^{n}\left(m_i\Delta_i^2\right)/\sum_{i=1}^{n}\left(m_i\Delta_i\right) = \frac{1.47}{21.21} = 0.069m\ ;\ m_e = \sum_{i=1}^{n} m_i\left(\frac{\Delta_i}{\Delta_d}\right) = \frac{\sum_{i=1}^{n} m_i\Delta_i}{\Delta_d} = \frac{21.21}{0.069} = 306.0t$$

$$H_e = \sum_{i=1}^{n}\left(m_i\Delta_i H_i\right)/\sum_{i=1}^{n}\left(m_i\Delta_i\right) = \frac{274.44}{21.21} = 12.94m$$

Table 8-10 – Design properties of 6-story frame based on DDBD (Config. 2/Case EC2-0.05g)

Story, i	H_i, m	m_i, t	Δ_i, m	$m_i\Delta_i$, tm	$m_i\Delta_i^2$, tm^2	$m_i\Delta_i H_i$, tm^2
6	18.5	55.6	0.0925	5.14	0.48	95.07
5	15.5	60.0	0.0817	4.90	0.40	75.93
4	12.5	60.0	0.0693	4.15	0.29	51.91
3	9.5	60.0	0.0552	3.31	0.18	31.45
2	6.5	60.0	0.0395	2.37	0.09	15.41
1	3.5	60.0	0.0222	1.33	0.03	4.67

Based on the assessment of the existing frame by Pushover analysis, as in Figure 8-16, the yield drift of the existing frame is determined. The ductility of the existing frame can be readily determined from ratio between the target drift and the yield drift of the existing frame. In this example, because the target drift is lower than the yield drift the ductility of the existing frame is equal to 1, meaning that the EVD of the existing frame is equal to 5%.

Step 3: Assuming the unit base shear acting on the retrofitted frame; proportioning this base shear to the RC frame and to the EMP system; determining the shear story on EMP system

To calculate the EVD of the EMP system, it is necessary to know the shears and the ductility of EMP at each story. This can be done by using strength assignment to the RC frame and the EMP system. This is based on the approach proposed by Paulay (2002). Assuming that the total base shear acting on retrofitted system is equal to one with ten percent of the base shear assigned to the existing frame, the remaining will be assigned to the EMP system. Based on the target displacement profile calculated in step 2, the shear story on the RC frame and on the EMP system can be distributed as in Table 8-11.

Table 8-11 – Distributing the total base shear to the RC frame and to the EMP system and calculation of the shear story on the RC frame and on the EMP (Config. 2/Case EC2-0.05g)

Story, i	$F_{i,total}$	$V_{i,total}$	$F_{i,MRF}$	$V_{i,MRF}$	$F_{i,EMP}$	$V_{i,EMP}$
6	0.242	0.242	0.024	0.024	0.218	0.218
5	0.231	0.473	0.023	0.047	0.208	0.426
4	0.196	0.669	0.020	0.067	0.176	0.602
3	0.156	0.825	0.016	0.083	0.141	0.743
2	0.112	0.937	0.011	0.094	0.101	0.843
1	0.063	1.000	0.006	0.100	0.057	0.900
SUM	1.000	4.147	0.100	0.415	0.900	3.733

Step 4: Choosing the yield drifts for the EMP; determining ductility of EMP system and EVD of the EMP system

The global ductility of EMP system is dependent on the local ductility at each story, which is in turn dependent on the target and yield drifts of EMP on that story. The target drifts over the height of the retrofitted frame is already determined. The yield drifts of EMP on each story can be chosen from 0.12% to 0.4% as presented in Chapter 4 and 5. In the current example, EMP yield drifts for all stories have first

been chosen to be equal to 0.3%. From this drift and the shear story on EMP system, one can calculate the yield displacements as well as the ductility of EMP on each story. The global ductility of the EMP system is then determined by weighting the ductility and shear story on each story. This is presented in Table 8-12.

Table 8-12 – EMP design ductility demand calculation summary (Config. 2/Case EC2-0.05g)

Story, i	Story height	$\theta_{y,EMP}$ (rad)	$\mu_{i,EMP}$	$\Delta_{y,EMP}$ (m)	$V_{i,EMP}$	$V_{i,EMP}\theta_{i,EMP}$	$V_{i,EMP}\theta_{i,EMP}\mu_{i,EMP}$
6	3	0.003	1.20	0.009	0.218	0.0008	0.00094
5	3	0.003	1.38	0.009	0.426	0.0018	0.00244
4	3	0.003	1.56	0.009	0.602	0.0028	0.00441
3	3	0.003	1.74	0.009	0.743	0.0039	0.00676
2	3	0.003	1.92	0.009	0.843	0.0049	0.00935
1	3.5	0.003	2.12	0.0105	0.900	0.0057	0.01210
					Σ	0.0198	0.03600

The overall ductility of the EMP system is (Equation 8-30):

$$\mu_{dEMP,sys} = \frac{\sum V_{EMP,i}\theta_{EMP,i}\mu_{EMP,i}}{\sum V_{EMP,i}\theta_{EMP,i}} = \frac{0.036}{0.0198} = 1.82$$

The EVD of the EMP system is then calculated analogously to that of the MRF, following Equation 8-27:

$$\xi_{EMP} = 0.05 + 0.444\left(\frac{\mu_{dEMP}-1}{\mu_{dEMP}\pi}\right) = 0.1135 = 11.35\%$$

Step 5: Determining OTM of both EMP and existing frame and calculating the Equivalent Viscous Damping of the retrofitted RC-MRF with EMP

The EVD of the dual system will be calculated based on the EVD of the individual systems by weighting their EVD and OTM corresponding to the shear story of each system, as in Equation 8-29.

Table 8-13 – Overturning moment calculation from equivalent force profiles (Config. 2/Case EC2-0.05g)

Story, i	Story height	H_s	F_{total}	M_{total}	F_{MRF}	M_{MRF}	F_{EMP}	M_{EMP}
6	3	18.5	0.242	4.484	0.024	0.448	0.218	4.035
5	3	15.5	0.231	3.581	0.023	0.358	0.208	3.223
4	3	12.5	0.196	2.448	0.020	0.245	0.176	2.203
3	3	9.5	0.156	1.483	0.016	0.148	0.141	1.335
2	3	6.5	0.112	0.727	0.011	0.073	0.101	0.654
1	3.5	3.5	0.063	0.220	0.006	0.022	0.067	0.198
		Σ	1.000	12.942	0.010	1.290	0.900	11.648

The proportions of overturning moment resisted by each system is determined using statics, together with Equation 8-21 for the distribution of the equivalent lateral force acting on the dual system, as presented in Table 8-13, the EVD of the dual system can be obtained by weighting the values of EVD of the individual system:

$$\xi_{sys} = \frac{M_{OTM,MRF}\xi_{MRF} + M_{OTM,EMP}\xi_{EMP}}{M_{OTM,MRF} + M_{OTM,EMP}} = \frac{1.29\times 5.0\% + 11.648\times 11.35\%}{1.29 + 11.648} = 10.7\%$$

Step 6: Inelastic design spectra and DDBD design base shear

From the dual-system EVD, the spectrum reduction factor, R_ξ, is determined:

$$R_\xi = \left(\frac{0.10}{0.05 + \xi_{EVD}} \right)^{0.5} = \left(\frac{0.10}{0.05 + 0.107} \right)^{0.5} = 0.80$$

Using this reduction factor to reduce the design spectrum, the effective period, T_{eff}, can be found from the design displacement, Δ_d, and the reduced spectrum as demonstrated in Figure 8-17.

The effective, K_e, and subsequently the design base shear are then calculated:

$$K_e = \frac{4\pi^2 m_e^2}{T_e^2} = \frac{4\pi^2 \times 306032}{1.35^2} = 6629180\,kN/m;\ V_{base} = K_e \Delta_d = 459324\,N = 459.3\,kN$$

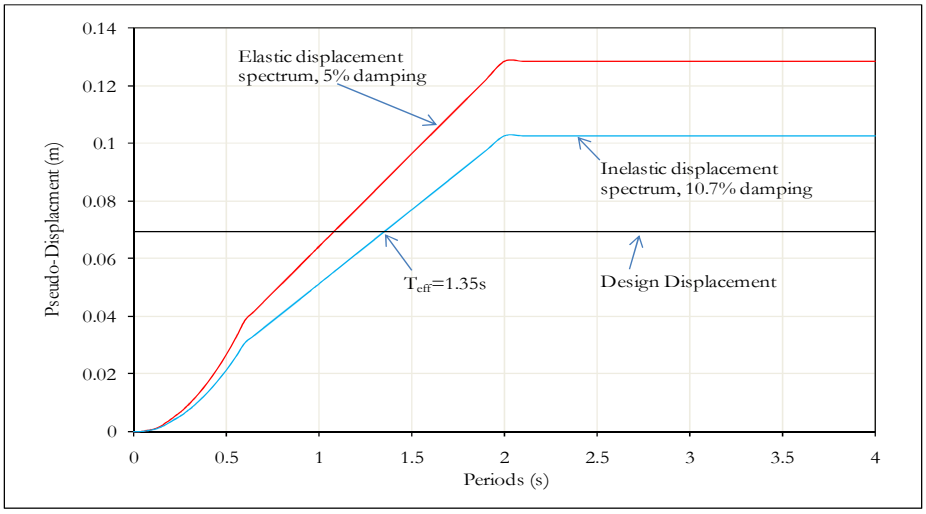

Figure 8-17 – Obtaining effective period, T_{eff}, from design displacement, Δ_d, and reduced displacement design spectrum

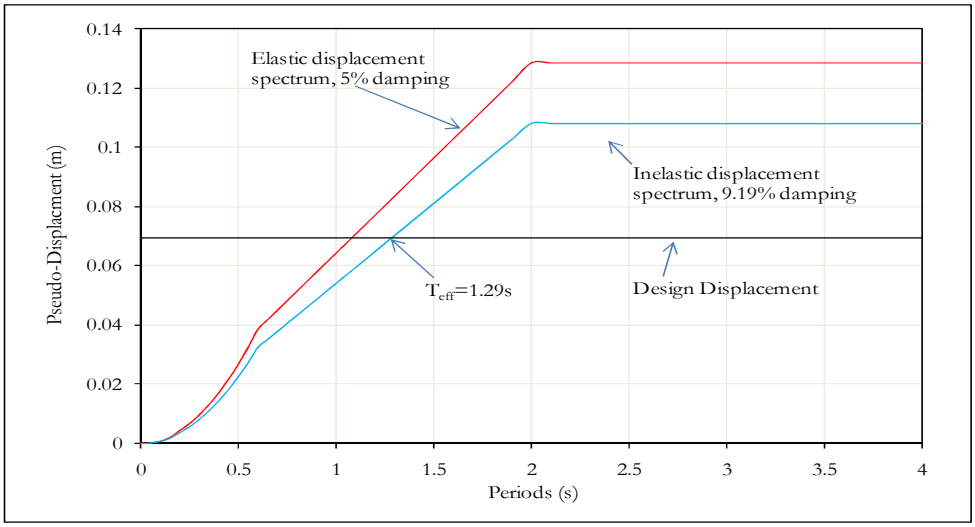

Figure 8-18 – Obtaining effective period, T_{eff}, from design displacement, Δ_d, and reduced displacement design spectrum

Comparing the shear resistance of the RC frame, chosen in step 1, with the total base shear acting to the dual system, calculated above, we can see that the RC frame contributes about 37% of the resistance to the dual system, not 10% as already assumed (170/459.3 = 37%). Therefore, it is necessary to reassume the contribution of the RC frame to the retrofitted system. After three iterative steps, the shear resistance of the RC frame contributing to the total shear resistance of the retrofitted frame is found to be 34%. The

damping of the dual system is 9.19% and the effective period of the substituted SDOF system is 1.29s, as shown in Figure 8-18. The effective stiffness and design base shear are found to be 7260189 kN/m and 503.1kN, respectively.

Step 7: Distributing the total base shear to each story and selecting and distributing the EMP throughout the structure

Having obtained the total base shear acting on structure, the shear forces acting on each story over the height of the case study frame can be determined by using Equation 8-21. Based on these shear forces, the shear story acting on EMP system can be calculated based on shear proportions to EMP assumed in step 6. The kinds of EMP in each story can be selected with the help of Table 4-1. Due to the symmetry in geometry, EMP shall be put at the middle span of the frame. Table 8-14 shows the selected EMP and their properties for each story in the current example.

Table 8-14 – Selection of EMP through out the frame (Config. 2/Case EC2-0.05g)

Story	$F_{i,total}$ (kN)	$V_{Ed,total}$ (kN)	$V_{Ed,EMP}$ (kN)	Type of EMP	$V_{Rd,EMP}$ (kN)
6	160.0	160.0	105.6	1A21-12-17-15	110.2
5	104.6	264.6	174.7	2A28-25-15-10	174.9
4	88.7	353.3	233.2	2A16-7-18-10	247.0
3	70.7	424.0	279.8	3A31-16-23-15	301.0
2	50.6	474.6	313.2	1A43-23-45-30	325.0
1	28.5	503.1	332.0	1A43-23-45-30	340.0

Step 8: Making an elastic analysis of the retrofitted frame and comparing the properties of the retrofitted frame with the design criteria

According to the proposed procedure in retrofitting the existing frame using EMP, the retrofitted frame will be elastically analysed under a set of shear forces determined from the previous steps. It should be noted that the stiffness of beam and column elements is reduced by 50% taking into account the cracking of the concrete, as required by EC8. In addition, in accordance with DDBD, the stiffness of EMP will be taken as the secant stiffness, corresponding to the target displacement or target drift of the retrofitted frame. The values of initial stiffness and secant stiffness of EMP at each story are given in Table 8-15.

Table 8-15 – Stiffness of EMP through out the retrofitted frame (Config. 2/Case EC2-0.05g)

Story	Type of EMP	$V_{Rd,EMP}$ (kN)	Yield displacement (m)	$\mu_{dEMP,i}$	Initial stiffness (kN/m)	Secant stiffness (kN/m)
6	1A21-12-17-15	110.2	0.009	1.20	12249.1	10997.4
5	2A28-25-15-10	174.9	0.009	1.38	19436.5	14070.3
4	2A16-7-18-10	247.0	0.009	1.56	27439.8	17572.0
3	3A31-16-23-15	301.0	0.009	1.74	33442.2	19200.4
2	1A43-23-45-30	325.0	0.009	1.92	36110.0	18778.5
1	1A43-23-45-30	340.0	0.0105	2.12	32379.2	15294.0

Under lateral shear forces determined, by performing the linear analysis of the retrofitted frame using SAP2000 with EMP modelled as linear link elements with elastic stiffness taken as secant stiffness given in Table 8-15, the top displacement of the retrofitted structure is found to be 0.0116 m and the total base shear acting on the RC-MRF is found to be 270.6 kN.

It is clear that the top displacement under designed PGA is not much different from the selected target displacement. However, the total base shear acting on the RC frame is much larger than the shear resistance of the existing frame, which is equal to 170.0 kN. In addition, the ratio of this base shear and

the total base shear on retrofitted frame is found to be 53%, different from 34% assumed in the preliminary design process.

Clearly, it is necessary to reassume the target displacement at top and the yield drifts of EMP of the retrofitted frame. It is worth stressing that the total base shear on the retrofitted frame is more sensible to the effective period of the equivalent SDOF system than the target displacement. This effective period is dependent on the ductility of the EMP system and of the existing frame, which is, in turn, related to chosen yield drifts of the EMP and the target drift of the retrofitted frame. Because of that in some cases, many iterative steps have been performed to obtain a reasonable target drift of the retrofitted frame and the yield drifts of the EMP system. In the current example, the final target drift is found to be 0.48% and the yield drifts of the EMP are taken as 0.4%. The profiles and effective secant stiffness of selected EMP used to retrofit the existing frame are given in Table 8-16. The final displacement of the retrofitted frame from linear analysis is equal to 0.0091m (0.49% drift) and the total base shear acting on the RC frame is found to be 165 kN, which is lower than the shear resistance of the existing frame. The RC frame contributes about 27% of the total base shear acting on the retrofitted system.

Table 8-16 – Profiles, shear resistance and secant stiffness of selected EMP through out the retrofitted frame (Config. 2/Case EC2-0.05g)

Story	Type of EMP	$V_{Rd,EMP}$ (kN)	Yield displacement (m)	$\mu_{dEMP,i}$	Initial stiffness (kN/m)	Secant stiffness (kN/m)
6	1A86-46-43-30	136.7	0.012	1.00	15487.4	15487.4
5	2A16-7-18-10	247.0	0.012	1.00	27979.7	27979.7
4	1A43-23-45-30	325.0	0.012	1.12	36820.5	32749.0
3	2A51-27-35-30	303.0	0.012	1.25	34294.6	27347.0
2	2A62-34-45-30	437.3	0.012	1.38	49547.4	35805.7
1	4A21-12-17-15	462	0.014	1.52	49153.4	32245.4

8.5.3. Verification of the proposed method and seismic evaluation of the case study RC-MRFs retrofitted by EMP using Pushover and NLTH analyses

To assess the validity of the proposed design method, Pushover and NLTH have been performed using the program SAP 2000 under the four seismic accelerogram records generated by GOSCA (Denoel, 2001).

8.5.3.1. Modelling of RC-MRFs and seismic input for nonlinear analyses

Beams and columns were modelled as linear beam elements with nonlinear properties of material considered as concentrated plastic hinges at two ends. Pivot model (Wilson, 1982) was used to represent the hysteretic loops of this element. Geometrical nonlinearities with P-delta effects and large displacement are also taken into account.

8.5.3.2. Modelling of EMP for nonlinear analyses

It can be seen from the study on EMP that under shear monotonic loading post buckling behaviour governs the performance of EMP. Post buckling behaviour of EMP under shear can be regarded as a tension field action corresponding to a band having a certain effective width with the same thickness and mechanical properties. Under cyclic shear loading, within a cycle the behaviour of EMP is also represented by a tension band corresponding to each direction of loading. The transition between each direction of loading is marked by pinching effect. The stiffness and resistance of EMP before redeveloping the tension field in the reversed direction is very low. Apparently, EMP can be modelled as an element having some characteristics: (1) initial stiffness being equal to the ratio between yield shear and yield displacement; (2) strength equivalent to a tension band having a certain effective width; (3) pinching effects accounting for the degradation of the stiffness when the load is reversed. With SAP 2000, EMP can be modelled by using two-node link elements with pivot hysteresis model, suggested by Dowell et al. (1998). This model is graphically explained in Figure 8-19.

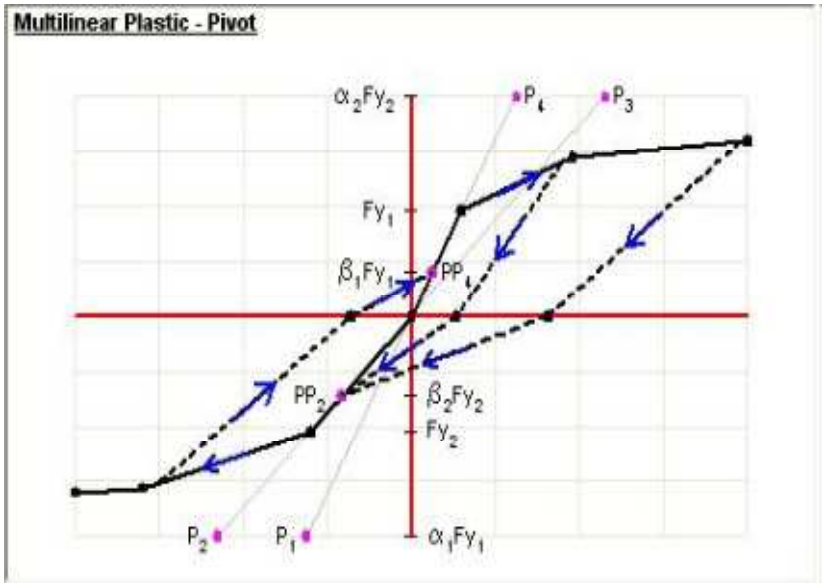

Figure 8-19 – Pivot hysteresis model in SAP 2000 for EMP (Dowell et al., 1998)

The parameters used in the model are explained hereafter:

• $\alpha 1$, which locates the pivot point for unloading to zero from positive force, taken as 1; $\alpha 2$, which locates the pivot point for unloading to zero from negative force, taken as 1

• $\beta 1$, which locates the pivot point for reverse loading from zero toward positive force, taken as 0.1, meaning that stiffness of the elements is reduced 90% compared to the elastic stiffness. $\beta 2$, which locates the pivot point for reverse loading from zero toward negative force, taken as 0.1, meaning that stiffness of the elements is reduced 30% compared to the elastic stiffness.

• η, which determines the amount of degradation of the elastic slopes after plastic deformation, taken as 0, meaning that unloading slope is equal to elastic slope.

8.5.3.3. Seismic response of the retrofitted frames in comparison with the ones before retrofitting of the two examples by Pushover and NLTH analyses

The left figures in Figure 8-20 and Figure 8-21 show the maximum interstory drifts and their average values under individual accelerograms corresponding to design PGAs (0.3g and 0.15g) of the retrofitted system established by NLTH and Pushover analyses. The target interstory drifts in design steps calculated from target displacement at the top of the retrofitted frame is presented by dashed lines in those figures. The lines in green in the figure depict the interstory drift profiles of the retrofitted frame at target displacement under design PGAs of 0.3g and of 0.15g, established by Pushover analysis. The original interstory drifts at the selected target displacements of the original frames, established by Pushover analysis, are also presented by the black lines. As mentioned in the design process, the main purpose of retrofitting the existing frame using EMP is to limit the deformations of the frame within a safe margin, which is based on its seismic assessment. From the figures, one can observe that the target interstory drift profiles, represented by the design line, are not much different from the ones, established by NLTH analysis. Also, the average interstory drifts from NLTH analysis (the red lines) are close to the interstory drifts of the frame before being retrofitted (the black lines). This means that the purpose of design process to limit the deformation of the retrofitted frame under a given earthquake at a selected deformation is obtained. It is also observed from the figures that the results of Pushover and NLTH analysis of the retrofitted frame are slightly different. Pushover analysis overestimates the interstory drifts of the frame.

The right figures in Figure 8-20 and Figure 8-21 present displacement profiles of the frame before being retrofitted at selected target displacement (the curves in black). The curves in red expresse the average displacement profiles of the retrofitted frame performed by NLTH analysis under 4 accelerograms corresponding to design PGAs. The cyan dashed curves depict the target design displacements of the retrofitted frame. The curves in green show the displacement profiles of the retrofitted frame from Pushover analysis. Observing the real and target displacement profiles of the frame before and after being

retrofitted, it is easily seen that all these curves fit well together. Under the design earthquake, the displacement of the retrofitted frame is nearly the same as the target displacement selected in the design process. The proposed design method in relevance with DDBD gives a useful tool to retrofit the frame using EMP. It is also observed that the results from Pushover analysis are greater than those from NLTH analysis.

Figure 8-22 shows the resulting shear forces and shear resistance of the frame before and after being retrofitted at design PGA from Pushover analysis. The dashed lines in cyan in the figures express the design story shears obtained by the proposed method, presented above. The continuous lines in green show that resulting story shears at target displacement (corresponding to the design PGA of 0.3g and of 0.15g) of the retrofitted frame from Pushover analysis. Clearly, they fit rather well together. The lines in red and in yellow are corresponding to the shear forces of the RC frame and of the EMP system at the target displacement obtained by Pushover analysis. The sum of these two lines at each story is corresponding to the lines in green in those figures. The black lines in the figures are the shear resistance at each story of the existing frame at the selected target displacement. These lines are obtained by Pushover analysis of the existing frame, presented in Chapter 7. One can see that under the design earthquake the story shears in the RC frame (the red lines) after being retrofitted are less than or approximately equal to the story shear resistance of the existing frame.

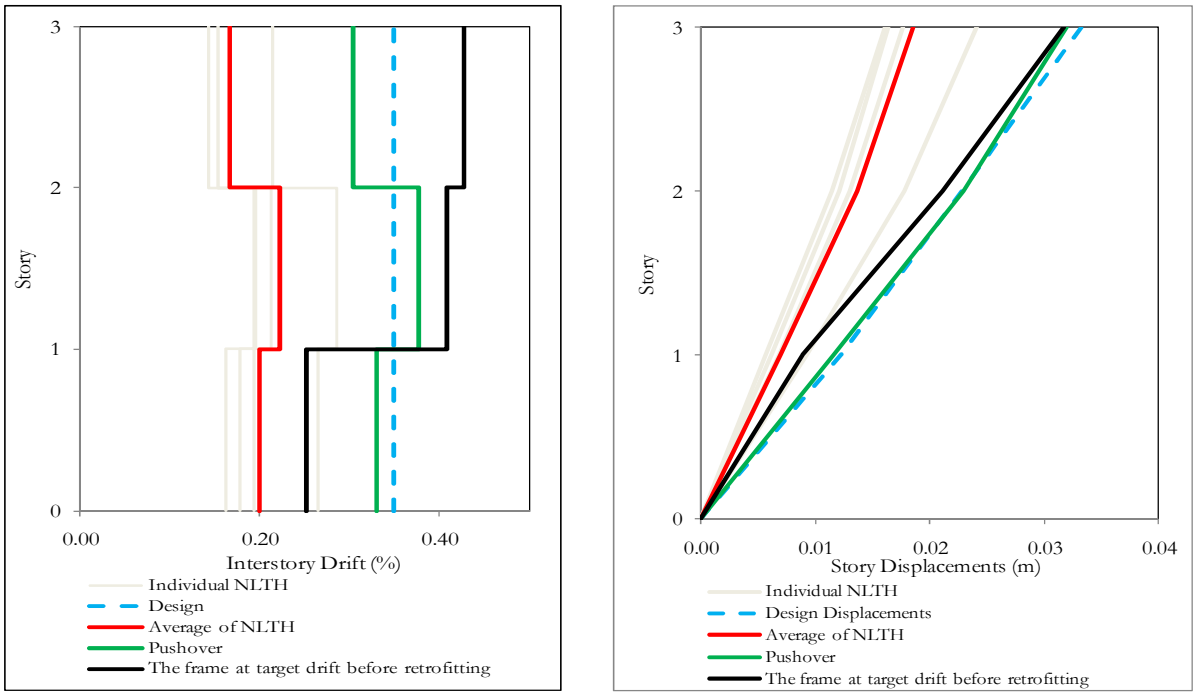

Figure 8-20 – Interstory drift and shear forces in retrofitted frame of the example Case 1/EC2-0.3g under earthquake at design PGA=a_{gR}=0.3g established by Pushover and NLTH analyses (left: the interstory drifts; right: displacement profiles)

Figure 8-23 and Figure 8-24 show the Pushover curves of the original and retrofitted frames using EMP. The performance points at design PGAs of 0.3g and of 0.15g of the frames are also given. Continuous curves are the behaviour of the frames before and after retrofitting until the failure due to crushing of concrete at beam-column joints. The dashed parts present their behaviour if it is assumed that beam-column joints are well retrofitted. It is clear that brittle failure due to the collapse of the beam-column joints governs the behaviour of the systems. In both Pushover and NLTH analyses, the brittle failure occurs at the stage at which the first plastic hinges have occurred at the ends of the intermediate beams. However, there an essential difference between two frames. For the non retrofitted one, the frame cannot reach the performance point caused by the earthquake having PGAs of 0.3g (for the Case 1/EC2-0.3g) and of 0.15g (for the Case 2/EC2-0.05g) due to premature failure of the joint. On the contrary, the retrofitted frame is able to reach the performance point under the design earthquake having similar PGAs of 0.3g and of 0.15g. The brittle failure due to the collapse of the beam-column node can occur but at a higher earthquake. As clearly observed in the figures, EMP significantly increases the stiffness and the

strength for the existing frame. This leads to lower displacement and more energy dissipated in the retrofitted one than in the original one under the similar seismic action.

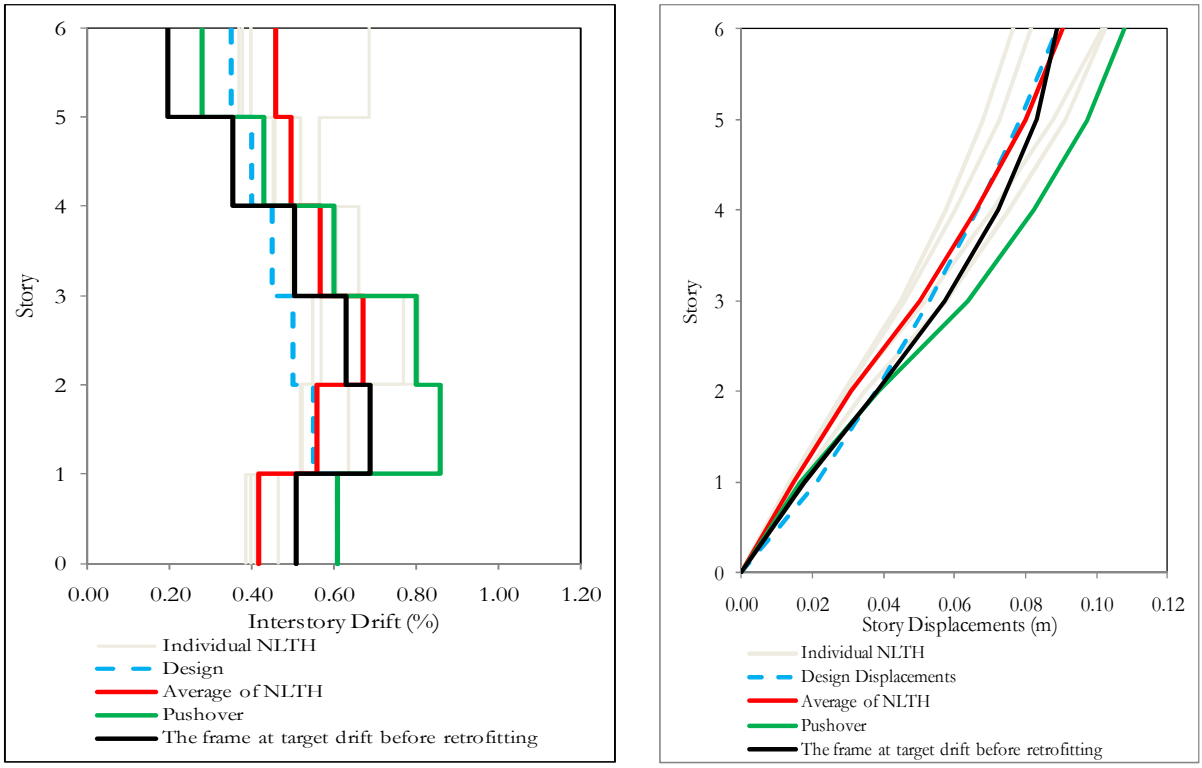

Figure 8-21 – Interstory drift and shear forces in retrofitted frame of the example Case 2/EC2-0.05g under earthquake at design PGA=a_{gR}=0.15g established by Pushover and NLTH analyses (left: the interstory drifts; right: displacement profiles)

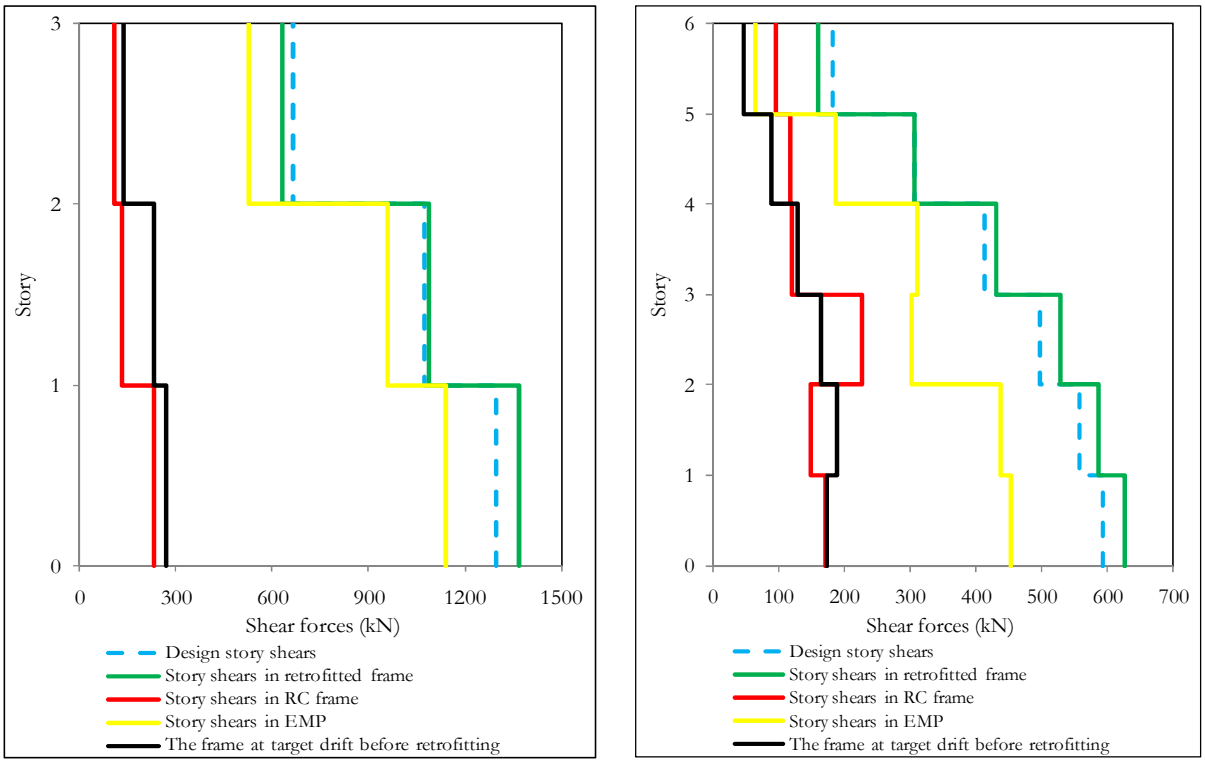

Figure 8-22 – Story shears of the examples under design PGA established by Pushover analysis (left: Case 1/EC2-0.3g; right: Case 2/EC2-0.05g)

In conclusion, the proposed design method using DDBD gives an acceptable solution for designing EMP retrofitting. The advantage of this method comes from its ability to obtain a desired or target displacement for the retrofitted frame under a given earthquake. Therefore, it is possible to select a safe limit of deformation as the target displacement for the existing frame based on its seismic assessment. Nevertheless, there are still some differences in interstory drifts between the values in design steps and real ones. In addition to that the failure at beam-column joints is inevitable. This needs a combination of EMP and some other retrofitting solutions. Although there are still some shortcomings, DDBD may be an efficient method in choosing the properties of EMP for the retrofitting process.

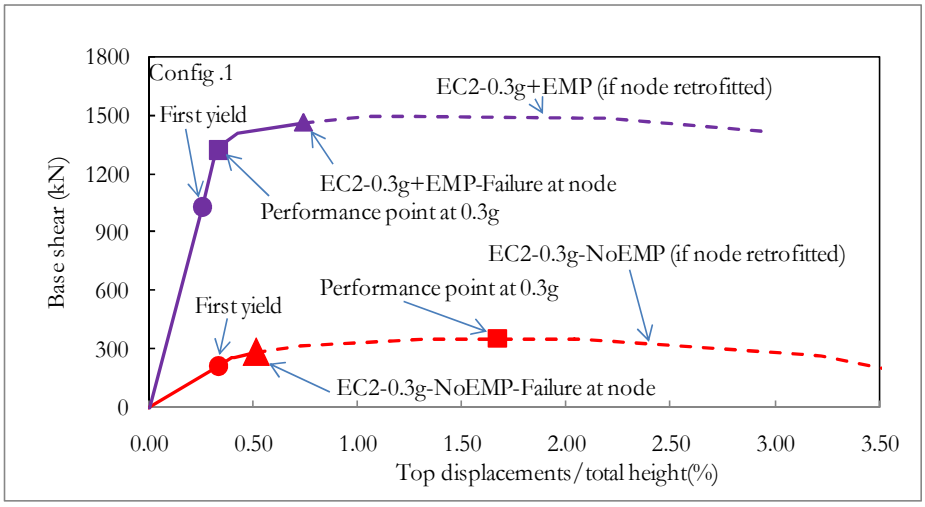

Figure 8-23 – Seismic performance of the frame Case 1/EC2-0.3g before and after being retrofitted by Pushover analysis

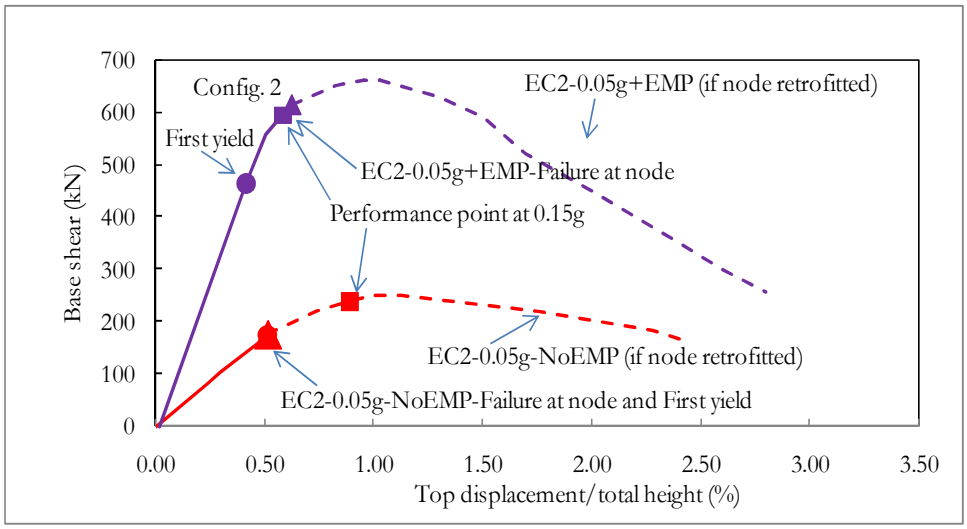

Figure 8-24 – Seismic performance of the frame Case 2/EC2-0.05g before and after being retrofitted by Pushover analysis

8.5.4. General results of retrofitting design of the existing frames based on DDBD

8.5.4.1. RC-MRFs in EC2 group

In this group, twelve frames in 4 configurations have been designed according to EC2. These frames are supposed to be located in three seismicity zones, having PGA of 0.05g, 0.15g and 0.3g and soil C, as defined in EC8. All frames have been evaluated by using pushover and NLTH analyses. Due to not having been designed in accordance with EC8, therefore there is some undesirable failure modes detected at the earthquake intensity of unity, such as soft-story or incomplete load path. To assess the necessity of retrofitting the EC2 frames under seismic actions, Pushover is adopted. Table 8-17 presents the maximum resistible PGA of the existing frames from Pushover results and the check of necessity of

retrofitting/upgrading the existing frames. Clearly, despite not being designed to EC8 the EC2 frames in low seismic zones having PGA of 0.05g are able to sustain the earthquake at PGA of 0.05g. Therefore, these frames do not need to be retrofitted. The remaining frames in zones with PGA of 0.15g and 0.3g will collapse if the earthquake at design PGA occurs due to node failure. It is necessary to retrofit them and they are considered as the subject of the next sections.

Table 8-17 – Check of the necessity of upgrading the existing frames in EC2-group

Configuration/Case	PGA causing failure (g)	PGA to be sustained by retrofitted structures (g)	Failure criteria	To be upgraded or Not
Conf.1/EC2-0.05g	0.06	0.15	Node	YES
Conf.1/EC2-0.15g	0.08	0.15	Node	YES
Conf.1/EC2-0.3g	0.09	0.30	Node	YES
Conf.2/EC2-0.05g	0.08	0.15	Node	YES
Conf.2/EC2-0.15g	0.08	0.15	Node	YES
Conf.2/EC2-0.3g	0.12	0.30	Node	YES
Conf.3/EC2-0.05g	0.11	0.15	Node	YES
Conf.3/EC2-0.15g	0.11	0.15	Node	YES
Conf.3/EC2-0.3g	0.11	0.30	Node	YES
Conf.4/EC2-0.05g	0.10	0.15	Node	YES
Conf.4/EC2-0.15g	0.10	0.15	Node	YES
Conf.4/EC2-0.3g	0.19	0.30	Node	YES

Determination of the properties of the equivalent SDOF of the retrofitted frames

It is expected that the retrofitted RC-MRFs using EMP are able to resist a given earthquake (defined in the third column in Table 8-17). Following the design steps introduced in Figure 8-12, the properties of the retrofitted frames can be addressed based on the target drifts or target displacements, on their target displacement profiles and on the Equivalent Viscous Damping of individual systems (the frames and the EMP) and of the retrofitted frames. Table 8-18 to 20 show these properties of the "substitute" SDOF systems. It is clear from this table that the ductility of the EMP is exploited much more in the tall frames than in the low ones. Moreover, in most cases, the ductility of the EMP is activated. However, the ductility of the existing frames is only activated in a few cases.

Table 8-18 – Properties of the "substitute SDOF" structures

Configuration/Case	% base shear assigned to EMP	Target design drift (%)	Effective height (m)	Effective mass (ton)	Design Displ. (m)	μ_{MRF}	μ_{EMP}
Conf.1/EC2-0.05g	77	0.40	7.37	150.7	0.029	1.00	1.33
Conf.1/EC2-0.15g	70	0.45	7.35	153.5	0.033	1.71	1.50
Conf.1/EC2-0.3g	85	0.35	7.31	157.2	0.026	1.04	1.00
Conf.2/EC2-0.05g	73	0.48	12.9	320.8	0.066	1.00	1.31
Conf.2/EC2-0.15g	73	0.48	12.9	320.8	0.066	1.00	1.31
Conf.2/EC2-0.3g	80	0.60	12.8	333.5	0.080	1.35	4.26
Conf.3/EC2-0.05g	60	0.37	16.64	437.4	0.066	1.00	2.64
Conf.3/EC2-0.15g	60	0.37	16.64	437.4	0.066	1.00	2.64

Table 8-19 – Properties of the "substitute SDOF" structures (continued)

Configuration/Case	% base shear assigned to EMP	Target design drift (%)	Effective height (m)	Effective mass (ton)	Design Displ. (m)	μ_{MRF}	μ_{EMP}
Conf.3/EC2-0.3g	80	0.50	16.6	437.4	0.090	1.00	3.57
Conf.4/EC2-0.05g	75	0.30	20.5	541.4	0.066	1.00	2.69
Conf.4/EC2-0.15g	75	0.30	20.5	541.4	0.066	1.00	2.69
Conf.4/EC2-0.3g	70	0.60	20.3	592.9	0.132	1.00	4.32

Table 8-20 – Properties of the "substitute SDOF" structures

Configuration/Case	Equivalent viscous damping (EVD) of RC-frames (%)	EVD of EMP (%)	EVD of 'dual-systems' (%)	Effective period, T_e (s)	Design base shear (kN)	Base shear/Seismic weight (%)
Conf.1/EC2-0.05g	5.0	8.5	8.00	0.56	559.6	33.1
Conf.1/EC2-0.15g	12.5	9.7	10.3	0.65	474.1	27.5
Conf.1/EC2-0.3g	5.7	5.0	5.1	0.35	1296.1	73.5
Conf.2/EC2-0.05g	5.0	8.4	7.5	1.19	592.2	16.2
Conf.2/EC2-0.15g	5.0	8.4	7.5	1.19	592.2	16.2
Conf.2/EC2-0.3g	9.7	15.8	14.6	0.90	1340.7	35.4
Conf.3/EC2-0.05g	5.0	13.8	10.3	1.26	720.9	14.2
Conf.3/EC2-0.15g	5.0	13.8	10.3	1.26	720.9	14.2
Conf.3/EC2-0.3g	5.0	15.2	13.2	0.97	1643.7	32.3
Conf.4/EC2-0.05g	5.0	13.9	11.7	1.37	755.5	11.8
Conf.4/EC2-0.15g	5.0	13.9	11.7	1.37	755.5	11.8
Conf.4/EC2-0.3g	5.0	15.9	12.6	1.35	1693.3	24.2

Selection and distribution of EMP through out the structure

Based on the base shear acting on the EMP and distributed over the height of buildings, the properties of EMP can be selected. Most frames in the case study structures are symmetrical in plan and elevation, therefore, EMP can be placed at the middle span of the frame.

8.5.4.2. RC-MRFs in EC8 group

Twenty frames in this group have been designed and detailed according to EC2 and EC8. They have been also situated in three seismic zones, having the PGAs of 0.05g, 0.15g and 0.3g. Due to the change of the seismicity, it is assumed that the magnitude of seismic action in these zones has been increased, as observed in some parts of the World such as in Turkey… Therefore, the structures which are located in those zones should be upgraded to be able to resist the increasing amount of earthquake actions. A question raised here is: is it necessary to upgrade the existing frames? In order to answer this question, the maximum resistible PGA of the existing frame will be compared with the 'new' PGA of the zones. Similarly to the frames of EC2 group, Pushover analysis is used to determine the maximum resistible PGA of the case study frames. Table 8-21 presents the maximum resistible PGA of the existing frames from Pushover results and the check of necessity of retrofitting/upgrading the existing frames.

Clearly, thanks to much over-strength in the design process, the real capacity of many existing frames in this group is greater than the required one, being almost the capacity of the frames of the Medium

Ductility Class. Therefore, these frames do not need to be upgraded. And from now on, only the frames needing upgrade are considered.

Table 8-21 – Check of the necessity of upgrading the existing frames in EC8-group

Configuration/Case	Design PGA (g)	PGA causing failure (g)	PGA to be sustained by retrofitted structures (g)	Failure criteria	To be upgraded or Not
Conf.1/EC8-0.05g-L	0.05	0.08	0.15	Node	YES
Conf.1/EC8-0.15g-L	0.15	0.13	0.15	Node	YES
Conf.1/EC8-0.05g-M	0.05	0.5	0.15	Global	No
Conf.1/EC8-0.15g-M	0.15	0.65	0.30	Global	No
Conf.1/EC8-0.3g-M	0.30	1.00	0.40	Global	No
Conf.2/EC8-0.05g-L	0.05	0.08	0.15	Node	YES
Conf.2/EC8-0.15g-L	0.15	0.09	0.15	Node	YES
Conf.2/EC8-0.05g-M	0.15	0.65	0.15	Global	No
Conf.2/EC8-0.15g-M	0.15	0.65	0.30	Global	No
Conf.2/EC8-0.3g-M	0.30	0.84	0.40	Global	No
Conf.3/EC8-0.05g-L	0.05	0.12	0.15	Node	YES
Conf.3/EC8-0.15g-L	0.15	0.16	0.30	Node	YES
Conf.3/EC8-0.05g-M	0.05	0.65	0.15	Global	No
Conf.3/EC8-0.15g-M	0.15	0.85	0.30	Global	No
Conf.3/EC8-0.3g-M	0.30	1.30	0.40	Global	No
Conf.4/EC8-0.05g-L	0.05	0.15	0.15	Node	No
Conf.4/EC8-0.15g-L	0.15	0.17	0.30	Node	YES
Conf.4/EC8-0.05g-M	0.15	0.80	0.10	Global	No
Conf.4/EC8-0.15g-M	0.15	0.84	0.30	Global	No
Conf.4/EC8-0.3g-M	0.30	0.84	0.40	Global	No

Selection of the capacity of the existing RC-MRFs contributing to the overall resistance of the dual systems

It can be seen from Table 8-21 that there are three frames in EC8 group which require an upgrade. They are all designed accordingly to Low Ductility Class. They collapse because of the failure at beam-column joints. Therefore they could not reach the performance point under the design earthquake. For these frames, similarly to the cases in EC2 group, depending on the failure displacements of each frame, the target displacements are selected as explained in Figure 8-6 and Figure 8-12. These values are presented in Table 8-22.

Determination of the properties of the equivalent SDOF

It is expected that under the design PGAs with use of EMP the retrofitted frame can reach the target displacement without any premature failure as observed in the frame before retrofitting. Because of that the target displacements are selected in the safe region as shown in Figure 8-6.

A target linear or nonlinear displacement profile (Equation 8-22 and Equation 8-23) with the selected target displacement is assumed for the first inelastic mode shape of the dual system. Table 8-22 and Table 8-23 show the properties of those "substitute" systems for the structures needing an upgrade.

Table 8-22 – Properties of the "substitute SDOF" structures

Configuration/Case	% base shear assigned to EMP	Target ultimate drift (%)	Effective height (m)	Effective mass (ton)	Design Displ. (m)	μ_{MRF}	μ_{EMP}
Conf.1/EC8-0.05g-L	70	0.40	7.37	150.7	0.029	1.0	1.33
Conf.1/EC8-0.15g-L	70	0.45	7.35	153.5	0.033	1.0	1.50
Conf.2/EC8-0.05g-L	60	0.48	12.94	306.0	0.066	1.0	1.70
Conf.2/EC8-0.15g-L	67	0.45	12.87	320.8	0.062	1.0	1.60
Conf.3/EC8-0.05g-L	57	0.40	16.64	437.4	0.072	1.0	2.85
Conf.3/EC8-0.15g-L	67	0.60	16.64	437.4	0.108	1.0	3.20
Conf.4/EC8-0.15g-L	67	0.55	20.50	541.4	0.122	1.0	4.94

Table 8-23 – Properties of the "substitute SDOF" structures

Configuration/Case	EVD of RC-frames (%)	EVD of EMP (%)	EVD of 'dual-systems' (%)	Effective period, T_e (s)	Design base shear (kN)	Base shear/Seismic weight (%)
Conf.1/EC8-0.05g-L	5.0	8.5	7.4	0.55	580.1	34.3
Conf.1/EC8-0.15g-L	5.0	9.7	8.2	0.58	556.4	32.0
Conf.2/EC8-0.05g-L	5.0	10.8	8.5	1.40	410.0	11.8
Conf.2/EC8-0.15g-L	5.0	10.3	8.5	1.31	458.1	12.5
Conf.3/EC8-0.05g-L	5.0	14.2	10.2	1.38	649.7	12.8
Conf.3/EC8-0.15g-L	5.0	14.7	11.5	1.20	1289.0	25.3
Conf.4/EC8-0.15g-L	5.0	16.3	13.5	1.30	1538.2	24.1

Selection and distribution of EMP through out the structure

Similarly to the Case in EC2-group, because all the studied frames are regular in plan and elevation EMP are placed at the middle spans of the frames.

8.6. Nonlinear response of the retrofitted structures in comparison with the structures before retrofitting

8.6.1. Periods

Table 7-3 shows the fundamental periods of the RC-MRFs before and after being retrofitted. The linear and nonlinear periods have been determined from time histories of top displacements as the average of four accelerograms of the ratios t/n, where n is the number of complete cycles of displacement and t the duration of the series from linear and nonlinear dynamic analyses (Carvalho, 1997).

It can be seen from Table 7-3 that although EMP has a very little elastic stiffness, however, thanks to its strength the stiffness of the dual system has been increased. Both the linear and nonlinear periods of the retrofitted frames with EMP or dual systems are lower than those of the original ones. The increase of the stiffness in the dual systems is dependent on the characteristics of the EMP. The higher base shears, requested to resist the seismic forces, the more EMP will be used. This leads to the increase of the stiffness in the dual system. Therefore, the period will be decreased.

It can also be observed that the values of nonlinear periods in most cases are greater than the elastic periods obtained by linear analysis. This is the result of the decrease of the structural stiffness, caused by

nonlinear behaviour in material and in geometry. However the increase due to nonlinear properties in the dual systems is not as much as in the original frames. This may be due to the fact that the stiffness of the dual system is not reduced much when coming to inelastic range. This also means that the plastic hinge rotations in the original frames are greater than those in the dual systems. In some cases of Configuration 1, the linear and nonlinear periods of the retrofitted frames are the same. This means that under the design PGAs the dual systems mostly work in the elastic range with small lateral deformations leading to very small effect of nonlinear geometry.

Table 8-24 – Fundamental periods of the RC-MRFs retrofitted in by linear and nonlinear time history analyses

Config.	Case	Fundamental periods (s)			
		Before retrofitting		After retrofitting	
		Linear dynamic	Nonlinear dynamic	Linear dynamic	Nonlinear dynamic
1	EC2-0.05g	1.25	1.25	0.58	0.58
	EC2-0.15g	0.96	1.10	0.59	0.59
	EC2-0.3g	0.84	0.91	0.34	0.36
	EC8-0.05g-L	1.25	1.25	0.59	0.59
	EC8-0.15g-L	0.96	0.97	0.59	0.60
2	EC2-0.05g	1.99	1.99	1.16	1.19
	EC2-0.15g	2.07	2.11	1.16	1.19
	EC2-0.3g	1.74	1.80	0.67	0.70
	EC8-0.05g-L	1.99	1.99	1.23	1.32
	EC8-0.15g/L	2.07	2.09	1.16	1.29
3	EC2-0.05g	1.67	1.67	1.02	1.10
	EC2-0.15g	1.67	1.72	1.02	1.10
	EC2-0.3g	1.90	2.00	0.87	0.87
	EC8-0.05g-L	1.67	1.67	1.10	1.10
	EC8-0.15g/L	1.67	1.70	0.91	0.93
4	EC2-0.15g	1.84	2.05	1.15	1.18
	EC2-0.3g	1.79	2.20	1.15	1.19
	EC8-0.15g/L	1.84	2.03	1.19	1.22

8.6.2. Comparison of nonlinear response of the studied RC-MRFs before and after retrofitted

The nonlinear behaviour of retrofitted systems in comparison with the original frames is presented from Figure 8-26 through Figure 8-60. The advantage and disadvantage of EMP on retrofitting or upgrading the existing RC-MRFs is discussed herein based on assessing the seismic performance of the frames before and after being retrofitted. This is done with the aid of Pushover and NLTH analyses.

Figure 8-26 to Figure 8-32 depict the capacity curves of all frames before and after being retrofitted. The reasons of failure of the frames and performance points at the design earthquake are also given in these figures. It is clear from the figures that the advantage of EMP comes from its capacity in increasing the strength and stiffness of the systems. Thanks to that, all frames after being retrofitted can reach the target

displacements expressed by the performance points before the failure of beam-column joints. It can also be observed from these figures that the top displacements at failure of some retrofitted frames are greater than those of the ones before retrofitting although their selected target displacements at top are less than the failure displacements at top of the original frames. It can be explained by the fact that the failure at beam-column joints is governed by interstory drifts not by the top displacements. The local failure due to the crushing of the concrete at beam-column joints is still the prominent failure mode in the retrofitted frames. However, all these brittle failures occur after the retrofitted frames have reached the target displacements under design earthquakes.

It can be seen from Figure 8-26 to Figure 8-32 that some retrofitted frames have exhibited little nonlinear response at failure. This is because they have worked in the elastic range with small values of lateral deflections. It is also observed that the first plastic hinges in most retrofitted frames have occurred at smaller drifts than those in the frames before being retrofitted, leading to greater ductility for the dual system.

If it is supposed that all beam-column joints have been retrofitted and failure is attained in plastic hinges, the typical failure mechanisms are presented in Figure 8-33. For the frames in EC2-group, the distribution of plastic hinges does not change much when comparing with the frames before retrofitting, scattered in both beams and columns, as observed in both Pushover and NLTH analyses. The positive effect of EMP is to delay the failure of the frame at much larger deformation. This leads to the increase of the capacity of the frames with EMP. For retrofitted frames in EC8-group, plastic mechanisms are not changed. The EMP also increases the deformation capacity for the retrofitted structures. Observing the distribution and plastic deformation of plastic hinges of frames before and after retrofitting from Figure 8-33, it can be seen that EMP can reduce the damage of the plastic hinges. The two pictures in Figure 8-33 are plotted at the same top displacements established by Pushover. Before retrofitting, at failure, sway of two first stories is observed with rotations of plastic hinges at base being in Collapse Prevention, which is close to collapse. After retrofitting, with the presence of EMP, plastic hinges in frames are distributed more uniformly than those in the frames without EMP. The rotations of four plastic hinges at base are reduced, compared to those before retrofitting. This means that EMP has played a role to redistribute the seismic actions in the structures. In addition, it is also observed that the sway of two first stories does not occur in retrofitted frames, leading to lower P-Δ effects on the structures. However, it should be noted that this preferred response has not been observed for all retrofitted frames. The distribution of EMP in the frames has a significant influence on the plastic redistribution of the structures. This needs further work to optimise the selection of EMP.

Figure 8-35 and Figure 8-38 show the target or maximum displacements at top of the frames at design PGA before and after being retrofitted from Pushover and NLTH analyses. It should be noted that these figures can only be obtained if it is assumed that failure of beam-column joints does not occurs or these joints are stiffened and strengthened to have more strength and ductility. It is clear that with the presence of EMP the displacements at top of the frames have been reduced significantly. In some cases, the displacements are reduced about 50%. Like in nonlinear analyses of the frames without EMP, the results between Pushover and NLTH are not consistent. Pushover overestimates the responses of the structures, especially for the long period frames.

Figure 8-39 and Figure 8-42 present the base shears generated in the frames before and after being retrofitted under design earthquakes in comparison with their design base shears with the assumption that there is no failure at beam-column joints for the frames before being retrofitted. It is necessary to note that for some EC8-L frames because their 'new design PGAs' are greater than those for the original frames; therefore their design base shears in the original frames are not considered. In addition, for the EC2 frames before retrofitting, because they have not designed according to EC8 their design base shears are equal to zero. The term 'design PGAs' mentions about the PGAs used to design EMP for the dual system. It should also be recalled that for structures before retrofitting, the Force Based Design method was adopted and for retrofitted structures, the DDBD method was used to design EMP for retrofitted frames. As observed in Figure 8-39 and Figure 8-42, for all studied frames, the base shears generated in the frames at design PGAs before retrofitting are much smaller than those generated in the ones after retrofitting. This is logical because EMP has increased the stiffness and masses of the retrofitted structures. Thus it leads to greater pseudo-accelerations and the inertia forces in retrofitted frames than the original ones. In most retrofitted frames, the design base shears are less than those generated in the

structures at design PGAs obtained by Pushover and NLTH analyses. This means that EMP has been selected in the conservative side. This may also be due to the fact that there is not enough product of EMP to completely fit the shear forces generated in the story in design process.

Figure 8-45 and Figure 8-47 show the maximum interstory drifts of the structures before and after being retrofitted. Comparing the maximum interstory drifts of the frames with and without EMP, it is apparent that EMP limits the interstory drifts of the structures, especially for the frames designed only according to EC2. Thanks to this advantage, the frames can resist bigger earthquakes. This is illustrated in Figure 8-55 and Figure 8-58. All retrofitted frames can reach the target displacements under design PGAs. It is necessary to stress that with the use of EMP the retrofitted frames are stiffened and strengthened, which are expressed by lower top displacements and smaller interstory drifts, and they can reach the target displacements under design PGAs. However, at higher PGAs all retrofitted frames still collapse because of the failure at beam-column connections. This means that EMP cannot increase the capacity of the beam-column joints. To obtain better seismic performance for the frames, some additional work should be made in order to increase the deformation capacity at joints of the frames.

Figure 7-32 and Figure 8-52 illustrate the ratio between maximum interstory drifts and drifts at top of the retrofitted frames. It is known that this ratio reflects the influence of second order effects on the structures. It is rather clear that this ratio in the retrofitted systems is smaller than in the original frames without EMP. This explains that EMP can also contribute to limiting the P-delta effects on the systems.

Figure 8-55 and Figure 8-58 present the maximum resistible PGAs of the studied frames before and after retrofitting. These PGA have been established by Pushover analysis. In spite of the fact that node failure still governs the response of the retrofitted frames, it can be seen that in many cases EMP are efficient in reducing the action effects on the frames. The maximum resistible PGAs of those retrofitted frames are greater than design PGAs. The node failure occurs after the retrofitted frames attain the target displacements. In some cases, such as Configuration 1-EC8-0.15g-L, Configuration 3-EC8-0.15g-L, the resistible PGAs are increased about 60%.

Based on Pushover analysis, Figure 8-60 plots the ratios of maximum resistible PGAs of the retrofitted frames in two cases: (1) partial retrofit with only EMP and (2) full retrofit with EMP and node retrofitted and the maximum resistible PGAs of the original frames.

Also resulting from Pushover analysis, Table 8-25 presents characteristics of the retrofitted systems in comparison with not retrofitted ones: first yield displacement ($\Delta_{1,y}$) and corresponding base shear ($V_b^{1,y}$); ultimate base shear (V_b^u) and the corresponding displacement (Δ_m); energy dissipated in the systems (E) at failure; the failure mechanisms of the systems at ultimate state; the over-strength factors of the systems, computed as $\frac{V_b^u}{V_b^{1,y}}$. These characteristics have been calculated based on the ductility of the 'equivalent' SDOF structures and over-strength of the original MDOF frames. It is clear that the over-strength factors of the retrofitted systems are much higher than those of the original ones. The increase of these over-strength factors obviously comes from the EMP, which enables to increase both ductility and strength of the systems.

It is important to note that the analysis ignores that the EMP in retrofitted frames introduce additional internal forces in the beams and columns in the spans where EMP are placed. Indeed, if EMP are placed in successive stories, the beams connected two EMP in two successive stories are less influenced by the additional effects from EMP than the ones connected with only one EMP.

In conclusion, with the presence of EMP, the failure modes of the retrofitted systems are the same as those of the existing frames: incomplete load path and soft story mechanisms. EMP increases the stiffness and strength of the structures and help absorbing the seismic energy, which results in an increase of safety. This is expressed by the fact that all retrofitted frames are able to reach the target displacements under design PGA without any premature failure. However, at the PGAs higher than design ones, the brittle collapse due to rupture of beam-column joints are still observed. In order to have a more complete retrofitting solutions with EMP, beam-column joints should be retrofitted as well. Some existing solutions of retrofitting beam-column nodes are presented in section 8.8.

Table 8-25 – Response of the frames by pushover analysis at the ultimate limit state

Case	Group	$V_b^{1,y}$ (kN)	$\Delta_{1,y}$ (m)	V_b^u (kN)	Δ_u (m)	E (kNm)	Criteria of failure	Over-strength
1	EC2-0.05g-NoEMP	184.6	0.056	184.6	0.056	5.18	Node	1.00
	EC2-0.15g+EMP	615.2	0.056	615.2	0.056	16.8	Node	1.00
	EC2-0.15g-NoEMP	100.7	0.03	172.6	0.060	5.52	Node	1.71
	EC2-0.15g+EMP	371.9	0.027	521.6	0.057	19.3	Node	1.40
	EC2-0.3g-NoEMP	213.8	0.03	283.7	0.050	7.73	Node	1.33
	EC2-0.3g+EMP	1027.5	0.024	1462.6	0.071	75.7	Node	1.42
	EC8-0.05/L –No EMP	186.0	0.057	186.0	0.057	5.26	Node	1.00
	EC8-0.05/L +EMP	680.6	0.057	680.6	0.057	19.0	Node	1.00
	EC8-0.15/L –No EMP	346.1	0.09	346.1	0.090	31.2	Node	1.0
	EC8-0.15/L +EMP	538.7	0.040	790.7	0.130	70.3	Node	1.47
2	EC2-0.05g-NoEMP	174.7	0.10	174.7	0.100	8.29	Node	1.0
	EC2-0.05g+EMP	564.6	0.08	615.0	0.120	38.7	Node	1.09
	EC2-0.15g-NoEMP	174.7	0.10	174.7	0.100	8.29	Node	1.0
	EC2-0.15g+EMP	564.6	0.08	615.0	0.120	38.7	Node	1.09
	EC2-0.3g-NoEMP	264.9	0.08	354.7	0.130	25.0	Node	1.34
	EC2-0.3g+EMP	422.7	0.023	1576.3	0.190	219.0	Node	3.73
	EC8-0.05/L –No EMP	174.7	0.10	174.7	0.100	8.29	Node	1.00
	EC8-0.05/L +EMP	439.3	0.12	439.3	0.120	32.7	Node	1.00
	EC8-0.15/L –No EMP	360.9	0.20	180.3	0.100	8.84	Node	-
	EC8-0.15/L +EMP	345.8	0.059	660.7	0.190	78.3	Node	1.91
3	EC2-0.05g-NoEMP	114.6	0.04	355.1	0.140	28.8	Node	3.10
	EC2-0.05g+EMP	593.5	0.054	733.0	0.140	66.4	Node	1.24
	EC2-0.15g-NoEMP	356.5	0.14	356.5	0.140	27.1	Node	1.0
	EC2-0.15g+EMP	264.5	0.03	787.0	0.160	80.3	Node	2.98
	EC2-0.3g-No EMP	356.5	0.14	356.5	0.140	27.1	Node	1.0
	EC2-0.3g+EMP	369.9	0.027	1709.2	0.180	202.0	Node	4.6
	EC8-0.05/L –No EMP	268.3	0.09	357.2	0.140	27.0	Node	1.33
	EC8-0.05/L +EMP	493.5	0.054	733.0	0.140	66.4	Node	1.49
	EC8-0.15/L –No EMP	547.4	0.18	294.8	0.100	14.4	Node	-
	EC8-0.15/L +EMP	888.2	0.073	1661.0	0.214	228.0	Node	1.87

Table 8-26 – Response of the frames by pushover analysis at the ultimate limit state (continued)

Case	Group	$V_b^{1,y}$ (kN)	$\Delta_{1,y}$ (m)	V_b^u (kN)	Δ_u (m)	E (kNm)	Criteria of failure	Over-strength
4	EC2-0.05g-No EMP	245.9	0.11	245.9	0.110	13.3	Node	1.0
	EC2-0.05g+EMP	295.8	0.037	874.8	0.156	85.4	Node	3.56
	EC2-0.15g-No EMP	245.9	0.11	245.9	0.110	13.3	Node	1.0
	EC2-0.15g+EMP	295.8	0.037	874.8	0.156	85.4	Node	3.56
	EC2-0.3g-No EMP	620.2	0.23	620.2	0.230	72.3	Node	1.0
	EC2-0.3g+EMP	1546.7	0.13	1922.3	0.309	425.0	Node	1.29
	EC8-0.15g/L-No EMP	504.3	0.22	447.7	0.196	43.9	Node	-
	EC8-0.15g/L+EMP	715.8	0.07	1644.4	0.230	229.0	Node	2.30

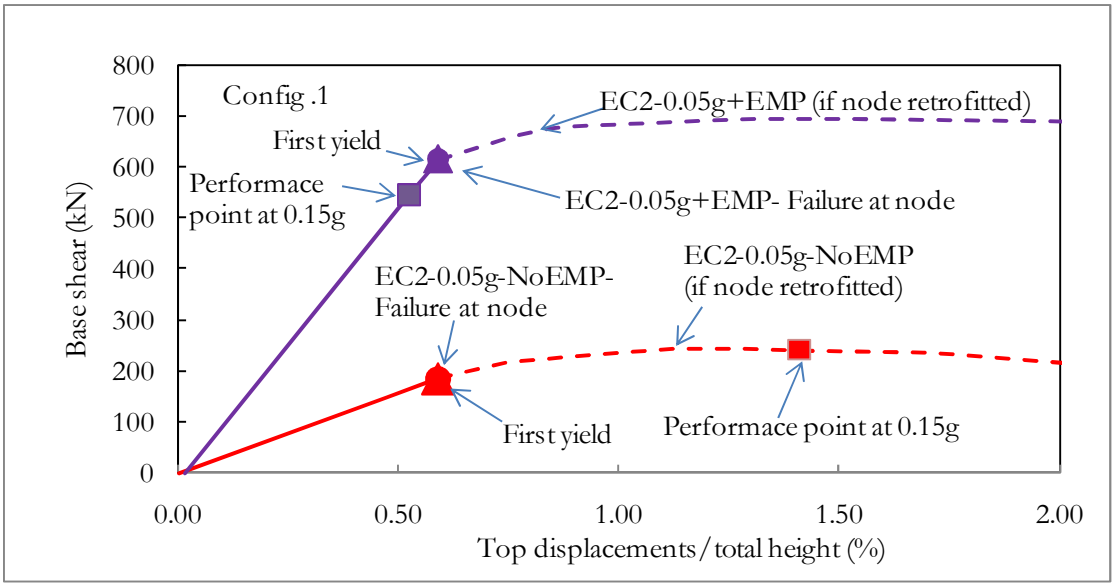

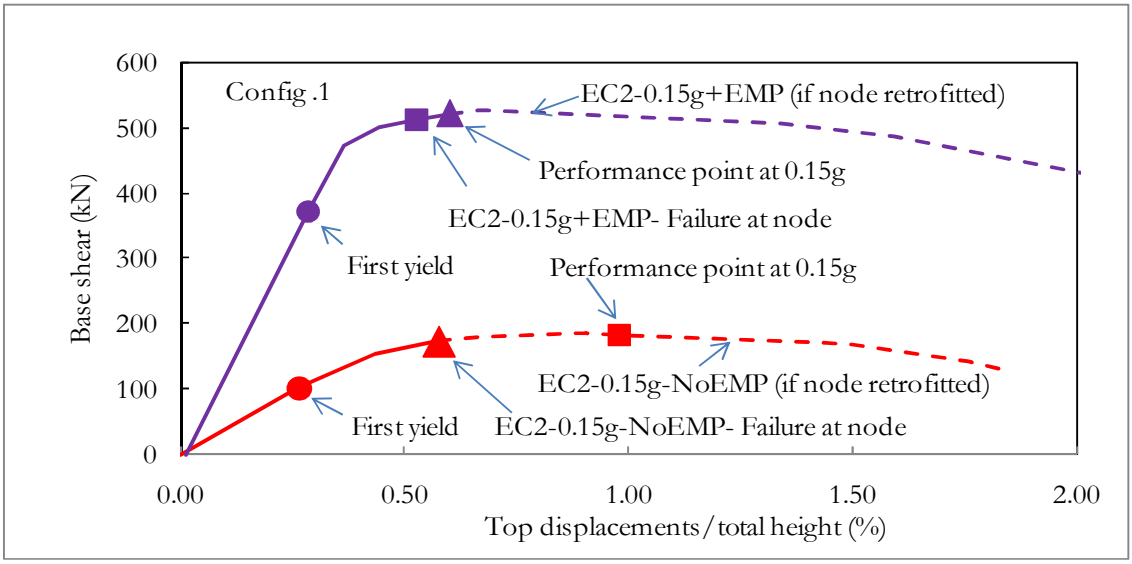

Figure 8-25 – Pushover curves and target drifts by Pushover analysis of RC-MRFs of Configuration 1

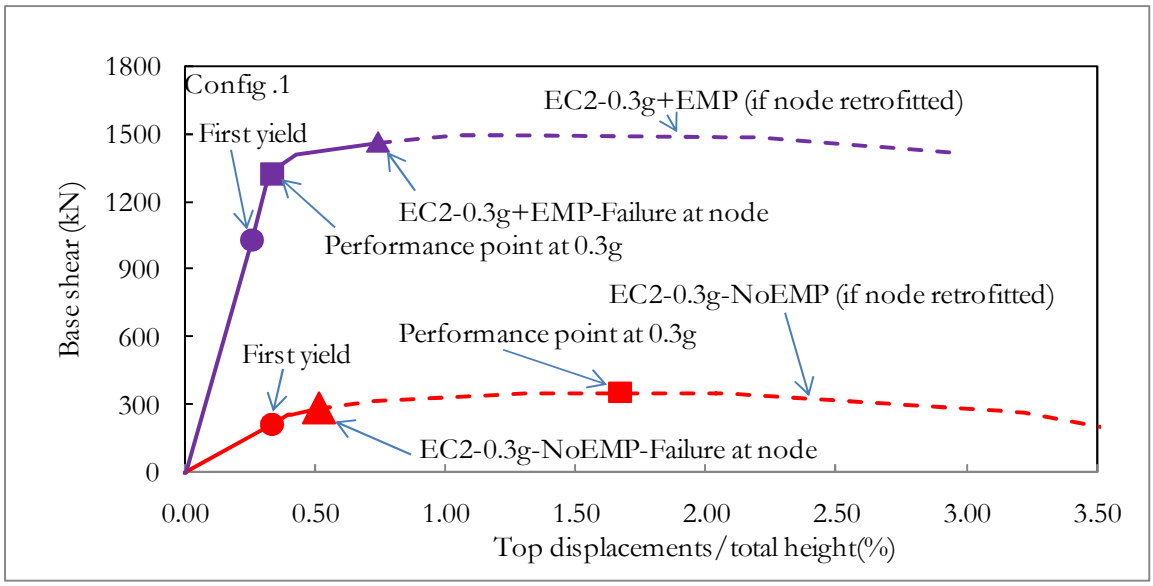

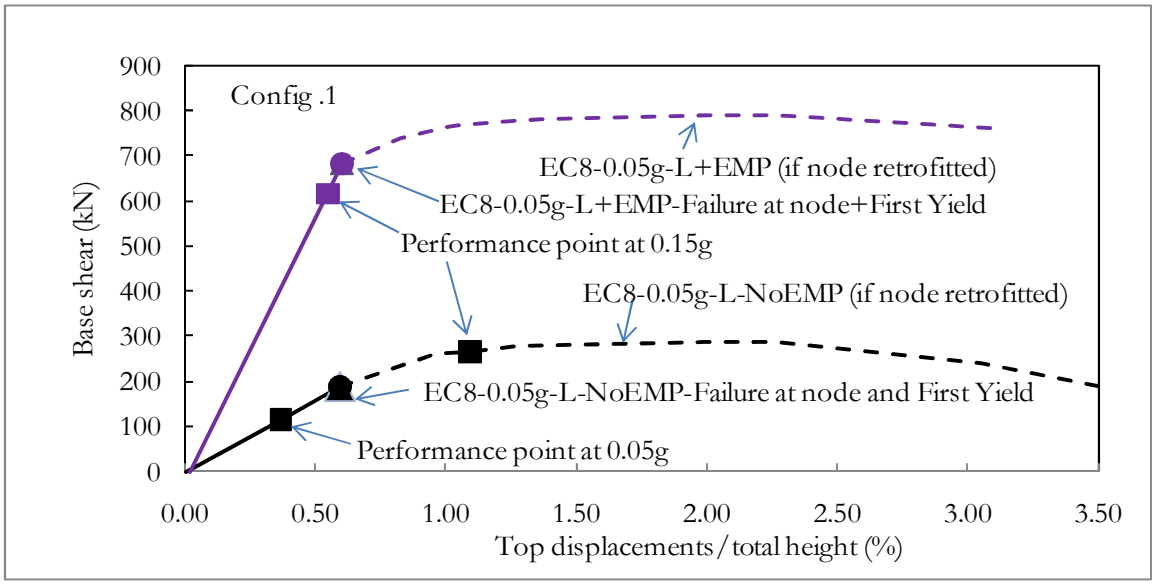

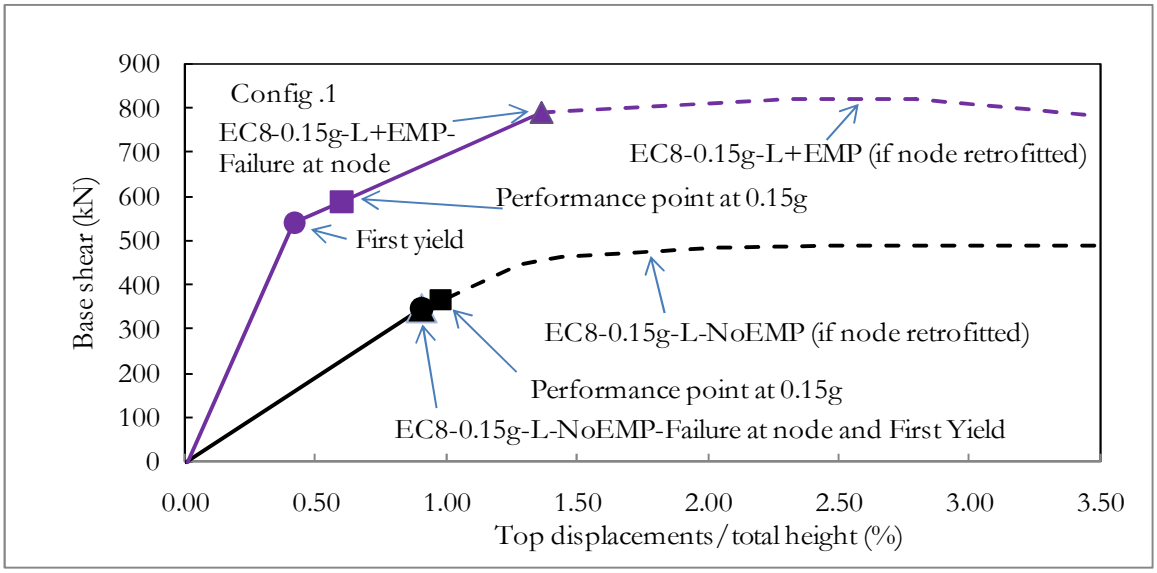

Figure 8-26 – Pushover curves and target drifts by Pushover analysis of RC-MRFs of Configuration 1 (continued)

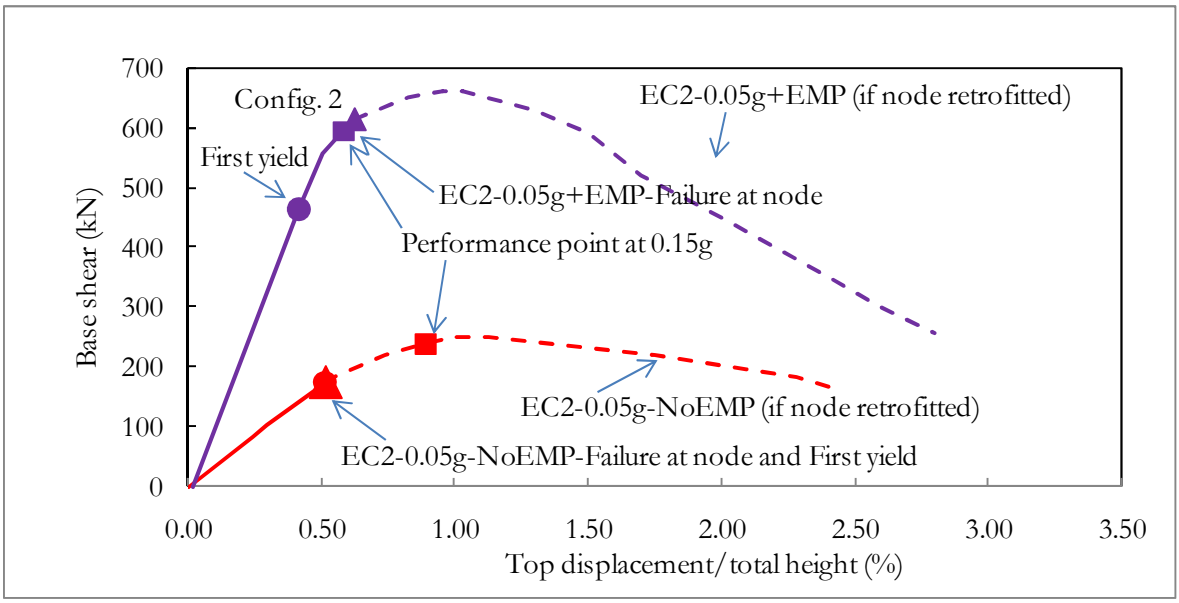

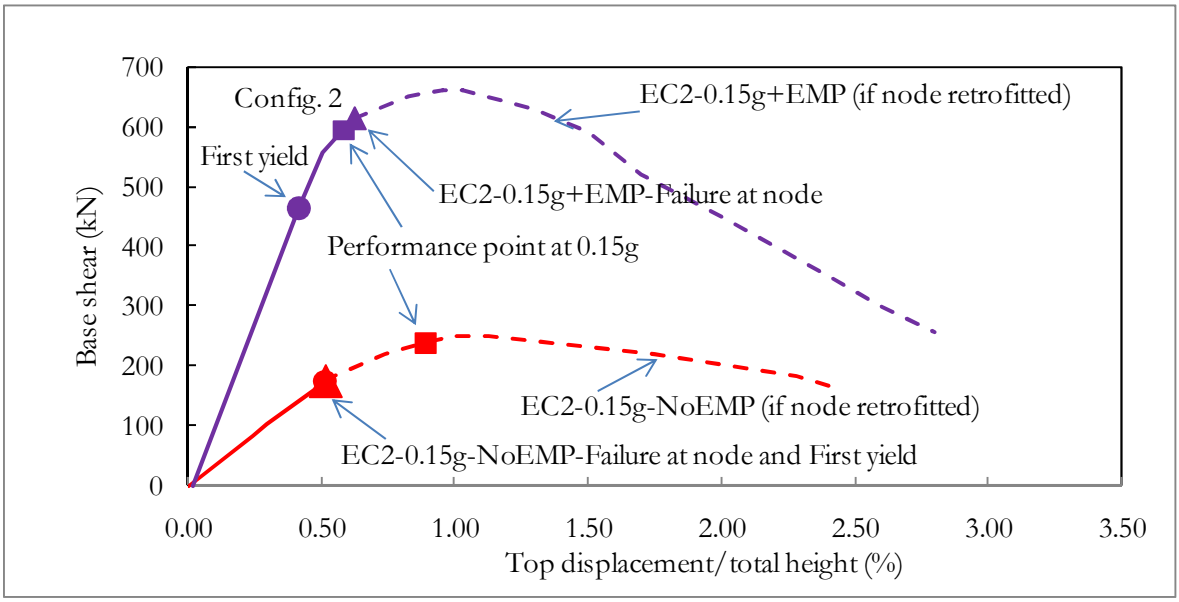

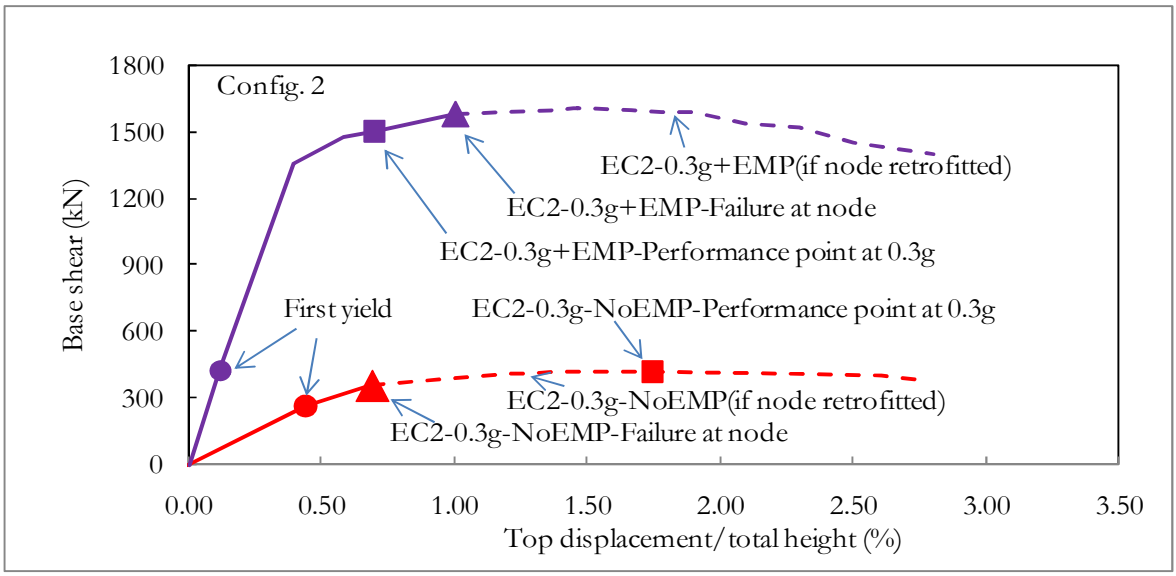

Figure 8-27 – Pushover curves and target drifts by Pushover analysis of RC-MRFs of Configuration 2

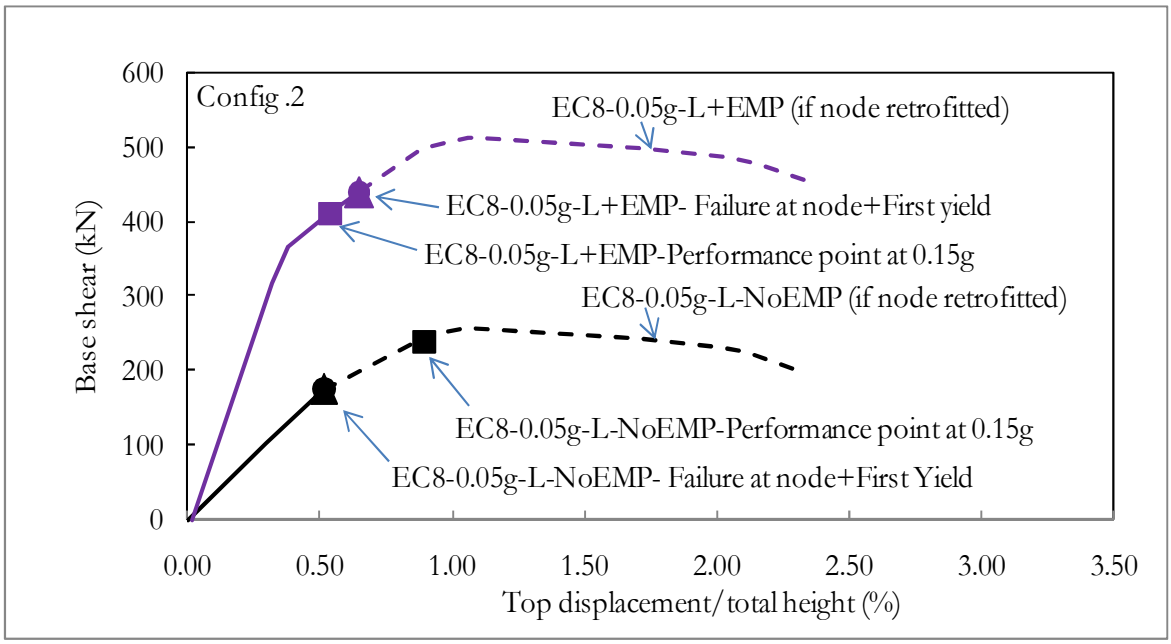

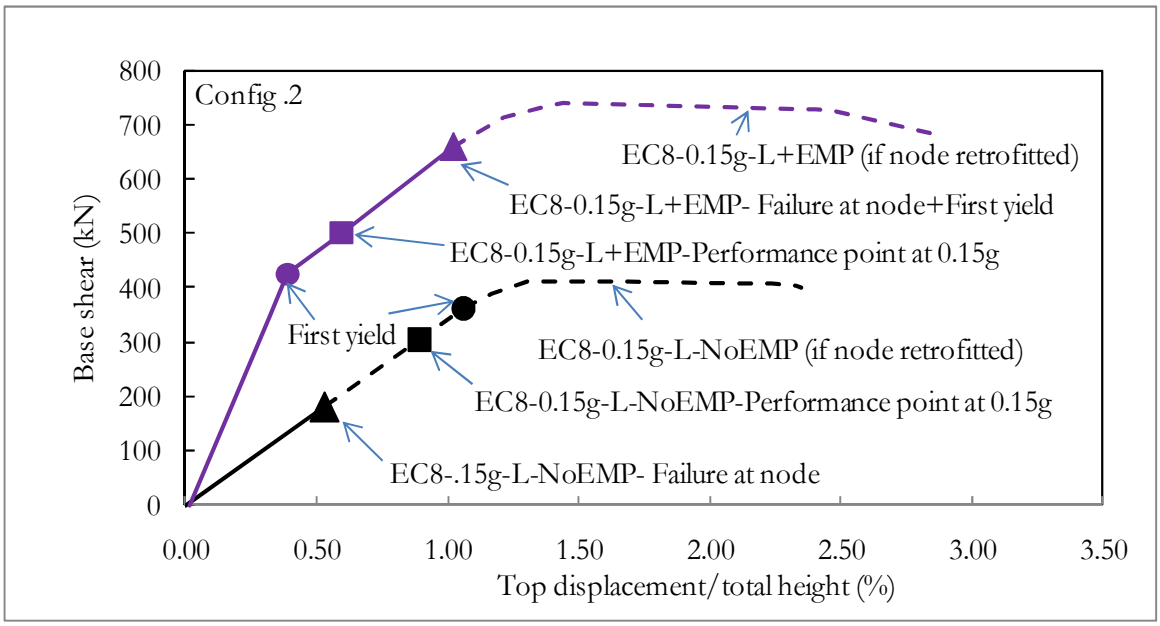

Figure 8-28 – Pushover curves and target drifts by Pushover analysis of RC-MRFs of Configuration 2 (continued)

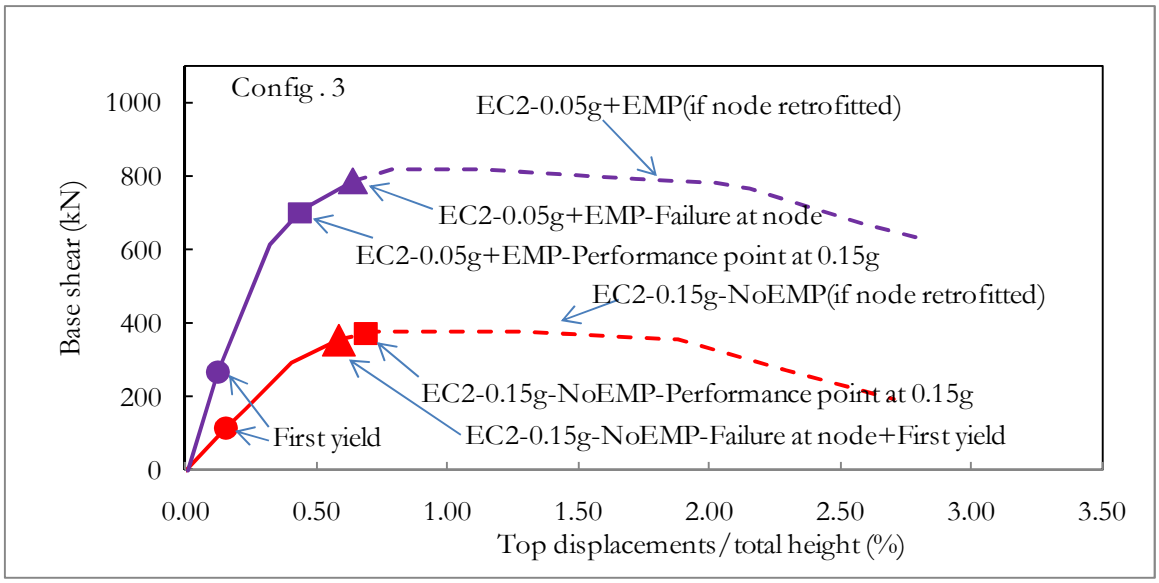

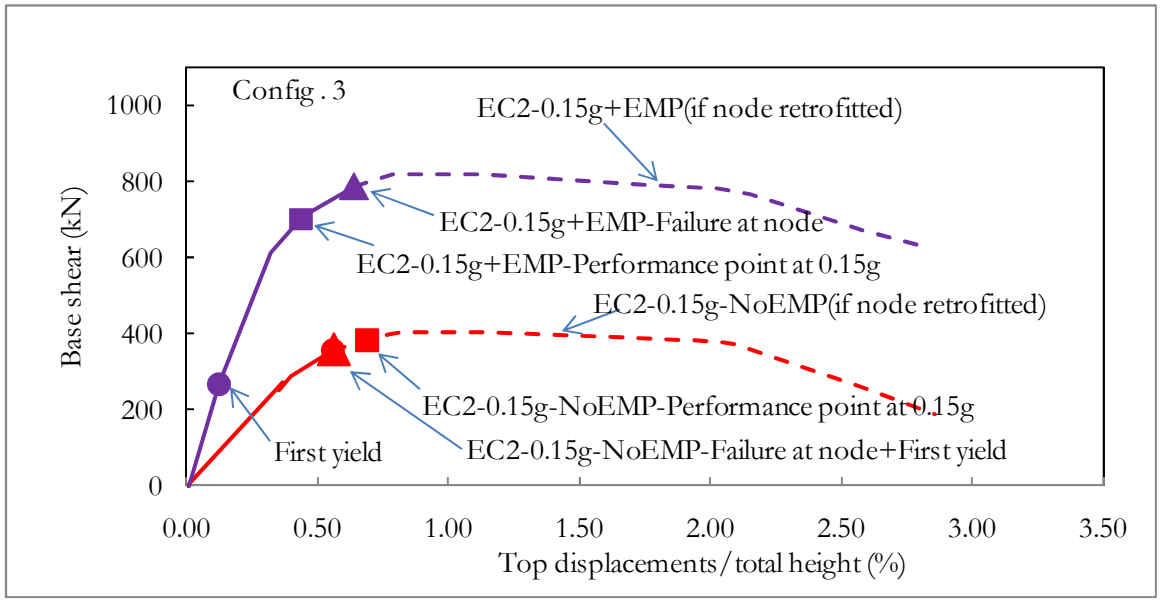

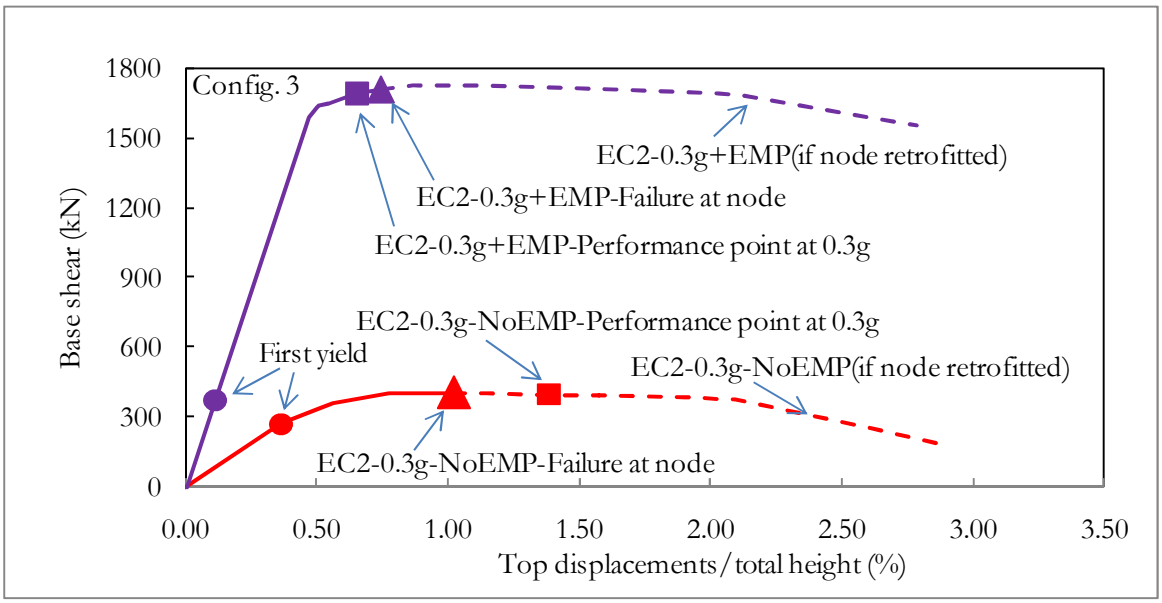

Figure 8-29 – Pushover curves and target drifts by Pushover analysis of RC-MRFs of Configuration 3

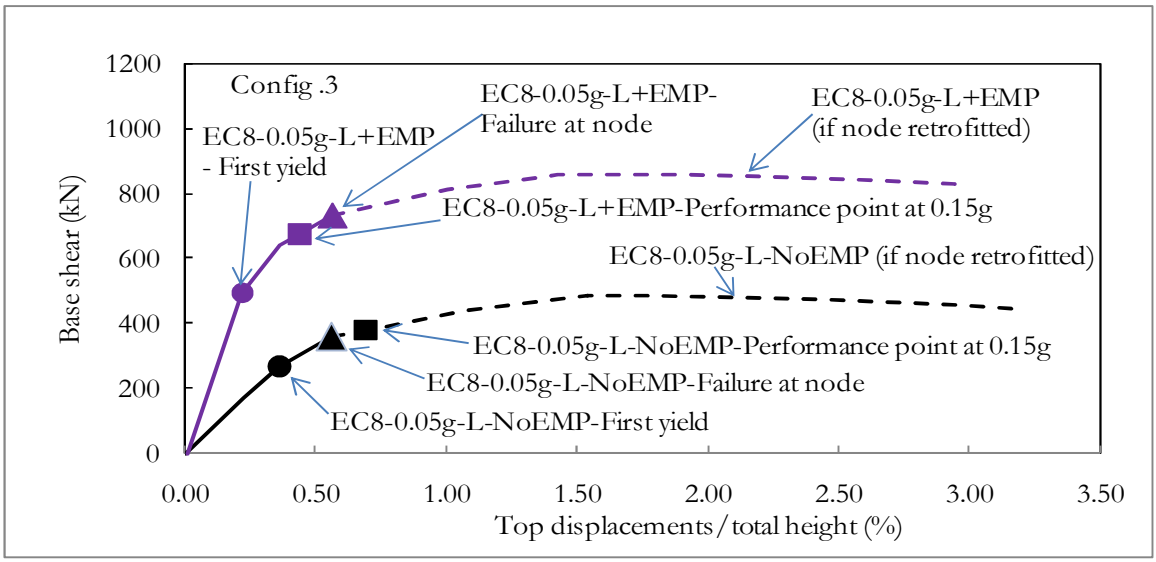

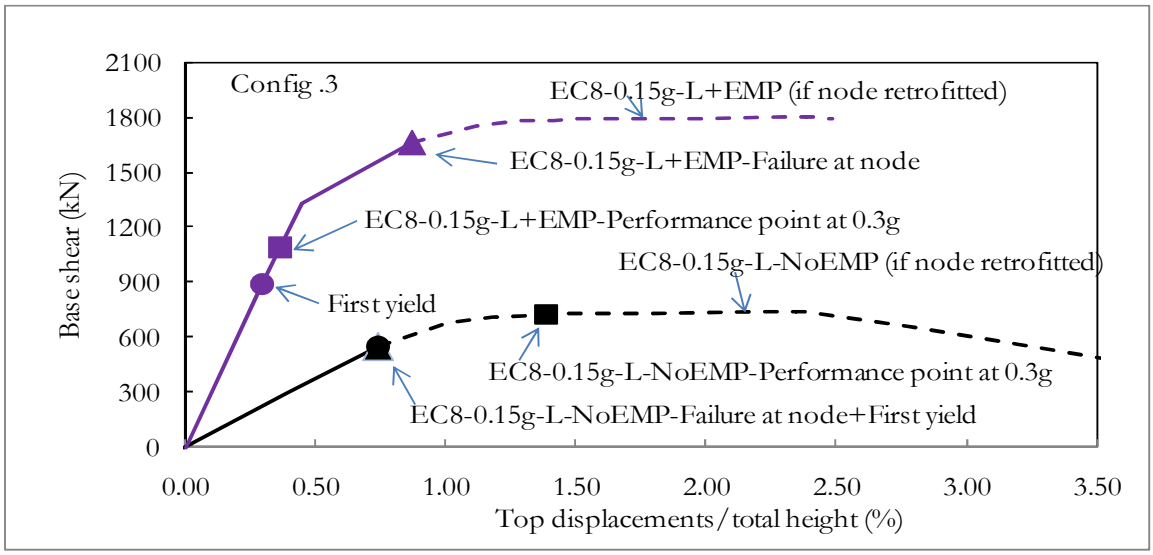

Figure 8-30 – Pushover curves and target drifts by Pushover analysis of RC-MRFs of Configuration 3 (continued)

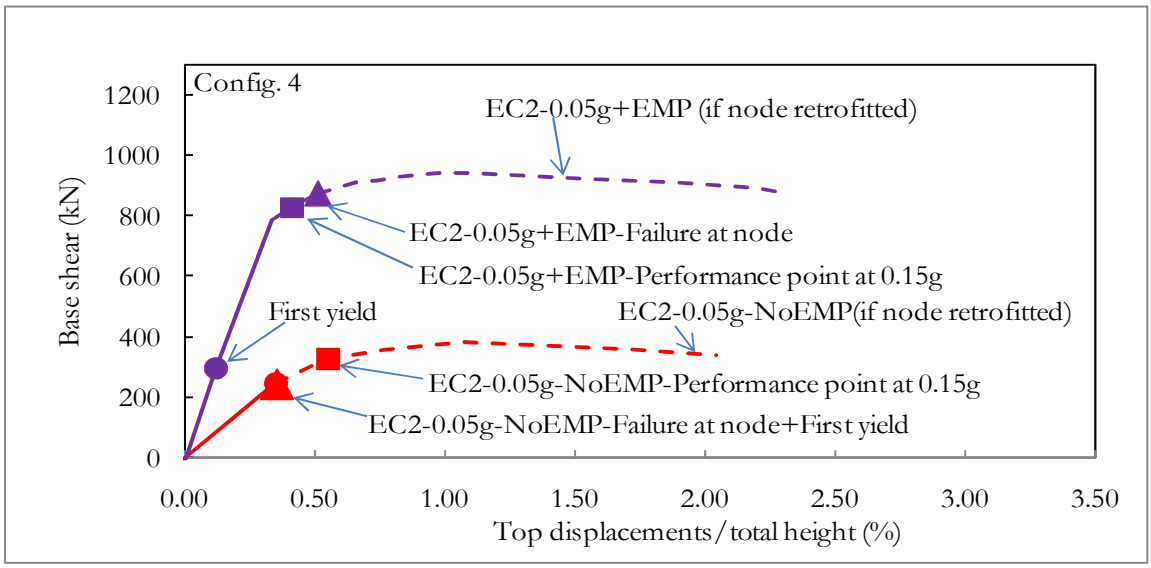

Figure 8-31 – Pushover curves and target drifts by Pushover analysis of RC-MRFs of Configuration 4

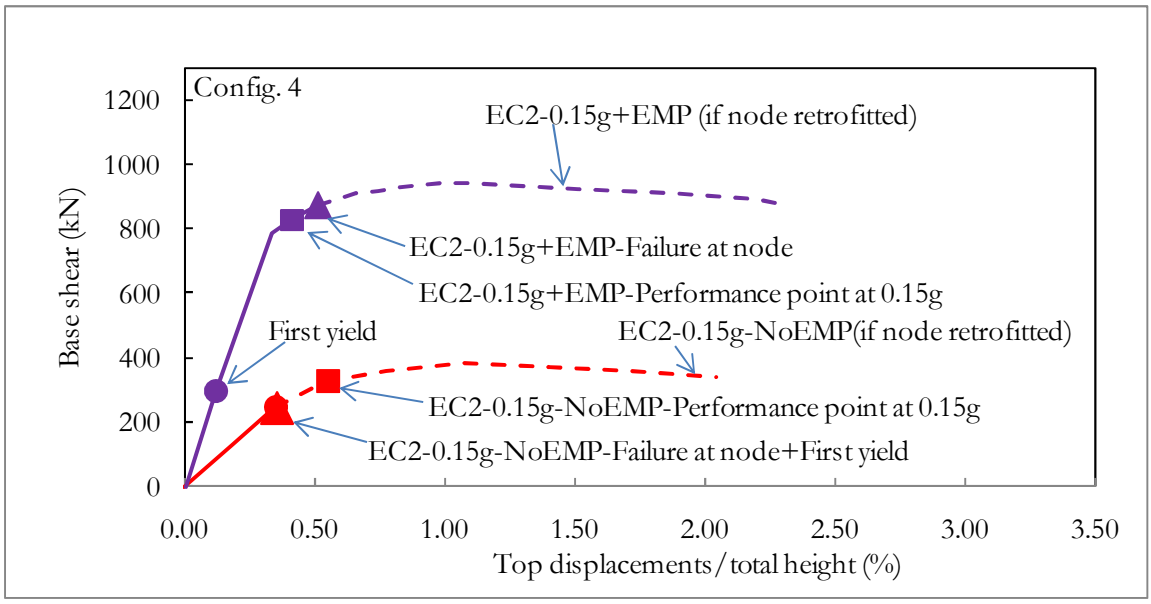

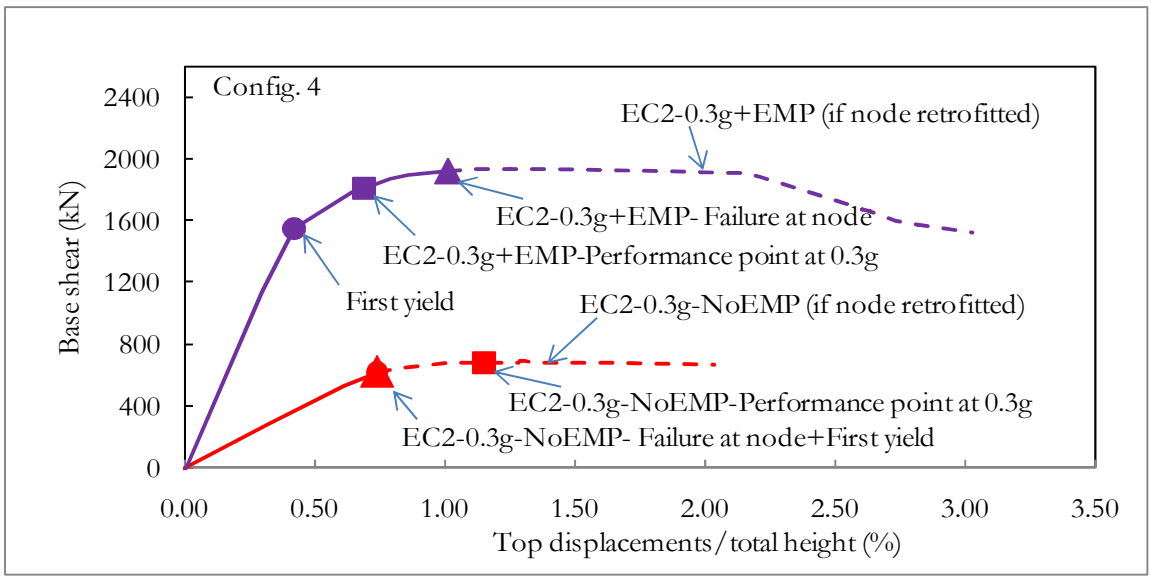

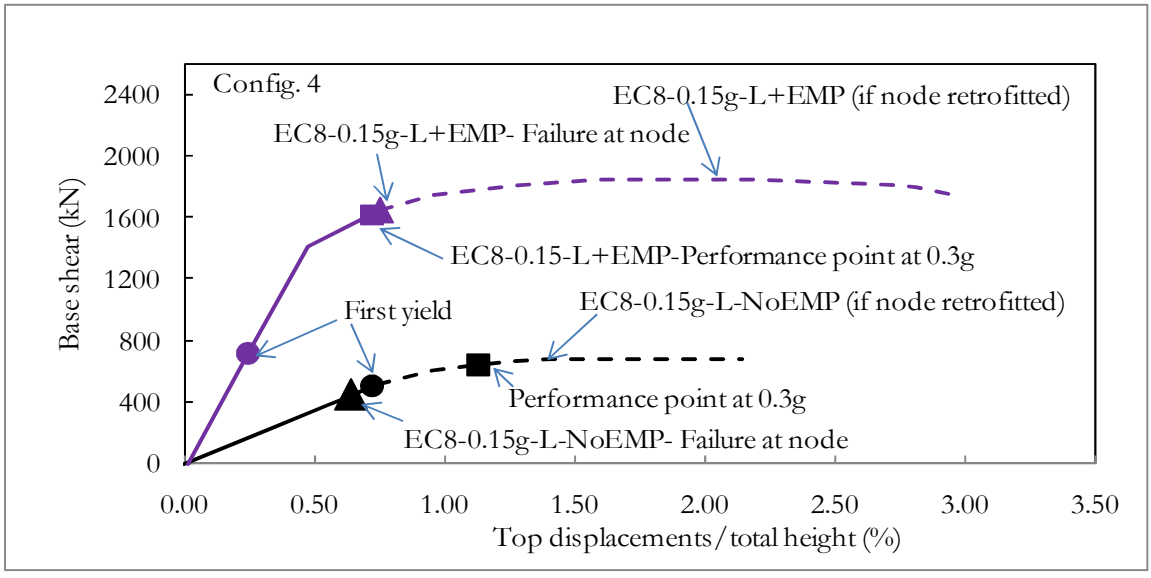

Figure 8-32 – Pushover curves and target drifts by Pushover analysis of RC-MRFs of Configuration 4 (continued)

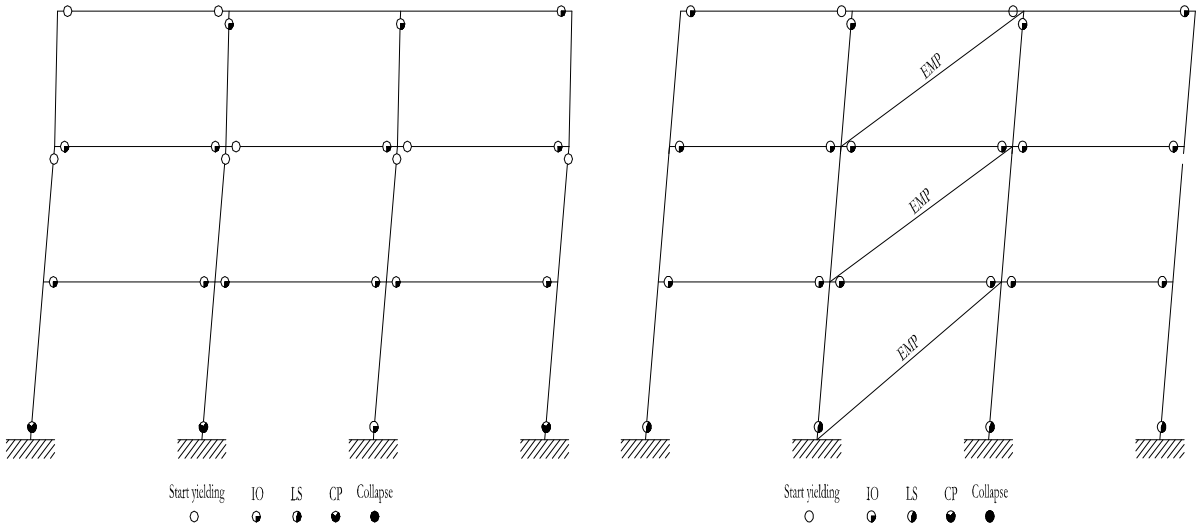

(a) – without EMP (b) with EMP

Figure 8-33 – Typical failure mechanisms if all beam-column joints are well retrofitted

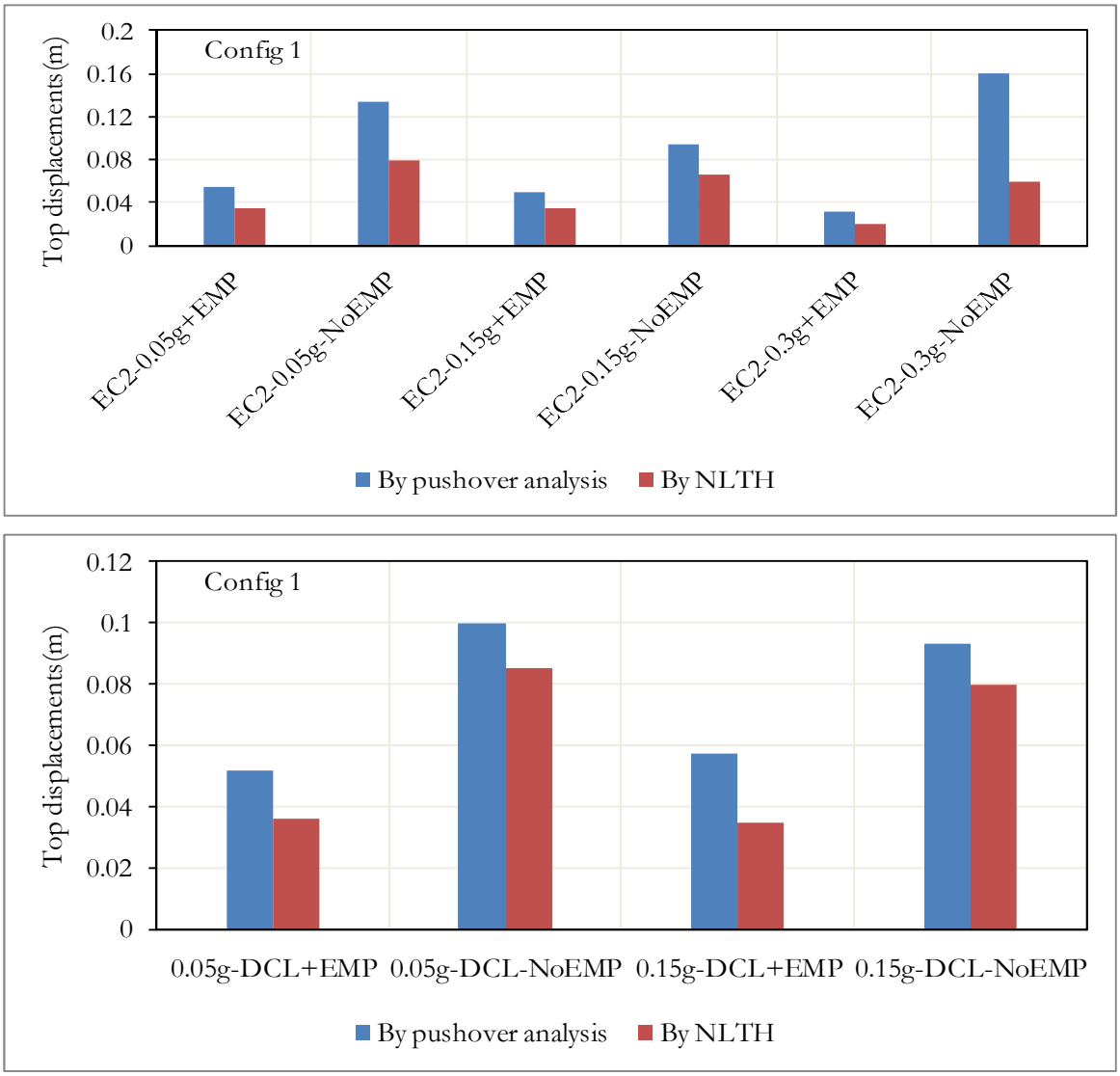

Figure 8-34 – Maximum values of top displacements of all RC-MRF studied under designed PGA by Pushover and NLTH analyses – Configurations 1

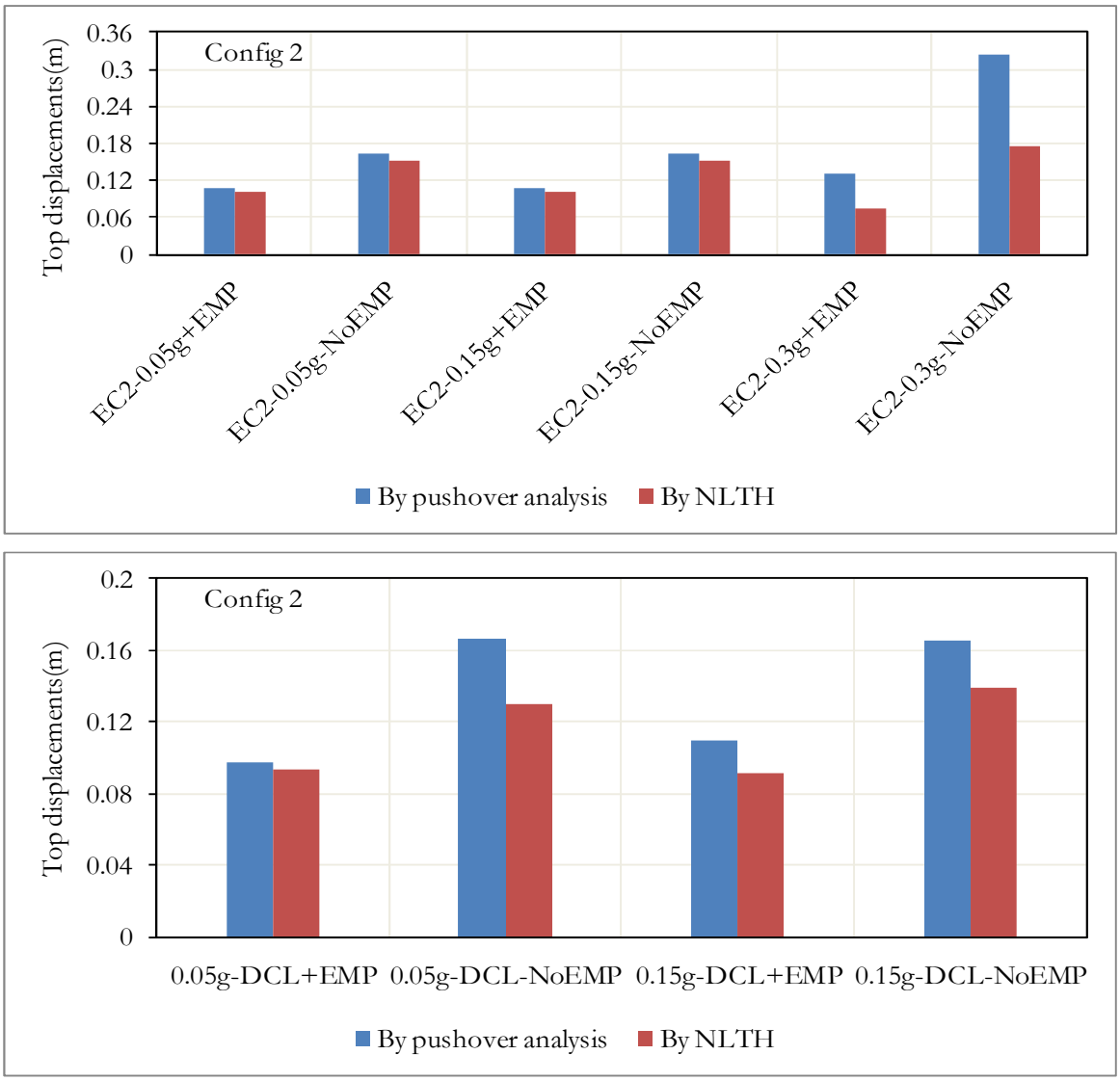

Figure 8-35 – Maximum values of top displacements of all RC-MRF studied under designed PGA by Pushover and NLTH analyses – Configuration 2

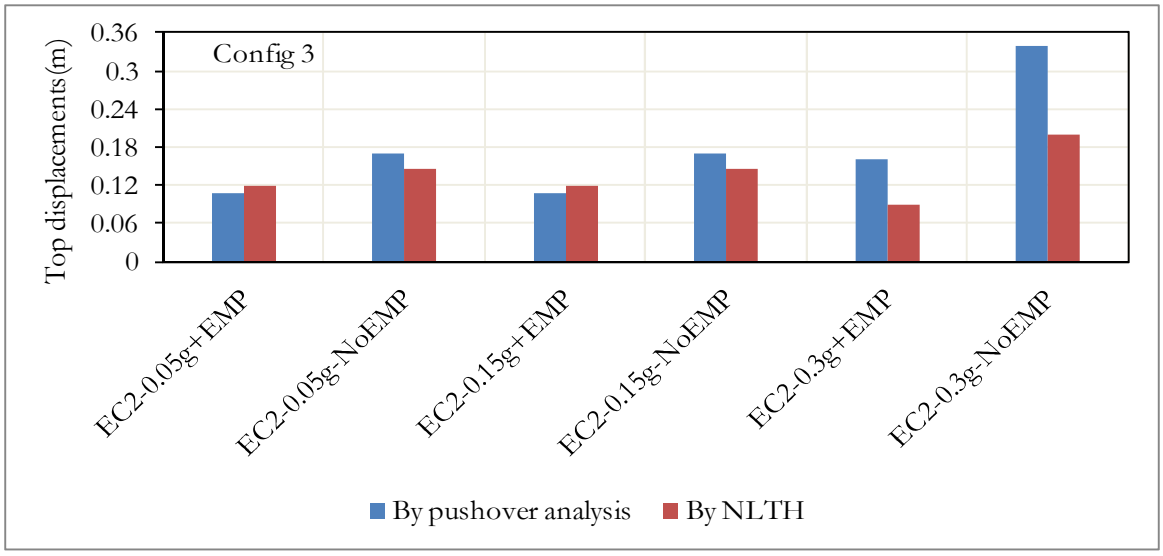

Figure 8-36 – Maximum values of top displacements of all RC-MRF studied under designed PGA by Pushover and NLTH analyses – Configurations 3

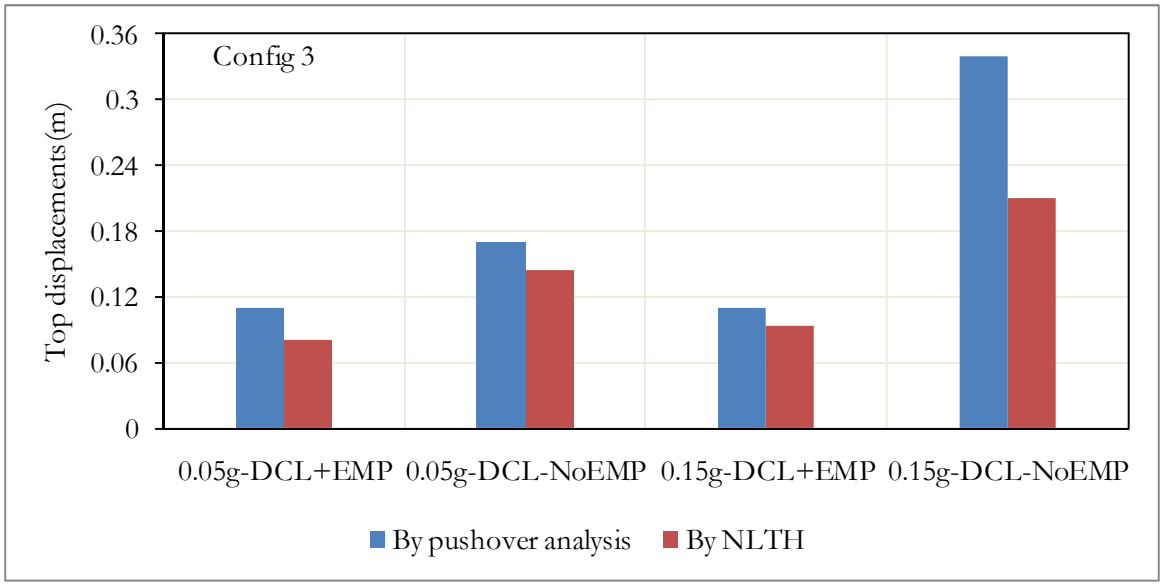

Figure 8-37 – Maximum values of top displacements of all RC-MRF studied under designed PGA by Pushover and NLTH analyses – Configurations 3 (continued)

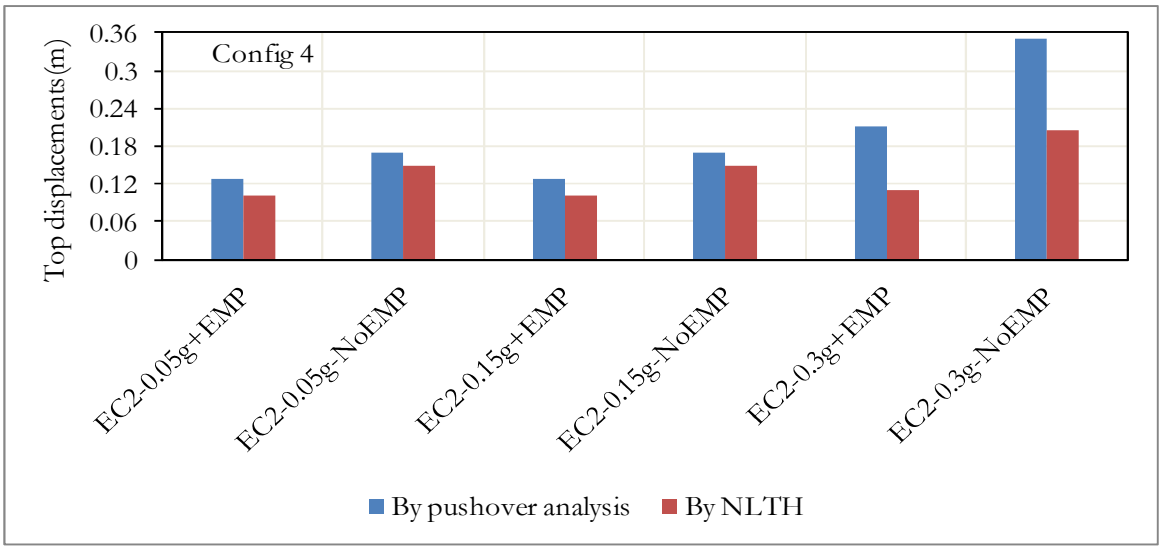

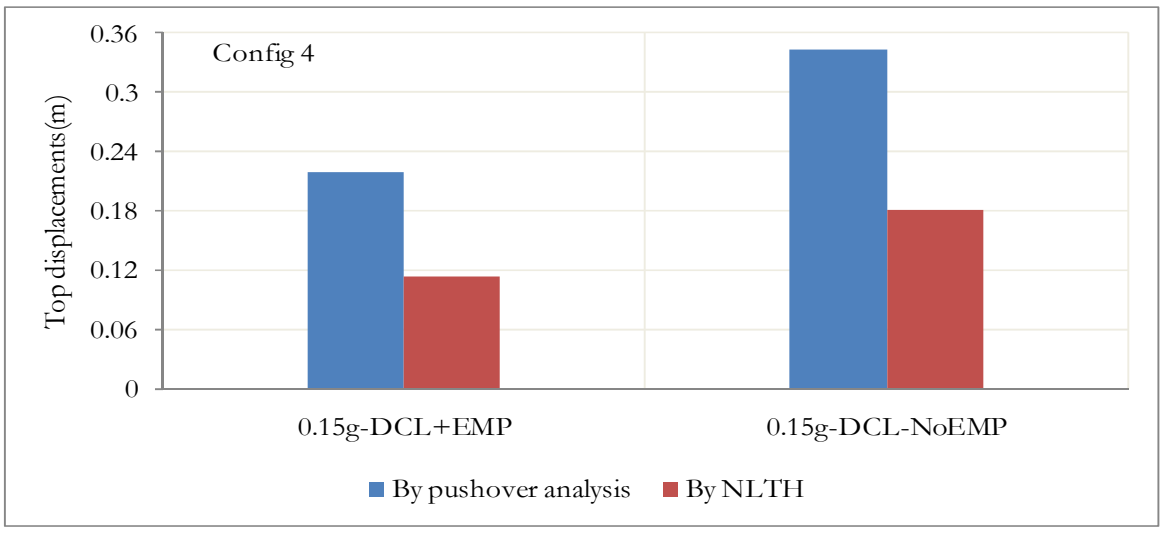

Figure 8-38 – Maximum values of top displacements of all RC-MRF studied under designed PGA by Pushover and NLTH analyses – Configurations 4

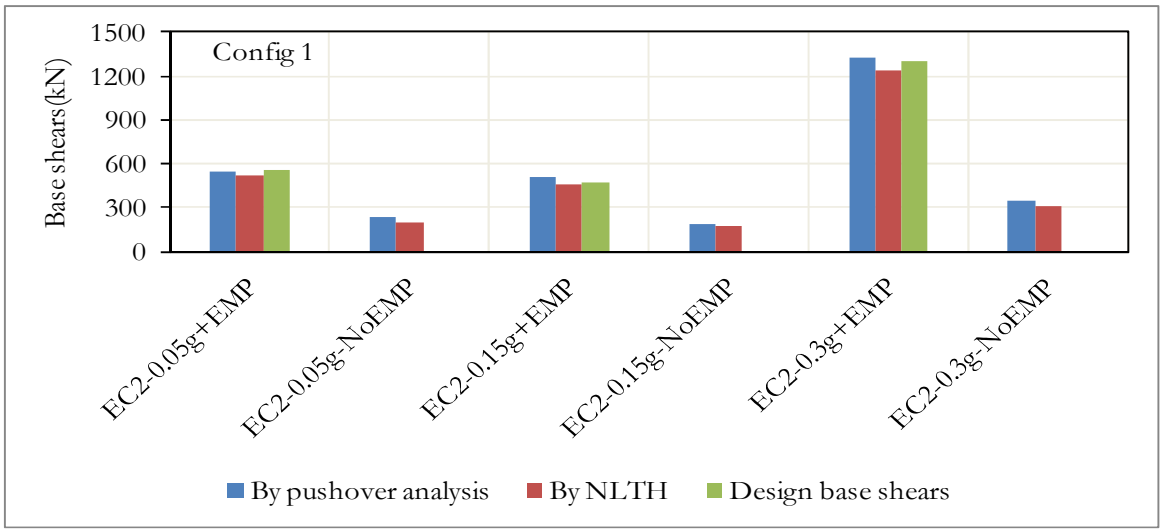

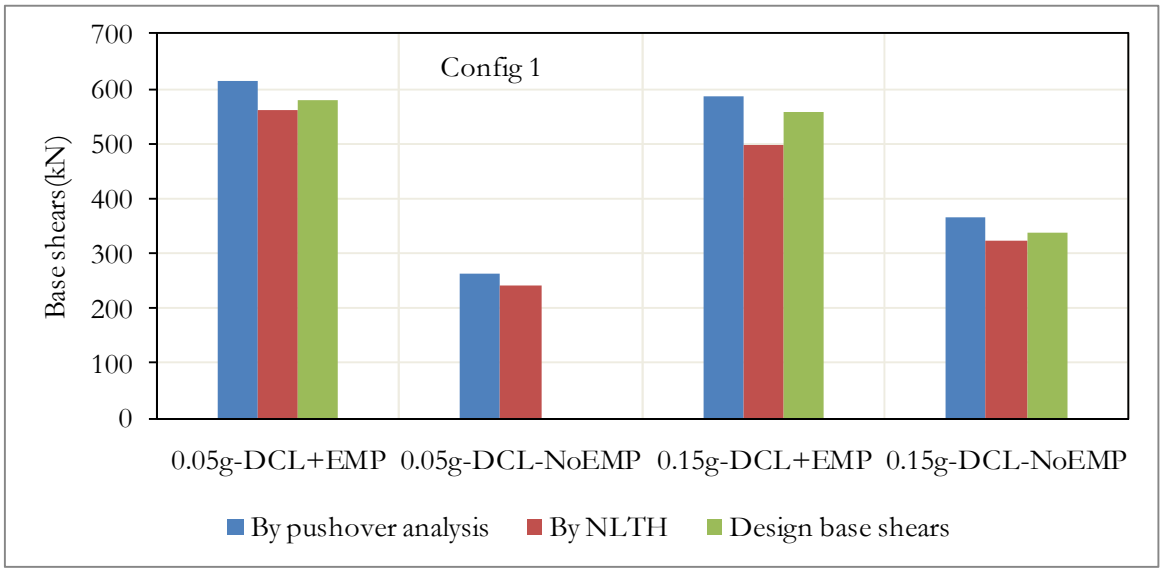

Figure 8-39 – Design base shears and base shears generated in studied RC-MRFs at target displacements under design earthquakes established by Pushover, NLTH analyses – Configurations 1

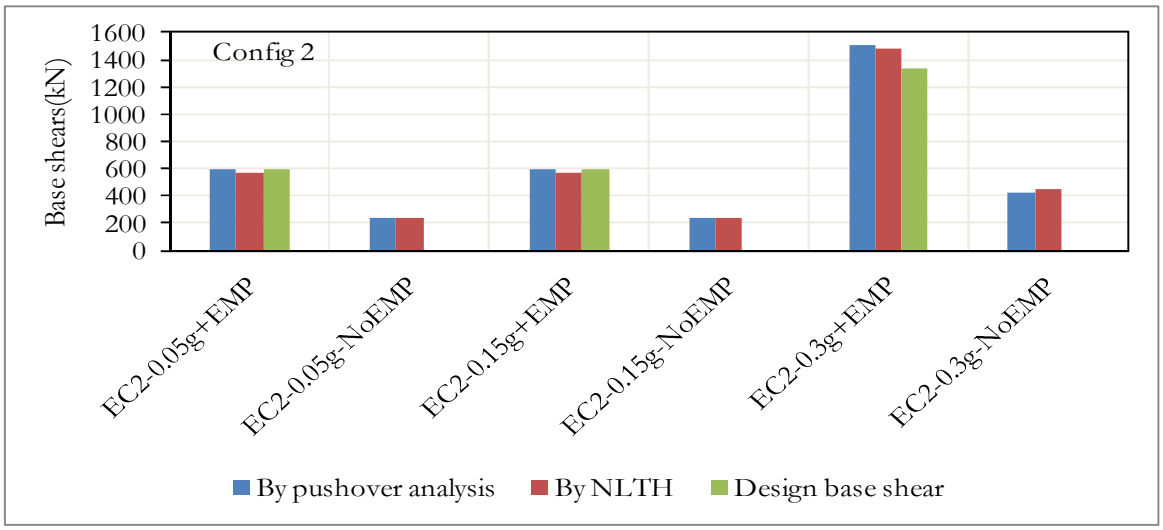

Figure 8-40 – Design base shears and base shears generated in studied RC-MRFs at target displacements under design earthquakes established by Pushover, NLTH analyses – Configurations 2

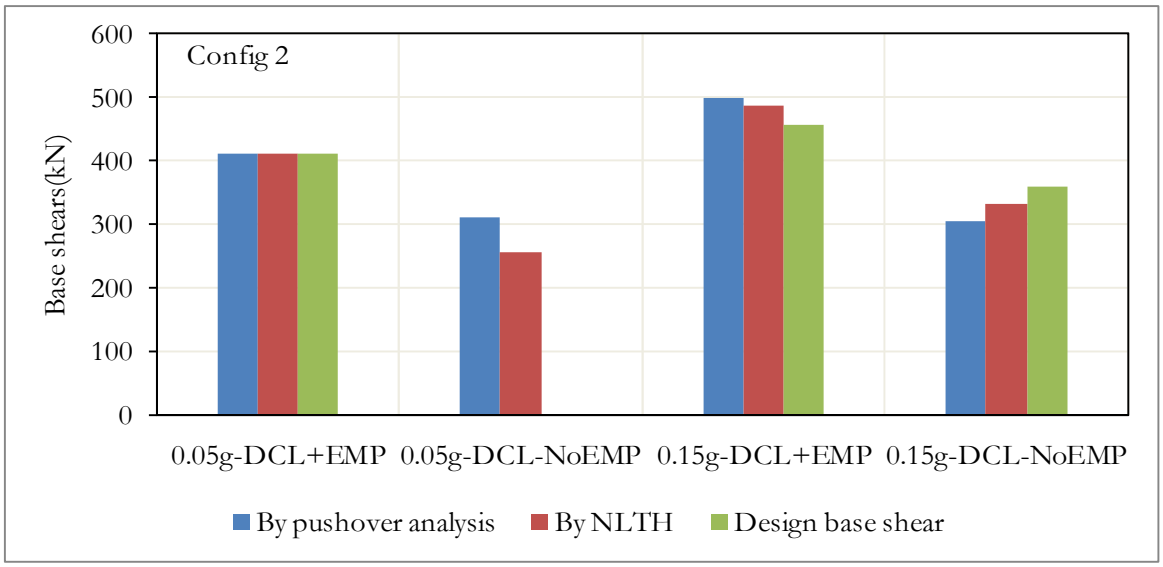

Figure 8-41 – Design base shears and base shears generated in studied RC-MRFs at target displacements under design earthquakes established by Pushover, NLTH analyses – Configurations 2 (continued)

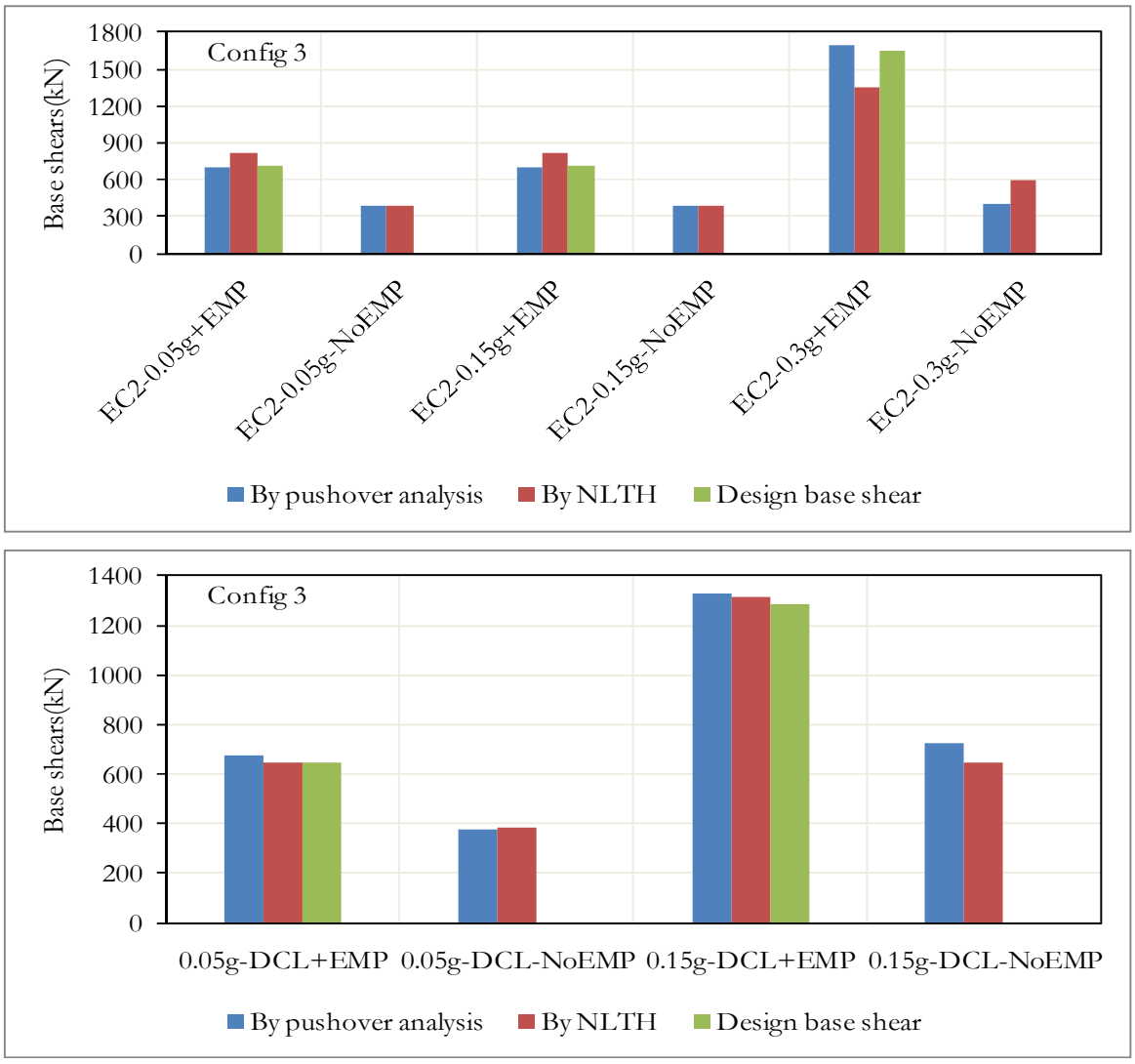

Figure 8-42 – Design base shears and base shears generated in studied RC-MRFs at target displacements under design earthquakes established by Pushover, NLTH analyses – Configurations 3

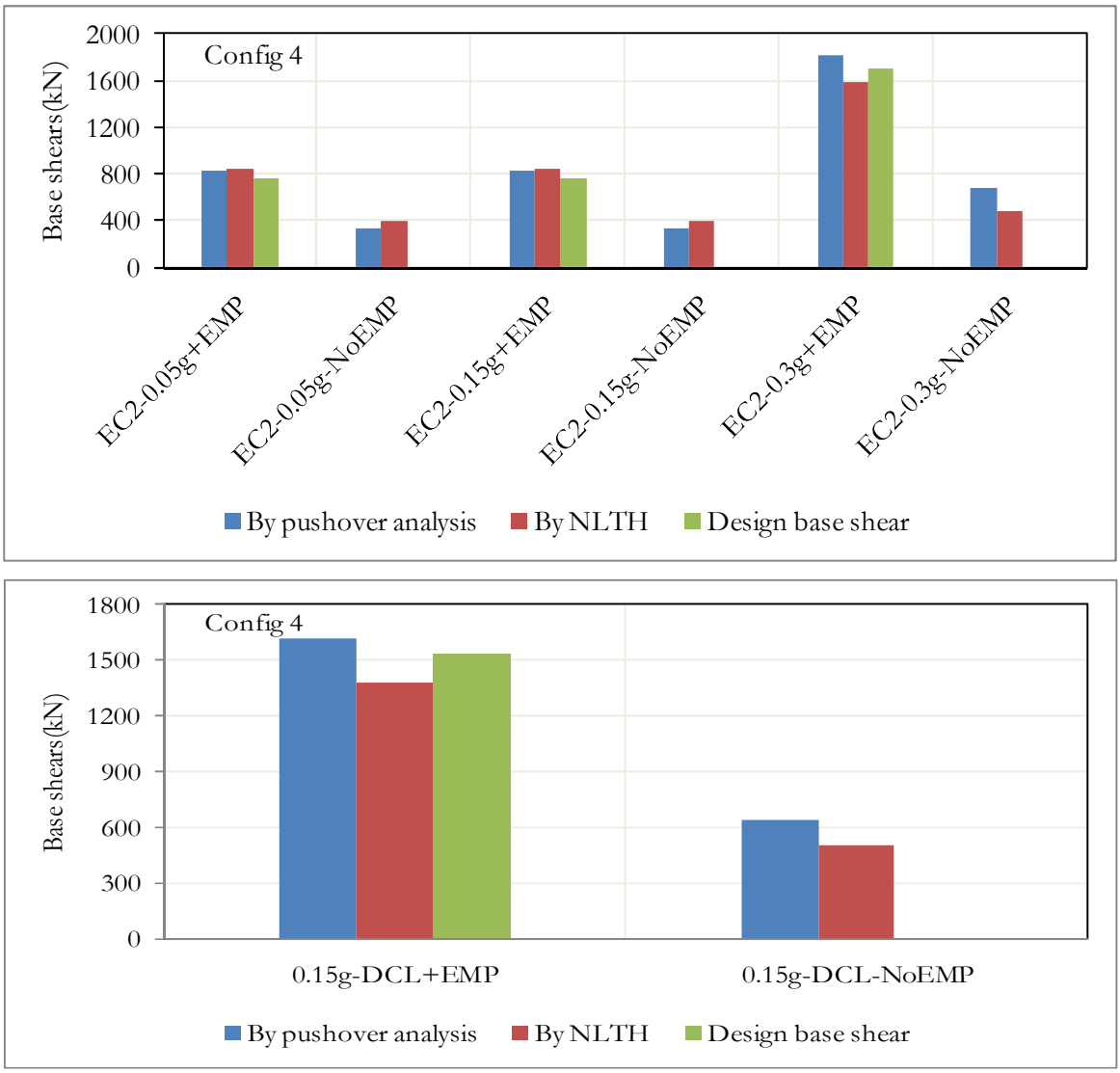

Figure 8-43 – Design base shears and base shears generated in studied RC-MRFs at target displacements under design earthquakes established by Pushover, NLTH analyses – Configurations 4

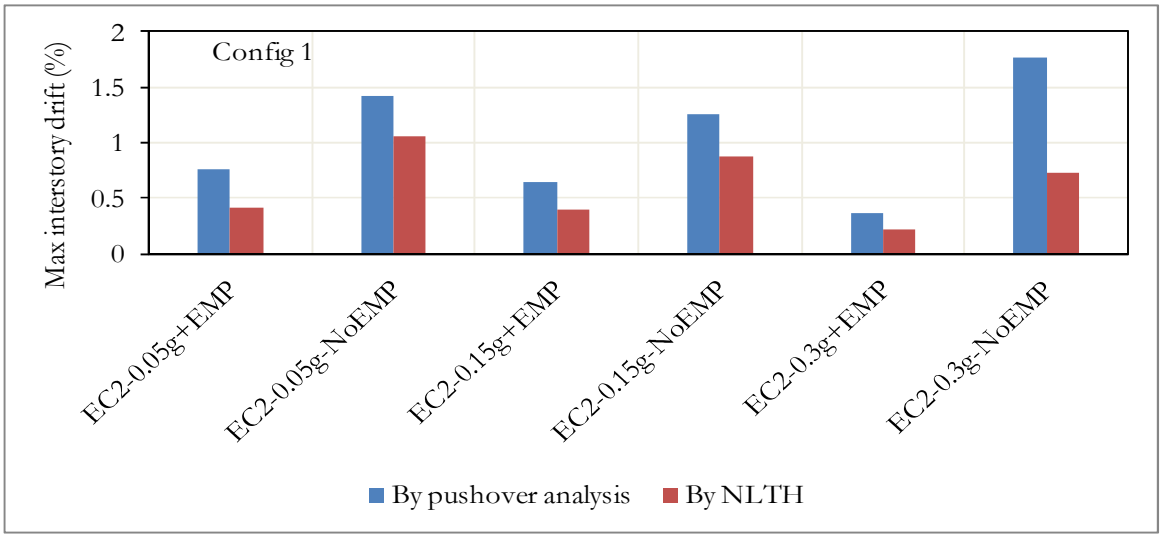

Figure 8-44 – Maximum interstory drift ratios at target displacements of studied RC-MRFs under design PGA established by Pushover and NLTH analyses – Configurations 1

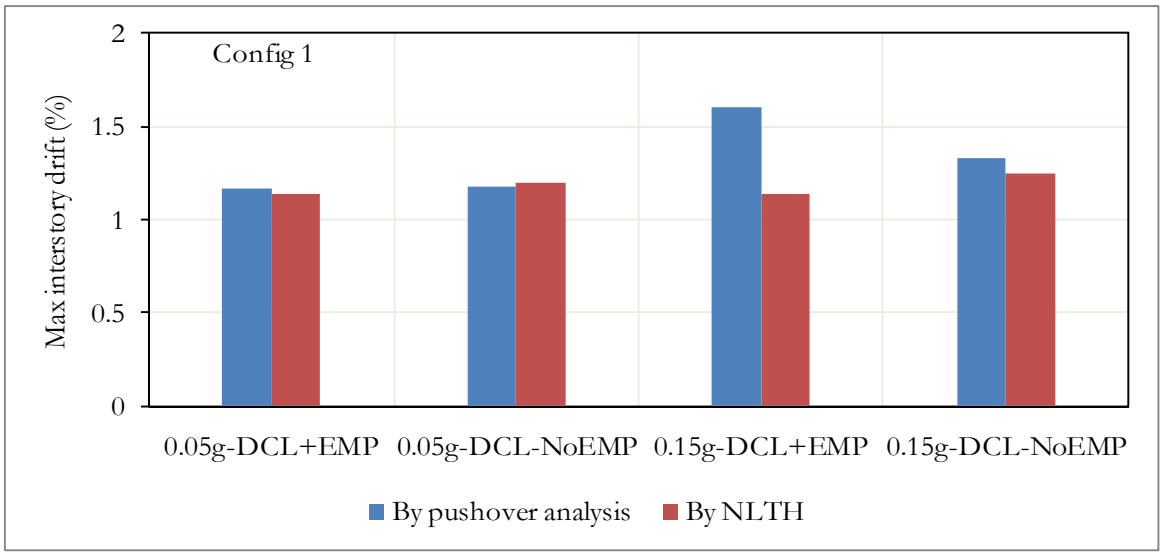

Figure 8-45 – Maximum interstory drift ratios at target displacements of studied RC-MRFs under design PGA established by Pushover and NLTH analyses – Configurations 1 (continued)

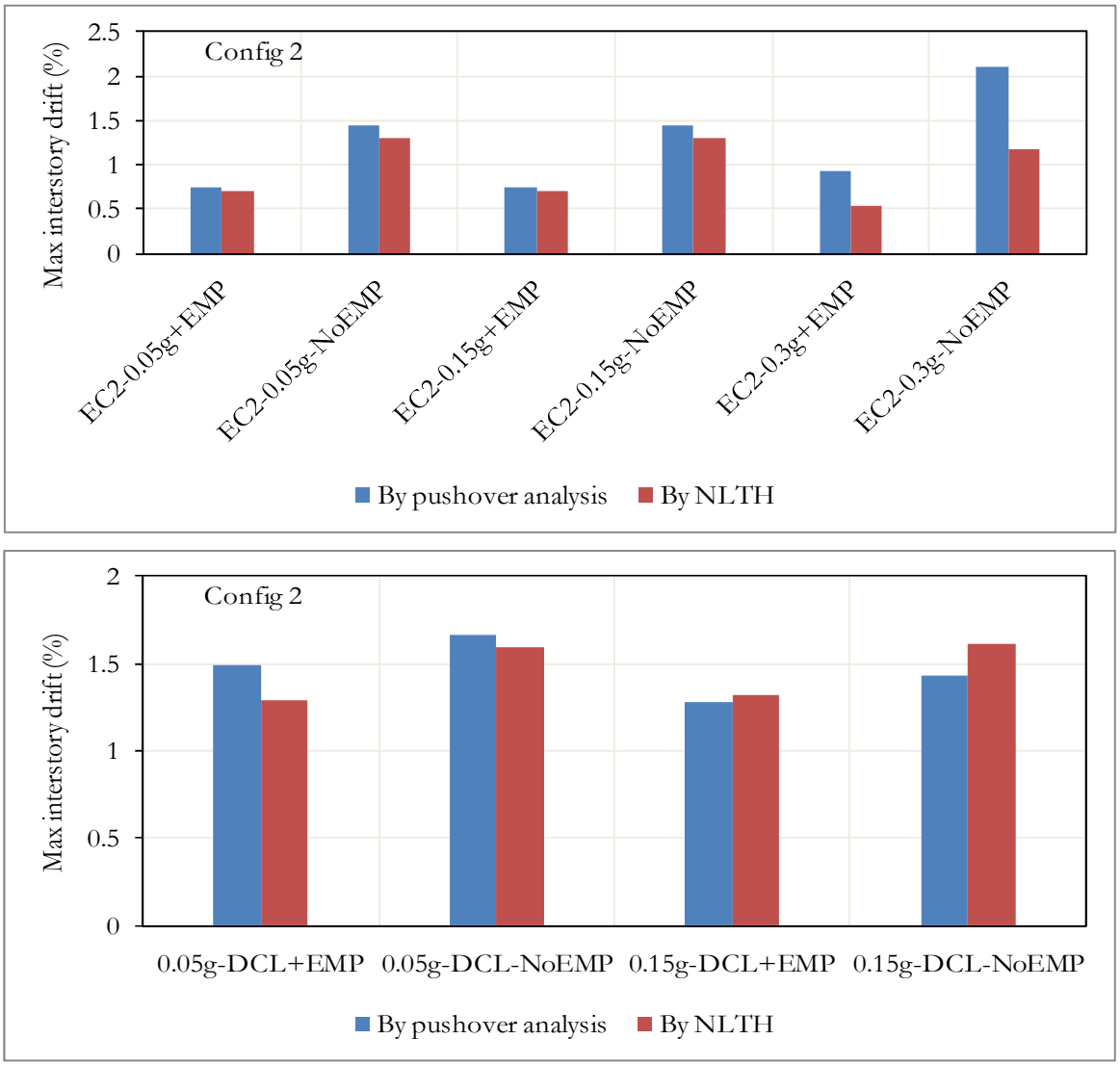

Figure 8-46 – Maximum interstory drift ratios at target displacements of studied RC-MRFs under design PGA established by Pushover and NLTH analyses – Configurations 2

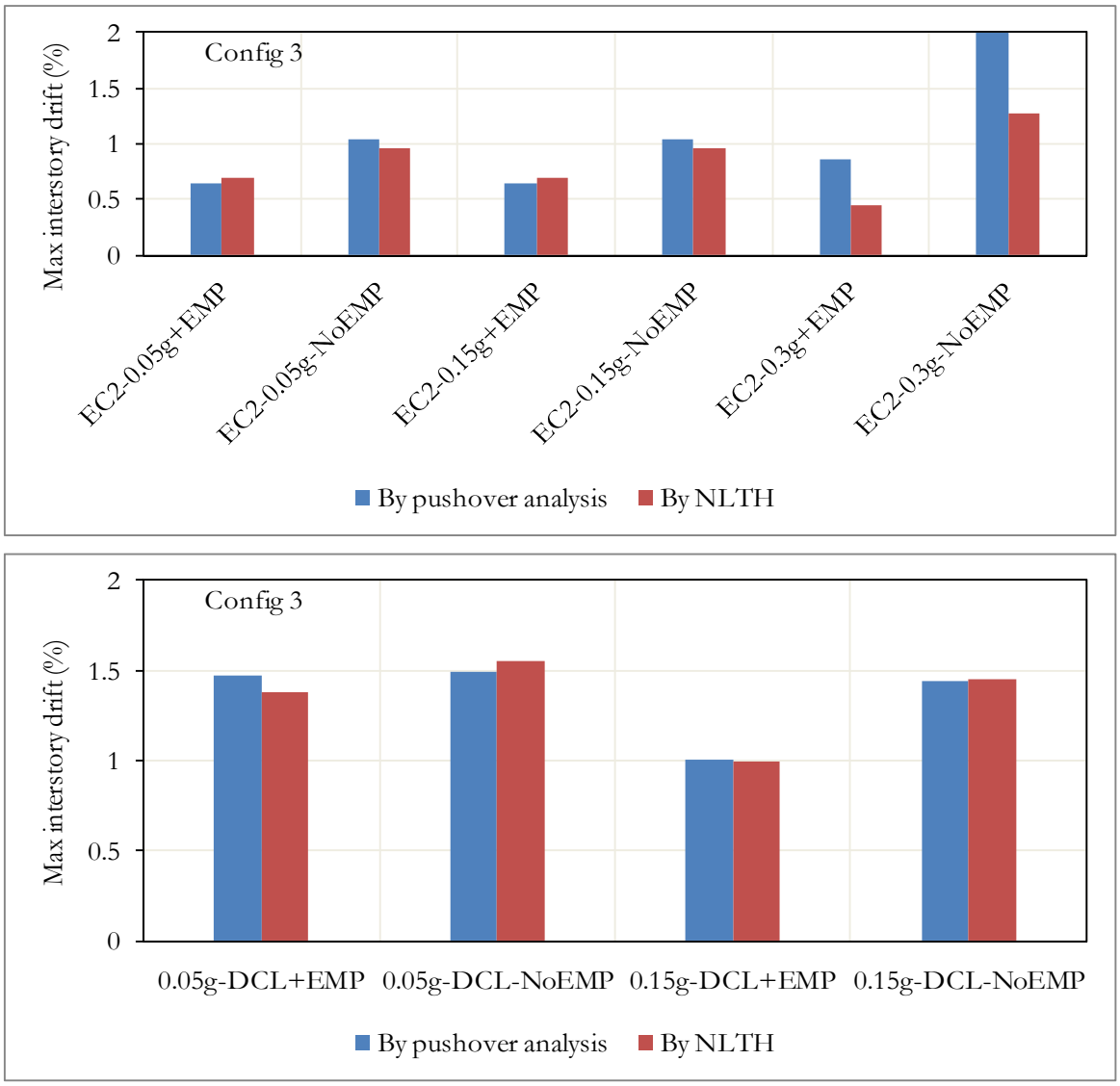

Figure 8-47 – Maximum interstory drift ratios at target displacements of studied RC-MRFs under design PGA established by Pushover and NLTH analyses – Configurations 3

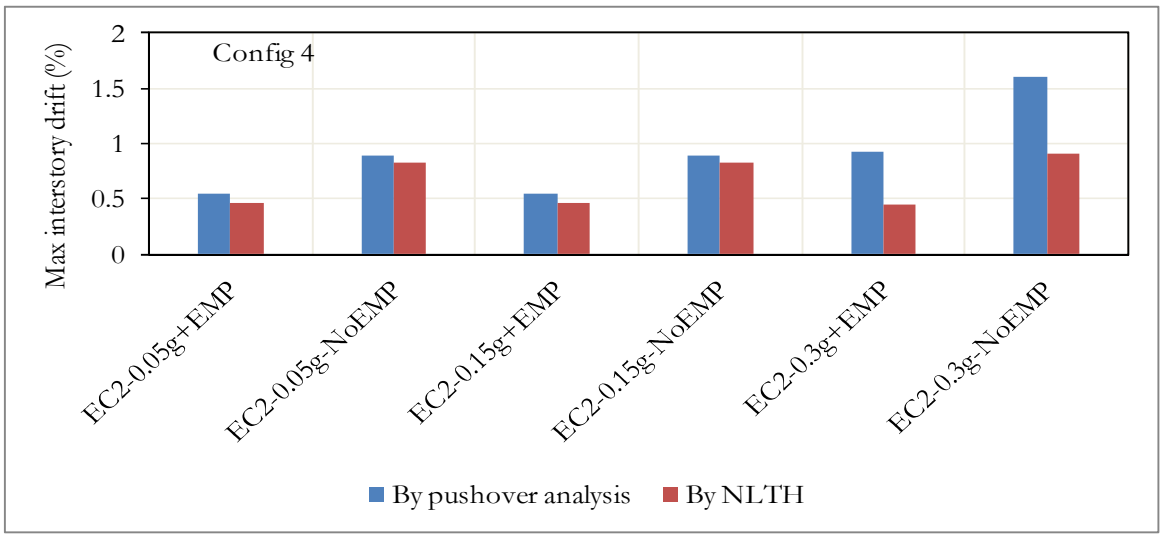

Figure 8-48 – Maximum interstory drift ratios at target displacements of studied RC-MRFs under design PGA established by Pushover and NLTH analyses – Configurations 4

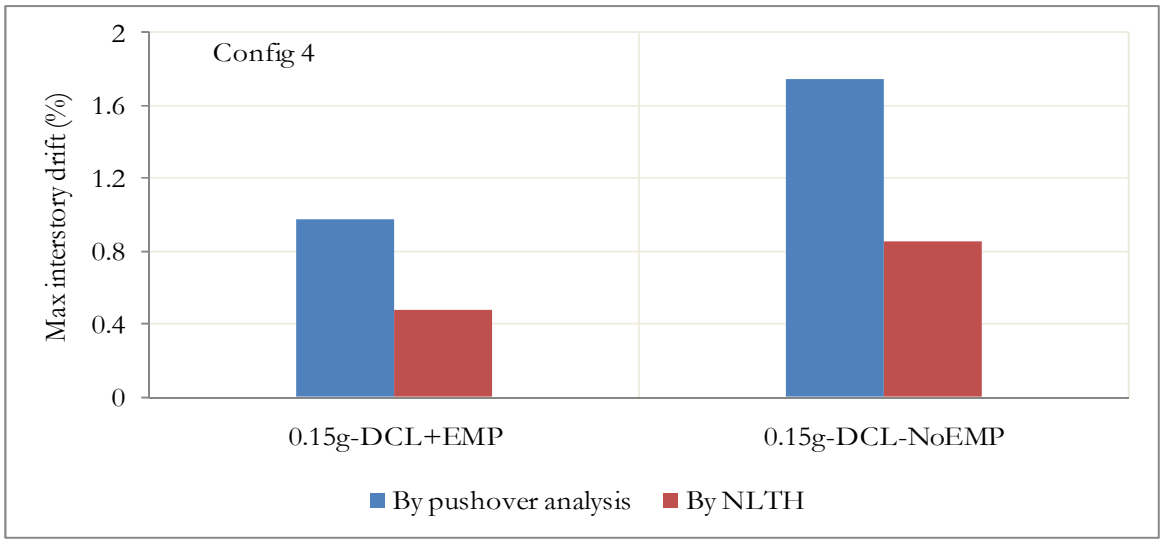

Figure 8-49 – Maximum interstory drift ratios at target displacements of studied RC-MRFs under design PGA established by Pushover and NLTH analyses – Configurations 4 (continued)

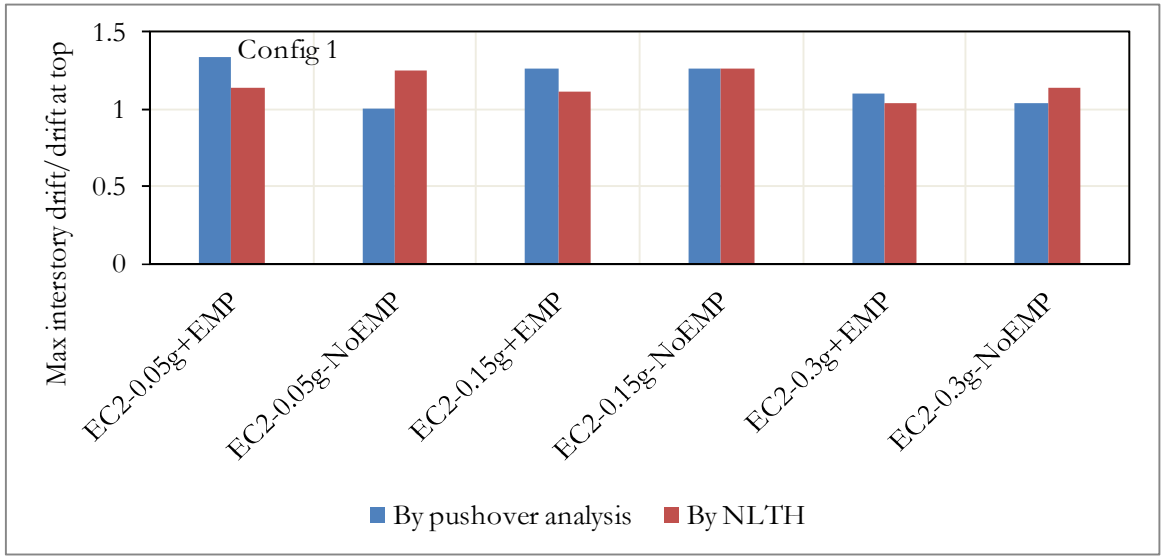

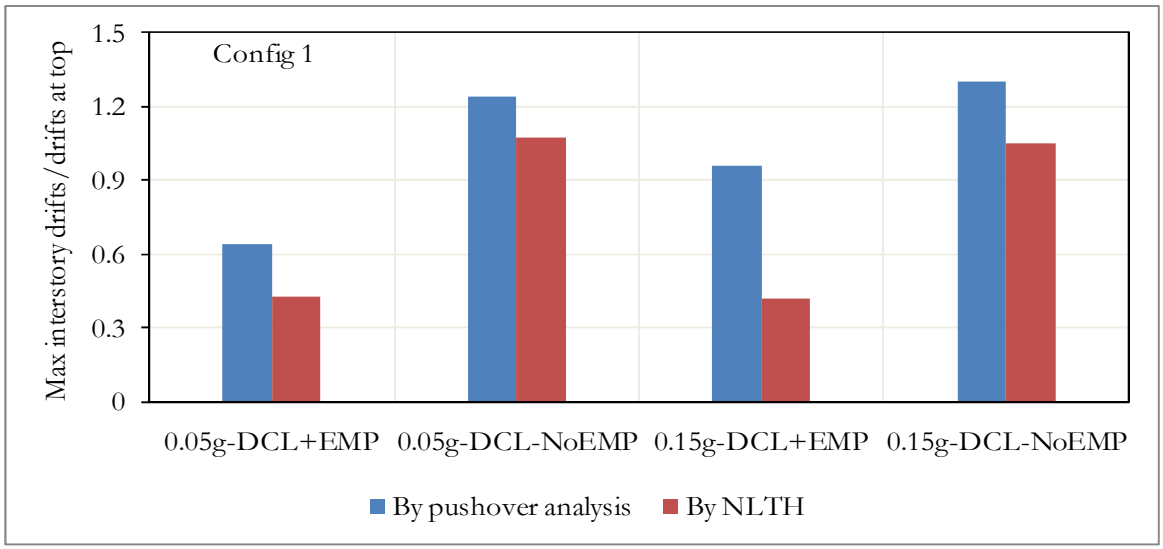

Figure 8-50 – Ratios between maximum interstory drifts and top drifts at target displacements of studied RC-MRFs under design PGA established by Pushover and NLTH analyses – Configurations 1

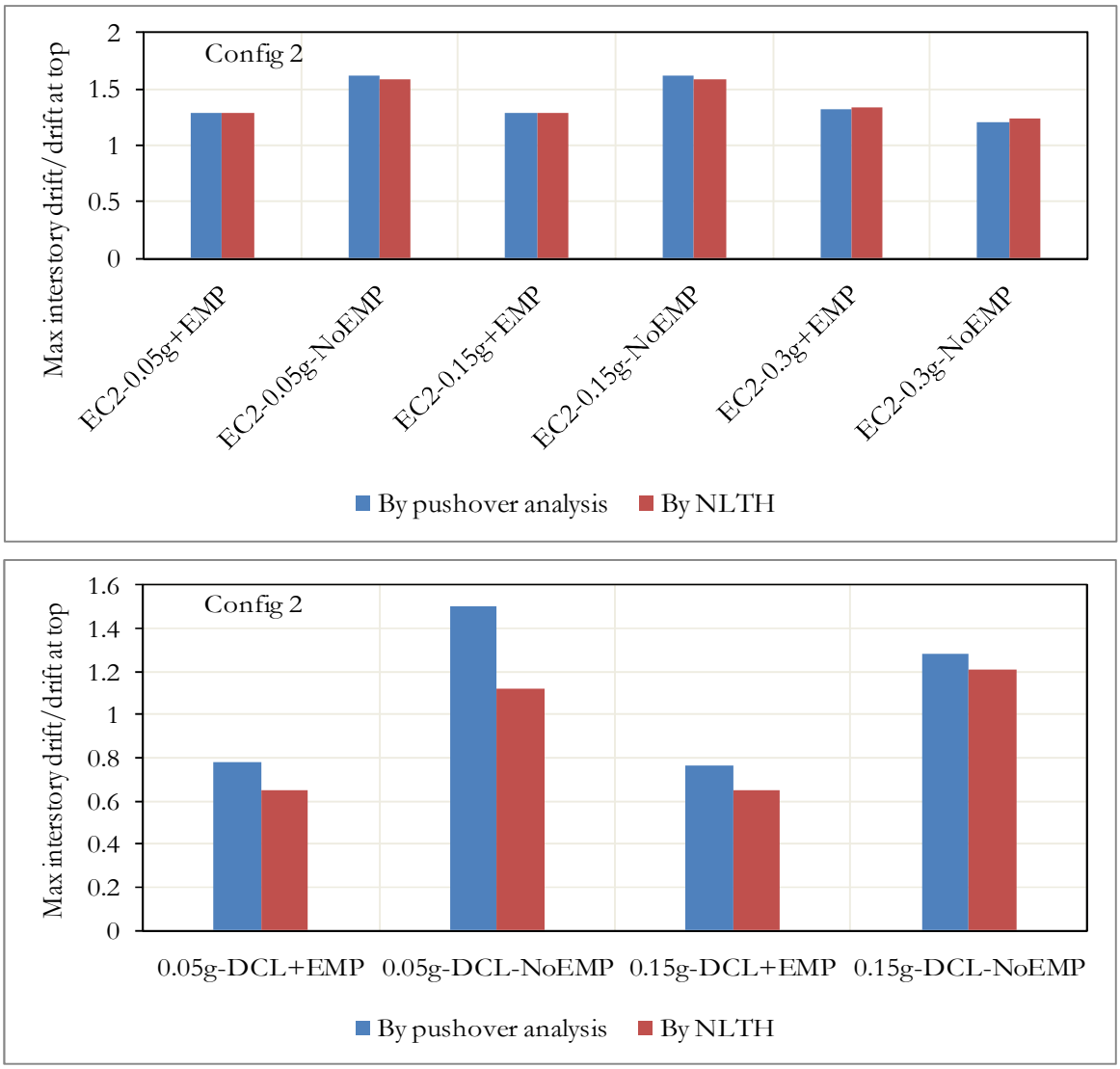

Figure 8-51 – Ratios between maximum interstory drifts and top drifts at target displacements of studied RC-MRFs under design PGA established by Pushover and NLTH analyses – Configurations 2

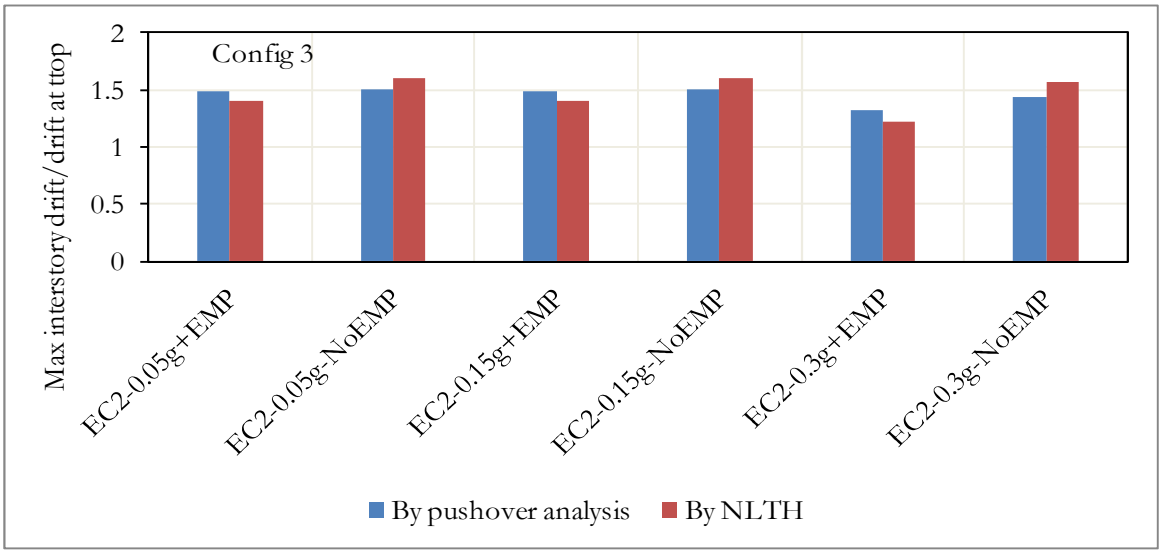

Figure 8-52 – Ratios between maximum interstory drifts and top drifts at target displacements of studied RC-MRFs under design PGA established by Pushover and NLTH analyses – Configurations 3

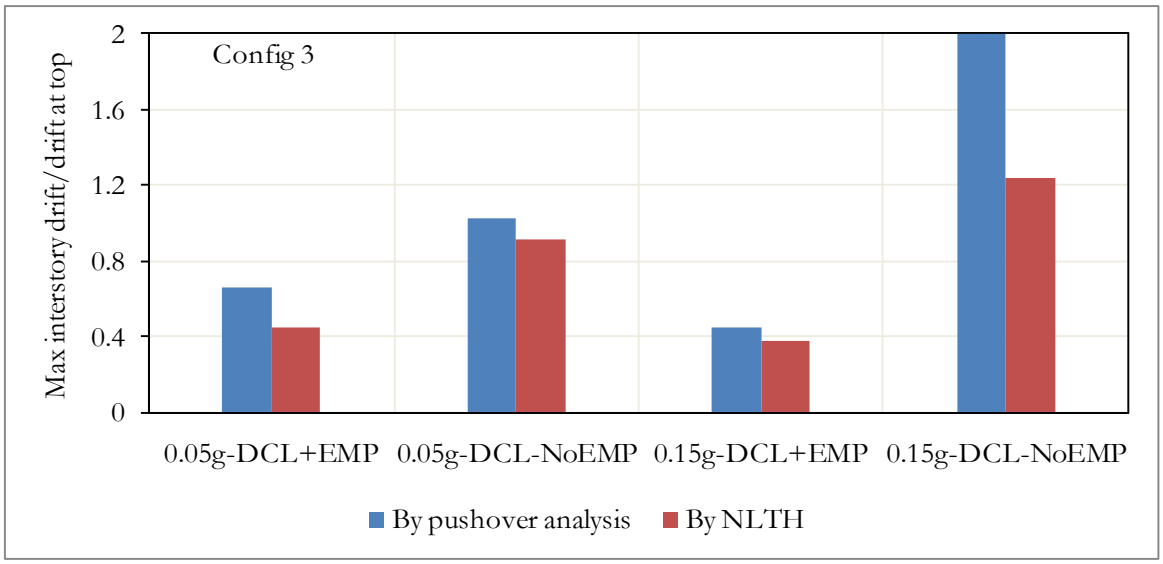

Figure 8-53 – Ratios between maximum interstory drifts and top drifts at target displacements of studied RC-MRFs under design PGA established by Pushover and NLTH analyses – Configurations 3 (continued)

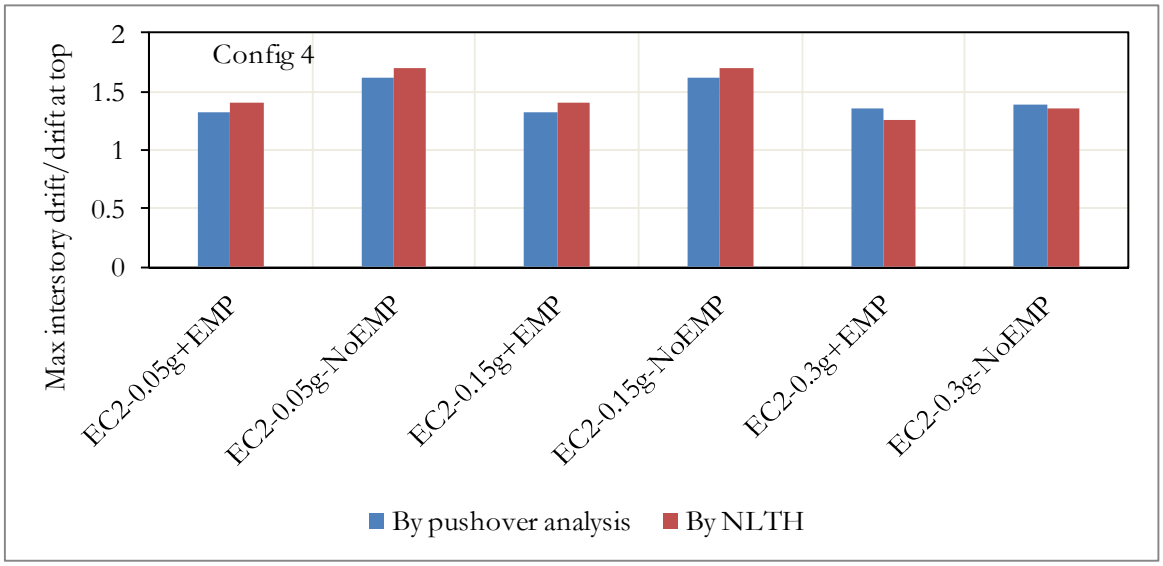

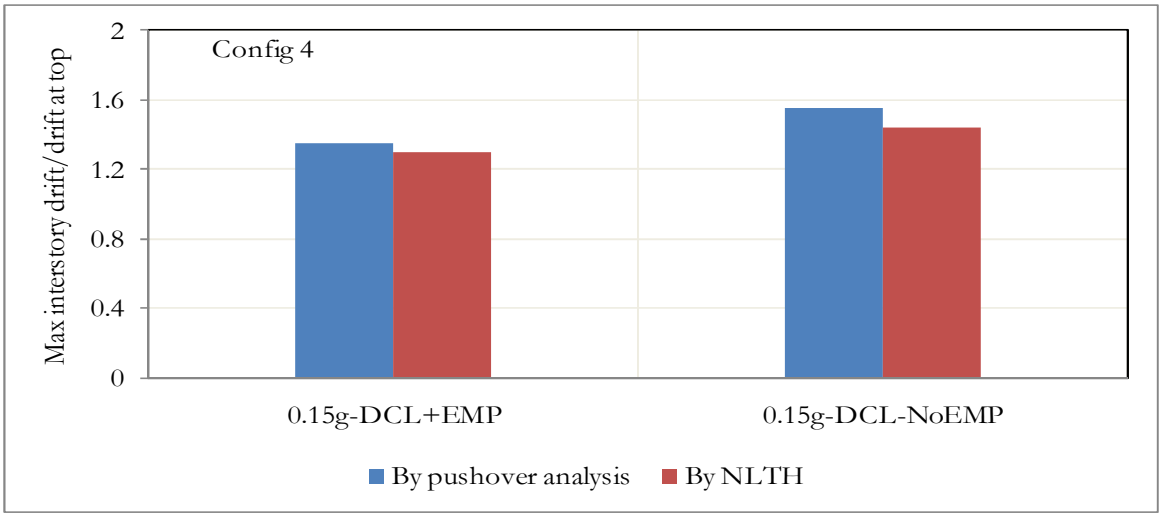

Figure 8-54 – Ratios between maximum interstory drifts and top drifts at target displacements of studied RC-MRFs under design PGA established by Pushover and NLTH analyses – Configurations 4

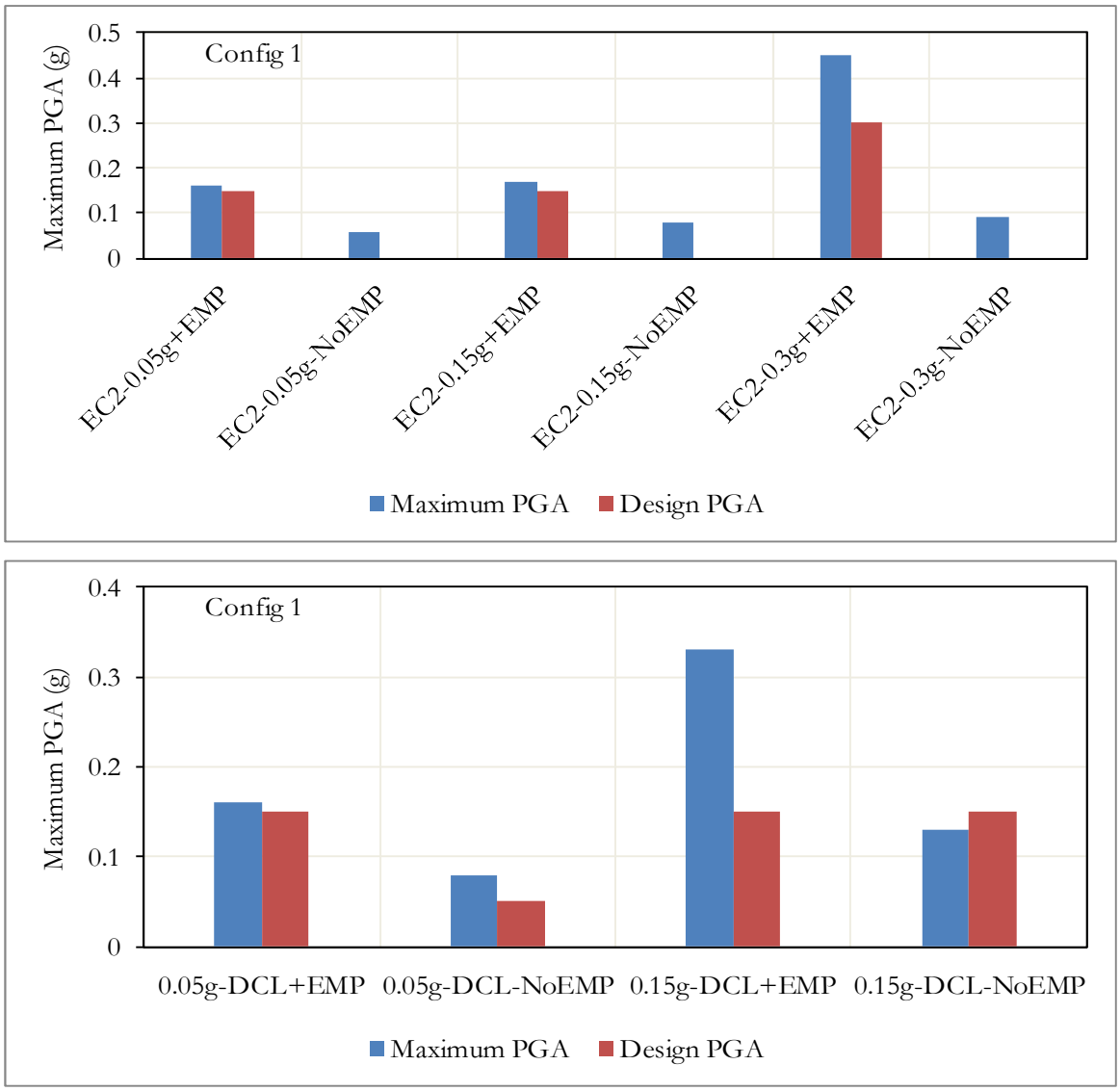

Figure 8-55 – Design and maximum resistible PGA of retrofitted RC-MRFs by Pushover analysis – Configurations 1

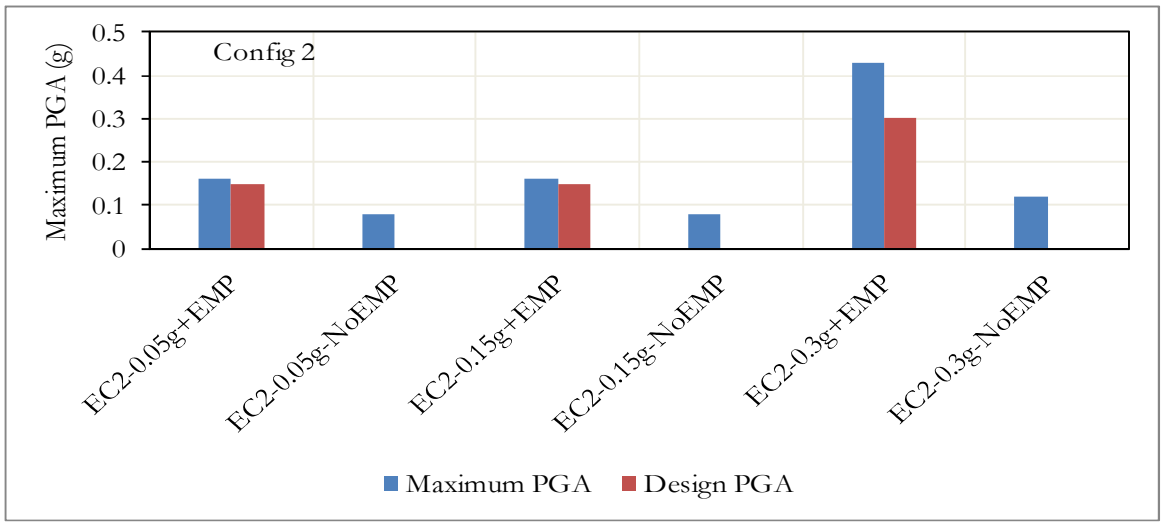

Figure 8-56 – Design and maximum resistible PGA of retrofitted RC-MRFs by Pushover analysis – Configurations 2

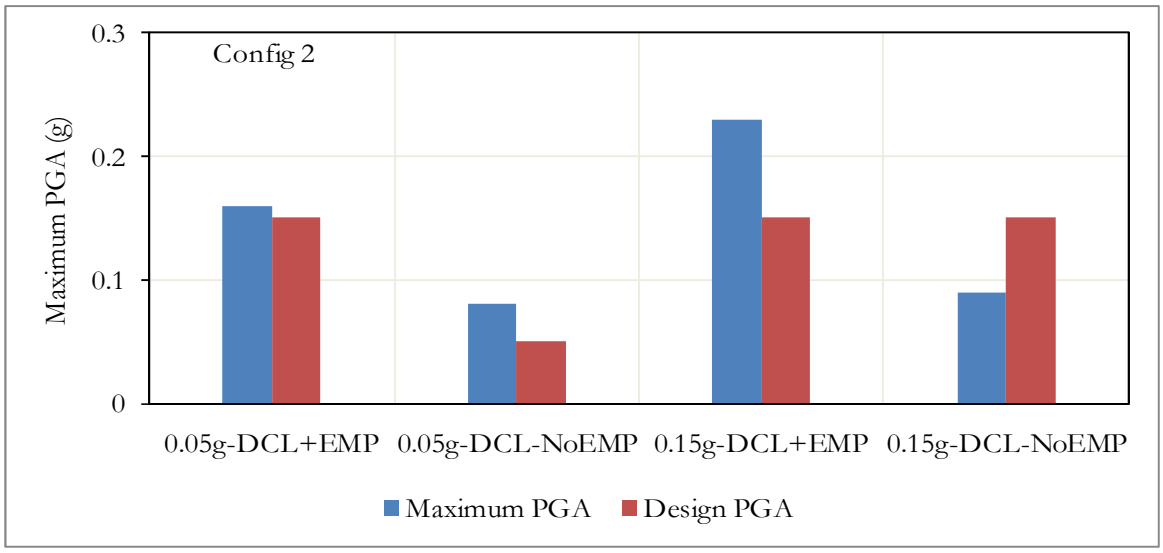

Figure 8-57 – Design and maximum resistible PGA of retrofitted RC-MRFs by Pushover analysis – Configurations 2 (continued)

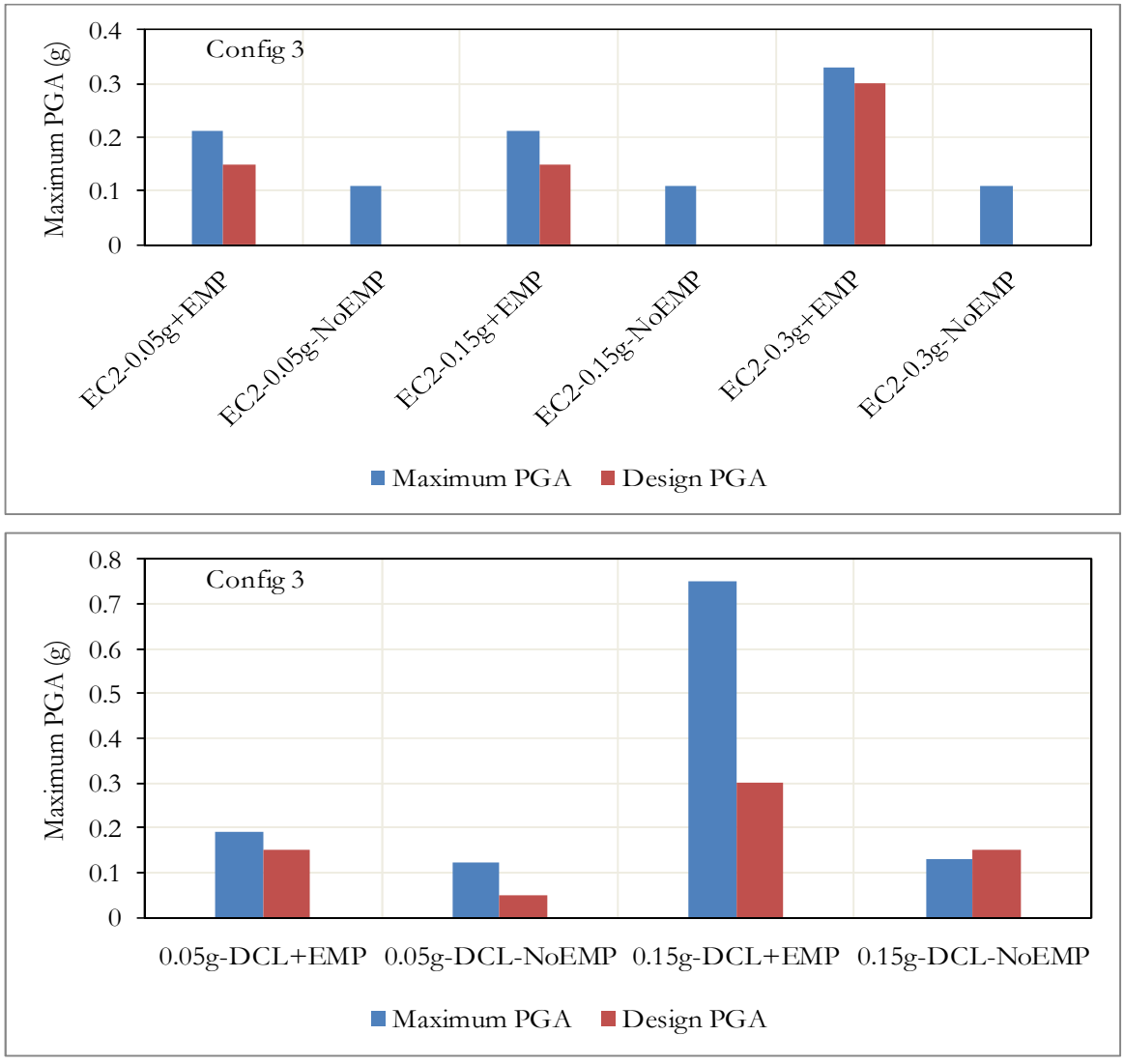

Figure 8-58 – Design and maximum resistible PGA of retrofitted RC-MRFs by Pushover analysis – Configurations 3

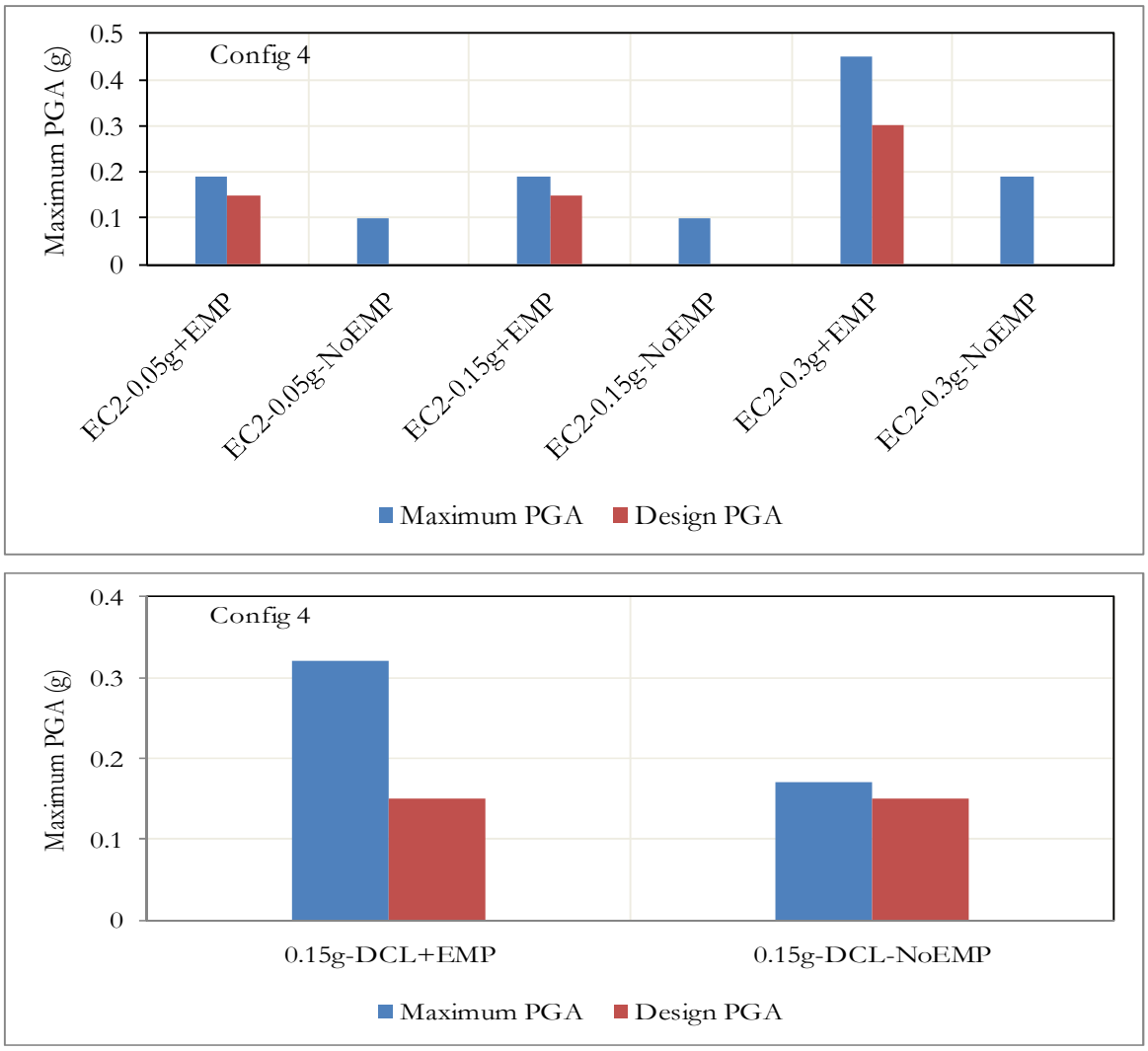

Figure 8-59 – Design and maximum resistible PGA of retrofitted RC-MRFs by Pushover analysis – Configurations 4

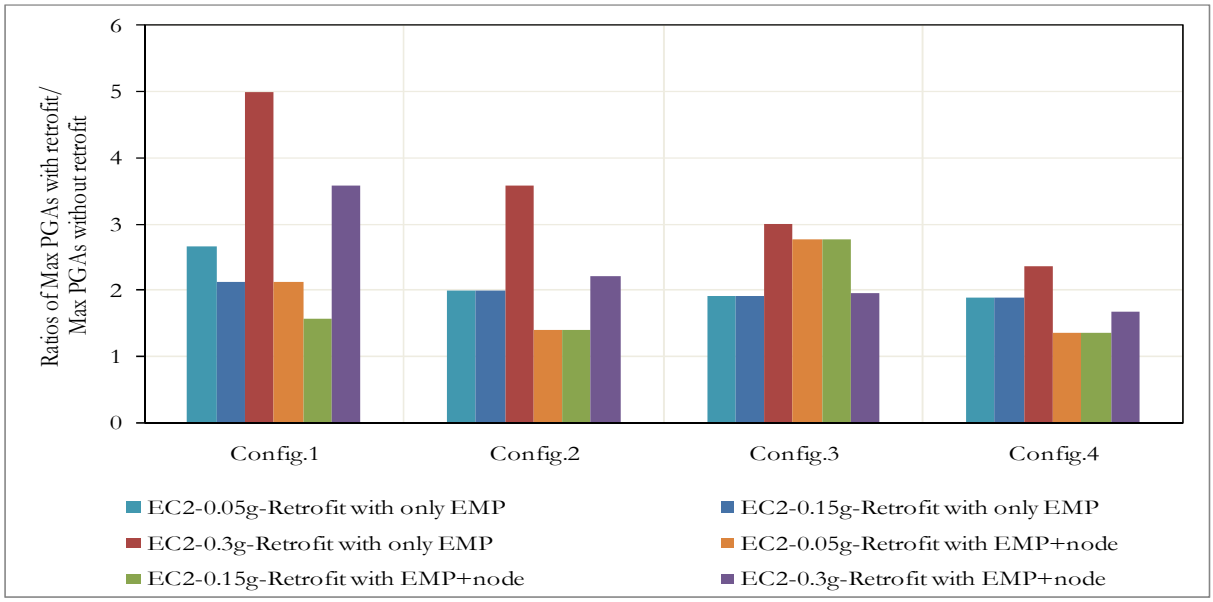

Figure 8-60 – Ratios of maximum resistible PGAs of RC-MRFs retrofitted using only EMP by Pushover analysis

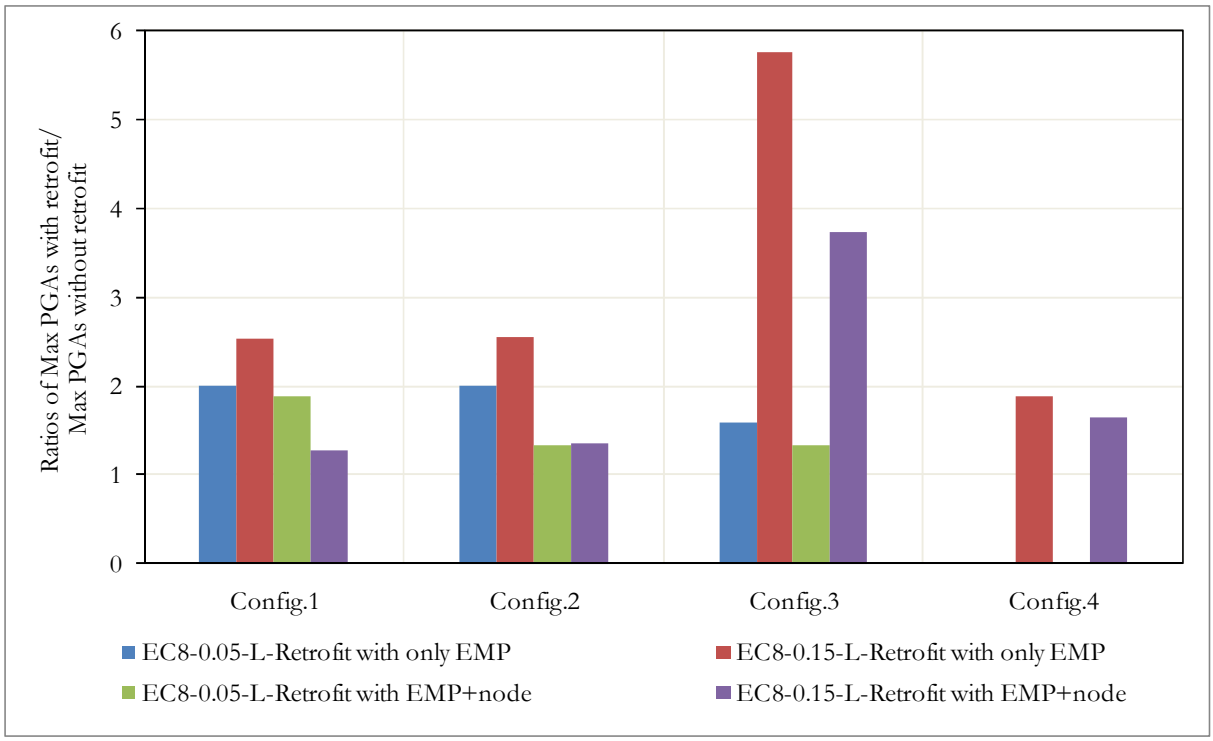

Figure 8-61 – Ratios of maximum resistible PGAs of RC-MRFs retrofitted by EMP and node retrofitted established by Pushover analysis

8.7. Some existing practical solutions to retrofit beam-column nodes or to increase shear resistance of RC beams and columns

With the use of EMP, the capacity of the retrofitted frames has been increased. However, the brittle failure due to shear leading to crushing of the concrete at critical regions of beams and columns or at beam-column nodes still governs the seismic behaviour of RC-MRFs designed to EC2 or EC2+EC8 with Low Ductility Class. Therefore, besides using EMP as the main seismic retrofitting system, some additional solutions to increase the strength and stiffness for shears of beams, columns and beam-column joints are necessary. The study on seismic retrofit of RC elements such as beams, columns or beam-column joints collapsed with brittle failure due shear is out of scope of the present thesis. Some practical methods are presented hereafter for the completeness of the retrofit work with EMP.

In order to increase the shear strength of beam-column nodes, a practically applicable solution is presented in Figure 8-62. The strength of compression strut of the joints is strengthened by using external prestressed bars with Dywidag type. These bars go through beams around the nodes in both directions. They are placed along the height of the beams, from their bottom to the lower edge of slab. Number of bars is dependent on the height of the beams and the required strength under seismic actions. To fix the bars, some additional angle profiles are used. The L profiles are placed close to the beams if the dimensions of columns are equal to or less than widths of the beams or close to the four corners of columns if the dimensions of the columns are greater than widths of the beams as shown in Figure 8-62. These L profiles run along the height of the beams. To adjust the positions of the L-profiles, mortar is used. In general, with this solution, the shear strength of the beam-column nodes can be increase about three to four (over even more) times higher than the original strength.

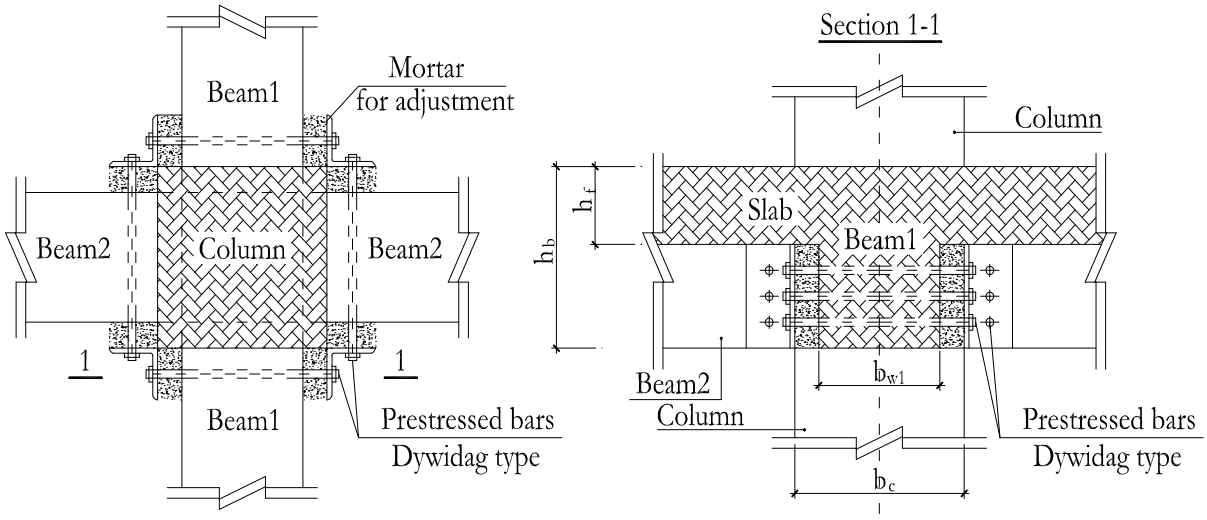

Figure 8-62 – Retrofit of beam-column joints by using external prestressed bars with Dywidag type

For retrofitting critical regions of beams or columns collapsed by shear, a solution presented in Figure 8-63 can be used. This method also uses some additional bolts or prestressed bars. These bars are put outside of the critical regions and they are parallel to the stirrups. Number and distance of the bars are determined by the required shear strength generated due to seismic actions. In addition, the cracks of concrete due to shear can be fixed by injecting epoxy to the cracks. The retrofitted shear strength can be about three to four times greater than the strength without retrofitting.

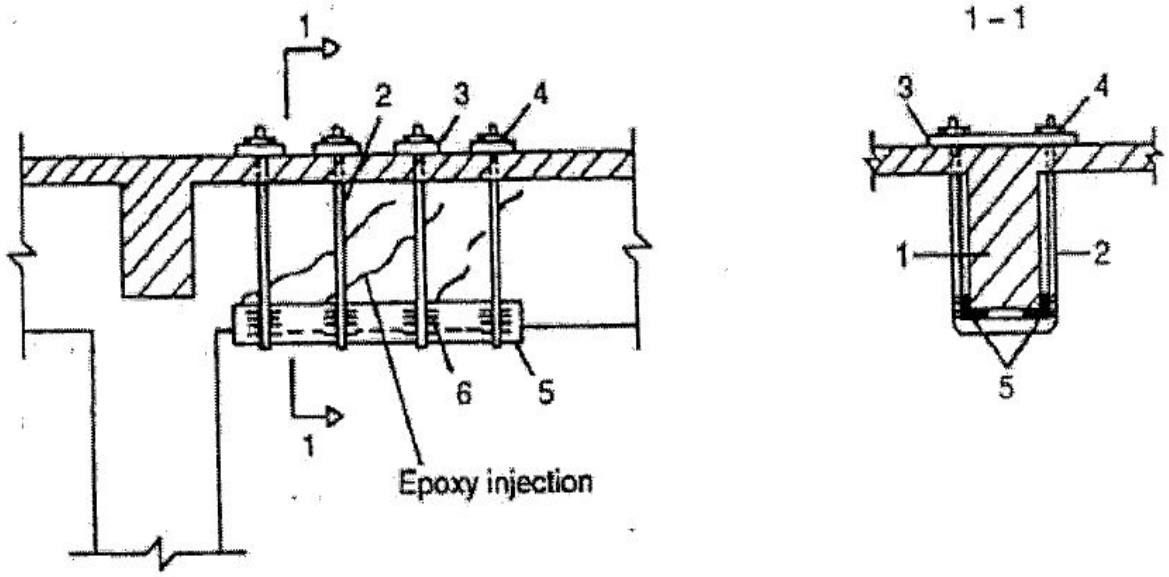

Figure 8-63 – Retrofit of beams at critical regions with brittle failure due to shears by using external bolts or bar with epoxy injection to the cracks of concrete

8.8. Design of connections of EMP with boundary elements of the frames

The study on EMP has proved that EMP is efficient in reducing the influence of the seismic actions on the structures by increasing their stiffness and strength and by absorbing the seismic energy. A practical problem raised here is that how to connect the EMP with the beams and columns on the RC-MRFs? A complete study on this issue has not been done to date. This section introduces a simple procedure that can be used to complete this difficult job on a conservative side. An example of designing the connections is also presented.

8.8.1. Description of the connection between EMP and the frame elements

A complete connection between an EMP and the frame's elements is shown in Figure 8-64 and Figure 8-65. Depending on the real dimensions of the spans and story height in the frame, an EMP can be made from several original EM sheets (number 15 in Figure 8-64 and Figure 8-65) and some complimentary steel plates or steel T profiles (numbers 3, 4 5 in Figure 8-64 and Figure 8-65). These EM sheets are connected together by welding them to the addition plates or by gluing them with the flat plates using epoxy. These solutions of connection have been well tested and used in the experiments on EMP, as presented in Chapter 3, 4 and 5. It should be noted that in order to stiffen the EMP for erection, some other plates are used (number 8 in Figure 8-64 and Figure 8-65). They will be taken out after completing the fabrication process.

In order to connect the beams and columns of RC-MRFs with a complete EMP (EM sheets and complimentary plates), some more components are used. First, there are four plates (number 11 and 12 in Figure 8-64 and Figure 8-65), rigidly attached to the beams and columns by means of bolts as seen in Figure 8-64. Then, plates with numbers 9 and 10 are connected to the plates numbers 11 and 12 by fillet weld. The EMP is connected to the frames by bolting with the plates 9 and 10. It should be noted that the positions of steel plates 9 to 12 should be adjusted so that the EM sheets of EMP are in plane.

8.8.2. Design of the connections between EMP and the frame's elements

There are two separate fabrication processes to install EMP in the existing RC-MRFs. The first process is about making a complete EMP and the second one is to connect the EMP with the beams and columns of the frame. Steps to design the connection between EMP and the frame's elements should consider these two processes.

8.8.2.1. Design of the connection between EM sheets to obtain a complete EMP

Figure 8-66 presents five steps of the design of a complete EMP from individual EM sheets and additional plates. Geometrical and material properties of all components in an EMP, such as dimensions of plates, the properties of connection materials or the length of the connection are determined by Capacity Design with reference to the EMP resistance. The tension resistance of the individual bars of the selected EM sheet is the key parameter in the design process.

Step 1 is to determine the characteristics of the EMP on each story. This is based on the shear forces which are distributed on each story level. The determination of these shear forces can be carried out by DDBD approach. The characteristics of the EMP can be selected with the aid of Table 4-1 and formulae in Equation 8-1.

Step 2 mentions about the determination of how many EM sheets and additional plates will be used to construct a complete EMP that fits the real dimensions of the frames.

Step 3 is to choose the connecting material that is used to link EM sheets with the additional plates (plates number 5 in Figure 8-64).

Depending on the connecting material chosen in the previous step, step 4 and 5 are about selecting and determining the geometrical and mechanical properties of the middle and boundary plates (number 3, 4 and 5 in Figure 8-64). Step 4 is to calculate the maximum tension resistance of the individual bars if the EM sheets and the minimum properties of weld or epoxy glue properties such as length and throat thickness… A safety factor of 1.5 could be used to increase the length of connection. Maximum tension resistance of a bar in an EM sheet can be calculated by the following equation:

$$V_{Ru,barEMP} = A \times B \times f_{u,EMP} \qquad \text{Equation 8-30}$$

The weld or glue connection length can be determined based on the tension force $1.5V_{Ru,barEMP}$.

Based on the required connection length, middle and boundary plates can be selected, as mentioned in step 5. It is necessary to note that the dimensions of boundary plates are chosen not only based on the required length of connection but also based on the real dimensions of the spans and story height.

8.8.2.2. Design of the connection between EMP and the boundary frame elements

The procedure to design the connection between EMP and the boundary frame is shown in Figure 8-67. Like in the design of connection between EM sheets, the first and second steps are to determine the characteristics and maximum tension resistance of the complete EMP using Equation 8-1.

Having obtained the maximum resistance of tensile mechanism, two components in vertical and horizontal directions are determined by projecting the tension resistance of the EMP onto two ordinates. This is step 2.

Using a safety factor of 1.5, vertical and horizontal components of the tension resistance of the complete EMP are increased 50%. Based on these forces, the properties of two types of bolts (1) used to connect the EMP with the plates 9 and 10 (Figure 8-64 and Figure 8-65) and (2) used to connect the plates 11 and 12 with the beams and columns of the RC frames can be selected. The properties of welding used to connect the plates 9 and 10 with the plate 11 and 12 (in Figure 8-64 and Figure 8-65) can then be selected as well.

8.8.3. An example of designing the connections between EMP and the frame's elements

The following is an example of design of a complete connection between EMP and a RC studied frame in EC2 group, named Config. 2/EC2-0.15g. The design of connection is at the second story. On this story, the height of the story is 3m and the length of the span is 5m. EMP profile chosen for this story is A51-27-35-30.

8.8.3.1. Connection between EM sheets to obtain a complete EMP

With the beam span is 5m, in order to form a complete EMP, four EM sheets of the profiles A51-27-35-30 are used. Figure 8-64 and Figure 8-65 show a complete picture of the EMP and the boundary elements. Five steps used to design the connections between EM sheets are presented hereafter.

Step 1 and 2: Four EM sheets with profile A51-27-35-30 are used to form a complete EMP in the second story. The standard dimensions of this profile are 1250mm x 2500mm.

Step 3: The weld connection is selected.

Step 4: Determination of the weld properties to connect EM sheets together

Design weld resistance

According to 6.3.4.3 (EC3; ECCS, 1991), design resistance of a fillet weld shall be taken as follows:

$$F_{w.Sd} \le \frac{F_{w.Rk}}{\gamma_{Mw}}$$

$$F_{w.Rk} = \frac{f_u}{\sqrt{3} * \beta_w} * a * L$$

f_u – The ultimate strength of the weaker component → $f_u = f_{uMD} = 393MPa$

β_w – Correlation factor, $\beta_w = 0.824$ (interpolation between $f_u = 360$ and 430)

a – throat thickness

L – Fillet weld length → Weld resistance is

$$f_{uwd} = \frac{f_u}{\sqrt{3}} * \frac{1}{\beta_w * \gamma_{Mw}} = \frac{393}{\sqrt{3} * 0.824 * 1.25} = 220.3MPa$$

Ultimate resistance of a bar in EM sheet A51-27-35-30

The width of each bar (A) is 3.5mm and the real thickness of the bar (B) is 2.7mm.

Section area of each bar is: S = 3.5x2.7=9.45mm^2.

Yield stress of MD is f_y = 337MPa and ultimate stress of MD is f_u = 393MPa.

Plastic resistance of 1 bar is $R_{pl} = f_y * S = 3185N$.

Ultimate resistance of 1 bar is $R_{ul} = f_u * S = 3714N$.

Properties of the weld connection

The weld resistance must be greater than the maximum forces generated in each bar during loading. Therefore, the properties of weld will be determined by capacity design rules. Here, it is easier if we fix the throat thickness of weld first and then the length of weld will be determined. Because the thickness of expanded metal bar is B = 2.7mm, so throat thickness of each bar will be determined as follows: $\sin 45^0 = \frac{a}{2.7} \rightarrow a = 1.9mm$. The required weld lengths for each bar of each EM rhomb-shape stitch are given by $L_{weld,EMP} \geq \frac{1.5 \times 3714}{220.3 \times 1.9} = 13.35mm$. Finally, the chosen weld length is 20mm (10mm in each side of the bar).

Step 5:

8.8.3.2. Connection between EMP and the boundary frame elements

Following five steps, presented in Figure 8-67, the connection between a complete EMP having profile A51-27-35-30 and frame's elements is designed as hereafter:

Step 1 and 2: Similarly to the connection between EM sheets, this step is to determine the characteristics of EMP on each level of the frame. An EMP with four EM sheets (profile A51-27-35-30) and some supplementary T profiles is selected for second level of the frame.

Maximum tension resistance of the EMP:

Maximum shear resistance of a complete EMP, V, is calculated by Equation 8-1. Projecting this shear onto diagonal direction, the maximum tension resistance is determined. Similarly, the vertical maximum component is also calculated. This is graphically explained in Figure 8-68.

Some main characteristics of the EMP are: (1) diagonal length of the EMP l_{dia} = 5831 mm; (2) exterior length of the rhomb-shape stitch LD=51mm, interior length of the rhomb-shape stitch LD_{in}=41mm; (3) average length of the rhomb-shape stitch LD_{aver}=(51+41)/2=46 mm; (4) exterior width of the rhomb-shape stitch CD=27 mm; (5) interior width of the rhomb-shape stitch CD_{in}=20 mm; (6) average width of the rhomb-shape stitch CD_{aver}=(27+20)/2=23.5 mm; (7) length of a bar l_{bar}=25.8 mm; (8) $\alpha = \frac{A}{l_{bar}} = \frac{3.5}{25.83} = 0.136$. Maximum shear resistance of the EMP is V = 199 kN.

Step 3:

Design shear resistance per bolt:

Design shear resistance of a bolt shall be taken as 6.2.3.2 (EC3, ECCS, 1991):

$$F_{v.Rd} = \frac{F_{v.Rk}}{\gamma_{Mb}}; \; F_{v.Rk} = C_1 * f_{ub} * A_s \text{ or } F_{v.Rd} = \frac{0.8}{\sqrt{2}} * \frac{f_{ub}}{1.25} * A_s$$

Where: - f_{ub}: ultimate shear resistance of a bolt.

A_s: Section area of a bolt.

C_1: factor

For bolts M12 with type 10.9, which has f_{ub} = 1000MPa and A_s = 84mm², the design shear resistance per bolt is $F_{v.Rd} = \frac{0.8}{\sqrt{2}} * \frac{1000}{1.25} * 84 = 38014N$.

For bolts M16 with type 10.9, which has f_{ub} = 1000MPa and A_s = 157mm², the design shear resistance per bolt is $F_{v.Rd} = \frac{0.8}{\sqrt{2}} * \frac{1000}{1.25} * 157 = 71050N$.

Design bearing resistance per bolt

Design bearing resistance per bolt shall be taken as 6.2.3.1 (EC3, ECCS, 1991):

$$F_{b.Rd} = \frac{F_{b.Rk}}{\gamma_{Mb}}; \; F_{b.Rk} = 2.5*\alpha*f_y*d*t$$

Where: - f_y: yield resistance of plates

- d: diameter of bolt

- $\alpha = \min\left(\frac{e1}{3d_0}; \frac{p1}{3d_0} - \frac{1}{4}; \frac{f_{ub}}{f_u}; 1.0\right)$

- d_0 – hole diameter

- e1, p1, e2, p2 – as Figure 8-69

- t – Smaller thickness between plates.

For bolts M12, d=12mm and d_0 = 13mm, the plate made by steel S460, f_y = 460MPa, α=1, and the plate with 5mm thickness → design bearing resistance is $F_{b.Rd} = \frac{2.5*1*460*12*5}{1.25} = 55200N$.

For bolts M16, d=16mm and d_0 = 18mm, the plate made by steel S460, f_y = 460MPa, α=1, and with the thickness of 5mm → design bearing resistance is $F_{b.Rd} = \frac{2.5*1*460*16*5}{1.25} = 73600N$.

Number of bolts for horizontal and vertical connections

The maximum ultimate shear resistance is 199kN. For bearing-type connections, at the ultimate limit state, design resistance of bolts is $F_{v.Sd}$ = min ($F_{v.Rd}$ and $F_{b.Rd}$) = min (38014N and 55200N) for bolts M12 and $F_{v.Sd}$ = min (71050N and 73600N) for bolts M16.

The numbers of bolts are determined from two conditions:

- For shear resistance $F_{force} \le m*n*F_{v.Rd}$

Where: - F_{force}: the total force acting to the plates; m: numbers of shear surfaces; n: numbers of bolts.

F_{force} =1.5 x V = 298.5 kN (1.5 is a safety factor)

Number of bolts is $\frac{298.5\times10^3}{1\times38014} = 7.9$ if the bolt of M12 is used and $\frac{298.5\times10^3}{1\times71050} = 4.2$ if the bolt M16 is used.

- For bearing resistance $F_{force} \le n*F_{b.Rd}$

Where: - F_{force}: the total force acting to the plates

- n: numbers of bolts.

F_{force} =1.5 x V = 298.5 kN (1.5 is a safety factor)

Number of bolts is $\frac{298.5\times10^3}{1\times55200} = 5.4$ if the bolt of M12 is used and $\frac{298.5\times10^3}{1\times73600} = 4.1$ if the bolt M16 is used.

Step 4: In this step, the boundary plates used to connect EMP with the beams and columns are selected based on some criteria: (1) number of bolts used to connect EMP to beams and columns; (2) spans and story height of the frame; (3) cross-sectional dimensions of beams and columns; (4) reinforcement configuration of beams and columns.

Step 5: Weld properties to connect plates 9 and 10 with 11 and 12 in Figure 8-64 are easily determined based on the shear resistance of the EMP.

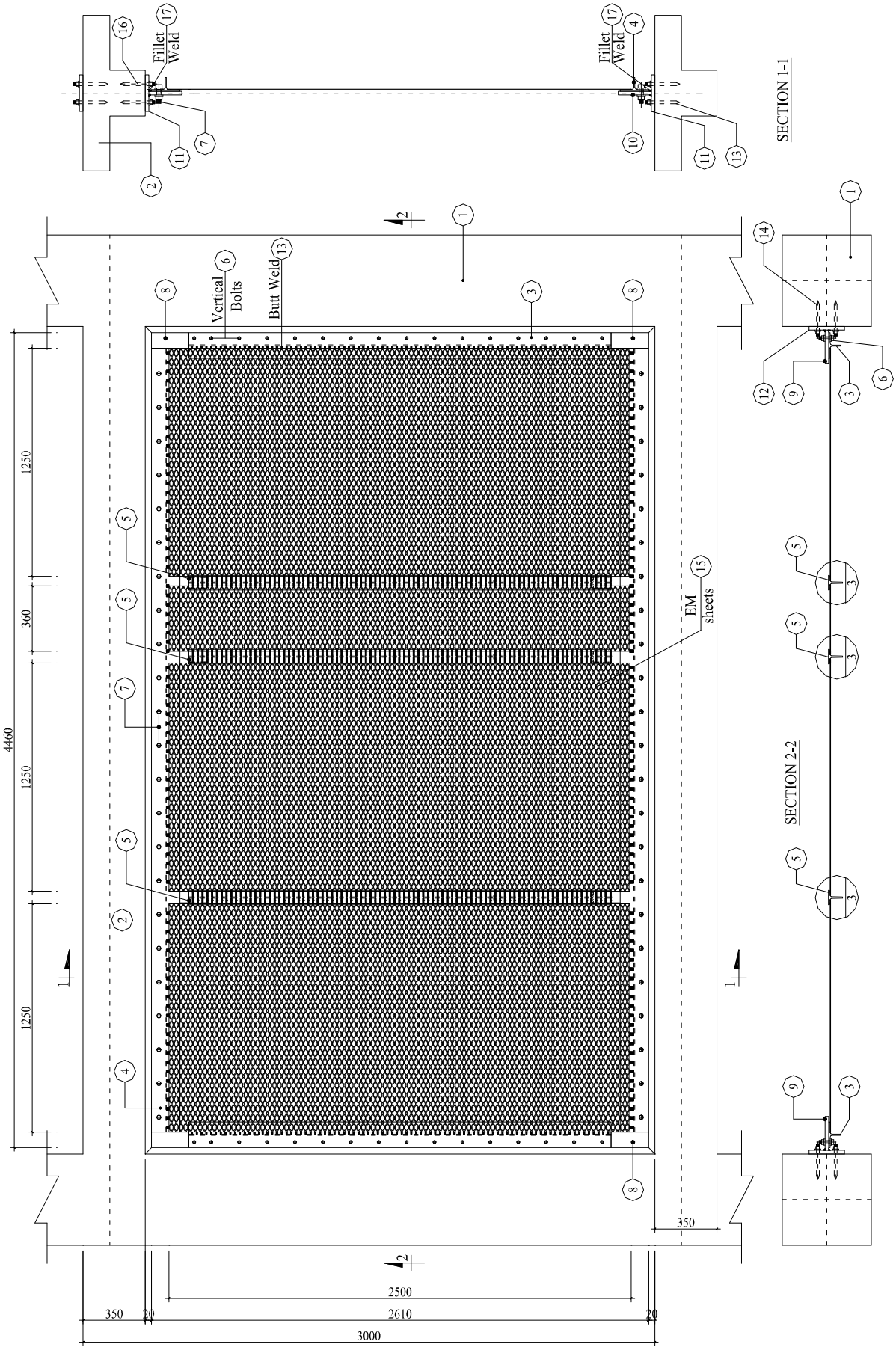

Figure 8-64 – Description of the connection between EMP and the frame's elements

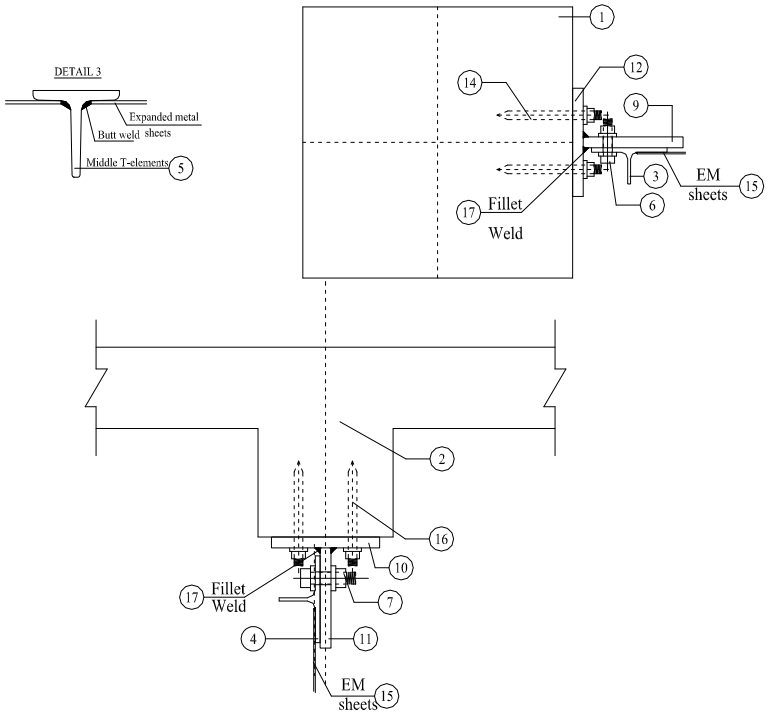

1 - Beams; 2 - Columns; 3 – Vertical plates of EMP; 4 – Horizontal plates of EMP; 5 – Plates used to connect EM sheets; 6 – Vertical bolts to connect EMP with columns; 7 - Horizontal bolts to connect EMP with beams; 8 – Temporary plates for EMP; 9, 10, 11, 12 – Plates used to connect EMP with beams and columns; 13 – Butt weld to connect EM sheets with plates 3 and 4; 14, 16 – Bolts to connect beams and columns with ; 15 – EM sheets; 17 – Fillet weld between plates 9 and 10 with 11 and 12

Figure 8-65 – Description of the connection between EMP and the frame's elements

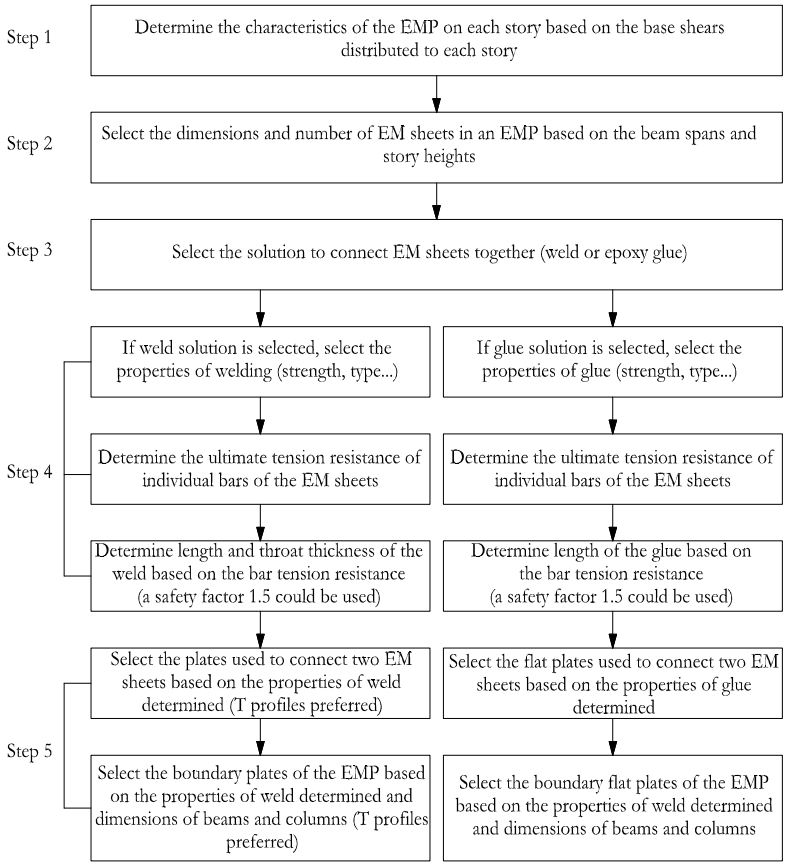

Figure 8-66 – Steps to design connection between EM sheets

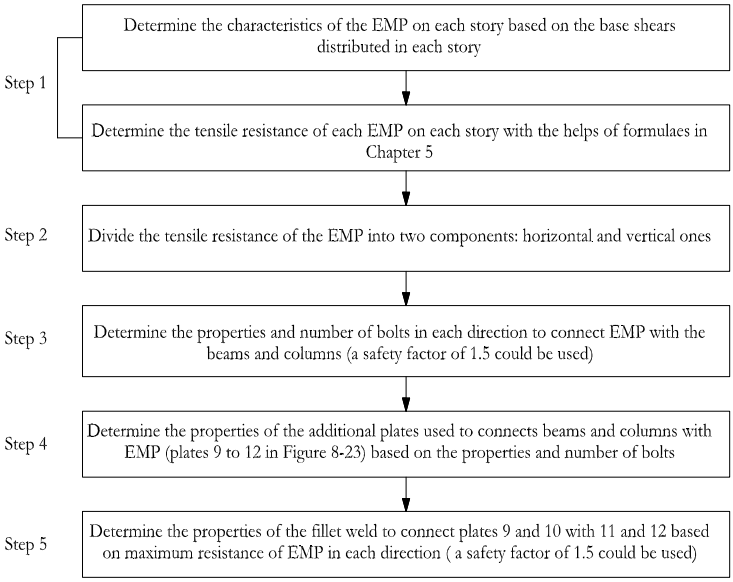

Figure 8-67 – Steps to design connection between EMP and the frame's elements

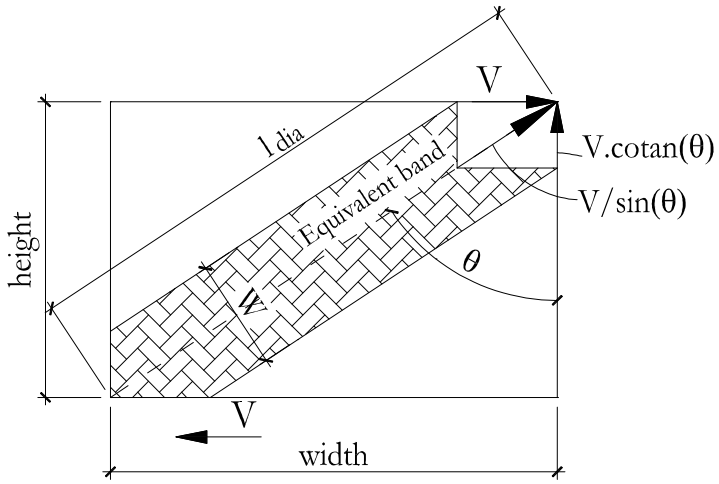

Figure 8-68 – Steps to design connection between EMP and the frame's elements

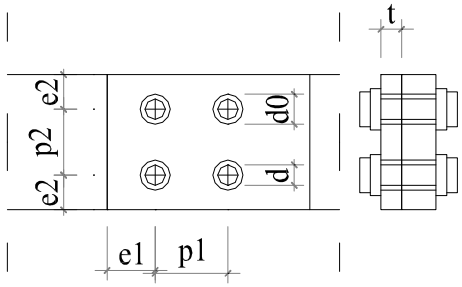

Figure 8-69 – Determination of bearing resistance per bolt

8.9. Concluding remarks

A complete study on the use of EMP to seismically retrofit the RC existing frames has been introduced. The design approach for determination of EMP is based on the DDBD method. All studied frames, designed and evaluated in Chapter 6 and 7, are verified with the aims to address the necessity of the retrofit. Thanks to the design in accordance with EC8, the frames with Medium ductility class do not have to be retrofitted. The remaining frames, including frames in EC2 group and EC8-DCL, are retrofitted with the application of EMP. The idea is to use EMP to carry some portions of the seismic forces

generated in the retrofitted frames. In order to connect individual EM sheets with the frame's elements, some solutions based on weld and epoxy glue connections have been proposed.

The main conclusions are drawn hereafter.

First of all, DDBD approach is a very useful tool in determining EMP for retrofitting an existing RC frame. The results from DDBD on retrofitting design are significantly affected by some typical parameters such as selected target displacements for the retrofitted frames and capacity of the existing frame contributing to overall resistance of the dual system, EVD of the EMP as well as geometrical dimensions of the existing frame. Verifying the retrofitting design results by means of Pushover and NLTH analyses has indicated that DDBD well predicts the response of structures at the ultimate limit state. The goal of design work is accomplished by using DDBD approach. However, in some cases, there are still some slight differences between design assumptions and exact response of the frames after being retrofitted. These may come from several reasons such as the limitation of the types of EMP in practice, leading to too conservative selection of the EMP for the retrofitting process. Studies on this design approach should be continued.

Second, all retrofitted frames are able to resist design earthquakes as expected. However, under bigger ones, the brittle failure of the frames designed accordingly to EC2 and to EC8-DCL still dominates the seismic response of the retrofitted frames. This failure is usually caused by crushing of the concrete due to shear at critical regions or due to shear at beam-column joints. It leads to the deficiency of incomplete load path of the structures. For the studied frames, failure of beam-column joints is observed in all frames not designed in accordance with EC8-DCM. In some cases, the failure is coincident with the first plastic hinges occurred at beams. With the use of EMP, the final failure mechanism of the retrofitted frames has not been improved. Brittle failure at beam-column joints is seen in all retrofitted cases, however, at rather large magnitude earthquakes compared with the design ones.

Third, the comparison of the seismic performance of the frames before and after being retrofitted has proved that EMP is able to reduce the influence of the earthquake on the original frames by increasing their strength and stiffness and by absorbing the seismic energy. This is proved by lower values of top displacements, of interstory drifts and of damage of the retrofitted frames compared with the original ones. If the brittle failure is fixed by other solutions, EMP can absorb about 40% of seismic energy generated in the retrofitted systems.

Finally, a design procedure for connection between EMP and the frames' elements is presented. It was verified in the experiments when connecting EMP with the steel frame. The design approach for the connection is based on capacity design rules, all starting with the maximum resistance of the bars in a rhomb-shape stitch of the EMP and tension field action developed in EMP during loading. However, it is necessary to do tests on the connections between EMP and the RC beams and columns.

9. CONCLUSIONS AND RECOMMENDATIONS

9.1. Conclusions

Seismic retrofit of RC-MRFs is a difficult task for structural engineers. This comes from many reasons such things as lack of knowledge of the existing structures, difficulties in assessing their seismic performance, in selecting and designing the appropriate seismic retrofitting strategies and systems. In this study, many seismic retrofitting systems to date have been summarised. Amongst those, Restrained Buckling Braces and Eccentrically Brace Frames have advantages over the other systems thanks to their capacity in obtaining a better hysteretic behaviour under seismic actions: stable hysteresis loops in both tension and compression without much degradation in stiffness and strength. However, the others, such as shear walls made from steel, aluminium or reinforced concrete or Concentric Conventional Braces …, also have their own advantages, mostly based on their capacity in more or less increasing the stiffness and strength, in absorbing the seismic energy and in low price of fabrication…

A complete study on pure shear behaviour of EMP under monotonic and quasi-static cyclic loading has been developed including experimental, theoretical and numerical investigations. Application of EMP in retrofitting RC-MRFs, which have been designed based on EC2 and EC8, is also examined as well. Furthermore, a procedure of designing EMP to seismically retrofit RC-MRFs as wells as suggestions of connecting EMP with the frame elements has been proposed. These retrofitting solutions using EMP have been evaluated using Pushover and nonlinear time history analyses.

There are two types of EMP, comprising flatten and normal ones An EMP, a product made from steel or other metals, looks like a flat plate with many voids. These voids have caused the lower weight for this product, leading to the lower cost compared with other metal plates. Currently, EMP is seldom applied for structural applications therefore mechanical properties of the used steel are not an important point for the manufacturer. However, as metal plates have been used in structural applications for the last decades, mostly in the field of earthquake resistance, playing as the parts of lateral resistance of the structures, EMP could have a similar use in retrofitting and upgrading structures for earthquake resistance.

From the experimental study, it is clear that under rather low shear forces the sheets are globally buckled, therefore the contribution of compression diagonal to the resistance of the sheets can be neglected. Under monotonic loading, the maximum shear resistance of EMP is dependent on the voids of the sheets. Besides, having nearly the same voids, maximum shear resistance of flattened type specimens are much greater than those of normal types. Under quasi-static cyclic loading, the hysteretic behaviour of all specimens is S-shaped with pinching effects. These effects on all specimens due to yielding in tension and to buckling in compression caused the degradation of stiffness of the sheets. In addition, in cyclic tests, the stiffness of the sheets is approximately equal to zero during the inversion of force. The deflection required to redevelop the tension field is based on the yielding displacements experienced by the sheets in the previous cycles. The ductility of panels is related to the ductility of the base material itself, which is not at present subject to get special control for manufacturer. For sure, if seismic applications of EMP are envisaged, a control of the steel material characteristics should be imposed. It was also observed for the experiments that out of two types of EMP, welding the flattened type with the boundary frames is more easily than welding the normal type with the frames. This advantage of the flattened type over normal one is due to the flatness in plane. Observing the tests in cyclic loading, it is clear that the observed hysteresis behaviour of the EMP is independent from the resistance of the panel before buckling because the elastic resistance of the panel is very small. The panel always buckles when the shear load is applied and this leads to pinching of the hysteresis loops. This behaviour is somewhat similar to conventional steel concentric braces, unstiffened steel plate shear walls and reinforced concrete elements. However, the behaviour of the EMP is more pinched than the others, leading to a smaller enclosed area of the loops and lower energy dissipated in the system. Based on the results from experiments, EMP seems to be suitable for the use in retrofitting structures subjected to in-plane shear thanks to some advantages such as strength and ductility. However, it is important for the fabricator to produce a much more constant mechanical product. Concerning the connection of the EMP with the boundary frames, it can be observed from the tests that both welded and epoxy-glued solutions are effective in connecting the EMP and the boundary frame elements.

Numerical simulations have been performed to analyse the experiments on the EMP loaded in shear and to make a parametric study with the aim of addressing a simplified model for shear behaviour of the EMP. There is a good correlation between the results obtained from the experiments and numerical simulations. FINELG, a fully nonlinear finite element code used for modelling the tests, is capable of predicting both monotonic and hysteretic responses of the EMP subjected to shear. The one inclined tension band model can be used with acceptable accuracy to evaluate the response of the EMP under shear loading. The characteristics of this tension band are dependent on the properties of the EMP, including geometrical and mechanical ones, on the boundary dimensions of the frames and on some fixed ratios which are related to the ratio between the length and the height of the boundary frame. If it is assumed that the EMP is fabricated with consistently mechanical product, having properties of the bands as mentioned above, the ductility of EMP under shear can range from 4 to 13. In addition to that, the ultimate drifts of the EMP can be about 3% to 3.5% and the yield drifts about 0.12% to 0.4%. To activate the capacity of EMP in absorbing energy, the drift the EMP should be less than 2%. The hysteresis behaviour of EMP is comparable to the hysteresis behaviour displayed by conventional steel concentric braces, by unstiffened steel plate shear walls or by reinforced concrete shear walls. Some existing hysteresis models from these three systems with little change on degradation factors on stiffness can be used for EMP in modelling with the real structures, such models as pivot (Dowell et al, 1998) or Takeda (1974)… The proposed hysteresis and monotonic behaviour can predict rather well the real behaviour of EMP loaded in shear with reasonable accuracy.

In order to develop the application of EMP in seismically retrofitting RC-MRFs, thirty two RC-MRFs have been designed in accordance with two codes EC2 and EC8. They are divided into two categories: EC2 and EC2+EC8 groups, depending on the design code referred to in design. These two groups consist of four configurations with different geometrical dimensions, representing the main structural resisting components for the buildings against both lateral forces and gravity loads. The buildings in each configuration have similar dimensions in plan and elevation. They are located in three seismicity zones, having the PGAs of 0.05g, 0.15g and 0.3g. In the zones having PGAs 0.05g and 0.15g, three frames have been designed: one only according to EC2 and two according to both EC2 and EC8 with two different Ductility Classes: Low and Medium. In the remaining zone, two frames have been designed corresponding to (1) one followed by EC2 and (2) one followed by EC2 and EC8 with Medium Ductility Class. The cross-sectional dimensions of the studied frames in the EC8 group have been selected as small as possible to comply with the damage limitations from EC8. In order to compare the steel content and responses of the frames under seismic actions, the cross-sectional dimensions of the frames in EC2 group have been selected the same as those of the EC8-L frames for the zones with PGAs 0.05g and 0.15g and similar to EC8-M frames for the zone with PGA 0.3g. Based on the comparison of the steel contents and local configuration of the resulting frames, it can be concluded that:

- The cross-sectional dimensions of frame components play a significant role on their steel configurations, not only affecting internal forces but also affecting the stiffness of the frames, which influence the total base shears for the frames in EC8 group. Moreover, the cross-sectional dimensions also influence the minimum steel contents required by the codes, especially for the frames belonging to the EC8 group.
- Steel contents of columns in the frames designed to EC2 are mainly dependent on the analysis. In addition to that, for the low-rise buildings, the steels of columns are usually governed by gravity loads and lateral forces (wind); however, for medium and high-rise buildings, due to larger cross-sectional dimensions, the steel contents of the columns are usually the minimum one from the code. On the other hand, for frames in EC8 group, the reinforcements in columns are determined by Capacity Design to obtain 'strong column – weak beam' mechanism. Comparing the steel contents of beams of the frames designed to EC2 or EC8, it is clear that the frames designed only in accordance with EC2 have lower steel contents than those of the frames designed according to both EC2 and EC8. This is obvious because the frames designed to EC8 must meet the requirements of EC2 as well.
- Based on the observation of the steel contents in the frames designed to EC8, it can be seen that different Ductility Classes change the steel contents in both beams and columns and the increase of the Ductility Class usually shifts steel from beams to columns. Moreover, it is clear that the slab plays a significant role in both cross-sectional dimensions and steel contents of the components of the RC-

MRFs. This is reflected through the effective width and reinforcements within this width of the slab contributing to both the stiffness and the bending resistance of the beams.

With aims at evaluating the seismic performance of the studied frames, general methods and common models used for seismic assessment of the existing RC-MRFs in relevance with EC8 have been summarised. The linear beam element with two concentrated plastic hinges at two ends of beams and columns has been adopted for evaluating the seismic response of the RC-MRFs. Besides, Pushover and NLTH analyses have been used to analyse the structures. Hysteretic behaviour of the nonlinear plastic hinges of beams and columns are based on the pivot model, proposed by Dowell et al. (1998). Performance criteria of the frames are based on FEMA 356 (2000). SAP 2000 has been adopted for performing the nonlinear static and nonlinear dynamic analyses. Four accelerograms, generated by GOSCA (Denoel, 2001), have been used as seismic input for NLTH analysis. All thirty two designed frames have been seismically assessed. Observing the seismic performance of the frames, designed in accordance with both EC2 and EC8, it is clear that the design goal is met, implying that the frames can reach the target displacements and develop the desired failure mechanisms. For the frames designed only in accordance with EC2, some prominent deficiencies are found, such as incomplete load path or the soft-story failure. A comparison of the results between Pushover and NLTH analyses has shown that Pushover analysis in conjunction with the N2 method, adopted by EC8, always overestimates the seismic performance of the existing frames compared with the results from NLTHs. The results of Pushover analysis for the large-period frames rather largely differ from the results obtained by NLTH analysis. The failures of studied RC-MRFs, obtained by Pushover, correspond to three situations: the local failure, the attainment of maximum base shear or the too large inter story drift ratio. Concerning the failure mechanisms of the studied structures, it is observed that the brittle failure of frames designed according to EC2 and to EC8-DCL dominates the response of the existing frames. This failure is usually caused by crushing of concrete due to shear at critical regions or due to shear at beam-column joints. It leads to the deficiency of incomplete load path of the structures. In many cases, the failure is coincident with the first plastic hinges occurring in beams. However, all frames in EC8 group perform favourable failure mechanisms represented by full or partial beam-sway mechanisms. Also based on the evaluation of the existing frames, it can be concluded that for the zones with low seismicity (PGA 0.05g in this study) it is possible not to design RC-MRFs in accordance with EC8 or to design the frames according to EC8 with Low Ductility Class because in all studied frames this zone can reach target displacements. However, for the higher seismicity zones (zones having PGA 0.15g and 0.3g in the current study) the RC-MRFs should be designed according to EC8 with medium ductility class to be able to resist the seismic actions. In addition to prediction of the deficiencies of the existing structures, their q-factors and maximum seismic capacity is also evaluated based on Pushover analysis. These q-factors are calculated based on equivalent SDOF systems having the same energy and maximum base shears as the existing MDOF ones. It is clear that q-factors obtained from Pushover analyses are about 1.2 to 2 times higher than that from the code.

Based on the knowledge of deficiencies of the existing frames obtained by Pushover and NLTH analyses, many attempts to exploit EMP to seismically retrofit the RC existing frames have been made. All frames designed in accordance with EC8 and Medium Ductility Class not need to retrofit because they can attain the target displacements under the earthquakes having magnitudes even much larger the design ones. All frames designed according to EC2 and EC8 with Low Ductility Class need to retrofit or upgrade because they cannot reach the target displacements due to premature failure of beam-column joints. In some frames, the failure of beam-column joints occurs at the state with rather low lateral displacement at the top of the frames. To retrofit these frames, Direct Displacement Based Design approach has been used to design the characteristics of EMP. The design is an iterative procedure, starting with the selection of the target displacements at the top. These target displacements are selected based on the results obtained from Pushover analysis. They are usually less than the limit displacements at which RC frames collapse due to crushing of the concrete at beam-column joints. The selected target displacements are corresponding to capacity of the existing frames which contributes to the overall resistance of the retrofitted frames. Based on the selected target displacements and capacity of the existing frames, following the steps in DDBD, properties of the SDOF equivalent systems of the retrofitted frames can be determined. Some hypotheses have been used to facilitate the design procedure such as: Equivalent Viscous Damping (EVD) of the EMP being calculated based on the Takeda thin hysteresis model (Priestley, 2007), EVD of the dual systems being determined based on strength assignment (Paulay, 2002)… Some excel sheets have been made to facilitate the design. The results from Direct Displacement Based Design on retrofitting are

significantly affected by some typical factors such as selected target displacements and capacity of the existing frames contributing to overall resistance of the retrofitted frames, EVD of the EMP as well as geometrical dimensions of the existing frames. The retrofitted design results, obtained by Pushover and NLTH analyses, have indicated that DDDB is a useful tool to seismically retrofit the existing frames using EMP. With the use of EMP, all retrofitted frames can reach target displacements under design earthquakes without any brittle failure as in cases of original frames. However, EMP cannot improve the behaviour of the beam-column joints. Under the earthquakes having magnitudes greater than design ones, failure of the nodes is still observed in all retrofitted frames. Besides, because of limitations of the types of EMP available in practice, in some cases EMP has been selected too conservatively, leading to too much overstrength for the retrofitted systems.

The comparison of the seismic performance of the frames before and after being retrofitted has shown that EMP is able to reduce the influence of the earthquake on the original frames by increasing their strength and stiffness and by absorbing the seismic energy. If the brittle failure at beam-column nodes can be fixed by some solutions such as using additional external stirrups, epoxy injections or carbon fibres…, EMP can absorb about 40% to 60% of the seismic energy generated in the retrofitted systems.

Proposed design procedure of connection between EMP and the frame elements is applicable. This was verified in the experiments when connecting EMP with the steel testing frames. The design approach for the connection is based on Capacity Design, all starting with the maximum resistance of the bars in a rhomb-shape stitch of the EMP and the tension field action developed in the EMP during shear loading. However, it is necessary to perform tests on the connections between EMP and the RC beams and columns. Also, improved practical details can be developed.

9.2. Recommendations

There are several types of EMP to date. The experiments on the normal and flattened types have been performed. The normal type has some disadvantages comparing with the flattened one, coming from difficulties in connecting the EMP with the frame elements if welded connection is used and of lower stiffness and strength. However, it has greater ductility than the flattened type. Therefore, more experimental, analytical and numerical studies on the normal types should be continued. In addition to that, the application of the normal type of EMP in order to seismically retrofit and/or upgrade RC-MRFs should be also investigated.

It is clear from the tests and numerical studies on EMP loaded in shear that pinching effects due to degradation of stiffness of the EMP when it buckles in compression govern the cyclic behaviour of EMP. This leads to limitations of EMP in absorbing the seismic energy. Therefore if the hysteresis behaviour of EMP can be improved by some means, the effectiveness of EMP in retrofitting the structures under seismic actions will be better. Some solutions that may be applied for improving the hysteresis behaviour of EMP under shear are to use stiffeners or combine EMP with concrete or mortal to have thicker plates with less degradation of stiffness in compression. This work should also be studied in future.

The selection of EMP to retrofit an existing RC frame under seismic actions and their distribution on the frame are still rather simple, based on the Direct Displacement Based Design method. Optimising the section of characteristics and positions of EMP on the frame is also necessary.

The study is limited to frames which are regular in both plan and elevation. Expanding the studies for irregular frames of RC-MRFs and for steel frames may be also interesting.

Another need is to perform some experimental shake-table tests of scaled building models in order to study the real behaviour of EMP with RC-MRFs and to calibrate better the numerical models.

REFERENCES

Amouri E. T. and Ghobarah A., **"Retrofit of RC Frames Using FRP Jacketing or Steel Bracing"**, Journal of Structural Earthquake Engineering, Vol 7., No. 2, pp 83-94

Astaneh-Asl Abolhassan, **"Seismic behavior and design of steel shear walls"**, Steel Tips: Structural Steel Educational Council / Technical Information and Product Service, july 2001

Astaneh-Asl Abolhassan, **"Composite steel plate shear walls"**, Steel Tips: Structural Steel Educational Council / Technical Information and Product Service, May 2002

ATC 19, **"Structural Response Modification Factors"**, Applied Technical Council 1995

ATC 33, ATC/BSSC, 1997b, *NEHRP* **"Commentary on the Guidelines for the Seismic Rehabilitation of Buildings"**, prepared by the Applied Technology Council (ATC-33 project) for the Building Seismic Safety Council, published by the Federal Emergency Management Agency, *FEMA 274 Report*, Washington, DC

ATC 40, **"Seismic evaluation and retrofit of concrete buildings"**, Report No SSC 96-01 – 11/1996

Basler, K., 1961, **"Strength of Plate Girders in Shear",** ASCE Journal of Structural Division, Vol. 87, No. ST7, pp. 151-180.

Bendimerad Fouad., **"The Boumerdes, Algeria, Earthquake of May 21, 2003",** Earthquake Engineering Research Institute EERI, October 2003

Bentz C. Evan **"Response 2000 – Reinforced Concrete Sectional Analysis using the Modified Compression Field Theory"**, Version 1.0.5, 2000

Berman Jeffrey, **"Plastic analysis and design of steelp plate shear walls"**, Department of Civil, Structural and Environmental Engineering, University at Buffalo

Berman Jeffrey W., Oguz C.Celik, Michel Bruneau, **"Comparing hysteretic behavior of light-gauge steel plate shear walls and braced frames"**, Engineering Structures vol. 27, 2005

Becker, Roy S.E, **"Seismic design of Special Concentrically Braced Steel Frames"**, Steel Tips, 1995

Becker Roy S.E, Michael Ishler, **"Seismic design Practice for Eccentrically Braced Frames based on the UBC 1994"**, Steel Tips, 1996

Bordea, Sorin. 2010. **"Dual Frame Systems of Buckling Restrained Braces"**, PhD thesis, University of Timosoara , Rumania.

Borzi B., Pinho R. and Crowley H., **"Simplified pushover-based vulnerability analysis for large-scale assessment of RC buildings",** Engineering Structures 30 (2008), pp 804–820, 7/2007

Borzi B., G.M. Calvi, A.S. Elnashai, E. Facciolic, J.J. Bommer: **"Inelastic spectra for displacement-based seismic design"**, Soil Dynamics and Earthquake Engineering 21 (2001), pp 47-61, 9/2000

Bracci Joseph M., Kunnath Shashi K., and Reinhorn Andrei M., **"Seismic Performance and Retrofit Evaluation of Reinforced Concrete Structures"**, Journal of Structural Engineering, January 1997/3

Caccese V., Elgaaly M., Chen R; (1993a), **"Experimental study of Thin Steel Plate Shear Walls under Cyclic Loads"**, Journal of Structural Engineering, ASCE, pp 573-587

Caccese V., Elgaaly M. And Du C. (1993), **"Post Buckling Behaviour of Steel Plate Shear Walls Under Cyclic Loads"**, Journal of Structural Engineering, ASCE, pp 588-605

Caccese, V. and Elgaaly, M., (1993) **"Experimental Study of Thin Steel-Plate Shear Walls Under Cyclic Load"**, *J. of Str. Engrg.*, ASCE, 119, n. 2, pp. 573-587

A.M. Chandler, P.A. Mendis, **"Performance of reinforced concrete frames using force and displacement based seismic assessment methods"**, Engineering Structures 22 (2000), pp. 352–363, 10/2008

Gian Michele Calvi, Timothy Sullivan, **"Development of a model code for Direct Displacement Based Seismic Design",** *The state of Earthquake Engineering Research in Italy: the ReLUIS-DPC 2005-2008 Project*, 141-171, © 2009 Doppiavoce, Napoli, Italy

Chopra, K. Anil, **"Dynamics of structures – Theory and Applications to Earthquake Engineering"**; Prentice-Hall, Inc; 1995

Chopra and Goel, 2002, **"A modal pushover analysis procedure for estimating seismic demand for buildings"**, Earthquake Engineering and Structural Dynamics, 31, 3, Mar. 2002, pp 561-582

Clough R. W., and Penzen J., **"Dynamics of Structures"** University of Berkeley, USA 1995

Cobden R., **"Aluminium : Physical Properties, Characteristics and Alloys"**, TALAT Lecture 1501, 1994

CSI, **"Analysis Reference Manual for SAP2000, ETABS, and SAFE"**, 4/2009

Dazio A., Beyer K., Bachmann H., **"Quasi-static cyclic tests and plastic hinge analysis of RC structural walls"**, Engineering Structures 31 (2009), pp 1556-1571

Dotreppe J-C., **"Béton armé"**, Université de Liège, Faculté des Sciences Appliquées

Dowell R.K., Seible F. and Wilson E.L. 1998., **"Pivot hysteresis model for reinforced concrete members"**, *ACI Structural Journal*, 95(5), 607-617.

Dubas, P. and Gehri E., **"Behaviour and Design of Steel Plated Structures"**, Edited by P. Dubas and E. Gehri, 1986

Driver Robert G., Geoffrey L.Kulak, D.J. Laurie Kennedy, Alaa E.Elwi, **"Cyclic test of four-story steel plate shear wall"**, Journal of Structural Engineering, February 1998

Earthquake Tip 23, **"Why are buildings with shear walls preferred in seismic regions?"**, Earthquake Tip 23, ITTK Indian Institute of Technology Kanpur, 2004

ECCS, **"Recommended Testing Procedure for Assessing the Behaviour of Structural Steel Elements under Cyclic Loads"**, ECCS Publication 1986

ECCS, **"Essential of Eurocode 3 – Design manual for steel structure in Buildings"**, ECCS Publication 1991

Elgaaly Mohamed, **"Thin steel plate shear walls behavior and analysis"**, Thin-Walled Structures vol. 32, 1998

Elgaaly, M. and Caccese, V., (1993) **"Post-buckling Behavior of Steel- Plate Shear Walls under Cyclic Loads"**, *J. of Str. Engrg.* ASCE, 119, n. 2, pp. 588-605

EN 1991-1, **"Eurocode 1 : Bases de calcul et actions sur les structures - Partie 1 : Bases de calcul"**, EUROCODE 1 (ENV 1991-1 : 1994)

EC2, EN 1992, Eurocode2 - 1: **"Design of concrete structures"**, December 2004

EC8, EC8-1, EN 1998-1, **"Eurocode 8 - Calcul des structures pour leur résistance aux séismes - Partie 1 : Règles générales, actions sismiques et règles pour les bâtiments"**, EUROCODE 8, 12/2004

EC8-3, EN 1998-3, **"Eurocode 8 – Design of structures for earthquake resistance - Partie 3 : Assessment and retrofitting of buildings"**, EUROCODE 8, 11/2004

EN 1993-1, **"Eurocode 3 : Calcul des structures en acier – Partie 1-1: Règles générales – Règles générales et règles pour les bâtiment**s", EUROCODE 3 (ENV 1993-1-1 : 1992 / A2)

Expanded Metal Manufacturers Association (EMMA) Division of the National Association of Architectural Metal Manufacturers (NAAM) **"EMMA 557-99: Standards for expanded metal"**, 1999

Fajfar P., **"Seismic Assessment of structures by a practiced-oriented method"**, Extreme Man-Made and Natural Hazards in Dynamics of Structures, 257-284, 2007 Springer

Fajfar and Fischinger, 1987, **"Nonlinear seismic analysis of RC buildings: Implications for a case study"**, European Earthquake Engineering

Fajfar and Fischinger, 1988, **"N2 – a method for nonlinear seismic analysis of regular buildings"**, 9th WCEE Tokyo, Kyoto, 1988

Fajfar and Gaspersic, 1994, **"A method for the prediction of seismic damage in RC buildings"** 10th WCEE, Vienna

Fajfar and Gaspersic, 1996, **"The N2 method for the seismic damage analysis of RC buildings",** Earthquake Engineering and Structural Analysis, 25, 1, Jan 1996, pp. 31-46

Fardis M. N.; Economu, S.N; Antoniou, A.N.; Komodromos, P.J.; Sfakianakis, M.G **"Damage measure and failure criteria. Part I – contribution of the University of Patras"**, Final report of the Cooperative Research on the Seismic Response of Reinforced Concrete Structures, 2nd phase, LNEC, Lisbon, 1993

Fardis M. N., Carvalho E., Elnashai Amr, Faccioli E., Pinto P. and Plumier A. **"Design if structures for earthquake reisistance. General rules, seismic actions, design rules for buildings, foundations an retaining structures"**, 2005

Fardis M. N., **"Seismic design, assessment and retrofitting of concrete buildings based on EN-Eurocode8"**, Springer, 2009

Filippou C. Filip, Ahmad Issa, **"Nonlinear Analysis of Reinforced Concrete Frames under Cyclic Load Reversals"**, Report No. UCB/EERC-88/12, Earthquake Engineering Research Centre, College of Engineering, University of California, Berkerly, 12/1998

FEMA 356, **"Pre-standard and Commentary for the seismic Rehabilitation of Building"**, November, 2000

FINELG, **"Nonlinear Finite Analysis Program"**, University of Liege, Version 8.5, 15/05/2002

Fujimoto, M., Wada, A., Saeki, E., Watanabe, A. and Hitomi, Y. (1988) **"A study on the un-bonded brace encased in buckling-restraining concrete and steel tube"**, *Journal of Structural Engineering,* 034B, 249–258 (in Japanese)

Fukuta, T., Nishiyama, I., Yamanouchi, H., and Kato, B. (1989). **"Seismic Performance of SteelFrames with Inverted V Braces."** ASCE Journal of Structural Engineering, 115(8), 2016–2028.

GOSCA [2001], Denoël, V. **"Calcul sismique des ouvrages d'art,"** *Individual Study*, Travail de fin d'études de l'Université de Liege, Belgium.

Horie, T., Yabe, Y., Hori, T., Nakamura, S. (1993). **"Elasto-plastic behavior of steel brace with restraint system for post buckling"**, *Journal of Steel Structures*, 1, 187–194 (in Japanese)

Inoue, K. and Sawaisumi, S. (1992). **"Bracing design criterion of the reinforced concrete panel including unbounded steel diagonal braces"**, *Journal of Structural and Construction Engineering*, 432, 41–49 (in Japanese).

Inoue, K. and Sawaisumi, S. (1992). **"Bracing design criterion of the reinforced concrete panel including unbounded steel diagonal braces",** *Journal of Structural and Construction Engineering*, 432, 41–49 (in Japanese)

Inoue, K., Sawaizumi, S., Higashibata, Y. and Inoue, K. (1993). **"Stiffening design at the edge of reinforced concrete panel including un-bonded steel diagonal braces"**, *Journal of Structural Engineering*, 443, 137–146 (in Japanese)

Inoue, K., Sawaisumi, S. and Higashibata, Y. (2001). **"Stiffening requirements for unbonded braces encased in concrete panels",** *Journal of Structural Engineering*, 127(6), 712–719

Jerome F.Hajjar, **"Composite steel and concrete structural systems for seismic engineering"**, Journal of Constructional Steel Research vol. 58, 2002

H.J. Judi, R.C. Fenwick & B.J. Davidson, **"Direct displacement based design – a definition of damping"**, NZSEE 2001, Conference

Kahn, L. F., and Hanson, R. D. (1976). **"Inelastic Cycles of Axially Loaded Steel Members."** ASCE Journal of the Structural Division, 102.

Kuwahara, S. and Tada, M. (1993). **"A study on stiffening capacity of double-tube members",** *Journal of Structural and Construction Engineering*, 445, 151–158 (in Japanese)

Lee, K.., and Bruneau, M. (2005). **"Energy Dissipation of Compression Members in Concentrically Braced Frames: Review of Experimental Data."** ASCE Journal of Structural Engineering, 131 (4), 552-559.

López W.A. and R. Sabelli, **"Seismic Design of Buckling Restrained Braced Frames",** 2004

Lubell Adam S., Helmut G.L.Prion, Carlos E.Ventura, Mahmoud Rezai, **"Unstiffened steel plate shear wall performance under cyclic loading"**, Journal of Structural Engineering, april 2000

Magliulo G., Maddaloni G., Cosenza E., **"Comparison between non-linear dynamic analysis performed according to EC8 and elastic and non-linear static analyses"**, Engineering Structures 29 (2007), pp. 2893–2900, 3/2007

Maheria M. R. and Ghaffarzadehb H., **"Connection overstrength in steel-braced RC frames"**, Engineering Structures 30 (2008), pp. 1938–1948, 2/2008

Maley Timothy J., Sullivan Timothy J. and Corte G. D., **"Development of a Displacement-Based Design Method for Steel Dual Systems with Buckling-Restrained Braces and Moment-Resisting Frames"**, Journal of Earthquake Engineering, 14(S1):106–140, 2010

Manabe, N., Shimokawa, H., Kamitani, M, Morino, S. and Kawaguchi, J. (1996). **"Elasto-plastic behavior of flat-bar brace stiffened by square steel tube"**, *Summaries of Technical Papers of Annual Meeting*, Architectural Institute of Japan, pp. 783–784 (in Japanese)

Mander J.B., Priestley M.J.N., Park R. [1988] **"Theoretical stress-strain model for confined concrete,"** *Journal of Structural Engineering*, Vol. 114, No. 8, pp. 1804-1826.

Maquoi R., **"Cours de constructions métalliques et mixtes"**, Université de Liège, Faculté des Sciences Appliquées, édition 2000

Maquoi R., F.Cerfontaine, **"Eléments de construction mixte"**, Notes de cours, Université de Liège, Septembre 2001

Marini A., Meda A., **"Retrofitting of R/C shear walls by means of high performance jackets"**, Engineering Structures, 2009, pp 3059-3064

Matteis G. De, R. Landolfo, F.M. Mazzolani, **"Seismic response of MR steel frames with low-yield steel shear panels"**, Engineering Structures vol. 25, 2003

Matteis G. De, Gianfranco, **"On the use of pure aluminium shear panels for seismic passive control of steel frames"**, Earthquake Engineering and Structural Dynamics, 2005

Matteis, G. De **"Effect of lightweight cladding panels on the seismic performance of moment resisting steel frames"**; Engineering Structures 27 (2005) 1662–1676

Matteis, G. De, Mazzolani, FM, Panico S. **"Pure aluminium shear panels as passive control system for seismic protection of steel moment resisting frames".** Proceedings of the 4th STESSA Conference (Behaviour of Steel Structure in Seismic Areas), 2003, Naples, Italy, pp. 599-607)

Matteis G. De, PanicoS., Formisano A., Mazzolani F.M. (2005). **"Experimental Tests on Pure Aluminium Shear Panels Under Cyclic Loading"**. Proceedings of the Int. Conference o, Earthquake Engineering in 21th Century (EE-21 C), Skopje, Macedonia, August

Matteis G. De, R. Landolfo, F.M. Mazzolani, **"Seismic response of MR steel frames with low-yield steel shear steel"**, Engineering Structure 25 (2003) page 155-168

Mazzolani, M. Federico, **"Seismic upgrading of RC buildings by advanced techniques, The ILVA-IDEM Research Project"**, Polimetrica International Scientific Publisher, 2006

Medhekar ManoJ.S., Lauri Kennedy D.J, **"Seismic evaluation of steel buildings with concentrically braced frames"**, 1997

Medhekar M.S., D.J.L. Kennedy, **"Displacement-based seismic design of buildings—theory"**, Engineering Structures 22 (2000), pp. 201–209, 8/1998

Medhekar M.S., D.J.L. Kennedy, **"Displacement-based seismic design of buildings—application"**, Engineering Structures 22 (2000), pp. 210–221, 8/1998

Métal Déployé Belge s.a., **"Le catalogue Métal Déployé"**, édition 10/2003

Mimura, H. and Akiyama, H., 1997 **"Load-Deflection Relationship of Earthquake Resistance Steel Shear Walls With a Developed Diagonal Tension Field"** Transactions, Architectural Institute of Japan, 260, October, pp 109-114

Montejo, A. Luis, Kowalsky J. Mervyn, **"CUBIA – set of codes for the analysis of reinforced concrete members"**, NC State University, Technical report No. IS 07-01

Mosley Bill, Bungey John and Hulse Ray, **"Reinforced Concrete Designed to Eurocode 2",** Palgrave Macmillan, Sixth Edition, 2007

Nagao, N. and Takahashi, S. (1990). **"A study on the elasto-plastic behavior of un-bonded composite bracing (Part 1: experiments on isolated members under cyclic loading)**", *Journal of Structural Engineering*, 415, 105–115 (in Japanese).

Nakagawa S, Kihara H, Torii S, Nakata Y, Matsuoka Y, Fujisawa K et al. **"Hysteretic behavior of low yield strength steel panel shear walls: experimental investigation"**. In: Proceedings of the 11th WCEE, Elsevier, CD-ROM, Paper No. 171. 1996

Nakashima, M. and Wakabayashi, M. (1992), **"Analysis and Design of Steel Braces and Braced Frames in Building Structures"** in Stability and Ductility of Steel Structures under Cyclic Loading, Fukumoto, Y. and Lee, G.C. editors, CRC Press, Boca Raton, FL, pp 309-321.

Nakashima Masayoshi, Satoshi Iwai, Mamoru Iwata, Toru Takeuchi, Shinzo Konomi, Takashi Akazawa, Kazuhiro Saburi, **"Energy dissipation behaviour of shear panels made of low yield steel"**, Earthquake Engineering and Structural Dynamics vol.23, 1994

Nakashima Masayoshi, **"Strain-hardening behavior of shear panels made of low-yield steel. I:Test"**, Journal of Structural Engineering, December 1995

Nilson Arthur H., Darwin David, Dolan Charles W., **"Design of Concrete Structure"**, 13th Edition, The McGraw-Hill Company, 2004

NEHRP, October 1997 **"Guidelines for the seismic rehabilitation of buildings",** *Federal Emergency Management Agency*, Washington, DC.

Oesterle, R.G., Fiorata, A. E., Aristizabal – Ochoa, J. D., and Corley, W. G., **"Hysteretic Response of Reinforced Concrete Structural Walls"**, PCA Research and Development Construction Laboratories, Stocky Illinois, June 1978

Otani Shunsuke, **"Nonlinear Dynamic Analysis of Reinforced Concrete Building Structures"**, Canadian Journal of Civil Engineering, Vol 7, pp. 333-344 (1980)

Patxi Uriz Stephen A. Mahin, **"Toward Earthquake-Resistant Design of Concentrically Braced Steel-Frame Structures",** PEER 2008/08, 11/2008

Park R. and Paulay T., **"Reinforced Concrete Structures",** A Wiley-Interscience Publication, 1974

Pecquet E., S.Cescotto, **"Mechanical behaviour of expanded metal sheets: critical and ultimate loads of square and rectangular sheets loaded in shear"**, 7th National Congress on Theoritical and Applied Mechanics, May 2006

Pecquet E., **"Simulations numériques et modèle analytique de tôles de metal déployé carrées sollicitées en cisaillement : comportements critique et ultime"**, Rapport intermédiaire n°4, Juillet 2005

Phung Ngoc Dung, André Plumier, **"Experiments of expanded metal panels under shear loading"**, 9th National Congress on theoretical and Applied Mechanics, May 2009.

Phung Ngoc Dung, André Plumier, **"Behaviour of expanded metal panels under shear loading"**, Proceedings SDSS 2010

Phung Ngoc Dung, André Plumier, **"Retrofitting and upgrading reinforced concrete moment resisting frame by using Expanded metal panels"**, Proceedings ECEE14, 2010

Pinho, Rui; Antoniou Stelios; Cassarotti, C.; Lopez, M. **"A displacement-based adaptive pushover for assessment of buildings and earthquake",** Advances in Earthquake Engineering for Urban Risk Reduction, 79-84, 2006 Springer

Plumier André, **"The dogbone - Back to the future"**, AISC Engineering Journal vol. 34, n°2, 1997

Plumier, A., Denoël, V., Sanchez, L., Doneux, C., Warnotte, V., Van Alboom, W. [2005] **"Seismic assessment and retrofitting of a S shape building with expansion joints"** *Seismic Performance Assessment and Rehabilitation of Existing buildings International Workshop*, pp. 253-267

Plumier, A., Warnotte, V., Van Alboom, W [2005], **"A case study of flexible reconnection over expansion joints in a buildings"** P*roceedings of 9th World Seminar on Seismic Isolation, Energy Dissipation and Active Vibration Control of Structures*, Kobe, Japan.

Plumier André, **"Constructions en zone sismique"**, Université de Liège, Faculté des Sciences Appliquées, édition 2010

Plumier André, **"Earthquake Resistant Steel Structures"**, Arcelor Mital Technical Brochure, 2008

Popov, E.P., **"Seismic behaviour of Structural Sub-assemblages"**, Journal of the Structural Division ASCE, V.106, No ST7, July 1980

Priestley M.J.N., Grant D.N., and Blandon C.A., **"Direct displacement-based seismic design"**, 2005 NZSEE Conference

Priestley, M. J. N., Calvi, G.M., Kowalsky, M. J., **"Displacement-Based Seismic Design of Structures"**, IUSS PRESS, Pavia, Italy, 2007

Riva P., A.Meda, E.Giuriani, **"Cyclic behaviour of a full scale RC structural wall"**, Engineering Structures vol. 25, 2003

Roberts T.M., S.Sabouri-Ghomi, « **Hysteretic characteristics of unstiffened perforated steel plate shear panels** », Thin-Walled Structures vol.14, 1992

Roberts, T.M., (1995) **"Seismic Resistance of Steel Plate Shear Walls"**, *Engineering Structures,* 17, no.5, pp. 344-351

Rocha P., Delgado P., Costa A. and Delgado R., **"Seismic retrofit of RC frames"**, Computers and Structures 82 (2004), pp. 1523–1534, 5/2004

Roeder Charles W. and Egor P.Popov, **"Eccentrically Steel Braced Frames for Earthquake"**, Journal of Structural Engineering, American Society for Civil Engineers, Volume 104, Number 3, March 1978.

Rueda M. J. E. and Elnashai, **"A novel technique for the retrofitting for the retrofitting of reinforced concrete structures"**, Engineering Structures, Vol 17, No. 5, pp 359-371, 1995

Rougier V.C., B.M. Luccioni, **"Numerical assessment of FRP retrofitting systems for reinforced concrete elements"**, Engineering Structures 29 (2007), pp. 1664–1675, 10/2006

Sabouri-Ghomi, S., and Roberts, T.M., (1992) **"Nonlinear Dynamic Analysis of Steel Plate Shear Walls Including Shear and Bending Deformations"**, *Engineering Structures,* 14, no.5, pp. 309-317

Sadjadia R., M.R. Kianousha and S. Talebi, **"Seismic performance of reinforced concrete moment resisting frames"**, Engineering Structures 29 (2007), pp. 2365–2380, 1/2007

SAP2000 [2004] **"Three dimensional static and dynamic finite element analysis and design of structures, Version 14.0."** *Computers & Structures, Structural and Earthquake Engineering Software, Berkeley*, California, USA

Sanchez Luiz, **"Seismic Performance of Ductile Moment Resisting Steel Frames. First Step for Eurocode 8 Calibration"**, Thèse de Doctorat. Faculté des Sciences Appliquées de l'Université de Liège, 2004

Saatcioglu, M., Gardner, N.J., and Ghobarah, A. (2001). **"1999 Turkey Earthquake Performance of RC Structures"**, *Concrete International*, **23**(3), 47-56.

Schumacher Ann, Gilbert Y.Grondin, Geoffrey L.Kulak, **"Connection of infill panels in steel plate shear walls"**, University of Alberta Department of Civil and Environmental Engineering, Structural Engineering Report n°217, August 1997

Seilie Ignasius F., John D.Hooper, **"Steel plate shear walls: Practical design and construction"**, Modern Steel Construction, April 2005

SEISMOSTRUCT, **"Nonlinear Finite Analysis Program"**, SEISMO Group, Version 5.0.1, 17/01/2010

Shanmugam N.E., **"Openings in thin-walled steel structures"**, Thin-Walled Structures vol.28 n°3/4, 1997

Shishkin Jonah J., Robert G.Driver, Gilbert Y.Grondin, **"Analysis of steel plate shear walls using the modified strip models"**, University of Alberta Department of Civil and Environmental Engineering, Structural Engineering Report n°261, November 2005

Shimizu, T., Fujisawa, K., Uemura, K. and Inoue, I. (1997) **"Design method to prevent buckling of low yield strength steel tube brace and fracturing of joints (Parts 1 and 2)"**, *Summaries of Technical Papers of Annual Meeting*, Architectural Institute of Japan, pp. 781–784 (in Japanese)

Sezen H., A.S. Whittaker, K.J. Elwood, K.M. Mosalam, **"Performance of reinforced concrete buildings during the August 17, 1999 Koaceli, Turkey earthquake, and seismic design and construction practise in Turkey"**, Engineering Structures vol. 25, 2003

Sokkary E. H., K. Galal, **"Analytical investigation of the seismic performance of RC frames rehabilitated using different rehabilitation techniques"**, Engineering Structures 31 (2009), pp. 1955_1966, 2009

Sridhara, B.N. (1990). **"Sleeved column as a basic compression member"**, *Proc. 4th International Conference on Steel Structures & Space Frames*, Singapore, pp. 181–188

T. J. Sullivan, G. M. Calvi, and M. J. N. Priestley, **"Initial Stiffness versus Secant Stiffness in Displacement Based Design",** 13th World Conference on Earthquake Engineering, Vancouver, B.C., Canada, August 1-6, 2004 Paper No. 2888

Suzuki, N., Asano, R. Tohata, Y., Sasaki, T. and Segawa, T. (1994) **"Experimental study on the H-section steel brace encased in RC or steel tube"**, *Summaries of Technical Papers of Annual Meeting*, Architectural Institute of Japan, pp. 1621–1622 (in Japanese)

Takahashi, Y., Takemoto, Y., Takeda, T., and Tagagi, M., 1973. **"Experimental study on Thin Steel Shear Walls and Particular Bracings Under Alternate Horizontal Load."**, Preliminary Report, IABSE Symposium on Resistance and Ultimate Deformability of Structures Acted on by Well-defined Repeated Loads, Lisbon , Portugal, pp. 185-191

Takeda, T.; Sozen, M.A. and Neisen, N. N. 1970 **"Reinforced concrete response to simulated earthquakes"** ASCE Journal of the Structural Division, 96 (ST12), pp. 2557-2573

Tanaka K, Torii T, Sasaki Y, Miyama T, Kawai H, Iwata M et al. **"Practical application of damage tolerant structures with seismic control panel using low yield point steel to a high-rise steel building"** In: Proceedings, Structural Engineering World Wide, Elsevier, CD-ROM, Paper T190-4. 1998

Tastani S.P., Pantazopoulou S.J., **"Detailing procedures for seismic rehabilitation of reinforced concrete members with fiber reinforced polymers",** Engineering Structures 30 (2008), pp. 450–461, 5/2008

Timber, P. A.; Kulak, G.L. **"Experimental study of Steel plate shear walls"**, Department of Civil Engineering, The University of Alberta , Edmonton, Alberta, Structural Engineering Report 114, 1983

Thorburn L. Jane, G.L Kulak and C.J Montgomery, **"Analysis of Steel plate shear walls"**, 1993; Structural Engineering Report No.107, University of Albert

Tremblay, R. (2002). **"Inelastic seismic response of steel bracing members"** Journal of Constructional Steel Research, 58, pp 665-701.

Tromposch, E. W. and Kulak, G. L., **"Cyclic and static behaviour of thin panel steel plate shear walls"**, April 1987, Structural Engineering Report No.145, University of Alberta

Tsai, K.C. and Lai, J.W. (2002). **"A study of buckling restrained seismic braced frame"**, *Structural Engineering*, 17(2) 3–32, (in Chinese)

Tsai, K.C., Hwang, Y.C., Weng, C.S., Shirai, T. and Nakamura, H. (2002), **"Experimental tests of large scale buckling restrained braces and frames"**, *Proceedings, Passive Control Symposium*, December 2002, Tokyo Institute of Technology, Tokyo, Japan.

Tsai, K.C., Hwang, Y.C. and Weng, C.S. (2004). **"Subassembly testing and analysis of buckling restrained brace for seismic resistance"**, *Structural Engineering*, 19(2)

Vian Darren, Michel Bruneau, **"Testing of special LYS steel plate shear walls"**, 13th World Conference on Earthquake Engineering Vancouver Canada, August 2004

Valipour H. R., Foster S. J., **"Nonlinear reinforced concrete frame element with torsion",** Engineering Structures 32 (2010) 988-1002, 15/1/2010

Verderamea, G.M., Giovanni Fabbrocinob and Gaetano Manfredi, **"Seismic response of r.c. columns with smooth reinforcement. Part I: Monotonic tests"**, Engineering Structures 30 (2008), pp 2277–2288, 3/2008

Verderamea, G.M., Giovanni Fabbrocinob and Gaetano Manfredi, **"Seismic response of r.c. columns with smooth reinforcement. Part II: Cyclic tests"**, Engineering Structures 30 (2008), pp 2277–2288, 3/2008

Wagner, H., 1931, **"Flat Sheet Metal Girders with Very Thin Webs, Part I – General Theories and Assumptions"** Technical Memo No.604, National Advisory Committee for Aeronautics, Washington D.C.

Wakabayashi, M., Nakamura, T., Kashibara, A., Morizono, T. and Yokoyama, H. (1973). **"Experimental study of elasto-plastic properties of precast concrete wall panels with built-in insulating braces"**, Summaries of Technical Papers of Annual Meeting, Architectural Institute of Japan, pp. 1041–1044

Warnotte, Vivianne "**Mitigation of pounding between adjacent buildings in earthquake situation"** Thèse de Doctorat présentée en vue de l'obtention du grade de Docteur en Sciences Appliquées, Université de Liège, 2008

Watanabe, A., Hitomi, Y., Yaeki, E., Wada, A. and Fujimoto, M. (1988). **"Properties of brace encased in buckling-restraining concrete and steel tube"**, *Proc. 9th World Conference on Earthquake Engineering*, Tokyo-Kyoto, Japan, Vol. IV, pp. 719–724.

Yamaguchi Tanemi, Toru Takeuchi, Toshimichi Nagao, Takahiko Suzuki, Yasuhiro Nakata, Takumi Ikebe, Akira Minami, **"Seismic control devices using low-yield-point steel"**, Nippon Steel Technical Report n°77,78, July 1998

Yokohama Japan, D.C.Rai, S.Jain, **"Inelastic buckling criteria for aluminium shear panels as energy dissipation devices"**, Proceedings of the Fifth International Conference on Behaviour of Steel Structures in Seismic Areas, August 2006

Youssefa M.A., H. Ghaffarzadehb and M. Nehdi, **"Seismic performance of RC frames with concentric internal steel bracing"**, Engineering Structures 29 (2007), pp. 1561–1568, 10/2006

Zayas, V. A., Mahin, S. A., and Popov, E. P. (1980a). **"Cyclic Inelastic Behavior of Steel Offshore Structures."** *UCB/EERC-80/27*, University of California, Berkeley, Berkeley,California.

Zayas, V. A., Popov, E. P., and Mahin, S. A. (1980b). **"Cyclic Inelastic Buckling of Tubular Steel Braces."** *UCB/EERC-80/16*, University of California, Berkeley, California